GAZİANTEP UNIVERSITY

3rd INTERNATIONAL ENERGY & ENGINEERING CONGRESS

UEMK 2018

CONTACT US

uemk2018@gmail.com

+90 (342) 3601200- 3933 -3999

http://uemk.gantep.edu.tr

18-19 October 2018
Faculty of Law
Gaziantep University
TURKEY

TC ENERJİ VE TABİİ KAYNAKLAR BAKANLIĞI · EPDK · SANKO ENERJİ · BÜYÜKŞEHİR GAZİANTEP · LİMİTSİZ ENERJİ · Springer

UEMK 2018
BİLDİRİ ÖZETLERİ KİTABI

18-19 Ekim 2018
Hukuk Fakültesi

GAZİANTEP ÜNİVERSİTESİ
ENERJİ SİSTEMLERİ MÜHENDİSLİĞİ BÖLÜMÜ
TÜRKİYE

© Copyright 2018 UEMK 2018

3rd INTERNATIONAL ENERGY & ENGINEERING CONGRESS PROCEEDINGS BOOK

3. ULUSLARARASI ENERJİ & MÜHENDİSLİK KONGRESİ BİLDİRİLER KİTABI

ISBN
978-975-7375-45-6

Date of Approval / Onaylanma Tarihi
2018-10-23 08:14:53

Editor / Editör
Doç. Dr. Adem ATMACA

Gaziantep Üniversitesi
Mühendislik Fakültesi
Enerji Sistemleri Mühendisliği Yayınları
Gaziantep/ TÜRKİYE

Tel: +90 342 360 1200
Fax: +90 342 360 1013
e-posta: uemk2018@gmail.com
web-site: http://uemk.gantep.edu.tr/

SPONSORS

T.C. ENERJİ VE TABİİ KAYNAKLAR BAKANLIĞI

EPDK ENERJİ PİYASASI DÜZENLEME KURUMU

SANKO ENERJİ

BÜYÜKŞEHİR GAZİANTEP

DOW

LİMİTSİZ ENERJİ "Doğandan Gelen Enerji"

Springer

HONORORIAL CHAIR

Prof. Dr. Ali GÜR
Rector of Gaziantep University
TURKEY

CHAIR

Assoc. Prof. Dr. Adem ATMACA
Energy Systems Engineering
Gaziantep University
TURKEY

INTERNATIONAL SCIENTIFIC BOARD

Assoc. Prof. Dr. Adem Atmaca - TURKEY
Dr. Alexander Hollberg - GERMANY
Prof. Dr. Arif Hepbaşlı - TURKEY
Prof. Dr. Benedict D. Ilozor - USA
Dr. Bert Liebold - GERMANY
Prof. Dr. Bin Chen - CHINA
Asst. Prof. Dr. Derya Bakbak - TURKEY
Assoc. Prof. Dr. Erdihan Tunç - TURKEY
Asst. Prof. Dr. Fatih Balcı - TURKEY
Assoc.Prof.Dr.Gillian F.Menzies - ENGLAND
Prof. Dr. Hüsamettin Bulut- TURKEY
Prof. Dr. Ignacio Acosta Garcia - SPAIN
Asst. Prof. Dr. Jitender Grover - INDIA
Prof. Dr. Joerg Baumeister - AUSTRALIA
Prof. Dr. Jürgen Ruth - GERMANY
Dr. Katrin Linne - GERMANY
Asst.Prof.Dr.Luis Martín Pomares- QATAR
Dr. Martin Brabant - AUSTRIA
Prof. Dr. Mehmet Kanoğlu - TURKEY
Prof. Dr. Metin Bedir - TURKEY
Asst. Prof. Dr. Mohammed Kamil - UAE
Asst. Prof. Dr. Mortaza Aghbashlo - IRAN
Assoc. Prof. Dr. Necip Fazıl Yılmaz - TURKEY
Assoc. Prof. Dr. Nihat Atmaca - TURKEY
Dr. Qian Yin - CHINA
Prof. Dr. Recep Yumrutaş - TURKEY
Prof. Dr. Sait Söylemez - TURKEY
Asst. Prof. Dr. Serap Sur Çelik - TURKEY
Prof. Dr. Tamara Nestorovic - GERMANY
Dr. Usep Surahman - INDONESIA
Prof. Dr. Yunus Çengel - TURKEY

ORGANIZING COMMITTEE

Assoc. Prof. Dr. Adem Atmaca - TURKEY
Prof. Dr. Bin Chen - CHINA
Dr. Fatih Balcı - TURKEY
Assoc. Prof. Dr. Nihat Atmaca - TURKEY
Dr. Serap Sur Çelik - TURKEY

Ahmet KILIÇ
Ayşe SARIOĞLU
Ayşegül ÖZTÜRK
Büşra Esra TÜRK
Cem YÜCEER
Ebru GEDİK
Fatma Zehra KARDAŞ
Ghaith ALQUDSI
Gökçe YÜREKLİ
Harun TAŞTAN
Kübra İBOLAR
Mehmet Latif ÖZTÜRK
Merve ÇAMCI
Miraç Anıl TUNÇ
Mücahit ÇALIŞKAN
Okan DENGİZ
Saturnin Floris KACKA SANGOLA
Serhat BAYKARA
Yurdagül DAĞLAR
Yusuf SAYGI
Zeynep Nur VERGİLİ

CONFERENCE TOPICS

Energy
Modeling of Energy and Systems
Energy Transport, Power & Fuels
Energy Systems
Energy Supply and Demand
Renewable Energy Resources and Technologies
Energy Audit and Rational Use of Energy
Advanced Energy Technologies
Energy-Saving Technologies
Electrical and Electronics Engineering
Civil Engineering and green buildings
Climate Change and Global Warming
Environmental engineering, Environmental Systems and Telecommunications
Environmental Safety and Health
Water Resources and Future Conflicts
Solid Waste, Waste Treatment and Management
Soil pollution
Air Pollution Control
Noise and Vibration Control
Planning & Sustainable Development Policy
Environmental Policy, Planning and Economy
Energy Policy, Planning and Economics.
Computer engineering
Global Climate Change
International cooperation to reduce carbon emissions
Industrial Engineering, Sustainable Materials
More Sustainable Product Design
Science for Sustainable Development
Social Security, Process Safety and Hazard Management
Waste Assessment and Treatment
Sustainable Urban Development
Mechanical Engineering
Mechanical and Structural Sustainability
Sustainable Chemical ProcessesTools to plan, design and operate integrated green technology
Adsorption and Gas Storage Materials
Sustainable Agriculture and Organic Farming; Green Agriculture Technology
Food engineering, Food Safety and Organic Food
Nanotechnology for Sustainability
Life Cycle Assessment
Computation, Modeling and Simulation, Ecological Sustainability
Management, Green Economy and Sustainable Economic Development
Natural Sciences

ÖNSÖZ

2018 yılında enerji sektörü dünyanın gündeminde yine ön sıralarda yer almayı sürdürmektedir. Son yıllarda özellikle ülkemize yakın coğrafyalarda yaşanan gelişmelerin uluslararası enerji politikaları üzerinde önemli etkileri olmaktadır. Sürekli artan enerji talebini karşılamak ve dışa bağımlılığımızı azaltmak için varolan bütün potansiyelimizi kullanmak, yerli ve yenilenebilirkaynaklarımızın tamamından yararlanmak durumundayız. Hedeflerimizi gerçekleştirmek için en önemli araç olan özellikle mühendislik alanında yapılacak AR-GE faaliyetlerinin sürdürülmesiyle hem dünyadaki teknolojik gelişmeleri ülkemize kazandırmak hem de kendi YERLİ teknolojilerimizi geliştirmemiz gerekmektedir. Gelişmiş dünya ülkeleri arasındaki yerimizi almak için 2023 hedefleri doğrultusunda, Ülke olarak tüm kaynaklarımızı en verimli bir şekilde kullanarak, çevreye duyarlı, sürdürülebiliryeni teknolojiler geliştirmemiz gerekmektedir. Türkiye son 10 yılda, dünyada doğalgaz ve elektrik talebinin Çin'den sonra en fazla arttığı ülke konumundadır. Ülkemizin önümüzdeki dönemde de enerji talebi artışı bakımından dünyanın en dinamik ekonomilerinden biri olmaya devam etmesi beklenmektedir. Ülkemizin enerji talebinin yaklaşık %74'ü yabancı kaynaklardan karşılanmaktadır. Bu durum yenilenebilir enerji kaynaklarından ciddi oranda yararlanılması gerektiği hususunu gözler önüne sermektedir. Önümüzde sürdürülebilir yerli enerji kaynaklarının kullanılması için atılması gereken büyük adımlar vardır. Uluslararası Enerji ve Mühendislik konferansının Gaziantep sanayisi ile akademisyenleri ortak bir platformda buluşturarak bu tip projelere kapılar aralamasını diliyorum.

Konferansımız 4 farklı salonda, toplam 13 oturumda yapılmış olup, 500'e yakın katılımcı hocamız yaklaşık 150 akademik bildiri sunmuştur. Konferansın gerçekleşmesinde emeği geçen herkese, özellikle ev sahibi Gaziantep Üniversitesi yöneticilerine, konferansın ta en başından beri sunduğu bütün imkanlar ve teşvik edici yardımlar için Sayın Rektörümüz Prof. Dr. Ali GÜR'e, Rektör yardımcıları Prof. Dr. Metin BEDİR'e, Mühendislik fakültesi dekanımız Sayın Prof. Dr. Mustafa GÜNAL'a, Organizasyonda emeği geçen Doç.Dr. Nihat ATMACA'ya, Dr. Serap ÇELİK ve Dr. Fatih BALCI'ya, destekleyen SANKO Enerji, Büyükşehir Belediyesi, DOW firması ve Limitsiz Enerji firmasına, bildiri sunan bütün akademisyenlere, ve matbaasından ağaç işlerine emeği geçen herkese, Yürütme Kurulu adına teşekkür eder, saygılarımı sunarım.

Organizasyon Komitesi Başkanı
Doç.Dr. Adem ATMACA
Enerji Sistemleri Mühendisliği Bölüm Başkanı
Gaziantep Universitesi
Ekim 2018

TABLE OF CONTENTS

THE HUMAN DEVELOPMENT RELIES ON RENEWABLE ENERGY: EVIDENCE FROM TURKEY 19

MEASUREMENT OF THE IMPACT OF ADP ON BLOOD COAGULATION USING PAPER BASED BIOSENSORS 28

MICROSTRUCTURE ASSESSMENT OF PULSED VACUUM OSMOTICALLY DEHYDRATED AND FRESH FIGS 34

INVESTIGATION OF SHELL MATERIALS EFFECTS ON CONVERSION EFFICIENCY OF TYPE-II QUANTUM DOT NANOCRYSTAL SOLAR CELLS 41

LIFE CYCLE ASSESSMENT OF RENEWABLE ENERGY SOURCES: A REVIEW FOR CARBON FOOTPRINT 42

A MODEL STUDY ON ENERGY PILES 53

IMPROVING SOME GEOTECHNICAL PROPERTIES OF AN ORGANIC SOIL USING CRUSHED WASTE CONCRETE 61

DESIGN AND PERFORMANCE COMPARISON OF FOUR-POLE BRUSHLESS DC MOTORS WITH DIFFERENT POLE/SLOT COMBINATIONS 71

NEURAL NETWORK ESTIMATION OF MUTUAL INDUCTANCE VARIATION FOR A SHADED-POLE INDUCTION MOTOR 82

OPTIMAL DESIGN OF HIGH PERFORMANCE INTERIOR PM MOTOR FOR ELECTRIC VEHICLE 92

EFFECT of CALCINED COLEMANITE ADDITION to COPPER CONVERTER SLAG in SILICA CRUCIBLE 101

HYDROMETALLURGICAL ASSESSMENT OF COPPER CONVERTER SLAG WITH DEEP EUTECTIC SOLVENT 108

SYNTHESIS AND CHARACTERIZATION OF QUATERNARY PERPENDICULARLY ALIGNED CXTS NANORODS 113

SYNTHESIS OF REFRACTORY METAL BASED CHALCOGENIDE NANOSTRUCTURES WITH USING LIQUID SULFUR SOURCES 115

A SMART HOME MODELING WITH LED SYSTEMS AND RENEWABLE ENERGY RESOURCES FOR MICROGRID FORMATION 117

A STUDY ON THE POSSIBLE USE OF INDUSTRIAL WASTE IN ROLLER-COMPACTED CONCRETE PAVEMENT 119

A STUDY ON THE WATER CONSERVATION MEASURES IN GREEN BUILDINGS 121

STRONGLY FLUORESCENT COMPLEXES: SYNTHESIS, CHARACTERIZATION, 3D HYDROGEN-BONDED, FLUORESCENCE STUDY, AND THEORETICAL ANALYSIS.....141

MODELING AND CONTROL OF ELECTRONIC COOLING SYSTEM IN IC ENGINE.....152

EXPERIMENTAL INVESTIGATION OF THE EFFECTS OF PILOT INJECTION ON NO_x EMISSION.....163

INVESTIGATION OF THE EFFECT AIR BUBBLE INJECTION ON CYCLIC VARIATIONS IN ENGINE COOLING SYSTEM WITH WAVELETS TECHNIQUE.....164

THE AIR FUEL RATIO CONTROL WITH GRAY PID IN SI ENGINES UNDER TRANSIENT CONDITIONS.....178

THE MATHEMATICAL MODEL OF THE EFFECT OF DIESEL ENGINE EGR GAS TEMPERATURE AND EGR RATIO ON NOx EMISSIONS.....180

AVAILABLE AND EMERGING METAL ADDITIVE MANUFACTURING TECHNIQUES FOR DIRECT METAL PART MANUFACTURING.....195

TRENDING TECHNIQUES IN ADDITIVE MANUFACTURING WITH THEIR ADVANTAGES AND DISADVANTAGES.....204

GREY WATER FOOTPRINT OF BIOENERGY: A CASE STUDY OF A UASB REACTOR.....224

EFFECT OF POROUS SLEEVE POSITION ON NATURAL CONVECTION IN A CONCENTRIC ANNULUS.....233

EXAM SCHDULING FOR MATHMATICAL MODEL.....247

UTILIZATION OF MANDARIN AND ORANGE ALBEDOS IN CAKE PRODUCTION.....258

DETERMINATION OF THE EFFECTS OF CRITIC SUNN PEST (HETEROPTERA: SCUTELLERIDAE) DAMAGE RATIO ON WEIGHT LOSS OF SOME WHEAT VARIETIES CULTIVATED IN TURKEY.....266

EFFECT OF CONTINUOUS UV-C PASTEURIZATION ON THE SHELF-LIFE AND TENDERIZING POWER OF ONION JUICE.....272

INVESTIGATION OF LIQUEFACTION DANGERS BY CONSIDERING TO LIQUEFACTION SUSCEPTIBILITY OF THE SOIL.....274

A COMPARATIVE STUDY ON VIBRATIONAL PROPERTIES OF GLASS FIBER REINFORCED EPOXY COMPOSITES WITH EFFECT OF OLIVE POMACE PARTICLES CONTENT.....284

SIMULATION OF GASIFICATION PROCESS USING RESTRICTED CHEMICAL EQUILIBRIUM METHOD.....294

DESIGN AND ANALYSIS OF INDUSTRIAL HEAT TREATMENT FURNACE.....295

FRESH PROPERTIES OF STEEL FIBER-REINFORCED SELF-COMPACTING CONCRETE.....305

DAILY HYDROGEN PRODUCTION EVALUATION USING SOLAR ENERGY IN BURSA, TURKEY 320

DESIGN and ANALYSIS of a MAGNETORHEOLOGICAL DAMPER 329

SUPERPLASTIC FORMING OF ALUMINUM ALLOYS 338

THE EFFECT OF GREEN ROOF ON URBAN HYDROLOGIC CYCLE 344

EFFECTS OF POSTHARVEST OXALIC ACID THE TREATMENT ON 'HİCAZNAR' POMEGRANATE ARILS QUALITY AND CHILLING INJURY 353

INFLUENCE OF GABA TREATMENT ON 'HİCAZNAR' POMEGRANATE ARILS QUALITY 370

FORECASTING OF PRIMARY ENERGY CONSUMPTION OF TURKEY AND SOME EUROPEAN COUNTRIES WITH GM(1,1) MODEL 371

DESIGN OF A LOW COST AND HIGH EFFICIENCY VERTICAL AXIS WIND TURBINE 380

DETERMINATION OF TILT ANGLES OF SOLAR PANELS: A STUDY ON GAZİANTEP 393

MODELING AND CONTROL OF DOUBLY FED INDUCTION GENERATOR WITH BACK TO BACK MODULAR MULTILEVEL CONVERTERS 402

REACTIVE POWER COMPENSATION IN THREE PHASE BALANCE LOADED SYSTEM BY USING STATCOM WITH DISPENSE OF THE INTERMEDIATE TRANSFORMER 411

TRIBOLOGICAL EFFECT OF BORIC ACID 426

EFFECT OF CONNECTING ROD BODY LENGTH, WIDTH AND WALL THICKNESS ON DESIGN PARAMETERS 427

OPTIMIZATION OF FATIGUE OF THE CNT REINFORCED GRP PIPES 428

NUMERICAL MODEL OF THE PRESSURE DISTRBUTION IN REINFORCED CONCRETE ELEVATED (RCE) FLUMES 429

INVESTIGATION OF SIMULTANEOUS EEG-fMRI ANALYSIS METHODS 445

EFFECT OF SOIL LAYER INCLINATION AND HYDRAULIC CONDUCTIVITY RATIO ON PRESSURE HEAD ALONG SHEET PILE FACE 459

MAGNESIUM OXIDE ADDING TO AL2024 ALLOYS 472

COBALT COATING OF CARBON NANOTUBE 479

SYNTHESIS AND CHARACTERIZATION OF $Ce_{1-x-y}Sm_xHo_yO_2$ CERAMIC ELECTROLYTES BY SOL-GEL METHOD 485

$Ce_{1-x-y}Sm_xHo_yO_2$ SERAMİK ELEKTROLİTLERİN SOL-JEL YÖNTEMİ İLE SENTEZ VE KARAKTERİZASYONU 486

QUALITY OF FRESH-CUT SULTANA TABLE GRAPE COATED WITH SODIUM ALGINATE DURING STORAGE.....487

***in vitro* PHYTOCHEMICAL and ANTIBACTERIAL PROPERTIES *of Peganum harmala* L.....501**

ENERGY DEMAND AND CLEAN ENVIRONMENT CHALLENGES: CHINA AS A SETTER OF BELT AND ROAD INITIATIVE.....510

DESIGN AND IMPLEMENTATION of A SMART CNC PLOTTER CONTROLLED BY MICROCONTROLLER.....511

NEW TOPOLOGY OF ASYMMETRICAL CASCADE H-BRIDGE MULTI-LEVEL INVERTER....519

EFFECT OF LED TEMPERATURES ON DRYING TIME OF HAZELNUT (CORYLUS AVELLANA L.) AT NATURAL CIRCULATION DRYING SYSTEMS.....534

STRUCTURAL PERFORMANCE OF REINFORCED CONCRETE CORBELS EXPOSED TO HIGH FIRE FLAME.....544

COMPRESSIVE STRENGTH OF CONCRETES PRODUCED WITH ANALCIME BLENDED CEMENTS.....555

THERMAL PERFORMANCE OF ZEOLITE AS AN INSULATION MATERIAL FOR EXTERNAL WALLS.....566

LIFE CYCLE ASSESSMENT OF MUNICIPAL SOLID WASTE INCINERATION POWER PLANT 571

INVESTIGATION ON THE TRACKING SPEED OF DC MOTOR UNDER DIFFERENT EXTERNAL TORQUE.....579

UTILIZATION OF WASTE PLASTIC IN MANUFACTURING OF BRICK 589

ASSESSMENT OF SEISMIC PERFORMANCE OF REINFORCED CONCRETE HIGH RISE BUILDINGS VIA TIME HISTORY ANALYSIS.....599

PRODUCTION OF SUSTAINABLE ENERGY VIA INTEGRATION OF DIRECT BOROHYDRIDE 613

EXPERIMENTALL STUDY OF THE EFFECT OF CONTRACTION RATIO ON BACKWATER BY USING BRIDGE PIER AS FLOW OBSTRUCTION 614

MONITORING OF ARSENIC FROM SPECIFIC POLLUTANTS IN DOWNSTREAM OF UZUNÇAYIR DAM LAKE (TUNCELİ).....627

DIGITAL MODULATION RECOGNITION BASED ON ANNS APPROACH 633

SMART GRID SYSTEMS in WIND ENERGY 641

SUSTAINABILITY ASSESSMENT OF ENERGY STORAGE ALTERNATIVES THROUGH AN INTEGRATED FUZZY-BASED MCDM METHODOLOGY.....654

PEANUT PRODUCTS USED in the FOOD INDUSTRY 664

IMAGE PROCESSING METHODS AND POROSITY MEASUREMENTS IN REEF-ROCKS 675

SINGLE BATHING DYEABILITY OF CATIONIC COTTON-WOOL MIXTURE 683

EXPERIMENTAL ANALYSIS OF MOISTURE ABSORPTION BEHAVIOR OF POLYPROPYLENE WOVEN FABRICS 691

MACHINE LEARNING BASED SENTIMENT ANALYSIS USING NAIVE BAYES ALGORITHM 700

A TECHNICAL ANALYSIS ON THE EFFECT OF EXFOLIATED VERMICULITE AGGREGATE ON THERMAL COMFORT PARAMETERS OF COMPOSITE MORTARS FOR INSULATION PURPOSES 706

FEATURE SELECTION FOR SMS SPAM FILTERING USING ROUGH SET THEORY 723

INVESTIGATION OF CHARGING AND DISCHARGING CHARACTERISTICS OF DIFFERENT TYPE BATTERIES ON HYBRID ELECTRIC VEHICLE MODEL 735

COMPARATIVE ANALYSIS OF SINGLE-SWITCH FORWARD CONVERTERS WITH PASSIVE SNUBBER 749

INVESTIGATION OF COOLING PERFORMANCE IN CHAMBER DESIGNED FOR TORREFIED BIOMASS 763

RELATION BETWEEN HARDNESS PARAMETERS AND MATERIALS THICKNESS AT HEAT TREATMENT OF CARBURIZED STEEL 764

THE EFFECT OF CARBURIZATION TIME ON THE HARDNESS AND MICROSTRUCTURE AT HEAT TREATMENT OF CARBURIZED STEELS 771

DESIGN AND SIMULATION DUAL-BAND FSS STRUCTURE BASED ON U-SHAPED COMPACT SLOT RESONATORS 778

***in vitro* ANTIMICROBIAL ACTIVITY OF *CEDRUS LIBANI* A. RICHARD TAR** 786

CURRENT ENERGY POTENTIAL OF THE MEDITERRANEAN SEA 794

EFFECTS OF POSTHARVEST GAMMA AMINO BUTIRIC ACID THE TREATMENT ON 'HİCAZNAR' POMEGRANATE FUNGAL ROT AND CHILLING INJURY 799

COMPARISON OF FEATURE SELECTION APPROACHES BASED ON GEOMETRIC FEATURES 826

EXPLORING THE POTENTIAL OF GIANT KING GRASS AS A BIOENERGY CROP IN MEDITERRANEAN ECOLOGICAL CONDITIONS 833

BIOFUEL CELL PLATFORMS 834

ELECTRICITY, MARKETS AND TURKEY'S PATH IN LIBERALIZATION PROCESS 835

A STUDY ON THE POSSIBLE USE OF INDUSTRIAL WASTE IN ROLLER-COMPACTED CONCRETE PAVEMENT **837**

EFFECT OF THERMAL TREATMENT ON PPO & POD ENZYME ACTIVITY AND SOME QUALITY PARAMETERS IN PEACH (*PRUNUS PERSICA* L. cv. MONROE) JUICE **859**

INVESTIGATION OF THE EFFECTS OF OIL AMOUNT ON THE DAMPING FORCE FOR THE SHOCK ABSORBERS **869**

RISK ANALYSIS WITH A PERSONNEL SURVEY OF A DRILLING FIELD AND EVALUATION IN TERMS OF WORK SAFETY **883**

TEMPERATURE TESTS IN ELAZIG BEYDAGI II GEOTHERMAL DRILLING WELL AND INVESTIGATION OF TEMPERATURE AND PRESSURE PROFILES BASED ON DEPTH **893**

COMPARISON OF SOIL ENZYMES AND SOIL PROPERTIES IN GRASSLAND, WHEAT AND PISTACHIO AGRICULTURAL LANDS IN ARABAN, GAZIANTEP PROVINCE **903**

OPTIMIZATION OF THE FLANGE TYPE DIFFUSER FOR WIND TURBINE WITH RESPONSE SURFACE METHOD **904**

USE OF VACUUM IMPREGNATION IN FOOD ENRICHMENT PROCESSES **913**

A PERSPECTIVE OF THE UTILIZATION OF ACTIVATED CARBON BASED FROM LIGNOCELLULOSIC BIOMASS SOURCES **920**

EFFECT OF BORON-CONTAINING CEMENT ON SULFATE ATTACK **932**

SYNTHESIS OF ACTIVATED CARBON BY HUMAN HAIR OF DIFFERENT AGES **944**

DIFFERENT E-PLL STRUCTURES FOR GRID-INTERFACED CONVERTERS: ANALYSIS AND COMPARISON **950**

INVESTIGATION OF THE CHARACTERISTICS OF OUTPUT BY USING MAGNETIC FLUIDS IN AIR GAPS FORMED IN THE CORE OF A SINGLE PHASE TRANSFORMER **964**

AN OVERVIEW OF BATTERY TECHNOLOGIES **974**

GRAPHENE AEROGEL SYNTHESIS AND CHARACTERIZATION FOR PEM FUEL CELLS **988**

APPLICABILITY OF INVESTMENT SAVINGS METHOD FOR DETERMINING OPTIMUM INSULATION THICKNESS IN TURKEY **997**

NUMERICAL INVESTIGATION OF MIXING in a STIRRED TANK by DIFFERENT TYPES of RADIAL and AXIAL IMPELLERS **1007**

EXPERIMENTAL INVESTIGATION OF DRYING CHARACTERISTIC OF EGGPLANT IN OSMANİYE PROVINCE CLIMATE CONDITIONS **1020**

IMPROVING ENERGY EFFICIENCY FOR LIGHTING SYSTEMS BY USING ARDUINO **1034**

IMPROVING ENERGY EFFICIENCY FOR LIGHTING SYSTEMS BY USING PWM TECHNIQUES AND ARDUINO 1041

COMPARISON OF THE FATIQUE ANALYSIS AND TEST RESULTS OF THE LIGHT COMMERCIAL VEHICLE SHOCK ABSORBER UNDER WORKING CONDITIONS 1042

USING THE LAYERED PRODUCTION IN THE DESIGN OF THE BODY COVER OF THE LIGHT COMMERCIAL SHOCK ABSORBER 1052

INCREASING THE PRODUCTIVITY WITH CHANGING OF SERPENTINE CONDENSING DESING IN STEAM DRYERS 1054

MAINTENANCE ROUTING AND SCHEDULING OF OFFSHORE WIND FARMS USING META-HEURISTIC METHODS 1063

THE SHEAR WALL EFFECT ON CONCRETE STRUCTURES 1064

EFFECT OF CURVED CROSS SECTIONAL TWISTED TAPES ON HEAT TRANSFER ENHANCEMENT 1075

EFFECT OF REVERSE CURVED CROSS SECTIONAL TWISTED TAPES ON HEAT TRANSFER ENHANCEMENT 1088

LINKAGE ANALYSIS FOR WATER-LAND RESOURCE IN MIDDLE REGION OF HEIHE RIVER BASIN: A NEXUS PERSPECTIVE 1100

OPTICAL PROPERTIES OF SPRAYED IRON OXIDE FILMS 1101

THE EFFECTS OF DIFFERENT DRYING TECHNIQUES ON MOISTURE AND COLOR OF THE TRADITIONAL EGGPLANT 1102

CALCULATION OF HEAT TRANSMISSION COEFFICIENT BY FUZZY ARTIFICIAL NEURAL NETWORKS 1103

SOIL POLLUTION: ESTIMATION OF THE CONTENT OF LEAD IN THE SOIL OF THE REGION OF THE TOWN OF SÉTIF 1114

STUDIES ON FLOWABILITY, COMPRESSIBILITY AND IN-VITRO RELEASE OF MIXED FRUIT POWDER TABLETS 1117

INVESTIGATION THE BEST FACTOR THAT EFFECT ON REDUCING COAGULANT DOSAGES IN WATER TREATMENT 1118

INVESTIGATION OF BIOACTIVE PEPTIDES THAT ARE RELEASED IN SILICO DIGESTION OF TARHANA PROTEINS 1120

TEXTURAL PROPERTIES OF HONEY CHOCOLATE 1121

PRODUCTION OF PRECIOUS POWDER METAL ALLOYS 1122

EVALUATION OF VALUABLE ORES IN WASTE CIRCUIT (PCB) CARDS OF MOBILE PHONES 1124

EVALUATION OF PRECIOUS ORE FROM WASTE CERAMIC CPU PROCESSORS 1125

ISOLATION AND MORPHOLOGICAL DETERMINATION OF THE AMF SPORES IN THE RHIZOSPHERE OF PUCCINELLIA DISTANS (L.) PARL (SALT LAKE) IN KONYA 1126

NUMERICAL INVESTIGATION OF 2D LID DRIVEN CAVITY FLOW 1143

ENERGY CONSUMPTION OF COMMERCIAL BUILDINGS……1148

FULL PAPERS, ABSTRACTS & POSTERs

THE HUMAN DEVELOPMENT RELIES ON RENEWABLE ENERGY: EVIDENCE FROM TURKEY

Asst. Prof. Dr. Elma SATROVIC
Çağ University, Turkey
Email: elmasatrovic@cag.edu.tr

ABSTRACT: The aim of this research is to provide empirical evidence on the relationship between human development and renewable energy. The time-series data are collected over the period 1992-2015 for the case of Turkey. Turkey is observed since it is considered to be one of the fastest growing energy markets in the world. In addition, Turkey reports impressive growth in terms of human development. In order to conduct empirical research we have applied time-series econometrics including Johansen test for cointegration and Granger causality test. The stationarity of variables is also tested. The Johansen cointegration test confirms that the null hypothesis on no co-integration (r = 0) is rejected by both the maximum eigenvalue and trace statistics. This indicates the existence of a long-run equilibrium relationship between economic terms of interest. Additionally, Granger causality test reports a unidirectional relationship between the economic terms of interest clearly indicating that renewable energy tends to contribute to human development. Human development is not found to foster the renewable energy in terms of Turkey. The findings of this paper suggest that Turkish decision makers need to make a stronger effort in order to foster renewable energy since it is found to have a significant contribution to the main dimensions of human development.

Key words: causal relationship, cointegration, human development, renewable energy

INTRODUCTION

The World Bank indicates that macroeconomic performance of Turkey has been tremendously increasing since the year 2000. This is due to the macroeconomic and fiscal stability that have decreased the unemployment rate and have increased income. In terms of poverty, the statistics is just impressive. The World Bank reports poverty incidence more than halved over 2002-2015. The exponential decrease of extreme poverty was also reported. In addition, Turkey became more urbanized, has opened borders for foreign trade and finance and has started following many European Union (EU) standards. Soytaş et al., (2001), Altınay and Karagöl (2005), Akpolat and Altıntaş (2013) indicate that economic growth in Turkey is strongly correlated with the energy consumption.

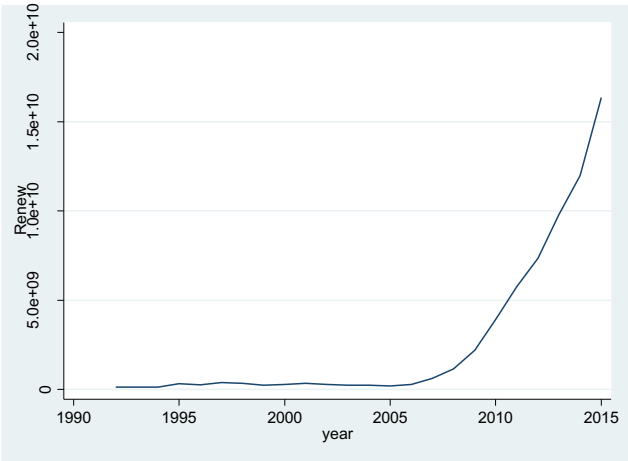

Graph 1. Electricity Production from Renewable Sources in Turkey
Source: Author

It is inevitable fact that developing countries require more energy to achieve economic growth. Turkey has become one of the fastest growing energy markets in the world. This is the result of impressive economic expansion, the rise in income per capita as well as urbanization. Energy demand is expected to increase by around 6 percent per annum through 2023 (Republic of Turkey Prime Ministry Investment Support and Promotion Agency). Hence, the research on the relationship between energy and economic performance is of great importance. Since Turkey aims to adopt many standards of EU, special attention should be paid to green economy and renewable energy. This is due to the fact that Turkey is one of the richest countries in the world in terms of renewable resources (Kamran, 2016).

Opportunities for renewable forms of energy production – hydro, wind, solar, and geothermal – are abundant (Republic of Turkey Prime Ministry Investment Support and Promotion Agency). In terms of geothermal energy, Turkey is ranked first in Europe and seventh in the world (Kamran, 2016). Installed capacity of wind energy in Turkey is increasing rapidly from 20MW in 2002 to 4503MW in 2015 (Kamran, 2016). Biomass and solar energy are also well developed. Erdem (2010) indicates that renewables can be regarded as supportive tools in sustainable development of Turkey. This is why this paper analyzes whether human development relies on renewable energy. Electricity production from renewable sources, excluding hydroelectric (kWh) is used as a proxy variable of renewable energy in this paper. In the period 1992-2005 the electricity production from renewable sources stagnates in Turkey. However, after the year 2005 it reports an impressive growth (Graph 1).

In terms of human development, UNDP suggests HDI (Human Development Index) as an appropriate proxy variable of this economic term. Therefore, there is a need to summarize statistics on HDI. UNDP reports HDI value to be 0.767 in Turkey in the last observed year (2015). Taking into account HDI value, Turkey is ranked as a country with high human development positioning it at 71 out of 188 countries and territories in the World. Between 1992 and 2015 (the observed period in this paper), Turkey's HDI value has increased from 0.586 to 0.767. This is the increase of 30.9 percent. An impressive increase is reported for all of the HDI elements. This positive trend is represented by Graph 2.

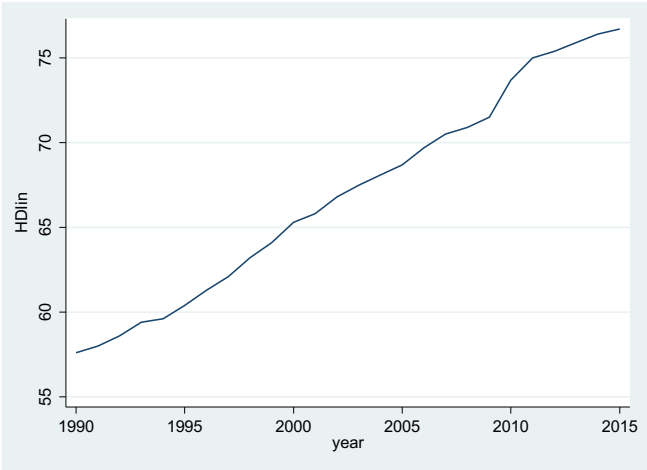

Graph 2. HDI in Turkey
Source: Author

The two major concerns in terms of energy nowadays are (Apergis and Danuletiu, 2014): the depletion of the most easily accessible energy resources (i.e., oil, gas, coal) and correspondingly, the problem of global warming caused by the rapidly increasing emissions of greenhouse gases such as carbon dioxide (CO2) and methane. Taking these issues into account there are worldwide initiatives directed to the increase in the production of renewable energy since it is inexhaustible, clean and safe. Therefore, it reports fast growth all over the world and it is expected to have a positive impact on sustainable development and human development. The empirical evidence on the matter is given below.

The paper proceeds as follows. Section 2 summarizes previous empirical studies on the relationship between the human development and renewable energy. Data, variables and methodology are described in detail in Section 3. Empirical results are reported and interpreted in Section 4. Main conclusions are summarized at the end of this paper.

LITERATURE REVIEW

A number of studies have analyzed the impact of energy on economic growth. Yet, the studies on the relationship between energy and human development are scarce. In addition, only few studies treat the relationship between human development and renewable energy from the best of our knowledge. This part of paper summarizes the most import empirical evidence on the relationship between economic terms of interest.

Pirlogea (2012) has analyzed the role of energy in development with the focus on human development. The author was also interested in giving evidence on the role of energy in sustainable and economic development. The author uses panel data for European Union countries. The observed countries report very high human development. Both fossil and renewable energy consumptions are included in the analysis in order to declare their capability of attaining human development in the

context of consequences on health and environment. The results indicate that, high levels of energy intensity treat human development.

Unlike previous renewable energy-growth studies, Apergis and Danuletiu (2014) examine for the first time the relationship between renewable energy and economic growth. They have collected annual panel data over the period ranging from 1990 to 2012 for the sample of 80 countries. They have applied Canning and Pedroni long-run causality test. The obtained results suggest a long-run positive causality running from renewable energy to economic growth. This is reported for the total sample of countries. Results are confirmed across regions. Findings of the paper indicate that renewable energy is important for economic growth and economic growth is found to foster the use of more renewable energy sources.

Meisen and Cavino (2007) indicate that China has reached impressive economic growth over the past several decades. This is due to the exponential increase in industry and production. Consequently, the quality of life has also been improved. The authors explore rural electrification, human development and the renewable energy potential of China and indicate that increased development of renewable fuels will prevent the deterioration of quality of life trends. Expansion of renewable resources is also expected to promote employment, alleviate pollution, reduce health risks and to contribute to the main dimensions of human development. The expansion of renewable fuels is in the economic as well as the political interest of China.

As the requirement for renewable energy increases, its relation with development becomes more controversial (Kazar and Kazar, 2014). The authors aim to explore the relationship between renewable energy and development. The have collected panel data over the period 1980-2010 to study the long-run relationship between economic terms of interest and the period 2005-2010 to study the short-run relationship. The findings indicate that development fosters the production of renewable energy in the long-run. In addition, a bidirectional relationship is found in the short-run between economic terms of interest.

DATA AND METHODOLOGY

Data

The data, used to estimate the causal relationship between human development and renewable energy in Turkey are collected over the period 1992-2015. The data sources are the World Bank and UNDP. The main criterion to select a time frame was the data availability. In addition, an attempt is made to include the most recent data. In order to give a detailed explanation of variables we start with human development. UNDP suggests that Human Development Index (***HDI***) is an adequate measure of human development. Hence, this institution defines HDI as `a summary measure of average achievement in key dimensions of human development: a long and healthy life, being knowledgeable and have a decent standard of living`. Human Development Report (2016) indicates that `human development is all about human freedoms: freedom to realize the full potential of every human life, not just of a few, nor of most, but of all lives in every corner of the world-now and in the future`.

On the other hand, there is a need to find appropriate proxy variable of renewable energy. Electricity production from renewable sources is assumed to be appropriate in this paper. The World Bank indicates that electricity production from renewable sources (***REN***) excludes hydroelectric but includes geothermal, solar, tides, wind, biomass, and biofuels. Since human development is all about human freedoms including freedom to realize the full potential of every human life, not just of a few, nor of most, but of all lives, this variable is suggested as appropriate. The necessity to analyze the relationship between aforementioned economic terms arose from the fact that, both human development and renewable energy report impressive growth in Turkey. Taking into account the potential of renewable energy in terms of Turkey, the positive impact on human development is expected.

Methodology

Methodology used in this paper can be summarized as follows. The analysis starts by calculating the most important measures of descriptive statistics. Moreover, the stationarity of variables will be explored using the appropriate tests. In addition, Johansen cointegration test will be used to examine the cointegrating relationship between human development and renewable energy in Turkey. Granger causality test will be used to examine the causal relationship between economic terms of interest (Satrovic and Muslija, 2017).

EMPIRICAL RESULTS

The empirical results section starts by presenting descriptive statistics. The highest value of REN is reported for the year 2015 while the lowest is reported for the year 1992. When it comes to HDI, the highest value of 76.7 is reported for the year 2015 while the lowest value of 58.6 is reported for the year 1995. Since standard deviations imply high volatility for the observed period and in order to ease interpretation, natural logarithm of the REN variable is calculated. Table 1 summarizes the obtained results.

Furthermore, information criterion procedures (Schwarz's Bayesian information criterion (SBIC), the Akaike's information criterion (AIC), and the Hannan and Quinn information criterion (HQIC)) are used to determine the number of lags needed. Table 2 summarizes the obtained results. The obtained results of all of the three criteria agree that the appropriate number of lags to be used in this research is 3 (Satrovic, 2017).

Table 1. Descriptive Statistics

stats	**HDI**	**REN**
mean	67.775	2620000000
sd	5.884	4440000000

max	76.700	16400000000
min	58.600	117000000
skewness	0.021	1.888
kurtosis	1.772	5.511

Source: Author

Table 2. The Number of Lags Needed

lag	LL	LR	Df	P	FPE	AIC	HQIC	SBIC
0	-76.1485				12.8147	8.22615	8.24298	8.32557
1	-12.2652	127.77*	4	0	.02357*	1.92265*	1.97313*	2.2209*
2	-9.06837	6.3936	4	0.172	0.026169	2.0072	2.09132	2.50427
3	-6.39897	5.3388	4	0.254	0.031562	2.14726	2.26503	2.84316
4	-2.12718	8.5436	4	0.074	0.033621	2.11865	2.27007	3.01338
5	-0.49381	3.2667	4	0.514	0.05078	2.36777	2.55284	3.46133

Source: Author

In addition, Augmented Dickey-Fuller (ADF) test is used to investigate the presence of unit root (Satrovic and Muslija, 2017). Table 3 summarizes the obtained results. The presence of unit root is also tested at the first differences and second differences in the case of REN. The results of the test indicate that the time series of HDI is stationary at the first differences (for 1% level of significance) while REN is stationary at the second differences (for 1% level of significance).

Table 3. Augmented Dickey-Fuller (ADF) Test

Variable		Test Statistics	1% Critical Value	5% Critical Value	10% Critical Value
HDI	Z(t)	-0.428	-3.750	-3.000	-2.630
	MacKinnon approximate p-value Z(t) = 0.9053				
D.HDI	Z(t)	-3.891	-3.750	-3.000	-2.630
	MacKinnon approximate p-value Z(t) = 0.0021				
lnREN	Z(t)	0.370	-3.750	-3.000	-2.630
	MacKinnon approximate p-value Z(t) = 0.9804				
D.lnREN	Z(t)	-1.978	-3.750	-3.000	-2.630
	MacKinnon approximate p-value Z(t) = 0.2962				
D2.lnREN	Z(t)	-4.689	-3.750	-3.000	-2.630
	MacKinnon approximate p-value Z(t) = 0.0001				

Source: Author

Moreover, econometric methodology in this paper proceeds to the application of Johansen test for cointegration (Satrovic and Muslija, 2017). Table 4 summarizes the obtained results. The empirical results confirm that the values of the trace tests and those of the maximum eigenvalue tests are greater than the critical values. This confirms that the null hypothesis on no co-integration (r = 0) is rejected by both the maximum eigenvalue and trace statistics. This indicates the existence of a long-run equilibrium relationship between economic terms of interest.

Table 4. Johansen Tests for Cointegration

maximum rank	parms	LL	eigenvalue	trace statistic	5% critical value
0	2	-28.547133	.	21.6299	15.41
1	5	-22.438203	0.42613	9.412	3.76
2	6	-17.732188	0.34807		
maximum rank	**parms**	**LL**	**eigenvalue**	**max statistic**	**5% critical value**
0	2	-28.547133	.	12.2179	10.07
1	5	-22.438203	0.42613	9.412	3.76
2	6	-17.732188	0.34807		

Source: Author

Since the Johansen cointegration test does not provide information regarding the direction of causality; the Granger causality test based on the VAR model is applied. Table 5 indicates the unidirectional relationship between the economic terms of interest clearly indicating that renewable energy tends to contribute to human development.

Table 5. Granger Causality Wald Tests

Equation	Excluded	Prob>chi2
D.HDI	D2.lnREN	0.138
D.HDI	ALL	0.138
D2.lnREN	D.HDI	0.000
D2.lnREN	ALL	0.000

Source: Author

However, human development is not found to foster the renewable energy in terms of Turkey. This is due to the fact that Turkey is positioned at 71 out of 188 countries and territories in the World in terms of HDI in the year 2015. Therefore, there is a long way ahead in terms of contribution to the main dimensions of human development. This is way for the time being human development is not found to Granger cause renewable energy.

CONCLUSION

It is inevitable fact that developing countries require more energy to achieve economic growth. The World Bank indicates that macroeconomic performance of Turkey has been tremendously increasing since the year 2000. This is due to the macroeconomic and fiscal stability that have decreased the unemployment rate and have increased income. As a result, Turkey has become one of the fastest growing energy markets in the world.

Opportunities for renewable forms of energy production – hydro, wind, solar, and geothermal – are abundant (Republic of Turkey Prime Ministry Investment Support

and Promotion Agency). In terms of geothermal energy, Turkey is ranked first in Europe and seventh in the world. Installed capacity of wind energy in Turkey is increasing rapidly. Biomass and solar energy are also well developed. Taking this into account, renewable energy can be regarded as supportive tool in sustainable development of Turkey. This is why this paper analyzes whether human development relies on renewable energy. The data are collected over the period 1992-2015.

The empirical results section starts by presenting descriptive statistics. The highest value of REN is reported for the year 2015 while the lowest is reported for the year 1992. When it comes to HDI, the highest value of 76.7 is reported for the year 2015 while the lowest value of 58.6 is reported for the year 1995.

Moreover, econometric methodology in this paper proceeds to the application of Johansen test for cointegration. The empirical results confirm that the values of the trace tests and those of the maximum eigenvalue tests are greater than the critical values. This confirms that the null hypothesis on no co-integration ($r = 0$) is rejected by both the maximum eigenvalue and trace statistics. This indicates the existence of a long-run equilibrium relationship between economic terms of interest.

Since the Johansen cointegration test does not provide information regarding the direction of causality; the Granger causality test based on the VAR model is applied. Table 5 indicates the unidirectional relationship between the economic terms of interest clearly indicating that renewable energy tends to contribute to human development.

Human development is not found to foster the renewable energy in terms of Turkey. This is due to the fact that Turkey is positioned at 71 out of 188 countries and territories in the World in terms of HDI in the year 2015. Hence, there is a long way ahead in terms of contribution to the main dimensions of human development. This is way for the time being human development is not found to Granger cause renewable energy and Turkish decision makers need to make a stronger effort in order to foster renewable energy since it is found to be a significant determinant of human development in present research.

REFERENCE LIST

Akpolat, A.,and Altıntaş, N. (2013). Enerji Tüketimi ile Reel GSYİH Arasındaki Eşbütünleşme ve Nedensellik İlişkisi: 1961-2010 Dönemi, Bilgi Ekonomisi ve Yönetimi Dergisi, Vol. 8(2), pp.15-127.

Altınay, G., and Karagöl, E. (2004). Structural Break, Unit Root, and The Causality between Energy Consumption and GDP in Turkey, Energy Economics, Vol. 26, pp.985-994.

Apergis, N. and Danuletiu, D.C. (2014). Renewable Energy and Economic Growth: Evidence from the Sign of Panel Long-Run Causality, International Journal of Energy Economics and Policy, Vol. 4, No. 4, pp.578-587.

Erdem, Z.B. (2010). The Contribution of Renewable Resources in Meeting Turkey's Energy-Related Challenges, *Renewable and Sustainable Energy Reviews*, Vol. 14(9), pp. 2710-2722.

Human Development Report 2016, (2016). UNDP.
Kamran, D. (2016). Hybrid Wind-Solar Reliable Solution for Turkey to Meet Electric Demand. *Balkan Journal of Electrical and Computer Engineering*. Vol. 4 (2), pp. 62-66.
Kazar, G. and Kazar, A. (2014). The Renewable Energy Production-Economic Development Nexus, *International Journal of Energy Economics and Policy*, Vol. 4, No. 2, pp. 312-319.
Meisen, P. and Cavino, N. (2007). Rural Electrification, Human Development and the Renewable Energy Potential of China, Global Energy Network Institute. Source: https://www.geni.org/globalenergy/research/china-development/china-development.pdf.
Pirlogea, C. (2012). The Human Development Relies on Energy. Panel Data Evidence, *Procedia Economics and Finance*, Vol. 3, pp. 496-501.
Satrovic, E. (2017). Financial Development and Human Capital in Turkey: ARDL Approach, *Cappadocia Academic Review*, Vol. 1(2), pp. 1-15.
Satrovic, E. and Muslija, A. (2017). Foreign Direct Investments and Tourism: Empirical Evidence from Turkey, ICPESS Proceedings, ISBN: 978-605-68010-0-6, Vol. 2, pp. 88-100.
Soytaş, U., Sarı, R., Özdemir, Ö. (2001). Energy Consumption and GDP Relation in Turkey: A Cointegration and Vector Error Correction Analysis, Economies and Business in Transition: Facilitating Competitiveness and Change in the Global Environment Proceedings, pp.838-844.
http://www.invest.gov.tr/en-US/sectors/Pages/Energy.aspx
http://www.worldwatch.org/system/files/ren21-1.pdf

MEASUREMENT OF THE IMPACT OF ADP ON BLOOD COAGULATION USING PAPER BASED BIOSENSORS

Tayyibe Gerçek
Gaziantep University
tayyibegercek@gmail.com

Kutay İçöz
Abdullah Gül University
kutay.icoz@agu.edu.tr

ABSTRACT: In recent years, paper based biosensors have been developed to detect various biomolecules. In this study, the impact of reactive materials to blood coagulation was measured using a paper based membrane. The membrane is made of nitrocellulose and two types of membranes having different pore densities were tested. Blood samples were mixed with different concentrations of reactive material (adenosine diphosphate) and added to the membranes. The adenosine diphosphate promotes blood coagulation and shorter travel distance on the membrane was measured. For the lower pore density membrane the control sample traveled 2.15 cm whereas 1 mM reactive material resulted in 1.5 cm travel. For the membrane having increased pore density, the control sample traveled 1.3 cm and 1 mM reative material resulted in 1.05 cm travel. These results reveal that lower pore density membranes are feasible to measure blood coagulation as a simple and low cost method.

Key words: blood coagulation measurement, paper based biosensors, lateral flow membranes, point-of-care, ADP

KAĞIT TEMELLİ BİYOSENSÖR İLE ADP'NİN KAN PIHTILAŞMASINA OLAN ETKİSİNİN ÖLÇÜLMESİ

ÖZET: Kağıt Temelli biyosensör sistemler son yıllarda farklı biyomoleküllerin algılanması için geliştirilmektedir. Bu çalışmada reaktif maddelerin kanın pıhtılaşmasına olan etkisini ölçmek üzere kağıt temelli membran kullanılarak ölçümler gerçekleştirilmiştir. Nitroselülozdan yapılmış farklı açıklık yoğunluğundaki iki membran üzerine farklı konsantrasyonlarda reaktif madde (adenozin difosfat) ile karıştırılmış kan ilave edilmiştir. Kanın artan adenozin difosfat konsantrasyonuna bağlı olarak pıhtılaşmanın çabuk gerçekleştiği ve membran üzerinde daha kısa mesafe ilerlediği ölçülmüştür. Düşük yoğunluklu açıklık yapısına sahip membranda kontrol deneyinde 2,15 cm ilerleyen kan 1 mM rekatif madde ile karıştırılınca 1,5 cm ilerlemiştir. Açıklık yapısı yoğunluğu daha fazla olan membranda kontrol deneyinde 1,3 cm, 1 mM reaktif madde ile karıştırılınca 1,05 cm ilerlemiştir. Bu sonuçlar düşük yoğunluklu açıklık yapısına sahip membranın kan pıhtılaşması ölçümleri için düşük maliyetli ve kolay bir yöntem olarak kullanılmasının uygun olduğunu göstermektedir.

Anahtar sözcükler: kan pıhtılaşması ölçümü, kağıt temelli biyosensörler, yatay akış membranlar, hasta başı ölçüm sistemleri, ADP

GİRİŞ

Kanın pıhtılaşma özelliği insan sağlığı için hayati öneme sahiptir. Kanın normalden hızlı yada yavaş pıhtılaşması düzensizlik olarak adlandırılır ve ciddi sağlık problemlerine yol açabilir. Damar içindeki kanın pıhtılaşması pıhtının kalp, beyin, karaciğer gibi organlara ulaşarak fonksiyonlarını durdurmasına, yada bir yaradan akan kanın pıhtılaşmaması aşırı kan kaybına hastanın bilincini ve yaşamını kaybetmesine neden olabilir. Düzensizliğe neden olarak karaciğerin fonksiyonlarını yerine getirememesi, thrombophilia (aşırı pıhtılaşma istidadı), hemofili (kanın pıhtılaşamaması) hastalıkları gösterilmektedir. Bu hastalıklar ve hastalıklara sebep olan faktörler üzerine tıbbi ve genetik araştırmalar yapılmaktadır (Triplett, 2000).
Trombosit (platelet) ve pıhtılaşma faktörlerinin etkileşimlerinin sonucunda kan pıhtılaşır. Kan pıhtılaşmasında düzensizlik pıhtılaşma testleri ile tespit edilir ve düzensizliğe sahip hastaların durumu bu testler ile izlenir. Testlerin amacı kanın pıhtılaşma istidadını ve zamanını ölçerek doktorlara düzensizlik olup olmadığına ve derecesine ait bilgi sağlamaktır. Trombosit fonksiyon testleri olarak adlandırılan bu testler farklı metotları kullanmaktadır (Akbiyik & Dikmen, 2014).

Günümüzde hastane laboratuvarlarında kullanılan, taşınabilir olmayan, pıhtılaşma testi cihazları olduğu gibi mikro akışkan temelli, taşınabilir ve ucuz, pıhtılaşma ölçümleri yapabilen cihazlar da geliştirilmektedir. Geliştirilme aşamasında olan yeni nesil cihazlar henüz laboratuvar cihazlarının sahip oldukları yetkinlikte değildirler. Mikro akışkan temelli testler ölçüm için az miktarda hasta örneğine ihtiyaç duyması, kısa sürece netice alınabilmesi, ucuz ve taşınabilir olması gibi özellikleri ile ilgi çekmektedir. Mikro/nano teknoloji tabanlı hasta başı (point-of-care) ölçüm cihazlarının en önemli avantajlarından birisi alınan örneğin analizin yapılması için başka bir yere taşınmasına gerek olmamasıdır. Pıhtılaşma testlerinde kanın laboratuvara taşınması yada bekletilmesi ölçüm sonuçlarını etkileyebilmektedir (Parolo & Merkoçi, 2013).
Günümüzde geliştirilen üretim teknikleri ile istenen şekilde ve boyutta mikro akışkan kanallar, zarlar tasarlamak ve üretmek kolayca gerçekleştirilebilmektedir. Bu çalışmaların bazıları ürüne dönüşmüş ve satın alınması mümkündür (Chin, Linder, & Sia, 2010).
Bu projenin amacı mikro akışkan temelli kullanımı kolay ve ucuz, hasta başı pıhtılaşma testi geliştirmek ve diğer araştırma guruplarının bu konuda yayınlanmış çalışmalarını ileri seviyeye taşıyarak bu alana bilimsel katkı sağlamaktır.

Kağıt Bazlı Hasta Başı (Point Of Care) Cihazlar

Hasta başı cihazlar, laboratuvara veya bir hastaneye gitmeye gerek kalmadan çok az miktarda örnekle ilgili testin sonucunu verebilen cihazlardır. Dünya Sağlık Örgütü tarafından tanı için kullanılacak point of care cihazlar için bir takım kriterler belirlenmiştir. Bu kriterler, ASSURED (Affordable, Sensitive, Specific, User-friendly, Rapid and robust, Equipment free, Deliverable to end-users) kısaltmasıyla anılan; kolay ulaşılabilir, ucuz; hassas, detaylı ölçüm yapabilen; kullanıcı dostu, uzman biri gerektirmeyen; çıplak gözle gözlemlebilen; dayanıklı olarak tanımlanmıştır (López-Marzo & Merkoçi, 2016).

Kağıt bazlı hasta başı cihazların avantajı ise üretiminin, elektrokimyasal elemanlarla entegrasyonunun ve uygulanmasının kolay olmasıdır (sunumdan). Bu sensörlerin 3 farklı çeşidi vardır: pH ölçmek için kullanılan daldırma çubukları, mikro PAD'ler (Paper Analytical Devices), yatay akış analizleri (LFA) (Parolo & Merkoçi, 2013). Bu çalışmada yatay akış analiz metodu kullanılarak reaktif maddenin kanın pıhtılaşmasının olan etkisinin ölçülmesi amaçlanmaktadır.

YÖNTEM

Kanın reaktif maddeler (Adenozin difosfat (ADP), Kollajen, Epinefrin, Ristosetin) ile karıştırıldıktan sonra laboratuvar cihazları ile ölçülmesi sayesinde trombosit miktarı değerlendirilmektedir (Büyükcoşkun, Özlük, & Sağdilek, 2006). Bu cihazlar taşınabilir ve ucuz değildir kullanımı uzman personel tarafından yapılmaktadır.

Kan pıhtılaşmasını ölçmek için 2014 yılında yapılan bir çalışmada (Han, Li, Pauletti, & Steckl, 2014), nitroselülozdan üretilmiş kağıtlar şerit şeklinde kesilip farklı $CaCl_2$ konsantrasyonları ile karıştırılan kan şeritler üzerine eklenmiştir. Parametrelerin optimizasyonu yapıldıktan sonra kanın kağıt üzerinde yayılım mesafesi ile $CaCl_2$ konsantrasyonu arasında lineer ilişki tespit edilmiştir. Bu çalışmada kanın Ca^{2+} eklenmesi ile pıhtılaşmasının tetiklenmesi ve pıhtılaşmanın ölçülmesini için Millipore firmasının ürettiği HF075 kodlu nitroselüloz zarı kullanılmıştır (Han, Li, Pauletti, & Steckl, 2014). Bahsi geçen yayında kullanılan yönteme benzer şekilde, kanın ve pıhtılaşmayı etkileyen reaktif maddenin (ADP) karıştırılması ve membrana uygulanmasını temel olan yöntem Şekil1'de gösterilmektedir. Önce 1:4 oranında sitrat ve kan örneği hazırlanıp serum fizyolojik ile seyrelttikten sonra farklı konsantrasyonlarda ADP çözeltisi eklendi. ADP konsantrasyonu 0,5-1 mM arası hazırlanarak ısıtılması için 5 dakika inkübasyona koyuldu. Kağıtlar 2 mm eninde eşit boylarda kesildi ve kanın yükleneceği yere glass fiber kağıdı konuldu. Hepsi eşit şekilde dizildikten sonra inkübasyondaki kan örneklerinden 18'er uL membranlara yüklendi ve 4 dakika beklenerek ilerlemesi gözlemlendi. Hazırlanan örnekleri farklı yoğunluktaki nitroselüloz membranlara (HF075 ve HF090) uygulanıp ne kadar ilerledikleri ölçüldü.

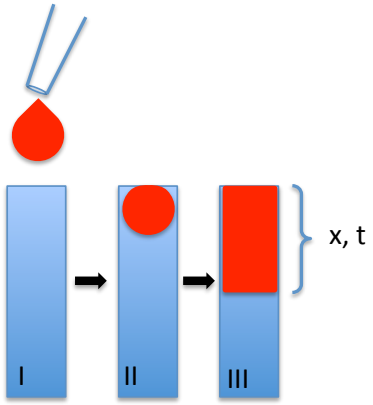

Şekil 1: Yapılacak ölçümleri gösteren çizim: ADP ile karıştırılan kan şerit şeklinde hazırlanan membranların ucuna eklenerek yayılması ve durduğu ana kadarki kat edilen mesafelerin (x) ve sürelerin (t) ölçülmesi.

BULGULAR

ADP'nin miktarını artırdıkça kanın daha hızlı pıhtılaştığını, ve buna bağlı olarak membran üzerinde ilerleme mesafelerinin azalması yapılan deneyler sonucunda gözlemlendi. Kontrollü deneylerde ADP konsantrasyonu dışında tüm parametreler aynı tutulmuştur.

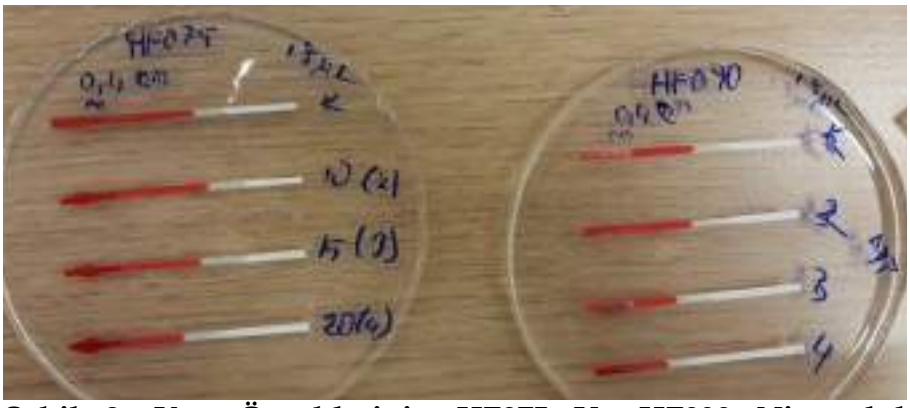

Şekil 2: Kan Örneklerinin HF075 Ve HF090 Nitroselüloz Membranlarında Yürütülmesi.

SONUÇ

Optimizasyon deneylerinden sonra elde edilen sonuçlar Şekil 2'de görüldüğü gibi ADP konsantrasyonu artırıldıkça kanın ilerlemesi azalmıştır. Şekil 2'deki deneyde kan örnekleri HF075 çeşidi membranda sırasıyla kontrol 2,15 cm, 0,5 mM konsantrasyonda 1,75 cm, 0,75 mM'da 1,6 cm; 1 mM konsantrasyonda 1,5 cm ilerlemiştir. HF090 çeşidi membranda ise sırasıyla kontrol 1,3 cm, 0,5 mM konsantrasyonda 1,3 cm, 0,75 mM'da 1,1 cm; 1 mM konsantrasyonda 1,05 cm ilerlemiştir. Deneylerin ortalama sonuçlarının grafiği Şekil 3'te gösterildiği gibidir. Beklendiği gibi ADP konsantrasyonu arttıkça pıhtılaşma kağıt membranlarda da daha hızlı olmaktadır. Aynı zamanda HF090 çeşidi kağıdın yapısı daha yoğun olduğu için onun üzerindeki ilerleme daha az olmuştur.

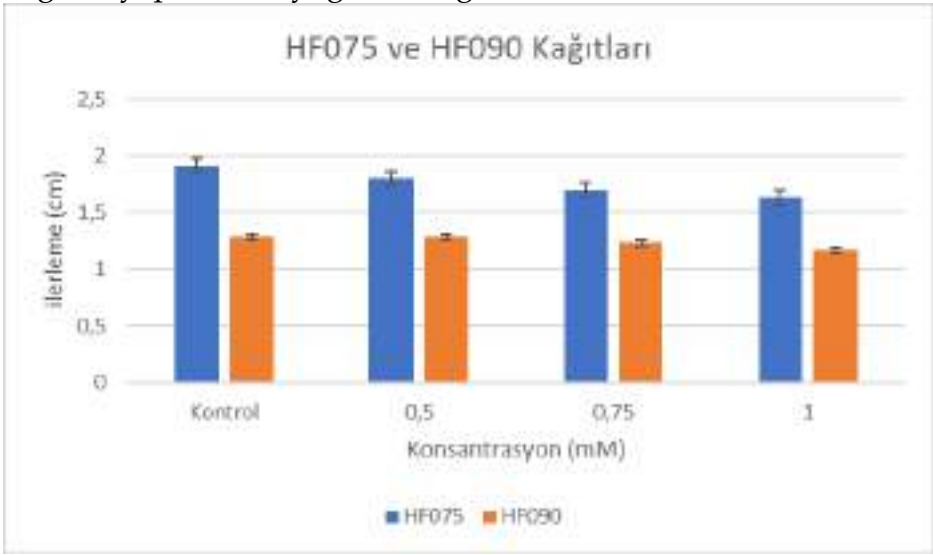

Şekil 3: HF075 Ve HF090 Nitroselüloz Membranlarında Yürütülen Örneklerin Konsantrasyon Artışına Göre İlerleme Mesafeleri

ÖNERİLER

Bu yöntemle pıhtılaşmayla ilgili hastalıkların tanısında kolaylık sağlanabilir. Hızlı, ucuz, kolay uygulanabilir bir yöntem olan kağıt temelli biyosensörler hastaların bulundukları yerde, laboratuvar veya hastaneye gitmeden ölçüm yapılmasını sağlayabilir.

KAYNAKLAR

Akbiyik, F., & Dikmen, Z. G. (2014). Trombosit fonksiyon testleri, *39*(September), 549–553. http://doi.org/10.5505/tjb.2014.17894

Büyükcoşkun, N. İ., Özlük, K., & Sağdilek, E. (2006). Trombositlerin Epinefrine Yanıtlarının Optik Agregometre ve PFA – 100 İle İncelenmesi, *32*(1), 15–20.

Chin, C. D., Linder, V., & Sia, S. K. (2010). Commercialization of microfluidic point-of-care diagnostic devices, (207890), 531–540. http://doi.org/10.1039/c3lc50564b.Please

Han, D., Li, H., Pauletti, G. M., & Steckl, A. J. (2014). Blood coagulation screening using a paper-based microfluidic lateral flow device. *Lab on a Chip*, *14*(20), 4035–4041. http://doi.org/10.1039/C4LC00716F

López-Marzo, A. M., & Merkoçi, A. (2016). Paper-based sensors and assays: a success of the engineering design and the convergence of knowledge areas. *Lab Chip*, *16*(17), 3150–3176. http://doi.org/10.1039/C6LC00737F

Parolo, C., & Merkoçi, A. (2013). Paper-based nanobiosensors for diagnostics. *Chem. Soc. Rev.*, *42*(2), 450–457. http://doi.org/10.1039/C2CS35255A

Triplett, D. A. (2000). Coagulation and bleeding disorders: Review and update. In *Clinical Chemistry* (Vol. 46, pp. 1260–1269).

THIS PAGE IS INTENTIONALLY

LEFT BLANK

MICROSTRUCTURE ASSESSMENT OF PULSED VACUUM OSMOTICALLY DEHYDRATED AND FRESH FIGS

Utkucan ŞAHİN
Muğla Sıtkı Koçman Üniversitesi, Teknoloji Fakültesi, Enerji Sistemleri Mühendisliği Bölümü, 48000, Muğla, Türkiye
usahin@mu.edu.tr

Harun Kemal ÖZTÜRK
Pamukkale Üniversitesi, Mühendislik Fakültesi, Makine Mühendisliği Bölümü, 20070, Denizli, Türkiye
hkozturk@pau.edu.tr

ABSTRACT: In this study, microstructure properties of pulsed vacuum osmotically dehydrated (pretreated) and fresh (non-pretreated) figs (Ficus carica L) were compared. In experiments, *Sarılop* variety figs were used as a whole. Before drying process, figs were osmotically dehydrated in sucrose solution at 50 °Brix and 50 °C with a solution/fruit mass ratio of 4/1. At the beginning of osmotic dehydration (OD) process, vacuum impregnation was applied at 130 mbar for 15 min. After the vacuum impregnation lasted, OD was continued at atmospheric pressure for 165 min thus, the pretreatment period took 180 min. Drying process was performed at 60 °C in a convective oven. Results showed that pulsed vacuum osmotic dehydration (PVOD) reduced the drying time of fig samples. Additionally, microstructure properties of dried (pretreated and non-pretreated) and fresh figs were observed by using scanning electron microscopy analysis. Consequently, PVOD caused changes such as damages in the structure of fig tissue. This study gives innovative information for food industry due to the having results of drying periods and microstructure analysis of figs.
Keywords: Fig, drying, pulsed vacuum osmotic dehydration, microstructure analysis.

VAKUM ALTINDA OZMOTİK DEHİDRASYON UYGULANMIŞ VE TAZE İNCİRLERİN MİKROYAPISININ DEĞERLENDİRİLMESİ

ÖZET: Bu çalışmada, vakum altında ozmotik dehidrasyon uygulanmış (önişlem uygulanmış) ve taze (önişlem uygulanmamış) incirlerin (Ficus carica L) mikroyapısı karşılaştırılmıştır. Deneylerde, bir bütün olarak Sarılop türü incirler kullanılmıştır. Kurutma işleminden önce, incirlere 50°Brix çözelti oranındaki ve 50°C çözelti sıcaklığındaki çözelti/ürün kütle oranı 4/1 olan sakaroz çözeltinde ozmotik dehidrasyon uygulanmıştır. Ozmotik dehidrasyon (OD) işleminin başlangıcında, 15dk boyunca 130mbar vakum uygulanmıştır. Vakum uygulama işleminden sonra, OD işlemi atmosfer basıncında 165dk devam etmiş ve böylece OD işlemi toplamda 180dk sürmüştür. Kurutma işlemi 60 °C'de bir kurutma fırınında gerçekleşmiştir. Sonuçlar, vakum altında ozmotik dehidrasyon (VAOD) yönteminin incir ürünlerinin kurutma süresini kısalttığını göstermiştir. Buna ek olarak, taramalı elektron mikroskobu analizi

ile kurutulmuş (önişlem uygulanmış ve önişlem uygulanmamış) ve yaş incirlerin mikroyapısal özellikleri gözlemlenmiştir. Sonuç olarak, VAOD yöntemi incir dokusunun yapısındaki hasarlar gibi değişikliklere neden olmuştur. Bu çalışma, incirin kurutma periyodu ve mikroyapısal analizi ile ilgili sonuçları içermesi bakımından gıda endüstrisi için yenilikçi bilgiler vermektedir.
Anahtar sözcükler: İncir, kurutma, vakum altında ozmotik dehidrasyon, mikroyapısal analiz.

GİRİŞ

Dünya Tarım Örgütü'nün (FAO) 2016 yılı verilerine göre, Dünya'da toplam kuru incir ihracatı 104757 ton olarak gerçekleşirken bu ihracatın %66.4'lük payını Türkiye oluşturmaktadır. Bununla birlikte, Dünya'da toplam 387 milyon $ değerinde kuru incir ihracatı gerçekleşmiş olup Türkiye %64.5'lik payıyla yine birinci sırada yer almaktadır (FAO, 2018). Ayrıca Gümrük ve Ticaret Bakanlığı'nın verilerine göre, 2016 yılı sonunda Türkiye kuru incir ve yaş incir üretiminde sırasıyla %56.5 ve %29.1'lik oranla Dünya'da ilk sırada yer almaktadır (Gümrük ve Ticaret Bakanlığı, 2018). Ege İhracatçılar Birliği'nin verilerine göre, 2017 yılında 63279 tonluk kuru incir ihracatı gerçekleşmiş olup bu rakam toplam kuru meyve ihracatının %12.8'ini oluşturmaktadır. Kuru incir, sırasıyla çekirdeksiz kuru üzüm ve kuru kayısıdan sonra en çok ihraç edilen üçüncü meyve ürünüdür. 2017 yılında, kuru incir ihracatından 253.5 milyon $'lık gelir elde edilirken bu miktar toplam kuru meyve ihracatının %19.8'lik payını oluşturmaktadır. Bununla birlikte, toplam kuru incir üretiminin ve ihracatının yaklaşık %84'lük kısmı Ege Bölgesi'nden sağlanmaktadır (EİB, 2018).

Yaş incirin gerek hasat süresinin kısa olmasından dolayı sebep olduğu bazı olumsuzlukların önüne geçmek gerekse de raf ömrünü uzatmak amacıyla incire kurutma işlemi uygulanmaktadır (Mujic ve diğ., 2014). Vinson ve diğ. (2005) tarafından yapılan bir çalışma, kuru incirin yaş incire kıyasla potasyum, kalsiyum ve demir mineralleri ile antioksidan miktarı açısından daha üstün olduğunu göstermiştir. Ancak kurutma işleminin gıda kalitesinde sebep olduğu bazı olumsuzluklar nedeniyle kurutma işleminden önce çeşitli önişlem yöntemlerinin uygulanması konusunda çalışılmıştır. Bu yöntemlerden biri de ozmotik dehidrasyon (OD) işlemidir (Sagar ve Suresh, 2010). OD işleminde, ürün ozmotik çözelti içerisine daldırılarak kütle transferi olarak adlandırılan üründen su kaybının ve çözeltiden ürüne katı kazanımının gerçekleşmesi amaçlanmaktadır (Zhao ve Xie, 2004). Bununla birlikte, OD işlemi sırasında kütle transferini hızlandırmak amacıyla vakum işlemi de uygulanmaktadır. Vakum altında ozmotik dehidrasyon (VAOD) işleminde, kurutulacak ürün ozmotik çözelti içerisine daldırıldıktan sonra kısa süreliğine (5-15dk) vakum altında bekletilir ve sonra OD işlemine atmosfer basıncında devam edilir (Chiralt ve Fito, 2003; Zhao ve Xie, 2004). Literatürde, kurutma işleminden önce VAOD yönteminin çeşitli gıda ürünlerinde uygulandığı çalışmalar vardır (An et al., 2013; Şahin ve Öztürk, 2016; Moreno ve diğ., 2016; Şahin ve Öztürk, 2018; Darvishi ve diğ., 2018). Bu çalışmanın amacı, kurutma işleminin ve kurutma öncesi uygulanan VAOD işleminin incirin mikroyapısı üzerindeki etkilerini incelemektir.

MATERYAL VE METOT

Şekil 1'de gösterilen vakum altında ozmotik dehidrasyon (VAOD) işlemi Pamukkale Üniversitesi, Temiz Enerji Evi'nde gerçekleştirilmiştir. Bu sistemde, deney düzeneği vakum pompası (Edward, RV8, New Jersey, ABD), vakum odası (Memmert VO-200,

Schwabach, Almanya) ve vakum odasından emilen nemli havayı yoğuşturmak için kullanılan bir ısı değiştirgecinden (Polyscience 9506, Niles, Illinois, ABD) oluşmaktadır.

Ozmotik dehidrasyon (OD) işlemi, 50°Brix çözelti oranındaki ve 50°C çözelti sıcaklığındaki çözelti/ürün kütle oranı 4/1 olan sakaroz çözeltinde uygulanmış ve OD işleminin başlangıcında, 15dk boyunca 130mbar vakum uygulanmıştır. Vakum uygulama işleminden sonra, OD işlemi atmosfer basıncında 165dk devam etmiştir. Bu sayede önişlem süresi 180dk sürmüştür. VAOD uygulanan incirler ile taze incirlerin kurutma işlemi 60 °C'de bir kurutma fırınında gerçekleşmiş ve ürünlerinin son nem içeriği yaklaşık %23'e (yaş bazda) ulaşıncaya kadar kurutma işlemi sürdürülmüştür.

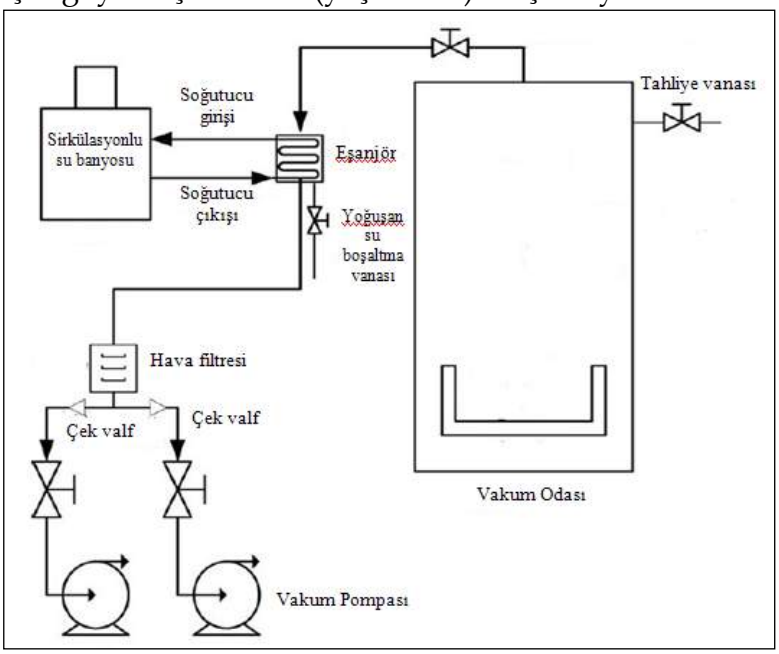

Şekil 1. Vakum sisteminin şematik gösterimi

Kurutulan ürünlerin nem oranı (MR) Eşitlik (1)'de verilen formülle hesaplanmaktadır.

$$MR = \frac{M - M_e}{M_o - M_e} \quad (1)$$

Burada, MR nem oranını (birimsiz), M herhangi bir t anındaki ürünün nem içeriğinin (kg su/kg kuru madde), M_o ürünün başlangıçtaki nem içeriğini (kg su/kg kuru madde) ve M_e ise ürünün denge nem içeriğini (kg su/kg kuru madde) belirtmektedir. İncirin denge nem içeriği M_e, GAB (Guggenheim-Anderson-De Boer) eşitliği ile hesaplanabilmektedir (Şahin ve Öztürk, 2016). GAB modeli Eşitlik (2) ile hesaplanabilmektedir.

$$M_e = \frac{\mathrm{M_m \cdot c \cdot k \cdot a_w}}{(1 - k \cdot a_w) \cdot (1 - k \cdot a_w + c \cdot k \cdot a_w)} \quad (2)$$

Burada, c ve k katsayıları sırasıyla Eşitlik (3) ve (4)'te verilmektedir.

$$c = c_0 exp\left(\frac{\Delta H_c}{R_g T_{mutlak}}\right) \quad (3)$$

$$k = k_0 exp\left(\frac{\Delta H_k}{R_g T_{mutlak}}\right) \quad (4)$$

Burada R_g üniversal gaz sabitini (8.314 J/(mol/K)) ve T_{mutlak} kurutma havasının mutlak sıcaklığını (K) belirtmektedir. GAB eşitliğindeki diğer katsayılar ise incir için $M_m = 11.7$ % (kuru bazda), $c_0 = 1.77$, $k_0 = 0.05$, $\Delta H_c = -1.55\ \mathrm{J/mol \cdot K}$ ve $\Delta H_k = 25.2\ \mathrm{J/mol \cdot K}$ olarak belirlenmiştir (Marinos-Kouris ve Maroulis, 2015). Buna ek

olarak, 60 °C'de kurutulan yaş incirlerin ve VAOD uygulanmış incirlerin su aktivitesi (a_w) ise sırasıyla 0.762±0.018 ve 0.753±0.009 olarak ölçülmüştür (Novasina LabSwift, İsviçre, ± 0.001).

Taramalı Elektron Mikroskobu (TEM) Analizi

Taze incirler ile kurutulmuş incirlerin mikroyapısı, FEI Quanta 450 FEG model Taramalı Elektron Mikroskobu (TEM) ile birlikte WetSTEM dedektörü kullanılarak (Hitit Üniversitesi Bilimsel Teknik Uygulama ve Araştırma Merkezi-HÜBTUAM, Çorum, Türkiye) incelenmiştir. Mikroyapısal analiz aşağıda belirtilen üç ürün grubuna uygulanmıştır.

Taze incirler,

VAOD uygulanmış ve 60 °C'de kurutulmuş incirler,

Önişlem uygulanmamış ve 60 °C'de kurutulmuş incirler

SONUÇLAR

Şekil 1'de taze incirler ile VAOD uygulanmış incirlerin 60°C'deki nem oranının kurutma süresince değişimi verilmektedir. Önişlem uygulanmamış incirlerin kurutma süresi 78h sürerken VAOD uygulanmış incirlerin kurutma süresi 53h sürmüştür. Başka bir ifadeyle, VAOD işlemi bu çalışma için kurutma süresini azaltmıştır. Elde edilen bu sonucun çeri domates (An ve diğ., 2013), kırmızı deniz kulağı (Pérez-Won ve diğ., 2016) ve yaban mersini (Moreno ve diğ., 2016) ile ilgili yapılan çalışmalarla da uyumlu olduğu tespit edilmiştir.

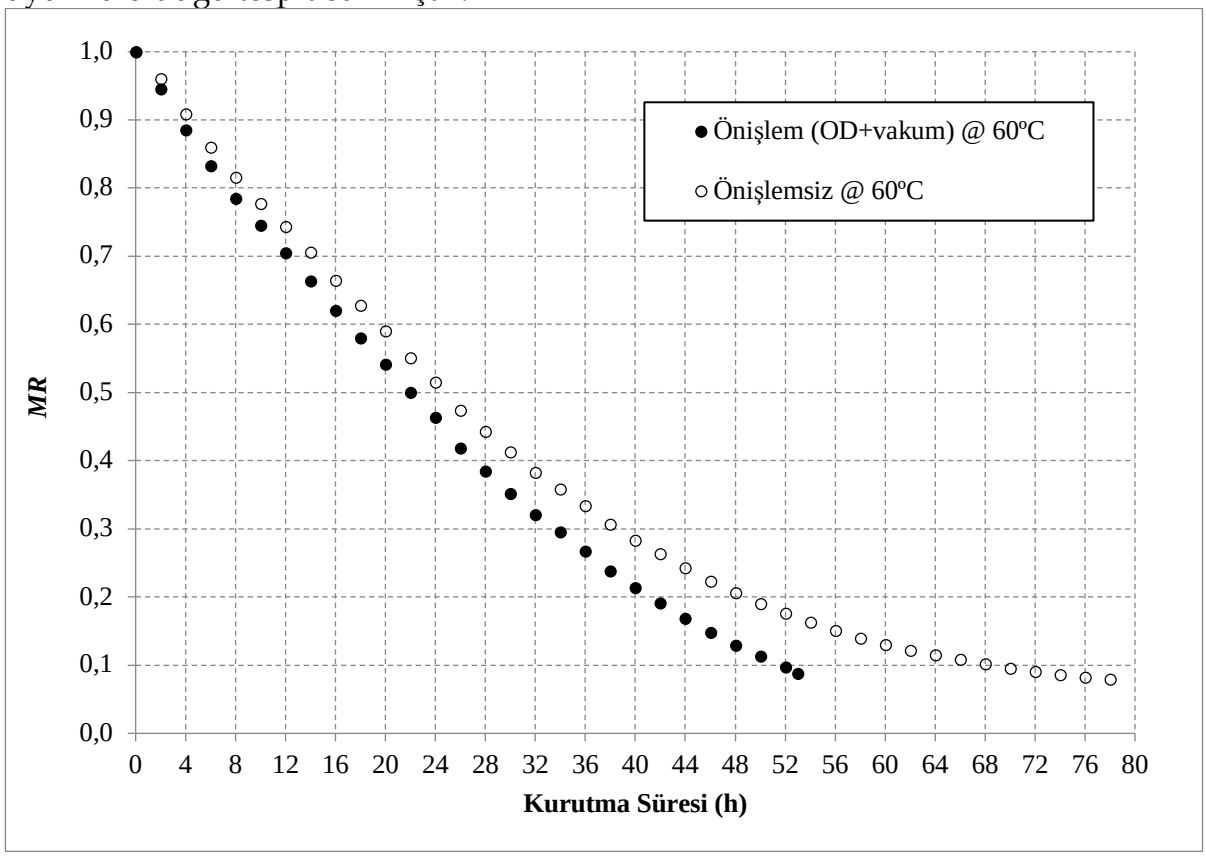

Şekil 2. Taze incirler ile VAOD incirlerin 60°C'de kurutulmasındaki nem oranı-kurutma süresi değişimi

Yaş incir örneklerinin mikroyapısı incelendiğinde (Şekil 3a), dokunun hücre duvarları ve hücrelerarası boşluklardan oluştuğu ve hücrelerin şişkin ve birbirlerine yakından bağlı olduğu söylenebilir. Önişlem uygulanmış ile önişlem uygulanmamış incirlerin kurutulması sonucu mikroyapısal farklılıklar Şekil 3b ve Şekil 3c'de gösterilmektedir. Önişlem uygulanmamış incirlerdeki (Şekil 3b) mikroyapısal durumun aksine, önişlem uygulanmış incirlerde (Şekil 3c) hücrelerin birbirlerine yakın bağlı olduğu söylenebilir. Ayrıca, önişlem uygulanmış incirlerin hücre yapısında deformasyon, çöküntü, hücrelerarası boşlukta daralma ve hücre duvarında bozulma olduğu ifade edilebilir. Bu sonucun, Nowacka ve diğ. (2014) tarafından ozmotik dehidrasyon önişlemi uygulanmış kivi meyvesinin kurutulmasıyla ilgili yapılan çalışma ile uyumluluk gösterdiği söylenebilir. Genel olarak, VAOD yöntemi incir dokusunun yapısındaki hasarlar gibi değişikliklere neden olmuştur. Bu durumun, VAOD yönteminin bir miktar suyun gıdadan uzaklaşmasını sağlaması ve gıdanın gözeneklerinden içeriye ozmotik çözeltinin girmesinden kaynaklandığı söylenebilir (Cháfer ve diğ., 2003; Chiralt ve Fito, 2003).

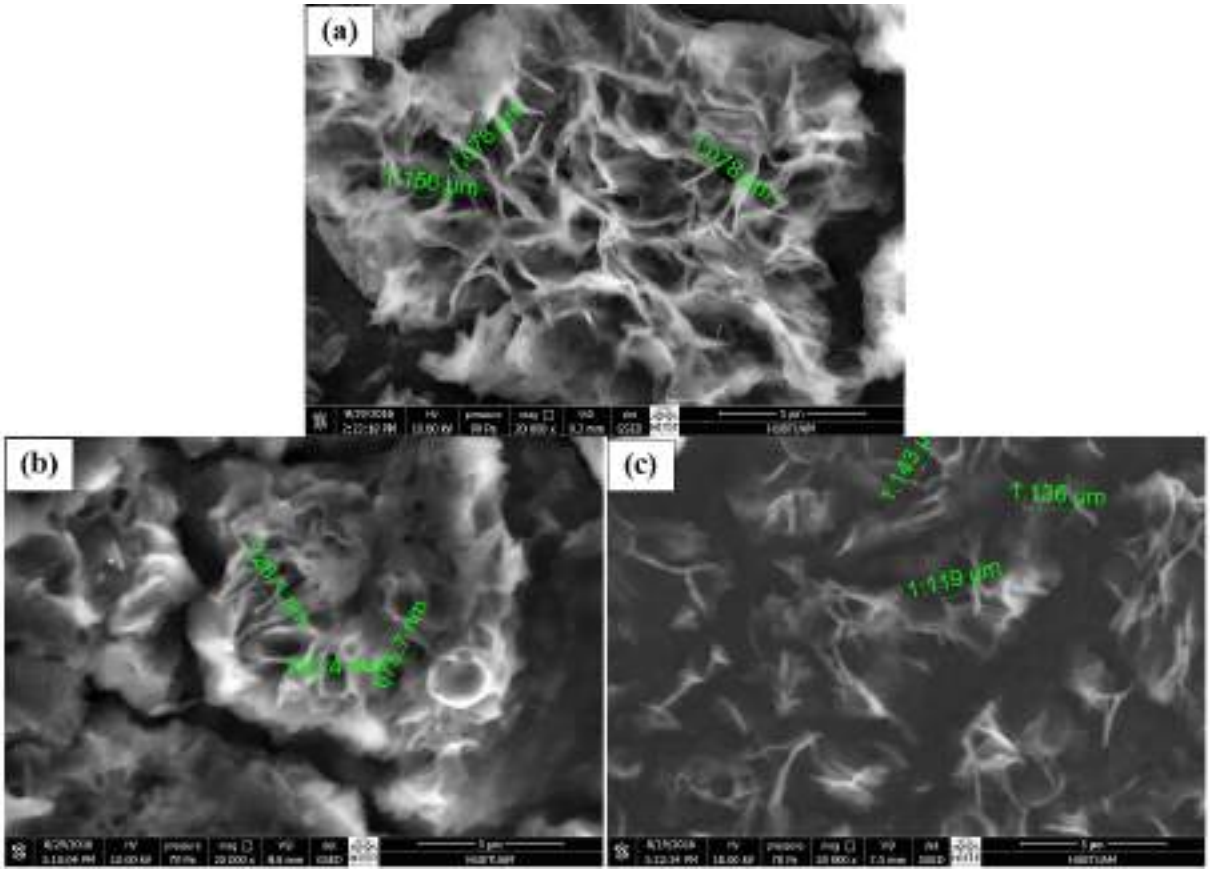

Şekil 3. 20000 kat büyütülmüş TEM görüntüleri (a) yaş incir, (b) VAOD uygulanmış ve 60°C'de kurutulmuş incir ve (c) önişlem uygulanmamış ve 60°C'de kurutulmuş incir.

TEŞEKKÜR

Bu çalışma, 2014FBE032 numaralı Pamukkale Üniversitesi Bilimsel Araştırmalar Doktora Tez Projesi tarafından desteklenmiştir.

KAYNAKLAR

An, K., Li, H., Zhao, D., Ding, S., Tao, H., Wang, Z., 2013. Effect of osmotic dehydration with pulsed vacuum on hot-air drying kinetics and quality attributes of cherry tomatoes. *Drying Technology: An International Journal*, 31, 6, 698-706.

Cháfer, M., Gonzáles-Martínez, C., Chiralt, A., Fito, P. (2003). Microstructure and vacuum impregnation response of citrus peels, *Food Research International*, 36, 35-41.

Chiralt, A., Fito, P. (2003). Transport Mechanisms in Osmotic Dehydration: the role of the structure, *Food Science and Technology International*, 9, (3), 179-186.

Darvishi, H., Azadbakht, M., Noralahi, B., 2018. Experimental performance of mushroom fluidized-bed drying: Effect of osmotic pretreatment and air recirculation, *Renewable Energy*, 120, 201-208.

EİB, 2018. Ege Kuru Meyve Mamulleri İhracatçı Birliği 2017/18 sezonu çalışma raporu ve faaliyet planı. <http://upload.eib.org.tr/20150512/00000000004779.pdf>. Erişim tarihi: 25.09.2018

FAO, 2018. Food and Agriculture Organization (Dünya Tarım Örgütü), FAOSTAT>data>food balance sheets. <http://www.fao.org/faostat/en/#data/TP>. Erişim tarihi: 25.09.2018

Gümrük ve Ticaret Bakanlığı, 2018. Gümrük ve Ticaret Bakanlığı Kooperatifçilik Genel Müdürlüğü, 2017 yılı kuru incir raporu, Nisan 2018. <http://koop.gtb.gov.tr/data/5ad0695fddee7dd8b423eb22/2017%20Kuru%20incir%20raporu.pdf> Erişim tarihi: 25.09.2018

Marinos-Kouris, D., Maroulis, Z.B., 2015. Transport properties in the drying of solids. In Mujumdar, A.S. (Ed.), *Handbook of industrial drying, fourth edition* (pp. 95-96). CRC Press.

Moreno, J., Gonzales, M., Zuniga, P., Petzold, G., Mella, K., Munoz, O., 2016. Ohmic heating and pulsed vacuum effect on dehydration processes and polyphenol component retention of osmodehydrated blueberries (cv. Tifblue). *Innovative Food Science and Emerging Technologies*, 36, 112-119.

Mujic, I., Kralj, M.B., Jokic, S., Jug, T., Subaric, D., Vidovic, S., Zivkovic, J., Jarni, K., 2014. Characterization of volatiles in dried white varieties figs (Ficus carica L.). *Journal of Food Science and Technology*, 51 (9), 1837-1846.

Nowacka, M., Tylewicz, U., Laghi, L. Dalla Rosa, M., Witrowa-Rajchert, D. (2014). Effect of ultrasound treatment on the water state in kiwifruit during osmotic dehydration, *Food Chemistry*, 144, 18-25.

Pérez-Won, M., Lemus-Mondaca, R., Tabilo-Munizaga, G., Pizarro, S., Noma, S., Igura, N., Shimoda, M., 2016. Modelling of red abalone (Haliotis rufescens) slices drying process: Effect of osmotic dehydration under high pressure as a pretreatment. *Innovative Food Science and Emerging Technologies*, 34, 127-134.

Sagar, V.R., Suresh, K.P., 2010. Recent advances in drying and dehydration of fruits and vegetables: a review, *Journal of Food Science and Technology*, 47 (1), 15-26.

Şahin, U., Öztürk, H.K., 2016. Effects of pulsed vacuum osmotic dehydration (PVOD) on drying kinetics of figs (Ficus carica L). *Innovative Food Science and Emerging Technologies*, 36, 104-111.

Şahin, U., Öztürk, H.K., 2018. Comparison between Artificial Neural Network model and mathematical models for drying kinetics of osmotically dehydrated and fresh figs under open sun drying. *Journal of Food Process Engineering*, 41 (5), e12804.

Vinson, J.A., Zubik, L., Bose, P., Samman, N., Proch, J., 2005. Dried Fruits: Excellent in Vitro and in Vivo Antioxidants, *Journal of the American College of Nutrition*, 24 (1), 44-50.

Zhao, Y., Xie, J., 2004. Practical applications of vacuum impregnation in fruit and vegetable processing. *Trends in Food Science and Technology*, 15, 434-451.

INVESTIGATION OF SHELL MATERIALS EFFECTS ON CONVERSION EFFICIENCY OF TYPE-II QUANTUM DOT NANOCRYSTAL SOLAR CELLS

Mehmet ŞAHİN
Materials Science and Nanotechnology Engineering, Abdullah Gül Üniversity, Kayseri 38080 Turkey, mehmet.sahin@agu.edu.tr

ABSTRACT: In this work, effects of the shell materials on the efficiency of the type-II quantum dot nanocrystal (QDNC) solar cells have been investigated in detail in frame of modified detailed balance model. The original detailed balance model, developed by Shockley and Queisser in 1961, is based on gap energy (E_g) only of solar cell material. This model is still used to calculate an upper limit for new generation core/shell QDNC solar cells. Since the original model established on E_g only, however, it can give no information about the effects of the core or shell material on the conversion efficiency of core/shell QDNC solar cells. Therefore, the original detailed balance model estimates the same efficiency values for all type solar cells, single crystal p-n junction, amorphous or third generation, if they have the same E_g values. In order to remedy this deficiency, the original detailed balance model has been modified by using of recombination oscillator strength in calculation of recombination current density. Later, the conversion efficiencies of the type-II core/shell QDNC solar cells have been calculated through the original and modified detailed balance model. In calculations, a few different QDNC structures with different shell materials have been taken into consideration to see clearly the effect of the shell materials on the conversion efficiency of the type-II QDNC solar cells. In results of the calculations, although there is no effect of the shell materials on the efficiency of QDNC solar cells according to the original model, the modified model has shown that the shell materials have strong influence on the efficiency values.

Key words: Detailed balance model, Shockley and Queisser limit, quantum dot nanocrystal, solar cell

References

[1] W. Shockley and H. J. Queisser, "Detailed Balance Limit of Efficiency of p-n Junction Solar Cells", J. Appl. Phys. **32**, 510 (1961).
[2] M.C. Hanna, M.C. Beard, J.C. Johnson, J. Murphy, R.J. Ellingson, and A.J. Nozik, "Quantum Dot Solar Cells with Multiple Exciton Generation", Conference Paper, NREL/CP-590-38992, Presented at the 2005 DOE Solar Energy Technologies Program Review Meeting November 7–10, 2005 Denver, Colorado, USA.
[3] A.J. Nozik, "Multiple exciton generation in semiconductor quantum dots", Chemical Physics Letters **457**, 3 (2008).
[4] S. Tomic, J.M. Miloszewski, E.J. Tyrrell, D.J. Binks, "Design of core/shell colloidal quantum dots for MEG solar cells", IEEE Journal of Photovoltaics **6**, 179 (2016).

LIFE CYCLE ASSESSMENT OF RENEWABLE ENERGY SOURCES: A REVIEW FOR CARBON FOOTPRINT

Pelin SOYERTAŞ YAPICIOĞLU
Harran University, Environmental Engineering Department, Şanlıurfa
pyapicioglu@harran.edu.tr

ABSTRACT: Growing concerns about the shortage of fossil fuels and climate change have motivated researches for new energy resources and sustainable energy technologies. Renewable energy sources are considered as the ideal alternative to fossil fuels because of their many advantages. To generate electricity, renewable energy resources have been used as production methods. Renewable energy resources contain biomass, hydropower, geothermal, solar, wind and marine energies. Renewable energy sources are in demand, clean, low risk, and inexhaustible when compared with other non-renewable energy sources. Non-renewable energy sources have many unfavorable and significant environmental impacts. They are the main contributor of the global warming and greenhouse effect due to their gas emissions and potential climate change effects. At the same time, renewable energy sources have less risk environmental impacts. It is crucial to detect the environmental impacts of renewable energy sources for a sustainable life. Life Cycle Assessment (LCA) is a methodology that enables the determination of the environmental impacts of a system or a product with the approach of from cradle to grave, worldwide. The life cycle assessment (LCA) of renewable energy resources is considered as the key indicator to observe their sustainability. A typical LCA include global climate change, ozone depletion, smog, acidification, eutrophication, natural resources consumption, human toxicity, ecotoxicity as the environmental impact indicators. In this paper, a review has been implemented considering global climate change indicator of LCA that contains carbon footprint. Carbon footprint is the main component of this methodology. This paper aims to prove that the importance related to life cycle assessment of renewable energy sources. According to the investigated studies, among renewable energy resources, biomass energy has the highest carbon footprint and offshore wind technologies has the minimum carbon footprint. The results of this review can ensure an assessment guide for the projects of renewable energy technologies.

Key words: renewable energy, life cycle assessment, environmental impact, carbon footprint

INTRODUCTION

In recent years, increasing greenhouse gas (GHG) emissions due to the combustion of fossil fuels has become a major global environmental challenge all over the world (Han and Kim, 2017). To reduce GHG emissions, many physical, biological, chemical, physicochemical and biochemical methods have been developed and investigated, worldwide (Qambrani et al., 2017). Trend to the renewable energy resources has been considered as a greenhouse gas emission mitigation method. Renewable energy is the alternative energy to non-renewable energy resources such as the fossil fuels (coal, petroleum etc.). Due to the environmental challenges of fossil fuel utilization,

renewable energy sources have gained the critical significance all around the world (Mao et al., 2015).

Renewable energy resources contain biomass, hydropower, geothermal, solar, wind and marine energies (Amponsah et al., 2014; Jacobson & Delucchi, 2011). Renewable energy resources have been regarded as a type of primary, low risk, clean and inexhaustible energy (Amponsah et al., 2014; Dincer, 2001; Bilgen et al., 2004). Along with these positive features, renewable energy resources could have also unfavorable environmental impacts. Sustainable development has been required the tools and methods to monitor and compare the environmental impacts of the systems, human activities and the products (Amponsah et al., 2014). Life cycle assessment is a widely-used environmental impact analysis and evaluation method, in recent years (Ghafghazi et al., 2011).

Life cycle assessment methodology includes cradle-to-grave analyses of production or service systems and supply benchmarked evaluations for all environmental impacts of inputs and outputs (Williams, 2009). LCA is a common preferred method to compare greenhouse gas (GHG) emission amounts of renewable energy resources. Carbon footprint can be defined as the total measure of GHG emissions caused directly and indirectly by a system, organization, event or product (Turkish Standards Institution, 2007). Carbon footprint is an indicator of the environmental damages and negative impacts to the environment that is a component of life cycle assessment methodology. Global warming potential (GWP) is an impact category of LCA method and carbon footprint is the definition of global warming potential (Uchiyam, 2007). It is important to know the net GHG emissions from renewable energy resources to compare with the others and to detect which energy system will be used and elected.

In this study, it is aimed to investigate the global warming potential of renewable energy resources. This paper reviews the current estimations of life cycle GHG emissions that is defined as the carbon footprint term of renewable energy resources in the literature.

RENEWABLE ENERGY

The increasing demand for energy day by day and the unfavorable environmental impacts of non-renewable energies cause the trend to the renewable energy systems (Guo et al., 2018; Montes et al., 2005; Yusaf et al., 2011; Kelly, 2011; Milbrandt et al., 2014; Nematollahi et al., 2016). Renewable energy resources are regarded as one of the remedies of the climate change and energy security (Harrison, 2008). So, renewable energy systems have gained attention due to these significant properties, in recent years. Renewable energy acts a crucial role in reducing GHG emissions. When renewable energy resources are used, the requirement for fossil fuels is decreased. There are many types of renewable energy resources, worldwide (Iyer et al., 2013).

Renewable Energy Resources

Renewable energy resources are continually replenished by the natural ways and derived directly from the sun such as solari thermal, photo-chemical, and photo-electric, indirectly from the sun such as wind, hydropower, and biomass or from other natural movements of the environment such as geothermal and wave energy or with other production methods such as hydrogen energy (T.C. MENR, 2018; Ellabban et al., 2014). Renewable energy does not contain energy resources derived from fossil fuels, waste products from fossil sources, or waste products from inorganic sources (Ellabban et al., 2014).

Biomass energy (bioenergy) is the transformation of biomass (wood and forest wastes, plants, animal manure, agricultural residues, sewage sludge etc.) into useful forms of energy such as heat, electricity and biofuels (Toklu, 2017). Geothermal energy is a powerful and efficient renewable energy type to extract energy from the earth by the natural processes. Geothermal energy is regarded as a cost effective, reliable, and environmentally friendly energy resource (Hammons, 2003).Geothermal energy resources comprise of thermal energy from the earth's interior stored in both rock and trapped steam or liquid water (Ellabban et al., 2014). Hydropower is a type of renerwable energy that is derived from the moving water. Moving water forms an energy that can be converted into electricity by using turbines. Hydropower is ensured from water flowing in the hydrological cycle with the help of solar radiation (Ellabban et al., 2014). The other renewable energy resource is the oceans. The renewable marine (ocean) energy consists of six sources that are waves, tidal range, tidal currents, ocean currents, ocean thermal energy conversion and salinity gradients (Aly & El-Hawary, 2011). Solar energy generation includes the use of the sun's energy to ensure hot water with solar thermal systems or electricity with solar photovoltaic (PV) and concentrating solar power (CSP) systems (Ellabban et al., 2014). Wind power is described as the conversion of wind energy by wind turbines into a useful form. There are two types of wind energy that contains onshore and offshore wind technologies. Onshore wind turbines are called as wind farms, although offshore wind energy technology has higher investment than onshore turbines (Islam et al., 2013; Eltamaly, 2013; Ellabban et al., 2014).

METHODS

This study is a purposeful review of peer-reviewed literature related to the use of LCA to estimate carbon footprint from renewable energy reosources to generate electricity. In many cases, the review was fulfilled with literature from web-accessible documents and projects. Carbon footprint is the indicator of the global warming potential. The global warming potential (GWP) is an impact category of LCA.

LIFE CYCLE ASSESSMENT (LCA)

Life cycle assessment is one of the methodologies of environmental impact evaluation worldwide, in recent years. Life cycle assessment (LCA) is described by ISO 14040 as the overview and the estimation of the environmental inputs, outputs and possible impacts of the systems during their life cycles (Turkish Standards Institution, 2006; Yapıcıoğlu & Demir, 2017). Life cycle assessments contain the cradle-to-grave

approach and this methodology enables benchmarking the environmental inputs and outputs and possible impacts (Williams, 2009). LCA methodology has four main stages that are goal and scope description, inventory analysis, impact assessment and interpretation (Guinee, 2004). In Figure 1., the definitions of the steps have been demonstrated.

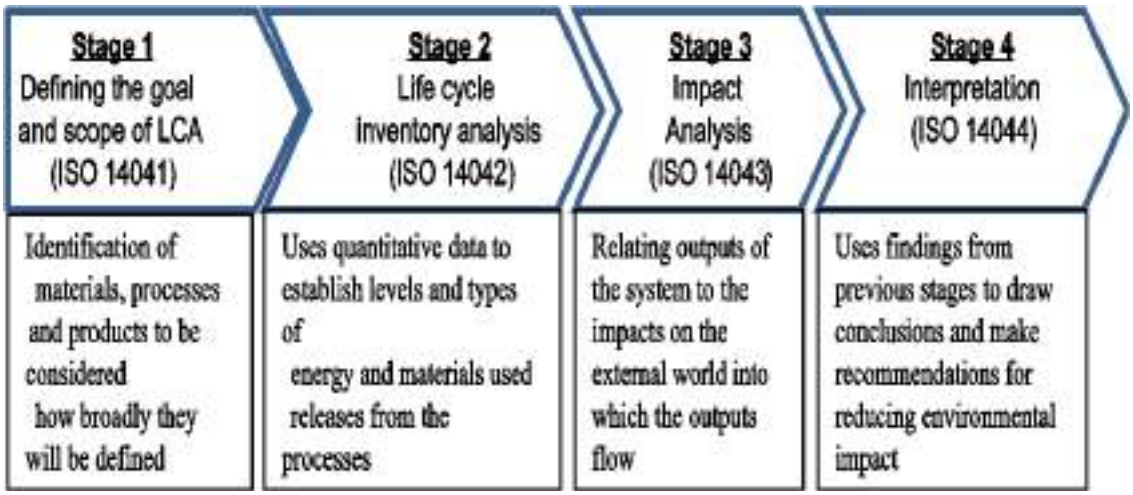

Figure 1. Stages of LCA (Liu and Jiang, 2011)

As seen in the figure, the first stage involves the description of the raw and auxiliary materials, processes and the by-products and end products of a system. In the second stage, the inventory provides quantitative data of the inputs and outputs. In this methodology, inputs are freshwater, energy and organic and inorganic chemical substances and outputs are air, dust and greenhouse gas emissions, wastewater and solid wastes. Impact analysis means the evaluation of the outputs and classifying them under an impact category. And the final stage is interpretation that is defined as creating the conclusions and suggestions for reducing environmental impacts (Rebitzer et al., 2004; Liu and Jiang, 2011).

Life Cycle Impact Assessment (LCIA) Methods

Life cycle impact assessment (LCIA) is the most crucial stage of LCA (Yapıcıoğlu & Demir, 2017). Impact assessment is carried out with various methods, database, models and commercial software. There are many LCIA methods that are based on different databases, recently. CML 2001, Cumulative energy demand, Cumulative exergy demand, Eco-indicator 99, Ecological footprint, Ecological scarcity 1997 and 2006, Ecosystem damage potential, Environmental Design of Industrial Products, EPS 2000, IMPACT 2002+, IPCC 2001 (climate change) and IPCC 2007 (climate change), ReCiPe (Midpoint and Endpoint approach), TRACI and USEt etc. are widely- used methods (Hischier et al., 2010).

Life Cycle Impact Categories

The major impact categories are global climate change, acidification, eutrophication, natural resources consumption, stratospheric ozone depletion, human toxicity, smog, ecotoxicity and noise (Turkish Standards Institution, 2006). The popular impact categories are global warming potential, photochemical oxidation potential, human toxicity, ecotoxicity, acidification potential, eutrophication potential, energy balance and terrestrial ecotoxicity (Rebitzer et al., 2004). Carbon Footprint is an indicator of the global warming potential.

Carbon Footprint Term and Greenhouse Gas Emissions

Over the last half century, climate change impacts have been felt most strongly all around the world (He et al., 2018). The emission of greenhouse gases (GHGs) is the major reason of global climate change (Luttropp and Lagerstedt, 2006; Metz et al., 2012; Wamsler et al., 2013). The carbon footprint measures and indicates the greenhouse gas emissions and its environmental impacts (Trappey et al., 2012; He et al., 2018). Main greenhouse gas emissions are carbon dioxide (CO_2), methane (CH_4) and nitrous oxide (N_2O) emissions related to many resources such as agricultural fields, industries, roads, buildings, waste and wastewater treatment plants, energy power stations, etc. on the earth, worldwide (IPCC, 2014). One of the greenhouse gas emission resources is renewable energy systems (IPCC, 2014).

RESULTS AND FINDINGS

CARBON FOOTPRINT OF RENEWABLE ENERGY SOURCES

Greenhouse Gas Emissions from Renewable Energy Sources

Renewable energy sources have not only positive environmental impacts, but also emit greenhouse gas emissions to the atmosphere. The amount of greenhouse gas emission can be calculated on the basis of the charged amount of energy obtained from the energy balance during the life cycle. In Table 1 greenhouse gas emissions (carbon footprints) that have been emitted to generate electricity related to various renewable energy sources have been demonstrated.

Carbon footprint is defined as for renewable energy sources with g CO_2-eq/ kWhe (gram carbon dioxide equivalent per kilowatt hour electricity) that is a standard unit in this review. For the detection of the minimum carbon footprint of the renewable energy resources, in the range, the least maximum value is considered. For the determination of the maximum carbon footprint of the renewable energy resources, in the range, the highest maximum value is regarded. The carbon footprint comparison of the renewable energy resources is given in Figure 2.

Figure 2. Carbon Footprint Comparison of the Renewable Energy Resources

Table 1. Carbon footprint of Renewable Energy Resources (Amponsah et al., 2014)

Renewable Energy Resource	Carbon Footprint (g CO_2-eq/kWh_e)	Reference
Onshore Wind	8-124	Gürzenich et al., 1999; Celik et al., 2007; Bojacá & Schrevens, 2010; Ardente et al., 2008.
Offshore Wind	5-24	Dolan & Heath, 2012; Proops et al., 1996; Vestas, 2006.
Hydropower	2-75	Goralczyk, 2003; Varun & Prakash 2012; Varun & Prakash 2010; Elsayed et al., 2003.
Wave	12-50	Varun & Prakash 2008; Carbon Trust, 2006.
Geothermal	11-78	Hondo, 2005; Moomaw et al., 2011.
Solar thermal	30-150	Velmurugan & Srithar, 2008; Lenzen, 1999.

Biomass	14-550	Larson, 2006; Curan, 2013.

CONCLUSION

Renewable energy systems are clean, low risk and environmentally friendly comparing with other non-renewable energy resources. Renewable energy systems play an important role in decreasing global climate change impacts.

Life cycle assessment is an environmental impacts assessment methodology that enables the determination of global warming potential of a system or a product. Life cycle assessment (LCA) is a widely-used methodology to detect the greenhouse gas emissions of renewable energy resources. Carbon footprint is the key indicator of emitting greenhouse gas emissions.

According to the investigated studies, among renewable energy resources, biomass energy (bioenergy) has the maximum carbon footprint with the value of 550 g CO_2-eq/kWhe, in any case offshore-wind energy has the least carbon footprint in value of 24 g CO_2-eq/kWhe to generate electricity.

RECOMMENDATIONS

Renewable energy resources emit greenhouse gas emissions, so carbon footprint estimation should be detected before the investment of the energy systems. There are limited case studies related to this topic, the investigations should be enhanced.

REFERENCES

Aly, H.H.H. & El-Hawary, M.E. Proceedings from CCECE '2011: State of the art for tidal currents electric energy resources. *24th Canadian conference on electrical and computer engineering (CCECE); 8–11May 2011.*
Amponsah, N.Y., Troldborg, M., Kington, B., Aalders, I., Hough, R.L. (2014). Greenhouse gas emissions from renewable energy sources: A review of lifecycle considerations. *Renewable and Sustainable Energy Reviews, 39,* 461-475.
Ardente, F., Beccali, M., Cellura, M., Lo Brano V. (2008). Energy performances and life cycle assessment of an Italian windf arm. *Renew Sustainable Energy Rev, 12(1),* 200–217.
Bilgen, S., Kaygusuz, K., Sari, A. (2004). Renewable energy for a clean and sustainable future. *Energy Sources, 26(12)*, 1119–1129.
Bojacá, C.R. & Schrevens, E. (2010). Parameter uncertainty in LCA: stochastic sampling under correlation. Int J Life Cycle Assess, *15(3),* 238–246.
Carbon Trust. (2006). *The carbon emissions generated in all that we consume*. Retrieved July 5, 2018 from https://www.carbontrust.com/media/84936/ctc603-the-carbon-emissions-generated-in-all-that-we-consume.pdf

Celik, A.N., Muneer, T., Clarke, P. (2007). An investigation into micro wind energy systems for their utilization in urban areas and their life cycle assessment. *Proc Inst Mech Eng A – J Power Energy, 221*, 1107–1117.
Curran, M.A. (2013). Life Cycle Assessment:a review of the methodology and its application to sustainability. *Curr Opin Chem Eng, 2(3),* 273–277.
Dincer I. (2001). Environmental issues:I-energy utilization. *Energy Sources, 23(1)*,69–81.
Dolan, S.L. & Heath, Ga. (2012). Life cycle greenhouse gas emissions of utility-scale wind power. *J Ind Ecol, 16*, 136–154.
Ellabban, O., Abu-Rub, H., Blaabjerg, F. (2014). Renewable energy resources: Current status, future prospects and their enabling technology. *Renewable and Sustainable Energy Reviews, 39,* 748–764.
Elsayed, M.A., Matthews, R., Mortimer, N.D. (2003). *Carbon and energy balances for a range of biofuels options.* Resources Research Unit, Sheffield Hallam Univ, 300.
Eltamaly, A.M. (2013). Design and implementation of wind energy system in Saudi Arabia. *Renewable Energy*, *60,* 42–52.
Ghafghazi, S.,Sowlati, T., Sokhansanj, S., Bi, X., Melin, S. (2011). Life cycle assessment of base-load heat sources for district heating system options. *International Journal of Life Cycle Assessment, 16(3),* 212–223.

Goralczyk, M. (2003). Life cycle assessment in the renewable energy sector. *Appl Energy*, 75, 205–211.
Guinée, J.B. (2004). *Handbook on life cycle assessment operational guide to the ISO standards.* Kluwer Academic Publishers, New York, USA.
Guo, S., Liu, Q., Sun, J., Jin, H. (2018). A review on the utilization of hybrid renewable energy. *Renewable and Sustainable Energy Reviews, 91*, 1121–1147.
Gürzenich, D., Mathur, J., Bansal, N.K., Wagner, H.J. (1999). Cumulative energy demand for selected renewable energy technologies. *Int J Life Cycle Assess, 4 (3),* 143–149.
Han, S. & Kim, J. (2017) An optimization model to design and analysis of renewable energy supply strategies for residential sector. *Renewable Energy*, *112*, 222-234.
Hammons, T.J. (2003). Proceedings from IEEE '2003: Geothermal power generation worldwide *IEEE Bologna power tech conference proceedings; 23–26 June 2003.*
Harrison, G. (2008). Life cycle assessment of renewable energy systems. Retrieved July 4, 2018 from http://www.bath.ac.uk/research/seminars/esrc/lca/GarethHarrisonLCAofRenewables.pdf
He, B., Pan, Q., Deng, Z. (2018). Product carbon footprint for product life cycle under uncertainty. *Journal of Cleaner Production, 187,* 459-472.
Hischier, R. & Weidema, B. (Editors) (2010). Implementation of Life Cycle Impact Assessment Methods. Retrieved July 6, 2018 from https://www.ecoinvent.org/files/201007_hischier_weidema_implementation_of_lcia_methods.pdf
Hondo, H. (2005). Life cycle GHG emission analysis of power generation systems: Japanese case. *Energy, 30(11–12),* 2042–2056.
IPCC, 2014. Mitigation of Climate Change Summary for Policy makers and Technical Summary. Retrieved July 5, 2018 from https://www.ipcc.ch/pdf/assessment-report/ar5/wg3/WGIIIAR5_SPM_TS_Volume.pdf

Islam, M.R., Mekhilef, S., Saidur, R. (2013). Progress and recent trends of wind energy technology. *Renewable and Sustainable Energy Review, 21*, 456–68.

Iyer, A.S., Couch, S.J., Harrison, G.P., Wallace A.R. (2013). Variability and phasing of tidal current energy around the United Kingdom. *Renewable Energy, 51,* 343-357.

Jacobson, M.Z. & Delucchi, Ma. (2011). Providing all global energy with wind, water, and solar power, Part I:technologies, energy resources, quantities and areas of infrastructure, and materials. *Energy Policy, 39(3),* 1154–69.

Kelly, G. (2011). History and potential of renewable energy development in New Zealand. *Renewable and Sustainable Energy Reviews, 15,* 2501–2509.

Larson, E.D. (2006). A review of life-cycle analysis studies on liquid biofuel systems for the transport sector. *Energy Sustain Dev,10(2),* 109–126.

Lenzen, M. (1999). Greenhouse gas analysis of solar-thermal electricity generation. *Sol Energy, 65(6),* 353–368.

Liu, S. and Meili, J. (2011). *Providing efficient decision support for green operations management: An integrated perspective (Chapter 13), In book: Efficient decision support systems - Practice and challenges in multidisciplinary domains,* InTech Publisher, Croatia.

Luttropp, C. & Lagerstedt, J., (2006). EcoDesign and the Ten Golden Rules: generic advice for merging environmental aspects into product development. *Journal of Cleaner Production, 14 (15),* 1396-1408.

Mao, C., Feng, Y., Wang, X., Ren, G. (2015) Review on research achievements of biogas from anaerobic digestion, *Renewable and Sustainable Energy Reviews*, *45*, 540-555.

Metz, B., Davidson, O.R., Bosch, P.R., Dave, R., Meyer, L. (2012). IPCC Fourth Assessment Report: Climate Change 2007. Working Group III Report "Mitigation of Climate Change". Consultado. Report. Retrieved July 5, 2018 from http://www.ipcc.ch/

Milbrandt, A.R., Heimiller, D.M., Perry, A.D., Field, C.B. (2014). Renewable energy potential on marginal lands in the United States. *Renewable and Sustainable Energy Reviews, 29,* 473–481.

Montes, G.M., López, M.D.M.S., Gámez, M.D.C.R., Ondina, A.M. (2005). An overview of renewable energy in Spain. The small hydro-power case. *Renewable and Sustainable Energy Reviews, 9,* 521–534.

Moomaw, W., Yamba, F., Kamimoto, M., Maurice, L., Nyboer, J., Urama, K., Weir T. (2011). *IPCC special report on renewable energy sources and climate change mitigation.* Cambridge, United Kingdom and NewYork,USA:Cambridge University Press, 161–208.

Nematollahi, O., Hoghooghi, H., Rasti, M., Sedaghat, A. (2016). Energy demands and renewable energy resources in the Middle East. *Renewable and Sustainable Energy Reviews, 54,* 1172–1181.

Proops, J.L., Gay, P.W., Speck, S., Schröder, T. (1996). The life time pollution implications of various types of electricity generation. An input-outputa nalysis. *Energy Policy, 24(3),* 229–237.

Qambrani, N.A., Rahman, M.M., Won, S. et al., (2017). Biochar properties and eco-friendly applications for climate change mitigation, waste management, and wastewater treatment: A review. *Renewable and Sustainable Energy Reviews,79*, 255–273.

Rebitzer, G., Ekvallb, T., Frischknecht, R. et al. (2004). Life cycle assessment Part 1: Framework, goal and scope definition, inventory analysis, and applications. *Environment International*, *30*, 701 – 720.

T.C. Republic of Turkey Ministry of Energy and Natural Resources, (T.C. MENR) (2018). Renewable Energy Sources. Retrieved July 4, 2018 from http://www.yegm.gov.tr/

Toklu, E. (2017). Biomass energy potential and utilization in Turkey, *Renewable Energy 107*, 235-244.

Trappey, A.J.C., Trappey, C.V., Hsiao, C.T., Ou, J.J., Chang, C.T. (2012). System dynamics modelling of product carbon footprint life cycles for collaborative green supply chains. *Int. J. Comput. Integrated Manuf., 25 (10)*, 934-945.

Turkish Standards Institution (2006*). ISO 14040: Environmental management, life cycle assessment, principles and framework*. *Ankara, Turkey.*

Turkish Standards Institution (2007*). ISO 14064: Greenhouse gases -- Part 1: Specification with guidance at the organization level for quantification and reporting of greenhouse gas emissions and removals*. Ankara, Turkey.

Uchiyama, Y. (2007). Life cycle assessment of renewable energy generation technologies. *IEEJ, 1*, 44-48.

Varun, Bhat, I.K. & Prakash, R. (2008). Life cycle analysis of run-of river small hydro power plants in India. *Open Renew Energy J, 1*,11–16.

Varun, Bhat, I.K. & Prakash, R. (2010). Life cycle energy and ghg analysis of hydroelectric power development in India. *Int J Green Energy, 7,* 361–75.

Varun, Bhat, I.K. & Prakash, R. (2012). Life cycle greenhouse gas emissions estimation for small hydropower schemes in India. *Energy, 44(1),* 498–508.

Velmurugan, V. & Srithar, K. (2008). Prospects and scopes of solar pond: a detailed review. *Renew Sustain Energy Rev, 12(8),* 2253–2263.

Vestas, (2006). Life cycle assessment of offshore and onshore sited windpower plants based on Vestas V90-3.0 MW turbines, Denmark.

Wamsler, C., Brink, E., Rivera, C. (2013). Planning for climate change in urban areas: from theory to practice. *Journal of Cleaner Production, 50*, 68-81.

Williams, A. S. (2009). *Life Cycle Analysis: A step by step approach, ISTC Reports.* Champaign, IL: Illinois Sustainable Technology Center, Champaign, USA.

Yapıcıoğlu, P. & Demir, Ö. (2017). Life Cycle Assessment of Sewage Sludge Treatment - An Overview. *Harran Üniversitesi Mühendislik Dergisi, 2,* 78-92.

Yusaf, T., Goh, S., Borserio, J.A. (2011). Potential of renewable energy alternatives in Australia. *Renewable and Sustainable Energy Reviews, 15,* 2214–2221.

A MODEL STUDY ON ENERGY PILES

Pınar Sezin ÖZTÜRK KARDOĞAN
Gazi University
sezinozturk@gazi.edu.tr

Stefano STACUL
Pisa University
stefano.stacul@for.unipi.it

Mehmet İnanç ONUR
Eskişehir Technical University
mionur@anadolu.edu.tr

ABSTRACT: The world energy politics affects civil engineering as well as all other sectors. Especially, minimum energy consumption and the use of renewable energy are gaining popularity. In accordance with this objective, design and application of civil engineering is also continuously developing. Just as the world, the implementation of civil engineering should be observed in the direction of national energy policies in our country. Pile foundation is used when the modern high structures' subsoil bearing capacity inadequate. Energy piles are pile foundation systems that are constructed by integrating collector lines to take advantage of geothermal energy. Energy piles are used for both heating and cooling purposes. In this study, a model study on energy piles, one of the most beautiful examples of renewable energy applications, was performed. Possible benefits were discussed in the case of a sample pile foundation project if design as energy piles in Eskişehir soil conditions.

Key words: energy piles, geothermal energy, pile foundations.

ENERJİ KAZIKLARI ÜZERİNE BİR MODEL ÇALIŞMASI

ÖZET: Dünya enerji politikaları tüm diğer sektörleri olduğu gibi inşaat mühendisliğini de etkilemektedir. Özellikle enerjinin minimum tüketilmesi ve yenilenebilir enerji kullanımına yönelik çalışmalar oldukça popülerlik kazanmaktadır. Bu amaç ile uyumlu olarak inşaat mühendisliği tasarım ve uygulamaları da sürekli gelişmektedir. Dünyada olduğu gibi ülkemizde de ulusal enerji politikaları doğrultusunda inşaat mühendisliği uygulamalarının gözden geçirilmesi gerekmektedir. Modern yüksek yapıların inşa edileceği zeminlerin taşıma gücü olarak yetersiz kaldığı durumlarda kazık temeller kullanılmaktadır. Enerji kazıkları ise jeotermal enerjiden yararlanmak amacıyla kolektör hatları entegre edilerek imal edilen kazık temel sistemleridir. Enerji kazıkları hem ısıtma hem de soğutma amacıyla kullanılmaktadır. Bu çalışmada, yenilenebilir enerji uygulamalarının en güzel örneklerinden olan enerji kazıkları üzerine bir model çalışması yapılmıştır. Eskişehir

ili zemin koşullarında örnek bir kazık temel projesinin enerji kazıkları olarak tasarlanması durumunda olası faydalar tartışılmıştır.

Anahtar sözcükler: enerji kazıkları, jeotermal enerji, kazıklı temeller.

INTRODUCTION

The concept of energy has become a rather important topic with the rapid growth of population and industrialization particularly in Turkey and generally in the world. With the increasing demand for energy, not only the cost has increased but also the existing resources have started to run out. Since this energy demand in the world is generally obtained through fossil fuels such as coal, natural gas and oil, these fuels have the potential to be depleted soon. Because of the increased energy consumption, the amount of CO2 in the atmosphere has increased rapidly, resulting in permanent damage to the environment. This constantly increasing energy consumption brings about the concept of sustainable energy and makes it necessary to find permanent solutions.

Geothermal energy is one of the first things which come to mind when it comes to sustainable energy. Although it is hard and costly to reach deep geothermal energies by using today's technology, it is easier to use shallow geothermal energy (Ozkaya, 2016). Geothermal energy in shallow depth is utilized with heat pumps. The shallow geothermal energy system consists of three main components: (i) Geothermal heat pump, (ii) Ground heat exchanger (GHE) and (iii) Ducting system distributing the conditioned air in the building (Akrouch et al., 2016).

The most common element used in geotechnical engineering with the ground source heat pump which is not affected by the seasonal temperature changes of the ground is the energy piles. Energy piles are pile foundation systems which are manufactured by integrating collector lines to benefit from geothermal energy. Deep foundation applications are used in the areas lack of bearing capacity and settlement problems. The most commonly used foundation application is the pile foundation. Pile foundations with increasing energy demand can be manufactured in such a way that they can obtain heat as well as being used for ground conditions which cannot carry the loads from the superstructure.

The growing demand for energy in recent years has led to an increase in the studies on energy piles. Research on energy piles was first used in Switzerland and Austria in the early 1980s and then widely applied in Europe. (Amis, 2010). Energy piles were used in the Main Tower, Frankfurt (Laloui et al, 2006) and the terminal-E construction of the Zurich International Airport (Pahud and Hubbuch, 2007). It has also been tested for usability by applying energy piles in England (Suckling and Canon, 2004), Switzerland, Germany, Austria (Unterberber et al, 2004) and China (Gao et al, 2008). In the past, numerical analyzes were also conducted to examine the performance of energy piles (Abdelaziz et al, 2011).

BEHAVIOR OF ENERGY PILES

In the use of energy piles, it is necessary to store the subsoil energy and transfer this energy out of the ground (Ennigkeit & Katzenbach, 2001). During the seasonal thermal storage, heat load and unloading can be performed by energy piles. The seasonal thermal storage cycle is shown in Figure 1; (Katzenbach et al, 1998).

The system consists of energy piles in the ground, heating systems of the building and cooling systems of the building. In this way, piles can be used as heating elements in winter and as cooling elements in summer. The liquid in the piles is circulated by the heat pump.

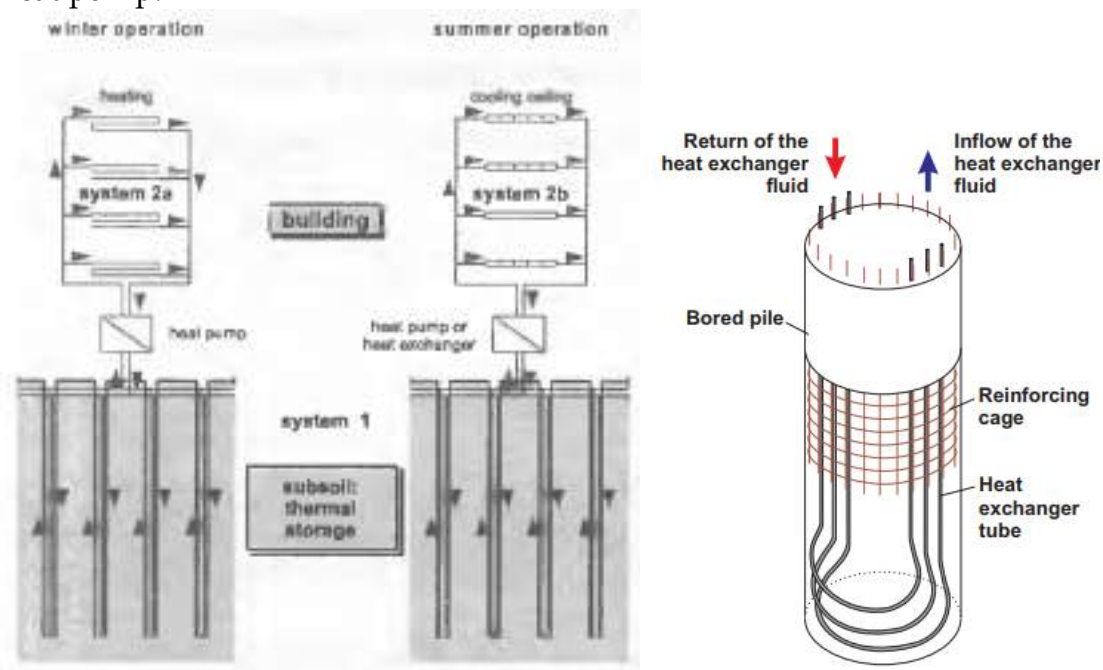

a) b)

Figure 1. a) Seasonal thermal storage system (Katzenbach et al.,1998), b) The figure of energy pile (Katzenbach et al., 2009).

The energy piles are thermo-active elements which provide heat exchange with the ground by means of the liquid circulating in the pipes, while the heat conduction in the energy piles is through molecular interaction, the heat cycle is formed by cyclic flow between the thermodynamic systems moving relative to each other (Olgun et al., 2010). The heat transfer mechanism in the energy piles is shown in Figure 2 schematically; and Table 1 shows the variables related to the heat transfer mechanism. The black arrow marks indicate the heat transfer due to cooling, while the white arrow marks indicate the heat supply for heating purposes. The components of the heat transfer between the fluid in the circulating pipe and the pile and ground (Abdelaziz, et al,2011);

Heat convection between circulating fluid and the inner surface of the pipe (Econv1)
Heat conduction through the circulation pipe wall (Econd1)
Heat conduction within pile (Econd2)
Heat conduction within the in-situ soil (Econd3)
Heat convection generated by groundwater flow, if it is available- convection (Econv2)

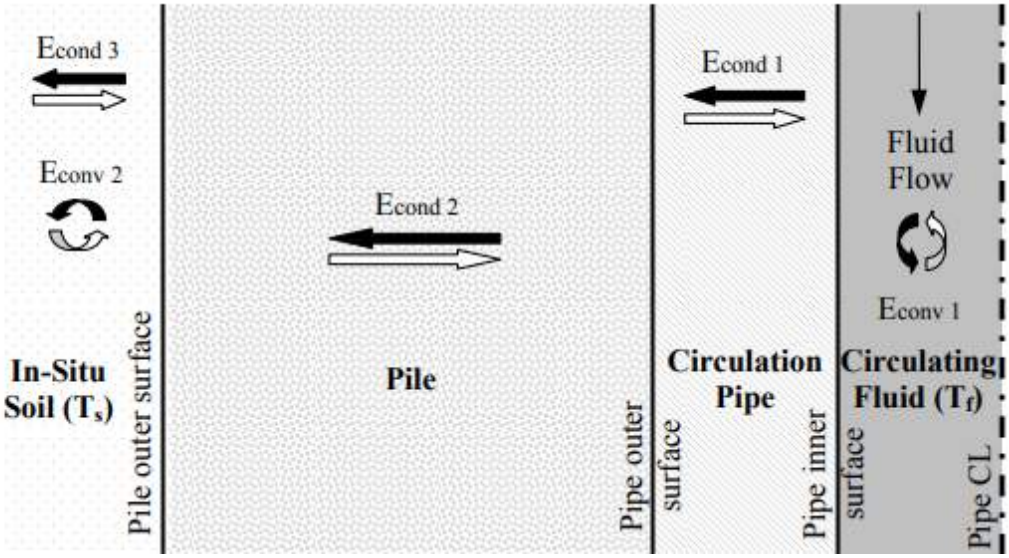

Figure 2. Heat Transfer Mechanisms in Geothermal Energy Pile (Abdelaziz, et al,2011).

Table 1. Factors Affecting the Thermal Design of Geothermal Heat Exchangers and Energy Piles Classified with Respect to the Corresponding Heat Transfer Mode (Abdelaziz et al., 2011)

Heat Transfer Mode	Controlling Factor
Heat Conduction	Thermal conductivity of the materials; circulating fluid, pipe walls, pile and in-situ soil
Heat Convection	Fluid flow conditions (flow rate of circulation fluid, laminar vs. turbulent flow) Diameter of the circulation pipe Properties of the circulation fluid (dynamic viscosity, density, heat capacity etc.) Ground water flow

Studies in the literature show that some changes have occurred in the structure of the subsoil due to the heating-cooling cycles in the energy piles; as a result, it is stated that additional stresses will occur in the piles, increase or decrease in the axial load of the piles and the decreases in pile frictional resistance may occur (Laloui et al, 2006; Bourne-Webb et al, 2009). For this reason, it has been emphasized that an increase should be made by increasing the service load of the piles under the effect of heating-cooling cycles and by increasing the safety coefficient of the frictional resistance. The

safety factor used in the design of energy piles is at least twice the safety factor used for conventional piles, resulting in additional costs (Xiao et al, 2016).
In this study, a model study was carried out on energy piles, one of the best examples of renewable energy applications. The potential benefits are discussed in case of a pile foundation project in Eskişehir province subsoil conditions designed as energy piles.

A STUDY ON SAMPLE ENERGY PILE MODEL

Depending on the structure of the subsoil, geothermal resources can be encountered at very close to the surface or accessible depths. However, the temperature levels of these geothermal sources vary. It is known that the temperature change on the earth is effective up to a certain depth and then the temperature of the underground thermal welding remains constant. It is known from the past studies that this depth is between 10 and 15 meters for our country.
It is stated by the General Directorate of Meteorology that; the average temperature for Eskişehir province is 10.9° C, the lowest average temperature is 5.3°C and the average maximum temperature is 17.4°C. Additionally, in a special area known as "thermal waters location" in the province, there is a thermal resource where the baths and similar facilities are installed. The temperature of the water extracted from this region is close to 50° C.
As a sample model for this study, if the foundation system of the congress center construction planned to be built in Eskişehir province planned as energy piles, the benefits to be obtained have been investigated. For the sample structure, 757 pieces 80 cm diameter and 30-meter-long bored piles have been planned. The project also includes heating and cooling systems for the congress center. Cost analysis for the current situation is given in Table 2. As the site of construction of the sample study, an area other than the aforementioned "thermal waters location" was selected.
Table 2. Analysis of current situation

Work and Energy Items	Consumption Values
Pile Foundation Processing	7.500.0000,00 TL
Installation of Heating Systems	325.000,00 TL
Cooling Systems Installation	1.275.000,00 TL
Total Manufacturing Cost	9.100.000,00 TL
Heating and Cooling Systems Total	12-hour x 200 kW = 2400 kWh
Average Daily Energy Consumption	365-day x 2400 = 876.000 kWh
Annual Energy Consumption	0,45 TL x 876.000 = 394.200,00 TL

Cost analysis for the new situation is given in Table 3 in case of manufacturing with energy piles.

Table 3. New Situation Analysis

Work and Energy Items	Consumption Values
Energy Pile Manufacturing	16.500.0000,00 TL

Installation of Heating Systems	515.000,00 TL
Cooling Systems Installation	1.875.000,00 TL
Total Manufacturing Cost	18.890.000,00 TL
Energy Stakes for Heating & Cooling	110 kW
Energy to be Obtained	12-hour x 110 kW = 1320 kWh
Energy Stakes for Heating & Cooling	2400 - 1320 = 1080 kWh
Daily Energy	365-day x 1080 = 394.200 kWh
Energy Required	0,45 TL x 394.200 = 177.390,00 TL

Within the scope of the study, it was tried to determine the potential benefits in the case where the foundation system of the congress center to be constructed in Eskişehir province is manufactured as energy piles instead of the conventionally manufactured bored piles. For this purpose, the costs of the old type of system and the new type of system were calculated. Then, two systems were compared by determining the cost difference. Table 4 shows comparison analysis. As can be seen from the table, the annual energy cost difference between the two systems is estimated as 216,810 Turkish Liras, which corresponds to an annual saving of around 55%. However, compared to the initial installation costs of the system, the cost difference is about 2 times higher. The reason for this is the high costs of the necessary parts due to the foreign exchange of the equipment required for the installation of the new system and the fact that it is not yet widespread. The depreciation period for two systems is calculated as approximately 45 years. However, these values are taken into consideration by considering the daily energy costs. Possible increases in energy costs over the years will reduce this depreciation period.

Table 4. Comparison Analysis

Details	**Total Cost**
Total Cost of Manufacturing System	9.100.000,00 TL
New System Total Manufacturing Costs	18.890.000,00 TL
Existing System Annual Energy Consumption Cost	394.200,00 TL
New System Annual Energy Consumption Cost	177.390,00 TL
Cost Difference & Earnings	394.200,00 TL – 177.390,00 TL = 216.810 TL
Earnings Amortization Time	9.790.000 / 216.810 = 45 years

CONCLUSION

Although there are many experiences on the benefits of energy piles, the system has not become widespread yet. It is clear for our country that it can be preferred to replace the traditional bored piles to be built especially in the regions where thermal resources are available. Moreover, high rates of savings can be achieved if localization of the necessary equipment and reduction of costs can be achieved by the widespread use of the system. The analysis made in this study was carried out for an exemplary model but since it may vary depending on the characteristics of each project and region, cost

analysis is required for each project separately. Further analysis can be made with more analysis on energy piles.

REFERENCES

Özkaya, T. (2016). Enerji Kazıklarında Isıl Performansın Parametrik İncelenmesi ve Kazık Aralıklarının Isıl Performansa Etkisi. *İstanbul Teknik Üniversitesi, İnşaat Mühendisliği Anabilim Dalı Zemin Mekaniği ve Geoteknik Mühendisliği Programı*.

Akrouch, G.A., Sanchez, M., Briad, J. (2016). An experimental, analytical and numerical study on the thermal efficiency of energy piles in unsaturated soils. *Computers and Geotechnics* 71, p.207–220.

Amis,T (2010).Energy Piles and Diaphragm Walls. *Current and Future Research Into Ground Source Energy, GSHP Association Research Seminar*,London,UK.

Laloui, L. Nuth, M., Vulliet, L. (2006). Experimental and Numerical Investigations of the Behaviour of a Heat Exchanger Pile. *International Journal for Numerical and Analytical Methods in Geomechanics*, Vol. 30, 8, 763-781

Suckling,T, and Cannon, R., (2004). Energy Piles for Pallants House, Chichester, UK. *Ground Engineering*, Vol, 37, 7, 27-29.

Unterberger, W., Hofinger, H., Grünstaudl, T., Adam, D., Markiewicz, R. (2004). Utilization of Tunnels as sources of Ground Heat and Cooling-Practical Applications in Austria. *Proceedings of the ISRM International Syposium 3rd ARMS*, Ohnishi and Aoki eds, 421-426.

Pahud, D. and Hubbuch, M., (2007). Measured Thermal Performances of Energy Pile System of the Dock Midfield at Zurich Airport. *Proceedings of European Geothermal Congress*, Unterhaching, Germany, 1-7

Gao, J., Zhang, X., Liu, J., Li, K., Yang, J., (2008). Numerical and Experimental Assessment of Thermal Performance of Vertical Energy Piles: An Application. *Applied Energy*, Vol.85, 901-910.

Olgun, G.C., Sezen, A., Martin, J.R., Abdelaziz, S.L. (2010). Temel Mühendisliğinde Yenilenebilir Enerji Uygulamaları. *Zemin Mekaniği ve Temel Mühendisliği 13. Ulusal Kongresi*, 30 Eylül-1Ekim 2010, İstanbul Kültür Üniversitesi, İstanbul.

Xiao, J., Luo, Z., Martin, J.R., Gong, W., Wang, L. (2016). Probabilistic geotechnical analysis of energy piles in granular soil. *Engineering Geology*, 209, 119–127.

Ennigkeit , A., Katzenbach, R.,(2001). The Double Use of Piles as Foundation and Heat Exchanging Elements. *15th International Conference on Soil Mechanics and Geotechnical Engineering*, Istanbul, Vol.2, pp.893-896.

Katzenbach, R., Arslan, U, Rückert, A., (1998). The Principle of The Seasonal Thermal Storage. *5th Darmstadt Geotechnical Conference 19. March, Darmstadt Geotechnics No.3, Institute and Laboratory of Geotechnics*, Darmstadt,Germany, 3-15.

Katzenbach,R., Ramm, H., Waberseck, T., (2009). Recent Developments in Foundation and Geotermal Engineering. *2nd International Conference on New Developments in soil Mechanics and Geotechnical Engineering*, Near East University Nicosia, North Cyprus, 464-471.

Abdelaziz, S.L., Olgun, C.G., Martin, J.R., (2011). Design and Operational Considerations of Geotermal Energy Piles. *Geo-Frontiers, ASCE Conference,* Dallas, Texas.

Laoui, L., Nuth, M., Vulliet, L. (2006). Experimental and Numerical Investigations of the Behaviour of a Heat Exchanger Pile. *International Journal for Numerical and Analytical Methods in Geomechanics*, Vol. 30, 8, 763-781.

Bourne-Webb, P.J., Amatya, B., Soga, K., Amis, T., Davidson, C., Payne, P., (2009). Energy Pile Test at Lambeth College, London: Geotechnical and Thermodynamic Aspect of Pile Response to Heat Cycles. *Geotechnique,* Vol.59, 3, 237-248.

IMPROVING SOME GEOTECHNICAL PROPERTIES OF AN ORGANIC SOIL USING CRUSHED WASTE CONCRETE

Omar A. Adnan
Department of Civil Engineering, University of Gaziantep, 27310 Gaziantep, Turkey
omarcivileng84@gmail.com

A F. Cabalar
Department of Civil Engineering, University of Gaziantep, 27310 Gaziantep, Turkey
cabalar@gantep.edu.tr

M D Abdulnafaa
University of Mosul, College of Engineering, Mosul, Iraq
Mohammed_al_heyaly@yahoo.com

ABSTRACT: Many urban areas are now struggling with the high volume of solid wastes, especially the construction and demolition materials. In this study, the crushed waste concrete (CWC), which is considered as one of the biggest components of solid waste, was used to improve some geotechnical properties of an organic soil. The CWC at the ratios of 5%, 10%, 15%, and 20% were added to organic soil in order to conduct an intensive series of experimental tests. The laboratory tests included the consistency limits by fall cone, modified compaction, unconfined compressive strength (UCS), and swelling percentage. The results show that when the CWC percentages were increased to 50%, there were decreases of about 30% and 60% in liquid limit and plasticity index of clay, respectively. Increase of about 35% in γ_{drymax} for the organic soil was noticed when the CWC content was increased from 10% to 50%. A reduction of about 50% of w_{opt} for organic soil was shown by increasing the CWC percentage to 50%. The UCS values of the organic silt increases by around 25% by increasing the CWC percentage up to 50%. The swelling percentage increased by adding CWC up to 30%, and then decreased with the addition of CWC up to 50%.

1. INTRODUCTION AND PREVIOUS STUDIES

Organic soil is one of the most difficult soils with engineering problems. Due to the presence of organic soils in large areas and depths, geotechnical engineers are forced to deal with them and use them for construction. The low shear strength, low hydraulic conductivity, high consolidation and settlement are the most common problems faced in the organic soil, which do not make it very suitable option compared to inorganic soil. Therefore, they are classified as the hardest soil for engineering purposes (Coduto, 1999; Hwang et al., 2005). The using of organic soils or peat to construct the roadways can be hard and problematic due to the low shear strength and high compressibility (Edil, 1997). Some unexpected results from the engineering and geotechnical point of view may be observed, when conducting laboratory experiments on organic soils and peat. Den Haan (1997) showed that both the effective strength parameters and the undrained shear strength of different types of organic soils and peat increase with increasing the water content or decreasing the unit weight. The possible explanation for the apparently counter behaviour of organic soils and peat is due to the fibre

content, which generally increases with increasing of water content and decreasing of unit weight. Hashim and Islam (2008) concluded that peat and organic soil displays unique geotechnical properties in comparison with those of inorganic soils such as clay and sandy soils which are fabricated of only soil particles.

Geotechnical engineers have to deal with organic soils or peat for improving engineering properties of these types of soils. Improving organic soils or peat needs to be used in a comprehensive and in-depth study because of the increased volatility of the engineering properties of those of the soil when increasing the content of organic matter. For instance, organic soils are known to be more difficult to stabilize by chemical additive than inorganic soils (Hampton and Edil, 1998; Janz, and Johansson, 2002). Despite those evidences, some investigators use the liquid chemical to stabilize organic soil and the results shows suitable improvement regarding of strength of organic soil (Ali, 2012). The stabilization of organic soils or peat by cement or fly ash is considered as the most famous methods of stabilizing organic soils or peat (Huat and Mohamed, 2005; Kalantari and Huat, 2008, 2009, 2010, 2011; Kazemian et al., 2011; Tastan et al., 2011; Sing et al., 2011; Kolay et al., 2011a)

The use of waste materials to improve or stabilize organic and/or peat soils has two advantages; (i) the environmental and economic benefit of materials disposal with negative environmental impact, and (ii) the engineering benefit of stabilizing or improving soil properties with geotechnical problems. A limited number of papers in the literature was found on the use of waste materials in order to improve the properties of organic soils or peat. Kolay et al., (2011b) used pond ash (PA), obtained from a coal fired thermal power station, to stabilize tropical peat soil collected from Sarawak, Malaysia. The researchers explored the effect of different amount (i.e., 5, 10, 15 and 20%) of PA on the compaction and unconfined compressive strength (UCS) properties of peat soil. The results showed that with the increase in PA content, the maximum dry density (MDD) of peat soil increases, while the optimum moisture content (OMC) decreases. The UCS values of the peat soils increases significantly with the increase of PA content and with curing periods. This results on compressive strength of tropical peat soils indicates that the PA has a potential to be used as a stabilizer for tropical peat soil. Besides, the use of PA in soil stabilization helps in reducing the pond volume and achieving environment friendly as well as a sustainable development of natural resources.

In the presented study, the crushed waste concrete was used at the ratios of 10%, 20%, 30%, 40%, and 50% in order to improve the geotechnical properties of organic silt. No attempt has been made to investigate the use of crushed waste concrete to stabilize the organic soils and/or peat, although numerous investigations have been conducted the effects of using cement and fly ash to improve organic soils.

2. MATERIALS AND METHODS

2.1 Materials of Study

2.1.1 Organic Soil

An experimental procedure was employed to test the soil sampled from Sakarya region, Turkey. Visual inspection on the soil indicated that the soil was dark brown to black in colour. The SEM (at scale 1″=500 µm) of organic soil used in the study is shown

in Figure 1. Table 1 gives the chemical composition of organic soil. The index, chemical, and geotechnical properties of organic soil are shown in Table 2.

2.1.2 Crushed Waste Concrete (CWC)

Crushed waste concrete was obtained from the paving slabs used in the Gaziantep city. The CWC with a size of less than 4.75 mm were artificially sieved to provide uniform specimens for the conducted tests program. The CWC was bringing from the municipal of Gaziantep City-Turkey. The SEM (at scale 1″=500 µm) of CWC used in the study is shown in Figure 1. Table 1 gives the chemical composition of CWC used in the study as additive.

2.2 Experimental Methods

All the organic soil used in the laboratory tests was dried in a conventional oven and then mixed with dry CWC. The selected contents of the CWC were 10%, 20%, 30%, 40% and 50% by dry weight of the sample. The mixtures of organic soil and CWC were prepared at room conditions. In order to examine the effect of CWC on the index, geotechnical, and chemical properties of peat soil, an experimental tests program have been conducted. The index tests include water content, particle size analysis, consistency limits, and specific gravity. The fall cone test, used to determine the liquid limits of organic soil and organic soil-CWC mixtures was used to estimate the undrained shear strength of organic soil and organic soil-CWC mixtures. Hansbo (1957) gave the following equation (1) that can used to determine the undrained shear strength s_u for organic soil and organic soil-CWC mixtures:

$$s_u = k\frac{mg}{d^2} \quad (1)$$

Where, m is the cone mass (g), d depth of cone penetration in the sample (cm), and k is a constant, which changes based on the angle of the cone and is found to be 0.85 for the 30° British cone (Wood,1985). The chemical tests contain the organic content, fiber content, ash content, and soil acidity. Undrained shear strength was found from the full cone test. Shear strength is found out by unconfined compressive strength according to ASTM D2166, based on the maximum dry density and optimum moisture content of organic soil and organic soil-CWC mixtures. Table 1 give the standards of tests adopted in this study. To obtain an accurate description of the soil used in the study, they were classified by three different systems, two of which specialize in the classification of organic soils.

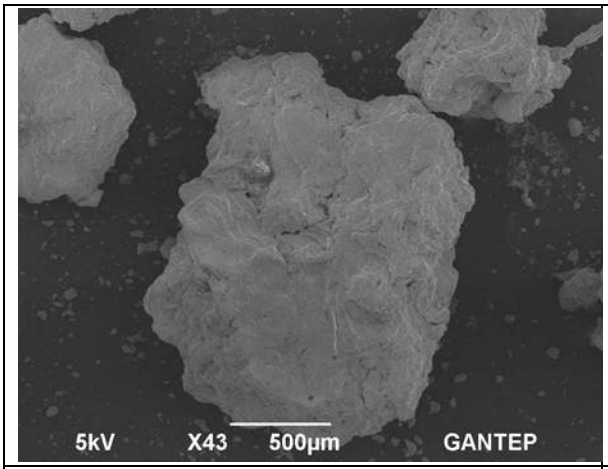

Figure1. SEM Picture of Organic Soil

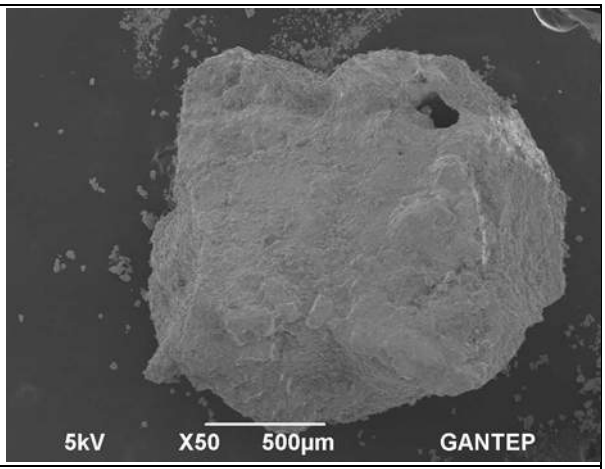

Figure2. SEM Picture of CWC

Table1. Chemical Composition of Organic Soil and CWC Using the Energy Dispersive X-Ray (EDX) Analysis

		Organic soil	CWC
Element	Unit	Concentration	Concentration
C	wt.%	14.057	12.934
O	wt.%	51.548	54.166
Na	wt.%	0.295	0.165
Mg	wt.%	1.144	0.468
Al	wt.%	9.068	1.402
Si	wt.%	19.127	2.420
S	wt.%	0.394	---
K	wt.%	1.127	0.227
Ca	wt.%	0.411	27.453
Ti	wt.%	0.287	---
Mn	wt.%	0.032	0.060
Fe	wt.%	2.511	0.707
		Total= 100.000	Total=100.000

Table2. Engineering Properties and Standard of Tests of Organic Soil Used in The

Properties	Standards	Values
Moisture content (%)	BS1377, Test 1(A)	
Specific gravity	ASTM D854	2.24
Liquid Limit (%)	BS 1337	68
Plastic limit (%)	ASTM D4318	45
Plasticity index (%)		23
Sand (%)	ASTM D422	25
Silt (%)	ASTM D422	67
Clay (%)	ASTM D422	8
Fibre content (%)	ASTM D1997	22.31
Ash content (%)	ASTM D2974	77
Acidity pH (%)	ASTM D2976	6.7
Organic content (%)	ASTM D2974	

ASTM classification	ASTM D5715	Sapric, High Ash, slightly
Unified soil classification		Organic silt soil with high
Von Post classification		H3
Maximum dry density ,γ_{dmax}	ASTM D1557-12	11
Optimum moisture content,	ASTM D1557-12	30

3. RESULTS AND DISCUSSION

3.1 Consistency Limits Tests, Classification, and undrained shear strength Results

Table 3 displays the consistency limits values (Atterberg limits) for organic soil and organic soil-CWC mixtures. Figure 3 illustrates the relation between the percentages of CWC addition and consistency limits. The data in Figure 3 and Table 3 show that there is decrease in liquid limits with increasing of CWC addition. The values of the plasticity limit slightly decreased with the increasing of CWC. The result of the change in the liquidity limit and plasticity limit values led to a significant decrease in the values of the organic soil plasticity index. One suitable explanation for the decreasing of plasticity limits, when adding CWC to organic soil is the physical compensation of a ratio of organic soil (by weight) with plasticity properties with non-plastic materials of a similar nature to sand or gravel. Table 3 also shows the classification of organic soil and organic soil-CWC mixtures, according to the unified soil classification system (USCS). Because of the gradual reduction in liquid limits and plasticity index of organic soil-CWC mixtures, the geotechnical classification of organic soil as OH (organic silt soil with high plasticity), changes at 50% CWC addition to the OL (organic silt soil with low plasticity).
The relationship between undrained shear strength su and water content for organic soil and organic soil-CWC mixtures, for comparison was given by Figure 4. The results showed that the undrained shear strength of the natural clay give the highest value at any specified water content. The organic soil-CWC mixtures are primarily controlled by the water content of mixture, used to calculate the liquid limit by full cone test. The additions of CWC, which are non-plastic materials of a similar nature to non-cohesive materials such as sand, reduce the su of natural clay with an increase in the proportion of CWC material.

3.2 Unconfined Compression Strength Test Results (UCS)

The density and water content of each UCS sample were calculated and showed in Table 3 and Figure 5. The optimum water content and maximum dry unit weight values of the specimens conducted for UCS are decreased with increases in CWC content as shown in Figures 6 and 7. The dry unit weight and Gs values of the CWC only were higher than those of the organic soils only. Therefore, the dry unit weight of the mixture increased. Figure 8 gives the variation of UCS as a function of water content for organic soil and organic soil-CWC mixtures. The peak compressive strength values of the specimens continuously increased as the amount of CWC increased as shown in Figure 9. As it has been noted, the UCS values of organic soil and organic soil-CWC mixtures were enhanced with similar increasing trends, comparing with UCS values of organic soil only.

3.3 Free Swelling Test Results

Table 3 and Figure 10 show that the swelling percentages increased when the CWC content increased in the oedometer test up to 30% CWC. This increase was due to the increase to the maximum dry density. After that, although the density continues to increase with the increase in the proportion of CWC, the swelling percentages begins to decrease because of the addition of heavy, non-plastic material, which obstructs the swelling process.

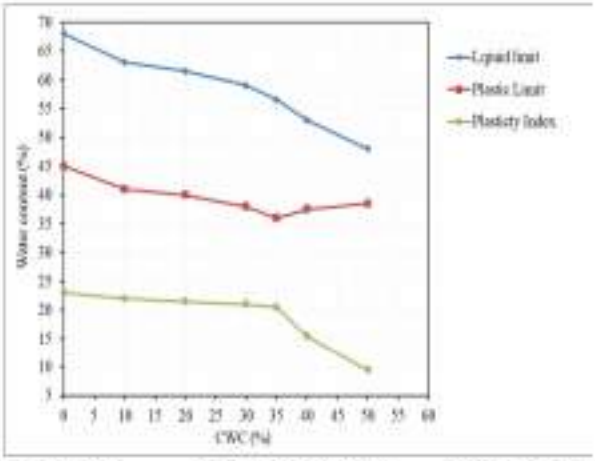

Figure3. Relationships Between Consistency Limits and CWC Content

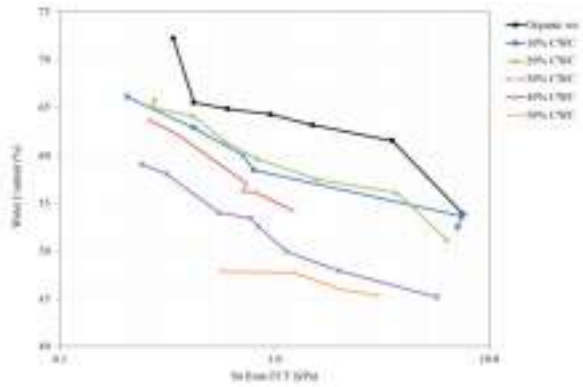

Figure4. Variation of Undrained Shear Strength as A Function of Water

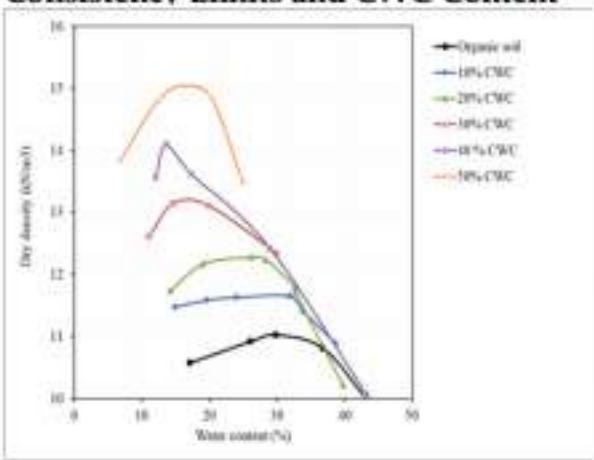

Figure5. Variation of Dry Unit Weight as A Function of Water Content for the

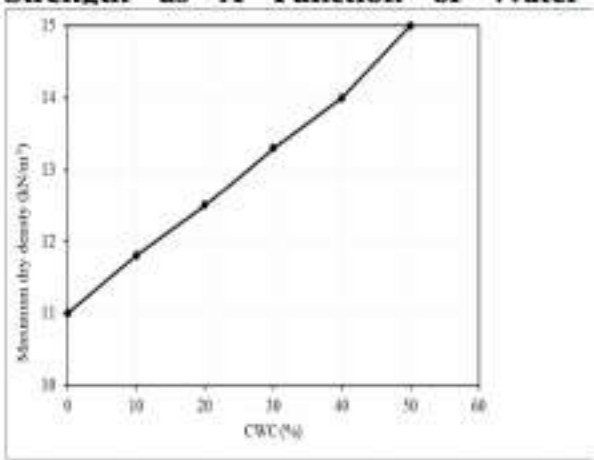

Figure6. Variation of the γ_{drymax} with the CWC Content

Table3. Summary of Study Results

Geotechnical properties	CWC%					
	Organic soil	10	20	30	40	50
Liquid limit (%)	68	63	61.5	59	53	48
Plastic limit (%)	45	41	40	38	37.5	38.5
Plasticity index (%)	23	22	21.5	21	15.5	9.5
Classification USCS	OH	OH	OH	OH	OH	OL
Maximum dry unit weight [a](kN/m³)	11.0	11.8	12.5	13.3	14	15
Optimum moisture content [b] (%)	30	28	22	17	16.5	16
Unconfined compression strength (kN/m³)	481	490	515	549	597	615
Optimum water content [c] (%)	25	23	22	16	15.5	13.8
Free swelling percentages	3.35	5.2	12.85	13.2	11.05	8.45

a: density calculated by specimens of UCS before testing, b: water content by specimens of UCS before testing,

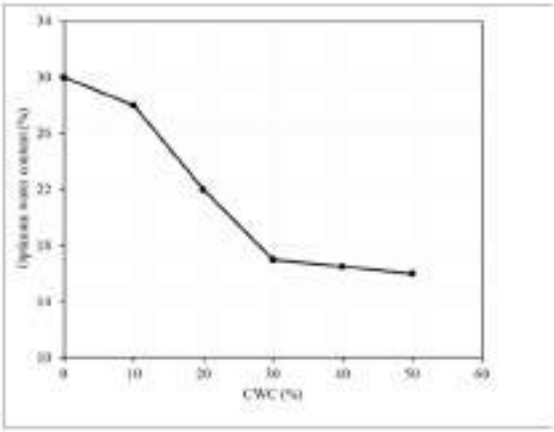

Figure7. Variation of the w_{opt} of compaction test with the CWC content

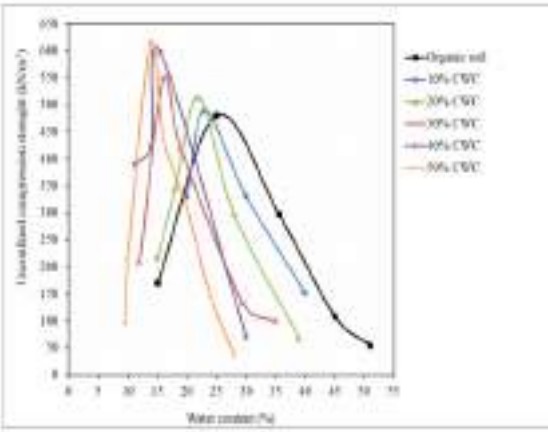

Figure8. Variation of UCS as a function of water content for the organic soil with

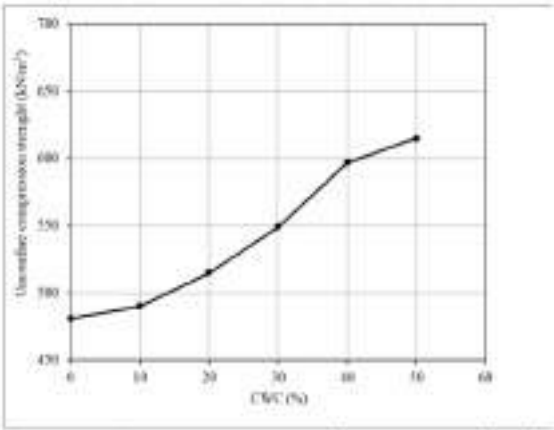

Figure9. Variations of unconfined compressive strength with the CWC

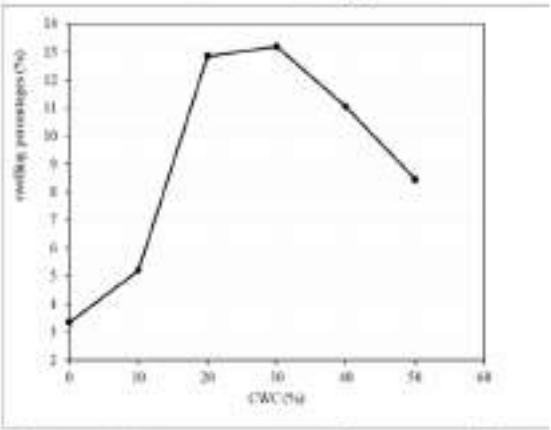

Figure10. Variations of swelling percentages with the CWC contents

4. CONCLUSIONS

This study aims to investigate the possibility to improve the geotechnical properties of organic soil using crushed waste concrete, some notable points can be concluded from the study results. The liquid limits and plasticity index of organic soil decrease as the CWC percentages increase. These decreases are reflected in the soil classification and strength. The increasing of the CWC content increased the maximum dry density of organic soil and causes increased swelling percentages to certain limit, then start to decrease. The strength of organic soil, as represented by UCS values, increased with increasing CWC percentages.

REFERENCES

Ali, F. (2012). Stabilization of residual soils using liquid chemical. Electronic Journal of Geotechnical Engineering, 17(BUNDLE B), 115-126.

ASTM, D. (1991). 2166. Standard test method for unconfined compressive strength of cohesive soil.

ASTM, D. (2003). Standard test methods for liquid limit, plastic limit, and plasticity index of soils. Annual Book of ASTM Standards, PA, 4(8), 482-593.

ASTM D 2974. (2007). Standard Test Methods for Moisture, Ash, and Organic Matter of Peat and Organic Soils.

ASTM D2976. (2013). Standard Test Method for pH of Peat Materials, ASTM International.

ASTM D1557. (2012). Standard Test Methods for Laboratory Compaction Characteristics of Soil Using Modified Effort (56,000 ft-lbf/ft3 (2,700 kN-m/m3)).

ASTM. D5715 (2014). Standard Test Method for Estimating the Degree of Humification of Peat and Other Organic Soils (Visual/Manual Method).

Coduto, D. P. (1999). Geotechnical engineering: principles and practices (M. Horton, Ed.).

Den Haan, E. J. (1997, March). An overview of the mechanical behavior of peats and organic soils and some appropriate construction techniques. In Proc. of the Conf. on Recent Advances in Soft Soil Engineering (Vol. 1, pp. 17-45).

Edil, T. B. (1997, March). Construction over peats and organic soils. In Conference on Recent Advances in Soft Soil Engineering (pp. 5-7).

Hampton, M. B., & Edil, T. B. (1998). Strength gain of organic ground with cement-type binders. In Soil improvement for big digs (pp. 135-148). ASCE.

Hansbo, S. (1957). A new approach to the determination of the shear strength of clay by the fall-cone test. Royal Swedish Geotechnical Institute.

Hashim, R., & Islam, M. S. (2008). Properties of stabilized peat by soil-cement column method. Electronic Journal of Geotechnical Engineering, 13, 1-9.

Huat, B. B., Maail, S., & Mohamed, T. A. (2005). Effect of chemical admixtures on the engineering properties of tropical peat soils. American Journal of Applied Sciences, 2(7), 1113-1120.

Hwang, J., Humphrey, A., Bobet, A., & Santagata, M. (2005). Stabilization and Improvement of Organic Soils. Final report. FHWA/IN/JTRP-2004/38, Purdue University.

Janz, M., & Johansson, S. E. (2002). The function of different binding agents in deep stabilization, 9th Report of Swedish Deep Stabilization Research Centre. Linkoping, Sweden.

Kalantari, B., & Huat, B. B. (2008). Peat soil stabilization, using ordinary Portland cement, polypropylene fibers, and air curing technique. Elect. J. Geotech. Eng., Bund. J, 1-13.

Kalantari, B., & Huat, B. K. (2009). Load-Bearing Capacity Improvement for Peat Soil. European journal of scientific research, 32(2), 252-259.

Kalantari, B., Huat, B. B., & Prasad, A. (2010). Effect of polypropylene fibers on the California Bearing Ratio of air cured stabilized tropical peat soil. Am. J. Engg. & Applied Sci, 3(1), 1-6.

Kazemian, S., Huat, B. B., Prasad, A., & Barghchi, M. (2011). Effect of peat media on stabilization of peat by traditional binders. International Journal of Physical Sciences, 6(3), 476-481.

Tastan, E. O., Edil, T. B., Benson, C. H., & Aydilek, A. H. (2011). Stabilization of organic soils with fly ash. Journal of geotechnical and Geoenvironmental Engineering, 137(9), 819-833.

Sing, W. L., Hashim, R., & Ali, F. (2011). Unconfined compressive strength characteristics of stabilized peat. Scientific Research and Essays, 6(9), 1915-1921.

Standard, B. (2004). 1377 (1990) Methods of test for soils for civil engineering purposes. British Standards Institution, London.

Standard, A. S. T. M. D854. 2014. Standard test methods for specific gravity of soil solids by water pycnometer. ASTM International, West Conshohocken, Pa.

Standard, A. S. T. M. (2007). Test method for particle-size analysis of soils. ASTM international, West Conshohocken, PA, DOI: 10.1520/D4513, 11.

Kolay, P. K., Aminur, M. R., Taib, S. N. L., & Zain, M. M. (2011a). Stabilization of tropical peat soil from Sarawak with different stabilizing agents. Geotechnical and geological engineering, 29(6), 1135.

Kolay, P. K., Sii, H. Y., & Taib, S. N. L. (2011b). Tropical peat soil stabilization using class F pond ash from coal fired power plant. International Journal of Civil and Environmental Engineering, 3(2), 79-83.

Wood, D. M. (1985). Some fall cone tests. Geotechnique, 35(1).

DESIGN AND PERFORMANCE COMPARISON OF FOUR-POLE BRUSHLESS DC MOTORS WITH DIFFERENT POLE/SLOT COMBINATIONS

Cemil OCAK
Gazi University
cemilocak@gazi.edu.tr

ABSTRACT: When the design process of the brushless motor is examined, attention must be paid to the correct choice of magnet material, internal or external rotor structure and the choice of core and winding structure. In addition to all these, the number of phases, the number of rotor poles, and the choice of slots configurations depending on them also have great importance. For this reason, to achieve optimum design, it is necessary to analyze all possible designs with different pole/slot configurations that can accommodate similar power and speed expectations. In this study, three different designs have been realized with different pole/slot configurations for four-pole, internal rotor brushless DC motors, which are frequently used in many different applications today. Designed motors have been analyzed with Finite Element Method to obtain the cogging torque, efficiency and active material costs. All motors that are analyzed have 100 W, 3000 rpm, 4/6, 4/12 and 4/15 pole/slot configurations respectively.

Key words: brushless DC motor, pole/slot combinations, efficiency, internal rotor

NOMENCLATURE

$v_{a,b,c}$	: Voltages of phases a, b, and c
$i_{a,b,c}$	: Currents of phases a, b, and c
$R_{a,b,c}$	: Winding resistances of phases a, b, and c
$e_{a,b,c}$	: Induced back-electromotive force
L_{aa}, L_{bb}, L_{cc}	: Total inductance of phase windings
L_{ab}, L_{bc}, L_{ca}	: Mutual inductances between phase windings
$\vec{H}$	: Magnetic field intensity
$\vec{J}$	: Current density
$\vec{E}$	: Electric field intensity
$\vec{B}$	: Magnetic flux density
$\vec{A}$	: Magnetic vector potential

INTRODUCTION

Although the moment-speed characteristic is linear in DC motors, the most important disadvantage of this type of motors is the realization of excitation by using brush and collector assembly. Due to the mechanical commutation, the motor requires frequent maintenance. Brushless DC motors (BLDC) have the moment-speed characteristic of brushed DC motors and eliminates the disadvantage of brush and collector mechanism by using electronic commutation (Hanselman, 2006; Saygın et al., 2015).

Recent developments in material science have allowed the production of magnets with high energy density. With the use of magnets which have high BH_{max} products, it was possible to obtain more power in a smaller volume. In addition, there has been a reduction in the cost of the switching elements due to the development of semiconductor technology. BLDCs have become more attractive with the increasing simplicity and reliability of electronic components, falling costs, and developments in material technology (Bayındır et al., 2011). BLDCs are almost maintenance-free and long-life electrical machines with a low moment of inertia. The absence of rotor windings in this type of motors lead to the absence of rotor copper losses and therefore to high efficiency. The BLDCs have a higher torque density than an asynchronous motor or brush motor for the same size. (Ehsani et al., 2003).
In the literature, effect of different pole slot combinations in the linear motor (Yuan & Niu, 2018), in the brushless doubly-fed generator (Zhang et al., 2019), in the interior permanent magnet synchronous motor (Carraro et al., 2018; Jun et al., 2017), in the surface-mounted permanent magnet machine (Zhu et al., 2014), and in the axial flux BLDC motor (Jafarishiadeh et al., 2016) have been discussed. Also, cogging torque parameter has been examined for different pole/slot combinations (4/6, 8/12 and 10/12) of permanent magnet synchronous motor. A proper cogging torque value can be obtained without any additional manufacturing process (Lee et al., 2014).

The relationship between the number of poles and slots in BLDC motors is quite popular. Even though it is thought that the today's mass-production motors have the pole/slot configurations which present the best performance, in fact, various computer-aided analyzes show that this is not always the case. For example, most 4-pole BLDC motors are produced as 12 stator slots. However, this type of design results in a very high cogging torque and large end turn lengths and thus high copper losses. In addition, the cost of winding and labour increases. For a lower cogging torque and a cost target, 4 pole/6 slot configuration can be preferred. If a motor with low cogging torque and a sinusoidal back emf is desired, 4 pole/15 slot configuration will be the best choice compared to the other alternatives mentioned above. In this study, as mentioned above, three BLDC motors rated 100W, and 3000 rpm have been designed with 4/6, 4/12 and 4/15 pole/slot configurations. Finite element method (FEM) has been used to analyze the proposed designs. As a result of performed analyzes, cogging torques, phase and line voltage waveform of motors have been obtained and compared according to the different pole/slot numbers given in the study. Thus, the effects of different pole/slot configurations have been obtained by computer-aided simulations for these motors which are widely used.

MATHEMATICAL MODEL OF BRUSHLESS DC MOTORS

The instantaneous power produced by the BLDC motor is equal to the back electromotive force multiplied by phase current. This is the power that is transferred from stator to rotor. When the friction losses are extracted from the transmitted power, the net power from the motor shaft can be determined. Since the friction losses of the BLDC motor are very small, the power value can be written as in Equation 1.

$$P_e = i_a e_a + i_b e_b + i_c e_c \tag{1}$$

Considering the 120° phase difference between the phases, the expression of the back electromotive force given in Equation 1 can be written as Equation 2.

$$\begin{aligned} e_a &= \omega\lambda(\theta) \\ e_b &= \omega\lambda\left(\theta - \frac{2\pi}{3}\right) \\ e_c &= \omega\lambda\left(\theta + \frac{2\pi}{3}\right) \end{aligned} \tag{2}$$

The resulting back electromotive force is in the form of a trapezoidal wave, which varies depending on the position. The value of the back electromotive force depends on the number of turns, magnetic field strength, rotor speed, and position. The equivalent circuit of the 3-phase star-connected BLDC motor is given in Figure 1.

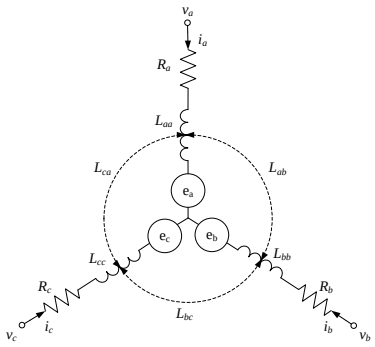

Figure 1. Three-Phase Equivalent Circuit of BLDC Motors

Voltage equation for the phase a is given in Equation 3 according to the equivalent circuit.

$$v_a = i_a R_a + L_a \frac{d\,i_a(t)}{dt} + e_a \tag{3}$$

The voltage equation for each phase of BLDC motor is expressed as Equation 4 (Çelik & Öztürk, 2017; Krishan, 2001; Aydoğdu, 2006).

$$\begin{bmatrix} v_a \\ v_b \\ v_c \end{bmatrix} = \begin{bmatrix} R_a & 0 & 0 \\ 0 & R_b & 0 \\ 0 & 0 & R_c \end{bmatrix} \begin{bmatrix} i_a \\ i_b \\ i_c \end{bmatrix} + \begin{bmatrix} L_{aa} & L_{ab} & L_{ca} \\ L_{ab} & L_{bba} & L_{bc} \\ L_{ca} & L_{bc} & L_{cc} \end{bmatrix} \frac{d}{dt} \begin{bmatrix} i_a \\ i_b \\ i_c \end{bmatrix} + \begin{bmatrix} e_a \\ e_b \\ e_c \end{bmatrix} \tag{4}$$

ELECTROMAGNETIC FINITE ELEMENT ANALYSIS

Analysis of electrical machines involves the solution of interrelated problems. Applying the finite element method (FEM) in the analysis of electrical machines enables the designer to obtain the behavior of the machine. It is possible to determine the electromagnetic parameters with a very high accuracy by applying a FEM method. In addition, applying this method gives the designer a considerable advantage over time and cost. (Hameyer & Belmans, 1999; Dalcalı et al., 2018).

The region to be solved in FEM is divided into a small number of finite regions. The desired value is assumed to be continuous over these small regions. In addition, it is assumed that the fundamental differential equation expressing the change of field is also valid on each element. In order to obtain the solution at a point in the region, the contributions of the elements surrounding the point must be taken into account. Therefore, the values of the corner points of all the elements in the region are chained together. As a result, a group of linear equation as much as the number of nodes is obtained. By solution of this equation set, the desired ones are calculated (Dalcalı & Akbaba, 2016; Dalcalı et al, 2018). The mesh structure of the proposed 12-slot motor is shown in Figure 2.

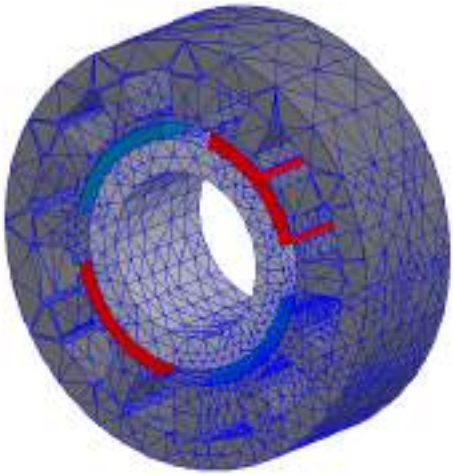

Figure 2. Mesh View of 4 Pole /12 Slot Motor

A. Analysis Model and Study of Proposed Design Combinations

In this section of the study, designs of the BLDC motor which is rated 100 W and 3000 rpm in different pole/slot combinations have been performed and their performances have been examined. Design parameters and materials of the motors are given in Table 1. When Table 1 is examined, it is seen that the materials and physical properties of the stator, rotor, and magnet are arranged to be the same for each design. The slot geometry has been arranged according to the different number of slots providing a maximum slot fill factor for each design. Thus, other parameters of the motor have not been changed to obtain a fair comparison while performing a comparative analysis.

Table 1. Design Parameters

Pole / Slot Combination		**4 pole/6 slot**	**4 pole/12 slot**	**4 pole/15 slot**
Stator	Outer diameter (mm)	90	90	90
	Inner diameter (mm)	55	55	55
	Length (mm)	30	30	30

	Core Material	M270-35A	M270-35A	M270-35A
Rotor	Outer diameter (mm)	54.2	54.2	54.2
	Inner diameter (mm)	35	35	35
	Length (mm)	30	30	30
Magnet	Core Material	ST37	ST37	ST37
	Type	N40UH	N40UH	N40UH
	Thickness (mm)	3	3	3
	Embrace	0.7	0.7	0.7
Slot	Slot clearance (mm)	5	2	2
	Width (mm)	28	13	9
	Net Slot Area ($mm^{2)}$	233.03	106.53	72.53

The view of the different pole/slot configurations of the designs has been presented in Figure 3. As can be seen from the Figure 3, rotor structures, stator inner and outer diameters and air gap distances are kept the same for the different configurations.

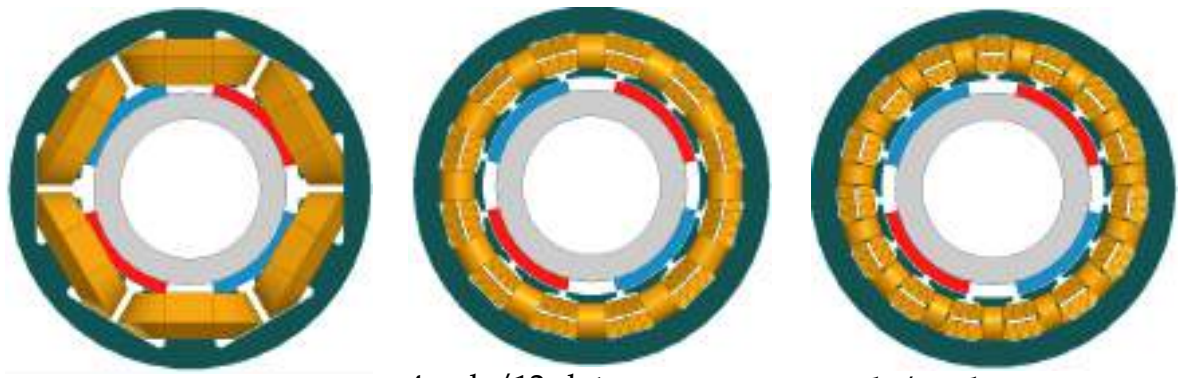

4 pole/6 slot 4 pole/12 slot 4 pole/15 slot

Figure 3. Views of Different Pole/Slot Configurations

B. Comparison of Load Performances and Flux Density Distributions

In this section, performance values and flux distributions have been examined comparatively by analyzing the motors at rated load and unloaded condition. The simulation results of full and no-load conditions are given in Table 2.

Table 2. Performance Values of Motors

Parameters		**4 pole/6 slot**	**4 pole/12 slot**	**4 pole/15 slot**
Full-load	Output power (W)	100	100	100
	Efficiency (%)	85.32	85.16	85.29
	Rated torque (Nm)	0.304	0.312	0.308
	Cogging torque (Nm)	0.107	0.204	0.05

No-load	Stator teeth flux density (T)	1.73	1.79	1.71
	Rotor yoke flux density (T)	1.65	1.71	1.74
	Stator slot fill factor (%)	51.0	51.3	51.6

When the output power values in Table 2 are examined, it is seen that all motors have been loaded to produce the same output power. The designs were aimed to provide the maximum slot fill factor and similar efficiency values to obtain balanced copper loss which is an important factor of efficiency between different designs. When the cogging torques values are compared, it is seen that the 4 pole/12 slot configuration has the highest cogging torque value. The lowest cogging torque value has been obtained in 4 pole/15 slot configuration. However, the winding and labour cost of this motor is higher than the other configurations. In the case of a cost-effective motor expectation, the 4 pole/6 slot motor can be preferred even if it has a high cogging torque compared to the 4/15 structure. When no load condition considered, it is also seen that stator and rotor flux densities are within the limit in each design and it can be modified by geometric changes. As mentioned before, the FEM is a very effective and frequently used method in the calculation of magnetic flux distributions. In electric machines, the magnetic field calculations are expressed by Maxwell's equations and the flux distribution obtained by the 3D analysis given in Figure 4 are found by the following equations. (Dalcalı & Akbaba, 2016; Ho & Fu, 1998; Dadpour & Ansari, 2013).

$$\nabla \times \vec{H} = \vec{J}$$
$$\nabla \times \vec{E} = -\frac{\partial B}{\partial t} \tag{5}$$

The magnetic vector potential can be expressed in terms of magnetic flux density in Equation 6.

$$\vec{B} = \nabla \times \vec{A} \tag{6}$$

The basic formulation of the vector potential for the magnetic field is expressed by Equation 7.

$$\nabla \times \left(v \nabla \times \vec{A} \right) = \vec{J} \tag{7}$$

$$\frac{\partial}{\partial x}\left(v \frac{\partial A}{\partial x} \right) + \frac{\partial}{\partial y}\left(v \frac{\partial A}{\partial y} \right) + \frac{\partial}{\partial z}\left(v \frac{\partial A}{\partial z} \right) = -\vec{J} \tag{8}$$

The magnetic flux density value is obtained from Equation 9.

$$B = \sqrt{B_x^2 + B_y^2 + B_z^2} \tag{9}$$

The magnetic flux distributions obtained by magneto-static analyzes are given in Figure 4. Only magnets were defined as a flux source to obtain no load condition. The upper limit of the color map for the flux density distributions is defined as 2T. Considering this definition, it can be seen that the flux densities of the cores are in line with the selected material and the limit.

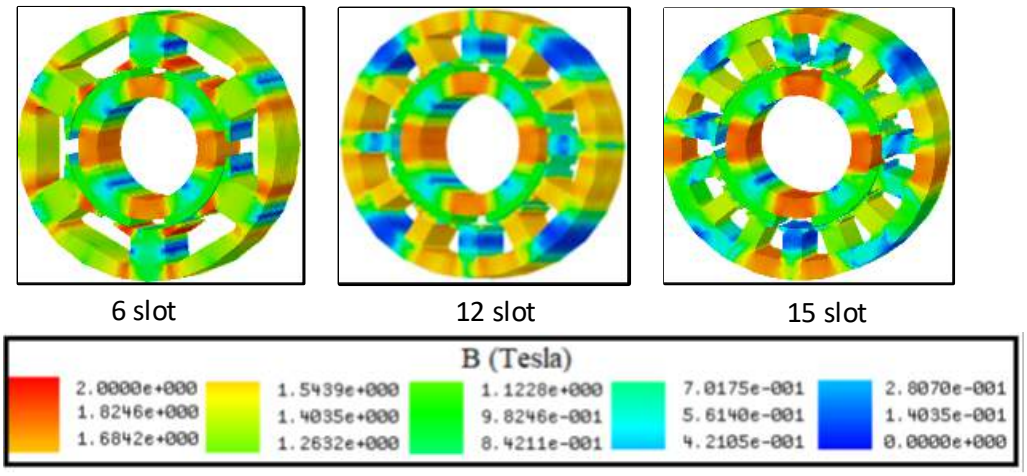

Figure 4. Magnetic Flux Density Distributions of Proposed Configurations

C. Cogging Torque

Cogging torque is the torque generated by the interaction between the stator slots and rotor magnets when no current applied on permanent magnet machines. The cogging torque is undesirable for electric machines because it causes noise and vibration by forcing rotation of the rotor.

The change of the cogging torque according to the electrical position of the rotor for each configuration is given in Figure 5. The lowest cogging torque value has been obtained in 4 pole/15 slot structure. Since the 4-pole/12-slot configuration has a very high cogging torque compared to other designs, this configuration should not be preferred. The 4-pole/6-slot configuration is acceptable for a cost-priority design.

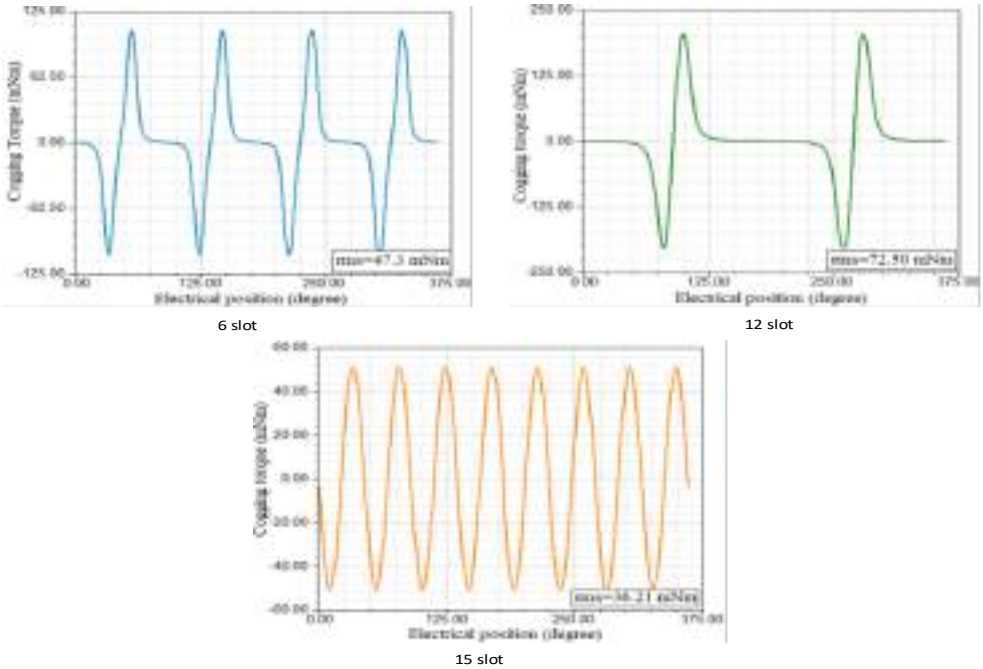

6 slot 12 slot 15 slot

Figure 5. Cogging Torque Values for the Different Pole/Slot Configurations

D. Induced Coil Voltage

The voltage equations of the BLDC motors have been previously given in Equations 3 and 4. According to the electrical position of the rotor, phase and line voltage values of phase A of the designed motor are given in Figure 6. The waveform of the induced voltage and air gap flux density are important in terms of core losses, especially for the high-speed motor designs.

The induced voltage waveforms of 4 pole/6 slot and 4 pole/12 slot configurations are far from the sinusoidal form. Furthermore, due to their high harmonic content, these designs should not be the first priority in applications with high-efficiency targets. In such a case, the 4-pole/15-slot configuration provides the best waveform with an almost sinusoidal waveform. This configuration offers superior performance values than the other two configurations when winding and labour cost are neglected.

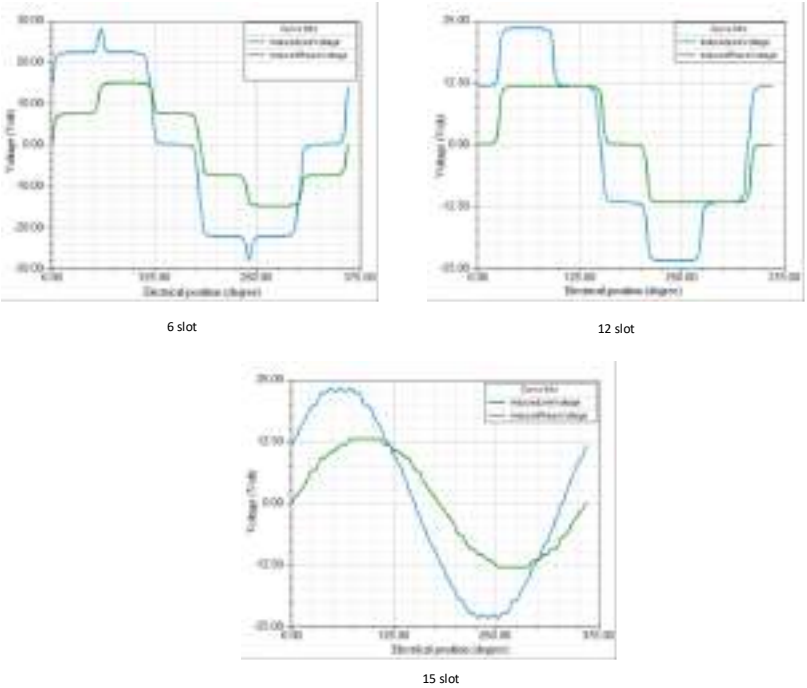

Figure 6. Line and Phase Voltage Waveforms for Different Pole/Slot Combinations

CONCLUSION

In the study, the designed motors are rated 100 W, 3000 rpm and have four-pole internal rotor structure. These machines have high torque density, robust structure, low loss, and low manufacture cost. In the design phase, pole/slot number has a dominant effect on machine performance. Three brushless DC motors have been compared in this study for revealing the effect of the pole/slot configurations on the characteristics.

Designed motors have been analyzed with FEM Method. Each motor has 4 pole and 6, 12 and 15 stator slots respectively. The lowest cogging torque value has been obtained in 4 pole/15 slot configuration compared to other designs. Therefore, the minimum torque fluctuation has been obtained in 4 pole/15 slot configuration. 4 pole/12 slot configuration has the worst performance values in terms of both cogging torque and induced voltage waveforms. The 4-pole / 6-slot configuration has a relatively low cogging torque and total cost. Therefore, these motors are often preferred in many applications such as an electric screwdriver and similar power tools.

On the other hand, where more specific working conditions such as the defense industry and where efficiency is more important, despite a small increase in cost, a 4-pole/15-slot configuration is preferable because of its low cogging torque and sinusoidal waveform.

REFERENCES

Aydoğdu, Ö. (2006). *Fırçasız doğru akım motorlarının genetik tabanlı bulanık denetleyici ile sensörsüz kontrolü*. Doktora Tezi, Selçuk Üniversitesi Fen Bilimleri Enstitüsü, Konya.

Bayındır, R., Ocak, C., & Topaloğlu, İ. (2011) Investigation of the effect of magnet thickness on output power and torque of PM BLDC machines using parametric approach method. *Proceedings of the 2011 International Conference on Power Engineering, Energy and Electrical Drives*, Spain.

Carraro, E., Zhang, S., & Koch, M. (2018). Design and performance comparison of fractional slot concentrated winding spoke type synchronous motors with different slot-pole combinations. *IEEE Transactions on Industry Applications, 54*(3), 2276-2284. doi: 10.1109/TIA.2018.2807382

Çelik, E., & Öztürk, N. (2017). A new fuzzy logic estimator for reduction of commutation current pulsation in brushless DC motor drives with three-phase excitation. *Neural Comput & Application,* 1-10. doi: 10.1007/s00521-017-3083-8

Dadpour, A., & Ansari, K. (2013). Conversion of shaded-pole induction motor to switched reluctance motor and effects of pole shoe and notch on SRM noise", *IEEE XXXIII International Scientific Conference Electronics and Nanotechnology*, Kiev.

Dalcalı, A., & Akbaba, M. (2016). Comparison of 2D and 3D magnetic field analysis of single-phase shaded pole induction motors. *Engineering Science and Technology, An International Journal, 19*(1), 1–7. doi: 10.1016/j.jestch.2015.04.013

Dalcalı, A., Kurt, E., Çelik, E., & Öztürk., N. (2018). Cogging torque reduction by using the skewing and separated magnet techniques. *6th Eur. Conf. Ren. Energy Sys., 24*(6), Istanbul, Turkey.

Ehsani, M., Gao, Y., & Gay, S. (2003). Characterization of electric motor drives for traction applications. *The 29th Annual Conference of the IEEE Industrial Electronics Society,* Montreal.

Hameyer, K., & Belmans, R. (1999). *Numerical modelling and design of electrical machines and devices*. Southampton, Boston: WIT Press.

Hanselman, D. (2006). *Brushless permanent magnet motor design (2nd Ed.)*. Ohio: Magna Physıcs Publishing.

Ho, S. L., & Fu, W. N. (1998). Review and future application of finite element methodes in induction motors. *Electric Machines & Power Systems, 26* (2), 111–125. doi: 10.1080/07313569808955811

Jafarishiadeh, S., Ardebili, M., & Marashi, A.N. (2016). Investigation of pole and slot numbers in axial-flux pm BLDC motors with single-layer windings for electric vehicles. *24th Iranian Conference on Electrical Engineering (ICEE)*, Shiraz, Iran.

Jun, H.W., Seol, H.S., & Lee, J. (2017). Effect of pole–slot combination on eddy-current formation in pmsm rotor assembly ıncluding retaining plate structure. *IEEE Transactions on Magnetics, 53*(11). doi: 10.1109/TMAG.2017.2707559

Krishan, R. (2001). *Electric motor drives: modeling, analysis and control*. New Jersey: Prentice Hall, Inc.

Lee, S.J., Kim, S.I., & Hong, J.P. (2014). Characteristics of PM synchronous motors according to pole-slot combinations for eps applications. *International Journal of Automotive Technology, 15*(7), 1183−1187. doi: 10.1007/s12239-014-0123-6

Saygın, A., Ocak, C., Dalcalı, A., & Çelik, E. (2015). Optimum rotor design of small PM BLDC motor based on high efficiency criteria. *ARPN Journal of Engineering and Applied Sciences*, *10*(19), 9127-9132.

Yuan, M., & Niu, S. (2018). Design and analysis of a novel modular linear double-stator biased flux machine. *IEEE Transactions on Magnetics, Early Access*, 1-5. doi: 10.1109/TMAG.2018.2842098

Zhang, F., Yu, S., Wang, Y., Jin, S., & Jovanovic, M.G. (2019) Design and performance comparisons of brushless doubly fed generators with different rotor structures. *IEEE Transactions on Industrial Electronics, 66*(1), 631-640. doi: 0.1109/TIE.2018.2811379

Zhu, Z.Q., Wu, J., & Modh Jamil, M.L. (2014). Influence of pole and slot number combinations on cogging torque in permanent-magnet machines with static and rotating eccentricities. *IEEE Transactions on Industry Applications, 50*(5), 3265-3277. doi: 10.1109/ECCE.2013.6647069.

NEURAL NETWORK ESTIMATION OF MUTUAL INDUCTANCE VARIATION FOR A SHADED-POLE INDUCTION MOTOR

Emre ÇELİK
Düzce University
emrecelik@duzce.edu.tr

ABSTRACT: Shaded-pole induction motors (SPIMs) are often preferred in small power applications owing to their ability to work with single-phase power source, simple structure and low-cost properties. Such motors are within the class easy to manufacture, but the most difficult to analyze mathematically due to the fact that they have a variable air gap and elliptical rotating magnetic field, which leads to highly complex inductance calculations. Considering that the identification accuracy of phase variables is directly related to the correct knowledge of inductances in AC machines, the authors of this article attempt to realize a neural network (NN)-based inductance estimation in-between the stator and rotor, and also in-between the shading ring (shaded-pole winding) and rotor loop for an industrial SPIM. For this aim, corresponding inductance measurements are made first experimentally in terms of each 3.6^{o} electrical position, and as such, a total of 101 data samples have been collected. %70 of them are considered as training data to train the NN while the remainder is adopted for testing the generation capability of NN. Results in comparison with the actual values have affirmed the excellence performance of the introduced NN in simultaneous estimation of the concerned two important inductances.

Key words: Shaded-pole induction motors, shaded-pole, rotor loop, neural network, inductance estimation

INTRODUCTION

Shaded-pole induction motors (SPIMs) have a salient pole stator and a squirrel cage rotor. Although SPIMs have a simple structure in terms of manufacturing, the analysis of these machines is known to be quite hard owing to the elliptically rotating magnetic field generated in the machine air gap. There is no universally accepted technique for modelling this type of motor and implementing the motor performance analysis (Dalcalı, 2017; Dalcalı & Akbaba, 2017a). The mutual inductances of SPIMs between stator and rotor loop, and also between shading ring and rotor loop are significant and exhibit a nonlinear variation depending upon the rotor angular position and motor phase current.

Artificial neural networks (ANNs) or neural networks (NNs) in short, are computing systems dedicated to mimic the essential behavior of biological neural system, which have seen much attention due to their capabilities in solving nonlinear problems by learning ability. They have some other unique properties such as excellent generalizing and learning capability from experience and examples, adaptation to changing situations, massive parallelism, and identification without exact knowledge. Via many nonlinear computational elements operating in parallel and connected to

each other in between layers with intensive interconnections, NNs are able to accomplish the task of approximating the nonlinear behavior between input and output data of a nonlinear model without prior knowledge about those data. They are very efficient and useful when the equations representing the respective model are nonlinear, complex, distributed in nature, and particularly vague or totally unknown with uncertain parameters (Çelik et al., 2017). As an alternative to neural network-based modelling, there are also studies adopting fuzzy logic for prediction of output parameters of a process according to its input parameters (Wang et al., 2003; Shabgard et al., 2012; Simoes & Bose, 1993; Yılmaz et al., 2006; Rodic et al., 2014). However, there are many parameters to be considered during the design of fuzzy logic system such as scaling factors, fuzzy-expert rules, membership functions etc. Determination of these parameters is still an ill-defined problem and based upon the experiences and knowledge of a skilled operator who gives several manual iterations over the considered system. Therefore, development of fuzzy-based prediction algorithm is tedious and time-consuming.

NNs have proved their remarkable contribution in a variety of applications, such as cover pattern recognition, control, diagnostic problems, fault detection, power electronics, forecasting, function approximation. Since the topic of this paper is related to the estimation property of neural network, giving some introductory literature survey about this topic would be to the point. So far NN approach has been successfully employed in various estimation problems, such as estimating the output power and efficiency of a new-designed axial flux permanent magnet synchronous generator based on its rotational speed and the load connected to its terminals (Çelik et al., 2017), online estimation for the rotor and stator resistances of an induction motor (Karanayil et al., 2007), predicting burr height produced in a sheet metal blanking process according to tool wear state and punch-die clearance (Hambli, 2002, estimation of the distorted waveforms in power electronics (Kim et al., 1995), wind power generation estimation as a diagnostics tool (Li et al., 2001), position estimation task in a speed sensorless switched reluctance motor drive system (Paulson & Prabhu, 2015), finding the optimal tilt angle of PV panels in order to maximize the solar power from the sun (Chatterjee & Keyhani, 2012), prediction of the nonlinear behavior of a newly designed wind energy harvester (Çelik et al., 2018a), and estimation of the clearance effect on blanking force, smooth sheared/fractured rate and burr height in the blanking process of CuZn30 sheet metal (Çelik et al., 2018b). Nonetheless, the utilization of NN strategy to resolve the estimation concern of varying inductance parameters of a shaded-pole induction motor (CPIM) is currently open in the literature. That being said, this research paper may be considered as the first contribution of NN to estimate the challenging inductance values of a CPIM, which exhibit a nonlinear behavior in nature depending upon the angular position.

In the present paper, a total of 101 data samples including mutual inductance between stator and rotor (M_{ar}) and between shading ring and one rotor loop (M_{br}) have been collected from the experimental test bench with respect to the angular rotor position (θ) in steps of 3.6°. 70 samples of the observed data is used as the training data to train the developed network while the remaining samples are reserved for testing the generalization ability of previously trained network. For training, a well-known back propagation (BP) learning algorithm is employed. At the end of the study, outputs of

the network, which are the predicted inductance values, are compared to their actual values for the test data, and the results have demonstrated that presented NN is able to establish a promising relationship among the outputs (M_{ar} and M_{br}) and the input variable of rotor position.

SHADED POLE INDUCTION MOTOR

Single-phase asynchronous motors are widely preferred for small power applications as they operate on single-phase grid with a robust and low-cost structure, which is manufactured easily and requires less maintenance. Their size increases at high powers, which degrades the ability of these machines to compete with their three-phase counterparts owing to the increased cost (Saygın et al., 2015). They have an important advantage of being fed from a single-phase grid without need for a drive. Nonetheless, the inability to alter the direction of angular rotation, low starting torque along with low efficiency are among the main disadvantages of SPIMs with single shading ring (Parasitili et al., 2014; Gao et al., 2005; Dalcalı & Akbaba, 2017b). The electrical and physical specifications of SPIM that we consider in this article are reported in Table 1.

Table 1. SPIM Parameters Under Consideration

Parameter	Value	Parameter	Value
Nominal	15	Rotor type	Squirrel
Nominal	220	Rotor radius, mm	22
Nominal	0.375	Slot number	26
Frequency, Hz	50	Stator winding	580
Pole number	4	Core depth, mm	25
Rotor speed,	1305	Core size, mm	25×25

MUTUAL INDUCTANCES OF SPIM

In AC machines, the identification accuracy of phase variables is directly related to the correct knowledge of inductances. Calculation of the inductances of SPIMs with variable air gap is quite difficult, and due to the variation of reluctance and saturation effect of the material used in the core, inductance in electric machinery is a nonlinear function of rotor position and phase current (Çınar et al., 2005; Akçayol, 2002). Inductance values in-between stator and rotor, and also in-between shading ring (shaded-pole winding) and rotor loop are acquired using a principle in (Dalcalı, 2017), and they are used as the same in this article. In this sense, a lookup table that contains 101 data samples including the corresponding inductance values as output and rotor position as input is generated in which the sampling period of rotor position is 3.6°. In order to obtain the inductances at certain steps without disrupting the air gap, the test setup shown in Fig. 1 is established. In this setup, the SPIM is mechanically coupled to a PIC 16F877A controlled stepper motor which has a 1.8° step angle (200 steps/revolution). This means an electrical angle of 3.6° in SPIM.

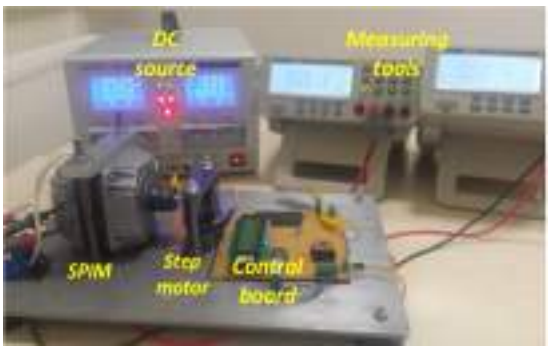

Figure 1. Test Setup for the Determination of Mutual Inductance

The respective changes of stator-rotor loop mutual inductance (M_{ar}, mH) and shading ring-rotor loop mutual inductance (M_{br}, μH) as a function of angular rotor position are given in Fig. 2.

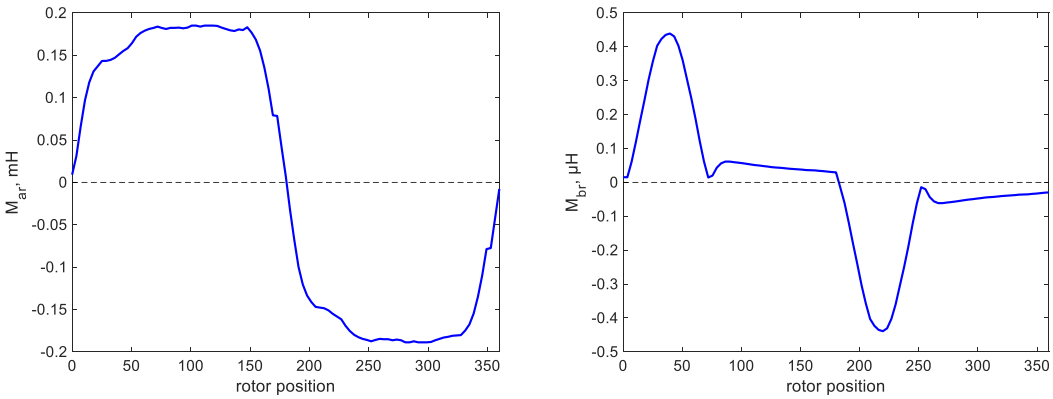

(a) (b)

Figure 2. Mutual Inductance Variation in a) Stator-Rotor Loop b) Shading Ring-Rotor Loop

THE DEVELOPED NEURAL NETWORK

One of the distinct characteristics of the NN is its ability to learn and generalize from experience and examples and to adapt to changing situations. NNs are able to map causal models (i.e. mapping from cause to effect for estimation and prediction) and inverse mapping (i.e. mapping from effect to possible cause). A NN is basically expressed by three kinds of parameters:

1. The interconnection pattern between different layers of nodes (or neurons, biologically)
2. The learning process for adjusting the weights of interconnections
3. The activation function that transforms a node's weighted input to its respective output

These parameters can be explained as follows: the connection weights connecting nodes in different layers each other influence the network performance crucially. Each node is usually connected with all of the previous and the next layer nodes. Modelling the relationship between the input and output patterns is realized by the training progress. Therefore, the input-output pattern matching is enabled when the network

is trained successfully. The NN training progress essentially involves presenting a set of examples with known outputs and calculating error between the actual output pattern and the desired output pattern (Hambli, 2002). The connection weights are adjusted iteratively by an algorithm, i.e. BP algorithm until the presented input-output pattern matching is completed in a certain success in that the error falls below an acceptable value for the whole training sets. After the training is successfully finished, the generalization capability of the network is tested with examples that are not applied to the network before during training. A satisfactorily trained network is expected to be able not only to remember all the training examples, but to predict the required output adequately for an unseen input data which is onto the universe covered by the example patterns. Finally, the ability of a network to imitate nonlinear mapping property closely corresponds to the nonlinearity of the selected activation function. There are many types of transfer functions, such as threshold type, signum type or linear threshold type, or they can vary nonlinearly in a continuous form, such as sigmoid, inverse-tan, hyperbolic or Gaussian type. More particularly, user-defined activation functions can be declared for specific applications.

In our analysis, a three-layer network as illustrated in Fig. 3 is arranged with feedforward architecture which is the most widely use scheme today. The nodes of this network are indicated by the circles and the weights by the dots in the connections. The input variable is rotor position (θ, degree) while the quantities to be estimated from the input variable are selected as stator-rotor loop mutual inductance (M_{ar}, mH) and shading ring-rotor loop mutual inductance (M_{br}, μH), respectively. There are 18 neurons in the 1st hidden layer with hyperbolic tangent activation function, 11 neurons in the 2nd hidden layer with linear activation function which is also used for the output node. The input and output layers have nodes equal to the respective number of variables. Thus, such particular network can be defined as 1-18-11-2 network. There is not a systematic way for deciding the number of hidden layers, the number of nodes and the type of activation functions. They are usually selected in an arbitrary fashion depending on both the complexity of problem being solved and the desired accuracy. In this paper, we used the trial and error method by observing the network testing performance.

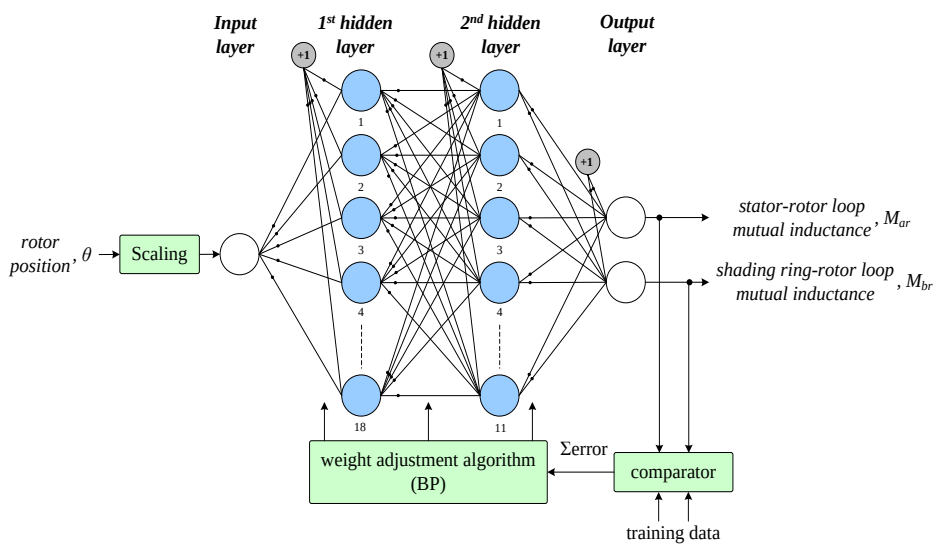

Figure 3. The Developed 1-18-11-2 Network Configuration

The aforementioned design is trained by employing BP algorithm. As the rotor position varies from 0° to 360°, which is a relatively greater range with respect to those of the NN output values, the range of the rotor position is transformed into the interval of [0, 1] prior to training process using Eq. 1. Such data normalization has proved to be useful and effective for the betterment of network estimation performance and also simplifying the computations significantly. In this equation, x_r and x_n are the actual and normalized value of a variable while x_{max} and x_{min} symbolize the maximum and minimum values of the respective variable.

$$x_n = \frac{x_r - x_{min}}{x_{max} - x_{min}} \qquad (1)$$

As mentioned earlier, the total number of collected experimental data is 101, which is graphically visualized with regard to the rotor position in Fig. 2. The number of training samples that we use during training is 70 which are picked up homogenously from the whole experimental dataset, and the trained network is tested by the remaining 31 samples which are not used during training. For convenience, six of the training and test data are tabulated in Table 2.

Table 2. Twelve Examples in the Experimental Dataset Used for Training and Test Purposes

Dataset	**θ (degree)**	**M_{ar} (mH)**	**M_{br} (µH)**
Training set	0.0	−0.009069	−0.015221
	25.2	−0.143319	−0.357259
	100.8	−0.185018	−0.056588
	198.0	−0.133576	−0.241127
	277.2	−0.186357	−0.061289
	360.0	−0.007714	−0.029547
Test set	7.2	−0.065789	−0.060707
	64.8	−0.181039	−0.121772
	144.0	−0.179756	−0.039397
	237.6	−0.179861	−0.249365
	306.0	−0.186357	−0.044769
	342.0	−0.134794	−0.035367

Moreover, to provide a better picture concerning the training samples and test samples observed for M_{ar} and M_{br}, their evolution with respect to the rotor position is depicted in Fig. 4, where the training samples are specified by blue "○" marks and test samples by red "□" marks.

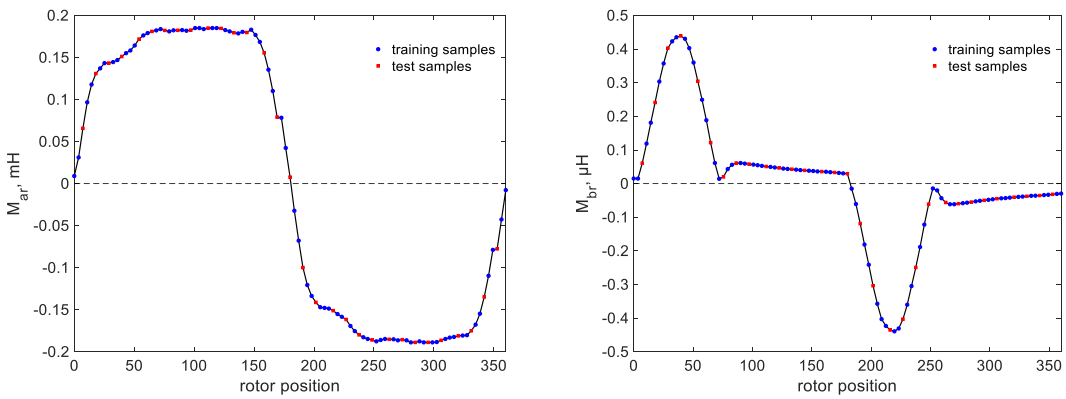

(a) (b)

Figure 4. Collected Training and Test Samples for (a) M_{ar} (b) M_{br}

INDUCTANCE ESTIMATION RESULTS AND PERFORMANCE ASSESSMENT

After the network is trained successfully, the network learning and generalizing capability of rotor position-inductance relations are checked for the case the test data includes unseen input rotor position values and the corresponding inductance values as output. To attain a well performed NN, we choose very small learning and momentum rates, and a very large number of training epochs which help the training error to converge gradually toward a minimal value in a stable trend. Fig. 5 shows the performance assessment criterion, namely, root mean-squared error (RMSE) for the training data as a function of iteration number. In line with what we desire, the RMSE drops from 0.6964 abruptly at first, then it approaches to a value of 0.01194 without any undesirable oscillation, signifying that the NN learns and gains the generalization property of rotor position-inductance relations as the training progresses. Also notice that after iteration 1×10^6, the error curve becomes almost stabile, and only very small amount of improvement is achieved after this point. If the training time is a concern and/or the results are satisfactory, the training process could be terminated here.

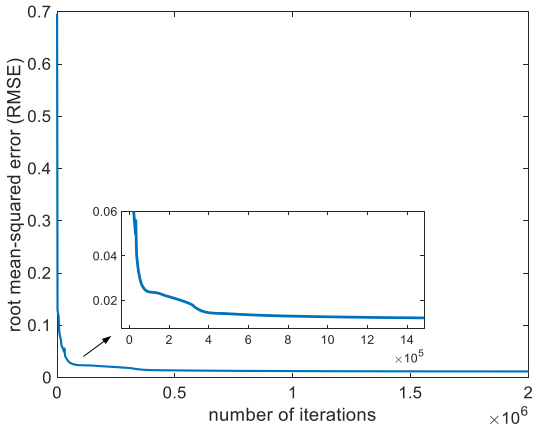

Figure 5. Root Mean-Squared Error during Training as a Function of Iteration Number

The experimental and the predicted values of stator-rotor loop mutual inductance by the designed NN model are shown in Fig. 6(a) in a superimposed manner for the test data. In addition, the percentage difference D_{MN} between the measured inductance L_M and the predicted inductance L_N by the NN model ($D_{MN} = (L_M - L_N)/ L_M$ %) is also given in Fig. 6(b) for each test sample. As seen from Fig. 6(a), there is a promising matching between the experimental results and the NN estimation. Except for the few cases, the percentage error rates are found to be very low. The mean error rate is calculated as 5.7% and it is to be noted that most of the error values favorably fall behind that mean error line.

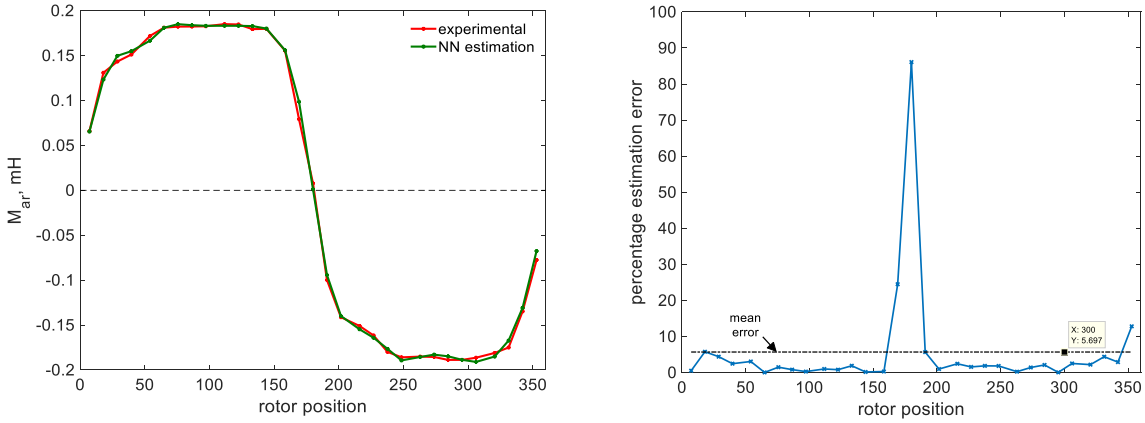

(a) (b)

Figure 6. Testing results for the Estimation of M_{ar} (a) Experimental and NN Estimated M_{ar} Variation (b) Percentage Error

Finally, the NN estimation results regarding the shading ring-rotor loop mutual inductance along with the experimental observations are presented in Fig. 7(a), from which it is evident that the NN estimation curve is in good agreement with the experimental results. It is remarkable from Fig. 7(b) that the presented approach can estimate the shading ring-rotor loop mutual inductance value with a mean error rate of 14.7%. Similar to the previous case, many of the error values are far below the mean error line.

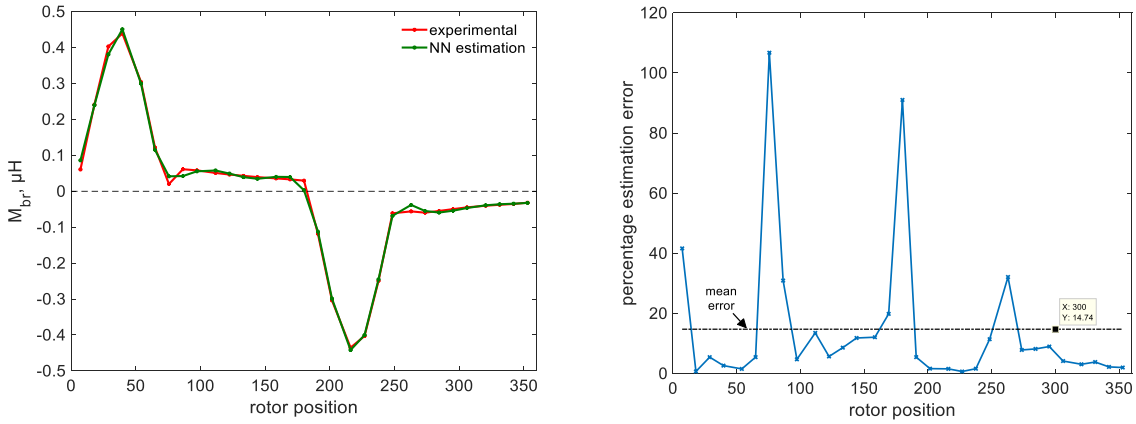

(a) (b)

Figure 7. Testing results for the Estimation of M_{br} (a) Experimental and NN Estimated M_{br} Variation (b) Percentage Error

CONCLUSION

Due to the ability to work with single-phase power source, simple structure and low-cost properties, SPIMs are still in use today in small power applications. Since they have a variable air gap and elliptical rotating magnetic field, inductance calculations of such motors, which influence the identification accuracy of phase variables, are highly complex. For this reason, two important inductance parameters, such as stator-rotor loop mutual inductance (M_{ar}) and shading ring-rotor loop mutual inductance (M_{br}.) are estimated with respect to the angular position θ in this paper by the employment of NN strategy. A three-layer feedforward NN is designed in which rotor

position is the input while the respective outputs are M_{ar} and M_{br}. Based on the real data collected from the experimental setup, the presented NN is trained by BP algorithm on a forward manner, which has produced satisfactory training results. Obtained results affirm the reliability and excellence of the proposed neural modeling in predicting the experimental test results with mean error rates less than 15%. Increasing the number of sampling data and iteration number can improve the results further. Moreover, more nodes can be included in the hidden layers and other activation function can be tried out in lieu of hyperbolic tangent and linear activation function.

REFERENCES

Akcayol, M. A. (2002). Anahtarlamalı relüktans motorun endüktans değişiminin sınırsel - bulanık modellenmesi. *Politeknik Dergisi, 5*(4), 287–292.

Chatterjee, A., & Keyhani, A. (2012). Neural network estimation of microgrid maximum solar power. *IEEE Transactions on Smart Grid, 3*(4), 1860-1866. doi: 10.1109/TSG.2012.2198674

Çelik, E., Çavuşoğlu, O., Gürün, H., & Öztürk, N. (2018), Estimation of the clearance effect in the blanking process of CuZn30 sheet metal using neural network−A comparative study. *Bilişim Teknolojileri Dergisi, 11*(2), 187-193.

Çelik, E., Gör, H., Öztürk, N. & Kurt. E. (2017). Application of artificial neural network to estimate power generation and efficiency of a new axial flux permanent magnet synchronous generator. *International Journal of Hydrogen Energy, 42*(28), 17692-17699. doi: 10.1016/j.ijhydene.2017.01.168

Çelik, E., Uzun, Y., Kurt, E., Öztürk, N., & Topaloğlu, N. (2018). A neural network design for the estimation of nonlinear behavior of a magnetically-excited piezoelectric harvester. *Journal of Electronic Materials, 47*(8), 4412-4420. doi: 10.1007/s11664-018-6078-z

Çınar, M. A., Gündoğan, Ç., & Kuyumcu, F. E. (2005). Taşıt tahriğinde kullanılacak bir anahtarlı relüktans motor tasarımı ve analizi. *Elektrik-Elektronik-Bilgisayar Mühendisliği 11. Ulusal Kongresi*, İstanbul.

Dalcalı, A. (2017). *Gölge kutuplu asenkron motorların yeni bir matematiksel modeli ve uzay harmonikli eşdeğer devresi*, Doktora tezi, Karabük Üniversitesi, Karabük.

Dalcalı, A. & Akbaba, A. (2017a). Detection of the space harmonics of the shaded pole induction motor. *Journal of Engineering Research 5*(4), 95-105.

Dalcalı, A. & Akbaba, M. (2017b). Comparison of the performance of bridge and bridgeless shaded pole induction motor using FEM. *International Journal of Applied Electromagnetics and Mechanics, 54*(3), 341-350. doi: 10.3233/JAE-160133

Gao, Y., Chau, K. T., & Ye, S. (2005). A novel chaotic-speed single-phase induction motor drive for cooling fans", *Fourtieth IAS Annual Meeting. Conference Record of the 2005 Industry Applications Conference*, Hong Kong.

Hambli, R. (2002). Prediction of burr height formation in blanking processes using neural network. *International Journal of Mechanical Sciences, 44*(10), 2089-2102. doi: 10.1016/S0020-7403(02)00168-6

Karanayil, B., Rahman, M.F., & Grantham, C. (2007). Online stator and rotor resistance estimation scheme using artificial neural networks for vector controlled speed

sensorless induction motor drive. *IEEE Transactions on Industrial Electronics, 54*(1), 167-176. doi: 10.1109/TIE.2006.888778

Kim, M.H., Simoes, M.G., & Bose, B.K. (1995). Neural network based estimation of power electronic waves. *21st International Conference on Industrial Electronics, Control, and Instrumentation*, Orlando, FL, USA.

Li, S., Wunsch, D.C., O'Hair, E.A., & Giesselmann, M.G. (2001). Using neural networks to estimate wind turbine power generation. *IEEE Transactions on Energy Conversion, 16*(3), 276-282. doi: 10.1109/60.937208

Parasiliti, F., Villani, M., & Castello, M. (2014). PM brushless DC motor with exterior rotor for high efficiency household appliances. *International Conference on Electrical Machines,* Berlin.

Paulson, F., & Prabhu, V.V. (2015). Back propagation based ANN technique for rotor position estimation of 8/6 switched reluctance motor. *International Conference on Innovations in Information, Embedded and Communication Systems, Coimbatore*, India.

Rodic, D., Gostimirovic, M., Kovac, P., Radovanovic, M., & Savkovic, B. (2014). Comparison of fuzzy logic and neural network for modelling surface roughness in EDM. *International Journal of Recent advances in Mechanical Engineering, 3*(3), 69-78. doi: 10.14810/ijmech.2014.3306.

Saygın, A., Ocak, C., Dalcalı, A., & Çelik, E. (2015). Optimum rotor design of small PM BLDC motor based on high efficiency criteria. ARPN Journal of Engineering and Applied Sciences, *10*(19), 9127-9132.

Shabgard, M.R., Badamchizadeh, M.A., Ranjbary, G., & Amini, K. (2012). Fuzzy approach to select machining parameters in electrical discharge machining (EDM) and ultrasonic-assisted EDM processes. *Journal of Manufacturing Systems, 32*, 32-39. doi: 10.1016/j.jmsy.2012.09.002

Simoes, M.G., & Bose, B.K. (1993). Application of fuzzy logic in the estimation of power electronic waveforms. *IEEE Industry Applications Conference Twenty-Eighth IAS Annual Meeting*, Toronto, Ontario, Canada.

Wang, K., Gelgele, H., Wang, Y., Yuan, Q., & Fang, M. (2003). A hybrid intelligent method for modelling the EDM process. *International Journal of Machine Tools and Manufacture, 43*, 995-999. doi: 10.1016/S0890-6955(03)00102-0

Yilmaz, O., Eyercioglu, O., & Gindy, N.Z. (2006). A user-friendly fuzzy-based system for the selection of electro discharge machining process parameters. *Journal of Materials Processing Technology, 172*(3), 363-371. doi: 10.1016/j.jmatprotec.2005.09.023.

OPTIMAL DESIGN OF HIGH PERFORMANCE INTERIOR PM MOTOR FOR ELECTRIC VEHICLE

Adem DALCALI
Bandırma Onyedi Eylül University
adalcali@bandirma.edu.tr

ABSTRACT: Interior permanent magnet synchronous motors (IPMSMs) are widely used in electric vehicles (EVs) due to their electrical and mechanical characteristics. In addition to the magnetic torque generated by the magnets in the IPMSM motors, a higher torque density is achieved by generating reluctance torque resulting from the inductance variation of the rotor on the d-q axes. Therefore, rotor and magnet geometry have significant effects on the motor performance. In an IPM design, it is often desirable to have maximum torque and flux weakening capability, minimum torque ripple, and low rotor harmonic losses. For this reason, rotor geometry is the most important part that affects the overall performance of the motor. In this study, a 100kW, single layer design V-shape structure IPMSM has been designed. The motor is optimized by considering important geometric data such as rotor geometry, magnet dimensions, bridge and flux barrier. Thus, it is aimed to design an optimum IPM traction motor considering efficiency criterion and cost in terms of magnet consumption. Also, the study provides design criteria that can meet low leakage flux and low cogging torque requirements for rotor topologies with V-shaped structures. 2D finite element analyzes have been used to verify the theoretically optimized designs.

Key words: electric vehicle, interior magnet motor, flux barrier, FEM

INTRODUCTION

Today, designing and using practical, efficient and environmentally friendly products is an inevitable necessity. Electric bicycles, electric motorcycles, and electric cars are among the best examples of these products. In electric vehicles, the torque transferred to the wheels is produced by the electric motor used in the vehicle. Therefore, the performance of the electric vehicles is directly related to the selection of the electric motor used. Synchronous, asynchronous, reluctance, and DC motors can be used in electric vehicles. Although DC motors are easily controlled among these machines, having a commutator and brush cause them to need frequent maintenance. The torque fluctuations of reluctance motors lead these motors to be disadvantageous in this kind of applications. In asynchronous motors, the power density is smaller than permanent magnet brushless motors and limits the use of these machines for high power density applications (Ehsani et al., 2003). The developments in the field of power electronics and the permanent magnet materials accelerated the development of permanent magnet synchronous motors compared to other electric machines. These motors are preferred in many applications in the industry because of their high efficiency, low volume, and high torque/weight ratios (Ocak, 2013). In the literature, permanent magnet synchronous motors (PMSM) with different topologies were compared especially for electric vehicles (Zhang et al., 2016; Seo & Choi, 2014). And also, different

rotor structures (spoke-type PMs, tangential-type PMs, U-shape PMs, and V-shape PMs) have been examined for electric vehicles. V-shape rotor structure was found to be superior to others (Liu et al., 2016). Also, the V-shape structure has the lowest value in terms of magnet consumption. In W-shape, high efficiency can be obtained in wide speed range (Wang et al., 2011). In terms of magnet placement technology, surface mounted permanent magnet motors (SMPMSM) do not have enough overload capacity compared to buried ones. Interior permanent magnet (IPM) motors can be also disadvantageous in terms of production costs because of the need for a high number of stator slots to control their harmonic losses (Pellegrino et al., 2012). It was determined that IPM machines give higher efficiency at low speeds, and surface mounted ones give higher efficiency at high speeds (Reddy et al., 2012).

In this study, the design of a 100 kW IPM motor with V-shape rotor for electric vehicles has been performed and optimization of rotor geometry which is aiming different design criteria has been realized. As with other electrical machines, the geometric components that constitute the magnetic circuit in electric motors with high-performance expectations have a significant impact on motor performance. For this reason, the parameters that constitute the rotor geometry of a V-shape IPM motor have been defined as variables. Geometric parameters have been obtained which provide the most suitable designs for maximum power, maximum efficiency/cost ratio, and maximum efficiency criteria. Also, different analyzes and comparative studies have been implemented.

ELECTRIC VEHICLES

Electric vehicle (EV) technology has been available since the invention of the car. However, in the early 1900s, the internal combustion engines were more attractive due to their low weight to power ratio and the high energy density of the petroleum used for fuel. Although electric drive systems are superior to the internal combustion system, they were in the background until the 1970s due to the low energy density of the batteries. The oil crisis that occurred in 1970 resulted in an increase in oil prices and attention to the electric vehicles have been reawakened (Ocak, 2013).

In 1997, Toyota was developed the Prius which was the first modern hybrid electric vehicle. Then Honda Insight and Honda Civic hybrid electric vehicles were produced. Generally, there are three different drive technology in EVs. First one is a battery-powered electric vehicle (all-electrical), the second one is classic internal combustion vehicles and the third one is hybrid electric vehicles with more than one drive unit. Figure 1 shows the principle of three types of structures.

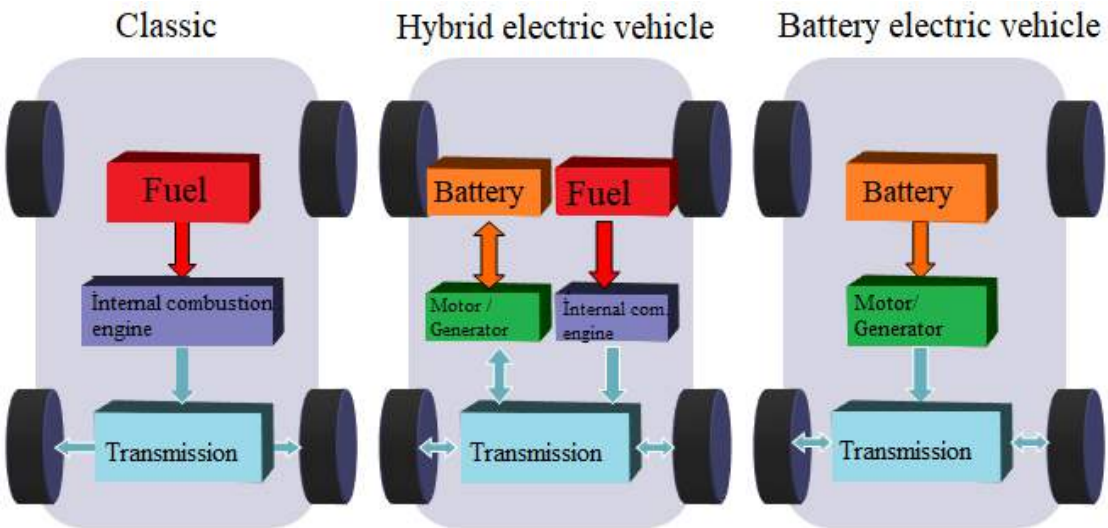

Figure 1. Details of Vehicles According to Drive Unit and Operation (Ocak, 2013)

In the battery electric vehicles (BEV), the wheels are driven by electric motor. In this structure, the power of the electric motor is only supplied by the batteries. Since BEV do not use fossil fuels, they do not release emissions. Furthermore, fuel and maintenance costs are also lower than others (Andwari et al., 2017; Choi et al., 2018; Momen et al., 2018). In the hybrid electric vehicle (HEV), in addition to the all-electric system, an internal combustion engine has been added. In this type of vehicles, fuel efficiency is significantly increased and emission values are reduced compared to conventional vehicles (Dnyandeo et al., 2018; Fiori et al., 2018).

DESIGNED INTERIOR PM MOTOR

The designed motor has an internal rotor and V-shape buried structure. In the permanent magnet synchronous motors (PMSM), there is no rotor winding losses because the rotor magnetic field is obtained from magnets instead of rotor conductors. Moreover, PMSMs are preferred in many areas because of their high power and torque density (Jeong et al., 2017; Athayele et al., 2016; Dalcalı & Ocak, 2018). Despite the high cost of rare earth magnets, permanent magnets (PM) are preferred especially for high efficiency and power density applications (Jeong & Hur, 2017). There are already different types of PM materials in the industry. PMs consist of iron, nickel and cobalt alloys. PMs have a wide BH curve, high magnetic remanence and coercive force (Galioto et al., 2015, Ocak et al., 2016). The maximum energy product value (BH_{max}) of a magnet is expressed by the product of the magnetic field intensity (H) and the magnetic flux density (B). In the study, high-temperature NdFeB type magnets with high BHmax are preferred. The characteristics of the initial design are given in Table 1.

Table 1. Parameters of the Initial Design

Parameter	Value	Unit
Rated output power	100	kW
Supply voltage	425	V
Rated frequency	300	Hz
Rated speed	4500	rpm

Number of poles		8	-
Number of slots		48	-
Stator	Outer diameter	245	mm
	Inner diameter	170	mm
	Length	120	mm
	Material	M210-35A	-
	Coil pitch	5	-
Rotor	Outer diameter	168.5	mm
	Inner diameter	110	mm
	Material	M210-35A	-
Magnet	Material	N40UH	-

2D and 3D models of the initial design are given in Figure 2. In order to see the motor structure in more detail, the motor is given in a split structure.

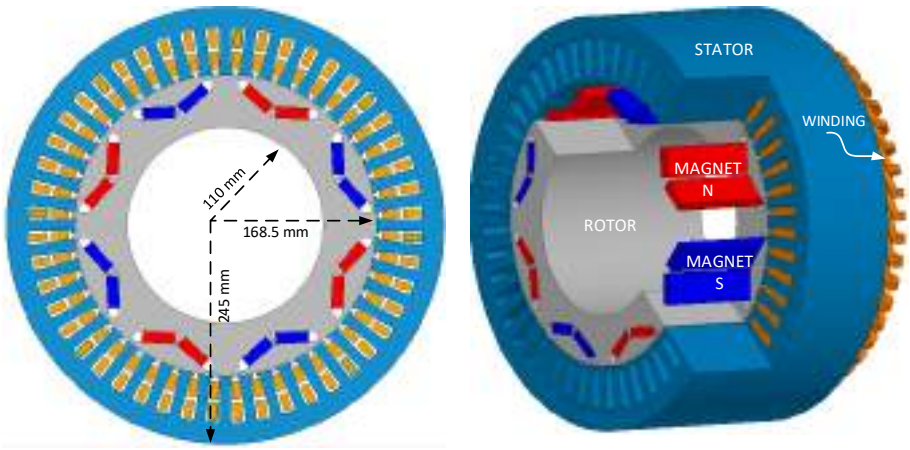

Figure 2. 2D and 3D View of Initial Design

Some criteria should be taken into account when designing an electrical machine. These criteria can be classified as design that is low-cost, efficient, and balanced with high-power density. In this study, motor designs with different rotor geometries have been performed considering maximum power, maximum efficiency/cost ratio and maximum efficiency criteria. In PM machines, the most important component of the cost is the magnet material. For this reason, total magnet weight needs to be optimized in order to obtain low-cost design. In some specific applications, instead of the best efficiency, maximum output power may be at the forefront due to the requirement of a low-volume motor. On the other hand, designs aimed to get higher efficiency often bring about an increase in motor cost. For this reason, maximum efficiency/cost ratio can be the most important criterion to be taken into account for a motor especially used in EV applications. In order to provide the three criteria mentioned above, each of the rotor geometry parameters is defined as a variable. For the case study, the upper and

lower limits of the design variables have been determined within the mechanical limitations and are given in Table 2.

Table 2. Defined Variables and Their Values for the Rotor Geometry

Parameter	Value
Magnet thickness	from 5 mm to 8 mm, step = 1 mm
Magnet width	from 20 mm to 40 mm, step = 1 mm
R_{ib}	from 10 mm to 15 mm, step = 1 mm
O2	from 5 mm to 13 mm, step = 1 mm

The defined variables are shown on the rotor geometry in Figure 3. R_{ib} is the distance between magnet barriers and O2 is the distance between the magnets and rotor inner diameter. In addition, magnet width and thickness are defined as other variables.

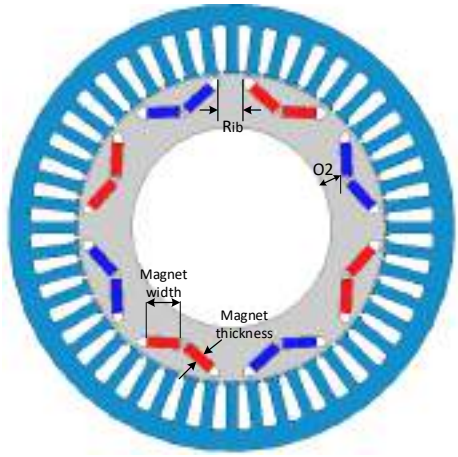

Figure 3. View of the Defined Variables on the Rotor Geometry

ANALYSIS RESULT

Parametric solution method used in optimization of electric motors is a result oriented, fast and practical. In this method, geometric parameters of the motor are defined as design variables. By determining the lower and upper limits of the variable, the analysis is carried out in the desired solution steps. The solution range directly affects solution accuracy and analysis time. As the step sensitivity increases, analysis time will be longer as expected. (Bayındır et al., 2011). In the study, a total of 4536 different analysis have been performed. This number varies according to the sensitivity of the variables. Since the general trend of geometric variables is the primary target, the steps for the solutions have been expressed in 1mm intervals. According to the analysis results, maximum output power, highest efficiency/cost ratio and the best efficiency design have been obtained and given in Table 3.

Table 3. Obtained Parameters Satisfying the Given Design Criteria

Maximum Output Power	Maximum Efficiency/Cost Ratio	Maximum Efficiency (Design C)

Parameter	Value	Parameter	Value	Parameter	Value
Magnet thickness	8 mm	Magnet thickness	5 mm	Magnet thickness	7 mm
Magnet width	40 mm	Magnet width	26 mm	Magnet width	31 mm
O2	5 mm	O2	9 mm	O2	9 mm
R_{ib}	15 mm	R_{ib}	15 mm	R_{ib}	10 mm

By using symmetrical boundary conditions, 1/8 symmetrical view of the three different motors which have been optimized is given in Figure 4. Solution time was reduced by the boundary conditions applied to the motor model.

Figure 4. Views of A, B and C Designs

The performance of the motors for Design A, Design B, and Design C has been given in Table 4. Design A is the design that fulfils maximum power criteria. The motor geometry which provides maximum output power criteria need a higher magnet consumption so this leads to higher cost as expected. Design C has the highest efficiency among the solutions. Design B is the design that which fulfils maximum efficiency/cost ratio. In all design variations, 100 kW output power is the minimum requirement to be a valid design. For this reason, designs that cannot provide this output power have not been taken into consideration even if they have lower costs or higher efficiency. Since the cost function has been expressed directly as the amount of magnet consumption, Design B has been considered to be the most suitable candidate for electric vehicle applications.

Table 4. Motor Performances Satisfying the Proposed Criteria

Structure	Efficiency (%)	Total magnet consumption (kg)	Maximum output power (kW)
Design A	94.31	2.27	234
Design B	95.65	0.92	102.8
Design C	97.91	1.54	147.4

The motor models which successfully passed the analytical design and optimization criteria have been subjected to finite element analysis. The finite element method (FEM) is a method in which an approximate solution of general differential equations in a specified region has been performed. With this method, heat transfer, solid and

liquid mechanics and electromagnetic problems can be solved. The use of FEM in electrical machines gives the designer a great advantage both time and economy. In addition, electrical and electromagnetic parameters of the machine have been analyzed with high accuracy rate with this method. (Dalcalı & Ocak, 2018). The magnetic flux density distribution for the obtained three designs have been given in Figure 5.

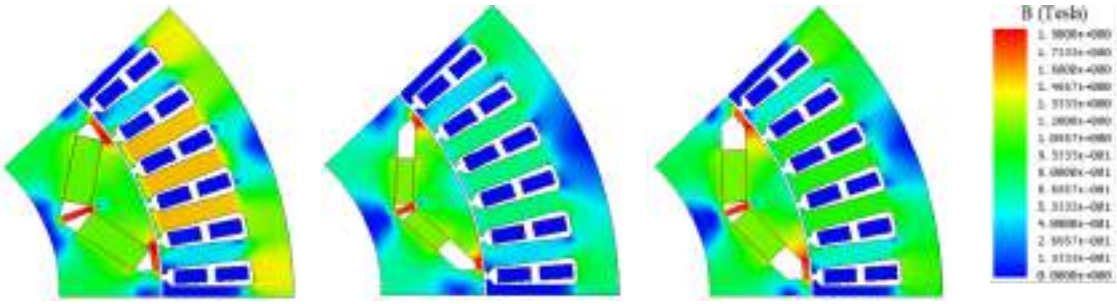

Figure 5. 2D Magnetic Flux Density Distributions for Designs A, B, and C

When the magnetic flux densities are examined, the flux density increases partly as the magnet thickness increases due to decreasing core cross section. It is seen that when considering the M210-35A core material, the flux values fulfil the requirements.

CONCLUSION

This paper has presented the design details and rotor geometry optimization which fulfils different design criteria of interior permanent magnet synchronous motors for electric vehicles. Motor models have been created which provide the best efficiency, highest output power, and best efficiency/cost ratio criteria by using a parametric approximation method. The performances of three different designs have been obtained with the help of finite element analysis. Considering the results of the study, it is viewed that designs targeting maximum output power result in high cost and relatively low efficiency. In addition, it is observed that providing the highest efficiency criteria alone would not be the right approach and usually result in very high costs. It has been seen that the maximum efficiency/cost ratio criterion is the most appropriate approach. The uncertain fluctuation in magnet prices leads to an increase of the studies that focus on the reduction of the magnet consumption. In the systems fed by the battery, efficiency is the most important performance value. As a result, the study provided a geometry-based optimization approach to the studies that can be performed to achieve maximum efficiency with minimum cost.

ACKNOWLEDGMENT

This study was supported by Scientific Research Project Unit of the Bandırma Onyedi Eylül University under Project No: BAP-18-MF-1009-080.

REFERENCES

Andwari, A.M., Pesiridis, A., Rajoo, S., Botas, R.M., & Esfahanian, V. (2017). A review of battery electric vehicle technology and readiness levels. *Renewable and Sustainable Energy Reviews*, *78*, 414-430. doi: 10.1016/j.rser.2017.03.138

Athavale, A., Sasaki, K., Gagas, B.S., Kato, T., & Lorenz, R.D. (2016). Variable flux permanent magnet synchronous machine (VF-PMSM) design methodologies to meet electric vehicle traction requirements with reduced losses. *IEEE Energy Conversion Congress and Exposition*. Milwaukee, WI, USA.

Bayındır, R., Ocak, C., & Topaloğlu, İ. (2011). Investigation of the effect of magnet thickness on output power and torque of pm bldc machines using parametric approach method. *Proceedings of the 2011 International Conference on Power Engineering, Energy and Electrical Drives*. Malaga.

Choi, H., Shin, J., & Woo, J. (2018). Effect of electricity generation mix on battery electric vehicle adoption and its environmental impact. *Energy Policy, 121*, 13-24. doi: 10.1016/j.enpol.2018.06.013

Dalcalı, A., & Ocak, C. (2018). Farklı Mıknatıs Malzemelerinin Yüzey Mıknatıslı Doğrudan Tahrikli Sabit Mıknatıslı Senkron Motor Performansına Etkisi. *III. International Rating Academy Congress on Applied Sciences*. Lviv, Ukraine.

Dnyandeo, P.A., Keshav, T.R., & Dilip, R.P. (2018). Hybrid electric vehicle. *International Research Journal of Engineering and Technology*, *5*(5), 4034-4036.

Ehsani, M., Gao, Y., & Gay, S. (2003). Characterization of electric motor drives for traction applications. *The 29th Annual Conference of the IEEE Industrial Electronics Society*. Roanoke, VA, USA.

Fiori, C., Ahn, K., & Rakha, H.A. (2018). Microscopic series plug-in hybrid electric vehicle energy consumption model: model development and validation. *Transportation Research Part D, 63*, 175-185. doi: 10.1016/j.trd.2018.04.022

Galioto, S.J., Reddy, P.B., El-Refaie, A.M., & Alexander, J.P. (2015). Effect of magnet types on performance of high-speed spoke interior-permanent-magnet machines designed for traction applications. *IEEE Transactions on Industry Applications*, *51*(3), 2148-2160. doi: 10.1109/ECCE.2014.6954019

Jeong, C.L., & Hur, J. (2017). Optimization design of PMSM with hybrid-type permanent magnet considering irreversible demagnetization. *IEEE Transactions on Magnetics*, *53*(11). doi: 10.1109/TMAG.2017.2707102

Jeong, C.L., Kim, Y.K., & Hur, J. (2017). Optimized design of PMSM with hybrid type permanent magnet for improving performance and reliability. *IEEE Energy Conversion Congress and Exposition*. Cincinnati, OH, USA.

Liu, X., Chen, H., Zhao, J., & Belahcen, A. (2016). Research on the performances and parameters of interior PMSM used for electric vehicles. *IEEE Transactions on Industrial Electronics*, *63(*6), 3533-3544. doi: 10.1109/TIE.2016.2524415

Momen, F., Rahman, K., & Son, Y. (2018). Electrical propulsion system design of Chevrolet Bolt battery electric vehicle. *IEEE Transaction on Industry Applications*, Early Access. doi: 10.1109/TIA.2018.2868280

Ocak, C. (2013). *Elektrikli araçlar için üç kademeli yeni bir fırçasız da motoru tasarımı, analizi ve uygulaması*. Gazi Üniversitesi, Ankara.

Ocak, C., Tarımer, İ., & Dalcalı, A. (2016). Advancing Pole arc offset points in designing an optimal PM generator. *TEM Journal, 5*(2), 126-132.

Pellegrino, G., Vagati, A., Guglielmi, P., & Boazza, B. (2012). Performance comparison between surface-mounted and interior pm motor drives for electric vehicle application. *IEEE Transactions on Industrial Electronics*, *59*(2), 803-811. doi: 0.1109/TIE.2011.2151825

Reddy, P.B., El-Refaie, A.M., Huh, K.K., Tangudu, J.K., & Jahns, T.M. (2012). Comparison of interior and surface pm machines equipped with fractional-slot concentrated windings for hybrid traction applications. *IEEE Transactions on Energy Conversion, 77*(3), 593-602. doi: 10.1109/ECCE.2011.6064067

Seo, J.H., & Choi, H.S. (2014). Cogging torque calculation for IPM having single layer based on magnet circuit model. *IEEE Transactions on Magnetics, 50*(10). doi: 10.1109/TMAG.2014.2327204

Wang, A., Ji, Y., & Soong W.L. (2011). Comparison of five topologies for an interior permanent-magnet machine for a hybrid electric vehicle. *IEEE Transactions on Magnetics, 47*(10), 3606-3609. doi: 10.1109/TMAG.2011.2157097

Zhang, Y., Cao, W., McLoone, S., & Morrow, J. (2016). Design and flux-weakening control of an interior permanent magnet synchronous motor for electric vehicles. *IEEE Transactions on Applied Superconductivity, 26*(7). doi: 10.1109/TASC.2016.2594863

EFFECT of CALCINED COLEMANITE ADDITION to COPPER CONVERTER SLAG in SILICA CRUCIBLE

Mehmet Ali TOPÇU
Karamanoğlu Mehmetbey University, Department of Metallurgical and Material Engineering, Karaman, Turkey
topcumali@kmu.edu.tr

Aydın RÜŞEN
Karamanoğlu Mehmetbey University, Department of Metallurgical and Material Engineering, Karaman, Turkey
aydinrusen@kmu.edu.tr

ABSTRACT: Copper losses to slag ranging from 4% to 8% in the copper converting process are very crucial. In this study, it was investigated to minimize the copper losses in converting stage by the adding of colemanite addition as a fluxing agent. Firstly, the converter slag obtained from the Eti Copper Co. was analyzed in terms of the physical, chemical and mineralogical by using various devices. After the characterization of converter slag, calcined colemanite addition (0, 2 and 4%) was selected as a variable parameter and the effects of the parameters were investigated in silica crucible at 1250 ^{o}C reaction temperature for 3 hours under nitrogen atmosphere. According to the characterization results, it was determined that the converter slag with the main phases of fayalite and magnetite contains 22.1% SiO_2, 44.3% Fe, 4.45% Cu and 3.15% Zn. Experimental results show that the amount of copper losses to the converter slag can be decreased from 4.45% to 4.1 % Cu only by adding 2% calcined colemanite at the temperature of 1250 ^{o}C and 3 hours reaction time.

Key words: Converter Slag, Colemanite, Pyrometallurgy, Characterization

INTRODUCTION

Considering that more than 80% of the world's copper ores are sulfides, pyrometallurgical method which consists of concentration, smelting, converting and refining steps is more widely used for copper production. In converting stage, matte with 40-50% Cu converts to blister copper (up to 98-99 % Cu) with sequential reactions; i) slag formation stage and ii) blister copper formation step (Schlesinger et al., 2002). In slag formation stage, the iron sulphite (FeS) in the matte phase is selectively oxidized by air blown into matte layer through the lance in order to form FeO and SO_2 as following reaction:

$$2FeS_{\text{(in matte)}} + 3O_{2\text{ (in blast)}} + SiO_{2\text{ (flux)}} \rightarrow 2FeO.SiO_{2\text{ (slag)}} + 2SO_{2\text{ (off-gas)}} + \text{heat} \quad \text{(Rx. 1)}$$

The consisted FeO combines with the silica flux to form fayalite – type slag. This slag, generally including 4 – 8% Cu, is granulated then sent to back to the smelting furnace for copper recovery. As a result of this step, the FeS in the matte is removed and white

metal of copper sulphide (Cu_2S) remains. In blister copper formation stage, oxygen is blown on Cu_2S. Thus, the sulfur contained in the white metal is removed as SO_2 and blister copper is formed as following reaction (Davenport, 2002);

$Cu_2S_{(in\ matte)} + O_{2(in\ blast)} \rightarrow 2Cu_{(molten\ copper)} + SO_{2(in\ off\text{-}gas)} + heat$ (Rx. 2)

One of the most important targets in the converter stage is to keep the copper losses to slag at minimum level. Copper losses to the slag in the pyrometallurgical copper production constitute a major problem as indicated previous studies (Jalkanen et al., 2003; Imris et al., 2005; Rüşen et al., 2012). There are two types of copper losses to slag namely mechanical and physico-chemical losses. While the mechanical losses are mainly related to the viscosity of slag, the physico-mechanical losses are directly associated with the solubility of copper in sulphides and oxides forms in slag. Copper converter slag is a byproduct that should be evaluated due to its high copper content. In the world, copper converter slags are generally re-processed in the production to gain copper from the slag (Altundoğan et al., 2004).

As stated above, in converter stage, SiO_2 are used as fluxing agent. Although the best matte – slag separation occurs at saturation of silica, excessive amount SiO_2 leads to increase in the viscosity of slag which affects more mechanical copper lost. According to the previous studies (Timuçin et al., 1986; Topkaya et al., 2004) in the steel industry, colemanite ($2CaO.3B_2O_3.5H_2O$) usage as flux showed that its addition decreases the viscosity and melting temperature of slag and a result decreasing viscosity the copper losses were decreased. Therefore, in this paper, it is aimed to investigate minimization of copper losses to converter slag by adding calcined colemanite at specified temperature after mineralogical and chemical characterization of the slag.

MATERIAL AND METHOD

Converter slag used in this study was obtained from Eti Bakır Inc. from Samsun Province (Turkey). Before experimental works, chemical and mineralogical structures of converter slag were determined by inductively coupled plasma mass spectrometer (ICP – MS) and X-Ray powder diffraction (XRD), respectively. Colemanite was supplied from Eti Bakır Inc., and used in the experiments as a flux agent after calcination at 400 ^oC for 2 hours. By this way, its chemical bonded water was removed from the structure.

Fig. 1 indicates the SiO_2 – Fe_2O_3 – FeO triple phase diagram which is proper to the converter slag structure, a fayalite type slag. This triple phase diagram represents the slag formation area consisting of silica saturated (SiO_2) – magnetite saturated (Fe_3O_4) – iron oxide saturated (FeO) boundaries. In this study, it was preferred to use silica crucibles in order to work especially in the vicinity of the silica saturated zone. Considering the triple phase diagram, pure silica dust also was added to the slag system in sufficient quantity because of the low silica content (22%) of the converter slag.

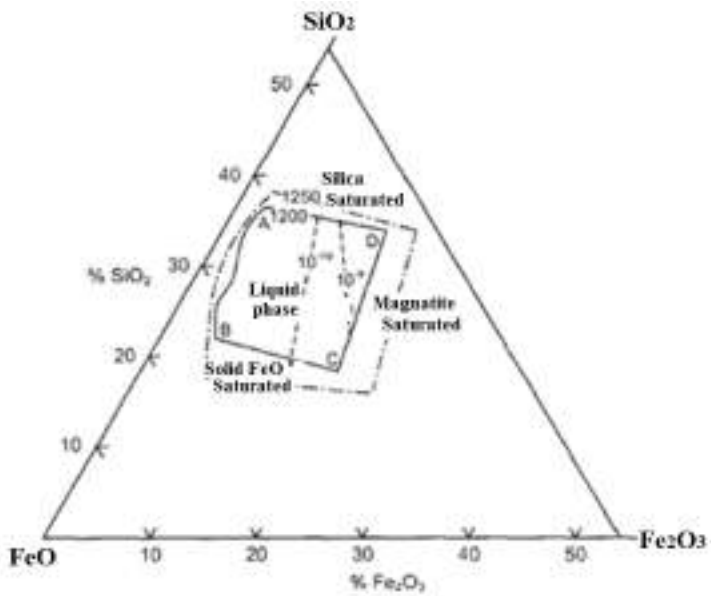

Figure 1. FeO-Fe_2O_3-SiO_2 Triple Phase Diagram (Davenport et al. 2002)

Thus, the effect of colemanite addition (0%, 2%, 4%) at elevated temperature (1250 ^oC) on copper losses to slag was investigated in the silica saturated conditions. Taking into account the capacity of the silica crucibles, the experiments were carried out by adding 10 g of blister copper to 60 g converter slag and adding sufficient amount of calcined colemanite.

RESULTS

Chemical and Mineralogical Analysis of Converter Slag

The chemical analysis of copper converter slag is given in Table 1. As stated previous study (Rüşen & Topçu, 2017) and seen in elemental analysis, copper converter slag is primarily composed of iron and silicon with high content. Apart from these elements, remarkable amount of copper and zinc are present in the converter slag.

Table 1. Elemental Analysis of Copper Converter Slag

Element	Si	Fe	Cu	Zn	S	Pb	Al	Ca	Na	K	Mg
Amount (wt. %)	11.1	44.3	4.45	3.39	1.09	0.45	0.87	0.65	0.54	0.5	0.7

XRD pattern of the slag is illustrated in Fig. 2, which reveals that copper converter slag is mainly composed with Fe_2SiO_4 and Fe_3O_4. In this study, copper and zinc deposit phases could not be determined in the XRD graph due to high density of $FeSiO_4$ and Fe_3O_4 phases. However, according to the previous studies, copper and zinc in converter slag can be found in different form. While copper can be present in the slag

as dignite, bornite, chalcopyrite and metallic copper, zinc can form as franklinite ($ZnFeO_4$) and zinc silicates (Muravyov et al., 2012).

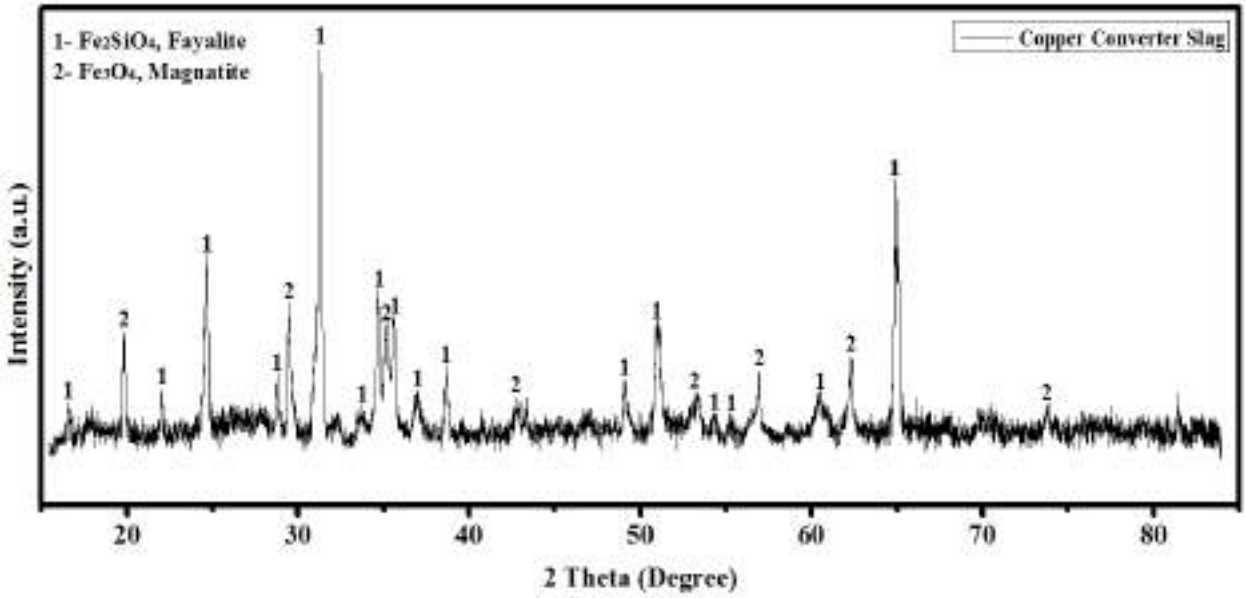

Figure 2. XRD Graph of Copper Converter Slag

Experimental Results

In this study, the effect of calcined colemanite addition on copper losses to slag was investigated at different temperatures in silica crucibles. The results could not be obtained after experimental studies conducted at 1200 °C and 1300 °C in the presence of mixture of blister copper and converter slag. It was observed that the mixture did not melt completely at 1200 °C and overflow from silica crucible at 1300 °C. For this reason, the samples obtained from these experiments were not subjected to analysis. Therefore, only the results for 1250 °C are presented in Table 2 and Fig. 2.

Table 2. Elemental Analysis of Experimental results

Experimental Conditions		Elemental Analysis of Copper Converter Slag (wt. %)					
Temp. (°C)	Colemanite Addition (%)	Cu	SiO_2	Fe	S	Al_2O_3	B_2O_3
1250 °C	0	7,83	45,8	25,0	0,01	0,44	-
	2	4,10	48,8	24,9	0,03	0,84	1,11
	4	4,92	45,5	24,5	-	1,22	1,99

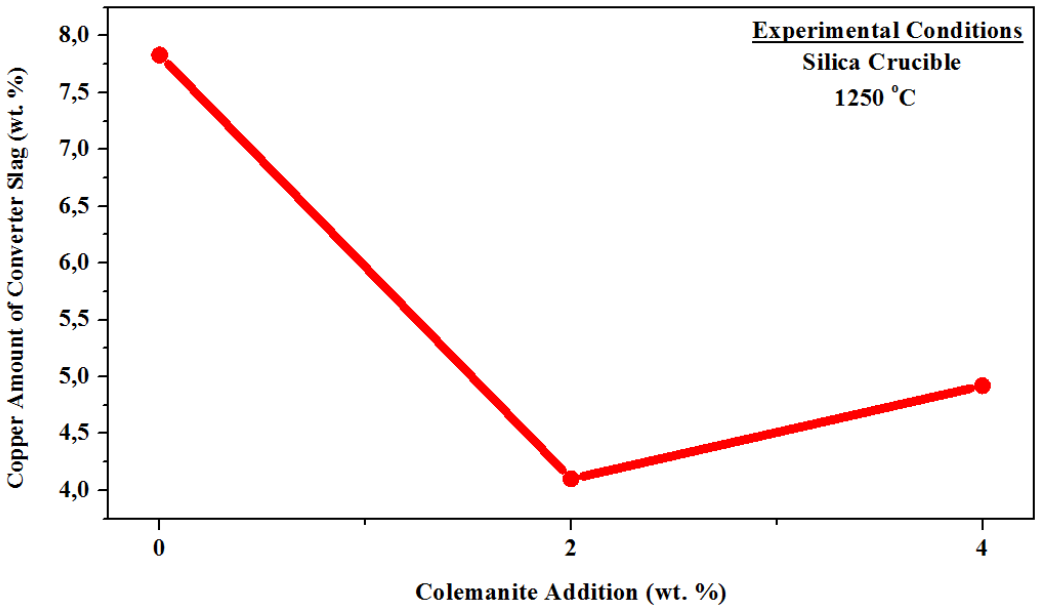

Figure 2. Effect of Colemanite Addition on Copper Losses to Slag

As a result of experiments, in the silica crucible (with addition of extra silica to form a saturated system to silica) without adding colemanite, the copper value in the slag is reached up to 8%. However, with addition of 2% calcined colemanite, the ratio of copper in the slag decreased to around 4%. It was observed that the more calcined colemanite addition beyond 2% affects the more copper losses in the system. It is thought that the addition of more colemanite to the slag causes the slag to become more fluid, which results in an increase in copper losses due to more scattering blister copper in the slag.

Furthermore, experimental works were carried out under constant temperature (1250 ^{o}C) with addition of converter slag and predetermined boron compound (0%, 2%, 4%) without blister copper addition. Thus, it is aimed to reveal positive and negative effects of blister copper on the system apart from the slag. However, at the end of the experiments performed under the specified conditions, it was determined that converter slag climbed in the crucible. Therefore, the samples obtained from these experiments were not evaluated to analysis. Images of samples obtained at the end of the experiments are shown in Fig. 3.

Figure 3. Images of silica crucible obtained after experiments without blister addition

CONCLUSIONS

In this study, the effect of calcined colemanite addition on copper losses to converter slag was investigated in silica crucible under the predetermined conditions. According to the experimental results, meaningful results were obtained at 1250 ^{o}C, but undesirable results revealed after the experiments carried out at 1200 ^{o}C and 1300 ^{o}C due to insufficient melting and overflow of the slag, respectively. As a conclusion, minimum copper content in converter slag could be obtained as 4.10% with the addition of 2% of calcined colemanite at 1250 ^{o}C for 3 hours under nitrogen atmosphere.

Acknowledgment
This work was supported by Karamanoglu Mehmetbey University Scientific Research Projects (BAP) Coordinatorship with project ID: 28 – M – 16. Also, the authors would like to thank the Scientific and Technological Researchers Application and Research Center for characterization of copper converter slag.

REFERENCES

Altundogan, H. S., Boyrazli, M., & Tumen, F. (2004). A study on the sulphuric acid leaching of copper converter slag in the presence of dichromate. Minerals engineering, 17(3), 465-467.

Davenport, W. G., King, M. J., Schlesinger, M. E., & Biswas, A. K. (2002). Extractive metallurgy of copper. Elsevier.

Imris, I., Sanchez, M., & Achurra, G. (2005). Copper losses to slags obtained from the El Teniente process. Mineral Processing and Extractive Metallurgy, 114(3), 135-140.

Jalkanen, H., Vehviläinen, J., & Poijärvi, J. (2003). Copper in solidified copper smelter slags. Scandinavian Journal of Metallurgy, 32(2), 65-70.

Muravyov, M. I., Fomchenko, N. V., Usoltsev, A. V., Vasilyev, E. A., & Kondrat'eva, T. F. (2012). Leaching of copper and zinc from copper converter slag flotation tailings using H_2SO_4 and biologically generated $Fe_2(SO_4)$ 3. Hydrometallurgy, 119, 40-46.

Ruşen, A., Geveci, A., Topkaya, Y. A., & Derin, B. (2012). Investigation of effect of colemanite addition on copper losses in matte smelting slag. Canadian Metallurgical Quarterly, 51(2), 157-169.

Rüşen, A., & Topçu, M. A. (2017). Thermal and Mineralogical Investigation of Copper Converter Slag. Microscopy, 3(10).

Timucin, M., Sevinc, N., Topkaya, Y. A., & Eric, H. (1986). Use of Colemanite in the Production of Iron and Steel.

Topkaya, Y., Sevinc, N., & Günaydın, A. (2004). Slag treatment at Kardemir integrated iron and steel works. International journal of mineral processing, 74(1-4), 31-39.

HYDROMETALLURGICAL ASSESSMENT OF COPPER CONVERTER SLAG WITH DEEP EUTECTIC SOLVENT

Mehmet Ali TOPÇU
Karamanoğlu Mehmetbey University, Department of Metallurgical and Material Engineering, Karaman, Turkey
topcumali@kmu.edu.tr

Aydın RÜŞEN
Karamanoğlu Mehmetbey University, Department of Metallurgical and Material Engineering, Karaman, Turkey
aydinrusen@kmu.edu.tr

ABSTRACT: Copper converter slag which includes remarkable amount of copper, zinc and cobalt, is produced as a by-product in copper production industry. Until today, different metals have been recovered from copper converter slag with hydrometallurgical methods by using different leaching reagents such as sulphuric acid, nitric acid, ferric chloride, ferric sulphate, ammonia and cyanide. Considering the environmental impact of these solvents, researchers have continued to search for environmentally sensitive solvents on metal recovery from slag. Therefore, in this study, a new generation solvent which called deep eutectic solvents (DES) is proposed to recover copper from converter slag by hydrometallurgical method. For this purpose, 100 ml deep eutectic solvent was prepared by mixing choline chloride [$(CH)_3N(Cl)CH_2CH_2OH$] and urea [NH_2CONH_2] with 1:2 molar ratio. Leaching experiments were carried out in the range of 2, 8, 16, 32, 48 and 72 hours at 95 ^oC and 1/20 g/mL solid-liquid ratio. Experimental results showed that copper recovery from slag was increased with increasing leaching time in the presence of DES, and the highest recovery rate of copper (86.80%) was obtained at the leaching duration of 72 h.

Key words: Converter slag, deep eutectic solvent, leaching

INTRODUCTION

Copper converter slag formed during the pyrometallurgical copper production and contains remarkable amount of valuable metals such as copper, zinc and cobalt. (Rudnik et al., 2009). During the process, converter slags are usually sent back to smelting stage to reduce the copper lost. However, as the volume and viscosity of the slag increase, higher copper losses occur in the converter stage. (Altundoğan et al., 2004) In recent years, hydrometallurgical processes were used to recover the valuable metals from copper converter slags. In these studies, various chemical agents were used for metal extraction such as sulphuric acid (Anand et al., 1983), nitric acid (Basir and Rabah, 1999), ferric chloride (Anand et al., 1980), ferric sulphate (Altundoğan & Tümen, 1997), ammonia (Rudnik et al., 2009). Unfortunately, these chemicals affect negatively to the environment such as toxicity, corrosion, etc. To overcome the negative effects of these conventional solvents, a new environmentally friendly solvent called Deep Eutectic Solvent (DES) has proposed by scientists a number of years ago.

DESs can be synthesized easily by mixing two safe components which are cheap, renewable and biodegradable to form a eutectic mixture (Zhang et al., 2012).
DES is based on combination of choline chloride with hydrogen bond donor such as urea, ethylene glycol, malonic acid and so on. Choline chloride is one of the most common components due to its low cost, biocompatibility and non-toxic structure. Nowadays, DESs which formed with ChCl and hydrogen bond donors have become of growing interest thanks to their low cost and ecological advantages (Smith et al., 2014). According to previous studies (Abott et al., 2009; Bakkar 2014), the solubility of metal oxides (especially zinc and copper oxides) was considerably high in deep eutectic solvents based on ChCl and urea. Therefore, in this study, the effect of leaching time on copper recovery from copper converter slag was studied with hydrometallurgical route by using DES as leach agent which prepared with choline chloride and urea.

MATERIALS AND EXPERIMENTAL METHODS

Leaching experiments were conducted using a converter slag from Eti Bakır Inc., Turkey. Quantitative analyses of the converter slag were performed by Inductively Coupled Plasma Mass Spectrometer (ICP – MS) in chemistry laboratory of Eti Bakır Inc., X-ray Powder Diffraction (XRD) at Karamanoğlu Mehmetbey University and the major oxides composition was detected by X-Ray Fluorescence Spectroscopy (XRF). The oxide composition of the slag sample is given in Table 1.

Table 1. Oxide Composition of Converter Slag (wt. %)

Oxide	Fe_2O_3	SiO_2	CuO	ZnO	SO_3	Al_2O_3	MgO	K_2O	CaO	Na_2O	PbO
Amount	61.5	20.9	5.32	4.13	2.41	1.42	1.01	0.841	0.831	0,463	0,426

As seen XRD pattern of converter slag (Fig. 1), the main structure of the converter slag consists of fayalite ($FeSiO_4$) and magnetite (Fe_3O_4) phases. It is also seen from XRD graph that the converter slag contains some amorphous structure. In addition, the minor and trace phases in the copper converter slag was identified by Scanning Electron Microscope (SEM). According to the SEM analysis from previous study (Rusen & Topcu, 2017), the copper converter slag includes metallic copper and complex (Cu-Fe-Zn) sulfides besides magnetite and fayalite.

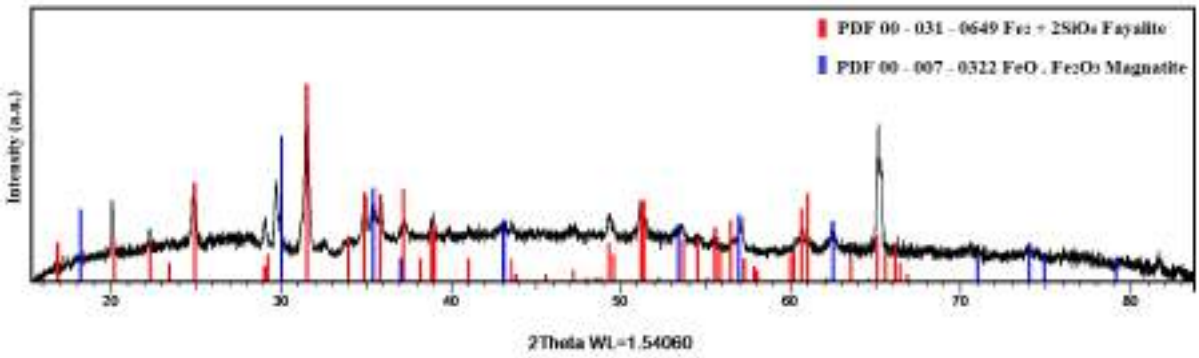

Figure 1. XRD Pattern of Converter Slag

Choline chloride (>98%) and urea (>99%) supplied commercially from Merck were used without further purification to prepare deep eutectic solvent. Choline chloride and urea were mixed in a glass baker with a stoichiometric eutectic molar ratio of 1:2, respectively and heated gently up to 90 °C using hot plate with magnetic stirrer until a homogenous colorless liquid was obtained. Then, 5 gram of converter slag was added to 100 ml of DES at 95 °C and stirred during leaching at 600 rpm. Leaching duration was selected in the range of 2, 8, 16, 32, 48 and 72 hours. After the filtering of the leaching experiments, the leach liquor was diluted with 0.1 M HCl. After that, leach solution was analyzed by using Perkin Elmer PinAccle 900T model Atomic Absorption Spectroscopy (AAS).

RESULTS

Effect of leaching time on copper recovery from copper converter slag with DES reagent was investigated at 95 °C reaction temperature, 1/20 solid/liquid ratio and 600 rpm stirring speed. Experimental results are summarized in Fig. 2.

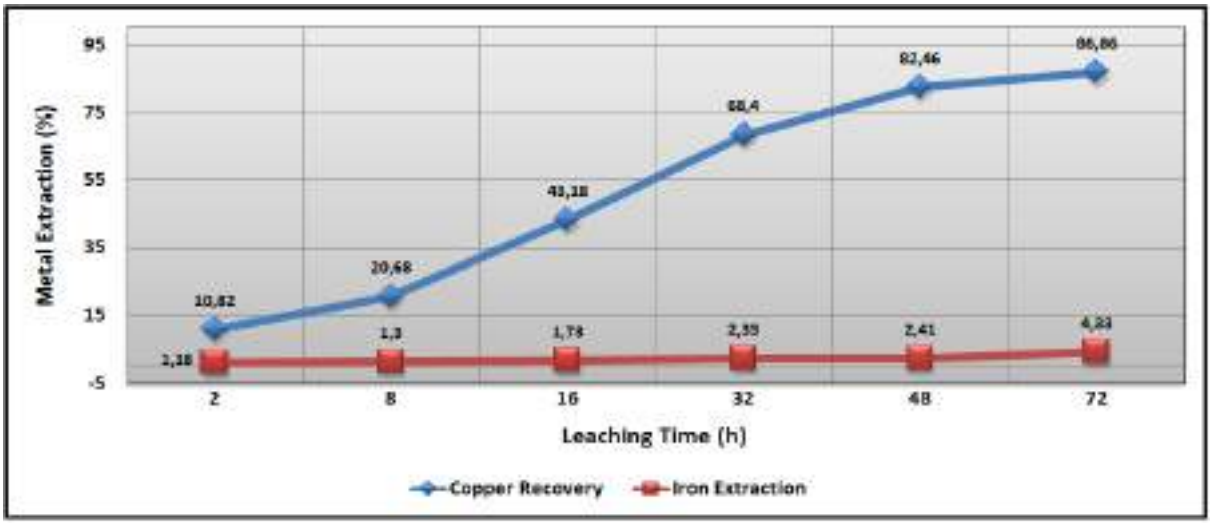

Figure 2. Effect of Leaching Time on Copper Recovery from Copper Converter Slag

As seen in Fig. 2, copper recovery increased significantly with the increasing of leaching time in deep eutectic solvent system and reached to nearly 87% after the

leaching of 72 hours. Although very low copper recoveries were obtained at less leaching durations, the rate of recovery was increased with increasing time, and the highest leaching efficiency was obtained after 72 hours of leaching time as 86.86%. According to the experimental results, only 4.4% of rising was achieved after leaching of 48 hours. That is, the increase of leach recovery of copper was not considerable beyond this point. Therefore, it can be said that leaching duration of 48 hours was sufficient for applicable copper recovery from copper converter slag by using DES agent.

On the other hand, Fig. 2 shows that iron dissolution from copper converter slag remains very low level and it does not changed with the leaching duration. From Fig. 2, it can be seen that deep eutectic solvents can be used to recover copper from copper converter slag with high ratio. Considering the low iron (Fe) dissolution even longer leaching duration, DES appears to be a good candidate for copper recovery from converter slag.

CONCLUSIONS

Deep eutectic solvent formed with choline chloride and urea was investigated for copper recovery from copper converter slag which includes remarkable amount of copper. According to the mineralogical determination, copper converter slag mainly composed with $FeSiO_4$ and Fe_3O_4 apart from other minor phases. After the leaching trials, it was determined that copper recovery increased by increasing leaching time and reached up to approximately 87%. It can be concluded that copper converter slag could be treated by using deep eutectic solvent with high copper recovery and low iron dissolution. The studies continue to determine the optimum leaching conditions for other leaching parameters such as temperature, solid/liquid ratio and stirring rate in DES solutions.

Acknowledgment

This work was supported by Karamanoglu Mehmetbey University Scientific Research Council (BAP) with project no KMU-BAP-17-M-18.

REFERENCES

Abbott, A. P., Collins, J., Dalrymple, I., Harris, R. C., Mistry, R., Qiu, F., ... & Wise, W. R. (2009). Processing of electric arc furnace dust using deep eutectic solvents. Australian journal of chemistry, 62(4), 341-347.

Altundoğan, H. S., & Tümen, F. (1997). Metal recovery from copper converter slag by roasting with ferric sulphate. Hydrometallurgy, 44(1-2), 261-267.

Altundogan, H. S., Boyrazli, M., & Tumen, F. (2004). A study on the sulphuric acid leaching of copper converter slag in the presence of dichromate. Minerals engineering, 17(3), 465-467.

Anand, S., Rao, P. K., & Jena, P. K. (1980). Recovery of metal values from copper converter and smelter slags by ferric chloride leaching. Hydrometallurgy, 5(4), 355-365.

Anand, S., Rao, K. S., & Jena, P. K. (1983). Pressure leaching of copper converter slag using dilute sulphuric acid for the extraction of cobalt, nickel and copper values. Hydrometallurgy, 10(3), 305-312.

Bakkar, A. (2014). Recycling of electric arc furnace dust through dissolution in deep eutectic ionic liquids and electrowinning. Journal of hazardous materials, 280, 191-199.

Basir, S. A., & Rabah, M. A. (1999). Hydrometallurgical recovery of metal values from brass melting slag. Hydrometallurgy, 53(1), 31-44.

Carranza, F., Romero, R., Mazuelos, A., Iglesias, N., & Forcat, O. (2009). Biorecovery of copper from converter slags: slags characterization and exploratory ferric leaching tests. Hydrometallurgy, 97(1-2), 39-45.

Rudnik, E., Burzyńska, L., & Gumowska, W. (2009). Hydrometallurgical recovery of copper and cobalt from reduction-roasted copper converter slag. Minerals Engineering, 22(1), 88-95.

Smith, E. L., Abbott, A. P., & Ryder, K. S. (2014). Deep eutectic solvents (DESs) and their applications. Chemical reviews, 114(21), 11060-11082.

Zhang, Q., Vigier, K. D. O., Royer, S., & Jerome, F. (2012). Deep eutectic solvents: syntheses, properties and applications. Chemical Society Reviews, 41(21), 7108-7146.

Rusen & Topcu 2017, thermal and mineralogical characterization of Converter slag JMESS.

SYNTHESIS AND CHARACTERIZATION OF QUATERNARY PERPENDICULARLY ALIGNED CXTS NANORODS

Adem SARILMAZ, Faruk ÖZEL

Department of Metallurgical and Materials Engineering, Faculty of Engineering, Karamanoğlu Mehmetbey
University, 70200, Karaman, Turkey.
adem.sarilmazz@gmail.com

ABSTRACT: In recent years, earth-abundant quaternary chalcogenides have been extensively studied due to their properties such as low-cost production and alternatives for conventional photovoltaic materials, which can significantly decrease the cost of devices (Mokurala et al. 2016, Ozel et al. 2016). In this study, we have successfully synthesized CXTS (X: Co, Zn, Mn and Ni) nanorods by a facile hot-injection method. Hot injection method provides to decrease reaction time and required pressure, therefore this process enables to achieve saving vast amount of energy and time. The resulting nanorods were characterized with X-ray diffraction (XRD), transmission electron microscopy (TEM), ultraviolet-visible (UV–Vis) spectroscopy and fourier transform infrared spectra (FTIR) techniques to investigate the crystal structure, composition, morphology, and band gap. All characterization results show that all of the synthesized nanorods showed good crystallinity with an average edge length ranging from 5 to 15 nm.

The authors would like to thank TUBITAK (P. No:217M212) for supporting this work.

Key words: Chalcogenides semiconductors, Nanorods, CXTS

REFERENCES

Mokurala, K., Mallick, S. & Bhargava, P. (2016). Alternative quaternary chalcopyrite sulfides (Cu_2FeSnS_4 and Cu_2CoSnS_4) as electrocatalyst materials for counter electrodes in dye-sensitized solar cells. *J. Power Sources, 305*, 134–143.
Özel, F., Sarılmaz, A., İstanbullu, B., Aljabour, A., Kuş, M., & Sönmezoğlu, S. (2016). Penternary chalcogenides nanocrystals as catalytic materials for efficient counter electrodes in dye-synthesized solar cells. Scientific reports, 6, 29207.

THIS PAGE IS INTENTIONALLY LEFT BLANK

SYNTHESIS OF REFRACTORY METAL BASED CHALCOGENIDE NANOSTRUCTURES WITH USING LIQUID SULFUR SOURCES

Adem SARILMAZ, Faruk ÖZEL

Department of Metallurgical and Materials Engineering, Faculty of Engineering, Karamanoğlu Mehmetbey
University, 70200, Karaman, Turkey.
adem.sarilmazz@gmail.com

ABSTRACT: Transition metal based chalcogenides are of great interest because of their suitable optical and electrical properties. The properties of these materials exhibit such qualities as semiconductor, narrow band-gap and high photocatalytic. Recently, refractory metal based sulfides which are one of the ternary compound materials have been used as photocatalyst for hydrogen production and dye sensitized solar cell (Gulen et al. 2018, Ozel et al. 2016). In this study Cu_2WS_4 (CWS) nanostructures a family of sulfide based ternary compound have been synthesized with liquid sulfur sources (Dodecanethiol and *Tert*-Dodecanethiol) by hot-injection method. Crystal structure, morphology and optical properties of synthesized nanostructures have been analyzed by X-ray diffraction (XRD), transmission electron microscopy (TEM) and ultraviolet-visible (UV–Vis) spectroscopy. The characterization results showed that the nanostructures were observed with good crystallinity and lacking of impurity. These results lead to the possibility of synthesizing a new generation of nanostructures with minimized reaction time as alternative energy conversion materials. In addition, high-quality nanostructures can be obtained with this method.

Key words: Chalcogenides semiconductors, Cu_2WS_4, Hot-injection synthesis

REFERENCES

Gulen, M., Sarilmaz, A., Patir, I. H., Ozel, F., & Sonmezoglu, S. (2018). Ternary copper-tungsten-disulfide nanocube inks as catalyst for highly efficient dye-sensitized solar cells. *Electrochimica Acta, 269*, 119-127.

Ozel, F., Aslan, E., Sarilmaz, A., & Hatay Patir, I. (2016). Hydrogen Evolution Catalyzed by Cu_2WS_4 at Liquid–Liquid Interfaces. *ACS applied materials & interfaces, 8(39)*, 25881-25887.

THIS PAGE IS INTENTIONALLY LEFT BLANK

A SMART HOME MODELING WITH LED SYSTEMS AND RENEWABLE ENERGY RESOURCES FOR MICROGRID FORMATION

Mehmet GÜÇYETMEZ
Ahi Evran University, Electric-Electronic Engineering Department, Kırşehir, Turkey
mgucuyetmez@ahievran.edu.tr, mehmetgcy@gmail.com

Mehmet Fatih TEFEK
Ahi Evran University, Department of Computer Technologies/ Computer Programming, Kırşehir, Turkey
mftefek@gmail.com

Serkan KESER
Ahi Evran University, Department of Electronic and Automation/ Electronic Technologies, Kırşehir, Turkey
skeser@ahievran.edu.tr

Mehmed Furkan YILMAZ
Ahi Evran University, Electric and Energy Department/ Electric, Kırşehir, Turkey
mehmedfurkanyilmaz@gmail.com

ABSTRACT: In the process of transition from conventional electricity networks to smart networks, it is first necessary to construct a microgrid structure. In the microgrid structure, the generation of electricity, the LED systems and the storage of the energy are the most important components. On the other hand, houses have an important place in microgrid architecture. Because a house that can not use its own energy optimally will not be efficient in the electricity distribution system. In this respect, it is important to establish a smart house model in which energy is generated from renewable energy sources such as wind and solar energy, the communication system is present, and at the same time all these components, which are stored and recalled, work in harmony with the conventional electricity grid.
Looking at the studies on smart home models, there are no studies based on energy efficiency, as there are studies related to control and automation of parts gas leak, humidity, window, garage door, etc. In this study, firstly the different studies about smart houses are mentioned and thus the last situation reached on these models is revealed. Then developed smart home energy generation, storage, communication has been mentioned. A software that controls the energy related to the model has been developed and information about this software has been given. The study will also form a model for the creation of larger projects and houses that have a large share in the transition to micro and smartgrids.

Key words: Smart home, microgrid, smartgrid, renewable energy, energy control

This work was supported by Ahi Evran University with MMF.A4.18.016 project number.

THIS PAGE IS INTENTIONALLY LEFT BLANK

A STUDY ON THE POSSIBLE USE OF INDUSTRIAL WASTE IN ROLLER-COMPACTED CONCRETE PAVEMENT

Gökhan KAPLAN[1], H.Yılmaz ARUNTAŞ[2], Rüya KILIÇ DEMİRCAN[2], A.Burcu GÜLTEKİN[3]
[1]Kastamonu University, Kastamonu Vocational School, Kastamonu/TÜRKİYE
[2]Gazi University, Faculty of Technology, Department of Civil Engineering, Ankara/TÜRKİYE
[3]Ankara University, Faculty of Applied Sciences, Department of Real Estate Development and Management, Ankara/TÜRKİYE

ABSTRACT: Pavement is categorized under two headings: asphalt (flexible) pavement and concrete (rigid) pavement. In the last decade, the use of concrete pavement has increased due to its superior durability and longer life cycle when compared to asphalt pavement. Moreover, the materials used to produce concrete pavement are supplied conveniently and in a more cost-effective manner in comparison. Today, roller-compacted concrete pavement (RCCP) is the method commonly preferred for road construction. RCCP is a zero-slump (dry-mix) concrete mixture. The most important advantages of RCCP over traditional concrete are the reduced time needed for construction and its low cost. RCCPs do not lend themselves to application of load transfer devices such as dowels or keyed joints and do not require surface finishing. Another quality of RCCP, as distinguished from traditional concrete, is the use of reduced cement and increased mineral additive content of the mix. The use of active mineral additives such as fly ash (FA) in RCCPs bears environmental significance. The use of industrial waste such as fly ash (FA), silica fume (SF) and blast-furnace slag (BFS) as additives in concrete production has been increasing with an emphasis on environmental sustainability and they have become components of concrete. Also known as artificial pozzolans, these mineral additives are proven to offer important benefits to the concrete technology, in terms of both economy and environment. Among the technical reasons behind the use of mineral additives are the workability of fresh concrete and the durability of hardened concrete. In some cases, economic and environmental aspects may prevail over technical ones. With the use of artificial pozzolans, it is possible to reduce the amount of cement used for concrete production which translates into positive economic and environmental outcomes. Nevertheless, most of the mineral additives consist of industrial by-products which can be considered as waste material. This study explored the characteristics of a number of industrial waste materials which can be used in RCCP applications. The effect of the use of industrial waste matter such as FA, BFS, SF, rice husk ash, biofuel ash, electric arc furnace slag, sewage sludge ash, glass powder and waste marble powder on fresh and hardened concrete properties is analyzed. Moreover, durability of the industrial waste used in concrete pavement is explored in the literature review.

Keywords: Industrial Waste, Roller-Compacted Concrete, Ecology, Sustainability

SİLİNDİRLE SIKIŞTIRILMIŞ BETON YOL KAPLAMALARINDA ENDÜSTRİYEL ATIKLARIN KULLANIM OLANAKLARININ İNCELENMESİ

Gökhan KAPLAN[1], H.Yılmaz ARUNTAŞ[2], Rüya KILIÇ DEMİRCAN[2], A.Burcu GÜLTEKİN[3]
[1]Kastamonu Üniversitesi, Kastamonu Meslek Yüksekokulu, Kastamonu/TÜRKİYE
[2]Gazi Üniversitesi, Teknoloji Fakültesi, İnşaat Mühendisliği Bölümü, Ankara/TÜRKİYE
[3]Ankara Üniversitesi, Uygulamalı Bilimler Fakültesi, Gayrimenkul Geliştirme ve Yönetimi Bölümü, Ankara/TÜRKİYE

ÖZET: Yol kaplamaları; kullanılan malzemelere göre asfalt (esnek) kaplama ve beton (rijit) kaplama olarak iki sınıfa ayrılmaktadır. Son yıllarda, beton kaplamaların kullanımı, asfalt kaplamalara göre üstün dayanıklılık ve daha uzun yapısal ömürlerinden dolayı artış göstermektedir. Ayrıca beton kaplamalarda kullanılan malzemelerin temin edilmesi nispeten daha kolay ve ucuzdur. Günümüzde beton yol yapımında genellikle silindir ile sıkıştırılmış beton (SSB) yollar tercih edilmektedir. SSB, nemli ve katı kıvama sahip (sıfır slump) bir beton türüdür. SSB beton yolların geleneksel beton yollara göre en büyük avantajı yapım hızı ve maliyetinin düşük olmasıdır. SSB'lerde kalıp, bağlantı demiri ve yüzey bitirme işlemine ihtiyaç duyulmaz. SSB'yi geleneksel betondan ayıran en önemli özelliklerden bir tanesi de, karışımda düşük çimento ve yüksek mineral katkı kullanılmasıdır. SSB yol kaplamalarında, uçucu kül (UK) gibi aktif mineral katkılarının kullanılması çevresel açıdan büyük önem taşımaktadır. Çevresel sürdürülebilirlik açısından UK, silis dumanı (SD) ve yüksek fırın cürufu (YFC) gibi endüstriyel atık katkı malzemelerinin beton üretiminde kullanımı büyük oranda artış göstermiş ve betonun bileşenlerinden biri haline gelmiştir. Aynı zamanda yapay puzolan olan bu mineral katkılar teknik, ekonomik ve çevresel açıdan beton teknolojisine büyük yararlar sağlamaktadır. Mineral katkı kullanımının teknik sebepleri arasında taze betonun işlenebilirliği ve sertleşmiş betonun dayanıklılığı bulunmaktadır. Bazı uygulamalarda ekonomik ve çevresel nedenler teknik nedenlerden daha önemli olabilmektedir. Yapay puzolanlar, beton üretiminde kullanılan çimento miktarının azaltılmasını sağlayarak hem ekonomik hem de çevresel faydalar sağlamaktadır. Ayrıca, mineral katkı maddelerinin çoğu atık olarak kabul edilebilecek endüstriyel yan ürünlerden oluşmaktadır. Bu çalışmada, SSB uygulamalarında kullanılabilecek bazı endüstriyel atıkların özellikleri ele alınacaktır. UK, YFC, SD, pirinç kabuğu külü, biyoyakıt külleri, elektrik ark fırını cürufları, arıtma çamuru atığı külleri, cam tozu ve mermer tozu gibi endüstriyel atıkların taze ve sertleşmiş beton özellikleri üzerindeki etkileri ortaya konulacaktır. Ayrıca, beton yollarda kullanılan endüstriyel atıkların durabilite ile ilişkisi literatür taraması kapsamında incelenecektir.

Anahtar Kelime: Endüstriyel Atıklar, Silindirle sıkıştırılan beton, Ekoloji, Sürdürülebilirlik.

A STUDY ON THE WATER CONSERVATION MEASURES IN GREEN BUILDINGS

A.Burcu GÜLTEKİN[1], Gökhan KAPLAN[2*], Rüya KILIÇ DEMİRCAN[3], H.Yılmaz ARUNTAŞ[3]

[1]Ankara Üniversitesi, Uygulamalı Bilimler Fakültesi, Gayrimenkul Geliştirme ve Yönetimi Bölümü, Ankara/TÜRKİYE
[2*]Kastamonu Üniversitesi, Mühendislik-Mimarlık Fakültesi, İnşaat Mühendisliği Bölümü, Kastamonu/TÜRKİYE gkaplan@kastamonu.edu.tr
[3]Gazi Üniversitesi, Teknoloji Fakültesi, İnşaat Mühendisliği Bölümü, Ankara/TÜRKİYE

ABSTRACT:71.7% of the Earth's surface is covered with water. However, only 3% of this vast amount of water is potable. Today, water conservation is gaining more and more importance with the rapid increase in the world's population. There is a growing focus on green buildings on a global scale in order to minimize the use of natural resources, to eliminate the adverse impact on the ecology and to restore the environment. Due to the increasing need for water, certification authorities included water conservation as one of their fundamental assessment measures for green building certification. A number of rating systems are developed for green buildings in different nations depending on the level of environmental targets. Green buildings are currently assessed for measures such as their energy efficiency, water conservation, and indoor air quality. Among these measures, water is a finite resource and it is of importance to reduce water consumption. The concept of water conservation resonates with both the reduced water consumption and the water efficiency. Among the commonly used building technologies for water efficiency is water-efficient fittings. Moreover, recycling and harvesting of rainwater and greywater reuse contribute to water conservation. Greywater is the wastewater obtained from bathroom and kitchen areas with a high level of organic matter content. After being recycled, greywater can be reused thanks to its reduced organic matter content. This study explores the assessment measures included to green building certification systems in relation with water conservation. In this context, the water conservation measures available in BREEAM, LEED, DGNB and CEDBIK Certification systems are studied and compared.
Keywords: Green building, wastewater, water conservation, greywater, black water

YEŞİL BİNALARDA SU KORUNUMU ÖLÇÜTLERİNİN İNCELENMESİ

A.Burcu GÜLTEKİN[1], Gökhan KAPLAN[2*], Rüya KILIÇ DEMİRCAN[3], H.Yılmaz ARUNTAŞ[3]

[1]Ankara Üniversitesi, Uygulamalı Bilimler Fakültesi, Gayrimenkul Geliştirme ve Yönetimi Bölümü, Ankara/TÜRKİYE
[2*]Kastamonu Üniversitesi, Mühendislik-Mimarlık Fakültesi, İnşaat Mühendisliği Bölümü, Kastamonu/TÜRKİYE gkaplan@kastamonu.edu.tr

[3]Gazi Üniversitesi, Teknoloji Fakültesi, İnşaat Mühendisliği Bölümü, Ankara/TÜRKİYE

ÖZET: Dünya yüzeyinin %71.7'si su ile kaplıdır. Ancak toplam suyun sadece %2,5'i içme suyu olarak kullanılabilmektedir. Günümüzde nüfusun hızla artışı ile suyun korunumu büyük bir önem kazanmıştır. Doğal kaynakların kullanımını en aza indirmek, ekoloji için zararlı etkileri azaltmak ve temiz bir çevre yaratmak için dünya çapında yeşil binaların yapımı hız kazanmıştır. Artan su talebi sonucunda yeşil binaların tasarımında su korunumu ilkesi, yeşil bina sertifika sistemlerinde temel değerlendirme ölçütlerinden biri konumuna gelmiştir. Bazı ülkelerde yer alan yeşil binalarda, çevresel hedeflerin derecesine göre farklı derecelendirme sistemleri geliştirilmiştir. Yeşil binalar; enerji verimliliği, su korunumu, iç mekan hava kalitesi gibi ölçütlere göre derecelendirilmektedir. Bu ölçütler içerisindeki su, sınırlı bir kaynak olduğundan tüketilen suyun korunumu büyük önem taşımaktadır. Su korunumu, suyun kullanımındaki azalmanın yanı sıra su israfındaki azalmayı da ifade etmektedir. Binalarda su tasarrufu esaslı teknolojiler ağırlıklı olarak su tasarruflu armatürleri içermektedir. Ayrıca yağmur suyunun biriktirilerek geri dönüşümü ve gri suyun yeniden kullanımı da su korunumuna katkı sağlamaktadır. Bu çalışmada, suyun korunumu için yeşil bina sertifika sistemlerinde yer alan değerlendirme ölçütleri dikkate alınmıştır. Bu kapsamda; BREEAM, LEED, DGNB ve ÇEDBİK Konut Sertifikası sistemlerinde su korunumuna ilişkin ölçütler incelenmiş ve karşılaştırılmıştır.

Anahtar Kelimeler: Yeşil bina, atık su, su korunumu, su verimliliği, gri su, siyah su.

1.GİRİŞ

Dünya üzerinde toplam su miktarı 1,4 milyar km^3'tür. Dünyanın dörtte üçünü kaplayan ve oldukça fazla görünen bu miktara rağmen su sorunu yaşanmaktadır. Bunun nedeni, dünyada toplam su miktarının %97,5'inin okyanuslar ve denizlerde tuzlu su olarak yer almasıdır. Geriye kalan %2,5'lik miktar ise dünya üzerindeki tatlı su miktarına karşılık gelmektedir. Hesaplamalar ışığında dünya üzerinde toplam tatlı su miktarının sadece 35,2 milyon km^3 olduğu söylenebilir. Bu kadar az olan tatlı su kaynaklarının da %90'ının kutuplarda ve yer altında hapsedilmiş olarak bulunması sebebiyle insanoğlunun kolaylıkla yararlanabileceği elverişli tatlı su miktarının ne kadar az olduğu anlaşılmaktadır (Atalık 2007).

Su, içme ve kullanma, sulama, enerji üretimi ve ekosistem için vazgeçilmezdir. İnsan nüfusunun son 20 yıl içinde belirgin biçimde artmasıyla su kaynaklarına olan talep de giderek artmaktadır. Bu durum, insanları su kaynaklarını daha planlı, etkin ve verimli şekilde kullanmak için çeşitli çareler aramaya yöneltmiştir. Tüm dünyada olduğu gibi Türkiye'de de hızlı nüfus artışı, kentleşme ve sanayileşme ile kullanılabilir suya talep artmıştır. Bu talepler doğrultusunda; su kaynakları ve potansiyeli, suyun etkin şekilde kullanımı ve korunması, su yönetim planlamaları gibi konular büyük önem kazanmıştır (Özsoy 2009).

Türkiye su zengini bir ülke değildir. Kişi başına düşen yıllık su miktarına göre ülkemiz su kıtlığı yaşayan bir ülke konumundadır. Devlet Su İşlerinin (DSİ) su potansiyeli hesaplarına göre Türkiye kişi başına yıllık 1.652 m^3 su potansiyeline sahiptir.

Öngörülere göre Türkiye nüfusu 2030 yılında 100 milyona ulaşacak ve su potansiyeli kişi başına yıllık 1.120 m^3'e düşecektir. Türkiye su sıkıntısı yaşayan ülkeler arasında yer alacak ve kaynakların çok daha etkin kullanmayı amaçlayan politikalar izlemek durumunda kalacaktır (Çevre ve Şehircilik Bakanlığı, 2016). Tüm bu öngörüler doğrultusunda suyun etkin bir şekilde kullanımına ilişkin atık suyun yeniden değerlendirilerek kullanıma kazandırılması önemli bir boyut kazanmıştır (Şahin D 2016).

Artan su talebi, yükselen alternatif doğal su kaynakları fiyatları ve gelişen geri kazanma teknolojileri, atık suların tekrar kullanılmasını hem çevre ve hem de kaynakların ekonomik kullanımı yönünden cazip hale getirmektedir. Atık suların geri kazanılarak tekrar kullanılması potansiyelini artıran en önemli sebepler; şehirlerde nüfus oranlarının artması sebebiyle su ihtiyaçlarının belirli merkezlerde yoğunlaşması ve deşarj edilen atık sular için verilen deşarj standartlarının ve arıtma seviyelerinin giderek yükselmesi olarak ifade edilebilir (Aslan V. 2008).

Kentleşme ile suyun etkin şekilde kullanımı beraber düşünüldüğünde, akılcı kullanımları bir arada bulunduran yeşil bina kavramı ortaya çıkmaktadır. Yeşil binalar ekolojik, doğa dostu, konforlu, enerji tüketimini en aza indiren yani sürdürülebilirlik kavramının temel ilkelerini bir arada bulunduran yapı sistemleridir. Gelişmiş ülkelerde yaygın olmakla beraber, Türkiye'de de uygulanma sıklığı giderek artmaktadır. Günümüzde yeşil binalar için derecelendirme yapılmasına olanak sağlayan yeşil bina sertifika sistemleri bulunmaktadır. Bu sistemlerin dünya genelinde geçerlilikleri kabul görmüş olup yaygın şekilde kullanılanları İngiltere, ABD ve Almanya'da sırasıyla LEED (Leadership in Energy Efficiency Design), BREEAM (BRE Environmental Assessment Method) ve DGNB (Die Deutsche Gesellschaft für Nachhaltiges Bauen) sertifikalarıdır. Ayrıca, uluslararası sertifika sistemleri örnek alınarak Türkiye'de yerel koşullara uygun olarak geliştirilen ulusal ÇEDBİK (Çevre Dostu Yeşil Binalar Derneği) Konut Sertifikası mevcuttur. Gelişen teknoloji, değişen gereksinimler ve geliştirilen yeni stratejilere bağlı olarak süreç içerisinde kurumlar söz konusu sertifika sistemlerinin yeni sürümlerini oluşturmaktadır.

Atık suların arıtılarak geri kazandırılması, taze su kullanımının yüksek oranlarda düşürülmesi ve atık suyun yeniden kullanılmasını sağlayan yeşil binalar hakkında yapılan çalışmalar günümüzde önem kazanmıştır. Bu çalışmalarda geleneksel yöntemlerle inşa edilmiş binalar ile yeşil binalar arasından yapılan karşılaştırmalara göre göre, yeşil binalarda taze suyun tüketiminin %30-%50 oranında azaltılabileceği vurgulanmaktadır (Diang, G. 2008). Bu azaltım daha çok atık suyun geri dönüşümü sağlanarak kazanılmaktadır. Yeşil binalarda su korunumu; BREEAM, LEED, DGNB ve ÇEDBİK Konut sertifikası sistemlerinde farklı değerlendirme ölçütleri kapsamında sınıflandırılmaktadır. Bu çalışmada, yeşil binalarda uygulanan su korunumu ölçütlerinin söz konusu sertifika sistemleri çerçevesinde karşılaştırması yapılmıştır.

2. YEŞİL BİNALARDA SU KORUNUMU

Yüksek performanslı yeşil binalar, küreselleşen su problemlerine ve bina hidrolik döngüsüne ait iki temel bileşene hitaben, en azından kısmi çözümler getiren alışılmamış yeni yaklaşımlar geliştirmektedir. İçilebilir su temini ve atık suyun uzaklaştırılması bu iki ana bileşeni oluşturmaktadır. Binalarda su tüketiminin

azaltılması ve bina çevresi için kullanılan atık su stratejilerinin yeniden düşünülmesi, uygun su kaynaklarının kapsamını önemli ölçüde genişletmektedir. Geliştirilen stratejiler, insan sağlığına verilen değeri arttırmakta ve ekolojik sistem üzerindeki tehdidi azaltmaya katkı sağlamaktadır (U.S. Department of Energy 2001).

2.1. Binalarda Atık Su Oluşumu

Binalarda oluşan atık sular, siyah ve gri su olarak sınıflandırılabilir. Genel anlamda insan atıklarını içeren su, siyah su olarak tanımlanmaktadır. Ancak, içinde petrol yağı, yemek yağı ve yemek kırıntıları barındırdığı için mutfak lavaboları ve bulaşık makinelerinden gelen su da siyah su kapsamına alınabilmektedir. Küvet, duş, banyo lavabosu, çamaşır makinesi ve çeşmelerden gelen su, gri su olarak tanımlanmaktadır. Ayrıca soğutma ekipmanları ve klimalardan gelen yoğuşma suyu, sıcak küvet, havuz ve çeşme, sarnıç ve drenaj suları da gri su kapsamında ele alınmaktadır.

Mutfak ve banyo gibi mahallerde açığa çıkan yüksek oranda organik madde içeren evsel atık sular, gri su olarak tanımlanmaktadır. Gri su geri dönüştürüldükten sonra düşük organik madde içeriği sayesinde tekrar kullanılabilmektedir. Gri su, minimum miktarda kirlilik içermektedir. Bu sebeple, bazı peyzaj uygulamalarında yeniden kullanılabilmektedir. Bu konu, kamu sağlığı yetkilileri tarafından hala tartışma konusu olsa da, literatürde gri suyun geri kullanımının sebep olduğu herhangi bir hastalığa rastlanmamıştır. Gerek siyah su gerekse gri su insanların uzak durması gereken patojenler içermektedir. Ancak siyah suyun, su kaynaklı hastalıkların bulaşması konusunda çok daha yüksek risk taşıdığı söylenebilir (Kantaroğlu Ö 2011).

2.2. Yeşil Binalarda Atık Suyun Değerlendirilmesi

ABD'de yeşil binalarda geri dönüştürülmüş siyah su ve gri su genellikle sulama suyu olarak değerlendirilmektedir. Ancak, söz konusu atık suların potansiyel kullanım alanları sulamadan çok daha geniş bir alanı kapsamaktadır. Bu alanlar, içilebilir su temini, peyzaj ve tarımsal sulama, soğutma kuleleri, endüstriyel işlemler, tuvaletlerde sifon suyu temini, yangından korunma, kazan besleme, beton karıştırma, dekoratif özellikli çeşme ve fıskiyeler olarak sınıflandırılabilir (Kantaroğlu Ö 2011).

Gri suyun toplanması, gri suyu tuvaletler ve pisuarlardan gelen siyah sudan ayırma işlemini gerektirmektedir. Gri su, genellikle peyzaj sulaması için kullanılmakta olsa da tuvalet ve pisuarların rezervuarları da gri suyun kullanım alanları kapsamına girmektedir. Gri suyun kullanımında dikkat edilmesi gereken husus, kullanılmadan önce çok uzun süre saklanmaması gerektiğidir. Uzun süre saklanan gri suyun yapısındaki mikroorganizmaların organik maddeleri ayrıştırarak ortamdaki oksijeni hızlıca tüketmesi ve böylece anaerobik bakterilerin ortamı teslim almasıyla kötü koku problemi ortaya çıkabilmektedir (Ludvig A 1999). Ayrıca, birçok gri su sistemi için filtre bakımı da büyük bir sorun olarak ortaya çıkmaktadır. Patojenlere karşı tam bir koruma için gri suyun yerçekimi ile ya da yeraltındaki atık alanına pompalanarak akması sağlanmalıdır. Genel bir kural olarak gri suyun çimen, çiçek, ağaç ve çalıların yer altı sulamaları için kullanılabileceği ancak, meyve ve sebze bahçeleri için kullanılmasının uygun olmadığı ifade edilebilir (California Department of Water Resources 1995).

3. YEŞİL BİNA SERTİFİKA SİSTEMLERİ KAPSAMINDA ATIK SULARIN DEĞERLENDİRİLMESİ

Dünyada kullanılan farklı yeşil bina sertifika sistemleri incelendiğinde, su kullanımının her bir sistemde ayrı bir değerlendirme ölçütü başlığı olarak ele alındığı görülmektedir. Söz konusu ölçütlerde su kullanımının azaltılması, doğal su döngüsü ve su kaynaklarının korunması gibi stratejiler üzerinden değerlendirme yapılmaktadır. Hedeflenen stratejilerin gerçekleştirilmesiyle sağlanan su tasarrufu, atık su arıtma altyapısı yatırım maliyetlerinin azaltılmasına ve su faturalarına doğrudan yansıdığı için işletim maliyetlerinin büyük oranda düşmesine katkı sağlamaktadır (Web Kaynağı-1 2018). Bu çalışma kapsamında BREEAM, LEED, DGNB ve ÇEDBİK Konut Sertifikası sistemleri tarihsel sırayla ele alınmıştır. Söz konusu sistemler, genel değerlendirme ölçütleri başlıkları ve bu başlıklardan su verimliliğine ilişkin alt başlıklar kapsamında incelenmiştir.

3.1. BREEAM Sertifika Sistemi Kapsamında Atık Suların Değerlendirilmesi

İngiltere'de Yapı Araştırma Kurumu (Building Research Establishment-BRE) tarafından geliştirilerek 1990 yılında uygulamaya geçirilen BREEAM, ölçütlere dayalı yeşil bina sertifika sistemlerinin ilk örneğidir (Gültekin AB., Bulut B. 2015). BREEAM'i oluştururken kurumun hareket noktası, sürdürülebilir kalkınmanın en geniş kapsamlı bileşeni olan çevresel kalkınma olmuştur (Sev,A. Canbay N. 2009). Sistem, ilk başta konut dışındaki binalar için geliştirilmiş (Yapı Dergisi 2009) olsa da günümüzde imar planları, altyapı ve tüm binalar için kullanılan bir sürdürülebilir değerlendirme yöntemidir. BREEAM, BRE tarafından geliştirilen standartları kullanarak, bir varlığın çevresel, sosyal ve ekonomik sürdürülebilirlik performansının değerlendirmesini üçüncü taraf sertifikasyonu aracılığıyla gerçekleştirmektedir. Böylece yeni bina, kullanım ve yenileme evreleri dahil olmak üzere yapılı çevrenin yaşam döngüsü boyunca yüksek performanslı olmasına katkı sağlamaktadır (Web Kaynağı-2 2018).

BREEAM resmi internet sitesinden Kasım 2018 itibariyle alınan bilgiye göre günümüzde 78 ülkede, 565.890 adet sertifikalı ve 2.275.207 adet sertifikaya aday bina mevcuttur (Web Kaynağı-2 2018). BREEAM sertifika sistemine göre binaların çevresel performansları, ağırlıklı puan sistemi ile on farklı değerlendirme ölçütü kapsamında 110 puan üzerinden değerlendirilmektedir. Puanlar binanın her bir değerlendirme ölçütü için gösterdiği performansa göre belirlenmekte ve her bir ölçütün çevresel etkilerine göre ağırlık katsayısı atanmaktadır (BREEAM 2011). Söz konusu değerlendirme ölçütleri ve her bir ölçüte ait puanların Avrupa'daki ağırlıkları Çizelge 3.1'de sunulmaktadır. Su verimliliği ölçütünün diğer değerlendirme ölçütlerine göre oranı % 5.45'tir.

Çizelge 3.1. BREEAM genel değerlendirme ölçütleri başlıkları (Web Kaynağı-3)

BREEAM Değerlendirme Ölçütleri	**Puan (%)**
Enerji	19.0
Sağlık ve refah	15.0
Yenilikçilik	10.0
Arazi kullanımı	10.0
Malzemeler	12.5

Yönetim	12.0
Kirlilik	10.0
Ulaşım	8.0
Atık	7.5
Su	*6.0*
TOPLAM	110

BREEAM sertifika sisteminin su korunumu açısından amacı, temiz su kaynakları azalan dünyada su tüketimini azaltan sistemleri teşvik etmek ve bu konuda yapılan çalışmaları ödüllendirmektedir. Bu bağlamda, BREEAM sertifika sisteminde "su" değerlendirme ölçütü, binanın ve arsasının işletilmesinde sürdürülebilir su kullanımını teşvik etmektedir. Bu ölçütün alt başlıkları, binanın kullanım ömrü boyunca içme suyu tüketimini (iç ve dış) azaltmanın ve sızıntı yoluyla kayıpları en aza indirmenin yöntemlerini tanımlamaya odaklanmaktadır. Söz konusu alt başlıklar ve yöntemler, Çizelge 3.2'de verilmektedir.

Çizelge 3.2. BREEAM "su" değerlendirme ölçütü alt başlıkları (BREEAM 2018)

Alt başlıklar	**Yöntemler**	**Puan**
Su Tüketimi	Etkin sıhhi tesisat armatürleri, yağmur suyu toplama ve su geri dönüşüm sistemlerinin sağlanması yoluyla içme suyu ihtiyacının azaltılması	Asgari 5
Suyun Denetlenmesi	Binada suyun fazla kullanıldığı alanları belirlemek ve bu durumun olası nedenlerini araştırmak amacıyla binadaki su kullanımının yönetilmesini ve izlenmesini sağlayan su sayaçlarının tanımlanması, böylelikle su kullanımındaki azalmaların teşvik edilmesi	Asgari 1
Su Kaçağının Tespit Edilmesi	Sızıntılar nedeniyle istenmeyen su tüketiminin azaltılması için kaçak tespit sistemleri ve akış kontrol cihazları kurulması	2
Su Verimli Ekipmanlar	Bina dışı ölçekteki su tüketiminin azaltılması, etkin sistemler belirleyerek sıhhi olmayan suyun kullanımın sağlanması ve herhangi bir su kullanım işleminin tasarım verimliliğinin geliştirilmesi	1

BREEAM İngiltere ve BREEAM Avrupa versiyonlarında su ile ilgili değerlendirme yeni binalar, eklentiler, mevcut binaların iyileştirilmesi için %6 ve bina donanımları için %7 oranında ağırlığa sahip olup kendi içerisinde su ile ilgili krediler ve değerleri değişebilmektedir. Ancak, BREEAM Körfez Ülkeleri versiyonunda su ile ilgili değerlendirme %30 oranında ağırlığa sahiptir (Şahin Nİ 2010).

3.2. LEED Sertifika Sistemi Kapsamında Atık Suların Değerlendirilmesi

1998'de Amerikan Yeşil Bina Konseyi (USGBC) tarafından yeşil binaların sertifikalandırılmasına yönelik ortaya çıkan LEED, inşaat sektörünün sürdürülebilirlik konusunda kendisini geliştirmesi düşüncesiyle geliştirilmiş bir yeşil bina sertifika sistemidir. Amerika Yeşil Binalar Derneğinin (USGBC) yaptığı çalışmaya göre ABD'de binalar, tüm CO_2 salımlarının %38'ine, tüm içme suyu tüketiminin %13,6'sına ve ABD'deki elektrik tüketiminin % 73'üne sebep olmaktadır. Bu bağlamda, LEED

sertifikası kaynak verimli, yüksek performanslı, sağlıklı ve uygun maliyetli binaların tasarım, yapım, işletim ve bakımını teşvik etmektedir. Daha sağlıklı, daha üretken, enerji ve kaynak açısından daha verimli binaların üretilmesine; bina değerlerinin artmasına, kira oranlarının yükselmesine ve işletme maliyetlerinin azalmasına katkı sağlamaktadır. Ayrıca, LEED sertifikalı binaların 2018 yılı sonuna kadar ABD gayri safi yurtiçi hasılasına doğrudan 29,8 milyar dolar katkıda bulunacağı öngörülmektedir (Web Kaynağı-4 2018).

LEED resmi internet sitesinden Kasım 2018 itibariyle alınan bilgiye göre günümüzde toplam 15 milyar metrekareden oluşan 160 ülke ve bölgede, 79,000 adet LEED sertifikası mevcuttur. Ayrıca her gün ortalama 1.85 milyon metrekarelik inşaat alanı sertifikalandırılmaktadır (Web Kaynağı-4 2018). LEED sertifika sistemine göre binaların çevresel performansları sekiz farklı değerlendirme ölçütü kapsamında 110 puan üzerinden değerlendirilmektedir. Söz konusu değerlendirme ölçütleri ve her bir ölçüte ait puanlar Çizelge 3.3'te sunulmaktadır. Su verimliliği ölçütünün diğer değerlendirme ölçütlerine göre oranı % 10'dur.

Çizelge 3.3. LEED genel değerlendirme ölçütleri başlıkları (Gültekin AB., Bulut B. 2015)

LEED Değerlendirme Ölçütleri	**Puan**
Konum ve ulaşım	16
Sürdürülebilir araziler	10
Su verimliliği	*11*
Enerji ve atmosfer	33
Malzeme ve kaynaklar	14
Yapı içi çevre kalitesi	16
Tasarımda yenilikçilik	6
Bölgesel öncelik	4
TOPLAM	110

LEED sertifika sisteminin su verimliliği açısından amacı, verimli cihazlar ve armatürler ile iç mekanlarda ve su esaslı çevre düzenlemesi ile dış mekanlarda su tasarrufu sağlamaktır. Bu bağlamda, LEED sertifika sisteminde "su verimliliği" ölçütü, suyun içeride ve dışarıda daha akıllı kullanımını teşvik etmektedir. Bu ölçütün alt başlıkları, bina içi ekipmanların su tasarruflu seçilmesi, bina yaşam döngüsü boyunca bakım ve sulamada kullanılacak suyun asgari düzeyde tutulması, içme suyunun sulama ve tuvaletlerde kullanılmaması ve gri suyun arıtılarak yeniden kullanılması gibi yöntemleri tanımlamaktadır (Çelik E. 2009). Söz konusu alt başlıklar ve yöntemler, Çizelge 3.4'te verilmektedir.

Çizelge 3.4. LEED "su verimliliği" değerlendirme ölçütü alt başlıkları (The U.S. Green Building Council 2018)

Alt Başlıklar	**Puan**
Dış Mekan Su Kullanımının Azaltılması	Önkoşul
İç Mekan Su Kullanımının Azaltılması	Önkoşul

Bina Düzeyinde Su Ölçümü	Önkoşul
Dış Mekan Su Kullanımının Azaltılması	1-2
İç Mekan Su Kullanımının Azaltılması	1-7
Soğutma Kulesi Suyu Kullanılması	1-2
Su Ölçümü	1

3.3. DGNB Sertifika Sistemi Kapsamında Atık Suların Değerlendirilmesi

DGNB, binaların planlaması ve değerlendirilmesinde kullanılmak üzere Alman Yeşil Bina Derneği (DGNB) ve Ulaşım, İnşaat ve Kentsel İlişkiler Birleşmiş Bakanlığı ortaklığında ofis ve yönetim binaları için 2008 yılında oluşturulmuş bir yeşil bina sertifika sistemidir. Sistem zaman içerisinde geliştirilerek mevcut ve yeni binalar, eğitim kurumları ve ticari binalar dahil olmak üzere dokuz bina tipini kapsayacak duruma getirilmiştir (DGNB 2011). Uluslararası düzeyde uygulanabilir bir sistem olan DGNB'nin diğer sistemlerden farkı, binaları holistik bir yaklaşım ile tüm yaşam döngüleri boyunca değerlendirmesidir.

DGNB resmi internet sitesinden Kasım 2018 itibariyle alınan bilgiye göre günümüzde toplam 23 ülkede 1048 DGNB sertifikalı ve 283 DGNB ön sertifikalı bina mevcuttur (Web Kaynağı-5 2018). DGNB sertifika sistemine göre binaların ya da kentsel bölgelerin çevresel performansı altı farklı değerlendirme ölçütü kapsamında yüzdelik puan üzerinden değerlendirilmektedir. Binaların değerlendirmesi ısıl konfor, ulaşım, akustik konfor gibi farklı alt ölçütlere göre yapılmaktadır. Kentsel bölgelerin sertifikalandırılması için ise bölgesel iklim değişikliği, biyolojik çeşitlilik ve etkileşim, sosyal ve işlevsel çeşitlilik ölçütleri uygulanmaktadır (Web Kaynağı-6 2018). Söz konusu değerlendirme ölçütleri ve her bir ölçüte ait yüzdelik puanları Çizelge 3.5'te sunulmaktadır.

Çizelge 3.5. DGNB genel değerlendirme ölçütleri başlıkları (Web Kaynağı-7)

DGNB Değerlendirme Ölçütleri	**Binalar için Puan (%)**	**Kentsel Bölgeler için Puan (%)**
Çevresel Nitelik	22.5	22.5
Ekonomik Nitelik	22.5	22.5
Sosyo-Kültürel ve İşlevsel Nitelik	22.5	22.5
Teknik Nitelik	22.5	22.5
Süreç Niteliği	10	10
Arazi Niteliği	100	100

DGNB sertifika sisteminde su ile ilgili bir değerlendirme ölçütü başlığı yer almamaktadır. Ancak, su ile ilgili alt başlıklar her bir değerlendirme ölçütünün altına entegre edilmiştir. DGNB sertifika sisteminin su verimliliği açısından amacı, gri su ve yağmur suyunun kullanılması ile tatlı su tüketiminin azaltılmasını sağlamaktır. Bu bağlamda, DGNB sertifika sistemi temizlik ve bakımı kolay yapı elemanları ile az miktarda deterjan ve su kullanımını teşvik etmektedir.

DGNB sertifika sisteminde su korunumu için yangın suyunun temini, su tasarruflu sıhhi tesisatlar kullanılarak su tüketiminin azaltılması ve boru tesisatını optimize etmek için ıslak hacimlerin bina içerisinde mümkün olduğu kadar birbirine yakın olarak düzenlenmesi dikkate alınan diğer yöntemlerdir. Mülk bazlı atık su imha kavramı DGNB sertifika sisteminde yer alan bir diğer kavramdır. Bu kavramın, yapılacak inşaat projelerinin tasarımı için bir temel oluşturacağı böylelikle gelecekteki yapısal değişiklikleri de dikkate alarak tüm mülkler için genel bir drenaj sistemi geliştirilmiş olacağı öngörülmektedir. Ek enerji ve yüksek servis ihtiyacı nedeniyle atık su pompa istasyonlarından kaçınılması ve atık su pompalarında oluşan gürültü kirliliği nedeniyle ses yalıtımına önem verilmesi; DGNB sisteminde vurgulanan diğer hususlardandır. Ayrıca, sistem yapının kullanım evresindeki su tüketiminin periyodik olarak kaydedilerek analiz edilmesi ve güncel tüketim sonuçlarının önceki sonuçlar ile karşılaştırılmasına odaklanmaktadır (Federal Ministry for the Environment 2014).

3.4. ÇEDBİK Konut Sertifikası Sistemi Kapsamında Atık Suların Değerlendirilmesi

ÇEDBİK, Türkiye'de inşaat sektörünün sürdürülebilir ilkeler ışığında gelişmesine katkı sağlamak amacıyla 2007 yılında kurulmuş olan bir dernektir. Türkiye için yerel koşullara uygun Ulusal Yeşil Bina Sertifikası hazırlanmasına bu dernek öncülük etmiştir. Dernek üyelerinin katkısı ile BREEAM, LEED, DGNB gibi uluslararası yeşil bina sertifika sistemleri örnek alınarak yeni konutlar için ÇEDBİK Konut Sertifikası geliştirilmiş ve ilk defa 2013 Şubat ayında düzenlenen 2. Uluslararası Yeşil Bina Zirvesinde tanıtımı yapılmıştır (Aslan NC 2015). ÇEDBİK Konut Sertifikasının amacı; sağlıklı toplumlar, yaşanabilir bir çevre ve gelişmiş bir ekonomi yaratmaktır. Bununla birlikte bu sertifika, yapılı çevrede sürdürülebilirliği ölçerken bina standardında ideal duruma yaklaşarak çıtayı yükseltmeyi hedeflemektedir. Çevresel etkilerin, tasarımın ve inşaatın her adımında nasıl azaltılabileceği sorusuna odaklanmaktadır (Web Kaynağı-8).

ÇEDBİK Konut Sertifikası sistemine göre binaların çevresel performansları dokuz farklı değerlendirme ölçütü kapsamında 110 puan üzerinden değerlendirilmektedir. Söz konusu değerlendirme ölçütleri, her bir ölçüte ait puanlar ve etki oranları Çizelge 3.6'da sunulmaktadır. Su kullanımı ölçütünün diğer değerlendirme ölçütlerine göre oranı % 10,9'dur.

Çizelge 3.6. ÇEDBİK genel değerlendirme ölçütleri başlıkları (ÇEDBİK 2018)

ÇEDBİK Konut Sertifikası Değerlendirme Ölçütleri	Puan	Etki Oranı (%)
Bütünleşik yeşil proje yönetimi	9	8.2
Arazi kullanımı	13	11.8
Su kullanımı	*12*	*10.9*
Enerji kullanımı	26	23.6
Sağlık ve konfor	12	10.9
Malzeme ve kaynak kullanımı	15	13.6
Konutta yaşam	14	12.7
İşletme ve bakım	7	6.5
Yenilikçilik	2	1.8

TOPLAM	110	100

ÇEDBİK Konut Sertifikası sisteminin su verimliliği açısından amacı, doğal su döngüsünü ve su kaynaklarını korumak için kişi başına düşen su kullanımının azaltılmasıdır. Sisteme göre, kişi başına düşen kullanım suyu miktarının en fazla 210 m^3/yıl olması gerekmektedir. Bu bağlamda, ÇEDBİK Konut Sertifikası sisteminde "su kullanımı" ölçütü, atık suların proje alanı kapsamında arıtılması ve yeniden kullanılmasını teşvik etmektedir. Bu ölçütün alt başlıkları; kullanım suyunu azaltmak için az su kullanan armatürlerin ve tuvaletlerin seçilmesi, perlatör kullanılması, suyu verimli kullanan sertifikalı çamaşır ve bulaşık makinalarının seçilmesi gibi yöntemleri tanımlamaktadır. Ayrıca yağmur suyu toplama veya gri su geri kazanım sistemleri aracılığıyla geri kazanılan suyun sulamada ve rezervuarlarda kullanılması, sulamada kullanılan temiz su miktarını azaltmak için damlatmalı sulama uygulanması ve yerel iklim koşullarına uygun çok su istemeyen bitki türleri seçilmesi de diğer tanımlanan yöntemler arasındadır. ÇEDBİK Konut Sertifikası sisteminde, gerek yatırım gerekse işletme maliyetlerini büyük oranda düşüreceği öngörüldüğü için, atık suların arıtılması ve değerlendirilmesi özellikle önem verilen hususlardandır. Bu kapsamda atık suların proje alanında arıtılmasını ve yeniden kullanılmasını teşvik ederek hem atık suyun geri kazanımını daha kısa süre ve mesafede gerçekleştirmek mümkün olabilir, hem de arıtılan suyun sulama, rezervuarlar gibi işlerde kullanılması sağlanabilir. Sisteme göre kullanıcı sayısının 100 kişiden fazla olması durumunda evsel atık su arıtma yöntemi belirlenmelidir. Ayrıca, atık su karakterine uygun bir arıtma sistemi kurularak işletmeye alınması ve arıtma tesisi için uygun bir yer belirlenerek kullanılacak tesisin özelliklerinin sistemin tasarımcısı tarafından detaylandırılması gerektiği belirtilmektedir. Örneğin ÇEDBİK Konut Sertifikası sisteminde konutlardan kaynaklanan atık sular, evsel atık olarak tanımlanmaktadır. Atık suların arıtılmadan alıcı ortamlara deşarj edilmesi, su kalitesinin bozulmasına ve sucul canlıların yaşamının olumsuz etkilenmesine sebep olacaktır. Sisteme göre, bir atık su toplama ve arıtma sisteminin kurulması, atıkların ön arıtmaya tabi tutulduktan sonra şehir kanalizasyonuna bağlanması ve arıtılmış atık suların faydalı bir şekilde yeniden kullanılması gerektiği açıklanmaktadır. (ÇEDBİK 2018).

4. SONUÇ VE ÖNERİLER

Günümüzde nüfusun hızla artması ile su korunumu büyük önem kazanmıştır. Doğal kaynakların kullanımının asgari düzeye indirgenmesi ve çevresel etkilerin azaltılması için inşaat sektöründe küresel ölçekte yeşil binaların yapımı son yıllarda büyük hız kazanmıştır. Bu bağlamda, enerji ve su kaynaklarını daha verimli kullanan, sağlıklı ortamlar sunan, çalışanların performansını ve kullanıcıların konforunu artıran, işletim maliyetleri düşük olan binaların tasarımı ön plana çıkmıştır. Gün geçtikçe artan su talebi sonucunda yeşil binaların tasarımında su korunumu ilkesi, tüm yeşil bina sertifika sistemlerinde temel değerlendirme ölçütlerinden biri konumuna gelmiştir.

Bu çalışmada incelenen yeşil bina sertifika sistemlerinde su verimliliği açısından LEED %10, BREEAM %6 ve ÇEDBİK %12 oranında puanlama yapmaktadır. DGNB ekolojik nitelik değerlendirme ölçütü altında atık su için %22.5 oranında puan vermektedir. Su verimliliği açısından en düşük oranın BREEAM sertifika sisteminde olduğu görülmektedir. Ancak, BREEAM sertifika sistemi suyun daha çok önemli olduğu

körfez ülkeleri için hazırladığı kılavuzda su verimliliğini %30 oranında puanlama ile ele almaktadır.

Türkiye inşaat sektöründe, binalarda tüketilen temel doğal kaynaklardan biri olan suyun tüketim değerlerinin azaltılması için gerekli olan uygulamalara daha çok özen gösterilmelidir. Su tüketimi azaltıldığı takdirde atık su oluşumu da azalarak bina işletim maliyetleri düşecektir. Enerji ve su kullanımı ile uzun dönem işletme ve bakım maliyetlerinin azalması yeşil binaların para kazandıran özelliği olarak ifade edilebilir. Özellikle İstanbul ve Ankara gibi su tüketiminin fazla olduğu büyük şehirlerde yaygınlaştırılması gereken yeşil bina sertifika sistemleri ile su korunumunun/tasarrufunun önemi kamu ile paylaşılmalıdır. Yeşil bina sertifikalarının kullanım oranının artmasına yönelik olarak ilgili bakanlıklar ya da yerel yönetimlerin desteği ile yeni tasarılar, yönetmelikler ve şartnameler oluşturulmalı ve birtakım teşvik edici uygulamalar hayata geçirilmelidir.

KAYNAKLAR

Aslan NC., Yeşil Bina Projelerinde Tasarım Süreci için Bir Yaklaşım: Leed V4 Sertifikalandırma Süreci Modeli, Yüksek Lisans Tezi, İTÜ (2015).
Aslan V. "Türkiye'de Su Potansiyeli ve Atıksuların Geri Kullanımı" TMMOB 2. Su Politikaları Kongresi, 273-277, Ankara (2008)
Atalık, A., 2007, Su Sorunu ve Tarımda Sulama Suyu Kullanımı, TMMOB Ziraat Müh. Odası Mühendislik Dergisi, 81.
BREEAM, BREEAM New Construction, Non- Domestic Buildings, Technical Manual, BRE Global, 2011.
BREEAM, BREEAM New Construction, Non- Domestic Buildings, Technical Manual, BRE Global, 2018.
California Department of Water Resources Publications Office, "Graywater Guide." 1995, Sacramento: www.dwr.water.ca.gov
ÇEDBİK, ÇEDBİK-Konut Sertifika Kılavuzu (Versiyon 1) 2018.
Çelik E., Yeşil Bina Sertifika Sistemlerinin İncelenmesi Türkiye'de Uygulanabilirliklerinin Değerlendirilmesi, Yüksek Lisans Tezi, İTÜ (2009).
Çevre ve Şehircilik Bakanlığı, Çevresel Etki Değerlendirmesi, İzin ve Denetim Genel Müdürlüğü Çevre Envanteri ve Bilgi Yönetimi Dairesi Başkanlığı, "Türkiye Çevre Durumu Raporu 2016".
DGNB, (2011). Excellence Defined,Sustainable Building with a Systems
Ding, G. K. C., Sustainable Construction : The Role of Environmental Assessment Tools, Journal of Environmental Management, 86, 451-464. (2008).
Federal Ministry for the Environment, Nature Conservation, Building and Nuclear Safety, Guideline for Sustainable Building, 2014.
Gültekin AB., Bulut B., Yeşil Bina Sertifika Sistemleri: Türkiye İçin Bir Sistem Önerisi, 2nd International Sustainable Buildings Symposium, Ankara (28-30 Mayıs 2015).
Kantaroğlu Ö., Yüksek Performanslı Binalarda Su Stratejileri, MMO Enerji Dergisi (2011).
Ludvig A., "Builder's Greywater Guide", Santa Barbara, CA: Oasis Design, 1999
Özsoy S. 2009, Su ve Yaşam: Suyun Toplumsal Önemi, Yüksek Lisans Tezi, Ankara Üniversitesi.

Sev A. Canbay N., "Dünya Genelinde Uygulanan Yeşil Bina Değerlendirme ve Sertifika Sistemleri", Yapı Dergisi Yapıda Ekoloji Eki, 329: 42-47, 2009.
Şahin CD. 2016, Oteller Bazında Su Tüketiminin CBS Yardımıyla Belirlenmesi: İstanbul Örneği, Yüksek Lisans Tezi, İstanbul Teknik Üniversitesi.
Şahin Nİ, Binalarda Su Korunumu, Yüksek Lisans Tezi, İTÜ (2010).
U.S. Department of Energy, "Greening Federal Facilities: An Energy, Environmental and Economic Resource Guide for Federal Facility Managers and Designers", 2nd ed. May 2001. Washington, DC: Federal Energy Management Program, Office of Energy Efficiency and Renewable Energy, DOEIGO-102001-l 165. www.1.eere.energy.gov/femp/pdfs/29267-O.pdf.
The U.S. Green Building Council, "LEED v4 for Building Design And Construction) 2018.
Yapı Dergisi, «Yapıda Ekoloji: Ekolojik Mimarlıkta Somut Adımlar,» Nisan 2009.
Web kaynağı-1 http://www.maviprogram.com.tr/yesil-bina-sertifikasyonunda-suyun-onemi/ (11.10.2018)
Web kaynağı-2 https://www.breeam.com/ (19.10.2018)
Web kaynağı-3 https://www.breeam.com/discover/how-breeam-certification-works/ (19.10.2018)
Web kaynağı-4 http://leed.usgbc.org/leed.html (19.10.2018)
Web Kaynağı-5 https://www.dgnb-system.de/en/projects/ (19.10.2018)
Web Kaynağı-6 http://www.dgnb-system.de/en/certification/certification-process/ (19.10.2018)
Web Kaynağı-7 https://www.dgnb-system.de/en/system/version2018/criteria/ (19.10.2018)
Web Kaynağı-8 https://cedbik.org/tr/yesil-bina-7-pg/cedbik-konut-sertifikasi-12-pg.

THIS PAGE INTENTIONALLY LEFT BLANK

THIS PAGE INTENTIONALLY LEFT BLANK

THIS PAGE INTENTIONALLY LEFT BLANK

THIS PAGE INTENTIONALLY LEFT BLANK

THIS PAGE INTENTIONALLY LEFT BLANK

THIS PAGE INTENTIONALLY LEFT BLANK

THIS PAGE INTENTIONALLY LEFT BLANK

THIS PAGE INTENTIONALLY LEFT BLANK

STRONGLY FLUORESCENT COMPLEXES: SYNTHESIS, CHARACTERIZATION, 3D HYDROGEN-BONDED, FLUORESCENCE STUDY, AND THEORETICAL ANALYSIS

Ouahida Zeghouan,[a, b*] Seifeddine Sellami,[c] and Jean Claude Daran[d]

[a]Unité de Recherche Chimie de l'Environnement et Moléculaire, Structurale, 'CHEMS', Faculté des Sciences Exactes,Campus Chaabet Ersas, Université, Frères Mentouri Constantine 1, 25000 Constantine, Algérie, [b] Centre de Recherche en Biotechnologie, Constantine, Algérie
[c]Laboratoire Pollution et Traitement des Eaux, Département de Chimie, Faculté, des Sciences Exactes, Université, Frères Mentouri Constantine 1, 25000 Constantine, Algérie, and [d]Laboratoire de Chimie de Coordination, UPR-CNRS 8241, 205 route de Narbonne, 31077 Toulouse Cedex 4, France

Correspondence e-mail: ouahida.zeghouan@gmail.com

ABSTRACT: Due to their versatile coordination modes and metal-binding conformations, nitrogen-containing heterocyclic alcohols ligand can provide a wide range of possibilities for building coordination complexes with various physical or chemical properties. As part of our continuing interest in the coordination chemistry of the 2-(2-hydroxyethyl)pyridine((hep-H), the synthesis of the mononuclear, Diaqua[bis(2-(2-hydroxyethyl)pyridine-κ2 N,*O*) nickel (II)] dinitrate complex [{Ni(C_7H_8NO)$_2$ ·(H_2O)$_2$,(NO_3)$_2$}](**1**), and the poly[bis(2-(2-hydroxyethyl)pyridine-κ2 N,*O*)bis(μ-sulfato-κ2O,*O*)copper(II)],[{Cu(C_7H_8NO)$_2$,(SO_4)$_2$}n), (**2**) polymer complex have been realised under ambient condition. In the two complexes, the 2-(2-hydroxyethyl)pyridine ligand coordinate to the metal ions through the nitrogen atom of pyridine ring and the oxygen atom of hydroxyl group, creating a chelate ring. The Ni^{II} or Cu^{II} ion lies on an inversion centre and exhibits a slightly distorted MO_4N_2 octahedral coordination geometry, coordinated by O and N atoms from two ligand (hep-H) and two water molecules or two oxygen atoms belonging to sulfate anions. The sulfate anion bridge Cu^{II} ions forming a polymeric chain. This polymeric complex has been deposited as a CSD communication and later reported by different authors in the Journal of Molecular Structure. Only a short comparison between the structures of 1 and 2 is described in the manuscript. However, the photoluminescence properties of these complexes have been studied on as-synthesized samples. It reveals that both the compounds 1 and 2 displays a strong blue-light emission with maxima around 497 nm. In the detailed DFT/TDDFT (time-dependent density functional theory) studies, the blue emission appears to be derived from the ligand-to-metal charge-transfer (LMCT) excited state. In addition, the IR spectroscopic properties and thermogravimetric behaviours of both complexes have been investigated.

Keywords: Transition metal, fluorescence, blue-light emission, TD-DFT theoretical analysis.

Introduction

A wide variety of nitrogen-containing heterocyclic ligands has been used to construct coordination complexes, such as pyrrole, pyridine, pyrazine, and so on (Lin et al.,2015; Kim et al.,2015; Huang et al.,2015). In particular, pyridine alcohol derivatives and their metal complexes have been studied extensively in recent years, many research efforts has been focused on the rational design and synthesis of coordination monomers and polymers due to their intriguing structural features as well as potential applications in catalysis, fluorescence, and as chemical sensors (Ley et al.,2010). Moreover, luminescent compounds have attracted attention because of their applications, particularly in modern electronics, as materials for producing organic light emitting diodes (OLEDs) (Kelley et al., 2004). Nitrogen-containing heterocyclic alcohols ligands have proved to be extremely versatile, and can build extended networks with different coordination modes and mediate significant magnetic interactions between paramagnetic centers separated by more than 6Å (Carranza et al.,2004). This type of ligands is widely used as a core building material of polynuclear metal complexes (Stamatatos, Abboud et al.,2007) in the preparation of coordination compounds with a broad spectrum of biological activities comprising anti-cancer (Icsel et al.,2013), antimicrobial (Zienkiewicz et al.,2014) antioxidant functions (Zienkiewicz et al.,2013; Zienkiewicz et al.,2014), and as coordination compounds for modeling the structure or function of biomolecules (Scarpellini et al.,2008; Scarpellini et al.,2005). They adopt many variants of their donating capabilities: N-monodentate (N) (Martínez, et al.,2007), N, O-chelating (2N,O) (Antonioli, et al.,2007); and (ii) as deprotonated chelating (2N, O) (Antonioli, et al.,2007) and bridging (N: O)(Antonioli, et al.,2007),2N,O: O7and2N,O: O: O)(Wang, et al.,2010) or simultaneously 2N,O: O and 2N,O: O: O bridging (Stamatatos, Boudalis et al.,2007). We are interested in the hep-H (hep-H = 2 (2-hydroxyethyl) pyridine) , because of their special features, which have attracted much attention in biology and chemistry due to their model character and practical applications (Kong et al.,2009; Mobin et al.,2010). The hep-H ligand could be good candidate to construct simultaneous nitrogen heteroaromatic alcohols coordination, monomers and polymers with interesting magnetic behaviors.

On the other hand, with Ni(II) and Cu (II) metals, the 2 (2-hydroxyethyl) pyridine) could also be desirable candidate for fluorescent materials. The flexible coordination sphere around the Ni(II) and Cu (II) ion, in combination with steric and packing forces, is one of the effects that give rise to a wide structural diversity in NiII/CuII coordination chemistry (Comba, et al.,2003). The combination of multidentate ligands with suitable cations has led to a large number of novel mononuclear and polynuclear complexes. In this study, by employing flexible 2-(2-hydroxyethyl)pyridine ligand to react with Ni(NO3)2 ·6H2O or Cu(SO4)2 ·6H2O, we have successfully obtained the Ni monomer complex, namely Diaqua(bis(2-(2-hydroxyethyl)pyridine-κ2N,O)dinitrate nickel (II)] ,{Ni(C7H8NO)2.(H2O)2,(NO3)2},(1). In addition, IR spectra, thermostability, fluorescence properties and absorption by theoretical study using TDDFT calculations of this Ni complex and the related poly[bis(2-(2-hydroxyethyl)pyridine-κ2N,O)bis(μ-sulfato-κ2O,O)copper(II)], {Cu(C7H8NO)2,(SO4)2}n, (2) (Zeghouan et al., 2016; Zienkiewicz-Machnik et al., 2016) have been investigated.

Structural description

In the mononuclear Ni complex (**1**) as well as in the polymeric Cu complex (**2**) (Zeghouan *et al.*, 2016; Zienkiewicz-Machnik *et al.*, 2016), the metal ions are located on inversion centers with the hep-H neutral molecule acting as a bidentate ligand in a ^{2}N,O fashion and forming the equatorial plane of an octahedron, the apex of which being occupied by water molecules in the case of Ni complex or O atom of a SO_4 anion in the Cu complex (Fig. 1 and 2). The main difference between the two structure is the occurence of the SO_4 anion which links the Cu complexes forming a polymeric chain. Moreover, in the Cu structure the asymmetric unit contains two halves of the complex. In the Ni complex two nitrate anions balance the charges. The coordination environment around the nickel ions could be described as a nearly perfect octahedron. The O1-Ni1-N1, 88.68 (3)°, N1-Ni1-O1W, 90.75 (4)° and O1-Ni1-O1W, 89.25 (4)° are all very close to 90° (Table 2). The two hep-H ligands being in trans position with respect to each other. The hydroxyl O and the pyridine N atoms define the equatorial plane whereas the water molecules occupy the apices. In the case of the Cu complex the octahedron is slightly distorded with angle around the metal ranging from 83.39°(5) to 96.62°(5). This distorsion might result from the influence of the SO_4 linking the Cu complex to form a polymeric chain.
A search in the Cambridge Structural Database, version 5.36 (Groom & Allen, 2014) based on a $Ni(Hep\text{-}H)_2O_2$ fragment reveals 11 hits with closely related structure displaying octahedral Ni complex located on inversion center coordinated by two chelating N,O hep-H ligand located in the equatorial plane and two O atoms of different ligands at the apices. A comparison of the Ni-N, Ni-O bond lenght as well as the dihedral angle betweenn the equatorial NiO_2N_2 plane and the pyridine ring is displayed in Table 3. There are no notable difference between the Ni-O(H) which range from 2.057 (2)Å to 2.114 (1)Å and the Ni-O(ligand) ranging from 2.052 (1)Å to 2.112 (2) Å. Clearly the organic substituent attached to the O atom in axial position has no real influence on the Ni-O(R) bond length. The dihedral angle between the pryridine ring and the NiN_2O_2 basal square plane Δ range from 28.3° to 37.6°. The largest angle is observed for two polymer structures in which the succinato or adipato organic ligand bridge the Ni atoms forming a chain, it might be related to steric influence.A similar search on $Cu(Hep\text{-}H)_2O_2$ fragment reveals 7 hits, the major difference observed with the related Ni complexes is the large discrepancy for the Cu-O(H) which range from 2.012 (2) Å to 2.428 (2) Å and the Cu-O(R) ranging from 1.982 (1) Å to 2.387 (4) Å. The difference observed between the Cu-O(H) and Cu-O(R) bond length might be related to Jahn teller effect. The dihedral angles between the pryridine ring and the CuN_2O_2 basal square plane Δ ranging from 26° to 38° are of the same order than the values found in the Ni complexes.
In both complexes the chelate ring displays a twist-boat conformation with puckering parameters θ= 81.9° and φ= 162° (Cremer & Pople, 1975) for compound 1 and θ= 79.2° and φ= 159.9° and θ= 87.75° and φ= 176.08° for the two molecules of the Cu polymer 2. Similar twist-boat conformation is also observed in all Ni and Cu related complexes bearing the hep-H ligand (Table 3).
Although not coordinated to the Ni atom, the nitrate anion occurs in the building of the packing. Indeed, hydroxyl group and water molecules are involved in strong O-H⋯O hydrogen bonds with the O atoms of the nitrate anions resulting in the

formation of $R^4_4(12)$ and $R^4_4(16)$ graph set motifs (Bernstein *et al.*, 1995) as shown in Figure 3. These O-H ··O hydrogen bonds build up a three dimensional net work.

Thermogravimetric and differential thermal analysis

Thermal analyses were performed on a SETARM 92-16.18 PC/PG 1 instrument from 303 to 1273 K under a dynamic air atmosphere and under nitrogen at 200.0 ml min^{-1} with a heating rate of 283K min^{-1}. The stability of the two complexes was measured by TGA and the experimental results are in agreement with the calculated data.

The TG curve of the complex 1 (Fig.4a) shows that it was stable up to 424K and the first weight loss of 33.55% (calculated 34.21%) at 303 –438 K corresponds to the loss of two coordinated water and the organic molecule hep-H and the second loss of 47.51% (calculated 40.02%) at 438 –488 K corresponds to the loss of the second hep-H molecule and nitrate anion, and then the second nitrate anion decompose (DP/P = 12.14%, calculated =13.34%). In addition, the corresponding endothermic and exothermic peaks (at 424.26; 475.06 K and at 631.85 K) in the differential scanning ATD curve also record the processes of weight loss. As illustrated in Figure 4b, the TG curve of the polymer (2) shows that it was stable up to 470K and the first weight loss of 24.16% (calculated 23.66%) at 470 –483 K corresponds to the loss of the sulfate anion and the second loss of 29.42% (calculated 30.30%) at 483 –573 K corresponds to the loss of the first hep-H molecule, and then the second hep-H molecule decompose (DP/P = 28.55%, calculated =30.30%). In addition, the corresponding endothermic and exothermic peaks (at 473; 558 K and at 773K) in the differential scanning ATD curve also record the processes of weight loss.

Luminescent properties

Photoluminescence spectra were measured using a Cary Eclipse (Agilent Technologies) fluorescence spectrophotometer with quartz cell (1x1 cm^2 cross-section) equipped with a xenon lamp and a dual monochromator, the measurements were carried out at ambient temperature 298K with the slit $_{ex/em}$=10nm/10nm for all. The photoluminescence properties of complex (1), (2) and free hep-H in ethanol-water (V/V = 1:1) solution, were investigated in the visible region. As shown in Fig. 5, free hep-H displays a orange emission with band at 96.06 nm (excited at 269.70 nm) which may be assigned to the π-π* electronic transitions. When hep-H is combined with Ni^{II} or Cu^{II} in complex (1) and (2), an intense blue emission band is seen at $\lambda_{em}/\lambda_{ex}$=498.03nm/250.93 or 496.96 nm /250.00 nm respectively. This is should probably be assigned to the π-π* charge-transfer interaction of the hepH ligands. The observed blue shift of the emission maximum between complex (1), (2) and free hepH was considered to originate mainly from the influence of the coordination of the metal atoms to hepH ligand (Leitl, *et al.*, 2016). Thus, these compounds may be a candidate for blue light luminescent materials and it is believed that more metal transition pyridine alcohol compounds with good luminescent properties can be developed.

Theoretical analysis

In an effort to better understand the nature of the electronic transitions exhibited by compounds 1 and 2, DFT calculations using the Amsterdam Density function (ADF) software (Baerends *et al.*,1973) along with generalized gradient approximations, exchange and correlation functional GGA (PBE) (Perdew *et al.*,1997), employing the TZP (Triple Zeta Polarized) basis set were realized. Singlet excited state was optimized using the Time-Dependent Density Functional Theory calculations (TDDFT) (Bauernschmitt *et al.*,1996; Gross *et al.*,1990; Gross *et al.*,1996).

The ground state geometry of complexes 1 and 2 was adapted from the X-ray data. The calculated structural parameters show a good agreement with the original X-ray diffraction data. The computed absorption bands, dominant transitions, characters, and oscillator strengths (*f*) are given in table 6. As shown in table 6, two absorption features have been predicted for the monomer, an absorption feature mainly consists of an absorption peak that is located at λ = 286 and 280 nm, it results from a transition HOMO-2 to LUMO and the HOMO-3 to LUMO transition which is attributed to a ligand metal charge transfer (LMTC) (Fig.6a). Three absorption features have been predicted in polymer. An absorption feature mainly consists of an absorption peaks that are located at λ = 507, 443 and 244 nm, they result from HOMO-4 to LUMO, HOMO-5 to LUMO and the HOMO-2 to LUMO transition which are attributed to a ligand metal charge transfer (LMTC) (Fig.6b). The HOMO–LUMO energy gap was found to be 4.33, 4.42 and 2.44, 4.03 , 5.81ev for transitions of monomer (1) and polymer (2) respectively.

Crystallization

The infrared spectra was recorded on a Perkin–Elmer spectrometer at room temperature in the range of 4000-500 cm-1.
The 1-10 phenanthroline hydrate was obtained from commercial sources. The crystallization of the stydied copound was prepared by reaction of 1-10 phenanthroline hydrate (1g) in a mixture of ethanol–water (V/V = 1:1) . The solution was maintained under agitation during 4h at room temperature. Transparent prism were obtained by slow evaporation of the solvents within 2 days. The crystals formed were filtered and washed with 20ml of water.
IR (cm-1, the pure crystals of compounds without KBr):(1): 3400 (vs), 3084 (m), 1632 (w), 1617 (w), 1575(s), 1564 (m), 1502 (s), 1443 (w), 1414 (vs), 1340 (w), 1285 (vw), 1208 w), 1132 (m), 1082 (w), 1031 (w), 987 (m), 860 (vw), 764 (w), 733 (vs).

Refinement details

Crystal data, data collection and structure refinement details are summarized in Table 1. H atoms were placed at calculated positions with C-H = 0.93 Å (aromatic H atoms) and 0.97 Å (methylene H atoms), and refined in riding mode with $U_{iso}(H) = 1.2U_{eq}(C)$. The O-bound H-atoms were located in a Fourier map and refined with O-H restrained to 0.85 (1) Å, with $U_{iso}(H) = 1.5U_{eq}(O)$. For the water molecule a further H···H restraint of 1.39 (2)Å has been used.

Conclusion

A new monomeric NiII–hep-H complex, (**1**) has been synthesized and characterized by IR spectroscopie, single-crystal X-ray diffraction, thermogravimetric differential thermal analysis and a photoluminescence study. It was compared to some related Ni and Cu complexes. The crystal structures analysis of shows that the NiII atom lies on a centre of inversion, and is coordinated by hep-H ligand in a ^{2}N,O fashion. Intermolecular O—H···O and C—H···O hydrogen bonds link the molecules into a three-dimensional structure. Furthermore, photoluminescence studies of complex (**1**) and the already reported Cu complex (**2**) show a blue shift emission compared with

free hep-H ligand as a result of the influence of the coordination of the metal atom to the ligand, which is attributed to a ligand-to-metal charge-transfer (LMCT).

View of the Ni complex, with the atom-numbering scheme. Displacement ellipsoids are drawn at the 50% probability level and H atoms are shown as circles of arbitrary radii. [Symmetry code: (i): - x + 1, -y + 1, -z + 2]. Hydrogen bonds are shown as dashed lines

Partial view of the polymer chain in the Cu compound, with displacement ellipsoids drawn at the 50% probability level. [Symmetry code: (i) -*x* + 1, -*y* + 2, -*z* + 2; (ii)-*x*, -*y* + 1, -*z* + 1]. Hydrogen bonds are shown as dashed lines

Partial view of the packing in the Ni complex showing the O—H···O hydrogen bonds and the formation of the graph set $R^4_4(12)$ and $R^4_4(16)$ motifs. Atoms are represented as circles of different radii. Hydrogen bonds are shown as dashed lines. [Symmetry code: (i): - *x* + 2, -*y* + 1, -*z* + 2; (ii) -*x* + 1, -*y*, -*z* + 2].

The thermogravimetric (TG) and differential thermal analysis (DTA) curves (*a*) the monomer, (*b*) the polymer.

The fuorescence spectrum of hep-H ligand and the title compounds (excitation at 250 nm)

Plots of the molecular orbitals dominating the contribution of the low-energy transitions for (*a*) the monomer, (*b*) the polymer.

Experimental details

	(1)
Crystal data	
Chemical formula	C14H22N4NiO10
Mr	465.05
Crystal system, space group	Triclinic, P
Temperature (K)	293
a, b, c (Å)	7.782 (5), 8.185 (5), 8.811 (5)
α, β, γ (°)	96.785 (5), 113.856 (5), 109.140 (5)
V (Å3)	464.0 (5)
Z	1
Radiation type	Mo Kα
μ (mm−1)	1.11
Crystal size (mm)	0.18 × 0.11 × 0.08
Data collection	
Diffractometer	Bruker APEXII
Absorption correction	–
No. of measured, independent and observed [I > 2σ(I)] reflections	2478, 2478, 2471
Rint	0.019
(sin θ/λ)max (Å−1)	0.685

Refinement	
R[F2 > 2σ(F2)], wR(F2), S	0.018, 0.052, 1.13
No. of reflections	2478
No. of parameters	139
No. of restraints	4
H-atom treatment	H atoms treated by a mixture of independent and constrained refinement
Δρmax, Δρmin (e Å−3)	0.42, −0.28

Hydrogen-bond geometry (Å, °)

D—H···A	**D—H**	**H···A**	**D···A**	**D—H···A**
O1W—H2W···O3i	0.843 (9)	1.946 (9)	2.7870 (16)	175.9 (14)
O1W—H1W···O4	0.845 (8)	1.930 (9)	2.7720 (19)	174.0 (14)
O1—H1···O2ii	0.8184 (7)	1.8827 (11)	2.6954 (15)	171.83 (6)
C2—H2B···O3iii	0.97	2.64	3.378 (2)	132.7
C3—H3A···O1W	0.97	2.55	3.2278 (17)	127.2
C8—H8···O1iv	0.93	2.49	3.0136 (19)	115.5
C8—H8···O4iv	0.93	2.66	3.4448 (18)	143.0
C5—H5···O2v	0.93	2.41	3.3076 (19)	163.0
Symmetry codes: (i) −x+2, −y+1, −z+2; (ii) −x+1, −y, −z+2; (iii) x−1, y, z; (iv) −x+1, −y+1, −z+2; (v) −x+1, −y, −z+1.				

Comparison of seleted geometry for Ni and Cu complexes bearing the Hep-H ligand

Ref	**R-factor(%)**	**M-N (Å)**	**M-OH (Å)**	**M-O(R) (Å)**	**Δ(°)**	**θ(°)**	**φ(°)**
1	1.80	2.102 (1)	2.062 (1)	2.083 (2)	28.28 (4)	81.9 (1)	162.6 (1)
BOZJAD	3.80	2.102 (2)	2.065 (3)	2.084 (3)	28.4 (1)	80.6 (3)	163.4 (3)
HULYAO	3.22	2.073 (1)	2.064 (1)	2.085 (1)	30.37 (6)	78.7 (1)	156.3 (1)
EJEZEZ	2.58	2.082 (1)	2.089 (1)	2.090 (1)	30.88 (6)	99.0 (1)	346.8 (1)
FEFWIY	3.13	2.100 (2)	2.088 (1)	2.072 (2)	30.4 (1)	96.8 (2)	349.7 (2)

FEFWIY01	3.05	2.090 (1)	2.104 (1)	2.064 (1)	31.86 (8)	95.9 (1)	354.6 (2)
FEFWIY02	2.59	2.096 (1)	2.085 (1)	2.064 (1)	30.51 (7)	97.9 (1)	346.1 (1)
BOZJOR	3.75	2.078 (2)	2.096 (1)	2.063 (2)	37.6 (1)	89.2 (2)	175.3 (2)
BOZJUX	3.03	2.083 (1)	2.114 (1)	2.052 (1)	35.43 (8)	94.3 (1)	352.5 (2)
BOZKAE	4.36	2.098 (2)	2.096 (2)	2.064 (2)	29.9 (1)	81.9 (2)	160.4 (2)
RAJQOL	4.07	2.083 (2)	2.057 (2)	2.112 (2)	31.9 (1)	84.5 (2)	167.7 (2)
NABBEA012	1.9	2.025 (2)	2.012 (2)	2.380 (1)	28.5 (1)	79.2 (1)	159.9 (1)
		1.988 (2)	2.055 (1)	2.298 (1)	38.0 (1)	87.8 (1)	176.2 (1)
NABBEA	5.2	1.993 (4)	2.070 (4)	2.298 (4)	37.5 (2)	87.5 (3)	175.9 (3)
		2.031 (4)	2.016 (4)	2.387 (4)	28.8 (2)	100.3 (4)	340.6 (4)
HAYHAS	2.8	2.032 (2)	2.422 (1)	1.982 (1)	29.50 (7)	81.9 (1)	171.9 (1)
IRERED	4.04	2.017 (2)	2.385 (2)	2.025 (2)	31.0 (1)	94.4 (2)	356.0 (2)
OJOBAQ	2.35	2.009 (1)	2.041 (1)	2.312 (1)	33.96 (4)	98.6 (1)	340.0 (1)
SOJGAB	3.52	2.029 (2)	2.428 (2)	1.998 (1)	25.97 (8)	101.4 (2)	346.6 (2)
UGAROK	3.44	2.021 (2)	2.019 (2)	2.357 (2)	31.4 (1)	95.9 (2)	345.3 (2)
		2.030 (2)	2.024 (2)	2.346 (2)	32.5 (1)	80.6 (2)	167.0 (2)

Δ dihedral angle (°) between the basal square plane MO2N2 and the pyridine ring

BOZJAD, BOZJOR, BOZJUX, BOZKAE: Trdin & Lah (2015)

EJEZEZ : Yilmaz et al. (2011)

FEFWIY, FEFWIY01, FEFWIY02 : Trdin & Lah (2012)

HULYAO : Hamamci et al. (2002)

RAJQOL: Colak et al. (2017)

HAYHAS: Lapanje et al. (2012)

IRERED: Pothiraja et al.(2011)

NABBEA: Zienkiewicz-Machnik et al.(2016)

NABBEA01: Zeghouan et al.(2016)

OJOBAQ: Yilmaz et al. (2003)

SOJGAB: Caglar et al. (2014)

UGAROK: Yesilel et al. (2009)

- This work was supported by the Unité de Recherche de Chimie de l'Environnement et Moléculaire Structurale (URCHEMS), Université Frères Mentouri Constantine, Algérie; and Biotechnology research center (CRBt), Constantine, Algérie.
Thanks are due to MESRS and ATRST (Ministère de l'Enseignement Supérieur et de la Recherche Scientifique et l'Agence Thématique de Recherche en Sciences et Technologie, Algérie) *via* the PNR program for financial support.

References

Antonioli, B., Bray, D. J., Clegg, J. K., Jolliffe, K. A., Gloe, K. & Lindoy, L. F. (2007). *Polyhedron*, **26**, 673–678.
Baerends, E. J., Ellis, D. E. & Ros, P. (1973). *J. Chem. Phys.* **2**(1), 41–51.
Bauernschmitt, R. & Ahlrichs, R. (1996). *J. Chem. Phys.* **104**, 9047–9052.
Bernstein, J., Davis, R. E., Shimoni, L. & Chang, N.-L. (1995). Angew. Chem. Int. Ed. Engl. 34, 1555-1573.
Bruker (2006). *APEX2* and *SAINT*. Bruker AXS Inc., Madison, Wisconsin, USA.
Burla, M. C., Camalli, M., Carrozzini, B., Cascarano, G. L., Giacovazzo, C., Polidori, G. & Spagna, R. (2003). *J. Appl. Cryst.* **36**, 1103.
Burnett, M. N. & Johnson, C. K. (1996). *ORTEPIII*. Report ORNL-6895. Oak Ridge National Laboratory, Tennessee, USA.
Caglar, S., Saykal, T., Buyukgungor, O. & Sahin, E. (2014). *Synth. React. Inorg. Met.-Org. Nano-Met. Chem.* **44**, 1234–1242.
Carranza, J., Sletten, J., Brennan, C., Lloret, F., Cano, J. & Julve, M. (2004). *Dalton Trans.* pp. 3997–4005.
Colak, A. T., Gunay, H., Temel, E., Buyukgungor, O. & Colak, F. (2017). *Transition Met. Chem.* **42**, 85–93.
Comba, P. & Remenyi, R. (2003). *Coord. Chem. Rev.* **238**, 9–20.
Cremer, D. & Pople, J. A. (1975). *J. Am. Chem. Soc.* **97**, 1354–1358.
Farrugia, L. J. (1997). *J. Appl. Cryst.* **30**, 565.
Farrugia, L. J. (1999). *J. Appl. Cryst.* **32**, 837–838.
Groom, C. R. & Allen, F. H. (2014). *Angew. Chem. Int. Ed.* **53**, 662–672.
Gross, E. U. K., Dobson, J. F. & Petersilka, M. (1996). Density Functional Theory of Time Dependent Phenomena, edited by K. Hafner, K. N. Houk, I. J. M. Lehn, K. N.

Raymond, C. W. Rees, J. Thiem & F. Vogtle, in Topics in Current Chemistry – Density Functional Theory II, pp. 81–172. Berlin: Springer.
Gross, E. K. U. & Kohn, W. (1990). Adv. Quantum Chem. 21, 255–291
Hamamci, S., Yilmaz, V. T. & Thöne, C. (2002). *Acta Cryst.* E**58**, m700–m701.
Huang, Q.-Y., Yang, Y. & Meng, X.-R. (2015). *Acta Cryst.* C**71**, 701–705.
Icsel, C., Yilmaz, V. T., Ari, F., Ulukaya, E. & Harrison, W. T. A. (2013). *Eur. J. Med. Chem.* **60**, 386–394.
Kelley, T. W., Baude, P. F., Gerlach, C., Ender, D. E., Muyres, D., Haase, M. A., Vogel, D. E. & Theiss, S. D. (2004). *Chem. Mater.* **16**, 4413–4422.
Kim, Y.-I., Song, Y.-K., Kim, D. & Kang, S. K. (2015). *Acta Cryst.* C**71**, 908–911.
Kong, L.-Q., Ju, X.-P. & Li, D.-C. (2009). *Acta Cryst.* E**65**, m1518.
Lapanje, K., Leban, I. & Lah, N. (2012). *Acta Cryst.* E**68**, m599.
Leitl, M. J., Zink, D. M., Schinabeck, A., Baumann, T., Volz, D. & Yersin, H. (2016). *Top Curr Chem (Z)*, **374**(3), 1–34.
Ley, A. N., Dunaway, L. E., Brewster, T. P., Dembo, M. D., Harris, T. D., Baril-Robert, F. & Pike, R. D. (2010). Chemical Communications. 46 (25), 4565-4567
Lin, R.-G., Wang, Y.-L. & Liang, Q. (2015). *Acta Cryst.* C**71**, 44–47.
Macrae, C. F., Edgington, P. R., McCabe, P., Pidcock, E., Shields, G. P., Taylor, R., Towler, M. & van de Streek, J. (2006). *J. Appl. Cryst.* **39**, 453–457.
Martínez, A., Lorenzo, J., Prieto, M. J., Font-Bardia, M., Solans, X., Avilés, F. X. & Moreno, V. (2007). *Bioorg. Med. Chem.* **15**, 969–979.
Mobin, Sh. M., Ashwiniand, M. & Srivastava, K. (2010). *Dalton Trans.* **39**, 1447–1449.
Perdew, J. P., Burke, K. & Ernzerhof, M. (1997). Phys. Rev. Lett. 78 (7), 1396-1396
Pothiraja, R., Sathiyendiran, M., Steiner, A. & Murugavel, R. (2011). *Inorg. Chim. Acta*, **372**, 347–352.
Scarpellini, M., Gätjens, J., Martin, O. J., Kampf, J. W., Sherman, S. E. & Pecoraro, V. L. (2008). *Inorg. Chem.* **47**, 3584–3593.
Scarpellini, M., Wu, A. J., Kampf, J. W. & Pecoraro, V. L. (2005). *Inorg. Chem.* **44**, 5001–5010.
Sheldrick, G. M. (2015). *Acta Cryst.* C**71**, 3–8.
Spek, A. L. (2003). *J. Appl. Cryst.* **36**, 7–13.
Stamatatos, T. C., Abboud, K. A., Wernsdorfer, W. & Christou, G. (2007). *Angew. Chem.* **119**, 902–906.
Stamatatos, T. C., Boudalis, A. K., Pringouri, K. V., Raptopoulou, C. P., Terzis, A., Wolowska, J., McInnes, E. J. L. & Perlepes, S. P. (2007). *Eur. J. Inorg. Chem.* 5098–5104.
Trdin, M. & Lah, N. (2012). *Acta Cryst.* C**68**, m359–m362.
Trdin, M., Leban, I. & Lah, N. (2015). Acta Chim. Slov. 62, 249–254
Wang, F.-M., Lu, C.-S., Li, Y.-Z. & Meng, Q.-J. (2010). *Acta Cryst.* E**66**, m594.
Yesilel, O. Z., Erer, H., Soylu, M. S. & Buyukgungor, O. (2009). *J. Coord. Chem.* **62**, 2438–2448.
Yilmaz, V. T., Hamamci, S. & Thone, C. (2003). *J. Coord. Chem.* **56**, 787–795.
Yilmaz, V. T., Yilmaz, F., Guney, E. & Buyukgungor, O. (2011). *J. Coord. Chem.* **64**, 159–169.
Zeghouan, O., Bendjeddou, L., Dems, M. A. & Merazig, H. (2016). Private communication (refcode: 1481676). CCDC, Cambridge, England.
Zeghouan, O., Guenifa, F., Hadjadj, N., Bendjeddou, L. & Merazig, H. (2013). *Acta Cryst.* E**69**, m439–m440.

Zienkiewicz, M., Jabłon?ska-Wawrzycka, A., Szlachetko, J., Kayser, Y., Stad- nicka, K., Sawka-Dobrowolska, W., Jezierska, J., Barszcz, B. & Sá, J. (2014). *Dalton Trans.* **43**, 8599–8608.
Zienkiewicz, M., Szlachetko, J., Lothschütz, C., Hodorowicz, M., Jabłon?ska Wawrzycka, A., Sá, J. & Barszcz, B. (2013). *Dalton Trans.* **42**, 7761–7767.
Zienkiewicz-Machnik, M., Masternak, J., Kazimierczuk, K. & Barszcz, B. (2016). *J. Mol. Struct.* **1126**, 37–46.

MODELING AND CONTROL OF ELECTRONIC COOLING SYSTEM IN IC ENGINE

Alırıza KALELİ
Bayburt University
arizakaleli@atauni.edu.tr

Galip KALTAKKIRAN
Atatürk University
g.kaltakkiran@atauni.edu.tr

Hüseyin KÖKSAL
Bayburt University
hkoksal@atauni.edu.tr

ABSTRACT: Today, the use of internal combustion engines in the transportation sector is increasing day by day. This rise also requires the need for power and performance. The traditional engine cooling system, which has an important role in energy management, has not changed much in comparison to other systems that have developed despite the advance of technology. In this study, a modeling study was carried out on the renewed test system for the electronic engine cooling system by changing the traditional engine cooling system. Here, simulation programs are prepared for analysis and simulation of the cooling system. In the literature, engine cooling system modeling has been used with modeling methods realized with analytical and detailed model structured software. In this study, the use of control systems that regulate the behavior of the cooling system actuators was needed. Both methods have been applied in the simulation studies. In the modeling of the engine cooling system, GT Suite, which is a software model, is preferred. This provides a more detailed analysis of the changes in the system. This simulation program can accommodate all subsystems and components in the cooling system circuitry. In addition, the GT-Suite has the ability to work integrated with the MATLAB / Simulink program that will run above the designed control algorithms. In the GT-Suite, fluid properties and physical properties of mechanical cooling components were needed to model a basic cooling circuit. After these features are added to the workspace, they are entered into the program with the corresponding windows. In the study, the data of the components of the cooling system were obtained from the experiments performed under different engine operating conditions.

Key words: control simulation modeling, electronically controlled cooling, internal combustion engines

İÇTEN YANMALI MOTOR ELEKTRONİK SOĞUTMA SİSTEMİNİN MODELLENMESİ VE KONTROLÜ

ÖZET: Günümüzde taşımacılık sektöründe içten yanmalı motorların kullanımı her geçen gün artmaktadır. Bu yükseliş ayrıca güç ve performans ihtiyacını da

gerektirmektedir. Enerji yönetiminde önemli bir rol sahibi olan geleneksel motor soğutma sistemi, teknolojinin ilerlemesine rağmen gelişen diğer sistemlere kıyasla çok fazla değişiklik gösterememiştir. Buna istinaden bu çalışmada geleneksel motor soğutma sistemi üzerinde değişikliklere gidilerek elektronik motor soğutma sistemine yönelik yenilenen test düzeneği üzerinde modelleme çalışması yapılmıştır. Burada soğutma sisteminin analiz ve benzetim çalışması için simülasyon programları hazırlanmıştır. Literatürde motor soğutma sistemi modellenmesinde analitik ve ayrıntılı model yapısına sahip yazılımlarla gerçekleştirilen modelleme yöntemlerinden faydalanılmıştır. Bu çalışmada soğutma sistemi eyleyicilerinin davranışını düzenleyen kontrol sistemlerinin kullanımına ihtiyaç duyulmuştur. Bunun için yapılan simülasyon çalışmalarında iki yöntem de uygulanmıştır. Motor soğutma sisteminin modellenmesinde bir yazılım modellemesi olan GT Suite tercih edilmiştir. Bu sistem içindeki değişimlerin daha detaylı bir şekilde incelenmesini sağlamıştır. Bu simülasyon programı soğutma sistemi devresindeki tüm alt sistemleri ve bileşenleri bünyesinde barındırabilmektedir. Ayrıca GT-Suite tasarlanan kontrol algoritmalarının üzerinde koşturulacağı MATLAB/Simulink programı ile entegreli olarak çalışabilme özelliğine sahiptir. GT-Suite ortamında temel bir soğutma devresinin modellenmesi için akışkan özelliklerine ve mekanik soğutma bileşenlerinin fiziksel özelliklerine ihtiyaç duyulmuştur. Bu özellikleri çalışma alanına eklendikten sonra ilgili pencereler ile program içerisine girilmiştir. Çalışmada farklı motor çalışma koşullarında yapılan deneylerden soğutma sistemi bileşenlerine ait veriler elde edilmiştir. Bu veriler kullanılarak elektronik kontrollü soğutma sistemi için matematiksel model GT-suite ortamında oluşturulmuştur.

Anahtar sözcükler: kontrol simülasyon modelleme, elektronik kontrollü soğutma, içten yanmalı motorlar

GİRİŞ

Yarı iletken teknolojisinin gelişmesi ve maliyetlerin azalmasından dolayı günümüzde elektronik kontrollü soğutma sistemleri otomotiv sektöründe kullanılmaya başlanmıştır. Bu sistemlerde mekanik elemanlar yerine elektronik kontrol ünitesi tarafından denetlenebilen valfler, pompalar ve fanlar kullanılmaktadır. Motor termal yönetim sistemi termostatlar, radyatörler, fanlar ve pompalar gibi birçok bileşenin bir arada çalıştığı ve içerisinde farklı disiplinlerin olduğu karmaşık sistemlerdir. Bu sistemlerde tüm elemanlar birbiriyle uyumlu bir şekilde çalışmalıdır. Böyle bir yapıya sahip sistemler ile motor performansındaki azalmanın, egzoz emisyonlarında ki bozulmaların ve yakıt verimliliğindeki düşüşün önüne geçilebilmektedir (Allen et al. 2001; Wagner et al. 2003). Benzer şekilde Melzer ve arkadaşları yaptıkları çalışmada radyatör girişinde bulunan bölgeye bir eyleyici yerleştirerek soğutma suyunu debisini kontrol etmiştir (Melzer vd. 1999). Çalışma sonuçlarına göre geniş çalışma koşullarında motor yaklaşık olarak %5 oranında yakıt tüketiminde tasarruf sağlamıştır. Bu düşüşün nedenlerinin yüksek motor sıcaklığı ve su pompasının düşük güç tüketimi olduğunu belirtmişlerdir.

İçten yanmalı motorlarda soğutma sistemleri için kontrol algoritmaları ve optimizasyon yöntemleri model bazlı olarak elde edilmektedir. Bu modellemeler için

literatürde bazı modelleme çeşitleri yer almaktadır. Bu modelleme yöntemleri genel olarak iki ana başlıkta ayrılırlar. Birinci analitik yöntemler ve ikincisi daha ayrıntılı bir model yapısına sahip başka bir yazılımla gerçekleştirilen modelleme yöntemleridir. İkinci kısma dahil olan modeller genelde motor tasarımı aşamasında kullanılmalarına ek olarak uzun süren simülasyon zamanlamasına sahiptir. Yapılan bu çalışmada simülasyon çalışmaları esnasında her iki yöntem de uygulanmış ve motor soğutma sisteminin modellenmesinde ikinci yöntem kapsamında olan GT Suite ortamından faydalanılmıştır. Böylece sistemde var olan değişimlerin detaylıca incelenme imkânı elde edilmiştir.

Kontrollü motor soğutma sistemlerinde önemli yere sahip bir uygulama olan motor ısınma süresinin azaltılması ile ilgili başka bir çalışmada motorun termal sistemi toplu parametre prensibiyle modellenmiş ve elde dilen model kullanılarak hem kararlı hem de geçici motor çalışma şartlarındaki ısınma süresindeki değişken dinamikleri simülasyon ortamında incelenmiştir (Samhaber et al. 2001). Motor ısınma süresinin kısalması ve yakıt tüketiminin düşürülmesine yönelik olarak modelleme tekniklerine ek olarak motorun termal davranışının CFD analizler ile incelenmesi için dört kütle motor termal model kullanılmıştır. Bu model içerisinde soğutucu hacmi, motor kütlesi, motor yağı hacmi göz önünde bulundurulmuş ve modelin avantajı olarak motorun geçici çalışma bölgesindeki ısınma çevrimi sırasında soğutma sıvısı sıcaklığının yanı sıra yağlayıcı sıcaklığı %10 hata ile tahmin edilmiştir (Ranjan et al. 2016). Modelleme bazlı yapılan basşka bir çalışmada bir boyutlu modelleme ile 4 silindirli, 1.6 litrelik, turboşarjlı ve ara soğutmalı, benzinli motorun ısınma davranışı sayısal olarak modellenmiştir (Lahuerta et al. 2013). Oluşturulan bu model sayesinde motorun ısınma özelliklerinin incelenmesi için motor bloğu, silindir kafası ve soğutma sistemlerinde ısı aktarımı için modelleme yapılmıştır. Motorun ısınma fazının kısaltılması için yapılan bir başka çalışmada mekanik pompa yerine elektrikli pompa kullanılmıştır. Böyle bir değişimle birlikte ek kontrol donanımlarına ihtiyaç duyulmuştur. Yapılan bu çalışmada CO2 emisyonunun ve yakıt tüketiminin özellikle motorun ısınma fazı esnasında azaltılması için kontrol stratejisi geliştirilmiştir. Yapılan strateji ile beklenen iyileşmeler elde edilmiştir (Pizzonia et al. 2016). Bu çalışmaya benzer bir başka çalışmada ise kontrol edilebilir bir pompa ve değişken şartlara uyumlu bir fan ile yapılan çalışma stratejisinin motor ısınma süresini azalttığını ve mekatronik eyleyiciler ile klasik soğutma sisteme ne kıyasla güç tüketiminde %57 kadarlık bir iyileşme sağlanmıştır (Zhou et al. 2015).

Hazırlanan bu çalışmada simülasyon programlarından faydalanılarak soğutma sisteminin analiz ve benzetim çalışması yapılmıştır. Motor soğutma sisteminin modellenmesinde kullanılan GT-Suite programı bir bütünleştirilmiş CAE (Computer-Aided Engineering) tasarım aracıdır ve termal yönetim sisteminde yer alan transmisyon, yağlama devresi, ara soğutucu, ısıtıcı ve klima sistemi gibi tüm alt sistemleri ve bileşenleri kapsamaktadır. Bu program ile motor termal yönetim sistem tasarımı ve analizleri gerçekleştirilebilmektedir. GT-Suite programı, egzoz emisyonu motorun hızlı ısınması, motor ömrü, kabin ısıtma, parça boyutları ve sistem kontrolü gibi tüm gereksinimleri karşılamak için termal yönetim ile ilişkili tüm alt sistemleri bir arada modellenme kapasitesine sahip bir prgramdır. Soğutma sistemi hattındaki bileşenler ve hortumlardaki ısı transferini gösteren tek boyutlu akışkan dinamiği gerçekleştirilmektedir. Ayrıca GT-Suite programı kontrol algoritmaların üzerinde

koşturulduğu MATLAB/Simulink programı ile entegre çalışabilme özelliğine de sahiptir. Buna istinaden soğutma sisteminin simülasyon analiz ve benzetim çalışması üzerine yapılan bir araştırma çalışmasında motor soğutma sisteminin esnekliği ve entegre edilebilirliği GT-SUITE programı ile analiz edilmiştir (Minovski et al. 2014). Benzer şekilde bir çalışmada motor soğutma sistemlerinin yakıt tüketimi üzerine olan etkileri araştırılmıştır (Khanjani et al. 2014).

Bu çalışmada GT suite ortamında bir içten yanmalı motorun termal yönetim sistemi modellenmiş ve sistem içerisinde buluna elektrikli pompanın devir sayısı PID (Oransal integral türev) algoritması ile kontrol edilmiştir. Kontrolcü parametreleri belirlenirken Simulink paketi içinde bulunan Design optimization araç kutusu kullanılmış ve burada ardışık kuadratik programlama algoritması kullanılarak optimum parametreler belirlenmiştir. Daha sonra elde edilen motor çıkış sıcaklık grafikleri sabit ve sinüzoidal değişim gösteren ısı girişine karşılık elde edilmiş ve sonuçlar grafiksel olarak gösterilmiştir.

YÖNTEM

Motor termal yönetim sistemleri termostat, radyatör, fan, pompa ve diğer bileşenlerin birlikte çalıştığı ve kendi arasında farklı disiplinlerin olduğu karmaşık sistemlerdir. Tüm bu sistem bileşenleri kendi içerisinde uyumlu halde çalışmalarını sürdürmektedirler. Bu çalışmada elektronik kontrollü motor soğutma sisteminin modellenmesi ve kontrolü gerçekleştirilmiştir. Dolayısıyla öncelikle adı geçen donanımsal bileşenlerin laboratuvar koşullarında bulunan test motoru üzerine montajı yapılmıştır. Çalışma kapsamında mevcut deney düzeneğinde bulunan soğutma sistemi yeniden düzenlenmiştir. Düzenleme işleminde mevcut su pompası yerine elektrik motorlu su pompası, termostat yerine açıklığı ayarlanabilen kontrollü vana ile değiştirilmiş ve fan için bir kontrolcü eklenmiştir. Ölçüm yapmak için belirlenen noktalara ilgili sensörler yerleştirilerek sistem tasarımı yapılmıştır. Bu sistemin şematik gösterimi Şekil 1 ile gösterilmiştir. Elektronik kontrollü soğutma sistemi için gerekli ölçüm verilerini elde etmek için 4-stroklu, su soğutmalı, yakıt püskürtmeli, buji ateşlemeli Ford MVH418 tipi bir motor kullanılmıştır. Motora teknik özellikler Tablo 1'de gösterilmiştir.

Tablo 1. Deneylerde Kullanılan Motora Ait Teknik Özellikler

Motor Tipi	Ford MVH418, 4-Stroklu, Su Soğutmalı, Yakıt Püskürtmeli, Buji Ateşlemeli
Silindir Tipi ve Sayısı	Sıra Tipi, 4 Silindirli, Dohc-16V
Ateşleme Sırası, Sıkıştırma Oranı	1-3-4-2 10:1
Çap, Strok, Kapasite	80.6 mm, 88 mm, 1796 cm^3
Maksimum Güç	6250 d/dak'da 93 kW
Maksimum Moment	4500 d/dak'da 157 Nm

Rölanti Devri	900 ∓ 50 d/dak
Buji Ateşleme Açıklığı	1.3 mm
Yakıt	LPG - Kurşunsuz Benzin
Yakıt Emme Sistemi	BOSH KE-Jetronik

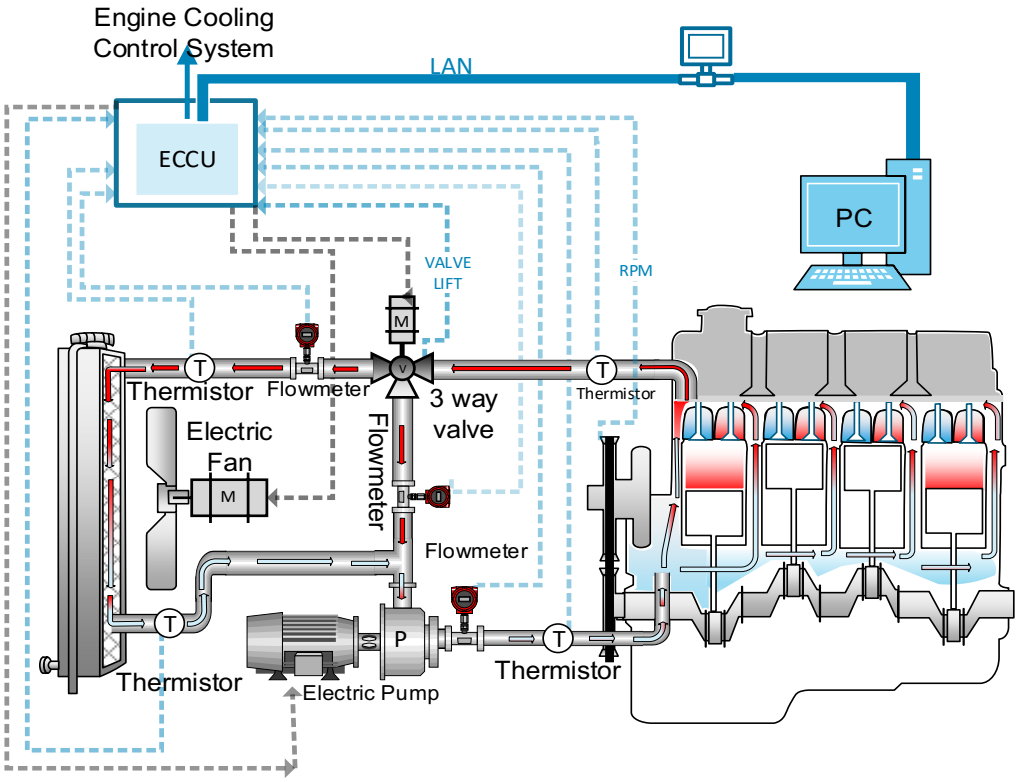

Şekil 1. Düzenlen Test Sisteminin Şematik Gösterimi

Çalışmalar kapsamında özellikle simülasyon çalışmalarında Matlab/Simulink yazılımı, gerçek zamanlı testler esnasında ölçümler ve kontrol algoritmaları Labview ortamında hazırlanarak gerçek zamanlı donanım üzerinde koşturulmuştur. Motor parametrelerinin ölçülüp kaydedilmesi amacıyla LabView ortamında hazırlanan yazılım kullanılmıştır.

İçten yanmalı motorların soğutma sistemlerinin kontrol algoritmaları ve optimizasyon yöntemlerinin modele dayalı olarak elde edilmektedir. Motor soğutma sistemlerinin modellenmesi için literatürde çeşitli modellenme teknikleri kullanılmıştır. Kullanılan bu yöntemler iki ana kısma ayrılırsa; birinci analitik yöntemler ve ikincisi ise daha ayrıntılı bir model yapısına sahip başka bir yazılımla gerçekleştirilen modellemelerdir. İkinci kısım modeller daha ziyade motor tasarımı aşamasında kullanılmalarının yanı sıra simülasyon süresi bakımından daha yavaş olarak çalışmaktadırlar. Çalışma kapsamında yapılan simülasyon çalışmaları esnasında iki yöntem de uygulanmış ve motor soğutma sisteminin modellenmesinde ikinci yöntem için GT Suite ortamı tercih

edilmiştir. Bu sayede sistem içindeki değişimleri daha detaylı bir şekilde incelenme imkânı elde edilmiştir.

Tasarlanan motor soğutma sistemi içerisinde denetlenebilen elektrikli pompa ve elektrikli üç yollu vana ve radyatör fanı olmak üzere üç önemli eyleyici bulunmaktadır. Dolayısıyla buradaki eyleyicilere uygun kontrol işaretlerinin gönderilebilmesi için elde edilen modellerin gerçek sistem üzerinden alınan veriler ile doğrulanması gerekmektedir. Dolayısıyla burada elde edilen modeller içinde bulunan parametrelerin ölçüm verileri kullanılmıştır. GT-Suite ortamında temel bir soğutma devresinin modellenmesi için akışkan özellikleri, soğutma devresinde kullanılan boruların giriş çıkış çapları, yüzey özellikleri gibi fiziksel özellikleri, kullanılan termostatın uzama miktarı, efektif alan gibi özellikleri, pompanı ve fanın fiziksel özellikleri ve ayrıca radyatörün özellikleri gibi verilere ihtiyaç duyulmaktadır. Burada sözü edilen her bir özellik bileşenler çalışma alanına eklendikten sonra ilgili pencereler ile program içerisine girilebilmektedir. Böylece soğutma sistemini oluşturan tüm bileşenlere ait veriler kullanılarak modelleme işlemi gerçekleştirilir.

BULGULAR

GT-Suite ortamında radyatör, master ve slave şeklinde isimlendirilen iki ayrı objenin birleşimi kullanılarak modellenir. Genel olarak, radyatörün modellenmesi için radyatörde meydana gelen ısı transferi iki forma ifade edilir. Birincisi, radyatörün giriş ve çıkışından alınan sıcaklık, basınç, akış debisinin yanı sıra radyatörün verimi, giriş çıkış sıcaklık oranı gibi değerlerin kullanılmasıdır. İkinci olarak, aşağıda ifade edilen ve Nusselt sayısı olarak bilinen denklemde katsayıların belirlenmesidir.

$$Nu = C\,Re^{m}Pr^{1/3} \qquad (1)$$

Deneysel sistem üzerinden toplanan gerçek veriler de kullanılarak motor soğutma sistemi GT-Suite ortamında oluşturulmuş ve ayrıca elde edilen model üzerinde kontrol algoritmalarının simülasyon yapıldığı Simulink ortamına aktarılması için oluşturulan model içerisine Simulink öğesi eklenmiştir. GT-Suite ortamında hazırlanan model Şekil 2 ile gösterilmektedir.

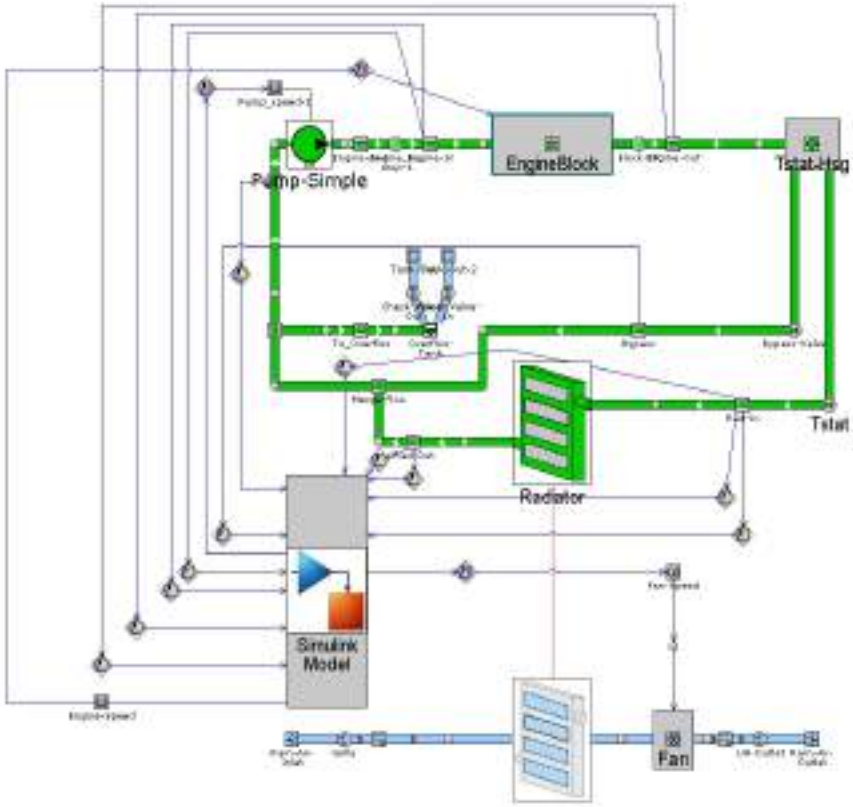

Şekil 2. Motor Soğutma Sistemi İçin Hazırlanan GT-Suite Ekran Görüntüsü

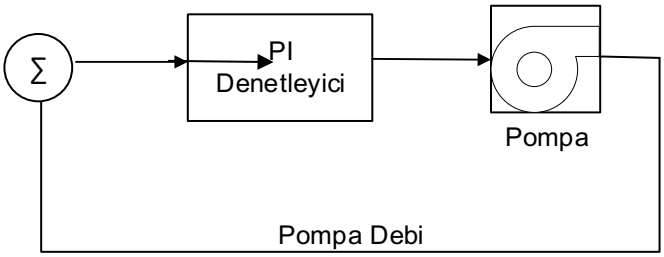

Şekil 3. Pompa Debisi İçin Tasarlanan Kontrolcü Blok Diyagramı

Elektronik kontrollü soğutma sisteminin mekanik tasarımının ardından sistem içerisinde bulunan elektrikli pompa ve 3 yollu valfe uygun kontrol işaretlerinin gönderilebilmesi için bu bileşenlerin ayrı ayrı matematiksel modellerinin elde edilesi gerekmektedir. Sistem içerisinde bulunan her bileşen için bir denetim algoritması tasarlanarak bu bileşenlerin her birinin ayrı ayrı istenen referanslara girdilere kaşı performansları incelenmiştir. Elektrikli pompa ve 3 yollu valfin matematiksel modellerinin elde edilmesi için Matlab içerisinde yer alan "Design optimization" modülü kullanılmıştır. Adı geçen modül için öncelikle pompa ve valf için giriş sinyalleri tanımlanarak pompa çıkışındaki debimetre ile debi, valf için ise açıklık oranı ölçülerek kaydedilmiştir. Daha sonra kaydedilen veriler Matlab ortamına aktarılarak adı geçen araç kutusu kullanılarak sistemin S düzleminde matematiksel eşitliği elde edilmiştir. Matlab ortamında hazırlanan ve GT-suite ile haberleşen program ise Şekil 4'te gösterilmiştir.

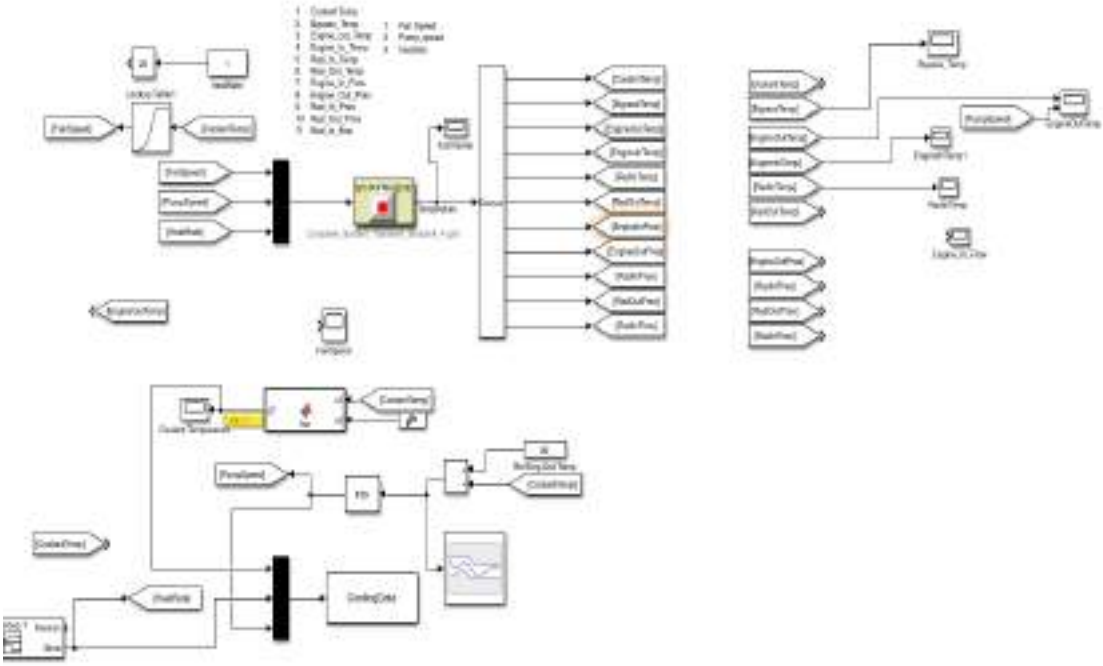

Şekil 4. Simulink Ortamında Hazırlanan Program

SONUÇ

Çalışma kapsamında kontrolcünün ve motorun termal modelinin performansını ortaya koyabilmek amacıyla öncelikle 20 kW'lık bir sabit ısı girişi daha sonra sinüzoidal değişim gösteren giriş uygulanmıştır. Her iki durum için motorun çıkış sıcaklık grafiği Şekil 5 ile verilmiştir.

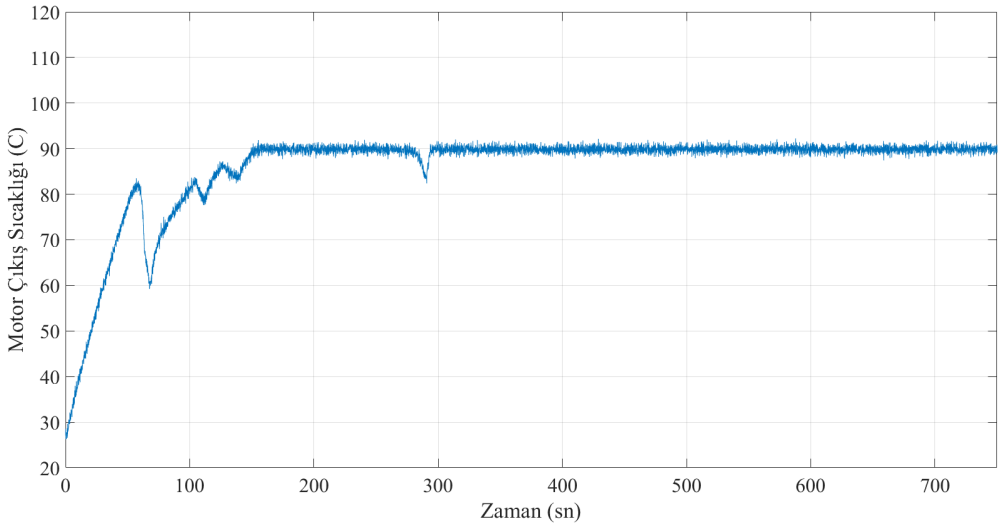

Şekil 5. 20 kw'lık Sabit Isı Girişi Sonucunda Elde Edilen Motor Çıkış Sıcaklık Grafiği

Şekil 5'ten görüleceği üzere motor çıkış sıcaklığı pompanın kontrolcüsü sayesinde motorun ısınma fazı boyunca yükselmiş ve daha sonra kontrolcü bloğuna referans sinyal olarak verilen 90 °C sıcaklık değerine oturmuştur. Yaklaşık 80.saniye civarında meydana gelen eğrideki düşüş termostatın açılması neticesinde sıcak suyun bir anda radyatörden geçirilip soğutulmasından kaynaklanmaktadır.

İkinci olarak kontrolcü performansı değişken bir ısı girişinin uygulanması sonucunda elde edilmiştir. Uygulanan değişken ısı girişi Şekil 6'da verilmiştir.

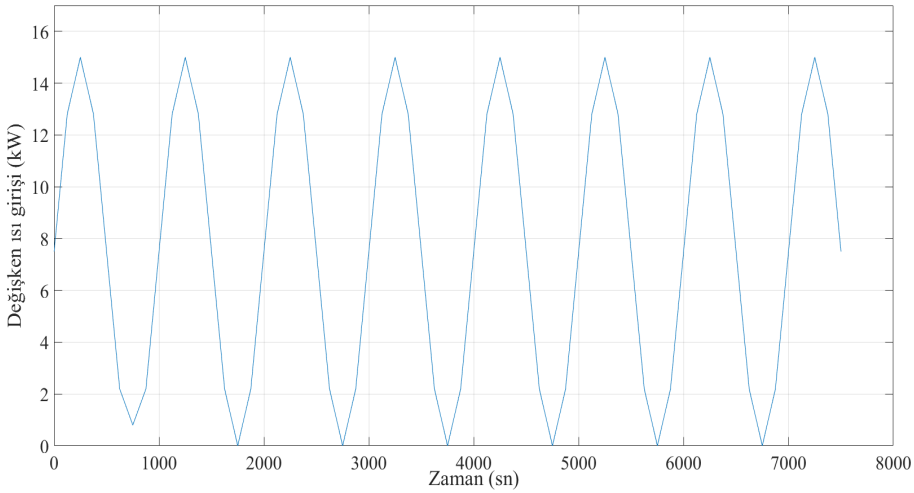

Şekil 6. Değişken Isı Girişi

Uygulanan bu ısı girişine karşılık elde edilen motor çıkış sıcaklık değişimi ise Şekil 7'de gösterilmiştir.

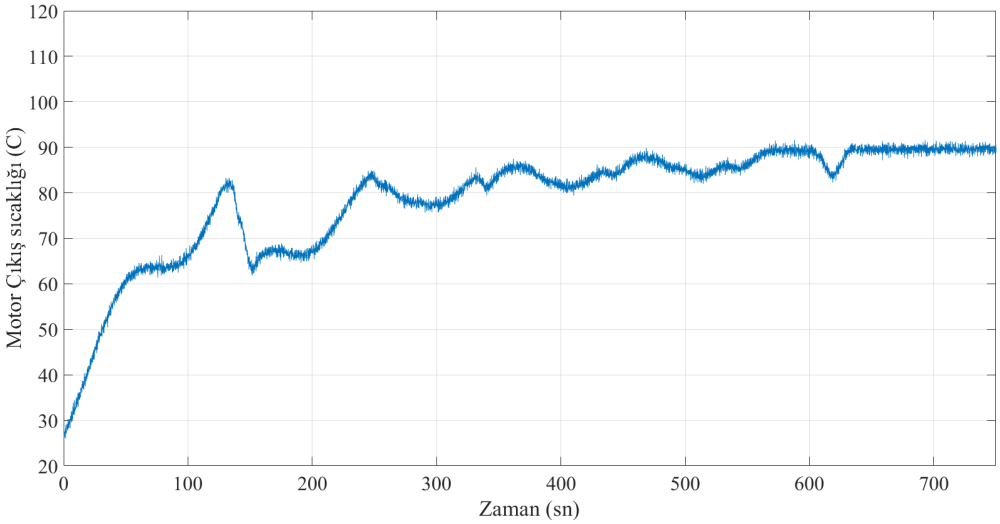

Şekil 7. Değişken Isı Girişine Karşılık Elde Edilen Motor Çıkış Sıcaklık Grafiği

Şekil 7'den görüleceği üzere değişken ısı girişi uygulandığı zaman motor çıkış sıcaklık değişimi dalgalı olmaktadır. Fakat dikkat edilirse kontrolcü sadece pompayı kontrol ederek sıcaklık değişimi 90 dereceye sabitlemeye çalışmaktadır. Bir içten yanmalı motorun gerçekte bu biçimde bir ısı üreteci olması mümkün değildir. Dolayısıyla burada sadece kontrolcünün performansının test edilmesi amaçlandığından kontrolcüyü zorlayıcı işaretler kullanılmıştır. Bunun sonucunda elde edilen işaret ise yeterli bulunmuştur.

ÖNERİLER

Bu araştır kapsamında yapılan modelleme çalışmasında bir içten yanmalı motor ısı üreteci şeklinde ele alınmış ve çıkışındaki akışkanın sıcaklığı kontrol edilmeye çalışılmıştır. İçten yanmalı motorlarda kullanılan klasik soğutma sitemlerinde akışkanını motor kanallarına göndermek için gücünü krank kayış mekanizmasından alan mekanik pompa kullanılmaktadır. Kullanılan mekanik pompanın devir sayısı doğrudan motora bağlı olduğundan pompanın istenen devir sayılarında çalıştırılması imkânsızdır. Bu amaçla mekanik yerine elektrikli pompanın kullanılmasıyla motora gereğinden fazla akışkanın gönderilip motorun ısınma fazının geciktirilmesi önlenir ve bu sayede motorda gereksiz yere soğutma sistemi yoluyla dışarı atılan ısı enerjisi azaltılabilir. Böylece motorun egzoz emisyonları dahi iyileştirilebilir. Örneğin; motorun en fazla NOx emisyonu saldığı an motorun soğuk çalıştırma koşullarıdır. Bu çalışma motorda sadece pompanın kontrol edilmesi ve gereksiz akışkan pompalamasının önüne geçirilerek motorun optimum termal çalışma koşullarına hızlı bir şekilde yükselmesi sağlanmış ve bu değerde sabit kalması sağlanmıştır. Bu çalışmanın sonraki aşamalarında ise diğer soğutma bileşenleri kontrol edilebilir düzenekler sağlanarak en zor çalışma koşullarında uygun denetleyici algoritmalarının test edilmesi sağlanabilir.

KAYNAKLAR

Allen, D. J., & Lasecki, M. P. (2001). Thermal Management Evolution and Controlled Coolant Flow. *SAE International*, 10.4271/2001-01-1732.

Khanjani, K., Deng, J., & Ordys, A. (2014). Controlling Variable Coolant Temperature in Internal Combustion Engines and its Effects on Fuel Consumption". *SAE Technical Paper*.

Lahuerta, J., & Samuel, S. (2013). Numerical Simulation of Warm-Up Characteristics and Thermal Management of a GDI Engine", *SAE International*, 10.4271/2013-01-0870.

Melzer, F., Hesse, U., Rocklage, G., & Schmitt, M. (1999). Thermomanagement". *SAE International*, 10.4271/1999-01-0238.

Minovski, B. B., & Lofdahl, L. (2014). Study of Software Integration for Transient Simulation of Future Cooling System for Heavy Truck Application. *SAE Technical Paper*.

Pizzonia, F., Castiglione, T., & Bova, S. (2016). A Robust Model Predictive Control for efficient thermal management of internal combustion engines. *Applied Energy* 169: 555-566.

Ranjan, R., Jha, K. K., Brahmasani, L., & Khan, P. (2016). Prediction of Engine Thermal Behavior during Emission Cycle Using 1D Four Point Mass Model. *SAE International*, 10.4271/2016-01-0197.

Samhaber, C., Wimmer, A., & Loibner, E. (2001). Modeling of Engine Warm-Up with Integration of Vehicle and Engine Cycle Simulation. *SAE International*, 10.4271/2001-01-1697.

Wagner, J. R., Srinivasan, V., Dawson, D. M., & Marotta, E. E. (2003). Smart thermostat and coolant pump control for engine thermal management systems. *SAE Technical Papers*.

Zhou, B., Lan, X. D., Xu, X. H., & Liang, X. G. (2015). Numerical model and control strategies for the advanced thermal management system of diesel engine. *Applied Thermal Engineering* 82: 368-379.

EXPERIMENTAL INVESTIGATION OF THE EFFECTS OF PILOT INJECTION ON NO_x EMISSION

Erdoğan GÜNER
Bayburt University
erdoganguner@bayburt.edu.tr

Alırıza KALELİ
Bayburt University
arizakaleli@bayburt.edu.tr

Kadir BAKIRCI
Atatürk University
abakirci@bayburt.edu.tr

ABSTRACT: Day-to-day stricted emission standards force vehicle manufacturers and researchers to reduce NO_x emissions. Pilot injection is a method used to reduce NO_x emissions. In this method, a part of the fuel is injected into the cylinder as a pilot injection and in-cylinder temperature is increased by the combustion of this fuel. Thus, the subsequent injection is carried out on a hotter mixture. In this case, the ignition delay and the amount of unburned fuel accumulated in the cylinder is reduced. Hence, the sudden pressure rise and high temperature inside the cylinder due to the ignition delay are somewhat reduced. As a result, this method reduces NOx emissions. In this study, experiments were carried out on a Ford diesel engine with 4 injections per cycle. Experiments were carried out with different injection angles and amounts. As a consequence, the effect of the injection strategy on NO_x emissions was observed.

Key words: pilot injection, no_x emissions, diesel engines

PİLOT ENJEKSİYONUN NO_x EMİSYONU ÜZERİNE ETKİSİNİN DENEYSEL İNCELENMESİ

ÖZET: Günden güne katılaşan emisyon standartları araç üreticilerini ve araştırmacıları NO_x emisyonunu azaltmaya yönelik çalışmalara zorlamaktadır. Pilot enjeksiyon uygulamak NO_x emisyonunu azaltmada kullanılan bir yöntemdir. Bu yöntemde yakıtın bir kısmı ön püskürtme olarak silindir içerisine enjekte edilir ve bu yakıtın yanması ile silindir içi sıcaklık artmış olur. Böylelikle, daha sonra gerçekleştirilen püskürtme daha sıcak bir karışımın üzerine gerçekleştirilmiş olur. Bu sayede tutuşma gecikmesi ve dolayısıyla silindir içerisinde biriken yanmamış yakıt miktarı azaltılmış olur. Yani tutuşma gecikmesinin sebep olduğu ani basınç artışının ve bu sebeple meydana gelen silindir içi yüksek sıcaklıkların bir miktar azaltılmış olur. Sonuç olarak NO_x emisyonları bir miktar azaltılmış olur. Bu çalışmada deneyler Ford marka bir dizel motor üzerinde her çevrimde 4 enjeksiyon uygulanarak gerçekleştirilmiştir. Deneyler farklı enjeksiyon açı ve miktarlarında yapılmıştır. Sonuç olarak, pilot enjeksiyonun NO_x emisyonu üzerindeki etkisi gözlemlenmiştir.

Anahtar sözcükler: pilot enjeksiyon, no_x emisyonları, dizel motorlar

INVESTIGATION OF THE EFFECT AIR BUBBLE INJECTION ON CYCLIC VARIATIONS IN ENGINE COOLING SYSTEM WITH WAVELETS TECHNIQUE

Galip KALTAKKIRAN
Atatürk University
g.kaltakkiran@atauni.edu.tr

Aliriza KALELİ
Bayburt University
arizakaleli@atauni.edu.tr

Hadi Ghasemi ZAVARAGH
Atatürk University
hghz2005@gmail.com

Kadir BAKIRCI
Atatürk University
abakirci@atauni.edu.tr

ABSTRACT: Advanced thermal management in internal combustion engines is effective as to the total fuel consumption and the improvement of engine exhaust emissions. It is also effective in the cyclic variations caused by variable combustion temperatures in the cylinder or in the improvement of irregular combustion between cyclic to cycles. Recently, a number of valuable studies have been conducted to assess and improve the cooling system and engine performance using various technologies. In this study, with a novel point of view, air-water mixture is employed to use in the cooling circuit of a spark-ignition internal combustion engine. The warm-up period of the engine is shortened and the cyclic variations are analyzed in the system which is formed by collecting pressure data with the inside of the cylinder pressure sensor during the warm-up period. In this study, Wavelet technique has been used to examine the effects of air injection strategy on the changes in cylinder pressure. An important factor in the preference of this technique is that the signal can be analyzed locally. Thus, the use of a small region for analysis of a large signal will be sufficient. In addition, the advantages of the designed system are presented in comparison with the classical system. The pressure data obtained from the designed system and classical cooling system are analyzed and the superior aspects of the designed system have been put there.

Key words: separator, air bubbles, cyclic variations, wavelets, engine cooling systems

INTRODUCTION

With regard to the innovative method of this study, there was no specific research directly related to the subject of the presented method. Therefore, different studies are combined. Air bubbles can be used as an effective tool in the cooling fluids to increase heat transfer and performance of heat exchangers. On the other side, over- injected air

into the heat exchanger can be an obstacle to efficient heat transfer to the coolant fluid. In coiled tube heat exchanger, the influence of air bubble injection on the heat transfer and the number of thermal units (NTU), have been experimentally investigated under different air flow rates. It was identified that the injected air bubbles cause to a significant increase in the NTU of the heat exchanger [Khorasani and Dandvand 2017]. Furthermore, the air flow rate is an important factor in the bubble production method which is examined in the heat exchanger shell and the coil sides. The various air flow rates were tested to find out an optimum state. Air flow rate increased heat transfer. The heat transfer coefficient was increased by 6-187% using air transfer method [Moosavi et al. 2016]. In order to better understand the flow properties, some air bubble injection and sub-cooled flow boiling experiments were performed. One example is the CFD model. Here it is used to estimate the overcooled flow boiling events in the fuel groups of pressurized water reactors [Samaroo et al. 2014]. In another study, the thermal performance of the upward simultaneous air-water flow in a narrow canal has investigated. The number of Reynolds in the experiment is in the range 800-6000 and the ratio of air-water mass is 0-0.05. As a result, the number of Reynolds and air-water flow have significant effects on heat transfer and pressure drop [Chang and Huang 2013].

Regarding the development of engine thermal systems, wax thermostats were introduced in 1950s and no significant change in vehicle cooling systems was observed. On the other hand, new methods to be used in engine cooling systems continue to be searched for the demands for more efficient operation of the engine. As a result of the studies carried out, new thermal components such as refrigerant flow valves, variable cooling water pumps, controlled thermostats, variable fans and heat exchangers are used [Shutty et al. 2013]. In a study, the double cooling circuit at different temperatures in the engine cooling system was examined as a new method and the mathematical model of the engine was developed. According to the results, significant improvements in engine fuel consumption, air supplementation and heating were obtained [Cipollone et al. 2013]. In another study, a special variable position electromagnetic thermostat is used in the engine cooling system to better control the coolant flow rate. In the advanced cooling system with the thermostat used, it was found that the engine warm-up time decreased and thus the values of exhaust emission gases such as CO_2, CO, THC and smoke opacity decreased [Mohamed 2016]. In a study in the literature, the original zero-dimensional model of an ICE cooling system was developed to precisely define onset of the nucleate boiling [Cipollone and Di Battista 2014].

In addition to the engine temperature and fuel consumption, the pressure changes in the cylinder must be fully understood. For this purpose, cyclical variations have been one of the important parameters to be considered during the design phase of internal combustion engines and the cyclic variations have to be kept at minimum values. Because, in engines where cyclical variations occur, the motor output power is reduced by about 10% for the amount of fixed fuel [Young 1981]. Understanding the characterization and control of cyclic variations in the combustion process in internal combustion engines helps to develop new strategies and control the changes in the cycle cycle. In defining and understanding this problem, it was seen that cyclical differences were higher in spark ignition engines than compression ignition engines.

Fluctuations in the cylinder are caused by charge movement in every cycle and the flow leads to changes in flame development and propagation [Heywood 1998]. In a study to understand the cyclical variations and to define the causes of them, they investigated the effects of hydrogen and gasoline fuels on exhaust emission, engine performance and cyclic variations for lean working conditions. The effects of different air-fuel ratios and the addition of variable amounts of H_2 to cyclical variations were investigated [Ceviz et al. 2012].

Some analysis techniques are used in the literature to describe the formation and characterization of cyclic variations Wavelet analysis is one of these techniques. Wavelet analysis has been used successfully to characterize cyclical variations for different parameters in internal combustion engines. The effects of different loads on the inside of the cylinder are analysed in long, medium and short periods in internal combustion engines by using continuous wavelet transform. As the engine speed increases, the cyclic variations are reduced due to the fact that the rotation speed becomes more effective with the increase in the piston speed and the combustion process is prolonged [Sen et al. 2008]. In addition, the analysis of temporal variations in mean effective pressure (IMEP) data series was also performed by wavelet analysis [Saxena and Maurya 2018].

When the literature studies are examined, a large number of studies have been carried out on cyclical variation and the use of wavelet analysis technique. In this study, with a novel point of view, air-water mixture is employed to use in the cooling circuit of a spark-ignition internal combustion engine. The warm-up period of the engine is shortened and the cyclic variations are analyzed in the system which is formed by collecting pressure data with the inside of the cylinder pressure sensor during the warm-up period. In addition, the advantages of the designed system are presented in comparison with the classical system. In the last sections of the study, the superior aspects of the system designed by analyzing the pressure data obtained in the classical cooling system and the designed system were put there. When the global wavelet spectra are examined, it is observed that the variations in the frequencies of all three signals used in the implementation of the designed system are reduced and thus the cyclical variation decrease. There is no doubt that this study will contribute to the literature in understanding the characteristics of cyclic differences along with the wavelet analysis technique.

METHODS

Detailed schematic layout of the test setup and the engine technical specifications are presented in Fig. 1 and Table 1 respectively. The experimental setup consists of a gasoline engine, air compressor, a control panel, a hydraulic dynamometer and measurement instruments as well as controllers, adjusting and actuator tools.

Table 1. Specifications of Test Set-up Engine.

Engine type	Ford MVH418, 4-Stroke, water cooling, fuel injected, spark ignition
Number of cylinders	4, Dohc-16 V
Firing order and Compression ratio	1-3-4-2 10:1
Bore diameter, Stroke, Total displacement	80.6 mm, 88 mm, 1796 cm^3
Maximum power	93 kW @ 6250 R.P.M
Maximum torque	157 Nm @ 4500 R.P.M
Idle speed	900
Fuel LPG –	Gasoline
Fuel injection type	BOSH KE-Jetronik

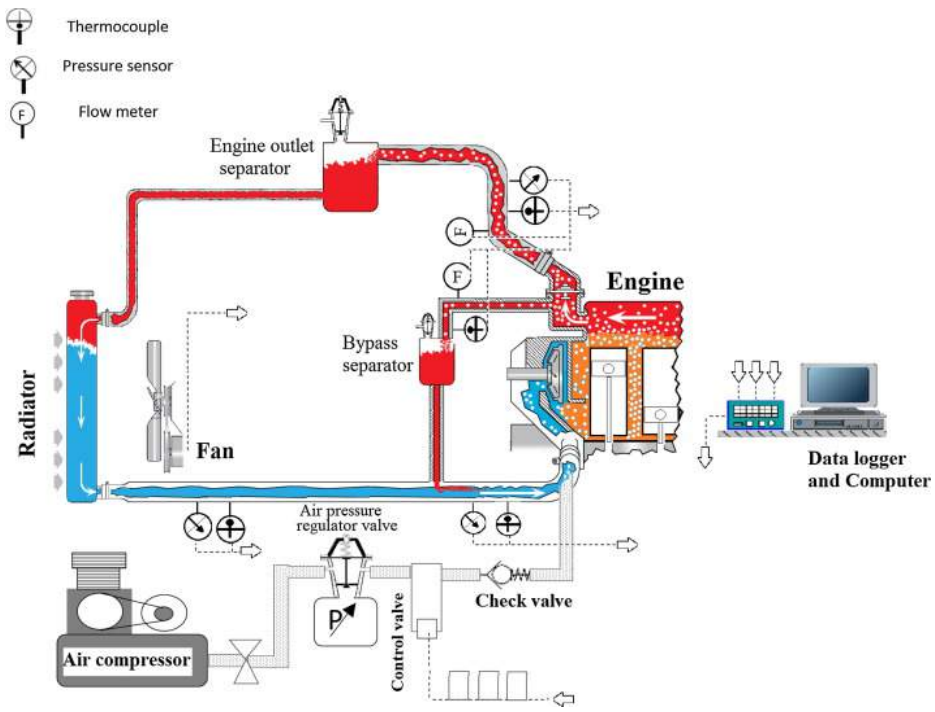

Figure 1. A Schematic Layout of the Test Set Up.

Some of the software and hardware components have used to obtain real-time data from the experiment setup. LabVIEW program has used for reading the in-cylinder pressure values, image processing and provisioning and saving of the instant data. All the data have monitored and recorded with the program we prepared in the laboratory. Sensors and measuring instruments are used as hardware. In the study, a piezoelectric pressure transducer has mounted on the engine cylinder head. The voltage signal corresponding to the cylinder pressure is recorded by the data acquisition system by the LabVIEW program. Engine speed was also measured with a built-in speed sensor which operates with photo electrical system by evaluating the

light that shines through a grid wheel. A FESTO controller valve (MPYE-5-1/8-HF-010-B) was used in the engine cooling circuit to control injected air flow rate.

Induced average effective pressure (IMEP), Induced work W_{ind} divided to displacement volume V_d ;

$$IMEP = \frac{W_{ind}}{V_d} \quad (1)$$

$$W_{ind} = \frac{2\pi}{360}\int_{-180}^{180}(P(\theta)\frac{dV}{d\theta})d\theta \quad (2)$$

Where, P shows the cylinder pressure and V the cylinder volume.

The change in the heat dissipation, which is another combustion parameter used in this study, is expressed by the following equation.

$$\frac{dQ(\theta)}{d\theta} = \left(\frac{1}{\gamma-1}\right)V(\theta)\frac{dP(\theta)}{d\theta} + (\frac{\gamma}{\gamma-1})P(\theta)\frac{dV(\theta)}{d\theta} \quad (3)$$

Where, Q is heat dispersion and γ is specific heat ratio. Total heat volatility is obtained from the integration of the pressure curve up to the point where the combustion starts. In this study, the change in cyclical differences is the maximum cylinder pressure.

Cyclic Variations in Engines

Cyclical variations are defined as irregularities occurring during combustion in the cylinder seen in both diesel and gasoline engines. The cyclical variations in the literature are often undesirable in engines because of the reduction in engine output, motor unstable operation, vibration and noise. 10% more power can be achieved at the same fuel consumption as preventing cyclical variations [Ozdor et al. 1994].

tra-cylinder pressure formation in internal combustion engines is closely related to the combustion process, and these variations in combustion processes in engine cycles cause significant changes. It is possible to see these differences both from the cycle and from the cylinder to the cylinder. The differences between the rollers are due to the same events that differ from the cylinder to the cylinder. These differences due to the combustion process are caused by the following reasons [Heywood 1998].

Change in the movement of the mixture inside the cylinder at the time of ignition,
Change in the amount of air-fuel feeding each cycle cylinder,
Especially the difference between the residual gas remaining in each cycle cylinder and the fresh filling mixture around the ignition advance,

An example of a cylinder pressure graph for cyclic differences occurring even when all engine operating parameters such as ignition advance, throttle opening ratio,

engine load is kept constant is shown in Figure 2. As can be seen from the graph, 50 motor pressure cycle spins are drawn on top of each other. Especially at the maximum pressure value and maximum value of the crankshaft angle from the firing time, there are differences in the conversion from the cycle.

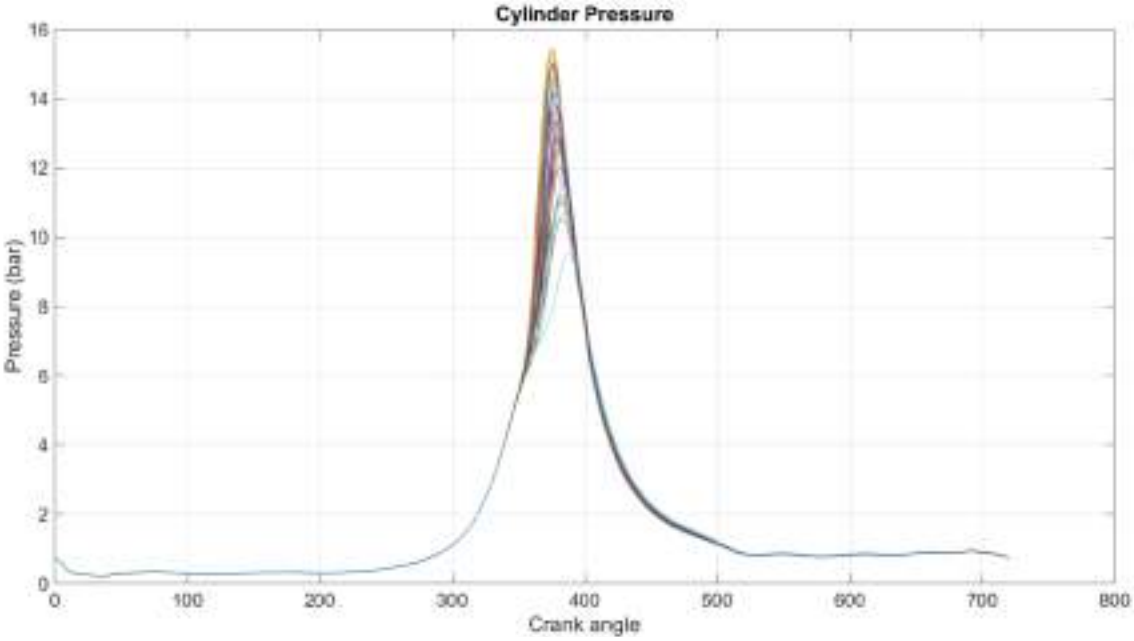

Figure 2. The Cyclical Differences of a Gasoline Engine in the 50 Cycles in the Cylinder.

Wavelet Analysis

In this study, the cooling time of the engine has been shortened by sending an air bubble to the coolant flow by a change in the cooling system of a spark ignition internal combustion engine. During the warm-up period, pressure data were collected by using the in-cylinder pressure sensor to analyse the cyclical differences in the generated system. In addition, the advantages of the designed system are presented in comparison with the classical system.

The calculation of the mathematical value known as the variation coefficient of the data in a time series is obtained by the ratio of the standard deviation of the data to the average. This value is very advantageous to compare the degree of variation between two time sequences statistically, even if the average values are quite different from each other. Although the expression of variance is meaningful for a time series with a constant frequency, the frequencies of the studied data are insufficient to define the variability over time. Since the data cannot reveal the spectral characteristics of the data, the frequency is insufficient in the analysis of the signals that change over time. Therefore, the variance value cannot fully characterize the examined mark. For this purpose, in the study, the pressure differences occurring in the cylinder by wavelet analysis method has been revealed spectral features.

Wavelet analysis is theoretically carried out in two ways: continuous wavelet transform (CWT) and discrete wavelet transform (DWT). In the continuous wavelet transform (CWT), the time-frequency spectra are matched in the time-frequency plane

where visualization of various periodicities from time-to-amplitude plane and their variation over time. The time-frequency plane uses a window of variable size to focus on the high-frequency components of this series, while an expanding window is used in the low-frequency features [Kumar and Foufoula-Georgiou 1997]. $\psi(t)$ continuous wavelet transforms for wavelet function (CWT);

$$CWT(a,b) = \frac{1}{\sqrt{|a|}} \int_{-\infty}^{\infty} x(t)\, \psi^{*}(t) \left(\frac{t-b}{a}\right), \quad a,b \quad \in R, a \neq 0 \tag{4}$$

Where, $\psi(t)^{*}, \psi(t)$ conjugate , it's a mother-type wavelet. $x(t)$ continuous signal and a, b coefficients.

WPS (Wavelet Power Spectrum) and GWS (Global Wavelet Spectrum) were used in the analysis of the differences in the cycle. WPS provides information on the fluctuation in the variance of the time warp at different frequencies or scales. The WPS expression is obtained by equality (5) by normalizing the series and dividing by standard deviation.

$$WPS = \frac{|CWT(a)|^2}{\sigma^2} \tag{5}$$

CWT is a complex function and WPS can easily show high variance in time series and their occurrence frequency. In addition, the time period of valid periods can be easily determined. GWS (Global Wavelet Spectrum) can be calculated by averaging WPS over time. In this way, the predominant prophesies of the time series studied can be easily demonstrated. GWS is calculated by the equation (6).

$$GWS = \frac{1}{N} \sum_{n=1}^{N} |CWT(a)|^2 \tag{6}$$

RESULT AND DISCUSSION

The superior aspects of the system designed by analyzing the pressure data obtained in the classical cooling system and the designed system have put there. After the data collection, the calculations have performed for the IMEP and total heat emission. A single engine operating point has chosen to prevent the subject from disintegrating. The aim of selecting this point was to be the most commonly used condition for vehicle drivers in urban traffic conditions. The test engine was set to 20 Nm with a speed of 2000 rpm and a light weight load. The comparison of the air bubble cooling system designed with the classic engine cooling system was previously performed on the temperature data and the findings were presented in a SCI journal [Zavaragh et al. 2017]. According to this, firstly the most important point of the designed system, which is the advantage of shortening the warm-up time, is shown in the study. In addition, the system, which is designed at different engine operating points, is compared with conventional engine cooling systems both in terms of warm-up times and exhaust emission values. In this study, the effects of the designed system on the in-cylinder pressure have investigated and the relevant results were given in this study. For this purpose, 1024 engine cycle crankshaft angle values in Figure 3, and Figure 4 shows the data of IMEP, PMAX and THR.

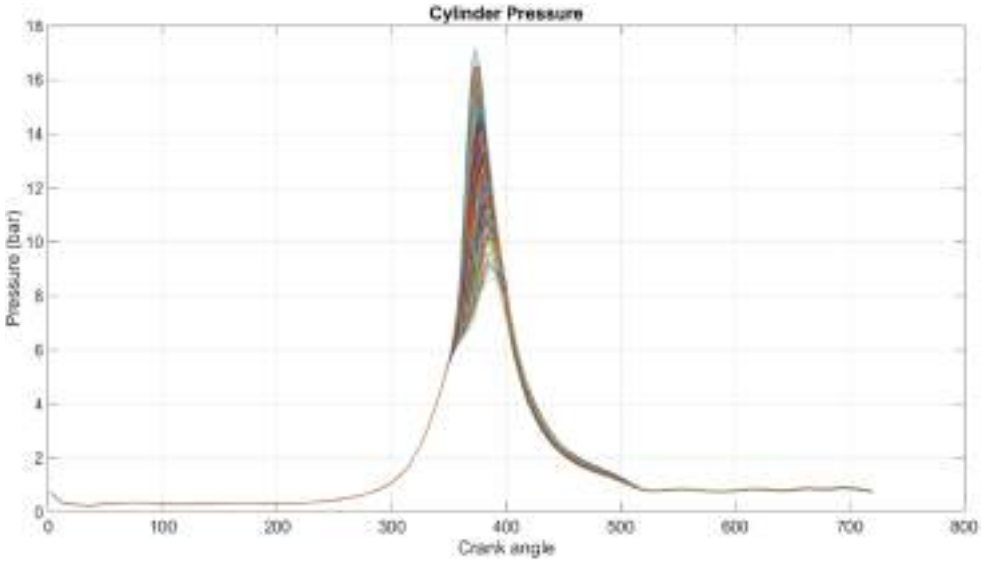

Figure 3. Pressure Change Graph for 1024 Engine Cycle Received from Classic System

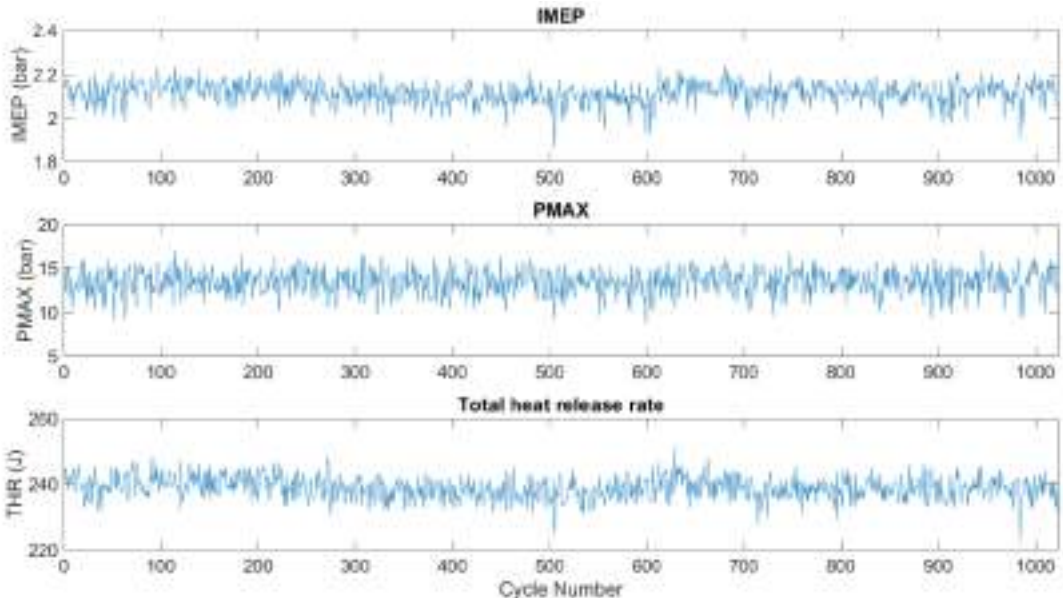

Figure 4. IMEP, Maximum Pressure and Total Heat Transmission Change Calculated From Classic Engine Cooling System At 20Nm and 2000 rpm Working Conditions

After this section, wavelet analysis results are given. The results of the classical system are given for the convenience of analyzing the results. Different wavelet analyzes have performed for both IMEP, maximum pressure and THR. Firstly, WPS and GWS graphs are shown in Figure 5 for the IMEP data received on the classical system. The colors seen in WPS indicate the energy of the signal and are defined as the amplitude of the wavelet function. The colors seen in WPS indicate the energy of the signal and are defined as the amplitude of the wavelet function. Here, the red color shows the highest energy and the blue color shows the lowest signal energy. In the Wavelet power spectrum graph, the black line and the u-shaped region define the values in the 95% confidence interval. The black curve defined in the Wavelet power spectrum shows the cone effect. The cone effect includes the edge effect when all time sequences are

matched. Therefore, regions outside of this curve are not evaluated and only the ones in the interior are evaluated.

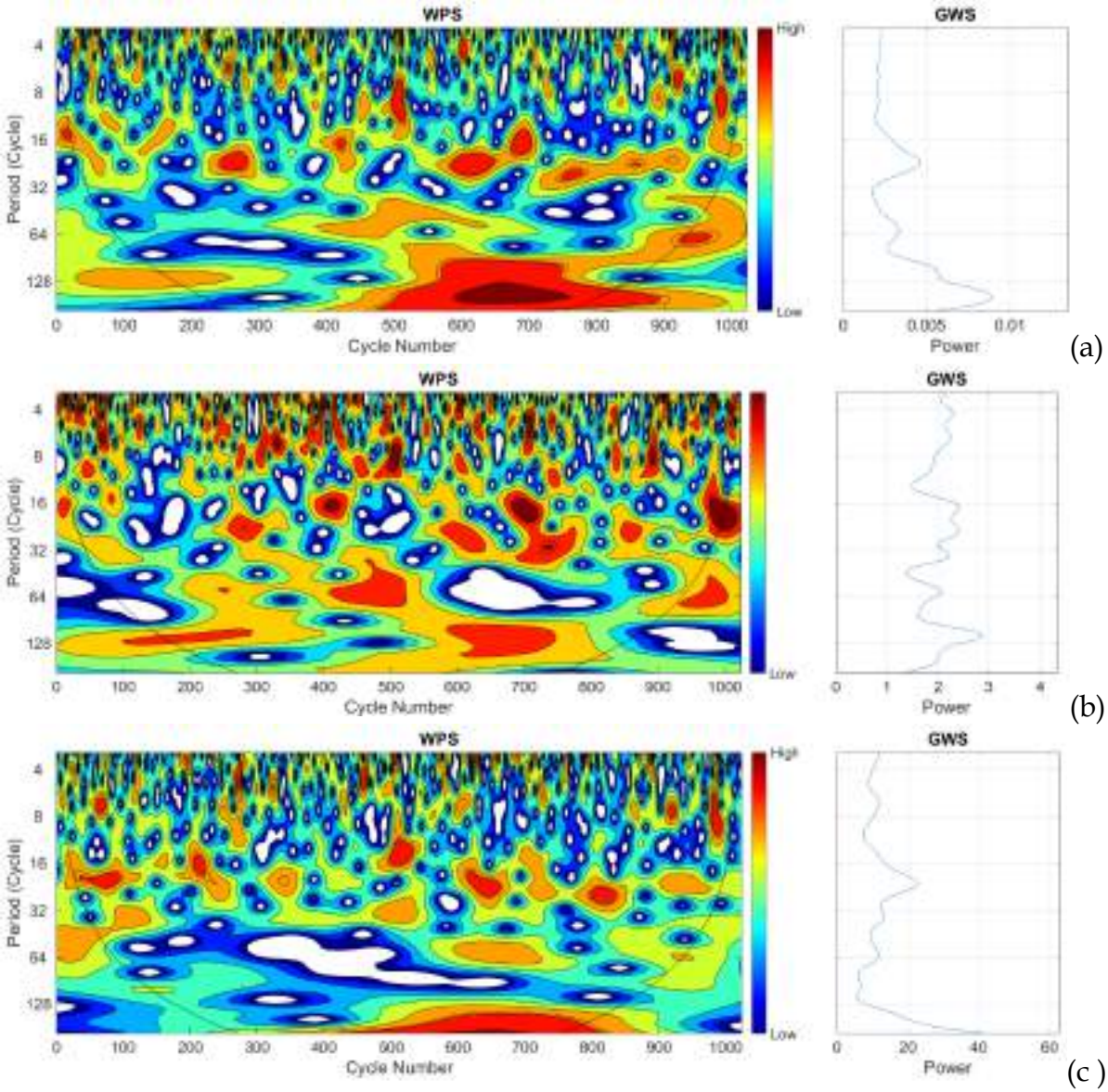

Figure 5. Analysis for WPS and GWS, IMEP (a), Maximum Pressure (b) And Total Heat Dissipation Changes (c) For Classic Cooling System At 20Nm and 2000 rpm Working

Figure 5a shows the WPS graph for the IMEP data received from the classic engine cooling system. Graphical analysis reveals a wide periodicity between 241-283 cycles in 18-24 periods, 498-513 cycles in 7-11 periods, 579-711 cycles in 13-28 periods, and in 586-756 cycles in 128-184 periods. Spectrum analysis is given for maximum pressure changes given in Figure 5b. Periodicity is observed between 18-28 cycles, in the range of 253-309, between 387-432 cycles in 14-20 periods, in cycles of 406-522 and in periods of 37-70 and between 479-515 cycles in 5-10 periods. In the 668-773 cycle range, between 13-37 periods and between 585-745 engine cycles in the period of 99-150 that there is a wide change in the frequencies of the signal and periodicity. The pressure data obtained from the classical system and the total heat emission obtained by

calculating the mathematical expression given by Equation (3) are given in Figure 5c. In the spectrum graph obtained for THR, between 37-93 cycles in 18-23 periods, in the 206-223 cycle range in 14-18 periods, between 493-530 cycles in 10-16 periods, in between 614 and 664 cycles in 17-26 periods, in between 796-836 cycles between 21-28 periods. The graph of the pressure change by applying the air bubble separator to the cooling system on the engine test system is given in Figure 6. Figure 7 shows the IMEP, maximum pressure and total heat diffusion curves.

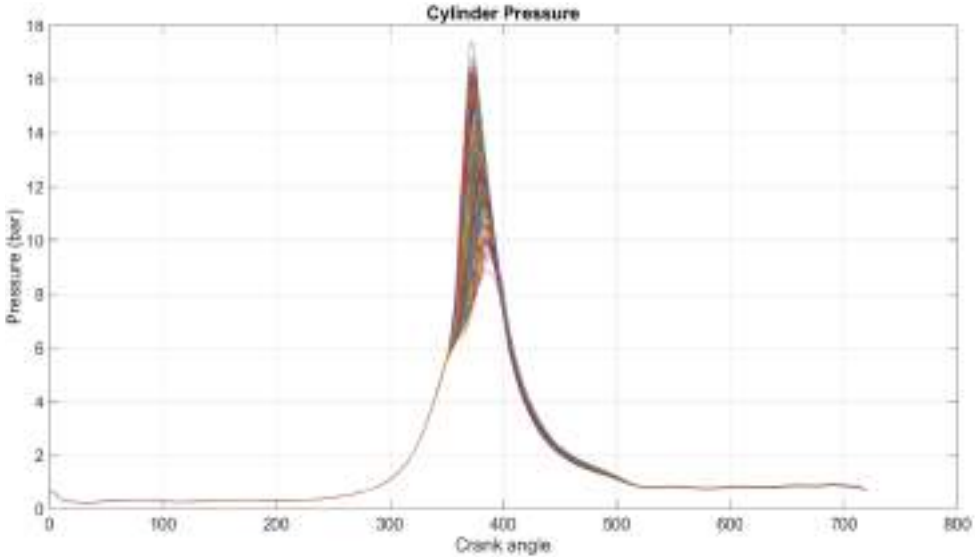

Figure 6. Engine Pressure Change Graph From Designed System

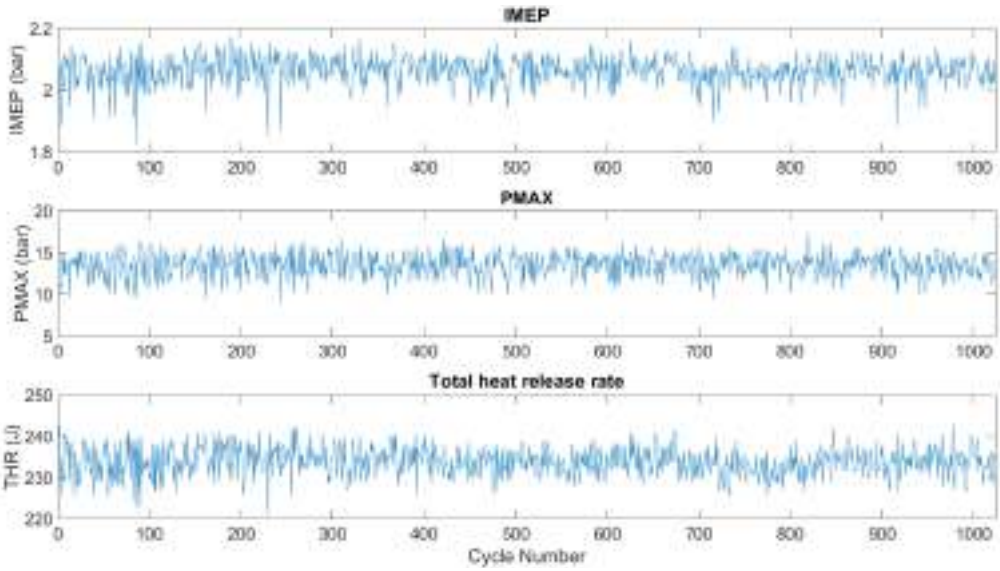

Figure 7. At 20Nm and 2000 rpm Working IMEP, Maximum Pressure and Total Heat Distribution from the Designed System

The cooling system is transferred to the fluid contained in the air bubble by the designed electronic device. Analysis of the in-cylinder data obtained by the wavelet method is given in Figure 8. Similar to the analysis in the classical system, firstly the IMEP data and then the maximum pressure and then the total heat dissipation (THR)

have analyzed. Then, periodic bands and engine cycles are aggregated in Table 2 for all systemic information for both systems.

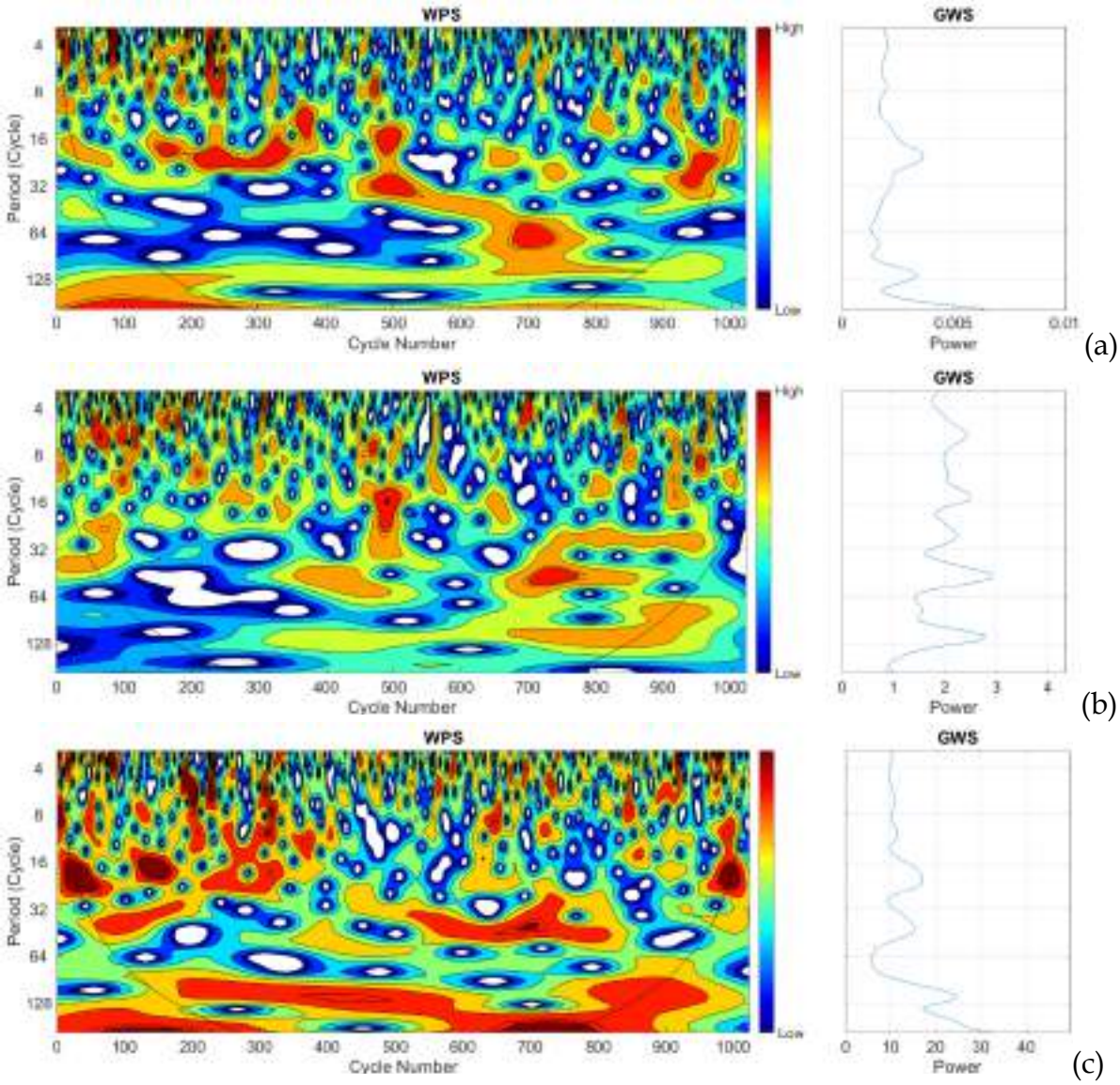

Figure 8. At Transfer of Air Bubbles for Cooling, At 2000 rpm and 20Mm load conditions, (a) IMEP, (b) Maximum Pressure and (c) Total Heat Dissipation Changes (THR) For WPS and GWS Analysis

When the WPS graph given in Figure 8a is examined, it is seen that there are periods of 26-34 in the range of 467-528 and in periods of 18-20 in the range of 151-181 and in periods of 16-24 in the range of 200-340. The maximum pressure changes given in Figure 8b are given. In spectrum analysis, periodicity is observed between 13-23 periods in the 476-503 cycle range and in the period of 42-51 in the 702-770 cycle range. Finally, the analysis for the total amount of heat dissipation is given in Figure 8c. In the spectrum graph obtained for THR, a signal frequency was observed between 120-167 cycles in 15-23 periods, and in the 675-715 cycle range in periods of 40-43.

Table 2. Periodic Range and Motor Cycles Table

	Periodic Range (Cycles)			Number of engine cycles (Cycles)		
	IMEP	**PMAX**	**THR**	**IMEP**	**PMAX**	**THR**
Classic engine cooling system	18-24 7-11 13-28 128-184	18-28 14-20 37-70 5-10 13-37 99-150	18-23 14-18 10-16 17-26 21-28	241-283 498-513 579-711 586-756	253-309 387-432 406-522 479-515 668-773 585-745	37-93 206-223 493-530 614- 664 796-836
	IMEP	**PMAX**	**THR**	**IMEP**	**PMAX**	**THR**
Designed System	18-20 16-24 26-34	13-23 42-51	15-23 40-43	151-181 200-340 467-528	476-503 702-770	120-167 675-715

Furthermore, when the global wavelet spectra in the graphs given in Figures 5 and 8 are examined, it is observed that the variations in the frequencies of all three signals used as a result of the implementation of the designed system are reduced, thus reducing the cyclical differences. Because the horizontal axis in the GWS graphs indicates the power axis. In addition, the predominant spectral modes of time series are predicted from the peaks in the GWS curves.

CONCLUSIONS

Variations of the IMEP, PMAX and THR time series from cycle to loop using continuous wavelet transform (CWT) were examined on a spark ignition engine. The effects of changes in cooling systems on the in-cylinder pressure were investigated. With the new design, the thermal efficiency of the engine has been increased by sending the air bubble to the coolant, which allows the engine to warm up more rapidly. This reduces the time required for cold starting conditions in which the internal combustion of the cylinder is unstable. In this way, the total duration of the in-cylinder combustion, which is unstable under cold start conditions, has been reduced. Thus, optimum combustion temperatures within the cylinder have been reached more quickly and cyclic differences or irregular burns between cycles have improved.

REFERENCES

Khorasani, S., & Dadvand, A. (2017). Effect of air bubble injection on the performance of a horizontal helical shell and coiled tube heat exchanger: an experimental study. *Appl. Therm. Eng.*, 111: 676–683.

Moosavi, A., Abbasalizadeh, M., & Sadighi Dizaji, H. (2016). Optimization of heat transfer and pressure drop characteristics via air bubble injection inside a shell and coiled tube heat exchanger. *Exp. Thermal Fluid Sci.* 78: 1–9.
Samaroo, R., Kaur, N., Itoh, K., Lee, T., Banerjee, S., & Kawaji, M. (2014). Turbulent flow characteristics in an annulus under air bubble injection and subcooled flow boiling conditions. *Nucl. Eng. Des.* 268: 203-214.

Chang, S., & Huang, B. (2013). Thermal performance improvement by injecting air into water flow. *Int. J. Heat Mass Transf.* 57 (2013) 439-456.

Shutty, J., Wenzel, W., Becker, M., & Bohan, S. (2013). Advanced Thermal Management of a Light Duty Diesel Vehicle. *SAE Technical Paper*, 2013–01- 0546.

Cipollone, R., Di Battista, D., & Gualtieri, A. (2013). A novel engine cooling system with two circuits operating at different temperatures. *Energy Convers. Manage.* 75: 581–592.

Mohamed, E. (2016). Development and analysis of a variable position thermostat for smart cooling system of a light duty diesel vehicles and engine emissions assessment during NEDC. *Appl. Therm. Eng*. 99:358–372.

Cipollone, R., & Di Battista, D. (2014). Sliding vane rotary pump in engine cooling system for automotive sector. *Appl. Therm. Eng.* 76: 157–166.

Young, M. B. (1981). Cyclic dispersion in the homogeneous-charge spark ignition- A Literature Survey. *SAE Technical Paper*, No:810020.

Heywood, J. B., (1998). Internal Combustion Engines Fundamentals, (*New York, McGraw Hill Education,* 1988), ISBN:978- 0070286375.

Ceviz, M. A., Sen, A. K., Küleri, A. K. & Öner, İ. V. (2012). Engine performance, exhaust emissions, and cyclic variations in a lean-burn SI engine fueled by gasolineehydrogen blends. *Applied Thermal Engineering* 36: 314-324.

Sen, A. K., Litak, G., Taccani, R., & Radu, R. (2008). Wavelet Analysis of Cycle-to-Cycle Pressure Variations in an Internal Combustion Engine. *Chaos, Solitons Fractals* 38:886-893.

Saxena, M. R. & Maurya R. K. (2018). Effect of Butanol Addition on Performance, Combustion Stability and Nano-Particle Emissions of a Conventional Diesel Engine, *SAE technical Paper*, 2018-01-1795.

Ozdor, N., Dulger, M. & Sher, E. (1994). Cyclic Variability in Spark Ignition Engines: A literature survey. *SAE Technical Paper*, No: 940987.

Kumar, P., & Foufoula-Georgiou, E. (1997). Wavelet analysis for geophysical applications. *Rev Geophys* 35: 385-412.

Zavaragh, H. G., Kaleli, A., Afshari, F., & Amini, A. (2017). Optimization of heat transfer and efficiency of engine via air bubble injection inside engine cooling system. *Applied Thermal Engineering*, *123*, 390-402.

THE AIR FUEL RATIO CONTROL WITH GRAY PID IN SI ENGINES UNDER TRANSIENT CONDITIONS

Hüseyin KÖKSAL
Bayburt University
hkoksal@bayburt.edu.tr

Alırıza KALELİ
Bayburt University
arizakaleli@bayburt.edu.tr

ABSTRACT: In internal combustion engines, improvements in engine output parameters and emissions can be achieved by setting the operating parameters such as air-fuel ratio, ignition advance, injection time, EGR ratio at an effective level. Ideal performance outcomes for spark ignition engines can be achieved when working with a stoichiometric air fuel ratio. This proportional value varies depending on the chemical composition of the fuel and should be 14.7 if gasoline is used. Thus, the conversion efficiency of the catalytic converter is kept at the maximum level and the emissions are reduced. It is possible to obtain a stoichiometric air fuel mixture at constant speed or load but it is more difficult for transient conditions. The change in the amount of air flowing through the cylinder under transient conditions, requires constant control of the amount of fuel injected. ECU is responsible for this setting in internal combustion engines. ECU uses datas such as engine speed, manifold pressure, air temperature, O2 signal to determine the injection duration. However, it becomes difficult to control the air fuel ratio with delays due to the system structure. Moreover, the cyclic variations that exist in motor dynamics restrict the effectiveness of the control structure. At this point, there is a need to design a real-time controller that can predict the behavior of these unwanted disruptive effects. In this study, mean value motor model was used and studied on 1-D engine model created in GT-Suite simulation platform. For the variable conditions obtained with the randomly generated throttle angle position information, the air-fuel ratio was controlled with the gray predictor based PID and compared to the traditional PID. It is aimed to create an alternative solution based on predictions for the rapid and effective control structure desired in the presence of uncontrollable and disturbance effects in a real-time system.

Key words: air fuel ratio, gray pid, transient conditions (keywords should not exceed 5 words)

BENZİN MOTORLARINDA DEĞİŞKEN ŞARTLAR İÇİN GRAY PID İLE HAVA YAKIT ORANI KONTROLÜ

ÖZET: İçten yanmalı motorlarda hava-yakıt oranı, ateşleme avansı, enjeksiyon süresi, EGR oranı gibi çalışma parametrelerinin etkin bir seviyede ayarlanması ile motor çıkış parametreleri ve emisyonlarda iyileşmeler elde edilebilmektedir. Buji ateşlemeli motorlarda istenilen maksimum performans çıktılarına stokiyometrik hava yakıt oranı ile çalışıldığında ulaşılabilir. Bu oransal değer yakıtın kimyasal bileşimine bağlı olarak değişir ve benzin kullanıldığı durumda 14.7 olmalıdır. Böylece katalitik konvertörün

dönüşüm verimliliği de maksimum seviyede tutularak emisyonlar azaltılmış olur. Sabit devir veya sabit yük şartlarında stokiyometrik hava yakıtı karışımını elde etmek mümkün olsa da, değişken koşullar altında bunu sağlamak daha zordur. Değişken şartlar altında her bir motor çevrimi için silindir içerisine yönelen hava miktarındaki değişim yakıtın enjeksiyon miktarının da sürekli olarak kontrol edilmesini gerektirir. İçten yanmalı motorlarda bu ayarlama işleminden motor kontrol ünitesi (ECU) sorumludur. ECU enjeksiyon süresini belirlerken motor devri, manifold basıncı, hava sıcaklığı, O2 sensörü sinyali gibi verileri kullanır. Fakat sistemin yapısından kaynaklanan gecikmelerle hava yakıt oranı kontrolü zorlaşmaktadır. Bununla beraber motor dinamiğinde var olan çevrimsel farklar kontrol yapısının etkinliğini kısıtlamaktadır. Bu noktada istenmeyen bu bozucu etkilerin davranışını öngörebilen bir kontrolcü tasarımına gereksinim duyulmaktadır. Bu çalışmada ortalama değer motor modeli kullanılmış ve 1 boyutlu GT-Suite simülasyon platformunda oluşturulan motor modeli üzerinde çalışılmıştır. Rastgele oluşturulan gaz kelebeği açı pozisyon bilgisi ile elde edilen değişken şartlar için hava yakıt oranı gray öngörü tabanlı PID kontrolcüsü ile denetlenmiş ve geleneksel PID ile karşılaştırılmıştır. Gerçek zamanlı bir sistemde kontrol edilemez ve bozucu etkilerin varlığında istenen hızlı ve etkin kontrol yapısı için öngörüye dayalı alternatif bir çözüm oluşturulmak hedeflenmiştir.

Anahtar sözcükler: hava yakıt oranı, gray pid, değişken koşullar

THE MATHEMATICAL MODEL OF THE EFFECT OF DIESEL ENGINE EGR GAS TEMPERATURE AND EGR RATIO ON NOx EMISSIONS

Halil İbrahim AKOLAŞ
Bitlis Eren University
hakolas@beu.edu.tr

Alırıza KALELİ
Bayburt University
arizakaleli@bayburt.edu.tr

Kadir BAKIRCI
Atatürk University
abakirci@atauni.edu.tr

ABSTRACT: Exhaust Gas Re-circulation System (EGR); It is one of the most effective methods to control NO_x emissions from diesel engines. Most of the diesel engines are equipped with the EGR system from light to heavy duty applications. In this method, a controllable portion of the exhaust gases is returned to the inlet air, and the displacement of these burned gases results in lower heat release and peak temperature, which reduces the formation of NO_x emissions. It is also possible to increase the engine life with EGR due to a decrease in cylinder temperature. When EGR is applied, the production of particulate emissions increases due to the decrease in the oxygen concentration in the cylinders. This is one of the most important problems in diesel engines using the EGR system and means that there must be a balance between NO_x and particulate emissions in the exhaust gases. The increase in input charge temperature is known to cause a decrease in volumetric efficiency and engine performance. The EGR gas must be cooled before mixing with fresh suction air to reduce the negative effects on the motor volumetric efficiency. EGR coolers are used in diesel engines to reduce the temperature of the exhaust gases to be recirculated. However, EGR cooler contamination reduces heat transfer performance over time. Pollution causes an increase in the pressure drop of the coolant and is the main problem of EGR coolers that affect EGR ratios, engine performance and exhaust emission characteristics In this study, the effects of exhaust gas temperature and EGR ratio on NOx emissions in a diesel engine were modeled by multiple regression technique and the results of the first and nonlinear models were compared with the actual data.

Key words: Diesel engine, Exhaust gas recirculation, Heat exchanger, NOx

DİZEL MOTORDA EGR GAZ SICAKLIĞI VE EGR ORANININ NOx EMİSYONLARI ÜZERİNE ETKİSİNİN MATEMATİKSEL MODELLENMESİ

ÖZET: Egzoz Gaz Re sirkülasyon Sistemi (EGR); Dizel motorlardan yayılan NO_x emisyonlarını kontrol etmede en etkili yöntemlerden biridir. Hafif hizmetten ağır hizmet uygulamalarına kadar dizel motorların çoğu EGR sistemi ile donatılmıştır. Bu

yöntemde, egzoz gazlarının kontrol edilebilir bir kısmı, giriş havasına geri gönderilir ve bu yanmış gazların yer değiştirmesi, daha düşük ısı salınımına ve NO emisyonunun oluşumunu azaltan tepe sıcaklığına neden olur. Ayrıca, silindir sıcaklığındaki düşüş nedeniyle motor ömrünün EGR ile arttırılması mümkündür. EGR uygulandığında, silindirlerdeki mevcut oksijen konsantrasyonundaki azalmaya bağlı olarak partikül emisyonlarının üretimi artar. Bu, EGR sistemini kullanan dizel motorlarda en önemli sorunlardan biridir ve egzoz gazlarında NO_xx ve partikül emisyonları arasında bir denge olması gerektiği anlamına gelir. Giriş şarj sıcaklığındaki artışın volumetrik verimde ve motor performansında bir azalmaya neden olduğu bilinmektedir. Motor hacimsel verim üzerindeki olumsuz etkileri azaltmak için taze emme havası ile karıştırılmadan önce EGR gazları soğutulmalıdır. EGR soğutucular, yeniden sirküle edilecek olan egzoz gazlarının sıcaklığını azaltmak için dizel motorlarda kullanılır. Bununla birlikte, EGR soğutucu kirlenmesi zaman içinde ısı transfer performansını azaltır. Kirlenme, soğutucunun basınç düşüşünde bir artışa neden olur ve EGR oranlarını, motor performansını ve egzoz emisyon özelliklerini etkileyen EGR soğutucularındaki ana sorundur. Bu deneysel çalışmada, EGR soğutucusu motor ana soğutma sisteminde ayırılmış ve NO_x emisyonlarını iyileştirmek için ikincil bir soğutma sistemi ile elektronik kontrollü olarak soğutulmuştur.
Bu çalışmada bir dizel motorda, emme manifolduna giren egzoz gazı sıcaklığı ve EGR oranının NO_x emisyonları üzerine etkisi çoklu regresyon tekniği ile modellenmiş ve birinci ve doğrusal olmayan modellerin sonuçlarının gerçek verilerle uyumları karşılaştırılmıştır.
Anahtar sözcükler: Dizel motor, Egzoz gaz devridaimi, Isı değiştirici, NO_x

GİRİŞ

İçten yanmalı motorlarda yakıtın yanması sonucu egzozdan; su buharı (H_2O), karbondioksit (CO_2), Azot oksit (NO_x), Partikül madde (PM), Hidrokarbon (HC) ve Karbon monoksit (CO_2) atmosfere salınır. Bunlardan su buharı hariç, diğerleri çevreye ve canlılara zararlı olan gazlardır. Sıkı bir şekilde uygulanan emisyon düzenlemeleri giderek ağırlaşmaktadır. Küresel ısınma, İklim değişikliği ve insan sağlığı üzerinde ciddi etkileri olan motorlu taşıt emisyonlarının gelecek nesillere ve tüm canlılara temiz bir yaşam alanı bırakılabilmesi için belirli uluslararası standartlar ve protokoller imzalanmıştır. Modern dünyamızda çevre ve insan sağlığı açısından ciddi zararlı etkilere sahip olan bu emisyonlar, uluslararası anlaşmalar ve yasalar ile giderek sınırlandırılmaktadır. Otomotiv üreticileri bu yasalar çerçevesinde ürettikleri motorlu taşıtlarda bu kriterleri dikkate almak ve bu yönde çalışmalar yapmak zorundadırlar. İçten yanmalı motorların çevreye yaydıkları zararlı emisyonları azaltmak adına pek çok araştırmacı ve motorlu taşıt üreten firmalar bu yönde çalışmalar yapmış ve yapmaya da devam edilmektedir. Gelecekte daha temiz bir çevre, canlılar için daha sağlıklı bir yaşam ortamı, küresel ısınmayı azaltmak, canlı yaşamı için gerekli besin ve enerji kaynaklarını korumak adına bu yönde yapılan bilimsel çalışmalar gelişmiş ve gelişmekte olan ülkelerde büyük bir hassasiyetle üzerinde durulan bilimsel araştırma konularıdır. Dizel motorlar genel olarak; ağır hizmetli iş makinelerinde, ulaşım araçlarında, yük taşıtlarında, gemilerde kullanılmasının yanı sıra; jeneratör, pompa ve kompresör gibi yardımcı sistem makinelerinde güç kaynağı olarak da kullanılmaktadır. Son yıllarda düşük yakıt tüketimi, düşük yakıt maliyetleri ve daha

az zararlı egzoz emisyonları açısından hafif hizmet taşıtlarında ve binek araçlarda da tercih edilir hale gelmiştir. Dizel taşıtlarında yakıt verimliliğinden ve performansından ödün vermeden optimum egzoz emisyonları elde edebilmek için günümüz dizel motorlarında; silindir içi yanma stratejilerinin (Harici EGR, İç EGR, Enjeksiyon stratejileri vb.) yanı sıra son işlem olarak SCR, DPF, DOC, LNT ve bu stratejilerin kombine kullanımları mevcut olup bu yönde çalışmalar halen devam etmektedir bk. Şekil 1.

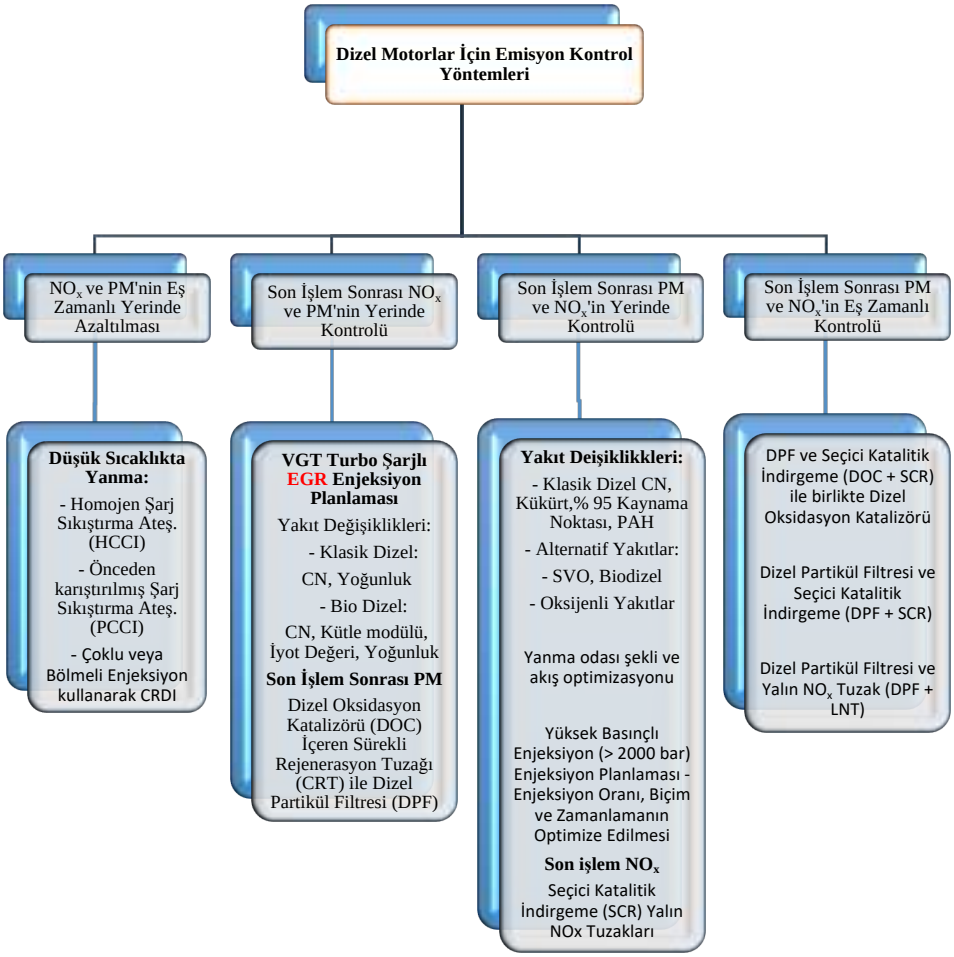

Şekil 1. Dizel Emisyon Kontrolü - Silindir İçi Ve Son İşlem Sonrası Seçeneklerin Özeti (Thangaraja and Kannan, 2016)

Dizel motorlarının hava-yakıt karışım oranları dikkate alındığında, fakir karışımla çalışan motorlardır. Genellikle tam yük koşullarında hava fazlalık katsayısı λ=1.5-1.8 arasında olup yük azaltıldığında ise λ değerinin daha yüksek değerlere çıkması NO_x oluşumuyla doğrudan ilişkilidir. Özellikle, dizel motorlarının silindir dolgusunda, yüksek oranda oksijen ve nitrojen varlığından dolayı, yanma odasında meydana gelen yüksek sıcaklık NO_x salınımlarının artmasına sebep olmaktadır (Zheng, Reader, and Hawley, 2004).

NO_x oluşum mekanizması

NO_2, keskin bir kokuya sahip olup kırmızı kahverengi karışımı renge sahip bir gazdır. Düşük yoğunlukta dahi akciğerlere, dokulara ve mukoza zarına zarar verir. MAK değeri 9 mg/m3'tür (Shafer 1995). NO_x yanma odası içerisinde yüksek sıcaklığın oluştuğu bölgede alev sonrası yanma işlemi sırasında ortaya çıkan bir kimyasal reaksiyondur. Yanma odası içerisinde meydana gelen kötüleşme ve NO_x oluşumu genişletilmiş Zeldovich Mekanizması ile açıklanabilir (Heywood 1998). Moleküler nitrojenden NO oluşumunu yöneten stokiyometrik yakıt-hava karışımındaki ana reaksiyon iyonları şunlardır:

$O + N_2 = NO + N$
$N + O_2 = NO + O$
$N + OH = NO + H$

Egzoz gaz re sirkülasyon sistemi

Günümüz dizel motorların üretim, bakım maliyetlerinde ki azalma, daha yüksek motor verimi nedeniyle dizel motorların kullanımı benzinli motorlara göre artmaktadır. Ancak diğer taraftan dizel motordan kaynaklanan NO_x emisyonları yüksektir. Dolayısıyla, motor performansını etkilemeden emisyonları azaltabilecek bir tekniğe ihtiyaç duyulmaktadır. Bu tekniklerden biri Egzoz gazı sirkülasyonudur (EGR). Sıkıştırma ateşlemeli motorlarda NO_x emisyonlarını azaltmak için en etkili yöntemlerden biri Egzoz Gaz Re sirkülasyon (EGR) Sistemidir. Bu sistemde bir miktar egzoz gazı, çevrim sırasında tekrardan emme manifolduna yönlendirilir (emme dolgusu basıncı ile egzoz gaz basınçları arasındaki fark dolayısı ile). EGR'nin uygulanması dizel motor yanmasını termal, kimyasal ve seyreltme olarak üç farklı şekilde etkiler (Hountalas, Mavropoulos, and Binder, 2008). Egzoz gazının çoğunluğunu su buharı ve karbondioksit oluşturduğundan emme dolgusunda O_2 konsantrasyonu azaltılır. Bu durum yanma odası içerisindeki maksimum yanma sıcaklığının azalmasına ve buna bağlı olarak NO_x oluşumunun azalmasına sebep olur bk. Şekil 2. Egzoz gazının diğer bir etkisi ise, kimyasal ayrışmadan ve egzoz gazının havaya göre daha yüksek özgül ısıya sahip olması ve yanma ürünlerinin varlığından dolayı O_2 ile buluşan ve reaksiyona giren azot moleküllerinin azalması. Buna bağlı olarak azalan yanma sıcaklığına karşılık NO_x değerlerinde azalma meydana gelirken EGR siz bir motora göre daha fazla duman üretimi oluşturur (Langridge and Fessler, 2002).

Egzoz gazı devridaim sistemine sahip olan bir dizel motoru üzerinde NO_x oluşumunu azaltmak adına kararlı yük ve standartlaştırılmış test çevrim koşullarında birçok araştırma çalışmaları yapılmış olup, bu çalışmalar EGR sistemi uygulanan motorlarda, NO_x oranında %50 ye varan azalma buna karşılık parçacık madde miktarında ise (PM) %100'e varan oranlarda artış olduğu gözlenmiştir (Satoh, Zhang, Hatanaka, Takatsuki, and Yokota, 1997; Shirakawa, Itoyama, and Miwa, 2001).

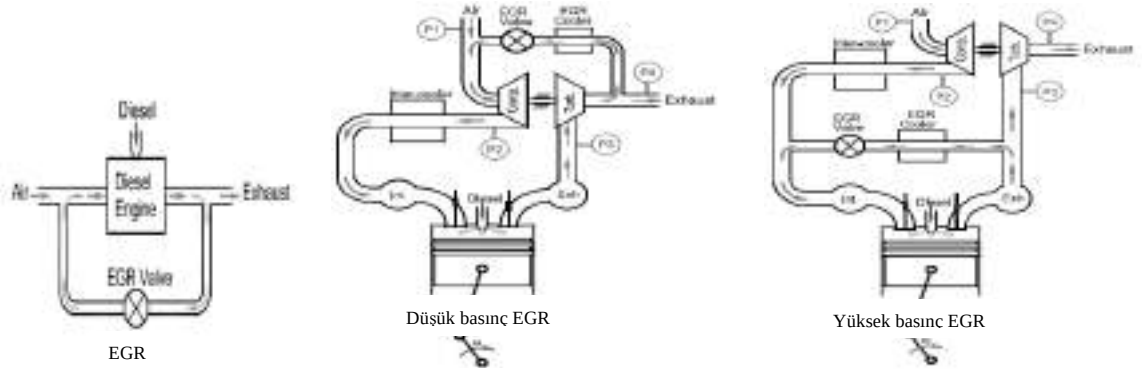

Şekil 2. Egzoz Gaz Re Sirkülasyon Sistemi Ve Türleri (Zheng et al., 2004)

EGR sisteminin kullanılması; kurum emisyonları açısından geleneksel motorlardan daha fazla yanmamış hidrokarbon (% 20-30) tüketir. EGR kullanan motorlar, EGR'siz motorlardan daha az miktarda egzoz gazı yayarlar, çünkü egzoz gazının bir kısmı yeniden sirküle edilir. Emme dolgu sıcaklığındaki artış, daima daha kısa tutuşma gecikmesine neden olur ve termal verimliliği yükseltebilir (Vivek Auti, Jachak, Pardesh, and Attar, 2017). Sirküle edilen gaz miktarının artması emme havası sıcaklığının artmasına ve taze şarj havasını azaltır. Bu, daha fazla duman oluşturur ve partikül maddesinin (PM) bozulmasına neden olur (Kakoi, Tsutsui, Ono, Umezawa, and Kondo, 1998). Resirküle edilen egzoz gazları doğrudan silindir içine yönlendirilirse "Sıcak EGR" bir ısı değiştiriciden geçirilip soğutulduktan sonra silindir içerisine gönderiliyorsa "Soğutulmuş EGR" adını alır (Zheng et al., 2004).

Soğutulmuş egr

EGR uygulandığında, silindirlerdeki mevcut oksijen konsantrasyonundaki azalmaya bağlı olarak partikül emisyonlarının üretimi artar. Bu, EGR sistemini kullanan dizel motorlarda en önemli sorunlardan biridir ve egzoz gazlarında NO_x ve partikül emisyonları arasında bir denge olması gerektiği anlamına gelir. Emme dolgusuna sıcak EGR ilavesi, giriş şarj sıcaklığını artırır ve termal yük nedeniyle emme yükü kütlesini azaltır. Bununla birlikte, EGR'nin soğutulması, hem yük kapasitesini hem de kütle akışını arttırır. Sonuç olarak, soğutulmuş EGR NO_x 'i sıcak EGR'den daha etkili bir şekilde azaltır (Ladommatos, Abdelhalim, Zhao, and Hu., 1998). Giriş yükü sıcaklığının azaltılması, yanma geciktirme süresini uzatır ve sonuç olarak yakıt buharı ve Oksijen sentezi arasında daha fazla homojenliğe yol açar (Ghassembaglou and Torkaman, 2016). Giriş şarj sıcaklığındaki artışın volumetrik verimde ve motor performansında bir azalmaya neden olduğu bilinmektedir. Motor hacimsel verim üzerindeki olumsuz etkileri azaltmak için taze emme havası ile karıştırılmadan önce EGR gazları soğutulmalıdır. EGR soğutucular, yeniden sirküle edilecek olan egzoz gazlarının sıcaklığını azaltmak için dizel motorlarda kullanılır.

Egr oranın hesaplanması

Emme dolgusuna gönderilen EGR gazlarının yüzde oranı hesaplanırken; emme dolgusuna yönlendirilen egzoz gazının kütlesinin toplam silindire giren emme dolgusunun kütlesine oranı olarak ifade edilir.

$$EGR(\%) = \frac{M_{EGR}}{M_{\text{i}}} x100$$

Emme giriş havası, ihmal edilebilir oranda CO_2 içerirken, egzoz manifoldu EGR akış oranı ve motor yükü ile artan yanma sonucu üretilen önemli miktarda CO_2 taşır. Bu yüzden, motor egzozundaki (CO_{2_exh}) ve emme manifoldundaki (CO_{2_EGR}) konsantrasyonlarının karşılaştırılması, EGR oranını belirlemenin pratik bir yoludur(De Serio, de Oliveira, and Sodré, 2017). EGR oranının belirlenmesi için emme manifoldundaki (CO_{2_EGR}) ve egzoz manifoldundaki (CO_{2_exh}) konsantrasyonları ölçmek için NDIR temelli sensörler kullanılarak % EGR oranı hesaplandı (Dangar and Rathod, 2012; Desantes, Galindo, Guardiola, and Dolz, 2010; Sutela, Collings, and Hands, 2000).

$$EGR = \frac{CO_{2_EGR} - CO_{2_atm}}{CO_{2_exh} - CO_{2_atm}}$$

Geleneksel olarak UEGO sensörleri, λ ve AFR ölçümü için test cihazlarında tezgah aletleri olarak ve aynı zamanda yağsız benzinli motorların üretiminde kullanılmaktadır.Son zamanlarda 80 ms tepki süresine sahip olmaları nedeni ile dizel motorlarda da kullanılmaya başlanmıştır. Bu sensörler sayesinde EGR oranı aşagıdaki gibi hesaplanmaktadir.(Hegarty, Dickinson, Cieslar, and Collings, 2013). Bu deneysel çalışmada EGR oranını hesaplamada emme ve egzoz manifoldlarındaki O_2 konsantrasyonlarını ölçmek için Bosch LSU 4.9 geniş bant lamda (oksijen) sensörleri kullanıldı.

$$EGR = \frac{O_{2_atm} - O_{2_int}}{O_{2_atm} - O_{2_exh}}$$

Çoklu regresyon modeli

Bu çalışmada kullanılan çoklu doğrusal regresyon modelinde, bağımlı değişenlerle bağımsız değişken arasındaki ilişkiler kullanılarak sistemin giriş değişkenlerinin çıkış değişkeni üzerindeki etkisinin matematiksel olarak ortaya konulması amaçlanmıştır. Ayrıca çalışmanın bu bölümü MATLAB ortamında hazırlanmış ve birinci ve doğrusal olmayan modellerden modeller oluşturularak model sonuçları gerçek verilerle karşılaştırılmıştır.

Çalışma kapsamında yapılan çoklu doğrusal regresyon modelinde, **birinci mertebenden model Y = b0+ b1X1+b2X2+ εi biçimindedir.** Modelde Y bağımlı değişken; X1, Emme manifolduna giren egzoz gaz sıcaklığı; X2 ise EGR oranı olmak üzere b0, regresyon eğrisinin y eksenini kesim noktası,b1 birinci bağımsız değişkenin regresyon katsayısı, b2 ikinci bağımsız değişkenin regresyon katsayısı, εi ise ortalaması sıfır, varyansı σ2 olan normal dağılışa sahip hata değişkenidir.

Çoklu doğrusal regresyon modellerin karşılaştırılmasında ise düzeltilmiş belirleme katsayısı (R^2), hata kareler ortalamasının karekökü (Root Mean Square Error-RMSE), ortalama mutlak sapma (Mean Absolute Deviation-MAD) ve ortalama mutlak yüzde hata (Mean Absolute Percentage Error-MAPE) kriterleri kullanılmıştır. Eşitlikler aşağıda ifade edilmiştir.

$$RMSE = \sqrt{\frac{\sum_{i=1}^{n}(\hat{y}_i - y_i)^2}{N}}, \quad MAD = \frac{\sum_{i=1}^{n}|(\hat{y}_i - y_i)|}{N}, \quad MAPE = \frac{\sum_{i=1}^{n}\left|\frac{(\hat{y}_i - y_i)}{y_i}\right|}{N}100$$

YÖNTEM

Yürütülen deneysel çalışmada; bir dizel motorda, emme manifolduna giren egzoz gazı sıcaklığı ve EGR oranının NO_x emisyonları üzerine etkisi çoklu regresyon tekniği ile modellenmiş ve birinci ve doğrusal olmayan modellerin sonuçlarının gerçek verilerle uyumları karşılaştırılmıştır. Emme dolgusuna sıcak EGR ilavesi, giriş şarj sıcaklığını artırır ve termal yük nedeniyle emme yükü kütlesini azaltır. Bununla birlikte, EGR'nin soğutulması, hem emme yük kapasitesini hem de kütle akışını arttırır. Sonuç olarak, soğutulmuş EGR NO_x 'i sıcak EGR'den daha etkili bir şekilde azaltır. EGR gaz sıcaklığını; EGR oranı, motor devri ve yük koşullarına göre optimum düzeyde NO_x salınımı için; EGR soğutucusu motor ana soğutma sisteminden ayırılarak harici elektronik kontrollü bir soğutma sistemi deney düzeneğine entegre edilmiştir. Deneyler dizel motorunun kararlı durum koşullarında 1200, rpm devrinde, yüklü koşullarda %5,10,15,20 EGR oranlarında gerçekleştirilmiştir.

Deney düzeneği ve sistem elemanları

Deney motoru ve teknik özellikleri

Deneyde Ford marka turbo şarjlı puma tip bir dizel motor kullanıldı bk. Şekil 3 . Teknik detaylar için bk. Tablo 1.

Tablo 1. Deney Motorunun Teknik Özellikleri

Dizel motor bilgileri	
Motor	Dizel yakıtlı Ford puma
Silindir sayısı	Sıra tipi 4
Motor gücü	125 PS
Tork	130 Nm

Motor hacmi	2198.1 cc
Çap	86 mm
Kurs boyu	94.6 mm
Sıkıştırma oranı	15.5:1

Şekil 3. Deneysel Çalışmada Kullanılan Ford Marka Dizel Motoru

Egr soğutucu için harici elektronik kontrollü soğutma sistemi ve sistem elemanları

EGR gazlarını soğutmak için; motor ana soğutma sisteminden bağımsız harici bir elektronik kontrollü soğutma sistemi tasarlandı. Bu soğutma sistemi bir elektrikli su pompası, elektrikli fan, termistör ve ısı değiştiriciden oluşmaktadır bk. Şekil 4 ve Şekil 5. Harici soğutma sisteminde egr soğutucu çıkışındaki akışkanın sıcaklık değeri bir termistör vasıtasıyla elektronik kontrolcüye gönderilir. Kontrol ünitesi okunan sıcaklık değerinin programlanan sıcaklık değerinde tutabilmek için fan ve devirdaim pompasına gerekli akımı sağlar yada keser. Egr soğutucudaki akışkan sıcaklığı bu çalışmada minumum 40 °C ile maksimum 100 °C aralığında, 10 °C artışlarla, EGR gaz çıkış sıcaklıkları optimum değerde tutlmaya çalışıldı.

Şekil 4. EGR Soğutucu İçin Harici Soğutma Sistemi **Şekil 5. EGR Soğutucu İçin Elektronik Kontrolcü**

Egzoz emisyon analizleri Bosh firmasına ait BEA 270 egzoz emisyon cihazı ile gerçekleştirildi. Veri toplama kartı olarak National Instrument firması üretimi olan PCIe-6363 modeli veri toplama (Data Acquisition) kartı kullanılmıştır. Sıcaklık ölçümü için kullanılan ısıl çiftlerden alınan veriler, devir sayısı, tork, egzoz emisyon değerleri ve yakıt tüketimi dataları veri toplama kartı ile ölçülmüştür ve alınan bu veriler LabView ortamında hazırlanan programlar ile işlenmiş ve veri kaydı yapılarak, analizler gerçekleştirilmiştir.

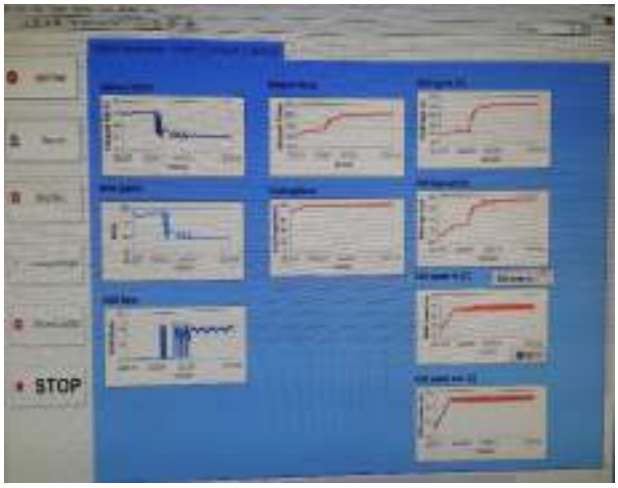

Şekil 6. Anlık Veri Kayıt Ekranı ve Verilerin Grafiksel Görünümü

Şekil 7. Test Düzeneğinin Genel Görünümü

BULGULAR

Yukarıdaki bölümlerde ifade edildiği gibi öncelikle bağımsız değişkenler tanımlanmış olup, bu değişkenler emme manifolduna giren egzoz gaz sıcaklığı ve EGR oranı şeklinde belirlenmiştir. Bu bağımsız parametrelerinin ağırlık oranları veya katsayıları şeklinde ifade edilen değerleri MATLAB ortamında hazırlanan programla belirlenmesiyle NO_x emisyonu üzerinde hangi parametrenin daha fazla etkiye sahip olduğu söylenebilecektir. Yapılan bu deneysel çalışmada motorun soğuk çalışma koşulları ele alınmayıp, motorun kararlı çalışma bölgesine gelinceye kadar beklenmiştir. Bundan sonra araştırmacılar tarafından tasarlanan veri toplama programları kullanılarak deneysel sistem üzerinden sıcaklık ve diğer motor parametre verileri toplanmıştır. Motorun kararlı hal çalışma bölgesi üzerinden 1 -1,5 dk boyunca 0,1 sn'lik aralıklarla veriler alınarak bu verilerin ortalama değerleri hesaplanmış ve modeller için bu ortalama değerler kullanılmıştır.

Öncelikle birinci mertebeden model ele alınmıştır. Aşağıda birinci mertebeden model verilmiştir.

$$f(x,y) = a + b * x + c * y$$

Burada a, b ve c katsayıları ifade ederken x, egzoz sıcaklığını, y ise EGR oranını gösteren veri dizilerini temsil etmektedir. Buna göre elde edilen denklem ve belirlenen katsayı değerleri aşağıda ifade edilmiştir.

$$f(x,y) = a + b * x + c * y$$

$$a = 105{,}6 \quad b = 2.421 \quad c = -3.936$$

Elde edilen bu model ile deneysel değerler birlikte 3 boyutlu grafikte **Şekil 8**'deki gibi gösterilebilir.

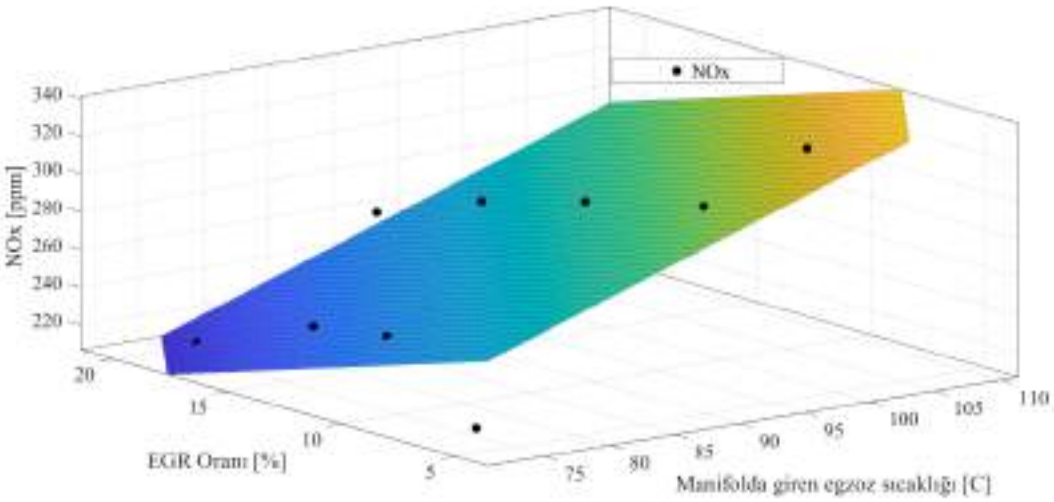

Şekil 8. Birinci Mertebe Model Ve Gerçek Değerlerin Karşılaştırılması

Şekil 8'de gösterilen grafikte verilerin kullanılıp modelin elde edilmesi sonucunda, yüzey şeklinde bir eğri elde edilmiştir. Grafik incelendiğinde noktalar şeklinde gösterilen NO_x emsiyon değerlerine yakın bir şekilde geçmesine rağmen elde edilen modelin gerçek verileri iyi bir şekilde kesmediği görülmektedir. Kullanılan X ve Y değişkenlerinin Z'deki toplam varyasyonu açıklayabilme oranını ifade eden belirtme katsayısı (R^2) açısından modelin değeri ise 0,7838' dir. Bilindiği üzere, bu değer 1'e yaklaştıkça modelin doğruluğu artmaktadır. Ayrıca **Şekil 9'**de ise gözlemlenen değerler ile model değerleri arasındaki farkı gösteren artık grafiği verilmiştir. Bu grafiktende görüleceği üzere birinci mertebeden regresyon modeli NO_x verisiyle yeteri kadar uyuşmamaktadır.

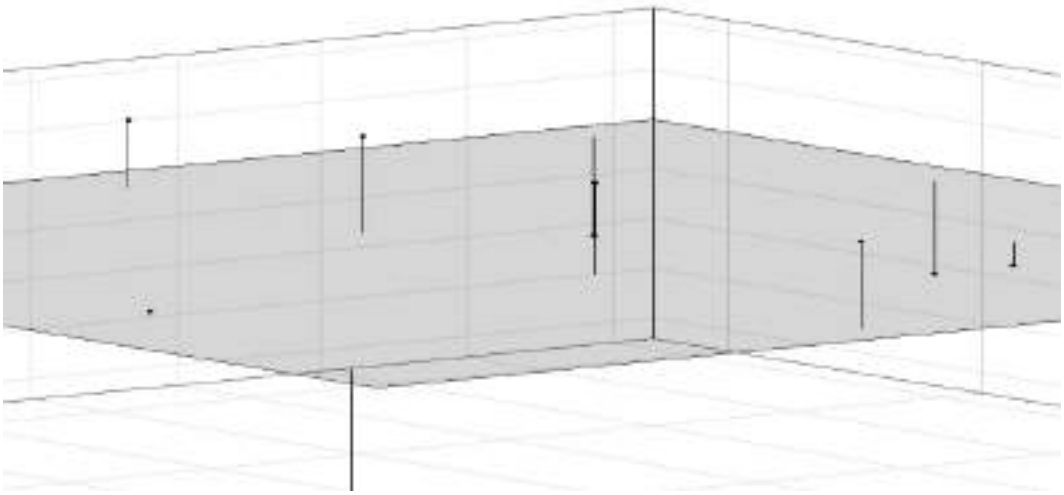

Şekil 9. Birinci Mertebeden Modelin Artık Grafiği

Bundan sonra, doğrusal olmayan bir model ele alınmış ve bağımsız değişkenle olan EGR oranı ve manifolduna giren egzoz gaz sıcaklığının, NO_x emisyonuna etkisi

araştırılarak istatistiksel model olarak ortaya konmuştur. Elde edilen regresyon modeli ve katsayılar ise aşağıdaki eşitlikte verilmiştir.

$$f(x,y) = p0 * a + p10 * b * x + p01 * c * y + p20 * d * x^2 + p11 * e * x * y + p02 * f * y\text{^}2$$

$$a = -863.8, \quad b = 23.08, \quad c = 4.277, \quad d = -0.1095,$$

$$e = -0.06392, \quad f = -0.08303$$

Şekil 10'da ise doğrusal olmayan modelin gerçek verilerle karşılaştırıldığı grafik gösterilmiştir.

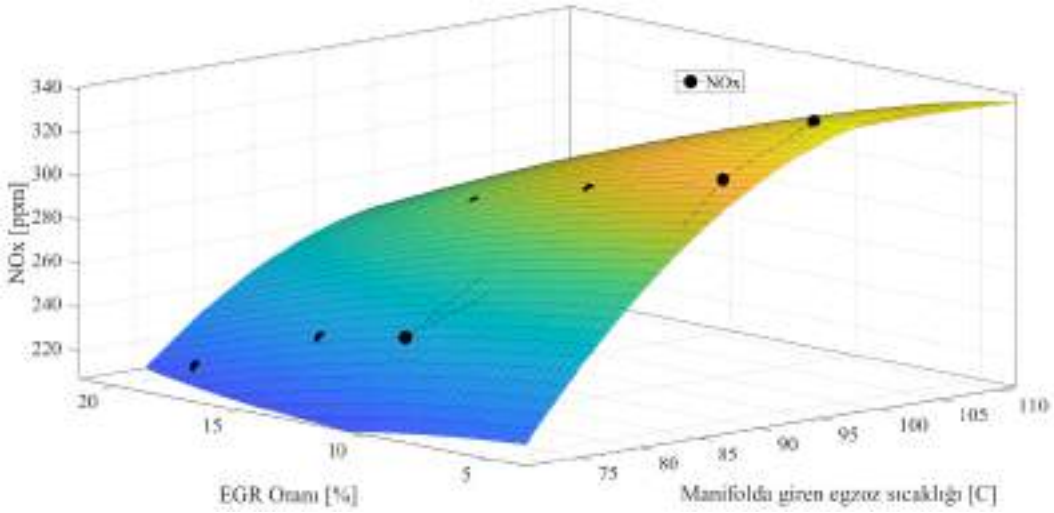

Şekil 10. Doğrusal Olmayan Bir Model İle Gerçek Değerlerin Karşılaştırılması

Ayrıca **Şekil 11**'de ise ikinci dereceden modelin artık analiz yapılmış olup birinci mertebeden olan modele göre oldukça gerçek verilerle uyumlu olduğu gözlemlenmektedir. Bu durum R^2 değeri açısından benzer bir sonucu vermiş olup 0,9797'dir. Her iki modelin karşılaştırılması sonucunda doğrusal olmayan modellernden modelin birinci mertebeye göre bu verilerle daha uyumlu olduğu görülmektedir.

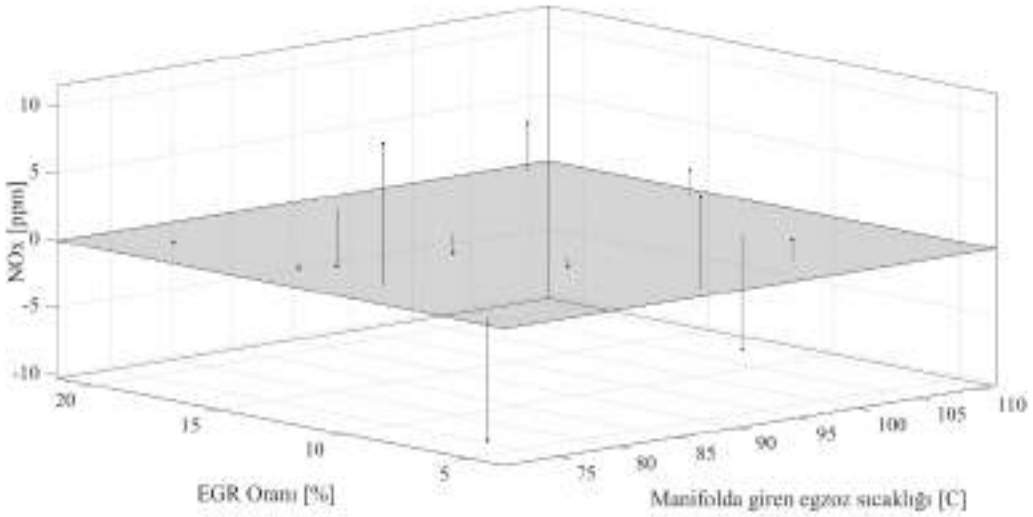

Şekil 11. Doğrusal Olmayan Modelin Artık Grafiği

Birinci modele göre doğrusal olmayan model daha karmaşık yapıya sahiptir. Buradaki zorluk daha fazla katsayısının tahmin edilme zorunluğunu ortaya çıkarmaktadır. Böylelikle doğrusal olmayan modellerden bir modelle daha iyi bir sonuç elde edilmiştir. Motor test sistemlerinin fiziksel olarak karmaşık yapıya sahip olması modeldeki karmaşıklığı da açıklamaktadır.

SONUÇ

Bu çalışmada, laboratuvar koşullarında bir dizel motorun NO_x emsiyonu üzerinde EGR oranının ve emme manifolduna giren egzoz sıcaklığının etkisi araştırılarak matematiksel model olarak regresyon modeli oluşturulmuştur. Farklı mertebelerden modellerin oluşturlarak deneysel verilerle karşılaştırma yapılıp modellerin doğruluk oranları analiz edilmiştir. İçten yanmalı motorlar üzerinde yapılan bu çalışmalar sayesinde stokastik bir yapıya sahip olan içten yanmalı motorlarda yanma olayının ve etkilerinin matematiksel ve istatistiksel modellerle ortaya konması, motorlarda parametre ayarlamalarını sadece deneme-yanılma yönteminden kurtarıp, daha modele dayalı yöntemlerle daha verimli kalibrasyon çalışması yapılabilme olanağı meydana getirmektedir.

SEMBOLLER

EGR	Egzoz Gaz Re sirkülasyon Sistemi
SCR	Seçici Kataliktik İndirgeme
DPF	Dizel Partikül Filtresi
DOC	Dizel Oksidasyon Katalizörü
LNT	Zayıf NO_x Tuzağı

MAK	Müsade Edilen Maksimum Konsantrasyon Dğeri
NO_x	Azotoksit
HC	Hidro Karbon
CO	Karbon Monoksit
CO_2	Karbon Dioksit
NO_2	Azot Dioksit
H_2O	Su
O_2	Oksijen
PM	Partikül Madde
ʎ	Hava Fazlalık Katsaysı

KAYNAKÇA

Dangar, H., and Rathod, G. P. (2012). Review on Combine Effect of Exhasust Gas Recirculation (EGR) *Advanced* and Inlet air pressure on Performance and Emission of Diesel engine. *International Journal of Engineering Research and Studies* doi:E-ISSN2249–8974

De Serio, D., de Oliveira, A., and Sodré, J. R. (2017). Effects of EGR rate on performance and emissions of a diesel power generator fueled by B7. *Journal of the Brazilian Society of Mechanical Sciences and Engineering, 39*(6), 1919-1927. doi:10.1007/s40430-017-0777-x

Desantes, J. M., Galindo, J., Guardiola, C., and Dolz, V. (2010). Air mass flow estimation in turbocharged diesel engines from in-cylinder pressure measurement. *Experimental Thermal and Fluid Science, 34*(1), 37-47. doi:https://doi.org/10.1016/j.expthermflusci.2009.08.009

Ghassembaglou, N., and Torkaman, L. (2016). Efficient design of exhaust gas cooler in cold EGR equipped diesel engine. *Alexandria Engineering Journal, 55*(2), 769-778. doi:https://doi.org/10.1016/j.aej.2016.01.023

Hegarty, K., Dickinson, P., Cieslar, D., and Collings, N. (2013). *Fast O2 Measurement using Modified UEGO Sensors in the Intake and Exhaust of a Diesel Engine*. https://doi.org/10.4271/2013-01-1051

Hountalas, D. T., Mavropoulos, G. C., and Binder, K. B. (2008). Effect of exhaust gas recirculation (EGR) temperature for various EGR rates on heavy duty DI diesel engine performance and emissions. *Energy, 33*(2), 272-283. doi:https://doi.org/10.1016/j.energy.2007.07.002

Kakoi, Y., Tsutsui, Y., Ono, N., Umezawa, K., and Kondo, N. (1998). *Emission Reduction Technologies Applied to High-Speed Direct Injection Diesel Engine*. https://doi.org/10.4271/980173

Ladommatos, N., Abdelhalim, S. M., Zhao, H., and Hu., Z. (1998). *Effects of EGR on Heat Release in Diesel Combustion*. https://doi.org/10.4271/980184

Langridge, S., and Fessler, H. (2002). *Strategies for High EGR Rates in a Diesel Engine*. https://doi.org/10.4271/2002-01-0961

Satoh, K., Zhang, L., Hatanaka, H., Takatsuki, T., and Yokota, K. (1997). Relationship between NO_x and SM emissions from DI diesel engine with EGR. *JSAE Review, 18*(4), 369-375. doi:https://doi.org/10.1016/S0389-4304(97)00037-4

Shirakawa, T., Itoyama, H., and Miwa, H. (2001). Study of strategy for model-based cooperative control of EGR and VGT in a diesel engine. *JSAE Review, 22*(1), 3-8. doi:https://doi.org/10.1016/S0389-4304(00)00100-4

Sutela, C., Collings, N., and Hands, T. (2000). *Real Time CO2 Measurement to Determine Transient Intake Gas Composition under EGR Conditions*. https://doi.org/10.4271/2000-01-2953

Thangaraja, J., and Kannan, C. (2016). Effect of exhaust gas recirculation on advanced diesel combustion and alternate fuels - A review. *Applied Energy, 180*(Supplement C), 169-184. doi:https://doi.org/10.1016/j.apenergy.2016.07.096

Vivek Auti, Jachak, S., Pardesh, T., and Attar, M. (2017). *A Review Study of the effect of Exhaust Gas Re*circulation (EGR) on performance and emission characteristics of diesel engine Paper presented at the National Conference "MOMENTUM-17", 14th and 15th February 2017 www.ijrat.org

Zheng, M., Reader, G. T., and Hawley, J. G. (2004). Diesel engine exhaust gas recirculation––a review on advanced and novel concepts. *Energy Conversion and Management, 45*(6), 883-900. doi:https://doi.org/10.1016/S0196-8904(03)00194-8

AVAILABLE AND EMERGING METAL ADDITIVE MANUFACTURING TECHNIQUES FOR DIRECT METAL PART MANUFACTURING

Volkan KORKUT
Adana Science and Technology University
vkorkut@adanabtu.edu.tr

Hakan YAVUZ*
Çukurova University
dr.hakanyavuz@gmail.com

ABSTRACT: Nowadays, Metal Additive Manufacturing (MAM) has become increasingly popular in automotive, space, aircraft and medical part manufacturing industries. This is mainly due to the advantage of the technique as it eliminates many time-wasting factors like tooling, fixing or cutting that are a part of the process in conventional methods. Furthermore, very complex structures can be manufactured by MAM with minimum amount of material. However, several drawbacks are still limiting this technology to become reachable because of high operational temperatures, high cost and not being suitable for the mass production. There are three dominating MAM methods based on adding layer upon layer using metals. Powder Bed Fusion technology is the leading method because of its relatively low-cost and high-resolution operation. The principle of this technique is to fuse nano-sized particles by focusing a laser beam to bond them. Powders may consist of the binder-metal mixture (Selective Laser Sintering) or single metal particles (Selective Laser Melting). Although those methods can be preferred for rapid prototyping, non-metal ingredients or high operating temperatures cause low density and degrades the strength of product. Another method is called Direct Energy Deposition which presents a functional part that can be used in a structure having high strength and relatively short post-processing. Electron beam or Ultrasonic waves are focused to the powder which is fed continuously to the same location, thus metal is melted over the substrate instantaneously. However, these setups require precisely controlled atmosphere and very expensive devices. Material Jetting (MJ) is the emerging type of MAM. Generally, material (metal or binder) is squeezed as tiny droplets before depositing. MJ could become very popular due to quick deposition, high resolution and high density properties achieved at the same time. However, this requires precise visualization as well as dealing with high temperatures.

Keywords: Metal additive manufacturing, Powder bed fusion, Direct energy deposition, Material jetting

INTRODUCTION

Nowadays, additive manufacturing (AM) technology has been adopted by the manufacturing industry. Because of reduced manufacturing costs and increased precision levels, direct part manufacturing become possible with this technology. Considering the wide-range of usage, the definition of AM technology has been standardized by American Society for Testing and Materials (ASTM) as "*a process of*

joining materials to make objects from 3D model data, usually layer upon layer, as opposed to subtractive manufacturing methodologies. Synonyms: additive fabrication, additive processes, additive techniques, additive layer manufacturing, layer manufacturing, and freeform fabrication" [1]. In addition to the polymers, ceramics and biological contents those are available for many years, the metallic compounds have started to take a place in AM industry since last decade. Aluminum, Steel, Titanium, Bronze, Nickel, Copper, Chromium and other traditional high melting point pure metals or alloys could also be processed in the automotive, spacecraft and medical tooling industries via different AM techniques [2-3]. As well as high melting point materials, low melting point metals such as soldering alloys with variable fractures of Lead, Tin and Bismuth could be used for various applications [4]. The usage of metal materials in the AM industry make possible to manufacture conventional products with higher precision. For instance, complex and multilayered circuit boards could be manufactured additively with high accuracy in shorter processing times [5]. In the field of MEMs, electronic packaging and flip-chip technology [6], various metal additive manufacturing (MAM) techniques are increasingly preferred due to the capability of manufacturing metallic objects directly from a CAD data. MAM techniques can be classified due to the material used, melting type and layering mechanism.

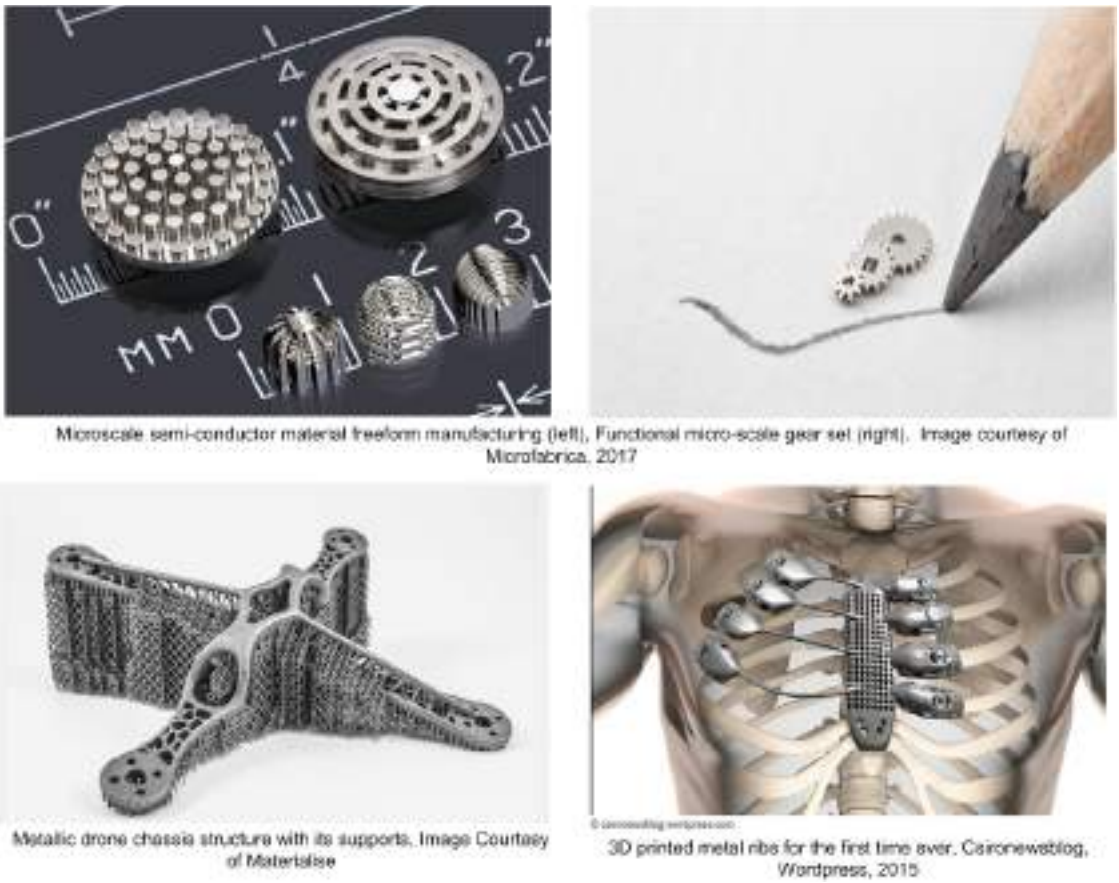

Figure 1: Various products manufactured via metal additive manufacturing techniques for different industries

All types of MAM provide different features on the final product generally listed in the literature as layer resolution, density, strength, functionality and surface finish quality [7]. However, these final product features cannot be achieved together at a

single process. Thus, the most desired property of the product as a top priority must be decided before the selection of MAM method in accordance with the demands and usage area. Also, the initial material conditions and properties play a major role in the method selection of MAM. In addition, the melting type, power requirement, deposition type, substrate and atmospheric conditions should also be taken into consideration during the selection of the method. Generally, MAM process could be routed as given below;

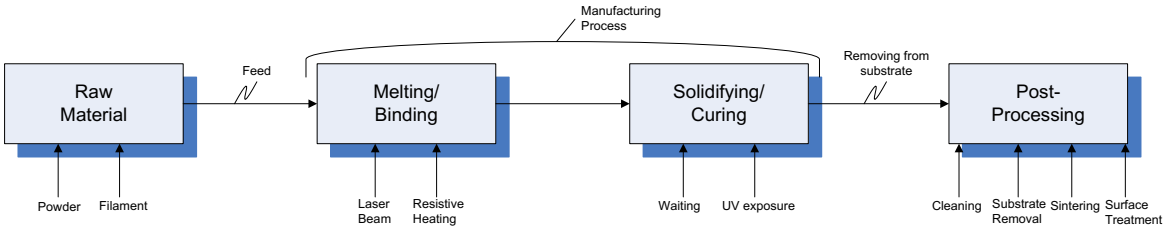

Figure 2: General steps of metal additive manufacturing operation

Beside the main steps of the manufacturing process, there are few more important issues which directly affect the final product condition. Firstly, the CAD model should be designed considering the actual manufacturing process in order to achieve the high quality product. Regarding the rough conditions of metal melting process at elevated temperatures, the boundary conditions of a geometrical design should be defined carefully taking into account the material response [8]. In addition, manufacturing atmosphere must be under control to avoid hazardous gas emissions, undesired chemical reactions and heat leakage during the melting process. Substrate material, which is a surface that the material will be deposited on, also should be chosen carefully. One reason is that the first few metal layers will directly interact with the substrate by the helpings of the high temperature. This interaction should not distort the chemical and the mechanical structure of the material. Moreover, the substrate should hold the material strongly enough not to cause undesired motion of the product during the process. In some cases, the product might be surrounded by support material that also solidifies with main product simultaneously to be able to beat the gravitational force. Support material must be removed after the AM process generally via conventional machining, heating or chemical resolving. The substrate should be durable enough to allow this kind of post processing without any deformation. Below, main methods of MAM and its sub-categories are given to be able to determine the suitable method according to the desired operation.

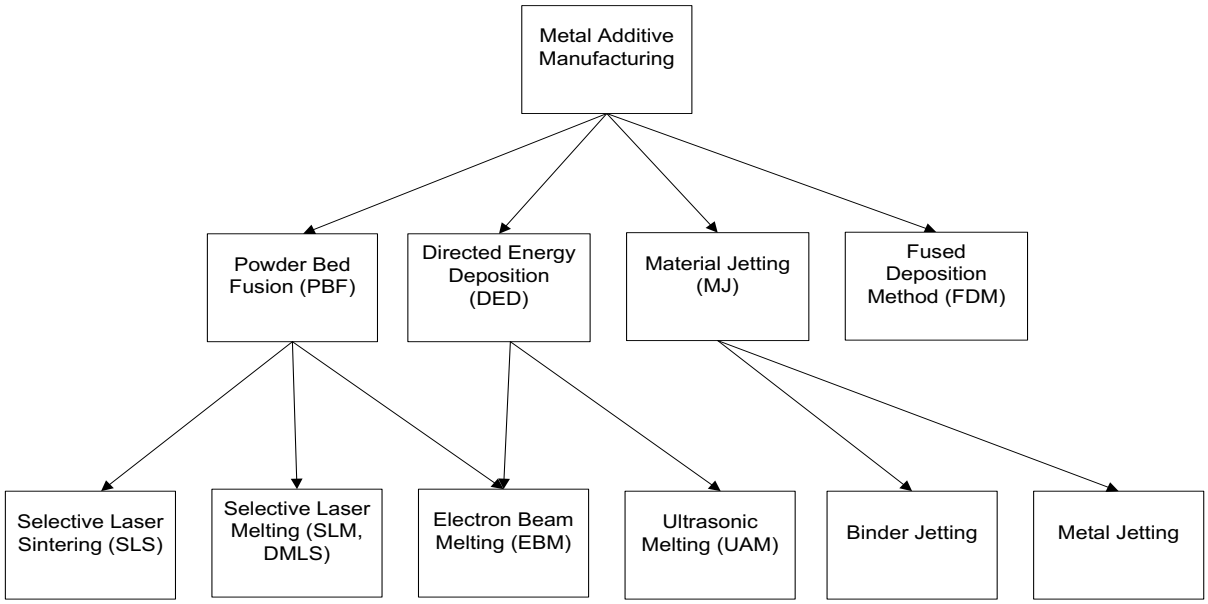

Figure 3: The classification of metal additive manufacturing with its main categories

In the following sections, the types of techniques are evaluated in more details with their advantages and disadvantages to be able to determine the best method for the final product with desired properties.

MAIN METHODS OF METAL ADDITIVE MANUFACTURING

Powder Bed Fusion

Powder Bed Fusion (PBF) is most commonly used technique for the metal manufacturing due to the capability of high layer resolution up to few microns. As a fundamental principle, the container (powder bed) full of fine powdered material is placed under a laser beam. Powder manufacturers pay intensive attention to the grain size during powdering process to achieve small and equivalent particles as much as possible. That is because the grain size (mostly in the scale of nanometer) and homogeneity of the powder directly affect the final product properties such as surface roughness, internal porosity and durability. Thus, the processed powder (powder cartridge) cost relatively high. The powder contains nearly 60 percent of metallic particles while the polymer occupies the rest. The duty of the polymer particles is to melt by the laser beam and hold the metal particles together in a desired shape layer by layer. By doing this, the shape is prepared for the sintering step. During the sintering, the most of the polymer content is decomposed from the metal particles by heating. Metallic particles are also partially melted and metallic bonding is achieved. As a result, a metallic part with the density of nearly % 60 is obtained [9]. This process is known as *Selective Laser Sintering (SLS)* in the MAM field. During the process, powder distribution is provided by a distributor stick called as "sweeper". The powder is spread homogeneously with the thickness of few micrometers after melting process is completed for the related layer. Sweeper technology is common mechanism in all types of PBF for mechanical powder distribution layer by layer. It should be capable of operating at micrometer scale for better layer resolution. It could be understood that SLS can provide high layer resolution. But expensive powder

cartridges, the density and the strength loss, and post processing requirement are the main limitations for this technology consequently.

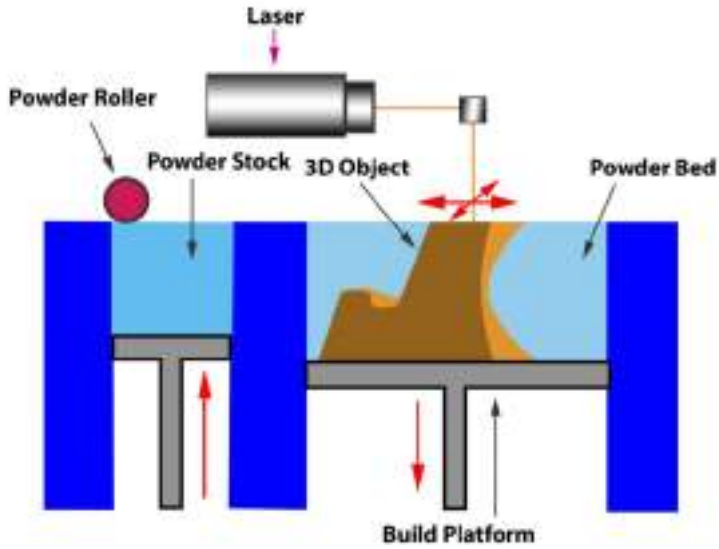

Figure 4: Schematic presentation of PBF process[10]

If higher density is demanded, hundred percent of metal powder could be melted without any polymer compound. This method is called both as Direct Metal Laser Sintering (DMLS) or Selective Laser Melting (SLM) in the MAM field. By using this method, near full density of metal product could be manufactured. However, a laser beam that requires much higher power must be employed to be able to melt the metal particles directly which also would increase the overall manufacturing cost. Furthermore, the melting process at high temperatures makes it difficult to control the material formation as another drawback of this technique.

Direct Energy Deposition

Direct Energy Deposition (DED) method relies on the similar concept to the PBF technology. The difference is that the powder is fed continuously to the focal area of the beam rather than being already placed in a powder bed container. DED represents much more durable final products fully made of metal particles. It is not necessary to use a binder material due to the direct melting of metal particles via high powered beams. Thereby, parts with high density and high strength could be manufactured with this method. Currently, automotive and aerospace [11] industries have already integrated this technique due to the result of intensive researches and developments in the field of DED. The beams mentioned above involve two main types. One, an electron beam, generated by an electron gun focused on to the powder to maintain the melting. The technique known as Electron Beam Melting (EBM) may provide high layer resolution due to precise melting in the scale of electron. On the other hand, high power necessity, requirement of human surveillance during the whole process which may last for days and highly strict atmospheric conditions are major drawbacks of this technology [12]. Moreover, mechanical equipment and controlling device costs are much above the budget of midsize companies. As a second type, Ultrasonic waves at high frequencies may be directed to the powder rather than electron beam which is

called as Ultrasonic Additive Manufacturing (UAM). Substantially, the principle, advantages and disadvantages of EBM are valid for the UAM method.

Fused Deposition Modeling

Fused Deposition Modeling (FDM) is a technique mostly used for thermoplastic manufacturing. The mechanism is based on extruding filament-type base material into the heater, liquefying then squeezing onto the substrate for solidification. Lately, metallic particles have been started to be added to the thermoplastic filaments at certain percentages. Therefore, FDM method could be associated with the MAM industry. There are several applications of FDM with metal filled filaments such as electronically conductive 3D parts with a high complexity, fine-line soldering and circuit board manufacturing. This method is capable of manufacturing relatively more durable parts due to the deposition by continuous beads. These individual beads collapse layer by layer, thus strong mechanical bonding is achieved. On the other hand, extra surface treatment is generally required after the deposition since the surface has a poor finish in this method. Furthermore, this method relies on heating until the glass transition of the base material rather than melting completely. Contrarily to thermoplastics, metals have very narrow range of glass transition temperature or do not have at all. This issue limits the FDM method to be used as a solid MAM technique.

Material Jetting

Material Jetting (MJ) method has many options in the name of MAM industry. The technique comes out of extruding the liquid material in form of a single droplet at a time repeatedly. Generated droplets are mechanically ejected with certain frequencies between 1 Hz and 25 kHz. The frequency and velocity of the ejection determine the total processing time. In this technique, liquid and droplet properties such as viscosity, surface tension, droplet diameter, excitation temperature and the velocity are dominant factors those determine the quality of the object to be deposited. Although there are many parameters need to be controlled simultaneously and precisely such as heat, pressure and power supply, actuation source and electrical inputs; many metal materials more than other methods could be deposited in MJ method. Due to the wide variety of usage areas, deposition via jetting can be called with different names such as Freeform Fabrication and Near-net Shape Manufacturing. This method is capable of providing complex metal shapes with high strength and density within reduced manufacturing times in a single process [13]. MJ involves depositing droplets in an array horizontally on the substrate, then, like any other AM methods, adding layer over layer vertically. In this method, operating temperature could be both low and high according to the process demanded. For instance, fully functional metal based assemblies in the scale of micrometer, high precision electronics and MEMs could be manufactured using low melting point materials such as Lead, Tin and Bismuth [14]. Besides, automotive and aerospace industries have a special interest on metal jetting techniques. This is because, highly complex and durable metal parts made of Steel, Aluminum, Titanium, Copper, Zinc or such Alloys could be manufactured within very short times comparing to the conventional methods with high accuracy. As another

reason, repairing broken parts benefiting from the CAD/CAM software could be possible without wasting time and material [15]. As another type of material jetting, polymer based materials could be deposited rather than liquid metals. Polymer based resins as a binder could be ejected over metallic powder layer if high density and strength are not required.

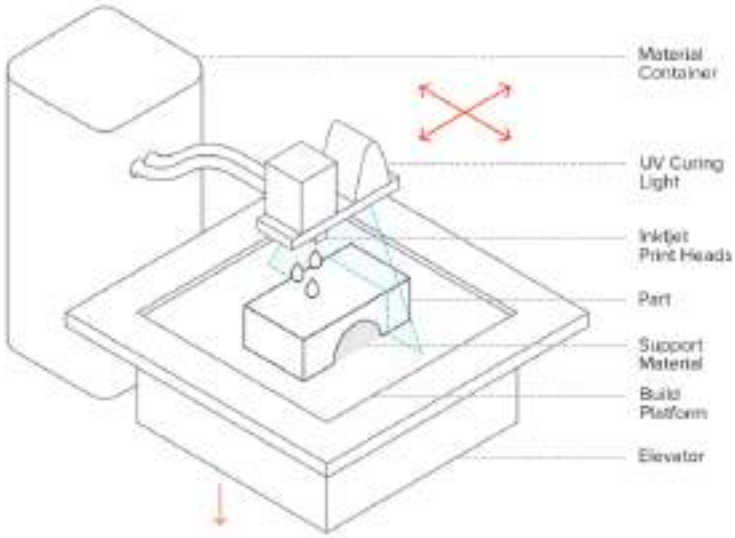

Figure 5: Schematical material (binder) jetting system components. Image courtesy of 3dhubs.com

Binder Jetting could be associated with the PBF but still resolution and strength values will be higher in jetting method due to the deposition droplet by droplet. Although many facilities about MJ, this technology is still under development because of relatively high cost of control equipment as well as advanced control engineering requirement.

RESULTS AND FINDINGS

Comparing the given methods due to the possibilities, MJ technology presents additional advantages over the other methods. Currently, ejecting the liquid by an actuation source with appropriate input parameters is the major issue need to be clarified in this method. Because the ejection step is a key parameter in order to generate droplets precisely in a desired form. For further, side factors such as pressure, heat and power supply need to be handled simultaneously during the process. To summarize, MJ involve many sensitive operational steps that need to be carried out by advanced control engineering. To summarize the information provided in this paper, a chart is given below showing the results of evaluation of the output properties for different MAM techniques.

Table 1: Expected final part properties and quality levels due to the method used.

	Leading time	Resolution	Strength	Density	Functionality	Prototyping
SLS	• • • •	• • • •	•	•	•	• • • • •
SLM	• • •	• •	• • • •	• • • •	• • • • •	•
EBM	•	• • • •	• • • •	• • • • •	• • • • •	•

UAM	• •	• • • • •	• • • •	• • • •	• • • • •	•
FDM	• • •	• •	• • •	• • •	• •	•
BJ	• • • •	• • • •	•	• •	•	• • • •
MJ	• • • • •	• • • •	• • • •	• • • •	• • • •	• • • • •

The chart is composed of the final features according to the characteristics of each method that are given in the previous sections of the paper.

CONCLUSION

Considering all advantages and disadvantages of all presented methods, MJ presents more features in a single process. Taking into account the possibilities of direct metal part manufacturing with increased functionality in crucial manufacturing industries, MJ is the future promising method. It should also be noted that there are still some issues that need to be taken care of in the jetting method. Many engineers and companies keep their research and development activities going due to the reduced cost of metal manufacturing with desired strength properties. As well as the opportunity of manufacturing a part with high complexity, which is not possible via conventional manufacturing methods, the availability of wide material options in MJ may reshape the future concept of metal manufacturing industry.

RECOMMENDATIONS

To be able to facilitate the difficulties of the MJ method during the process, simulations could be utilized using software such as Flow3D or Comsol. Since the droplet generation quality strongly depends on nozzle geometry and base material properties; the process could be simulated with a high rate of consistency without realizing the actual manufacturing. By doing this, total cost and leading times would be minimized in order to spread the usability of this method for many more industries.

REFERENCES

[1] ASTM F2792-12a, Standard Terminology for Additive Manufacturing Technologies, (Withdrawn 2015), ASTM International, West Conshohocken, PA, 2012, www.astm.org

[2] Vayre, B., Vignat, F., & Villeneuve, F. (2012). Metallic additive manufacturing: state-of-the-art review and prospects. Mechanics & Industry, 13(2), 89–96. https://doi.org/10.1051/meca/2012003

[3] Gao, W., Zhang, Y., Ramanujan, D., Ramani, K., Chen, Y., Williams, C. B., … Zavattieri, P. D. (2015). The status, challenges, and future of additive manufacturing in engineering. Computer-Aided Design, 69, 65–89. https://doi.org/10.1016/j.cad.2015.04.001

[4] Tseng, A. A., Lee, M. H., & Zhao, B. (2001). Design and Operation of a Droplet Deposition System for Freeform Fabrication of Metal Parts. Journal of Engineering Materials and Technology, 123(1), 74. https://doi.org/10.1115/1.1286187

[5] Hayes, D. J., Wallace, D. B., Boldman, M. T., and Marusak, R. M., 1994, ''Picoliter Solder Droplet Dispensing,'' Int. J. Microcirc. Electron. Packag., 16, pp. 173–180.
[6] Wallace, D. B., 1989, ''Automated Electronic Circuit Manufacturing Using Ink-Jet Technology,'' ASME J. Electron. Packag., 111, pp. 108–111.
[7] Frazier, W. E. (2014). Metal additive manufacturing: A review. Journal of Materials Engineering and Performance. Springer New York LLC. https://doi.org/10.1007/s11665-014-0958-z
[8] D.L. Bourell, M.C. Leu, and D.W. Rosen, Ed., Roadmap for Additive Manufacturing, University of Texas at Austin, Austin TX, 2009
[9] Badrinarayan, B., and Barlow, J. W., 1992, "Metal Parts From Selective Laser Sintering of Metal-Polymer Powders," Solid Freeform Fabrication Symposium, pp. 141–146.
[10] https://sdgmag.com/features/digital-eye-3d-print-technology
[11] Laptev A, et al. Study of production route for titanium parts combining very high porosity and complex shape. Powder Metall 2004;47(1):85–92.
[12] W. Lu, F. Lin, J. Han, H. Qi, et N. Yan, "Scan Strategy in Electron Beam Selective Melting," Tsinghua Science & Technology, vol. 14, Juin. 2009, p. 120-126.
[13] Beaman, J. J., Barlow, J. W., Bourell, D. L., Crawford, R. H., Marcus, H. L., and McAlea, K. P., 1997, Solid Freeform Fabrication: A New Direction in Manufacturing, Kluwer Academic, Boston, MA.
[14] Yokoyama, Y., Endo, K., Iwasaki, T., & Fukumoto, H. (2009). Variable-size solder droplets by a molten-solder ejection method. Journal of Microelectromechanical Systems, 18(2), 316–321. https://doi.org/10.1109/JMEMS.2008.2011154
[15] Geiger, M., Steger, W., Greul, M., & Sindel, M. (1994). Multiphase Solidification - a new process towards metal prototypes and a new data interface. Fraunhofer, 9–16.

TRENDING TECHNIQUES IN ADDITIVE MANUFACTURING WITH THEIR ADVANTAGES AND DISADVANTAGES

Volkan KORKUT
Adana Science and Technology University
vkorkut@adanabtu.edu.tr

Hakan YAVUZ*
Çukurova University
dr.hakanyavuz@gmail.com

ABSTRACT: Additive Manufacturing (AM) technology is a revolutionary technique which may shape the future of manufacturing industry. It can be integrated into various fields including biotechnology, MEMs, automotive, space and aeronautical applications. By using this technology, the difficulties faced in conventional methods such as precise manufacturing of complex parts could be overcome. The other advantage of additive manufacturing process is to be able to obtain a physical part directly from a CAD data. The process is done by adding material layer upon layer on desired locations rather than material removing process used in conventional methods. There are many techniques and material options available in this technology. Fused Deposition Method is the one, based on fusing the material, then depositing it continuously on the substrate. This method presents high strength and durable parts but poor surface finish quality. Powder Bed Fusion method allows various materials for deposition such as polymers, composites and alloys. Principally, a laser beam is directed to the fine-powdered material to bond particles together. Many advanced engineering fields have already focused on this method due to the wide material options. Compared to the conventional methods, prototyping of complex parts could be done in shorter times. However the equipment costs and the strength loss of material are the main limitations of this method. Stereolithography is a relatively low cost and more reliable technology for the parts with high complexity. This method provides high surface quality instead of high strength and durability. In this method, photosensitive materials are cured by UV light at desired coordinates. Material Jetting Technology is another method which may bring both high strength and high resolution at one time. The jetting is done by generating tiny droplets on demand which determines the total processing time and final part quality. Although the advanced control engineering requirement, the most advantageous sides of all other methods could be collected in this method such as high strength and surface quality in shorter processing times.

Keywords: Additive manufacturing, Fused deposition method, Powder bed fusion, Stereolithography, Material jetting

INTRODUCTION

Additive Manufacturing (AM) has growing popularity due to the capability of manufacturing a part using digital model directly. This feature enables to manufacture complex shapes those cannot be achieved via conventional techniques such as material

removing, cutting or bonding processes. AM process involves several steps to convert virtual model into a physical object. Fundamentally, it begins with modeling desired geometry using any professional 3D modeling software. Afterwards, the completed model file is exported into an appropriate file format (".stl" is the most commonly used) to be able to configure the model in the slicer software. Slicer software could be found in the market as both commercial and open-source form. Previously prepared and exported 3D model is first divided into horizontal layers by slicer software. This procedure is also called as "slicing step". During the slicing, software also simulates material adding action depending on the time and location. The data of time and location is then recorded in the form of G-code (".gcode") file. G-code file could be assumed as a universal code that maintains connection between digital processing and actual manufacturing processing. Although there are many different devices, materials and mechanisms available, the principle of operation relies on the g-code as the key feature of AM industry. Technically, the base material is deposited on a suitable substrate continuously layer by layer according the data received. This process continues until the last layer is completed. However base material and the method of deposition may differ depending on expectations from the final part [1].

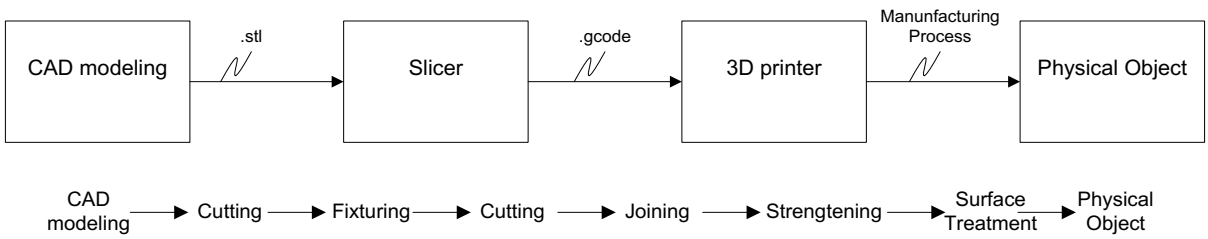

Figure 1: Main steps of Additive Manufacturing process (top) and conventional manufacturing steps (bottom).

The usage of AM method is widespread around many crucial fields currently. Automotive industry has started to use this technology since last decade for manufacturing complex parts. It is understood that the manufacturing times could be reduced to few days if AM technique is employed rather than conventional techniques which would take weeks for the same process. AM technique generally eliminates many conventional processes such as molding, machining, turning or milling. Also in-place repairing of the damaged parts has become possible instead of re-manufacturing the whole part again. In the fields of space and aeronautical industry, generally light-weighted and high strength parts are demanded. Therefore, these industries have started to manufacture parts using AM technology rather than conventionally manufactured ones; because AM technology also allows manipulation of strength distribution in a part which is not possible in traditional techniques. Regarding the high material costs used in these industries, material waste could also be minimized by employing topology optimizations before manufacturing. AM technique also attracted medical industry to itself because of its wide variety of operational capabilities relevant to the human health. AM provides; customizable prosthesis with almost hundred percent compatibility to the disabled body area, high precision medicine manufacturing and artificial tissue/organ manufacturing by leaving the

dangers of conventional transplantations behind. Moreover, the fields both mechatronics and MEMs have already adopted AM to their essential categories such as micro/nano assembling, electronic packaging and 3D circuit boards with high accuracy [2-5].

"Bionic Ear" made of mechanichal and electronical system. Photo by Frank Wojciechowski.

F1 brake pedal with hollow design made from EOS Ti64. Photographed by Michael Petch

Fully functional, micro fabricated metal gears, Captured by Neil Gershenfeld, MIT.

High-strength FDM thermoplastic (ULTEM) Image credit: Stratasys Direct Manufacturing

Figure 2: Four different examples of additively manufactured products.

In addition to the wide variety of usage areas, AM techniques also bring many base material options with itself such as polymers, low and high melting point pure metals, metal alloys, ceramics and biological contents. Whenever AM is required, the material is the first to be considered due to the expectations from the final product. Because the initial material properties tend to change during the heat or chemical treatments and directly affect the condition of the final product. Besides, the method of AM selected plays another major role over the properties of final product such as strength, density, surface finish and functionality [6]. One reason is that every method of AM involves different operational steps such as melting, curing, bonding and/or cooling. For this reason, there are time-dependent and dynamic factors like control of the mechanical system, heating type, power source, initial material form (liquid, powdered or filament). These are strongly determinant issues over the product to be used in the industry on demand. On the other hand, AM technology is still under development due to the need of understanding so many important issues such as reducing the cost of equipment, controlling the manufacturing atmosphere precisely and achieving the expected features of the product. Currently, dominant properties such as high strength, near-full density, high quality surface finish and high resolution cannot be achieved at the same time. Briefly, suitable method of AM method must be selected carefully in order to obtain a part with desired properties. In the following sections,

advantages and disadvantages of essential methods are evaluated for obtaining a final part with desired properties.

DIFFERENT METHODS OF ADDITIVE MANUFACTURING

Initially, AM process should first be categorized by its base materials. The general classification is given below in order to select the best method regarding the expected properties of the final product.

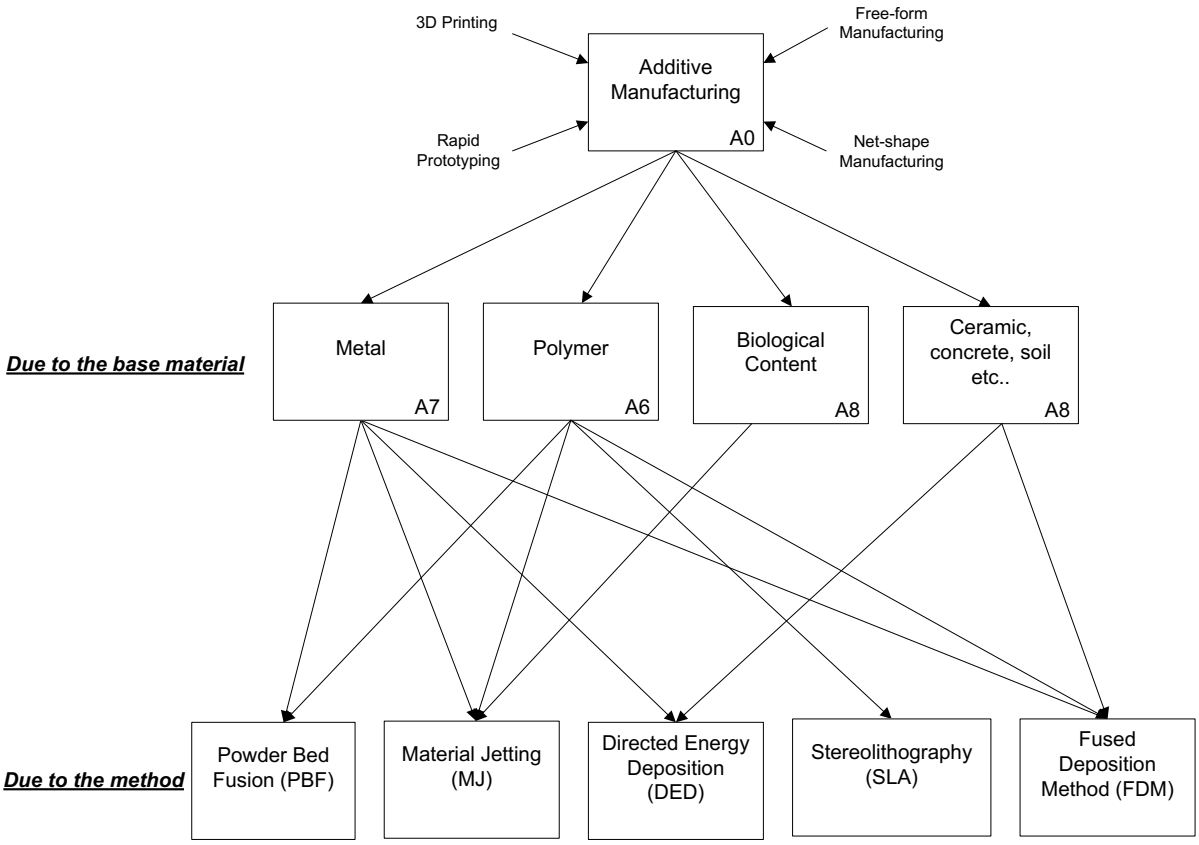

Figure 3: AM classification and categorization due to the base material and the method.

Powder Bed Fusion

Powder Bed Fusion (PBF) method includes several options inside. Generally, fine powdered initial material is placed inside a bed. Then high powered beam is focused into certain coordinates. The energy of the beam heats and melts (or cures in some cases) the material. Melted particles bond together and create a significant 3D physical object layer by layer.

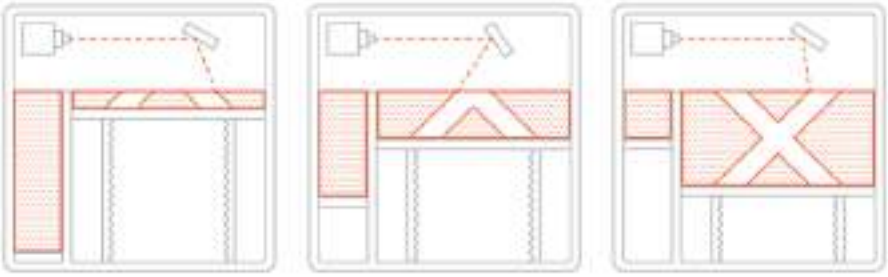

Figure 4: Representative images of PBF method (Images taken from the Knowledge Base of www.3dhubs.com, 2018 [7])

Alongside the binding process, the number of different applications is also available in this method. The type of both power source and base material mainly divide the PBF method into three main categories.

Selective Laser Sintering

Selective Laser Sintering (SLS) method relies on the laser beam melting which is directed precisely onto predefined coordinates. The beam fuses the particles in the focal area. Powdered material averagely consists of 50-60 percent of metal particles (as a base material) while the rest is polymer. The main use of the polymer, also called as *binder,* is to melt primarily, then to hold the metal particles in a desired shape and prepare the part for sintering step by solidifying quickly. Binding process may not be achieved by the melting process all the time. The UV light could be directed to the photo-sensitive polymers to be cured. By doing this, solidification is maintained by curing process rather than melting-cooling processes [8]. As a result, SLS brings generally almost half density of a final product that can be used just for precise prototyping rather than functionality. This concept is widely used in the automotive and aircraft industry for rapid prototyping and mold patterning [9]. SLS presents highly detailed prototyping which eliminates both the most of material removal processing and human factor. Although the advantages of high resolution and cost-effective processing, SLS has still limited use due to the low density of the final product. Unpredictable density dissipation of the product may also result in mismatch between the actual part and simulations.

Selective Laser Melting

Selective Laser Melting (SLM) or Direct Metal Laser Sintering (DMLS) allow direct metal manufacturing using almost similar principle to that of SLS. There is no binder material in the powder bed during the SLM process as a main difference from SLS. As a principle, hundred percent of metal particles are fused by the high powered laser beams. Thus, the full density of metal object could be obtained. However, high operating temperatures may cause material failures such as warping or cracking. In addition, the cost of equipment such as high powered laser head, power supply, control system and controlled atmosphere limit the usage of this method for low-cost manufacturing.

Electron Beam Melting

Electron Beam Melting (EBM) may provide very accurate manufacturing process due to the melting in the scale of almost electron size. As the principle of operation, electron gun (electron beam) with high frequency is focused on a certain point over the top layer of powder. The energy of the beam generates a heat enough to melt this small region and hold the particles together. Although the high accuracy and layer resolution, some limitations must be noted for this method. EBM operation requires experienced engineers to control the whole process. The manufacturing atmosphere

also needs to be controlled including the whole room to avoid any hazardous issue such as fire, gas emission or chemical reactions. Additionally, the high power consumption needs to be handled carefully. Although aircraft or automotive parts could directly be manufactured using this technique, this is a highly limited method due to the physical side-factors which also requires astronomical funding. Consequently, only companies with high budgets can afford this technology.

Directed Energy Deposition

Electron Beam Melting & Ultrasonic Additive Manufacturing

EBM and Ultrasonic Additive Manufacturing (UAM) have the same principle since the beam is directed to the same point with the material being fed in the form of powder. In the focal point, material is continuously melted by the high powered beam. EBM and UAM could be categorized under the same title together because these two methods slightly differ from each other just due to the melting mechanism. EBM uses electron bombardment to increase the kinetic energy and to melt the desired region while the high frequency ultrasonic waves are emitted over the particles to for the same reason in the UAM.
The principle of the methods both PBF and DED relies on directing a beam with enough energy to melt the powdered material. But DED provides higher accuracy in most cases due to the higher energy conservation because material feed rate could be adjusted according to the power emitted. Conversely, the energy focused on powder bed is dispersed out of the focal area boundaries which result in undesired melting in PBF.
On the other hand, DED requires advanced control engineering to be able to handle many parameters in harmony. Besides, setup of the whole system is expensive as much as PBF at least. These factors decrease this method's availability in the most industries. Currently, DED is mostly used in automotive, space and medical industries those require high precision.

Stereolithography

Stereolithography (SLA) stands for the very first AM method which uses photosensitive polymers (in the form of resin) as a base material. UV beam at a certain frequency is directed over the resin in order to cure the polymer at the focal area. The beam is continuously directed to the liquid resin layer by layer until the desired shape is obtained [10].

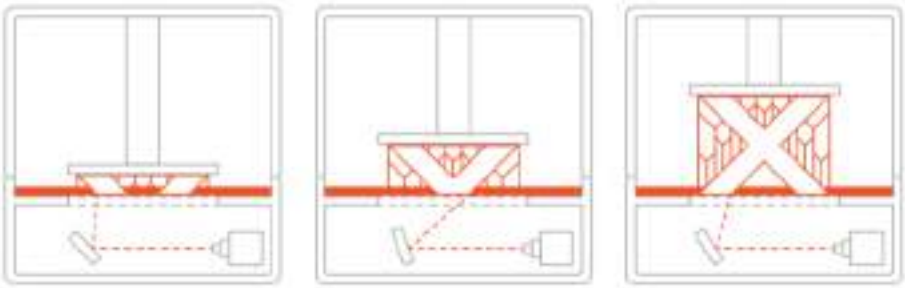

Figure 5: Representative images of SLA method (Images taken from the Knowledge Base of www.3dhubs.com, 2018 [7])

While this method provides a part with high quality surface finish, dynamically functional parts cannot be achieved due to the low strength values of the polymers. Although the durable compositions with polymers could be possible, the low density would still be a problem in SLA. Thus, this method is currently preferred in order to obtain complex prototypes with high resolution in the industry.

Fused Deposition Method

Fused Deposition Method (FDM) is most commonly used AM method which can provide a final product with relatively high strength due to the bulk deposition. In FDM, filament-type material is heated until its viscoelastic phase while being fed by an extruder motor. Then the heated material is squeezed from an orifice over a suitable substrate layer by layer like every other AM method.

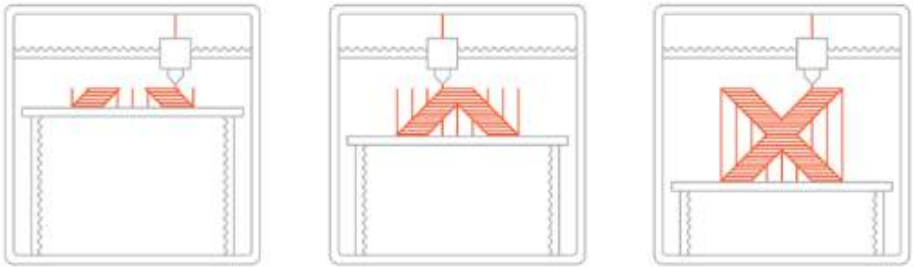

Figure 6: Representative images of FDM method (Images taken from the Knowledge Base of www.3dhubs.com, 2018)

It is possible to find various FDM devices in the market with the prices from 100 $ up to 500.000 $ mostly depending on the base material to be used. Resolution, consistency and homogeneity of the final product are other the major factors for determining the price. Many base materials are also available for FDM with different characteristic such as polymers (PLA, ABS, PETG), metal particle filled polymers (filled with bronze, gold, copper) and metals (solder wires) [11]. On the other hand, there are several drawbacks of this method. The temperature control plays a major role in the process since the temperature range of the viscoelastic material is very restricted. The extrusion rate must also be in harmony with the operating temperature. In addition, heating type, ambient type, temperature provided and substrate properties must also be determined specifically for every single material. Although the capability of depositing relatively high strength products, low quality surface finish and obligatory post processing requirement still limit the usage of this technology.

Material Jetting

Material Jetting (MJ) technology is a future promising method. This is due to the fact that it can be able to present durable parts with high resolution in much shorter leading times. As the principle, the liquid base material is first stored in a reservoir which has an orifice at the bottom. Then the liquid is pushed towards orifice. This pressure forces the liquid to squeeze out of the orifice and result in a droplet. As a result, the flow consisting equivalent droplets provides a continuous material deposition. The deposition is maintained droplet by droplet, then layer by layer respectively. MJ could be divided into two main categories due to the droplet generation frequency:

Continuous and Drop-on-Demand jetting [12]. In the continuous jetting, droplets separate from each other partially or do not separate at all due to the ejection at high frequencies. Thus, the heterogeneous but continuous groove is observed. In drop-on-demand jetting, droplets are generated and controlled individually. Although the deposition rates are generally lower than continuous jetting, more accurate manufacturing operation could be achieved via drop-on-demand technique.

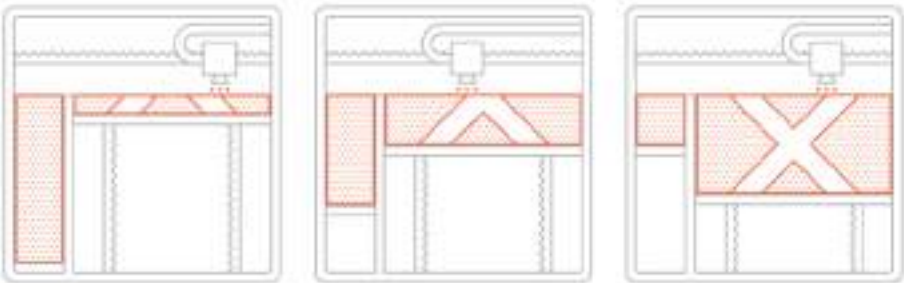

Figure 7: Representative images of MJ method (Images taken from the Knowledge Base of www.3dhubs.com, 2018)

In the MJ method, more material options than other AM methods are available such as polymer, metal, biological content and ceramic-like materials. Since the last decade, this method has already become subject of interest for some crucial industries such as medicine manufacturing, tissue engineering, MEMs, aerospace, electronic packaging, flip-chip technology and direct metal part manufacturing [13]. Although the wide usage area, there are still several limitations in this technology those need to be handled. The liquid ejection is the most important step of the jetting method. Achieving a high quality product strongly depends on the properties of a single droplet generated such as droplet volume, velocity, density and homogeneity. To be able to generate consistent array of droplets, other major parameters such as reservoir and orifice geometry, ejection method, power, heat and pressure supply must be accounted precisely. The droplet generation must be carried out at low tolerances since the droplets are expected to be in the scale of micro or nanometer. Operations at those scales require very sensitive actuators, controlling devices and inspection equipment which means an expensive setup. Nevertheless, possibilities in MJ methods are wider comparing to the other methods if sufficient control of the system could be carried out.

RESULTS AND DISCUSSION

Taking into account the advantages and disadvantages of all methods of AM mentioned previously, the selection of the method should be done firstly according to the base material demanded. According to the material, final expectations from the product such as strength, density, surface finish and functionality should also be considered. In order to achieve the best results of the material property a chart, in Table 1 with the main input and outputs, is provided for guidance.

Table 1: Comparison chart of the AM methods due to their possibilities and properties

	Main Methods	SLS	SLM	EBM	FDM	DED	SLA	MJ
Material	Polymer	x			x		x	x
	Metal		x	x	x	x		x
	Composite	x			x			x
	Ceramic	x				x		x
	Biological	x						x
Property (High...)	Strength		x	x	x	x		x
	Density		x	x	x	x		x
	Resolution	x		x		x	x	x
	Surface Finish			x		x	x	x
Energy Required	Ultra High		x	x		x		
	High	x				x		x
	Medium	x			x			x
	Low						x	
Usage Area	Prototyping	x			x	x	x	x
	Electronics	x	x	x		x		x
	Medical			x		x		x
	MEMs			x	x	x		x
	NanoFabrication		x	x		x		x
	Experience Req.	M	H	H	L	M	L	H
	Average Cost	M	H	H	M	H	L	H

It can be seen from the chart that the material options are wider in MJ method compared to the others. The material properties of the final product in a single operation tend to be better in both EBM and MJ methods than other. Considering lower energy consumption and the ease of controllability of the power supplement carries MJ method one step forward from EBM. Moreover, it is possible to modify the MJ system for many manufacturing industries which are capable of to change the future. However, MJ system is still not feasible for some applications due to the expensive equipment as well as advanced control technique requirements. If these drawbacks that stop this method to become widespread, MJ method could be more reasonable to choose rather than other AM methods.

CONCLUSION

To conclude, suitable AM method must be chosen to be able to obtain a product with desired strength, density, surface finish quality, tolerances and functionality in terms of AM technology. To initiate the AM process, firstly the base material must be considered for the job demanded. Secondly, the expectations from the product should

be determined as well as the equipment and experience needed for the operation. Keeping the current outcomes of MJ method in mind, it is a glittering method due to possess the most of the features of other AM method in a single operation.

RECOMMENDATIONS

Although AM technology shortens the long period of a multi-stage conventional manufacturing process, the operation still takes relatively long time to process a single part. To reduce the processing times as well as the material usage, topology optimizations could be employed. Topology optimizations are getting more popular day by day in the name of reducing time and material waste, for those reasons, the CAD software start to provide this module with themselves.

REFERENCES

[1] Gibson I, Rosen DW, Stucker B (2010) Additive Manufacturing Technologies: Rapid Prototyping to Direct Digital Manufacturing, Springer, New York
[2] Gao W, et al. The status, challenges, and future of additive manufacturing in engineering. Comput Aided Des 201
[3] Laptev A, et al. Study of production route for titanium parts combining very high porosity and complex shape. Powder Metall 2004;47(1):85–
[4] Melchels FP, et al. Additive manufacturing of tissues and organs. Prog Polym Sci 2012;37(8):1079–104
[5] F.G. Tseng, Microdrop Generators, in The MEMS Handbook, Mohamed Gad-el-Hak, Ed., CRC Press LLC, Boca Raton, FL, 2002, pp. 30-1, 30-30.
[6] Gao, W., Zhang, Y., Ramanujan, D., Ramani, K., Chen, Y., Williams, C. B. Zavattieri, P. D. (2015). The status, challenges and future of additive manufacturing in engineering. Computer-Aided Design, 69, 65–89. https://doi.org/10.1016/j.cad.2015.04.001
[7] Knowledge Base, www.3dhubs.com
[8] Deckard C. Method and apparatus for producing parts by selective sintering. US Patent 4,863,538, September 1989.
[9] Hejmadi, U., & Mcalea, K. (1996). Selective Laser Sintering of Metal Molds: The RapidTool(TM) Process. Proceedings of the SFF Symposium, 97–104.
[10] Hull C. Apparatus for production of three-dimensional objects by stereolithography. US Patent 4,575,330, March 1986
[11] Breyfogle A, Cormier D. Capability assessment of combining 3D printing (FDM) and printed electronics (aerosol jet) processes to create fully printed functionalized devices. In: RAPID, June, 2013.
[12] Lin, H.-J., Wu, H.-C., Shan, T.-R., & Hwang, W.-S. (2006). The Effects of Operating Parameters on Micro-Droplet Formation in a Piezoelectric Inkjet Printhead Using a Double Pulse Voltage Pattern. Materials Transactions, 47(2), 375–382. https://doi.org/10.2320/matertrans.47.375

[13] Tseng, A. A., Lee, M. H., & Zhao, B. (2001). Design and Operation of a Droplet Deposition System for Freeform Fabrication of Metal Parts. Journal of Engineering Materials and Technology, 123(1), 74. https://doi.org/10.1115/1.1286187.

THIS PAGE INTENTIONALLY LEFT BLANK

THIS PAGE INTENTIONALLY
LEFT BLANK

THIS PAGE INTENTIONALLY LEFT BLANK

THIS PAGE INTENTIONALLY LEFT BLANK

THIS PAGE INTENTIONALLY LEFT BLANK

THIS PAGE INTENTIONALLY LEFT BLANK

THIS PAGE INTENTIONALLY LEFT BLANK

THIS PAGE INTENTIONALLY LEFT BLANK

THIS PAGE INTENTIONALLY LEFT BLANK

GREY WATER FOOTPRINT OF BIOENERGY: A CASE STUDY OF A UASB REACTOR

Pelin SOYERTAŞ YAPICIOĞLU
Harran University, Environmental Engineering Department, Şanlıurfa
pyapicioglu@harran.edu.tr

ABSTRACT: Freshwater has the vital importance on earth. Due to growing population, there is concern in several regions and countries with limited and depleted water resources. So, water consumption and pollution have gained importance for these reasons. A tool has been developed by Water Footprint Network (WFN) for the assessment of water pollution capacity that is called as the grey water footprint (GWF). Industrial wastewater treatment plants (WWTPs) have been regarded as one of the freshwater pollutant configurations. Anaerobic treatment that contains Up flow Anaerobic Sludge Bed (UASB) reactor is implemented as the wastewater treatment method in a dairy industry. Because of biogas ensure in the result of the anaerobic treatment, it is a type of bioenergy. In this study, grey water footprint was calculated and investigated for a UASB reactor as a type of biomass energy. The main aim of this study is to determine the water pollution capacity of the biomass energy. Chemical oxygen demand (COD), oil and grease (O&G) and total suspended solids (TSS) are the main pollutant parameters for the UASB reactor. The results revealed that total grey water footprint of a UASB reactor was 6897.9 m^3/d. The major component of grey water footprint was footprint of oil and grease removal with the value of 3811.1 m^3/d and the minor component of grey water footprint was organic materials (COD) removal from wastewater in the value of 1300.7 m^3/d. According to the mass balance, influent wastewater flow rate is 2100 m^3/d and water pollution capacity (GWF) of this stream is 6897.9 m^3/d. The biogas amount is 2300 m^3/d and the GWF related to this volume of biogas is 6897.9 m^3/d. From this point of view, the grey water footprint of the bioenergy is 2.99 m^3/ m^3 biogas.

Key words: UASB reactor, bioenergy, grey water footprint, wastewater treatment

INTRODUCTION

Water resources have been consumed due to the climate change, in recent years (Ercin et al., 2013; IPCC, 2014). Water scarcity is described as the deficiency of available freshwater resources. Available freshwater resources have been utilized by several industries and energy technologies (Gerbens-Leenes et al., 2008). One of them is dairy industry that is considered as a huge freshwater consumer plant. Freshwater is the raw and auxilary material for these types of agro-industries as using process water and as the sanitation purpose. Also, dairy industries has generated crucial amounts of wastewater with relatively high organic content (Amini et al., 2013).

The dairy industry is one of the most pollutant plants due to the wastewater generated and discharging highly organic wastewaters (Ozturk et al., 2003; Demirel et al., 2005). Chemical oxygen demand (COD), oil and grease (O&G) and total suspended solids

(TSS) are the major pollution indicators of the dairy wastewaters. Also, this wastewater is a feedstock of the biomass energy as a renewable energy type. In the result of anaerobic treatment of dairy wastewater, biogas is ensured as the bio-energy (Speece, 1996; Yapıcıoğlu &Filibeli, 2017).

Up-flow Anaerobic Sludge Bed (UASB) reactors are the common anaerobic treatment configurations (Metcalf & Eddy, 2014). So, in order to obtain the bioenergy, a water contamination emits from the UASB reactors. To determine freshwater pollution capacity in wastewater treatment plants (WWTPs) a new indicator was developed named as the grey water footprint (GWF) by Water Footprint Network (WFN) (Hoekstra & Mekonnen, 2011).

In this study, for a full-scale UASB reactor that is operated in a diary wastewater treatment plant, grey water footprint (GWF) assessment has been carried out using WFN method for three parameters that contain COD, O&G and TSS. The main aim of the study is in order to determine the water pollution capacity for a type biomass energy.

METHODS

Description of the Dairy Industry

The dairy industry is located in an organized industrial zone in Turkey. The main products are drinking milk, fruit juice, cream, milk powder, yoghurt and butter. The wastewater charactrization of the dairy industry is given in Table 1. The wastewater analysis results were obtained using Standard Methods (APHA 1998). The wastewater treatment plant is a full-scale plant.

Figure 1 demonstrates the wastewater treatment process flow scheme in the plant. UASB reactor is used as the anaerobic treatment for organic and suspended materials removal. UASB reactor capacity is 400 m^3 and hydraulic retention time is 4.5 hours. UASB reactor is in cylindrical form and it has 4 m diameter and 8 m height. The average biogas that emits from UASB reactor is approximately 2300 m^3/d. In DAF process, oil, grease and suspended organic materials removal have been obtained. After wastewater is treated, then the effluent is discharged to the Organized Industrial Zone Central Sewage System.

Table 1. Influent Dairy Wastewater Characteristics

Parameter	Value
COD (mg/L)	12000
Oil & Grease (mg/L)	350
TSS (mg/L)	350
pH	6
Flow Rate (m^3/d)	2100

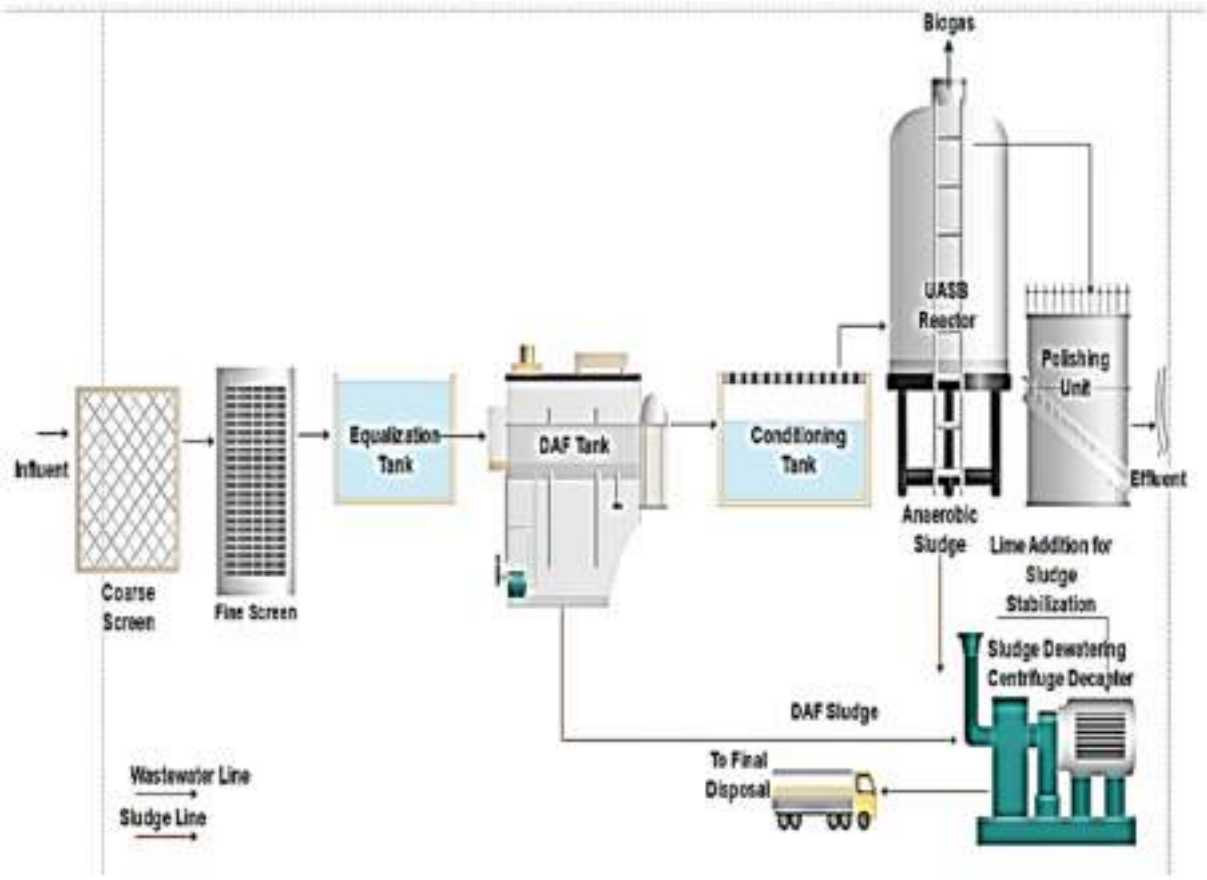

Figure 1. Wastewater Flow Scheme of the Dairy Industry WWTP

Grey Water Footprint Estimating

The grey water footprint (GWF) is an indicator parameter of freshwater pollution. Therefore, the GWF does not only determines the quantification of freshwater resources depleted, but it also figures out the freshwater pollution capacity.
It can be calculated by a simple equation from derived the mass balance named as WFN methodology (WFN, 2014). Eq. (1) shows the calculation.

GWF=(Qe x (Cmax-Ce)) / (Cmax-Cnat) (Eq. 1) (Morera et al., 2016)

In Eq. (1), Qe is the effluent flow rate (volume/time), Ce is the concentration of a pollutant in the WWTP effluent (mass/volume), Cmax is the maximum concentration of a contaminant allowed in the sewage system or receiver freshwater body, and Cnat is the natural concentration of a contaminant in the sewage system or receiver freshwater body (Morera et al., 2016). Ce values and Cnat values have been determined from wastewater analyses and Cmax values have been from Turkish Water Pollution Procedure (Official Gazette, 2004). Three pollutant indicators that contain COD, O&G and TSS have been considered for GWF accounting. Because, these three parameters are the major pollutant parameters for the dairy wastewaters.

Goals and Boundaries

The aim of the study is to determine GWF of a UASB reactor that operated in dairy WWTP using WFN methodology. The main goal is to estimate the water pollution capacity of biogas emitted from the UASB reactor in the plant. The system boundaries have been demonstrated in Table 2. COD and TSS analyses have been implemented by using Standard Methods (APHA, 1998) and O&G analyses have been conducted using EPA method (EPA, 2010).

Table 2. Data Set of GWF Assessment

Parameter	UASB Influent	UASB Effluent Ce	Sewage System Cmax	Sewage System Cnat
COD (mg/L)	4800	2900	4000	2224
Oil & Grease (mg/L)	10	5	250	115
TSS (mg/L)	200	170	500	112

RESULTS AND FINDINGS

Grey Water Footprint Assessment of UASB Reactor

Table 3 presents the GWF assessment results of this study. The highest GWF value corresponds to O&G parameter with the value of 3811.1 m^3/d. So, it can be said that oil and grease are the major pollutant parameter that leads to the water pollution for a UASB reactor. The following highest parameter is TSS that has GWF at the value of 1786.1 m^3/d.

Table 3. Grey Water Footprint Assessment Results

GWF	Value
GWF_{COD} (m^3/d)	1300.7
$GWF_{O\&G}$ (m^3/d)	3811.1
GWF_{TSS} (m^3/d)	1786.1
GWF_{Total} (m^3/d)	6897.9

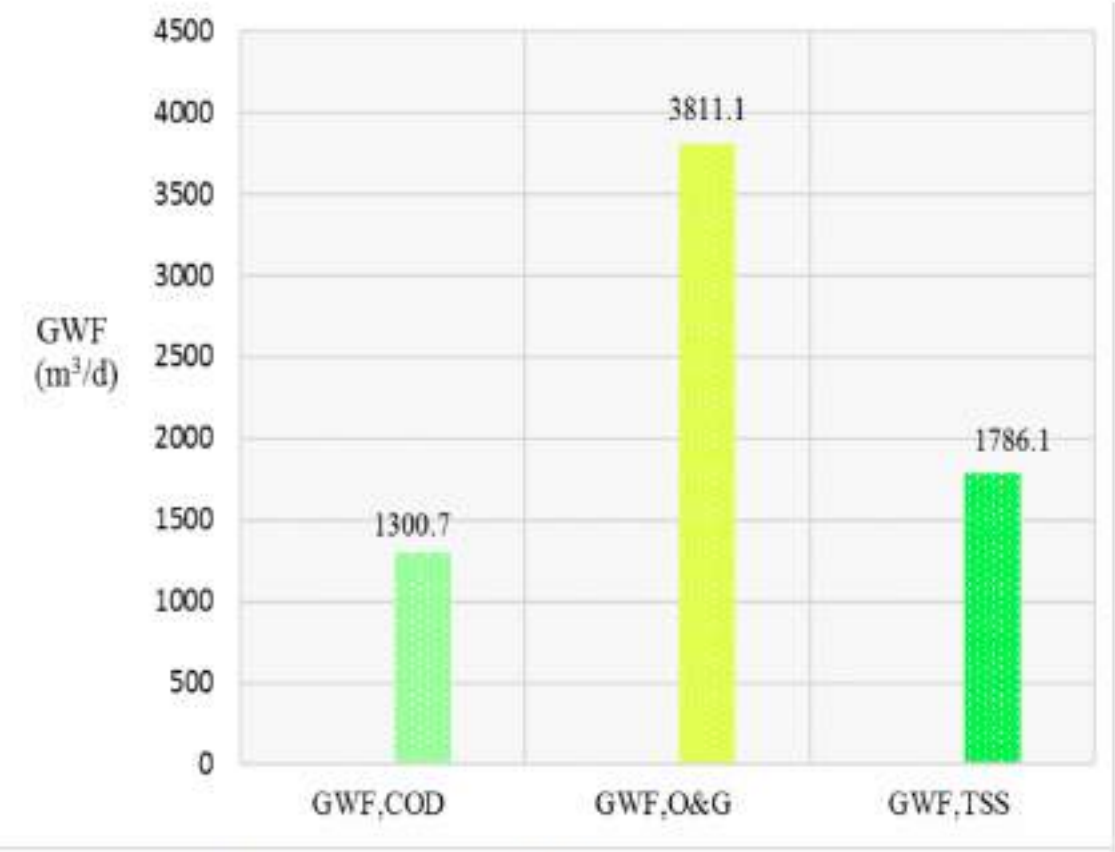

Figure 2. Grey Water Footprint Assessment

Figure 2 shows the comparison of three pollutant parameters. The lowest GWF corresponds to COD parameter, COD gives the least damage to the water resources for a dairy factory.

Mass Balance Results

Influent wastewater flow rate is averagely 2100 m^3/d but for this amount of treated wastewater, grey water is occurred in the value of 6879.9 m^3/d. This wastewater stream has an environmental impact on sewage system 3.3 times higher than the volume of influent wastewater. To generate 2300 m^3/d biogas, 2100 m^3/d wastewater should be treated and this wastewater creates total grey water footprint in the value of 6879.9 m^3/d in the central sewer system.

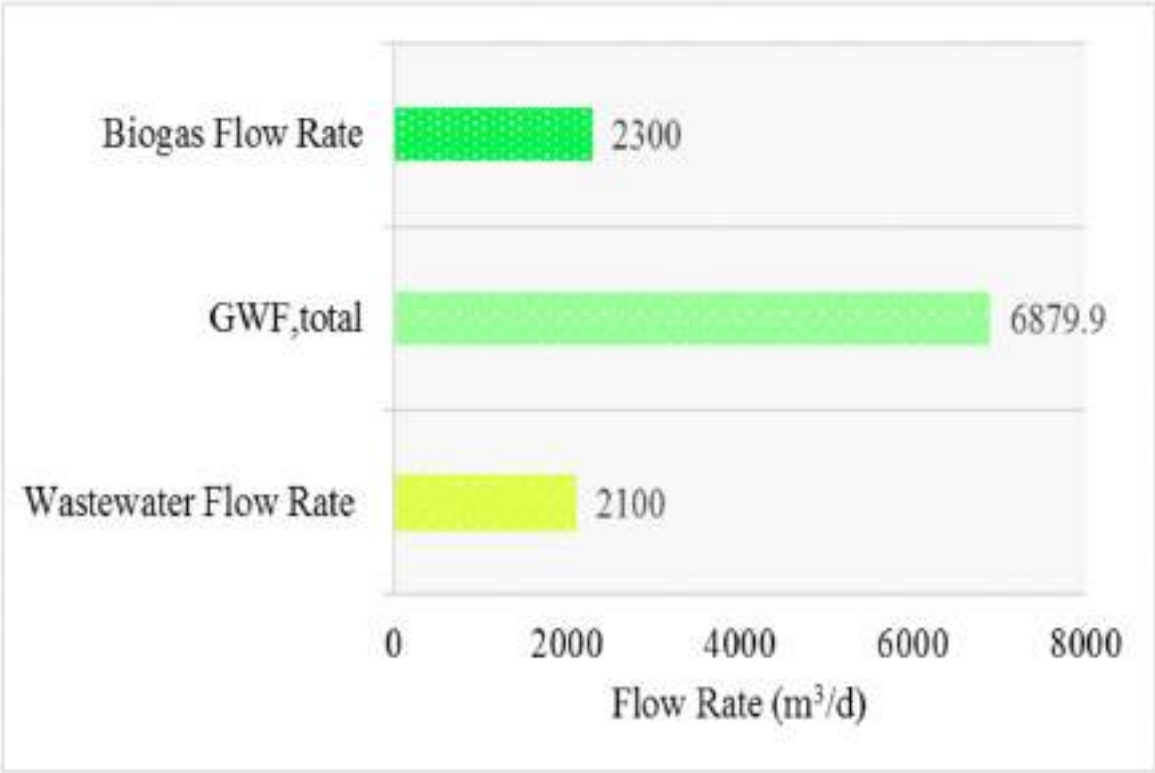

Figure 3. Mass Balance Assumption

CONCLUSION

Biogas that occurs in the result of anaerobic treatment is a type of bioenergy that leads to the grey water footprint. UASB reactors are mainly used anaerobic treatment technologies for dairy wastewater treatment. In the result of anaerobic treatment of dairy wastewater, biogas is obtained that is a resource of grey water footprint. So, dairy wastewater treatment plants can be regarded as one of the fresh water pollutant constructions.

Grey water footprint can be used as the indicator of the water pollution capacity of the industrial wastewater treatment plants. It can be figured out with a simple WFN methodology for dairy wastewater plants. Also, this tool can be used for other industrial wastewater treatment plants and other wastewater pollutant parameters.

The highest GWF value corresponds to O&G parameter with the value of 3811.1 m^3/d. So, this result demonstrates that oil and grease are the major pollutant parameter that causes the water pollution for a UASB reactor. The second highest parameter is TSS that has GWF at the value of 1786.1 m^3/d. The lowest GWF belongs to COD parameter, COD gives the least damage to the sewage system for a dairy industry WWTP with the value of 1300.7 m^3/d. According to the assessment results, total GWF is 6879.9 m^3/d for a bioenergy.

Mass balance has an importance for this assessment tool. Inlet flow rate is 2100 m^3/d in a full-scale dairy wastewater treatment plant and this flow rate leads to the grey

water footprint with the value of 6879.9 m^3/d in the sewage system. So, it has an effect that is 3.3 times higher than its initial quantification. In the result of dairy wastewater treatment that has 2100 m^3/d flow rate, 2300 m^3/d biogas is ensured. So, in order to generate the biogas, grey water footprint revealed in the value of 6879.9 m^3/d. From this point of view, the grey water footprint of the bioenergy that contains biogas energy is 2.99 m^3/ m^3 biogas.

RECOMMENDATIONS

In the literature, the water footprint assessment of renewable energies that contain the bioenergy are very limited. These researches on this topic should be increased.

REFERENCES

American Public Health Association, American Water Works Association, (1999). *Standard Methods for the Examination of Water and Wastewater,* USA.

Amini, M., Younesi, H., Zinatizadeh-Lorestani, A.A., & Najafpour, G. (2013). Determination of optimum conditions for dairy wastewater treatment in UAASB reactor for removal of nutrients. *Bioresource Technology*, *145*, 71–79.

Demirel, B., Yenigun, O., & Onay, T.T. (2005). Anaerobic treatment of dairy wastewaters: a review. *Process Biochemistry, 40 (8)*, 2583–2595.

EPA, (2010). United States Office of Water, *Environmental Protection Agency (4303), February 2010, Method 1664, Revision B: n-Hexane,* USA.

Ercin, A.E., Mekonnen, M.M., & Hoekstra, A.Y. (2013). Sustainability of national consumption from a water resources perspective: The case study for France. *Ecological Economics, 88*, 133–147.

Gerbens-Leenes, P.W., Hoekstra, A.Y. & Van Der Meer, T.H. (2008). *Water Footprint of Bio-energy and Other Primary Energy carriers.*Value of Water Research Report Series No.29, Delft, Netherlands.

Hoekstra, A.Y., & Mekonnen, M.M. (2011). The water footprint of humanity, *PNAS*, vol. 109, pp. 3232–3237.

Metcalf & Eddy, (2014). *Wastewater Engineering: Treatment and Resource Recovery* 5th ed, Boston, USA, McGraw-Hill.

IPCC (2014). Jimenez, B.E., Oki, T. N., Arnell, W., Benito, G., Conley, J.G., Döll, P., Jiang, T., & Mwakalila, S.S. Freshwater resources. In: Climate Change 2014: Impacts, Adaptation and Vulnerability. Contribution of Working Group II to the Fifth Assessment Report of the Intergovernmental Panel on Climate Change.

Morera, S., Corominas, L., Poch, M., Aldaya, M.M., & Comas, J. (2016). Water footprint assessment in wastewater treatment plants. *Journal of Cleaner Production, 112*, 4741–4748.

Ozturk, I., Eroglu, V., Ubay, G. & Demir, I. (2003). Hybrid upflow anaerobic sludge blanket reactor (HUASBR) treatment of dairy effluents. *Water Science and Technology*, *28*, 77–85.

Speece, R.E. (1996). Anaerobic biotechnology for industrial wastewaters, USA, Archae Press.

T.C. Official Gazette (2004) Water Pollution Control Procedure, Ankara, Turkey. Retrieved June, 25, 2018 from

http://www.mevzuat.gov.tr/Metin.Aspx?MevzuatKod=7.5.7221&sourceXmlSearch=&MevzuatIliski=0

Water Footprint Network, WFN, (2014) Retrieved from June 25, 2018 http://http://waterfootprint.org/

Yapıcıoğlu, P., & Filibeli, A. (2017). Proceedings from IATS '17: The 8th International Advanced Technologies Symposiu. Elazığ, Turkey.

THIS PAGE INTENTIONALLY
LEFT BLANK

EFFECT OF POROUS SLEEVE POSITION ON NATURAL CONVECTION IN A CONCENTRIC ANNULUS

Ali Azzam
Department of Mechanical Engineering, Graduate School, Korea Maritime and Ocean University, Busan, South Korea
aliazzam89@yahoo.com

Laith M. Jasim
Department of Mechatronics Engineering, University of Mosul, Mosul, Iraq
jasiml68@uomosul.edu.iq

Hudhaifa Hamzah
Department of Mechanical Engineering, Çukurova University, Adana, Turkey
hudhaifahamzah@gmail.com

ABSTRACT: Laminar convection flow through two concentric horizontal cylinders with a porous sleeve is numerically analyzed. Both cylinders are maintained at constant temperatures with the inner cylinder at slightly higher temperature than the outer one. The flow outside the porous medium is governed by Navier-Stokes equation, whereas the Brinkman–Forchheimer–extended Darcy model governs the flow through the porous medium. The working fluid is water, while the fiberglass is used as a solid phase. The main objective of this study is to examine the position effect of a constant volume porous sleeve on the average transfer of heat. This sleeve was press-fixed in two different positions: the outer face of the inner cylinder and the inner face of the outer cylinder. The effect of various values of modified Rayleigh number (25-500) is investigated, whereas the Porosity, Darcy and Prandtl numbers are considered constants and fixed at 0.9, 10^{-3} and 7 respectively. The results show that the fixed insulation materials on the inner cylinder in more effective than fixed it on the outer cylinder. Rayleigh number has a significant effect on the rate of heat transfer in both cases.
Key words: Porous sleeve, Natural convection, Concentric annulus, Thermal insulation.

INTRODUCTION

Natural convection heat transfers and fluid flow in a horizontal annulus have been recently studied extensively. The motivation of these studies is came from a wide range of their applications such as fluid movement in solar collectors, thermal insulators, cooling of electronic chips and underground electrical lines (for example, see Charrier-Mojtabi (1997)). The first study of a natural convection heat transfer in a horizontal concentric annulus was carried out by Beckmann (1931). Kraussold (1934) was extended that study. Kuehn and Goldstein (1976) experimentally and numerically studied the velocity, temperature distributions and local heat transfer coefficient of natural convection within the horizontal annulus.

Some studies were expanded to include the effect of the porous materials on the rate of heat transfer and fluid flow behavior. The effects of some important terms such as, inertia, boundary, and velocity on the heat transfer between two isothermal horizontal

cylinders filled by a saturated porous medium was studied numerically by Kaviany (1986). Natural convection flow in two and three- dimensional horizontal porous annulus was simulated numerically by Charrier-Mojtabi (1997). Mixed convection heat transfer in a horizontal annulus filled with a uniform fluid-saturated porous medium has been carried out numerically by Khanafer and Chamkha (2003). Their results obtained a significant role of the Richardson number on the heat transfer characterization within the annulus. Braga and de Lemos (2006) investigated numerically the laminar and turbulent flow and free convection heat transfer within a horizontal cylindrical annulus filled with a saturated porous medium. Natural convection in a horizontal annulus filled with porous medium was studied numerically by Aldoss (2009). In his study, he considers the effect of variable porous permeability in the radial and tangential directions. Alloui, and Vasseur (2011) numerically studied the natural convection in a horizontal annular cavity filled with a binary fluid. Sakr and Berbish (2012) numerically and Experimentally investigated the free convection heat transfer in a horizontal elliptic annulus filled with saturated porous media.

Regarding the natural convection in a horizontal annulus partially filled with a porous material, some studies have highlighted the effect of the porous sleeve thickness. The unsteady natural convection in a horizontal cylindrical annulus filled partially or completely with the fluid-saturated porous medium has been studied numerically by Kumari and Nath (2006). Their results obtained that the annulus completely filled with a porous medium has the best insulating effectiveness. However, in case of annulus partially filled with a porous material, insulating the region near the outer cylinder is more effective than insulating the region near the inner cylinder. Leong and Lai (2006) analytically analyzed the natural convection in concentric cylinders with a porous sleeve. The porous layer was positioned to the inner face of the outer cylinder. It was found that the greater strength of a convective cell achieved with a thinner porous sleeve. Khanafer et al. (2008) numerically investigated the natural convection in a horizontal annulus partially filled a fluid-saturated porous medium. In their analysis the porous layer was positioned to the inner surface of the inner cylinder. They explained that Nusselt number depends mostly on the thermal conductivity ratio for a relatively thick porous sleeve. The rate of heat transfer will decrease with an increasing the porous sleeve thickness if the thermal conductivity equal to unity. The effect of the porous sleeve thickness in a long horizontal annular cylinders has been studied numerically by Ait Saada et al. (2009). They divided, the annular region is divided into two sub-regions: the outer thicker sub-region is filled with a porous material, whereas the inner one is clear.

From above survey, there are many researchers have studied the natural convection in a horizontal annular cylinder either with a full field of porous materials or with the partial field of it. All these studies were focused on the effect of porous sleeve position with a constant thickness of a porous layer. The present work will study the effect of porous layer position at a constant volume of porous materials. Hence, the thickness of the porous sleeve if fixed on the inner cylinder, will be thicker than that when positioned on the outer cylinder.

PROBLEM DEFINITION AND MATHMATICAL MODEL

Problem Definition

The physical model that used in this work is shown in Fig. 1. The model consists of a heated (T_h) inner cylinder with radius (R_i) located inside a cold (T_c) outer cylinder with radius (R_o). The aspect ratio R has been taken to be 2. The study assumed that the amount of porous material is equal to half of the annulus section.

$$A = \sqrt{\frac{3}{2} + {R_i}^2} \quad (1)$$

If porous sleeve is fixed on the inner cylinder, $t_1 = A - R_i$ (2)

If porous sleeve is fixed on the outer cylinder, $t_2 = R_o - A$ (3)

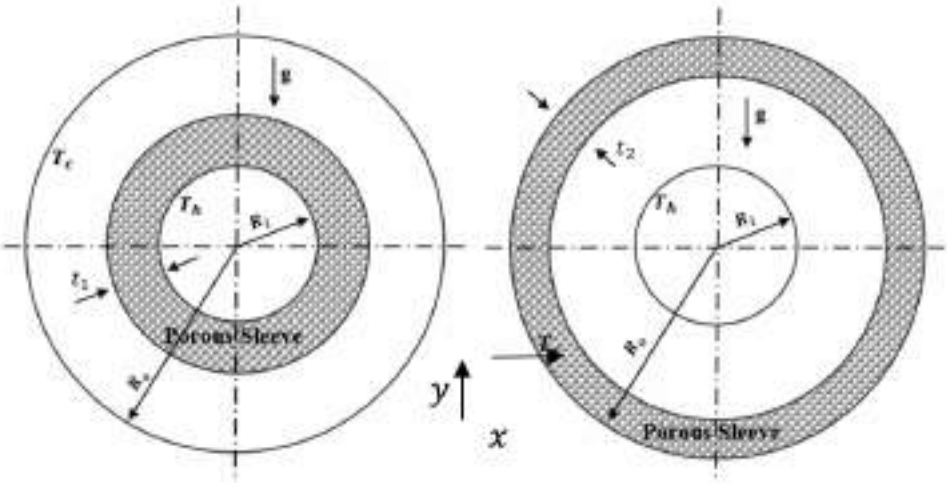

Figure 1. Schematic of the Physical Model and Coordinate System

Mathematical Model

The flow is assumed to be incompressible and laminar. All the physical properties of the fluid are assumed constant. The density variation as a function of temperature in the buoyancy term for which the Oberbeck-Boussinesq approximation is used "Bejan(2006)". As well as neglected the effect of the viscous dissipation.

$$\rho = \rho_o[1 - \beta(T - T_o)]g \quad (4)$$

Where, β is the coefficient of thermal expansion given by: (Khanafer, K. and Chamkha.,2003)

$$\beta = -\frac{1}{\rho_o}\left(\frac{\partial \rho}{\partial T}\right)_p \quad (5)$$

According to above assumptions, the dimensionless governing equations can be written as follows:

Continuity equation.

$$\frac{\partial u}{\partial x} + \frac{\partial v}{\partial y} = 0 \quad (6)$$

X - Momentum equation.

$$\frac{1}{\emptyset^2}\left[u\frac{\partial u}{\partial x} + v\frac{\partial u}{\partial y}\right] = -\frac{\partial p}{\partial x} - \frac{F}{\sqrt{Da}}\sqrt{u^2+v^2}\ u.S_p - \frac{Pr}{Da}u.S_p + \frac{Pr}{\emptyset}\left[\frac{\partial^2 u}{\partial x^2} + \frac{\partial^2 u}{\partial y^2}\right] \quad (7)$$

Y-momentum equation. Saada (2009), Mohammed and Dawood (2016).

$$\frac{1}{\emptyset^2}\left[u\frac{\partial v}{\partial x}+v\frac{\partial v}{\partial y}\right]=-\frac{\partial p}{\partial Y}-\frac{\mathrm{F}}{\sqrt{\mathrm{Da}}}\sqrt{u^2+v^2}\;v.S_p-\frac{\mathrm{Pr}}{\mathrm{Da}}v.Sp+\frac{\mathrm{Pr}}{\emptyset}\left[\frac{\partial^2 v}{\partial x^2}+\frac{\partial^2 v}{\partial y^2}\right]+\mathrm{Ra}^*\mathrm{Pr}.\theta \quad (8)$$

Energy equation.

$$u\frac{\partial\theta}{\partial x}+v\frac{\partial\theta}{\partial y}=\left[\frac{\partial^2\theta}{\partial x^2}+\frac{\partial^2\theta}{\partial y^2}\right] \quad (9)$$

Contracting the equations (7) and (8) to get the dimensionless vorticity-transport equation: Mohammed and Dawood (2016).

$$u\frac{\partial\omega}{\partial x}+v\frac{\partial\omega}{\partial y}=\frac{\mathrm{F}.\emptyset^2}{\sqrt{\mathrm{Da}}}\left[\frac{\partial|\mathrm{V}_m|}{\partial y}\;u-\frac{\partial|\mathrm{V}_m|}{\partial x}\;v\right].S_p-\frac{\emptyset^2.\mathrm{Pr}}{\mathrm{Da}}\omega.S_p-\frac{\mathrm{F}.\emptyset^2}{\sqrt{\mathrm{Da}}}|\mathrm{V}_m|\omega.S_p+\emptyset.\mathrm{Pr}\left[\frac{\partial^2\omega}{\partial x^2}+\frac{\partial^2\omega}{\partial y^2}\right]+\emptyset^2.\mathrm{Ra}^*.\mathrm{Pr}.\left(\frac{\partial\theta}{\partial x}\right) \quad (10)$$

The Dimensionless Stream function equation. (Al-Amiri 2000)

$$\omega=-\left(\frac{\partial^2\psi}{\partial x^2}+\frac{\partial^2\psi}{\partial y^2}\right) \quad (11)$$

The Forchheimer term is expressed by (Vafai, 1984)

$$\mathrm{F}=\frac{\mathrm{B}}{\sqrt{150\emptyset^3}} \quad (12)$$

Where, B is equal to 1.75, based on Ergun's (1952) experimental investigation. The Brinkman–Forchheimer–extended Darcy model turns up into the classical Navier–Stokes equation when the values of S_p and $\emptyset$ equal 0 to and 1 respectively.

The dimensionless terms and numbers were defined as follows:

$$\mathrm{Ra}=\frac{g\beta\,(T_h-T_c)\,R_i^3}{\nu\,\alpha_e},\quad \mathrm{Da}=\frac{\mathrm{K}}{R_i^2},\quad \mathrm{Pr}=\frac{\nu}{\alpha_e},\quad x=\frac{X}{R_i},\; y=\frac{Y}{R_i},\quad \theta=\frac{T-T_c}{T_h-T_c}\quad p=\frac{P}{\rho g\beta\,(T_h-T_c)\,R_i}$$

$$\mathrm{V}_m=\sqrt{u^2+v^2},\quad u=\partial\psi/\partial y,\quad v=-\partial\psi/\partial x,\quad \psi=\frac{\bar{\psi}}{\alpha_e},\quad \omega=\frac{\bar{\omega}\,.\,{R_i}^2}{\alpha_e},$$

The local Nusselt number on the surface of inner cylinder can be expressed as:

$$\mathrm{Nu}_i=-\partial\theta/\partial n \quad (13)$$

The average Nusselt number on the surface of inner cylinder is evaluated as:

$$\overline{\mathrm{Nu}}_i=\log_{10}(R)\int_0^S \mathrm{Nu}_i\,.ds \quad (14)$$

Where,

$$S=\int_0^{2\pi}\sqrt{1+(dy/dx)^2}\,.ds \quad (15)$$

Boundary Conditions

The boundary conditions for the present problem is expressed as:

Inner cylinder

$$\theta=1,\quad \psi=0,\quad \omega=-\partial^2\psi/\partial n^2$$

Outer cylinder

$$\theta=0,\quad \psi=0,\quad \omega=-\partial^2\psi/\partial n^2$$

NUMERICAL PROCEDURE

Solution Method

The governing equations (9) and (10) are solved using Alternative Direction Implicit method (ADI) based on the finite difference technique, whereas the equation (11) is solved by line successive method. The details can be found in the text by Hoffmann and Chiang (2000) and Petrovi´c and Stupar (1996). All the computational processes are based on the non-orthogonal mesh with denser lines near cylinder walls, as shown in Fig. 2. For more details about mesh and cluster function can be found in the text by Thomas and Middlecoff (1980), and Mohammed and Dawood (2016). The convergence criteria of the solution are satisfied when the residual for all dependent variables (ψ, ω, θ) get below (10^{-5}). The program code is created using Matlab software (M-file).

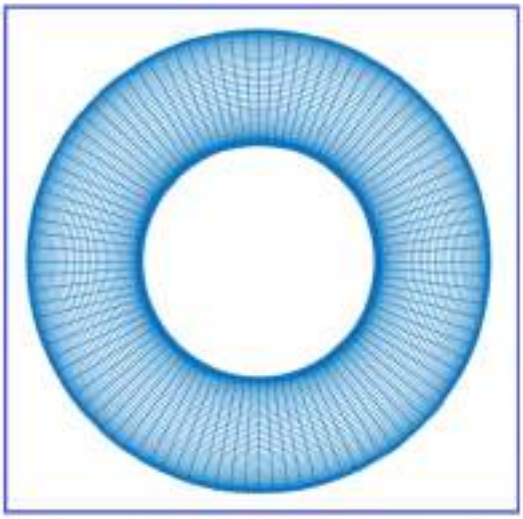

Figure 2. A Typical of Non-Orthogonal Mesh Distribution (101 x 51)

Grid Refinement

In order to guarantee grid independent solution, various mesh combinations are tested for the case of two concentric annulus filled with saturated porous materials at $\mathrm{Ra}^* = 500$, $\mathrm{Pr} = 7$, $\mathrm{Da} = 10^{-5}$ and $\emptyset = 0.9$ as shown in Table 1. It is observed that there is no significant change in the value of the average Nusselt number at a combination $(181x\ 101)$ with the improvement of the finer grid. Therefore, it is adopted in the all simulated cases.

Mesh Size	91x61	101x71	121x81	141x91	161x101	181x101	201x101
$\overline{\mathrm{Nu}}_i$	3.8356	3.8347	3.6894	3.6807	3.6738	3.6776	3.6778

Table 1. Grid Convergence Test For Various Mesh

Code Validation

The validation of the present study code is performed against numerical study of natural convection in a porous cylindrical annulus presented by Braga and de Lemos (2006) for the following operation conditions $R = 2$, $\mathrm{Da} = 3.125x10^{-7}$, $\mathrm{Pr} = 7$ and $\emptyset = 0.2$. The streamlines and Isotherms are showed excellent agreement, as demonstrated in Fig. 3.

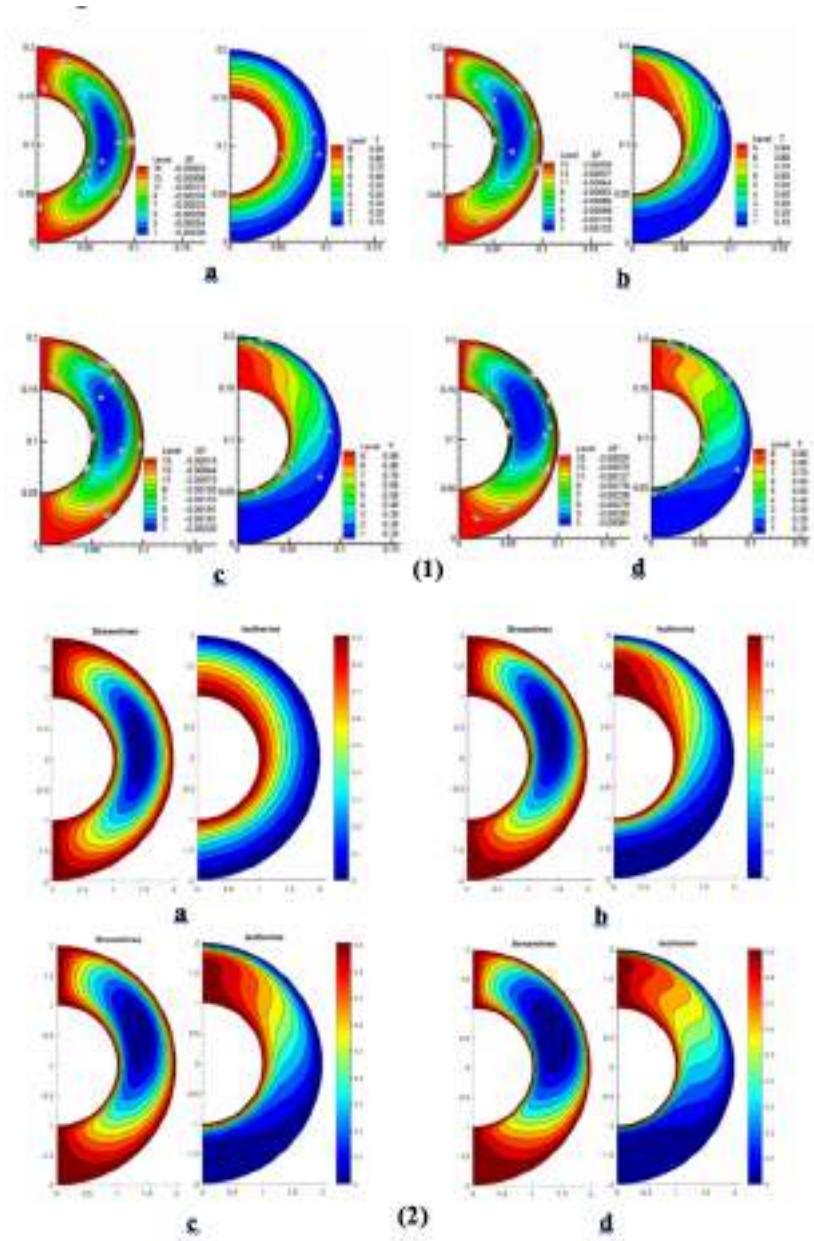

Figure 3. Comparison of The Streamlines and Isotherms for The Present Work (2) With Those of Braga and De Lemos (2006) (1), for Different Values of Rayleigh Number: (a) 25, (b) 100, (c) 200 and (d) 500.

The average Nusselt number around the inner cylinder ($\overline{\mathrm{Nu}}_i$) and the maximum value of stream function (ψ_{max}) are compared with those of Braga and de Lemos (2006), Caltagirone (1976) and Charrier-Mojtabi (1997) for the similar parameters mentioned above. The results are found to be in excellent agreement, as illustrated in Table 2.

Table 2. Comparison of Present Average Nusselt Number and Maximum Stream Function With Those of Previous Studies

Ra^*	Present Results		Caltagirone (1976)		Charrier-Mojtabi (1997)		Braga and de Lemos (2006)	
	$\overline{\mathrm{Nu}}_i$	ψ_{max}	$\overline{\mathrm{Nu}}_i$	ψ_{max}	$\overline{\mathrm{Nu}}_i$	ψ_{max}	$\overline{\mathrm{Nu}}_i$	ψ_{max}
25	1.0725	2.8985	1.0993	2.8921	-	-	1.1095	-
100	1.8246	9.9200	1.8286	9.7480	1.8670	-	1.8629	-
150	2.2623	13.3480	-	-	2.3090	-	2.3023	-
200	2.6327	16.1768	2.6256	15.8598	-	-	2.6764	-
500	4.1937	27.5734	4.1983	27.0995	-	-	4.2741	-

RESULTS AND DISCUSIONS

The present study is focused on the effect of a porous sleeve position with a constant volume of porous material on the fluid flow and heat transfer for a wide range of Rayleigh number ($25 - 500$). The Porosity, Darcy and Prandtl numbers are considered as constants and fixed at 0.9, 10^{-3} and 7 respectively. The thickness of porous sleeve when it is fixed on the inner and outer cylinder was taken as 0.58 and 0.42 respectively.

Effect of Rayleigh Number

In general, Rayleigh number reflects the influence of the temperature gradient between both two cylinders. Fig. 4 and 5 show the effect of Rayleigh number on the streamlines and isotherms when the porous sleeve is fixed on the inner and outer cylinders respectively. For a small Rayleigh number ($Ra^* < 100$), it can be seen from the streamlines contour that the flow field within the annulus is characterized by a regular eddy located near to the annulus center and the boundary layer thickness close to the surface of both cylinders is larger than other region. This is owing to the fact that the effect of the buoyancy force on the fluid motion is weak. The isotherms distributed in non-concentric circles around the inner cylinder. The thermal boundary layer at the top region is thicker than its thickness at the lower portion. In this case, the transfer of heat is dominated by conduction regime.

As Rayleigh number increases, the main eddy is driven upward to the top portion due to increasing of its rotational speed which can be seen through the maximum value of the stream function. This large eddy increased the flow motion activity at the top

portion as compared with its activity at the lower region which is considered as a stagnant region. The boundary layer thickness becomes thinner around the inner and outer cylinders. The isotherms become distorted and concentrated at the top portion of the annulus resulting an increase in the rate of heat transfer. This is attributed to dominate the buoyancy forces on the fluid motion and the convection regime on heat transfer.

The effect of Rayleigh number on the heat transfer for both two cases is illustrated in figure. 6, where average Nusselt number on the inner cylinder is presented. It can be seen a significant effect of Rayleigh number on the average heat transfer for both cases. The average Nusselt number significantly increase with increasing of Rayleigh number due to an increase of the effect of thermal convection. The effect of Rayleigh number on the rate of heat transfer is similar in both cases.

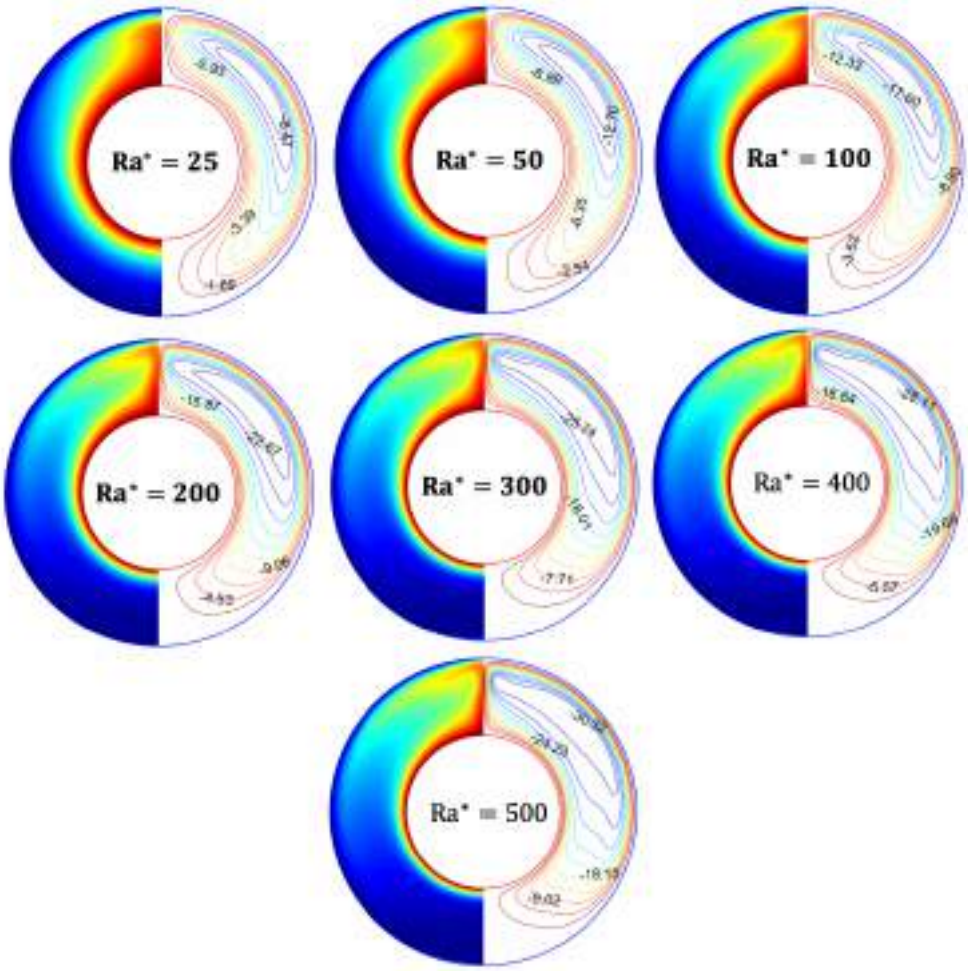

Figure 4. Streamlines (Right) and Isotherms (Left) for Different Values of Ra When The Porous Sleeve Was Fixed On the Inner Cylinder

Effect of Porous Sleeve

The effect of porous sleeve position on the streamlines and isotherms when the porous sleeve is fixed on the inner and outer cylinders can be seen in Fig. 4 and 5 respectively. For a constant volume of porous material, the thickness of the porous sleeve when fixed on the outer cylinder is smaller than that when fixed on the inner cylinder. Hence, the thickness of the air layer will be larger when the porous sleeve fixed on the outer cylinder than that thickness when the porous sleeve fixed on the inner cylinder. when the porous sleeve positioned on the inner cylinder, the velocity of fluid motion is very weak and the transfer of heat takes place by conduction. As is known, the thermal conductivity of air is smaller than that for the insulation materials at the same conditions, therefore the heat transfer by conduction will reduce according to Fourier's law when the porous sleeve fixed at the outer cylinder.

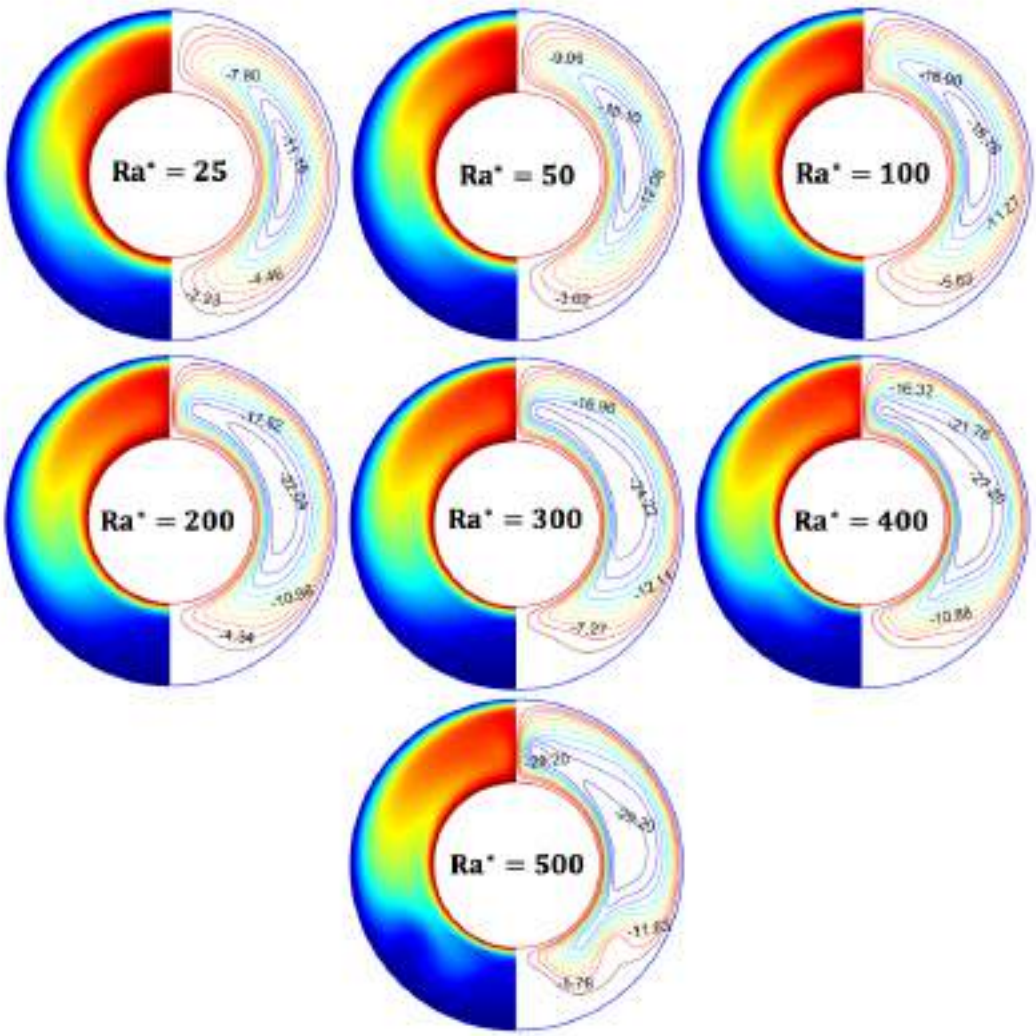

Figure 5. Streamlines (Right) and Isotherms (Left) for Different Values of Ra When The Porous Sleeve Was Fixed on The Outer Cylinder

As increases in air layer thickness, the velocity of fluid motion increase and the heat transfer is dominated by convection. This is confirmed in Fig. 6, which shows that the average heat transfer in case where the porous sleeve fixed at the outer cylinder larger than that when the porous sleeve positioned on the inner cylinder for all values of Rayleigh number. On the other hand, it can be said that fixed the porous sleeve on the surface of the inner cylinder gives better thermal insulation than that on the outer cylinder.

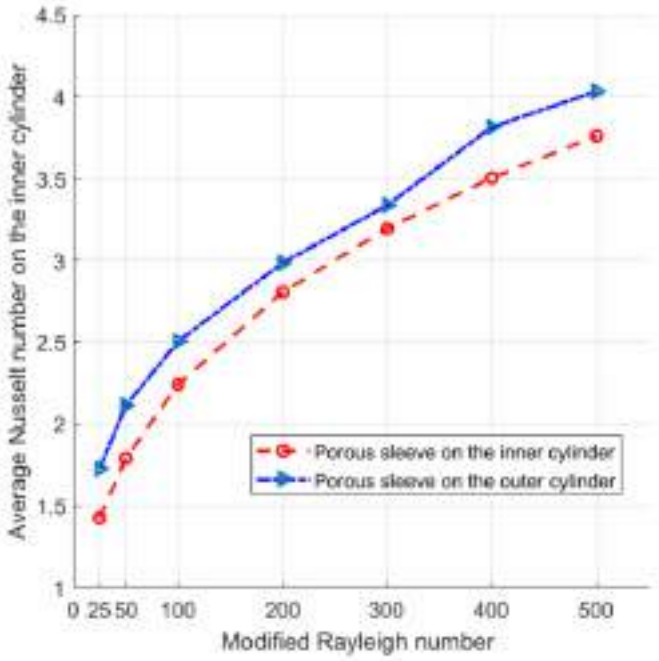

Figure 6. Average Nusselt Number at the Inner Hot Cylinder for Both Two Cases

CONCLUSION

The present study investigates the effect of porous sleeve position with a constant volume of porous material on laminar fluid flow and heat transfer in two concentric cylinders. The porous material has been fixed in two different positions, first on the outer cylinder and second on the inner cylinder. The effect of Rayleigh number on the average heat transfer along the inner hot cylinder has been studied. The results show that Rayleigh number has a significant effect on the average heat transfer for both two cases. It has been found that the maximum heat transfer was achieved when the porous sleeve was fixed on the outer cylinder. Hence, the best thermal insulation can be obtained when the porous sleeve is positioned on the surface of the inner cylinder.

Nomenclature

A	The half area of the annulus
c_p	Specific heat at constant pressure (J/kg. K)
Da	Darcy number
F	Forchheimer term
g	gravitational acceleration (m/s^2)
K	Permeability (m^2)
K	Thermal conductivity of the fluid $(W/m\,K)$
n	normal to surface
Nu	Nusselt number
p	Dimensionless pressure
P	Pressure (N/m^2)
Pr	Prandtl number
Ra	Rayleigh number
Ra^*	Modified Rayleigh number, $\mathrm{Ra}^* = \mathrm{Ra} \times \mathrm{Da}$
R	Dimensionless radial coordinate, $R = R_o/R_i$
R_i	Radius of the inner cylinder (m)
R_o	Radius of the outer cylinder (m)
S	Real length of the inner cylinder (m)
S_p	Porous factor
T	Temperature (C°)
t	Porous sleeve thickness (m)
u, v	Velocity components (m/s)
V_m	Mean velocity (m/s)
X, Y	Cartesian coordinates (m)
x, y	Dimensionless Cartesian coordinates

Greek symbols

β	Coefficient of thermal expansion(1/K)
ρ	Density (Kg/m^3)
ρ_0	Density at standard conditions (Kg/m^3)
α_e	Effective thermal diffusivity (m^2/s)
ν	Kinematic viscosity (m^2/s)
$\bar{\psi}$	Stream function (m^2/s)
ψ	Dimensionless stream function
$\bar{\omega}$	Vorticity $(1/s)$
ω	Dimensionless vorticity
Ø	Porosity
θ	Dimensionless temperature

Subscripts

h	Hot
c	Cold
i	Inlet
o	Outlet
p	pressure

REFRENCES

Khanafer, K. and Chamkha, A. J. (2003). Mixed convection within a porous heat generating horizontal annulus, *Int. J. Heat and Mass Transfer*, vol. 46, pp. 1725–1735.

Al-Amiri, A. M. (2000). Analysis of momentum and energy transfer in a lid-driven cavity filled with a porous medium, *Int. J. Heat Mass Transfer*, vol. 43, pp. 3513–3527.

Vafai, K. (1984). Convective flow and heat transfer in variable porosity media, *J. Fluid Mech.*, vol. 147, pp. 233–259.

Nield, D. A. and Bejan, A. (2006). Convection in Porous Media, 3rd ed., New York: Springer Science.

Ergun, S. (1952). Fluid flow through packed columns, Chem. Eng. Proc., vol. 48, pp. 89–94.

Hoffmann, K. A. and Chiang, S. T. (2000). Computational Fluid Dynamics I, Wichita, KS: Engineering Education System.

Thomas, P. D. and Middlecoff, J. F. (1980). Direct control of the grid point distribution in meshes generated by elliptic equation, *AIAA J.,* vol. 18, pp. 652–656.

Petrovi´c, Z. and Stupar, S. (1996). Computational Fluid Dynamics I, Belgrade: Mechanical Engineering Faculty, University of Belgrade.

Braga, E. J. and de Lemos, M. J. S. (2006). Simulation of turbulent natural convection in a porous cylindrical annulus using a macroscopic two-equation model, *Int. J. Heat and Mass Transfer,* vol. 49, pp. 4340-4351.

Caltagirone, J. P. (1976). Thermoconvective instabilities in a porous medium bounded by two concentric horizontal cylinders, *J. Fluid Mech.,* vol. 76, pp. 337–362.

Charrier-Mojtabi, M. C. (1997). Numerical simulation of two and three dimensional free convection flows in a horizontal porous annulus using a pressure and temperature formulation, *Int. J. Heat Mass Transfer*, vol. 40, pp. 1521-1533.

Mohammed, Ali, A. and Dawood, Amir, S. (2016). Mixed convection heat transfer in a ventilated enclosure with and without a saturated porous medium, *J. Porous Media*, vol. 19 (4), pp. 347-366.

Beckmann, W. (1931). Die Wärmeübertragung in zylindrischen Schichten bei naturlieher Konvektion, *Forsch. Geb. d. Ingenieurwesen*, vol.2 (5), pp.165-178.

Kraussold, H. (1934). Wärmeabgabe von zylindrischen Flüssigkeitsschichten bei natur- licher Konvektion, *Forsch. Geb. d. Ingenieurwesen*, vol. 5 (4), pp.186-191.

Kuehn, T. h. and Goldstein, R. J. (1976). An experimental and theoretical study of natural convection in the annulus between horizontal concentric cylinders, *J. Fluid Mech.*, vol.74, pp. 695-719.

Kaviany, M. (1986). Non-Darcian effect on natural convection in porous media confined between horizontal cylinders, Int. J. Heat Mass Transfer, vol.29, pp. 1513-1519.

Sakr, R. Y. and Berbish, N. S. (2012). Natural convection heat transfer in a horizontal concentric elliptic annulus containing saturated porous media, *J. Porous Media*, vol.15 (6), pp. 567-584.
Aldoss, T. K. (2009). Natural convection from a horizontal annulus filled with porous medium of variable permeability, *J. Porous Media*, vol. 12 (7), pp. 715-724.

Alloui, Z. and Vasseur, p. (2011). Natural convection in a horizontal annular porous cavity saturated by a binary mixture, *Computational Thermal Science*, vol.3 (5), pp. 407-417.

Kumari, M. and Nath, G. (2008). Unsteady natural convection from a horizontal annulus filled with a porous medium, *Int. J. Heat and Mass Transfer*, vol.51, pp. 5001-5007.

Leong, J. C. and Lai, F. C. (2006). Natural convection in a concentric annulus with a porous sleeve, *Int. J. Heat and Mass Transfer*, vol.49, pp. 3016-3027.

Khanafer, K., Al-Amiri, A. and Pop, I. (2008). Numerical analysis of natural convection heat transfer in a horizontal annulus partially filled with a fluid-saturated porous substrate, Int. J. Heat and Mass Transfer, vol. 51, pp. 1613-1627.

Ait Saada, M., Chikh, S. and Campo, A. (2009). Natural convection reduction in a composite Air/porous annular region with horizontal orientation, J. Heat Transfer, vol. 131.

EXAM SCHDULING FOR MATHMATICAL MODEL

Qayssar Al SAMMARRAIE
Gaziantep University/ Industrial Engineering
kaysariraq@gmail.com

Assoc.Prof.Dr. Eren Özceylan
Gaziantep University/ Industrial Engineering
erenozceylan@gmail.com

ABSTRACT: The educational institutions in the world are moving towards the automatic education of the educational process and these aspects are the scheduling of the exam and when there are a large number of students and classes and teachers and places in educational institutions and makes the process of scheduling manually long and boring and useless and in this paper was developed mathematical model to prepare the timetable for the final exams for the Iraqi private Emel Ninova International Schools in Turkey – Istanbul, has been implemented using the Matlab 2013 program. timetable were always difficult problems until (1976). In the appointment of examinations for different sections of the classroom.

Key words: Final Exam scheduling for Using Mathematical Model

INTRODUCTION

In view of the need for schools, universities and educational institutes to draft examination schedules within appropriate time periods without getting overlap in the dates of examinations and to ensure the completion of one exam a day and that the table covers all the lessons and all stages of study and the shortest period of time. And always get errors in the preparation of tables manually and the difficulty in preparing.

Accordingly, we recommend using the computer and applying the scientific programs to complete the task of preparing the examination schedules regardless of the number of stages of study, the number of students, the diversity of the curricula, and without any interference in performance.

This study has been prepared to prepare the final exam schedule for the Iraqi Ninawa School in Istanbul using the mathematical model and work on the matlab 2013 program. The mathematical model codes have been entered into the program and then the final table as well as the schedule and the details in subsequent chapters.

Despite the existence of these programs observed a large number of Iraqi schools and universities are preparing schedules of examinations and daily lessons by hand, which makes them fall a lot of errors and overlap in the exams and times.

Some studies have indicated the preparation of the examination tables using computer and software It has been shown that the preparation of tables depends on three basic points.

1. Time slots, during which Different examinations can be scheduled. Typically, these openings are uniform in duration Limited in number.
2. Resources: These are human and the logistics elements needed to complete the exam correctly in a manner (eg, halls, observers, etc.).
3. Scheduling Restrictions:

These are conditions that prevent concurrent scheduling Examinations. Sometimes it is not possible to schedule the exam at the time allotted is due to students who have multiple exams in at the same time, a certain number of tests the same day, or any other restrictions determined by the academic institution.

Problem Formulation

The sample in this study means the final exams for the Iraqi Nineveh school in istanbul, which consists of three stages of study and each stage of study a number of lessons. The interval was considered as time slots (sessions) Is equal to zero . which Each student takes only one exam per day and takes into account the number of observers and the number of classes. . The goal function that has been formulated reduces total The objective function that was formulated reduces the total number of classrooms and has to be conducted with the minimum amount of time allotted during the full test period .

Data and Method

The database of the Iraqi Emel Ninnova International Schools used in the model

Table 1: Lessons for primary Education

NU	Class 1	Class 2	Class 3	Class 4	Class 5	Class 6
1	Arabic	Arabic	Arabic	Arabic	Arabic	Arabic
2	Biology	Biology	Biology	Biology	Biology	Biology
3	Mathematics	Mathematics	Mathematics	Mathematics	Mathematics	Mathematics
4	Islamic religion	Islamic religion	Islamic religion	Islamic religion	Islamic religion	Islamic religion
5	English	English	English	English	English	English
				Socialism	Socialism	Socialism
6	sport	sport	sport	sport	sport	sport
7	Art	Art	Art	Art	Art	Art

Table 2: Lessons for Middle Education

NU	Class 1	Class 2	Class 3
1	Mathematics	Mathematics	Mathematics

2	Islamic religion	Islamic religion	Islamic religion
3	English	English	English
4		National	National
5	Sciences	Sciences	Biology
6	Arabic	Arabic	Arabic
7	Socialism	Geography	geography
8		History	history
9			physics
10			chemistry

Table 3: Lessons for Secondary Education

Nu	**Class 4 scientific**	**Class 4 literary**	**Class 5 scientific**	**Class 5 literary**	**Class 6 biology**	**Class 6 scientific**	**Class 6 literary**
1	Mathematics	Math	Math	Math	Math	Math	Math
2	Islamic religion	Islamic religion	Islamic religion	Islamic religion	Islamic religion	Islamic religion	Islamic religion
3	Arabic	Arabic	Arabic	Arabic	Arabic	Arabic	Arabic
4	English	English	English	English	English	English	English
5	Biology	geography	Biology	geography	chemistry	chemistry	geology
6	physics	history	physics	history	physics	physics	history
7	chemistry	philosophy	chemistry	philosophy	Biology	Biology	philosophy
8			geology	Economy			Economy

Table 4. Resources Available

constraints	**Emel Ninova International School**		
	P	M	S
Number of students for each type	63	70	52
Number of type exam	1575	1680	1300
Number rooms	16	16	16

Time exam for hours	2	3	3

METHODOLOGY

Mathematical model of the problem
Sets and parameters
Let z : departments {1,…,z}
Let j : grades {1,…,J}
Let k : exams {1,…,K}
Let g : days {1,…,G}
Let l : classrooms {1,…,L}
Let M : set for exams of grades of departments
Let Dl : capacity of classroom l
Let Czjk : number of students taking the exam k of grade j of Stages z
Let Ql : invigilator needed for classroom l
Let R : total number of invigilators
Decision Variables
ABzjkgs : 1 if the exam k of grade j of department z is assigned to session s on day g; 0 else
Azjkgsl : 1 if the exam k of grade j of department z is assigned to classroom l in session s on day g; 0 else

MATHMATICAL MODEL

$$\text{Min} \sum_{Z\in M} \sum_{j\in M} \sum_{k\in M} \sum_{g}^{G} \sum_{s}^{S} \sum_{l}^{L} A_{zjkgsl}$$

$$\sum_{s}^{S} \sum_{k\in M} A_{zjkgs} \leq 1 \quad zj\ M\ ;\ \forall g$$

$$\sum_{j\in M} \sum_{k\in M} AB_{zjkgs} \leq 1 \quad \forall\ z,g,s\ ;\ j,k\in M$$

$$\sum_{l}^{L} A_{zjkgsl}\ D_l\ C_{zjk}\ AB_{zjkgs} \quad \forall\ zjk\in M\ ;\forall gs$$

$$\sum_{Z\in M} \sum_{j\in M} \sum_{k\in M} A_{zjkgsl} \leq 1 \quad \forall g,s,l$$

$$\sum_{Z\in M} \sum_{j\in M} \sum_{k\in M} \sum_{l}^{L} (A_{zjkgsl} \times Q_l) \leq R \quad ;\forall gs$$

```
% departments
z={'Middle School','Primary Education','Secondary School'};
% grades
j={'Class 1','Class 2','Class 3','Class 4','Class 5','Class 6','Class 4 Literary','Class 4 Scientific','Class 5 Literary','Class 5 Scientific','Class 6 Biolo
% exams
k={'Arabic','Art','Biology','Chemistry','Economy','English','Geography','Geology','History','Islamic Religion','Mathematics','National','Philosophy','Physics
% days
g={1,2,3,4,5,6,7,8,9,10};
% classrooms
l={1,2,3,4,5,6,7,8,9,10,11,12,13,14,15,16};
% number of exams with thier specified classrooms
%16 classrooms  % 10 days
m=cell(16,10);
A=0;   % room flag
AB=0;  % day flag

for a=1:3 %type
for b=1:13 %classes
for e=1:17 %lessons
A=0;
for f=1:10   %days
AB=0;
for h=1:16    %classrooms
if isequal(z{a},'Primary Education')
switch j{b}
case {'Class 1','Class 2','Class 3'}
switch k{e}
case {'Arabic','Art','Biology','English','Islamic Religion','Mathematics','Sport'}
```

Figure 1. Data processing using the mathematical model and its application using the Matlab program

```
switch k{e}
case {'Arabic','Art','Biology','English','Islamic Religion','Mathematics','Sport'}
if isequal(isempty(m{h,f}),0)
if isequal(m{h,f}{1,1},z{a})&&isequal(m{h,f}{1,2},j{b})&&isequal(m{h,f}{1,4},f)
AB=1;
end
else
if AB==0&&A==0
AB=1; % day g is assigned
A=1; % classroom l is assigned
m{h,f}={z{a},j{b},k{e},g{f},l{h},AB,A};
end
end
end
case {'Class 4','Class 5','Class 6'}
switch k{e}
case {'Arabic','Art','Biology','English','Islamic Religion','Mathematics','Sport','Socialism'}
if isequal(isempty(m{h,f}),0)
if isequal(m{h,f}{1,1},z{a})&&isequal(m{h,f}{1,2},j{b})&&isequal(m{h,f}{1,4},f)
AB=1;
end
else
if AB==0&&A==0
AB=1; A=1;
m{h,f}={z{a},j{b},k{e},g{f},l{h},AB,A};
end
end
end
end
```

Figure 2. Data processing using the mathematical model and its application using the Matlab program

Table 4. Final Exam scheduling for primary Education class 1and2

Department	Class	Day	lesson	Room
Primary Education	1	1	Arabic	4
		2	Art	4
		3	Biology	4

		4	English	4
		5	Islamic	4
		6	Mathematic	4
		7	Sport	4
Primary Education	2	1	Arabic	5
		2	Art	5
		3	Biology	5
		4	English	5
		5	Islamic	5
		6	Mathematic	5
		7	Sport	5

Table 4.1 Final Exam scheduling for primary Education class 3 and 4

Department	Class	Day	lesson	Room
Primary Education	3	1	Arabic	6
		2	Art	6
		3	Biology	6
		4	English	6
		5	Islamic	6
		6	Mathematic	6
		7	Sport	6
Primary Education	4	1	Arabic	7
		2	Art	7
		3	Biology	7
		4	English	7
		5	Islamic	7
		6	Mathematic	7
		7	Sport	7

Table4.2Final Exam scheduling for primary Education class 5and6

Department	Class	Day	lesson	Room
Primary Education	5	1	Arabic	8
		2	Art	8
		3	Biology	8
		4	English	8
		5	Islamic	8
		6	Mathematic	8
		7	socialism	8
		8	Sport	8
Primary Education	6	1	Arabic	9

		2	Art	9
		3	Biology	9
		4	English	9
		5	Islamic	9
		6	Mathematic	9
		7	socialism	9
		8	Sport	9

Table 5. Final Exam scheduling for Middle Education class 1,2 and 3

Department	Class	Day	lesson	Room
Middle Education	1	1	Arabic	1
		2	English	1
		3	Islamic	1
		4	Mathematic	1
		5	Sciences	1
		6	socialism	1
Middle Education	2	1	Arabic	2
		2	English	2
		3	geography	2
		4	History	2
		5	Islamic	2
		6	Mathematic	2
		7	National	2
		8	Sciences	2
Middle Education	3	1	Arabic	3
		2	Biology	3
		3	chemistry	3
		4	English	3
		5	geography	3
		6	History	3
		7	Islamic	3
		8	Mathematic	3
		9	National	3

Table.6 Final Exam scheduling for Secondary Education class4

Department	Class	Day	lesson	Room
Secondary Education literary	4	1	Arabic	10
		2	English	10
		3	geography	10

		4	History	10
		5	Islamic	10
		6	Mathematic	10
		7	Philosophy	10
Secondary Education Sciences	4	1	Arabic	11
		2	Biology	11
		3	chemistry	11
		4	English	11
		5	Islamic	11
		6	Mathematic	11
		7	Physics	11

Table. 6.1 Final Exam scheduling for Secondary Education class5

Department	Class	Day	lesson	Room
Secondary Education literary	5	1	Arabic	12
		2	Economy	12
		3	English	12
		4	Geography	12
		5	History	12
		6	Islamic	12
		7	Mathematic	12
		8	Philosophy	12
Secondary Education sciences	5	1	Arabic	13
		2	Biology	13
		3	Chemistry	13
		4	English	13
		5	Geology	13
		6	Islamic	13
		7	Mathematic	13
		8	physics	13

Table. 6.2 Final Exam scheduling for Secondary Education class6

Department	class	Day	Lesson	Room

Biology Education	6	1	Arabic	14
		2	Biology	14
		3	Chemistry	14
		4	English	14
		5	Islamic	14
		6	Mathematic	14
		7	Physics	14
Secondary Education literary	6	1	Arabic	15
		2	Economy	15
		3	English	15
		4	Geography	15
		5	History	15
		6	Islamic	15
		7	Mathematic	15
		8	Philosophy	15
Secondary Education sciences	6	1	Arabic	16
		2	Biology	16
		3	Chemistry	16
		4	English	16
		5	Islamic	16
		6	Mathematic	16
		7	Physics	16

Function Name	Calls	Total Time	Self Time*	Total Time Plot (dark band = self time)
Exam_Scheduling_Final	1	1.133 s	0.991 s	
uitable	1	0.126 s	0.016 s	
arrayviewfunc	2	0.110 s	0.000 s	
arrayviewfunc>createCellArrayValue	1	0.110 s	0.000 s	
arrayviewfunc>reportValuesCallback	1	0.110 s	0.000 s	
arrayviewfunc>reportValues	160	0.094 s	0.000 s	
arrayviewfunc>reportValuesLogic	161	0.047 s	0.031 s	
...orka.mlmdgeta.array.ValueDataSection (Java method)	322	0.031 s	0.031 s	
strcat	121	0.016 s	0.016 s	
workspacefunc	122	0.016 s	0.016 s	
arrayviewfunc>getMLArrayRefClass	161	0.016 s	0.016 s	
codetools\private\dataviewerhelper	161	0.015 s	0.000 s	
...tenviewerhelper>isUnsignedIntegralType	161	0.015 s	0.015 s	
blanks	121	0 s	0.000 s	
uitools\private\uiewOdialog	1	0 s	0.000 s	
cell.strmatch	7	0 s	0.000 s	
iscellstr	175	0 s	0.000 s	
strmatch	7	0 s	0.000 s	
uitools\private\uitable_parseold	1	0 s	0.000 s	

Figure 3. Total Time For Exams

...pace.MatlabWorkspaceListener.swl(swl)	1	0 s	0.000 s	
workspacefunc>getCleanupHandler	1	0 s	0.000 s	
onCleanup>onCleanup.onCleanup	2	0 s	0.000 s	
...s.mlservices.WorkspaceVariableAdaptor (Java method)	2	0 s	0.000 s	
...pace.MatlabWorkspaceListener.swl(swl)	1	0 s	0.000 s	
workspacefunc>getWorkspace	1	0 s	0.000 s	
workspacefunc>getWorkspaceID	1	0 s	0.000 s	
onCleanup>onCleanup.delete	2	0 s	0.000 s	
...pace.MatlabWorkspaceListener.swl(swl)	1	0 s	0.000 s	
...pace.MatlabWorkspaceListener.swl(swl)	1	0 s	0.000 s	
workspacefunc>getShortValueObjectJ	121	0 s	0.000 s	
java.lang.String (Java method)	242	0 s	0.000 s	
arrayviewfunc>getBaseVariableName	1	0 s	0.000 s	
arrayviewfunc>getIndicesOfIndexingChars	1	0 s	0.000 s	
codetools\private\dataviewerhelper	161	0 s	0.000 s	
...taviewerhelper>isUnsignedIntegralType	161	0 s	0.000 s	
...athworks.mlservices.WorkspaceVariable (Java method)	161	0 s	0.000 s	
...orks.mlwidgets.array.ValueDataSection (Java method)	322	0 s	0.000 s	
arrayviewfunc>getAttributes	1	0 s	0.000 s	
...thworks.mlwidgets.array.ValueMetaInfo (Java method)	1	0 s	0.000 s	

Figure 4. Total Time For Exams

CONCLUSIONS

The purpose of this study is to use the mathematical model in solving the problems of timetables and timetables for the final exams, and we have not noticed their use at all in Iraqi schools, and note that it is best to use programs to avoid errors and difficulties faced by school administrations in determining the examination schedules. And reduce the time required to perform examinations according to the schedule.

RECOMMENDATIONS

Through the accuracy of our findings, we recommend using the specialized programs and programs in the scheduling area to avoid errors and shortening periods of time as short as possible.

REFERENCES

Al-Qahtani, A. S. (2017). Exam Scheduling. Jordan University of Science and Tech P.O, Jordan : Ali Shatnawi and Mohammad Fraiwan and Hadi S. Al-Qahtan.

Burke E.K., E. D. (1996). Examination timetabling in British. Springer,Berlin,: Mehmet Sevkli1 , Ozgur Uysal2 and Mustafa Sari3.

Burke, Q. a. (2005). Hybrid Variable Neighborhood HyperHeuristics for Exam. Vienna,: Mehmet Sevkli1 , Ozgur Uysal2 and Mustafa Sari3.

Christelle G., P. S. (2000). Applications of optimization with Xpress-MP. Paris,: Mehmet Sevkli1 , Ozgur Uysal2 and Mustafa Sari3.

S., B. E. (2002). Recent research directions in automated timetabling. Eur J Oper Res: Mehmet Sevkli1 , Ozgur Uysal2 and Mustafa Sari3.

UTILIZATION OF MANDARIN AND ORANGE ALBEDOS IN CAKE PRODUCTION

Mustafa Kürşat DEMİR
Necmettin Erbakan University, Faculty of Engineering and Architecture, Department of Food Engineering, Konya, Turkey
mkdemir@konya.edu.tr

Halef DİZLEK
Osmaniye Korkut Ata University, Faculty of Engineering, Department of Food Engineering, Osmaniye, Turkey
hdizlek@osmaniye.edu.tr

ABSTRACT: The citrus peels are by-product of food industry that has functional properties. These by-products used mainly for animal feed contains valuable nutrients. Citrus peels consist of two layers, namely, flavedo and albedo. Citrus albedo contains higher quality dietary fibres than cereal fibres. Dietary fibers are a layer of this shell that is used in most food products with the emergence of positive effects on human health. In this study, mandarin and orange albedos were used in cake formulation at different levels (0, 5 and 10 % w/w). As parameters, the physical (crust color, crumb color and firmness), chemical (ash, crude protein, crude fiber and mineral content [Ca, Mg, K, Fe and Zn]) and sensory properties of cake samples were determined. As a results, crumb and crust L^* (brightness) values decreased, a^*(redness) and b^* (yellowness) values increased with albedo addition. The ash and crude fiber contents of the cake increased with increasing amount of citrus albedos. Also, Ca, Mg, K, Fe and Zn contents increased at different degrees with albedo addition. Albedo addition affected overall acceptability of cake samples significantly. As a result, the use of citrus albedo in the production of cake has been found suitable for the improvement of sensorial and chemical properties.

Key words: Citrus, cake, dietary fiber, mineral, by-product.

PORTAKAL VE MANDALİNA ALBEDOLARIN KEK ÜRETİMİNDE KULLANIMI

ÖZET: Fonksiyonel özelliği sahip olan turunçgil kabukları, gıda endüstrisinin önemli yan ürünlerindendir. Genellikle bu yan ürünler, besinsel değeri yüksek hayvan yemi olarak değerlendirilmektedir. Turunçgil kabukları; albedo ve flavedo olarak isimlendirilen 2 tabakadan oluşmaktadır. Tahıl liflerine göre daha yüksek ve kaliteli diyet lifi içeriğine sahip olan albedo tabakaları, diyet lifinin insan sağlığa olumlu etkileri nedeniyle, birçok gıda ürününde kullanılmaya başlanmıştır. Bu çalışmada ise; portakal ve mandalinadan elde edilen albedolar, farklı oranlarda (%0, 5 ve 10) kek üretiminde kullanılmıştır. Üretilen keklerde de; fiziksel (kabuk rengi, iç rengi ve sertlik), kimyasal (kül, ham protein, ham lif ve mineral içeriği [Ca, Mg, K, Fe ve Zn] ve duyusal özellikler parametre olarak incelenmiştir. Sonuç olarak; kek örneklerinde albedo oranının artması ile kabuk ve iç rengi L^* (parlaklık) değerlerinin azaldığı, a^* (kırmızılık) ve b^* (sarılık) değerlerinin arttığı belirlenmiştir. Ayrıca, turunçgil albedo

miktarındaki artışlara bağlı olarak, kek örneklerinin kül ve ham lif miktarları ile Ca, Mg, K, Fe ve Zn mineral içerikleri de artış göstermiştir. Duyusal özellikleri açısından değerlendirildiğinde ise, albedo ikamesi genel kabul edilebilirlik değerleri üzerinde önemli etkide bulunmuştur. Sonuç olarakta; turunçgil albedolarının kek üretiminde kullanımı, gerek duyusal, gerek kimyasal özelliklerinin geliştirilmesi bakımından uygun bulunmuştur.
Anahtar sözcükler: Turunçgil, kek, diyet lifi, mineral, yan ürün.

GİRİŞ

Geçmiş yıllarda besin değeri olmadığı ve posa olarak adlandırılan diyet lif bileşiklerinin günümüzde sağlık üzerindeki olumlu etkileri ile teknolojik ve fiziksel özelliklerinin belirlenmesi sonucunda, gerek bu bileşiklere gerekse bu bileşiklerce zengin gıdalara olan ilgi artmıştır. Birçok gıdada lifçe zengin ürünlerin "fonksiyonel katkı" olarak katılması gündeme gelmiş ve bu amaçla da daha çok buğday, yulaf, arpa ve pirinç gibi tahılların kepekleri kullanılmıştır. Ancak buğday kepeği başta olmak üzere tahıl kepeklerinde fazla miktarda bulunan fitik asidin bazı mineraller ve proteinler ile olan interaksiyonu ve ayrıca kepeğin ürün kalitesi ve duyusal özelliklerindeki olası olumsuz etkileri başka lif kaynaklarının kullanım olanaklarının araştırılmasını gündeme getirmiştir (Türksoy, 2011; Demirel ve Demir, 2018). Sebze lif konsantrelerinin diyet lif içeriği bakımından daha zengin oldukları ve katıldıkları oranlara bağlı olarak bisküvileri bu değerler bakımından önemli derecede zenginleştirdikleri görülmüştür (Türksoy, 2011).

Türkiye'de turunçgillerin ticari olarak üretimi yapılan çeşitleri limon, portakal, mandalina ve greyfurttur. Turunçgiller, kabuklarının büyük bölümünü oluşturan albedo tabakasında mevcut bitkisel lif yoğunluğu ile bu amaçla kullanılabilecek önemli bir kaynak olarak görülmüşlerdir (Çoksever, 2009). Albedo denilen beyaz kısım ticari pektin üretiminde en yaygın olarak kullanılan hammaddelerden biridir (Koubala ve ark., 2008; Schiewer ve Patil, 2008). Türkiye'de 2015 yılında 1.816.798 ton portakal üretilmiş olup, portakal suyu üretim tesislerinde yaklaşık 760.000 ton atık portakal kabuğu oluştuğu tahmin edilmektedir. Oluşan atık portakal kabuklarının bir bölümünün hayvan yemi olarak kullanıldığı, bir kısmının kurutularak değerlendirildiği ve geri kalan kısmının ise kentsel katı atık depolama tesislerine götürüldüğü saptanmıştır. Bu durum özellikle narenciye üretimi yapılan yerleşim yerlerindeki belediyeler için önemli bir sorun oluşturmaktadır (Günkaya ve ark., 2016). Bu açıdan atık turunçgil kabuklarının gıda sektöründe kullanılması ve değerlendirilmesi ülkemiz için önemlidir.

Turunçgil kabukları; albedo ve flavedo adı verilen iki tabakadan oluşur. Flavedo, en dıştaki, renkli olan sarıdan turuncuya kadar değişen dış tabakadır. Bu katmanda karotenoid pigmentleri ile içerisinde uçucu yağ maddelerini üreten bezelerin bulunduğu lipit/yağ hücreleri bulunmaktadır. Flavedonun alt kısmında; bir devam tabakası olarak, beyaz/krem renkte, daha kalın keçeye benzeyen bir katman olan albedo bulunmakta olup, gevşek bir yapıda iri hücrelerden oluşmaktadır. Bu kısımda meyveye su ve besin maddelerini ileten damarlar yer almaktadır (Çoksever, 2009). Ayrıca albedo diğer bitkisel lif kaynaklarından daha yüksek kaliteye sahiptir. Bunun sebebi antioksidan özellikteki birleşik biyoaktif bileşenlerinin (flavonoidler ve C

vitamini) sağlık açısından düzenleyici etkilerinin bulunmasıdır. Albedo çok miktarda pektin ve hisperidin içeren büyük hücreler arası boşluklar ile yumuşak dokudan oluşur. Meyve gelişiminin ilk zamanlarında turunç meyvelerinin beyaz kısmı olan albedo, meyvenin su idaresi açısından önemlidir. Albedo ağırlığının %21'ini hücre duvarları oluşturmaktadır. Albedo tabakası meyvenin ilk oluşmaya başlamasından itibaren meyve ve yapraklar arasında suyun iletiminde görev alır. Olgunlaşma sonrasında ise suyu rezerve edici olarak görev yapar. Bileşenlerinin özellikleri albedonun nasıl izole edildiğiyle ilgili olarak değişiklik gösterir. Turunçgil kabuğunda %30-35 oranında bulunan pektinin %73'ü albedo tabakasında mevcuttur (Sinclair, 1984; Schröder ve ark., 2004; Çoksever, 2009; Demirel ve Demir, 2018).

Bu çalışmada da, tahıl bazlı gıdalarımızdan olan kek ürünü hedef alınmış, daha kaliteli ve yüksek besin değerine sahip yeni son ürünlerin üretilmesi amaçlanmıştır.

MATERYAL VE YÖNTEM

Materyal

Kek üretimde kullanılacak olan buğday un, Hekimoğlu un fabrikasından (Konya, Türkiye)'den temin edilmiştir. Kek formulasyonunda yer alan diğer bileşenler ise piyasasından satın alınmıştır. Ayrıca bileşimine ilave edilen turunçgil albedoları ise Konya piyasasından temin edilen turunçgillerden elde edilmiştir.

Yöntem

Deneme planı

Denemede 2 farklı turunçgilden (portakal ve mandalina) elde edilen albedolar, kek üretiminde buğday ununa, 3 farklı oranda (%0, 5 ve 10) ikame edilerek kullanılmıştır. Denemelerde (2 x 3) x 2 faktöriyel deneme desenine göre yürütülmüştür.

Albedoların üretimi

Denemelerde kullanılan portakal ve mandalinalardaki meyve kabukları (flavedo tabakası) bıçak yardımıyla ayrılmış ve albedo tabakası alınmıştır. Daha sonra bu albedo tabakaları, kurumanın kolaylaştırılması için bıçak yardımıyla küçük parçalara ayrılarak, 80 °C'de bir kurutma kabininde (Nüve KD-200, Ankara, Türkiye) kurutulmuştur. Kuruyan bu albedo tabakaları, laboratuvar tipi bir öğütücü (Trisa Coffee Mill, Tokyo, Japonya) yardımıyla öğütülmüştür.

Kek üretimi

Kek hamurları, Levent ve Bilgiçli (2013)'e göre hazırlanmıştır. Kek hamuru formülasyonunda; 100 g buğday unu, 75 g shortening, 75 g şeker, 75 g yumurta, 10 g mısır nişastası, 5 g yağsız süt tozu, 0.5 g tuz, 4.5 g kabartma tozu ve 0.5 g SSL kullanılmıştır. Öncelikle; yumurta ve şeker krema görüntüsü alıncaya kadar karıştırılmış, karışımın üzerine shortening ilave edilerek homojen bir yapı

sağlanıncaya kadar işleme devam edilmiştir. Sonra 30 ml su ile birlikte, diğer tüm bileşenler eklenip homojen bir kek hamuru elde edilmiştir. Kek hamurları mini fırında (LG MP-9485S, Seoul, Kore) 160˚C sıcaklıkta 50 d süreyle pişirilmiştir. Soğutulduktan sonra da, tüm kek örnekleri kilitli polietilen ambalajda muhafaza edilmiştir.

Hammadde ve kek analizleri

Renk okumaları *L**, *a** ve *b** değerleri cinsinden Hunter Lab Color Quest II Minolta CR-400 (Konica Minolta Sensing, Inc., Osaka, Japan) cihazı kullanılarak *L** değeri [(0) siyah-(100) beyaz], *a** değeri [(+) kırmızı- (-) yeşil] ve *b** değeri [(+) sarı-(-) mavi] cinsinden ölçülmüştür (Francis, 1998). Tekstür ölçümleri ise, tekstür analiz cihazı (TA-XT, Stable Micro Systems Ltd., Surrey, UK) kullanılarak gerçekleştirilmiştir (AACC, 1990). Ayrıca; su miktarı tayininde 135°C'de 2.5 s kurutma normuyla (AACC 44-19) yapılmıştır. Ham protein tayini; Kjeldahl yöntemiyle, protein miktarları kuru madde esasına göre, AACC 46–12'ye göre yapılmıştır (AACC, 1990). Kül tayini AACC 08-01, ham lif miktarı ise AACC 32-10 metoduyla belirlenmiştir (AACC, 1990). Toplam mineral madde içeriği belirlenirken, 0.5 g örnekler, 10 mL HNO_3+H_2SO_4 kullanılarak mikrodalga (Mars 5, CEM Corporation, USA) yaş yakma metoduyla yakılarak elde edilen süzüklerde mineral madde içerikleri ICP-AES (Inductively coupled plasma-atomic emission spectrometry) cihazında (Vista Series, Varian International, AG, İsviçre) tayin edilmiştir (Skujins, 1998). Pişirilen kek örneklerinin duyusal değerlendirmesinde ise; Necmettin Erbakan Üniversitesi Gıda Mühendisliği Bölümü öğretim elemanları ve lisansüstü öğrencilerinden oluşturulan, yaşları 21-35 arasında değişen ve konu ile ilgili kısa bir eğitime tabi tutulan 10 kişilik panelist grubu tarafından gerçekleştirilmiştir. Kek örnekleri; tat, renk, koku, görünüş ve genel beğeni özellikleri bakımından 5'lik hedonik skala ile değerlendirilmiştir (5 Puan: Çok iyi, 4 Puan: İyi, 3 Puan: Kabul edilebilir, 2 Puan: Yeterli değil, 1 Puan: Kötü).

İstatistiki analizler

Araştırma sonunda elde edilen veriler varyans analizine tabi tutularak, farklılıkları istatistiki olarak önemli bulunan ana varyasyon kaynaklarının ortalamaları ise Duncan çoklu karşılaştırma testi ile karşılaştırılmıştır (Düzgüneş ve ark., 1987).

BULGULAR

Kek üretiminde kullanılan portakal ve mandalina turunçgil albedolarının analitik analiz sonuçları Tablo 1'de verilmiştir. Tablo 1'e göre; turunçgil albedolarının özellikle ham lif içeriğinin yüksek miktarda oldukları açıkça görülmektedir. Ayrıca mineral içeriğini bakımından da tahıl unlarına nazaran daha zengin bir nitelikte oldukları görülmektedir.

Tablo 1. Portakal ve Mandalina Albedolarının Kimyasal ve Fiziksel Özellikleri

Özellikler	Portakal Albedo	Mandalina Albedo
Su (%)	7.39±0.23	7.97±0.26
Ham protein (%)	3.96±0.09	3.81±0.06
Kül (%)	2.70±0.05	2.87±0.16

Ham lif (%)		23.23±0.31	23.14±0.71
Renk	*L**	85.00±4.07	81.72±0.17
	*a**	-0.58±0.11	-0.71±0.02
	*b**	28.39±0.39	30.52±0.11
Mineral madde (mg/100g)	Ca	287.13±21.37	248.66±10.09
	K	653.24±31.41	634.12±15.56
	Mg	74.92±3.58	68.47±2.69
	Fe	8.55±0.27	7.57±0.17
	Zn	3.44±0.04	2.59±0.28

Üretilen kek örneklerinin kabuk ve iç rengi özelliklerine ait Duncan çoklu karşılaştırma testi sonuçları Tablo 2'de sunulmuştur. Tablo 2'ye göre; kontrol grubu örnekler, hem kabuk hem de iç renkte en yüksek parlaklık (*L**) değerlerini vermiştir. Albedo ikamesi ve bu ikamede de artışlara gidilmesi, renk parlaklık değerlerini önemli düzeyde ($P < 0.05$) azaltmıştır. Ayrıca ikameye bağlı olarak; kabuk ve iç renk değerleri yine önemli ölçüde değişime uğramıştır. Albedo ikameleri ile kabuk renginin daha kırmızı ve sarı renkli bir hal aldığı, iç renk *b** (sarılık) değerlerinin de bariz bir şekilde arttığı tespit edilmiştir. Demirel ve Demir (2018)'de yapmış olduğu bir başka çalışmasında; albedo ikamesi ile bisküvilerini *L** değerlerinin azaldığını, *a** değerlerinin ise arttığı tespit etmiştir. Sonuç olarak son ürünlerin, daha koyu renkli olduğu belirlenmiştir. Bunda da albedoların lif içeriğine yüksek olması etkili olmuştur. Yüksek lif içeren yapılarda; gerek renk verici bileşenlerin varlığı, gerekse fenolik ve karotenoid bileşenlerin miktarına bağlı olarak esmerleşme reaksiyonlarının artığı bilinmektedir (Can, 2015; Demirel ve Demir, 2018).

Tablo 2. Keklerin Renk Özellikleri Üzerine Turunçgil Albedoların Etkisi[1]

Albeo Tipi	Oran (%)	İç Rengi			Kabuk Rengi		
		*L**	*a**	*b**	*L**	*a**	*b**
Mandalina	0	72.36[a]	-2.44[c]	25.17[c]	54.28[a]	14.74[c]	23.37[c]
	5	70.18[b]	-1.55[b]	29.61[b]	51.36[b]	15.81[b]	25.12[b]
	10	67.41[c]	-0.36[a]	34.57[a]	48.69[c]	17.36[a]	26.91[a]
Portakal	0	72.45[a]	-2.40[c]	25.03[c]	54.39[a]	14.25[c]	23.14[c]
	5	70.68[b]	-1.46[b]	29.07[b]	50.68[b]	15.80[b]	24.68[b]
	10	68.06[c]	-0.24[a]	33.89[a]	47.39[c]	17.22[a]	26.47[a]

[1]Aynı sütunda farklı harf taşıyan ortalamalar birbirinden farklı (P <0.05), aynı harf taşıyan ortalamalar farksızdır (P >0.05).

Üretilen kek örneklerinin bazı fiziksel ve kimyasal özelliklerine ait Duncan çoklu karşılaştırma testi sonuçları ise Tablo 3'de sunulmuştur. Tablo 3'e göre; kontrol grubu kek örneklerinin kül, ham lif ve sertlik değerlerinin daha düşük olduğu, albedo ikamesi ile bu değerlerde istatistik olarak önemli düzeyde ($P < 0.05$) artışların gerçekleştiği belirlenmiştir. Ham protein ise ikame oranına bağlı olarak azaldığı tespit edilmiştir. Bu artış ve azalmaların muhtemel sebebi, albedoların kimyasal bileşimi ile ilgilidir. Tablo 1'e bakıldığında; özellikle albedo ham lif içeriklerinin %23 civarında olması, son ürünlere de yansımıştır. Yüksek lif içeriği ve ikameye bağlı olarak, nişasta seyrelmesi gerçekleşmiş, su tutma kapasitesi etkilenmiş ve daha sert yapıda son ürünler elde edilmiştir.

Tablo 3. Keklerin Bazı Fiziksel ve Kimyasal Özellikleri Üzerine Turunçgil Albedoların Etkisi[1]

Albeo Tipi	Oran (%)	Kül (%)	Ham Protein (%)	Ham Lif (%)	Sertlik (g)
Mandalina	0	1.41[c]	5.86[a]	4.13[c]	1278[c]
	5	1.52[b]	5.52[b]	5.26[b]	1453[b]
	10	1.63[a]	5.12[c]	6.27[a]	1562[a]
Portakal	0	1.40[c]	5.83[a]	4.12[c]	1274[c]
	5	1.50[b]	5.55[b]	5.29[b]	1461[b]
	10	1.61[a]	5.17[c]	6.31[a]	1549[a]

[1]Aynı sütunda farklı harf taşıyan ortalamalar birbirinden farklı (P <0.05), aynı harf taşıyan ortalamalar farksızdır (P >0.05).

Üretilen kek örneklerinin mineral madde içeriklerine ait Duncan çoklu karşılaştırma testi sonuçları ise Tablo 4'te sunulmuştur. Tablo 4'ye göre; albedo ikamesiyle keklerin mineral madde içeriklerinin arttığı tespit edilmiştir. Kontrol grubuna göre, %10 albedo ikameli kek örneklerinde ortalama Ca miktarı 1.78, K miktarı 1.36, Mg miktarı 1.50, Fe miktarı 1.92, Zn miktarı ise 1.55 kat artış göstermiştir. Demirel ve Demir (2018) turunçgil albedolarının buğday ununa göre oldukça yüksek mineral madde ve kül içeriğine sahip olduğunu bildirmiştir. Bu sonuçlarda bizim sonuçlarını destekler niteliktedir.

Tablo 4. Keklerin Mineral Madde İçerikleri Üzerine Turunçgil Albedoların Etkisi[1]

Albeo Tipi	Oran (%)	Mineral madde (mg/100g)				
		Ca	K	Mg	Fe	Zn
Mandalina	0	30.15[c]	136.48[c]	6.89[c]	0.76[c]	0.46[c]
	5	42.61[b]	159.62[b]	8.50[b]	1.10[b]	0.57[b]
	10	53.09[a]	185.46[a]	10.08[a]	1.45[a]	0.70[a]
Portakal	0	30.88[c]	136.40[c]	6.72[c]	0.77[c]	0.46[c]
	5	43.47[b]	161.21[b]	8.63[b]	1.15[b]	0.59[b]
	10	55.83[a]	187.64[a]	10.37[a]	1.49[a]	0.73[a]

[1]Aynı sütunda farklı harf taşıyan ortalamalar birbirinden farklı (P <0.05), aynı harf taşıyan ortalamalar farksızdır (P >0.05).

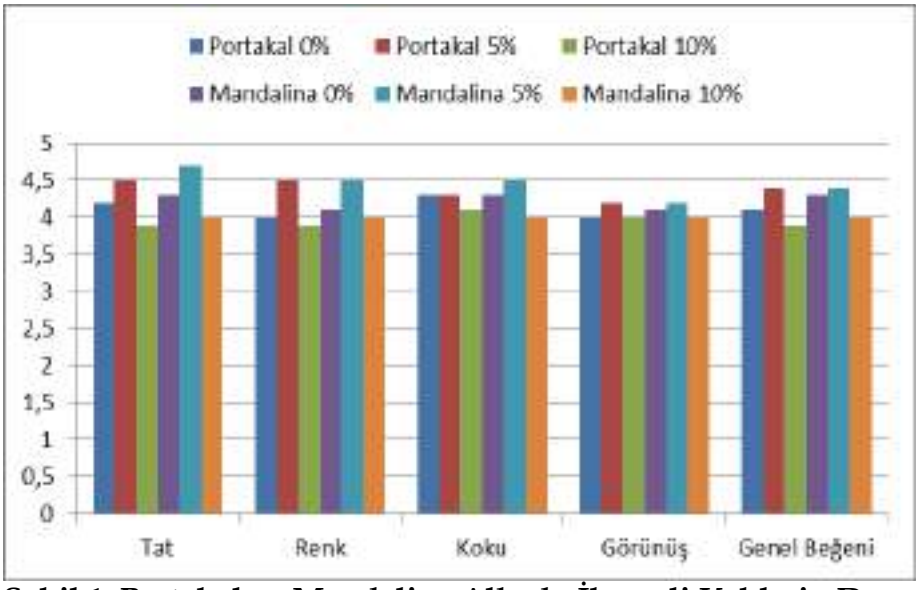

Şekil 1. Portakal ve Mandalina Albedo İkameli Keklerin Duyusal Özellikleri

Üretilen kek örneklerinin duyusal değerlendirme özelliklerine ait veriler Şekil 1'de özetlenmiştir. Şekil 1 incelendiğinde; kontrol grubu örneklere göre, %5 albedo ikameli keklerin daha çok beğenildiği, daha çok duyusal değerlendirme puanları aldıkları tespit edilmiştir. %5'in üzerinde ikame yapıldığında ise, aynı puanlama değerlerinin azaldığı belirlenmiştir. Portakal ve mandalina albedoların arasında ise, duyusal değerlendirme bakımından önemli bir farklılık gözlenmemiştir.

SONUÇ VE ÖNERİLER

Bu çalışmada; lif ve mineral maddelerce zenginliği ispatlanan portakal ve mandalina albedolarının kek üretiminde kullanılması ve son ürün kalitesi üzerine etkileri incelenmiştir. Elde edilen sonuçlara göre; kek üretiminde albedo ikamesinin kül, ham lif ve mineral madde içeriğini önemli ölçüde arttırdığı, son ürünlerin besinsel açıdan daha nitelikli hale geldiği, duyusal özellikleri geliştirmesi açısından da %5'e kadar kullanımının uygun olduğu tespit edilmiştir. Bu çalışmanın verileri ışığında; besinsel açıdan önemi ispatlanan ve turunçgil sanayinin yan ürünü niteliğindeki albedoların, tahıl ürünleri başta olmak üzere, birçok gıdada lif kaynağı olarak kullanılabileceği belirlenmiştir.

KAYNAKLAR

AACC (1990). American Association of Cereal Chemists, Approved Methods of the AACC. 8th Edition, Saint Paul, Minnesota, USA.

Can, F. (2015). Portakal kabuğu tozunun bisküvi hamuru ve bisküvi kalitesi üzerine etkilerinin incelenmesi. İnönü Üniversitesi Fen Bilimleri Enstitüsü Gıda Mühendisliği Anabilim Dalı Yüksek Lisans Tezi, Malatya.

Çoksever, E. (2009). Farklı oranlarda turunç albedosu ilavesinin sucuk kalitesi üzerine etkisi. Selçuk Üniversitesi Fen Bilimleri Enstitüsü Gıda Mühendisliği Anabilim Dalı Yüksek Lisans Tezi, Konya.

Demirel, H., & Demir, M. K. (2018). Farklı turunçgillerden elde edilen albedoların bisküvi üretiminde kullanımı. *Gıda Dergisi, 43*(3), 501-511.

Düzgüneş, O., Kesici, T., Kavuncu, O., & Gürbüz, F. (1987). *Araştırma ve Deneme Metodları*. Ankara Üniversitesi Ziraat Fakültesi Yayınları, Yayın No: 1021, Ankara, 381 s.

Francis, F. J. (1998). Colour Analysis. Food analysis. Gaithersnurg, USA: Aspen Publishers.

Günkaya, Z., Demirel, R., & Banar, M. (2016). Portakal kabuğu atıklarından üretilen biyokompozit ambalaj filminin aflatoksinlere karşı etkisinin incelenmesi. *Pamukkale Üniversitesi Mühendislik Bilimleri Dergisi*, *22*(6), 513-519.

Koubala, B. B., Mbome L. I., Kansci, G., Mbiapo, F. T., Crepeau, M. J., Thibault, J. F., & Ralet, M. C. (2008). Physicochemical properties of pectins from ambarella peels obtained using different extraction conditions. *Food Chemistry*, *106*(3), 1202-1207.

Levent, H., & Bilgiçli, N. (2013). Quality evaluation of wheat germ cake prepared with different emulsifiers. *Journal of Food Quality*, *36*(5), 334-341.

Schiewer, S., & Patil, S. (2008). Pectin-Rich fruit wastes as biosorbents for heavy metal removal: equilibrium and kinetics. *Bioresource Technology*, *99*(6), 1896-1903.

Schröder, R., Clark C. J., Sharrock, K., Hallett I. C., & MacRae, E. A. (2004). Pectins from the albedo of immature lemon fruitlets have high water binding capacity. *Journal of Plant Physiology*, *161*(4), 371-379.

Sinclair, W. B. (1984). The Biochemistry and Physiology of the Lemon and Other Citrus Fruits, Division of Agriculture and Natural Resources, University of California Publication, California, USA, 946 p.

Skujins, S. (1998). *Handbook for ICP – AES (Vartian-Vista)*. A short guide to vista series ICP – AES operation, Variant International, version 1.0, Switzerland.

Türksoy, S. (2011). Meyve ve sebze lif konsantreleri ilavesinin hamurun reolojik özellikleri ve bisküvi kalitesine etkileri. Ankara Üniversitesi Fen Bilimleri Enstitüsü Gıda Mühendisliği Anabilim Dalı Doktora Tezi, Ankara.

DETERMINATION OF THE EFFECTS OF CRITIC SUNN PEST (HETEROPTERA: SCUTELLERIDAE) DAMAGE RATIO ON WEIGHT LOSS OF SOME WHEAT VARIETIES CULTIVATED IN TURKEY

Mahmut İSLAMOĞLU
Uşak University, Faculty of Agriculture and Natural Sciences, Department of Plant Protection, Uşak, Turkey
mahmut.islamoglu@usak.edu.tr

Halef DİZLEK
Osmaniye Korkut Ata University, Faculty of Engineering, Department of Food Engineering, Osmaniye, Turkey
hdizlek@osmaniye.edu.tr

ABSTRACT: Wheat is the most important nutrient for human being, constitutes approximately 20% of the calories obtained from the food all over the world. The sunn pest, *Eurygaster* spp. (Heteroptera: Scutelleridae) is the most important harmful insect on wheat in Turkey. They are distributed on 75% of wheat fields in Turkey and their chemical control is carried out over an average of 1.2 million hectares every year. Both nymphs and adults of sunn pest cause plant damage, feeding on leaves, stems, and grains. Yield losses were estimated by 50 to 90% in wheat and 20 to 30% in barley. Apart from the direct yield reduction, the insect injects digestive enzymes during feeding which reduce the baking quality of the dough. If as little as 2 to 3% of the grain has been fed on, the entire grain lot may be rendered unacceptable for baking purposes because of poor quality flour. In the study, the effect of 3% sunn pest sucking rate which disrupts the bread quality on the weight loss of wheat mass, in 6 different wheat varieties, has been tested by applying the variance analysis. It was determined that the effect of critic sunn pest damage ratio (3%) of the different wheat varieties on the weight of thousand kernels was significant. The weight loss of samples showed differences according to the varieties. According to this, the highest weight loss of thousand kernel weight was determined as Ceyhan-99 variety with 1.33%. It was determined that Golia variety followed the Ceyhan-99 variety with 1.19%. Weight loss of thousand kernel weight was 1.027% in Ziyabey-98 wheat variety, followed by Zenit wheat cultivar with 0.55%. The weight loss of thousand kernel weight in Panda variety was 0.32%. It was found that the lowest weight loss in the rate of 3% sunn pest damage in thousand kernel weight was found in Adana-99 variety (0.16%).

Key words: wheat, wheat quality, sunn pest, weight loss

KRİTİK SÜNE (HETEROPTERA: SCUTELLERIDAE) EMGİ ORANININ TÜRKİYE'DE YETİŞTİRİLEN BAZI BUĞDAY ÇEŞİTLERİNİN AĞIRLIK KAYBINA ETKİSİNİN BELİRLENMESİ

ÖZET: Buğday, insanlar için en önemli gıda hammaddesi olup tüm dünyada gıdalardan sağlanan kalorinin yaklaşık %20'sini oluşturmaktadır. Süne, *Eurygaster* spp. (Heteroptera: Scutelleridae) Türkiye'de buğdaya zarar veren en önemli böcektir. Ülkemizde buğday tarımı yapılan alanların %75'inde süne zararı olmakta ve her yıl

ortalama 1.2 milyon hektar alanda süne mücadelesi yapılmaktadır. Sünenin hem yavruları hem de erginleri buğdayın vejetatif ve generatif aksamından beslenerek zarara neden olur. Verim kayıplarının buğdayda %50 ile 90, arpada ise %20 ile %30 arasında olduğu tahmin edilmektedir. Süne doğrudan verimde azalmaya yol açmasının yanı sıra, bitkiden beslenme sırasında sindirim enzimlerini enjekte eder ve bu da hamurun ekmeklik kalitesini düşürür. Buğday kitlesinin %2 ile %3'ü kadar küçük bir kısmı bile emilmişse (süne hasarına maruz kalmışsa), tüm tahıl lotu, düşük kaliteli un nedeniyle ekmeklik amaçlı kullanım için kabul edilemez hale gelebilir. Araştırmada 6 farklı buğday çeşidinde ekmeklik kaliteyi bozan %3'lük süne emgi oranının buğday kümelerinin ağırlık kayıpları üzerine etkisi varyans analizi uygulanarak test edilmiş ve %3'lük süne emgi oranının farklı buğday çeşitlerinin bin tane ağırlığı üzerine etkisi önemli bulunmuştur. Bin tanedeki ağırlık kayıplarının çeşitlere göre farklılık gösterdiği belirlenmiştir. Buna göre, bin tanedeki en yüksek ağırlık kaybının %1.33 ile Ceyhan-99 çeşidinde olduğu tespit edilmiştir. Ceyhan-99 çeşidini %1.19 ile Golia çeşidinin takip ettiği saptanmıştır. Ziyabey-98 buğday çeşidinde bin tanedeki ağırlık kaybının ise %1.027 olduğu, bunu %0.55 ile Zenit buğday çeşidinin izlediği belirlenmiştir. Panda buğday çeşidinde bin tanedeki ağırlık kaybının %0.32 olduğu saptanmıştır. %3'lük süne emgi oranının bin tanedeki en düşük ağırlık kaybının Adana-99 çeşidinde (%0.16) olduğu tespit edilmiştir.

Anahtar sözcükler: buğday, buğday kalitesi, süne, ağırlık kaybı

GİRİŞ

Ülkemizin temel gıda hammaddesi kaynağı olan buğday, ülkemizde ortalama ekiliş alanı 9 400 000 ha ve yıllık ortalama 21.000.000 ton üretim ile bitkisel ürünler içerisinde ilk sıradaki yerini korumaktadır (TUİK, 2016). Buğdayın teknolojik kalitesi ve verimi üzerine çeşidin genetik özellikleri ve yetiştirme koşullarının yanı sıra, hasat öncesindeki hastalık ve zararlılarının da etkisi çok büyüktür. Hasat öncesi buğdayın verimini ve kalitesini olumsuz yönde etkileyen zararlılarının başında süne (*Eurygaster* spp.) ve kımıl (*Aelia* spp.) gibi zararlılar gelmektedir (Lodos, 1961; Sivri, 1998). Süne, uzun yıllardır ülkemizde buğdaya verdiği zarar itibariyle önemli olmakta ve büyük boyutlarda ekonomik kayıplara yol açmaktadır (Rashwani ve Cardona, 1984; Talay, 1997; Şimşek ve ark., 2005). 1950'li yıllarda süne sorunu ülkemizde sadece Güneydoğu ile Güney Anadolu bölgesinde mevcut iken, günümüzde buğday üretimi yapılan alanın yaklaşık 3/4'ünü tehdit etmektedir (Şimşek, 1998). Süne zararının buğdayın teknolojik kalitesini bozmasının nedeni, hasat öncesi dönemde bu zararlının buğdayı emerek beslenirken taneye bıraktığı, yüksek proteolitik ve kısmen de amilolitik enzim aktivitesine sahip sindirim salgısıdır. Bu enzimler, buğday proteinlerini, özellikle gluten proteinlerini, parçalayarak buğdayın teknik değer ölçülerinin, bir diğer ifadeyle buğday kalitesinin önemli düzeyde gerilemesine yol açarlar (Dizlek, 2010).

Süne'nin buğday tanesinde emdiği bölgenin sabit bir alanla sınırlandırılamayacağı – tanenin hangi oluşum evresinde bulunmasıyla ilintili olarak – tane içeriğinin çoğunu emebileceği gibi, sadece bir kısmını da emebileceği bildirilmektedir (Corbellini ve ark., 2001; Dıraman, 2004; Özberk ve ark., 2005). 1000 adet buğday tanesi içerisinde 3-4 adet süne zararı görmüş tane bulunması halinde bile, buğdayın teknolojik kalitesinin bozulduğu ve salgın olduğu yıllarda zarar görülen bölgede hasat edilen ürünün

tamamının ekmek üretiminde kullanılamaz duruma geldiği bildirilmiştir (Yakovenko ve ark., 1973). Greenaway ve ark. (1965)'nın bildirdiğine göre Brooke (1936), %1-2 oranında; Swallow ve Every'nin (1991) bildirdiğine göre Kosmin (1933), nisbeten düşük düzeyde (yaklaşık %3) süne zararı görmüş buğdayın, sağlam buğdayın niteliklerini bozmak için yeterli olduğunu belirtmişlerdir. Ülkemizde süne konusunda çalışan ilk araştırıcılardan Tekeli (1964) ile Lodos (1980) ise buğday kitlesindeki süne emgi oranının %2 olması durumunda buğdayın teknolojik vasfının kaybolduğunu bildirmişlerdir.

Bu çalışmada, buğday kalitesini olumsuz yönde etkileyerek bozan kritik süne emgi oranı olarak %3 düzeyi ele alınmış ve bunun ülkemizde yetiştirilen bazı buğday çeşitlerinin ağırlık kaybına etkisinin belirlenmesine çalışılmıştır. Bu amaçla, hububat teknolojisinde önemli bir fiziksel kalite kriteri olan 1000 tane ağırlığı dikkate alınmış ve %3 süne emgili taneler ile aynı çeşidin sağlam taneleri birbiri ile mukayese edilerek kritik süne emgi oranının buğday kümelerinin olası ağırlık kaybına etkileri yüzdesel oran olarak ortaya konulmuştur.

YÖNTEM

Araştırmada 6 farklı buğday çeşidi (Golia, Panda, Adana-99, Ziyabey-98, Ceyhan-99 ve Zenit) kullanılmıştır. Söz konusu çeşitler olgunlaşma döneminden yaklaşık 10 gün sonra hasat edilerek laboratuvara getirilmiştir. 10 gün geç hasat yapılmasının nedeni çeşitlerin daha fazla süne zararına maruz kalmalarını sağlamaktır.

Laboratuvara getirilen buğday çeşitleri binoküler altında emgili ve emgisiz olarak gruplandırılmıştır (Köksel ve ark., 2002). Bunun için buğday örneklerinden yeterli miktarda olacak biçimde numune alınarak bu numunelerdeki süne zararına uğramış tanelerin seçimi elle yapılmıştır. Her bir buğday kitlesinde süne emgili tane kalmayıncaya kadar devam ettirilen ayıklama işlemi bitirildikten sonra 1000 tane ağırlığı analizinin belirlenmesinde kullanılan ve üzerine yerleştirilmiş metal levhada 500 tane oyuk bulunan kutudan yararlanılmıştır. Bu kutunun 500 oyuğu, her bir buğday çeşidi için ayrı ayrı olmak üzere süne emgili tanelerin ayıklanmasından sonra arta kalan sağlam buğday kitlesi ile doldurulmuş ve sonra hazırlanacak %3 emgili kitle düzeyine göre orantı yoluyla belirlenen 15 adet sağlam buğday tanesi bu oyuklardan çıkarılarak bunların yerine daha önceden ayıklanan ilgili çeşide ait süne emgili taneler (rastgele seçilerek) eklenmiştir. Bu işlem çok defa tekrar edilerek, her bir çeşide ait %3 emgili numuneler hazırlanmış, sonra her bir kitle kendi içerisinde homojen olacak biçimde iyice karıştırılmıştır. Böylece, her buğday çeşidinde iki farklı buğday grubu (emgisiz [kontrol] ve %3 emgili) oluşturulmuştur. Buğday gruplarının oluşturulmasında kırık ve çift emgili tanelerin elemine edilmesine özellikle dikkat edilmiştir.

Elde edilmiş %3 emgili grup ve emgisiz grup (kontrol) ile bin taneli buğday grupları oluşturulmuştur. %3 emgili ve emgisiz kitlelerden oluşturulan bin taneler hassas terazide tartılarak ağırlıkları kayıt edilmiştir (Uluöz, 1965). Emgili buğday kitlelerinin emgisiz olanlara göre bin tane ağırlığında meydana gelebilecek olası ağırlık kayıpları SPSS paket programı kullanılarak istatistiki analize tabi tutularak değerlendirilmiştir. Deneme, her bir buğday çeşidi için on tekerrürlü olarak yürütülmüştür.

BULGULAR

%3'lük süne emgi oranının farklı buğday çeşitlerinin bin tanedeki ağırlık kaybı üzerine etkisi önemli ($p<0.05$) bulunmuştur (Şekil 1). Bin tanedeki ağırlık kayıplarının çeşitlere göre farklılık gösterdiği belirlenmiştir. Buna göre, bin tanedeki en yüksek ağırlık kaybının %1.33 ile Ceyhan-99 çeşidinde olduğu tespit edilmiştir. Ceyhan-99 çeşidini %1.19 ile Golia çeşidinin takip ettiği saptanmıştır. Ziyabey-98 buğday çeşidinde bin tanedeki ağırlık kaybının ise %1.027 olduğu, bunu %0.55 ile Zenit buğday çeşidinin izlediği belirlenmiştir. Panda buğday çeşidinde bin tanedeki ağırlık kaybının %0.32 olduğu saptanmıştır. %3'lük süne emgi oranının bin tanedeki en düşük ağırlık kaybının Adana-99 çeşidinde olduğu tespit edilmiştir. Adana-99 buğday çeşidinde bin tanedeki ağırlık kaybının %0.16 olduğu saptanmıştır.

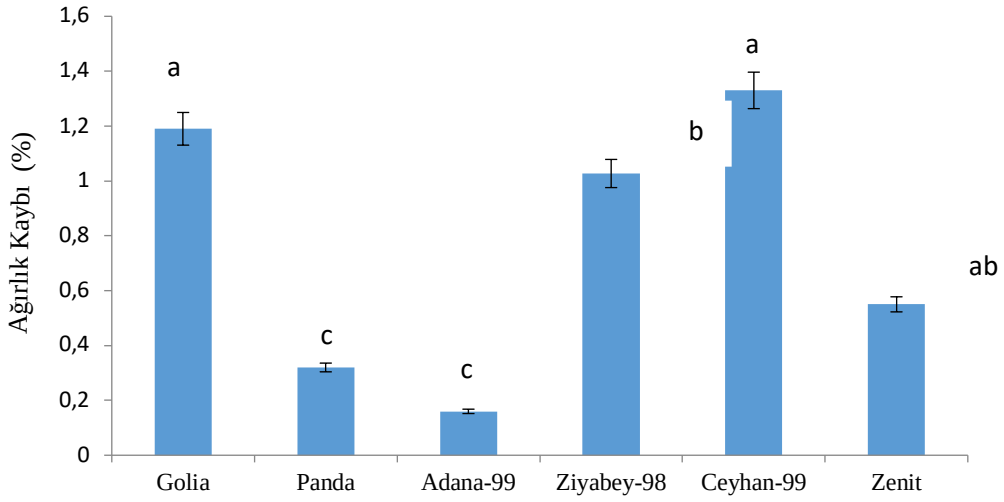

Şekil 1. Muhtelif Buğday Gruplarında %3 Süne Emgi Oranının Çeşitlerin Ağırlık Kaybı Üzerine Etkisi

Çeşitler arasında %3'lük emgi düzeyinin ağırlık kaybına etki bakımından farklılık olup oluşturmadığını test etmek amacıyla yapılan istatistiki değerlendirmede, Golia ve Ceyhan-99 buğday çeşitlerindeki % ağırlık kaybı aynı grupta yer alırken (a), Ziyabey-98 çeşidinin farklı grupta (b) yer aldığı tespit edilmiştir. Zenit buğday çeşidindeki % ağırlık kaybı ise, Golia ile Ceyhan-99 buğday çeşitlerinin oluşturduğu grup ile Panda ve Adana-99 buğday çeşitlerinin oluşturduğu grup arasında (ab) yer almıştır. Panda ve Adana-99 buğday çeşitlerindeki % ağırlık kaybının farklı bir grup (c) oluşturduğu belirlenmiştir (Şekil 1).

Bin tane ağırlığının buğday çeşidi için önemli bir kalite kriteri olduğu (Karababa ve Ozan, 1998) ve un verimi ile pozitif ilişkili olduğu (Lee ve ark., 1983) belirtmiştir. Bu çalışmadan elde edilen bulgularla uyumlu olarak Critchley (1998) ile Hariri ve ark. (2000) süne hasarı ile buğdayın bin tane ağırlığının azaldığını tespit etmişlerdir. Bununla beraber, Critchley (1998) bu azalmanın oransal olarak %8-22, Hariri ve ark. (2000) ise %24 düzeyinde olduğunu bildirmişlerdir. Çalışmadan elde edilen ağırlık

kaybı oranları ile diğer araştırıcıların bulguları arasındaki farklılığın, araştırmalarda ele alınan süne emgi düzeyinin ve buğday çeşitlerinin farklı olmasından, ayrıca buğday çeşitlerinin süne hasarına mukavemeti bakımından çeşitler arasında varyasyon olmasından kaynaklandığı düşünülmektedir.

SONUÇ

%3'lük süne emgi oranının farklı buğday çeşitlerinin bin tane ağırlığı üzerine etkisi önemli bulunmuştur. Buna göre denemede ele alınan ve buğdayın kalitesini bozduğu bildirilen %3 emgi düzeyinin buğdayların 1000 tane ağırlığında oransal olarak %0.16 ile %1.33 arasında gerilemeye yol açtığı saptanmıştır. Çeşitler arasında ağırlık kaybı bakımından varyasyon olduğu, bazı çeşitlerin (Ceyhan-99 ve Golia) süne zararından daha fazla etkilendiği tespit edilmiştir. Süne hasarının buğdayın sadece teknolojik, reolojik ve ekmeklik-makarnalık özelliklerini bozmadığı, aynı zamanda ağırlık kaybına yol açarak un verimi gibi kalite kriterlerini de sekteye uğrattığı tespit edilmiştir.

KAYNAKLAR

Corbellini, M., Vaccino, P., Boggini, G., & Spina, A. (2001). La cimice del grano: manifestazioni e danni arrecati alla coltura (the wheat bug: detection and damages caused to crops). *Tecnica Molitoria*, *52*(8), 743-747.

Critchley, B. R. (1998). Literature review of sunn pest *Eurygaster integriceps* Put. (Hemiptera, Scutelleridae). *Crop Protection*, *17*(4), 271-287.

Dıraman, H. (2004). Ekmeklik buğdaylarda bazı böcek (süne kımıl) enzimlerinin oluşturduğu zararın mekanizması ve biyokimyası. *Akademik Gıda Dergisi*, *2*(12), 27-32.

Dizlek, H. (2010). Süne zararına uğramış ekmeklik buğdayların bazı niteliklerinin incelenmesi ve iyileştirilmesi olanakları üzerine bir araştırma. Çukurova Üniversitesi Fen Bilimleri Enstitüsü Gıda Mühendisliği Anabilim Dalı Doktora Tezi, Adana.

Greenaway, W. T., Neustadt, M. H., & Zeleny, L. (1965). Communication to the editor: a test for stink bug damage in wheat. *Cereal Chemistry*, *42*(6), 577-579.

Hariri, G., Williams, P. C., & El-Haramein, F. J. (2000). Influence of pentatomid insects on the physical dough properties and two-layered flat bread baking quality of Syrian wheat. *Journal of Cereal Science*, *31*, 111-118.

Karababa, E., & Ozan, A. N. (1998). Effect of wheat bug (*Eurygaster integriceps*) damage on quality of a wheat variety grown in turkey. *Journal of the Science of Food and Agriculture*, *77*, 399-403.

Köksel, H., Atlı, A., Dağ, A., & Sivri, D. (2002). Commercial milling of suni bug (*Eurygaster* spp.) damaged wheat. *Nahrung/Food*, *46*(1), 25-27.

Lee, H. S., Cho, C. H., Song, H. S., & Chang, H. G. (1983). Studies on the variation of quality traits and its selection efficiency in *Triticum aestivum*. In: Sakamota, S. (ed.), Proceedings of the 6th international wheat genetics symposium, 835-841. 28 November-3 December 1983, Kyoto.

Lodos, N. (1961). *Türkiye, Irak, İran, Suriye'de süne* (*Eurygaster integriceps Put.*) *problemi üzerinde incelemeler*. E.Ü. Ziraat Fakültesi Yayınları No:51, Ege Üniversitesi Matbaası, İzmir.

Lodos, N. (1980). *Türkiye entomolojisi "genel uygulamalı ve faunistik"*. Cilt II E.Ü. Ziraat Fakültesi Yayınları No:429, Ege Üniversitesi Matbaası, İzmir.

Özberk, İ., Atlı, A., Pfeiffer, W., Özberk, F., & Coşkun, Y. (2005). The effect of sunn pest (*Eurigaster integriceps*) damage on durum wheat: impact in the marketplace. *Crop Protection*, *24*, 267–274.

Rashwani, A., & Cardona, C. (1984). Effect of suni bug (*Eurygaster integriceps* Put.) damage on the yields of Hammari and Gezira-17 durum wheats. *Rachis*, *3*(1), 21.

Sivri, D. (1998). Süne proteolitik enzimlerin izolasyonu, karakterizasyonu, saflaştırılması ve gluten proteinleri üzerine etkilerinin belirlenmesi. Hacettepe Üniversitesi Fen Bilimleri Enstitüsü Gıda Mühendisliği Anabilim Dalı Doktora Tezi, Ankara.

Swallow, W. H., & Every, D. (1991). Insect enzyme damage to wheat. *Cereal Foods World*, *36*(6), 505-508.

Şimşek, Z., Aktaş, H., Kondur, Y., Koçak, E., Özdemir, I., & Karaca, V. (2005). Ülkemizde hububatın önemli zararlısı süne (Eurygaster spp.) ile hububatta kök ve kökboğazı çürüklüğü hastalık etmenleri ve mücadele stratejileri. IV. GAP Tarım Kongresi. Bildiri Kitabı (1): 323–329. 21-23 Eylül 2005, Şanlıurfa.

Talay, M. (1997). *Ekmek bilimi ve teknolojisi*. Ray Filmcilik Matbaacılık, İstanbul.

Tekeli, S. T. (1964). *Hububat teknolojisi*. Ankara Üniversitesi Basımevi, Ankara.

Türkiye İstatistik Kurumu (TUİK). 2016. Bitkisel üretim istatistikleri. https://biruni.tuik.gov.tr/bitkiselapp/bitkisel.zu l (Erişim Tarihi: 18.04.2016).

Uluöz, M. (1965). *Buğday, un ve ekmek analiz metodları*. Ege Üniversitesi Ziraat Fakültesi Ofset Tesisleri, İzmir.

Yakovenko, V. A., Litvinov, A. M., & Stayanova, A. A. (1973). Characteristics of gluten protein of wheat attacked by the wheat bug. *Izv. Vyss. Uchebn. Zaved. Pishch. Tekhnol.*, No 4, 17-19.

EFFECT OF CONTINUOUS UV-C PASTEURIZATION ON THE SHELF-LIFE AND TENDERIZING POWER OF ONION JUICE

Hande DEMİR
Osmaniye Korkut Ata University
handedemir@osmaniye.edu.tr

Mehmet Onur ORAL
Osmaniye Korkut Ata University
monroral@gmail.com

ABSTRACT: Onion juice has gained attention as a natural meat-tenderizer in the marination of meat and fish in the last few years. Due to its natural initial microbial load, onion juice is required to be pasteurized before using as a marination agent for the principle of food safety. UV-C irradiation is a non-thermal process successfully used for the pasteurization of juices having relatively no negative effect on nutritional and sensorial quality of food products. The aim of this study is to investigate the effect of continuous UV-C pasteurization on the shelf-life of acidified onion (*Allium cepa* L.) juice that was pasteurized by a designed coiled-tube type UV-C reactor. For this purpose, a continuous UV-C reactor system (Figure 1) composed of four vertical 20 W (UVP XX-20S, 254 nm) low-pressure mercury lamps with coiled PTFE tubes were designed. A reflector and a cooling jacket were placed outside the coiled tube. The coiled-type UV-C system was supplied by a secondary eddy flow effect. The UV-C irradiated samples (38.09 kJ/L dose value, 1.26 L/min flow rate) were monitored for 6 weeks. Total aerobic mesophilic count, total mold and yeast count, color values, non-enzymatic browning index, pH, total titratable acidity, total soluble solid content and turbidity of the samples were analyzed by 15-day intervals. Additionally, the UV-C irradiated onion juice was used for marination of beefsteaks and the tenderizing effect of onion juice was measured by textural profile analysis of the marinated beefsteaks.

Key words: onion juice, UV-C reactor, shelf-life

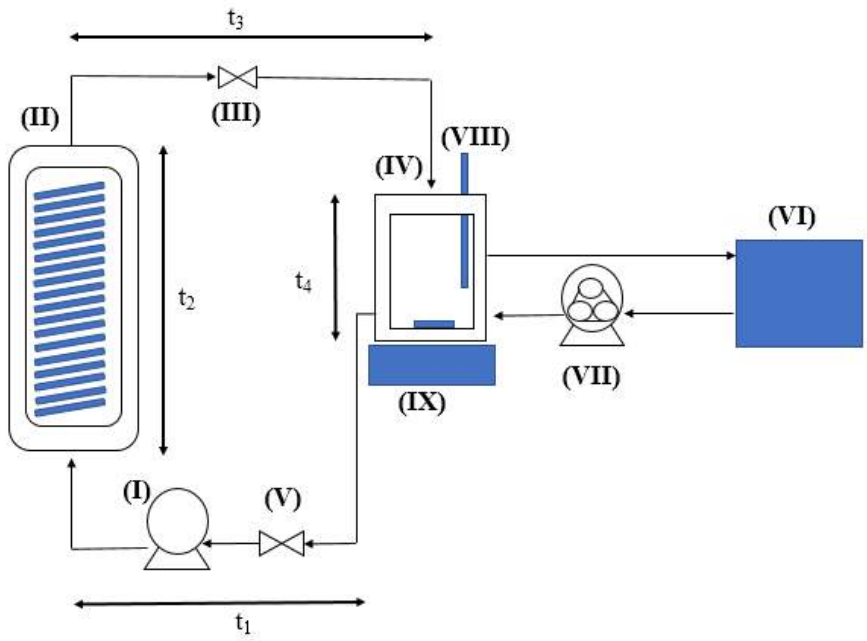

Figure 1. Scheme of Continuous System UV-C reactor and its Components (I: diaphragm pump, II: UV-C lamps coiled by PTFE tube and water jacket, III: outlet valve of reactor, IV: reservoir, V: outlet valve of reservoir, VI: water bath, VII: peristaltic pump, VIII: temperature, IX: magnetic stirrer)

INVESTIGATION OF LIQUEFACTION DANGERS BY CONSIDERING TO LIQUEFACTION SUSCEPTIBILITY OF THE SOIL

Mohammad Beykzade*
Department of civil engineering, Kharazmi University, Tehran, Iran
m.beykzade@gmail.com

Omid Reza Baghchesaraei
Department of civil engineering, Kharazmi University, Tehran, Iran
omidreza@baghchesaraei.com

Mohammad Heydari Torkamani
Department of civil engineering, Kharazmi University, Tehran, Iran
m@gmail.com

ABSTRACT: Liquefaction was first introduced by mogami & kubo in 1953. It is often considered as one of the most catastrophic consequences of the earthquake. Liquefaction has two types namely: flow liquidation and cyclic mobility (lateral spreading). Liquefaction is a phenomenon whereby pore water pressure is increased and effective stress of the soil layers are reduced. Even if there is no lack of soil bearing capacity, there is the possibility of structure settlement and disruption of the service state. Among the liquefaction problems are the rising soil surface, land subsidence, sand boil and the permanent set, which have been the subject of many researches over the past few decades. Since all soil types do not have the liquefaction susceptibility (they are not prone to liquefaction), the first step in assessing the risks of liquefaction is to assess the liquefaction potential. If the site's soil does not have liquefaction potential, the process of evaluating liquefaction can be terminated.

Key words: Liquefaction, flow liquidation, cyclic mobility, liquefaction potential

INTRODUCTION

Natural disasters, like earthquake, storm, tornado and flood, often cause financial and life damages. These bring about many consequences around the world every year. In today's human societies, earthquake is considered one of the most dangerous natural disasters. Soil is the upper layer of the earth and it is naturally a result of the interaction between geologic effects, vegetation and climate (Baghchesaraei, A., & Baghchesaraei, O. R, 2014). Soil liquefaction is an example of damages incurred by earthquake, in which the soil layers lose their resistance and flow like a fluid. In liquefaction, soil loses its resistance so that it couldn't withstand the weight of the above structures or even itself (Kramer). Liquefaction, which was first introduced by mogami & kubo (1953), means that due to sudden loading, the non-drained non-cohesive saturated soils tend to be highly compacted. So, the pore water pressure increases and the effective stresses decrease that lead to liquefaction.
Pursuant to the devastating earthquake in Niigata, Japan, 1964, in Alaska, 1964, in Lunzon, the Philippines, 1990, and Kocaeli, Turkey, 1999, the liquefaction

phenomenon has been observed on a large scale in a susceptible area, causing extensive damage to the buildings, roads, bridges and dams.

Liquefaction is often observed in fine to medium-grained non-cohesive saturated soils. According to laboratory results and local observations and studies, the most important causes of liquefaction are groundwater level, soil type, relative density, gradation, drainage, particle forms, geological age, and all-round pressure, based on which the most commonly used liquefaction feasibility methods are formulated (Siyahi & arsalan ,2008).

Grain aggregates tend to be compressed under seismic loads. In saturated masses, the mass-reduction tendency of the soil is resisted due to lack of pore water pressure, lack of drainage of soil and short loading time; so, the pore water pressure increases, which reduces the effective stress. It specially leads to a reduction in the shear strength and eventually to liquefaction, especially in non-cohesive soils (Jefferies & Been, 2015).

Liquefaction is divided into flow liquidation and cyclic mobility (lateral spreading). Flow liquefaction occurs when the shear stress required for static equilibrium of the soil mass (static shear stress) is greater than the shear strength of the soil, which can make a very large movement in the soil. Flow liquefaction has caused the destruction of many earth dams, including the Sheffield Dam, destroyed by the 1925 Santa Barbara earthquake (Figure1) and also of the foundation, for example the upstream foundation of the lower san Fernando dam which was destroyed by the san Fernando 1971 earthquake (Figure 2). Lateral spreading could make a lasting, unexpected deformation during the earthquake. Cyclic mobility (lateral spreading) is exactly opposite the flow liquefaction, because it occurs when the static shear stress of the soil mass is less than the flowing soil resistance. These deformations increase in the earthquake.

Figure 1. Liquefaction failure of Sheffield dam following the 1925 Santa Barbara earthquake (k. Steinbrugge collection; courtesy of EERC, University of California)

Figure 2. Lower San Fernando Dam following Liquefaction failure of its upstream

slope in the 1971 San Fernando earthquake (k. Steinbrugge collection; courtesy of EERC, University of California)

Figure 3. Lateral spreading of very flat ground toward the Motauga River following the 1976 Guatemala earthquake (Photo by G. plafker; courtesy of USGS

According to the above definition, one of the consequences of liquefaction in soils is lateral spreading, which, based on the previous earthquakes, has been significantly damaging (Bardet et al 1999, Youd & Hoose 1976). The lateral spreading caused by liquefaction occurs in gentle slopes (0.3 Up to 5%) with high groundwater levels and loose sand abounding in lower layers (non-cohesive soil susceptible to liquefaction). This happens during earthquakes and ends with it. It is noteworthy that the occurrence of liquefaction in areas with a moderate to steep slope leads to a massive flow liquidation, which causes a massive downward movement towards the slope at relatively long intervals. Meanwhile, the lateral spreading is reliant on the milder movements of the ground with low slope (Youd et al., 2002).

LIQUFACTION SUSCEPTIBILITY

Since all soils are not susceptible to liquefaction, the first step in assessing the liquefaction risk is the liquefaction susceptibility. If, at a construction area, the soil is not susceptible to liquefaction the liquidation evaluation process can be terminated. But if soil is susceptible to liquefaction, the underlying conditions of the liquefaction should be examined. Several criteria such as historical criteria, geologic criteria, compositional criteria, and state criteria

Background

A great deal of information can be obtained from post-earthquake field studies. It shows that if the soil and groundwater conditions are unchanged, liquefaction often occurs in the same place (1984a youd). Therefore, the historical cases of liquefaction can be used to identify specific sites or more general conditions that demonstrate the liquefaction susceptibility in the future. Field studies after the earthquake have shown that the effects of liquefaction over time are limited to areas with a clear distance from the source of the earthquake. Using shallow earthquakes around the world, Ambraseys 1988 obtained a focal length, beyond which liquefaction wasn't observed earthquakes with different magnitudes (following figure 4). The distance at which the liquefaction is expected increases greatly with magnitude, while the relationships

shown in the figure above do not guarantee that the liquefaction does not occur for greater distances, but are useful for assessing regional regression scenarios.

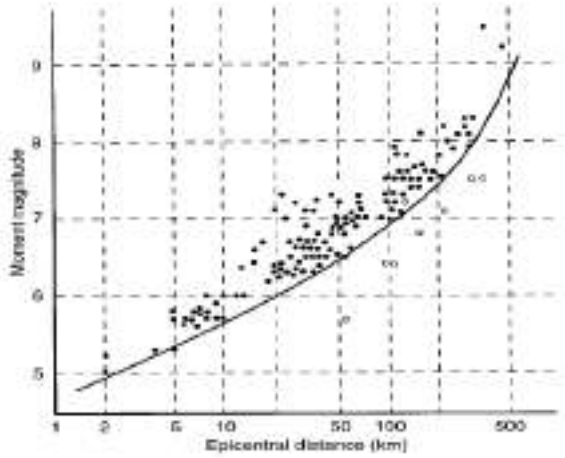

Figure 4. Relationship between limiting epicentral distance site at which liquefaction has been observed and moment magnitude for shallow earthquake(ambraseys 1988)

Structural criteria

In recent years, much has been written about the tectonic and structure, especially in reference to the engineering of what used to be termed the old world structure. It appears that less attention has been given to understanding the tectonics of the construction of the new brand construction (Baghchesaraei, A., & Baghchesaraei, O. R, 2014).

Since liquefaction necessarily occurs due to the increase in the pore water pressure, the liquefaction susceptibility is influenced by the characteristics with the high potential for volume change, like the particle size, form and gradation. Historically, liquefaction was assigned only to the sand, but in recent years, it has been also observed in the coarse grained soil.

In fine grained soils, non-plastic layer liquefaction was investigated both in the laboratory and in the field (Ishihara, 1984, 1985), which indicates that, in addition to gradation, the plastic characteristics also affect the susceptibility of liquefaction. Non-cohesive and non-plastic coarse grained layers are highly susceptible to liquefaction (Ishihara, 1993). Fine grained soils that meet the criteria in the following table face lower resistance to the liquefaction (Wang, 1979 and finn & et al. 1994).

Table 1. Fine-grained soil characteristics to reduce liquefaction resistance

Finn & et al 1994 (American)	Wang 1994 (China)
Fraction finder than 0.005 mm ≤10%	Fraction finder than 0.005 mm ≤15%
Liquid limit , LL≤ 36%	Liquid limit , LL≤ 35%
Natural water convent ≥0.92 LL	Natural water convent ≥0.9LL
Liquidity index ≤ 0.77	Liquidity index ≤ 0.75

In the field, Coulter & Migliaccio 1996, Chang 1978, Wong 1984, Uoud et al 1985, Yegian et al 1994, and in the laboratory Wong et al., 1975, Evans & 1987, investigated the course grained soils, and showed that the effects of the membrane penetration into the functional sample have been showing a high resistance to the liquefaction of the sandy soils.

State criteria

A soil may have all the prerequisites for liquefaction susceptibility, but it is not susceptible to liquefaction. This means that the soil's potential for liquefaction depends on the initial state of the soil, such as the stress and density, before the earthquake. Since the tendency to create overpressure in the pore in a given soil is hugely affected by the conditions of density and initial stress, the not liquefaction susceptibility is heavily dependent on the initial state of soil, contrary to the previous criteria for flow liquefaction and cyclic mobility (Kramer, 1996).

INVESTIGATION OF DAMAGED STRUCTURES BASED ON THE LIQUEFACTION PHENOMENON

Underground structures

Modern construction methods are a kind of building and infrastructure are its foundation, without an appropriate foundation the building will collapse (Baghchesaraei, A., & Baghchesaraei, O. R, 2014). Among the earthquakes that damaged the tunnels and underground structures were Loma prieta 1986 and the Tangshan 1976 earthquake in China. In Japan's Kobe earthquake in 1995, gas and water lines were seriously damaged, and about 234 gas leakages were reported, ultimately causing a massive fire in the city, burning seven thousand buildings (Scawthorn & Yanev, 1995). Damage to the gas pipelines in Taiwan's Chi-Chi earthquake in 1999 led to the gas outage at many industrial centers, with losses of about US $ 25 million as a result of exploitation of gas pipelines (Chen et al. 2000).

Buried structures in liquefied soils may suffer from subsidence or heave during earthquake (Chian & Madabhushi, 2012). Heave can be attributed to various reasons like the movement of liquefied soil under the structure and increase of the water pore pressure (Fugro, 2008). In the 2004 Chūetsu earthquake in Japan, about 37% of the manholes in the city were heaved, resulting in blockage of the city, traffic congestion, and access to urban roads and also barriers to rescue. In addition to causing damage to underground structures, these heaves caused damage to the ground structures (Tobita et al. 2009). In the 2009 Kushiraki earthquake, more than 20 manholes upraised from the ground to a height of 1.5 meters (Koseki Et al. 1997). Among the more recent earthquakes that caused soil heaving are ones in Kobe 1995, Chuetsu 2004, Maule 2010, Tohoku 2011, etc. (Ghayamghamian et al 2007; Chian and Tokimatsu 2012).

There has been a lot of research on soil heaving. Using a seismic table, it was observed that the higher the thickness of the liquefied soil layer, the higher the heaving observed (Tokida et al. 1993). In a subsequent experiment on a seismic table, it was shown that the total heave and subsidence of an object in a liquefied soil could occur in one of the following states: 1. Lateral deformation, 2. Pore water movement, 3. Reconsolidation, 4. Limited space total heave or subsidence (Figure 5). Koseki et al. 1997, and Ichii et al.

showed that the heaving velocity was higher at the beginning of loading and that, the percentage of fine grains is effective on the rate of heaving.

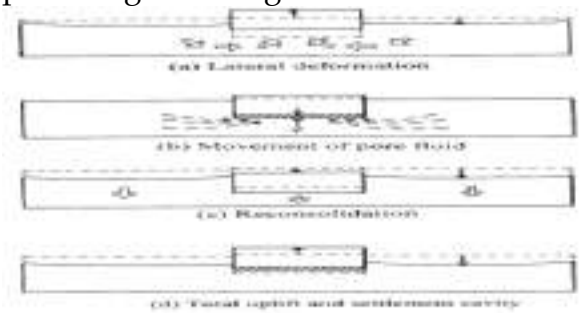

Figure 5. schematic diagram of behavior of surrounding subsoil and underground structure(Koseki et al 1997)

Ground structures

The first documented data on the reduction of load capacity and cumulative subsidence were related to the 1694 Niigata earthquake, in which about 340 RC structures on thick layers of a liquefied soil experienced subsidence and rotation. Observations have shown that subsidence was proportional to the height-to-width ratio and the weak effect of short piles on subsidence and load bearing capacity (Yoshimi, & Tokimatsu, 1997). Also, according to a study conducted in the 1990 Lazon earthquake in the Philippines, a number of structures that are placed on a thick layer liquefied soil experienced subsidence and rotation (Tokimatsu, et al. 1994).
The first investigation by seismic table on underground liquefaction and the shield enclosing effect to reduce the subsidence risks and increase the pore water pressure was made by Yoshimi, & Tokimatsu (1997). Subsequently, using centrifuge experiments, a number of researchers examined the effect of depth and density on reducing the risk of liquefaction. They investigated the positive effect of increasing the soil hardness in the presence of rock pillars on the decrease of subsidence due to liquefaction (Adalier & Elgamal, 2004).
An increase in the water pressure caused by earthquake can reduce the hardness and load bearing capacity of surface foundations. If the load bearing capacity of sand under water pressure exceeds the stress caused by the upper structure, failure due to the lack of load bearing capacity will not occur. But there is the possibility of extraordinary subsidence and getting out of service. Centrifugal investigations by the Dashti & Bray (2013) on a shallow foundation constructed in liquefied sands indicate the role of the shear strains due to the upper structure load and the interaction of the structure and the soil in general subsidence. However, geotechnical engineers estimated liquefaction-induced subsidence by measurements of the volumetric strains caused by the re-consolidation of sand obtained by using the results of triaxial and simple cycles.
Earth dams are among the most complex and ambiguous structures which should be analyzed and designed require a lot of information about the surrounding area. When exposed to severe earthquakes, dams and the embankments may cause failure of liquefaction. The location of the dam that has been saturated (usually upstream) may liquefy when vibrated more than a threshold. Liquefaction in earth dams usually occurs on the upstream and downstream of the dam so it is necessary to take practical actions to reduce liquefaction in these locations.

Conclusion

The following results can be found according to the above information and its analysis:

1. Liquefaction has been thought to be for the fine to medium-grained non-cohesive saturated soils, but recently, research on coarse-grained soils has also been considered.
2. The most important causes of liquefaction are groundwater level, soil type, relative density, gradation, drainage, particle forms, geological age, and all-round pressure.
3. The lateral spreading caused by liquefaction occurs in gentle slopes (0.3 Up to 5%) with high groundwater levels and in areas with a moderate to steep slope, flow liquefaction occurs.
4. Liquefaction does not occur in all soils. Some soils with liquefaction susceptibility have to be assessed by the historical, geological, compositional and state criteria.
5. In coarse-grained soils, the effect of plastic membrane penetration into the sample is the most important factor in showing high resistance to soil liquefaction.
6. Generally, liquidation causes damage to ground or underground structures. The subsidence or heave of soil in the manhole causes disturbances in traffic and, ultimately, is an obstacle to rescue.

REFERENCES

Adalier, K., & Elgamal, A. (2004). Mitigation of liquefaction and associated ground deformations by stone columns. *Engineering Geology*, 72(3-4), 275-291.

Ambraseys, N, N. (1988). Engineering seismology, *Earthquake Engineering and Structural Dynamics*, vol 17, 99. 1-105.

Baghchesaraei, A., & Baghchesaraei, O. R. *Tectonic knowledge impacts on design process*.

Baghchesaraei, A., & Baghchesaraei, O. R. (2014). *Essential Words for Architects and Structural Engineers*. Alireza Baghchesaraei & Omid Reza Baghchesaraei.

Baghchesaraei, A., & Baghchesaraei, O. R. (2014). *The Importance of Infrastructures in the Development of Modern Methods of Construction*. International Journal of Applied Engineering Research, 9(21), 11689-11692.

Bardet, J, P. Mace, N. Tobita, T. (1999). Liquefaction induced Ground deformation and Failure , *A report to PEER/PG&E, Task 4A, Phase 1, Civil Engineering Department, University of Southern California, Los Angeles.*

Chang, K. T. (1978). An Analysis of Damage of Slope Sliding by Earthquake Paiho Main Dam and its Earthquake Strengthening, *Tseng-hua Design Section, Dept. of Earthquake- Resistant Design and Flood Control Command of Miyna Reservoir, People Republic of China*

Chen, W. W., Shih, B. J., Wu, C. W., & Chen, Y. C. (2000). Natural gas pipeline system damages in the Ji-Ji earthquake (The City of Nantou). *In Proceedings of the sixth international conference on seismic zonation*. Palm Springs, Riviera Resort, CA.

Chian SC, Madabhushi SPG (2012) Effect of buried depth and diameter on uplift of underground structures in liquefied soils. *J Soil Dyn Earthq Eng* 41:181–190

Chian, S. C., & Tokimatsu, K. (2012). Floatation of underground structures during the M w 9.0 Tōhoku Earthquake of 11th March 2011. *In Proceedings of the 15th World Conference on Earthquake Engineering*, Lisbon, Paper ID (Vol. 3705).

Coulter, M. Migliaccio, L. (1996).'' Effect of the earthquake of March 27, 1964 at Valdez, Alaska. ''*Professional Paper 542-C, U.S. Geotechnical Survey*, U.S. Department of the Interior, Washington, D.C.

Evans, M. D. Seed, H. B. (1987).'' Underained cyclic triaxial testing of gravels; the effect of membrane compliance,'' *Report UCB/EERC -87/08, Earthquake Engineering Research Center*, University of California, Berkeley, California.

Finn, W. D. L., Ledbetter R. H., Wu. G., (1994). ''Liquefaction in Silty Soil: Design and Analysis,'' Ground Failures under Seismic Conditions, *Geotechnical Special Publication 44, ASCE*, New York, pp. 51- 76.

Ghayamghamian, M. R., Tobita, T., Iai, S., & Kang, G. C. (2007). Reconnaissance *Report of July 16, 2007 Niigata-Ken Chuetsu-Oki, Japan, Earthquake. Journal of Seismology and Earthquake Engineering*, 9(1-2), 73-84.

Cirella, A., Piatanesi, A., Tinti, E., & Cocco, M. (2008). Rupture process of the 2007 Niigata-ken Chuetsu-oki earthquake by non-linear joint inversion of strong motion and GPS data. *Geophysical Research Letters*, 35(16).

Ichii, K., Seto, N., & Kidera, H. (2008). Characteristics of uplifting velocity of a buried pipe in liquefied ground. *In Geotechnical Earthquake Engineering and Soil Dynamics IV* (pp. 1-10).

Ishihara, K. (1984). Post-earthquake failure of a tailing dam due to liquefaction of the pond deposit. Proceedings, *International Conference on Case Histories in Geotechnical Engineering*, University of Missouri, St. Louis, Vol. 3, pp. 1129-1143

Ishihara, K. (1985). Stability of natural deposits during earthquakes, Proceedings, *11th International Conference on Soil Mechanics and Foundation Engineering*,Vol. 1, pp. 321-376.

Ishihara, K. (1993). Liquefaction and Flow Failure During Earthquake, *Geotechnique*,Vol. 43, No. 3, pp. 351-415,

Jefferies, M. Been, K., (2015).'' Soil Liquefaction: A Critical State Approach''. *Second Edition CRC Press*,

Koseki, J., Matsuo, O., & Koga, Y. (1997). Uplift behavior of underground structures caused by liquefaction of surrounding soil during earthquake. *Soils and Foundations*, 37(1), 97-108.

Koseki, J., Matsuo, O., Ninomiya, Y., & Yoshida, T. (1997). Uplift of sewer manholes during the 1993 Kushiro-Oki earthquake. *Soils and Foundations*, 37(1), 109-121.

Kramer, S. L. (1996). Geotechnical earthquake engineering. In prentice–Hall international series in civil engineering and engineering mechanics. *Prentice-Hall*, New Jersey.

Mogami, T., AND Kubu, .k. (1953) ''the behavior of soil during vibration'' , *proceeding , 3rd International conference on mechanics and foundation Engineering, zurich*, Vol 1, pp. 152-155

Scawthorn, C., Yanev, PI,.(1995) ''Preliminary report 17 January 1995, *Hyogo-ken Nambu, Japanese Earthquake,'' Engineering Structure*, Vol. 17, No. 3, pp. 146-157

Sharp, M. K., & Adalier, K. (2006). Seismic response of earth dam with varying depth of liquefiable foundation layer. *Soil Dynamics and Earthquake Engineering*, 26(11), 1028-1037.

Siyahi B, Arslan H. (2008). ''Earthquake induced deformation of earth dams.'' *Bull Eng Geol Environ*. 67:397-403

Tobita, T., Iai, S., Kang, G. C., & Konishi, Y. (2009). Observed damage of wastewater pipelines and estimated manhole uplifts during the 2004 Niigataken Chuetsu, Japan, and earthquake. In TCLEE 2009: *Lifeline Earthquake Engineering in a Multihazard Environment* (pp. 1-12).

Tokida, K., Ninomiya, Y., & Azuma, T. (1970). Liquefaction potential and uplift deformation of underground structure. *WIT Transactions on The Built Environment*, 3.

Tokimatsu, K., Kojima, H., Kuwayama, S., Abe, A., & Midorikawa, S. (1994). Liquefaction-induced damage to buildings in 1990 Luzon earthquake. *Journal of Geotechnical Engineering*, 120(2), 290-307.

Yegian, M. K., Gharaman, V, G., Harutiunyan, R. N. (1994). ''Liquefaction and embankment failure case histories, 1988 Armenai earthquake,'' *Journal of Geotechnical Engineering*, ASCE, Vol. 120, No. 3, pp.581-596.

Yoshimi, Y., & Tokimatsu, K. (1977). Settlement of buildings on saturated sand during earthquakes. *Soils and Foundations*, 17(1), 23-38.

Youd, T, L. Hoose, S, N. (1976). Liquefaction During 1906 San Francisco Earthquake, *J.Geotech Engrg*. Div., ASCE, Vol. 102, NO. 5, May, pp. 425 – 439

Youd, T, L. Hoose, S, N. (1977).Liquefaction susceptibily and geologic setting. *Proceedings, 6th World Conference on Earthquake Engineering*, New Dehli, Vol. 3, pp. 2189 – 2194.

Youd, T, L. (1984). Recurrence of liquefaction at the same site. *Proceedings, 8th world Conference on Earthquake Engineering*, Vol.3 pp.231-238

Youd, T, L.(1991).Mapping of earthquake – induced liquefaction for seismic zonation, Proceedings, 4th *International Conference on Seismic zonation, Earthquake Engineering Research Institute, Stanford University*, Vol. 1, pp. 111-147

Youd, T. L., et al (1985). ''The Borah Peak, Idaho earthquake of October 28, 1983—liquefaction.'' *Earthquake Spectra*, Vol. 22, No. 1, pp. 71-89.

Youd, T, L. Hansen, C, M. Bartllet, S, F. (2002). Revised Multilinear Regression Equations for Prediction of Lateral Spread Displacement, J. *Geotech Geoenviron Eng*,. Vol. 128, No. 12, pp. 1007- 1017

Wang, W. (1979).'' Some findings in soil liquefaction,'' *Water Conservancy and Hydroelectric Power Scientific Research Institute,* Beijing, China.

Wong, W. (1984). Earthquake damages of earth dams and levees in relation to soil liquefaction and weakness in soft clays, Proceedings, *International Conference on Case Histories in Geotechnical Engineering*, Vol. 1, pp. 511-521.

Wong, R. T., Seed, H. B., Chan, C. K. (1975). ''Liquefaction of gravelly soil under cyclic loading conditions,'' *Journal of Geotechnical Engineering Division*, ASCE, Vol. 101, No. GT6, pp. 571-583.

A COMPARATIVE STUDY ON VIBRATIONAL PROPERTIES OF GLASS FIBER REINFORCED EPOXY COMPOSITES WITH EFFECT OF OLIVE POMACE PARTICLES CONTENT

Mohamad Alsaadi[1], Ahmet Erkliğ[2], Ahmed Shihan[2]
[1]University of Technology, Materials Engineering Department, Baghdad 10066, Iraq.
[2]Gaziantep University, Faculty of Engineering, Mechanical Engineering Department, Gaziantep 27310, Turkey.
phd.mohamadalsaadi@gmail.com, erklig@gantep.edu.tr

ABSTRACT: This work aims to study the effect of the mixing of natural particles of micro-size olive pomace (OP) on the vibrational properties of glass fiber reinforced polymer composite (GFRP). Hence, the vibrational behavior of recycled olive pomace filled glass fiber reinforced epoxy composites was examined in order to develop an engineering material for industrial applications. The modifying of GFRP composite was conducting by adding six weight fractions of olive pomace (0.5, 1, 2, 5, 10, and 15%) with grain size of (75 µm). The composite specimens were prepared by Hand-Lay-up technique and cut according to ASTM standards. It has found the maximum damping ratio was obtained at 10 wt% addition of olive pomace. Damping ratio is increased to the value of 0.407 with increment of 70 % higher than unfilled GFRP composite.

Key words: Glass fiber, olive pomace, epoxy, hybrid composite.

INTRODUCTION

Natural fibers like sisal, banana, jute, oil palm, kenaf, recycled jute and coir have been utilized as a reinforcement materials for advanced composite and used in engineering applications such as automobile, aerospace, consumer goods, furniture, and civil structures. Hence, the merge of reinforcement materials (particle and fiber) in brittle matrices can lead to new materials with outstanding mechanical characteristic include the features of both the fiber and matrix (Termonia 1990; Alsaadi et al. 2017, 2018; Bulut et al. 2018). Furthermore, it is becoming more and more significant in advanced engineering systems for enhanced vibration, noise control, dynamic stability plus fatigue and impact resistance. It is a necessary for reinforcement of damping in lightweight structural composite materials, So that they may be more utilized in the design of high-performance machines, tool and structures (Finegan 1999). Alaa Abd Mohammed (2015) studied the effect of data seeds (DS) and olive seeds (OS) particles filled epoxy resin on the tensile and impact characteristic. When powders of dates seeds and olive were added to the epoxy matrix at weight fraction of (0, 8, 13, and 18 wt%) with grain size of (300-450 and 600 µm), it's found the higher value of modulus of elasticity and tensile strength happened at (18 wt%) and grain size of (300 µm). Qutaiba (2011) studied the usage of powdered olive pits as a new filler material as a new series of sustainable reinforced polymer composite materials to be used with epoxy resin. It was found that the mechanical features of composites reinforced with treated olive pits were significantly improved as compared with that of composites reinforced with untreated olive pits. Rodrigo et al. (2012) investigated valorization of

some lignocellulose agro industrial remains to gain bio-polyols, The valorization of renewable and much resources (date seed, olive stone, corncob, rapeseed cake and apple pomace) from industrial activities was achieved by mild liquefaction utilize polyhydric alcohols to get bio-polyols that create an interesting optimal for industrial divisions specially polyurethanes. Karmaker et al. (1996) made composites by the use of jute, kenaf fiber and polypropylene resins. They stated that the mechanical characteristic of jute fiber is best than that of kenaf fiber. Ichazo et al. (2001) noticed that the addition of saline treated wood flour to PP produced a sustained increase in the tensile strength and the tensile modulus of the composite. Misra et al. (2002) studied the composites and their tensile stress-strain performance when fiber loading is 40% by weight. There was about 22% increase in tensile strength for alkali treated (5%) sisal polyester bio composite. Kenny et al. (1995) studied the nonlinear behavior of composite laminates, developed a micromechanical model including the plastic behavior of the matrix. They exhibited that there is an association between the plastic deformation and the increase of damping at high stresses. Hwang et al. (1987) studied the micromechanical modeling of both damping and hardness in composite offered a strain energy approach including the fiber/matrix interface. Chandra et al. (1999) highlighted the desirability of including damping as a restraint from their work on damping based design with composite materials. The case study result in lower weight configurations, improved dynamic performance, higher strength and stiffness of the composite structure.

As a conclusion on the summarized literature, the effect of fillers on the composite material can be clearly seen. Weight rate or volume rate of additive materials affect almost all properties of the composite material. Type of additives may affect with different weight rate/volume rate of olive pomace (additive) or different filler type. Also, the Mathematical model results show that the weight fraction of particle has a higher effect than grain size on the physical and mechanical properties of composite materials. The success of combining natural particulate fillers with polymer matrices results in the improvement of mechanical properties of the composites compared with the matrix materials. These fillers can be acquired from renewable sources and easily recyclable. Despite their little strength, they can produce composites with superior specific strengths.

MATERIALS AND PROCEDURES

Materials

The matrix Materials is epoxy resin (Momentive-MGS L285) used with hardener by a stoichiometric ratio of (100:40). The reinforcing Materials are glass fibers (E-Glass) and olive pomace particles (Figure 1). In the production of composite specimens, the olive pomace particles added in epoxy (Figure 2) with six various weight fractions as 0.5, 1.0, 2, 5, 10 and 15 wt. % with a grain size of (75 µm). Table 1 shows the chemical composition of olive pomace.

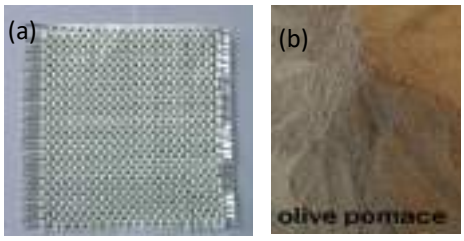

Figure 1 (a) Glass fibre and (b) olive pomace.

Figure 2 (a) Epoxy (b) Hardener (c) olive pomace.

Table 1 The chemical composition of olive pomace.

Crude protein	Crude fiber	Crude fat	Soluble carbohydrates	Ash
5.6%	57.5%	3.2%	20.7%	13.0%

Composites Production and Samples Preparation

The composites were prepared by adding particulate olive filler in epoxy resin with six different particle contents. Using a mechanical stirrer, the particulate filler quantity was mixed for 30 minutes with epoxy at a constant speed of 700 RPM to obtain a homogeneous particulate blend. Then hardener was mixed with particulate blend for quick setting of composite. Then, the particulate blend was applied to the fibers layer by layer until all the 8 layers were placed at room temperature 25°C. Afterward, modified laminated fabrics with dimensions of 150 mm × 200 mm were subjected to 0.3 MPa pressure in the flat molds for 1 h curing time with 80 °C temperature. Afterward, laminate were cooled to the room temperature under the pressure (Figure 3 shows production unit). After the production, the composite laminates were cut to produce vibration specimens with size of 200 mm × 12.7 mm according to ASTM standards. Figure 4.

Figure 3. Production unit.

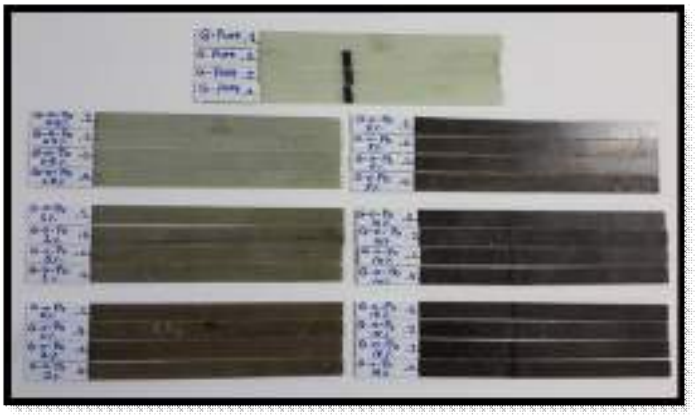

Figure 4. Vibration test specimens

Vibration and Damping Tests

The vibration properties of the olive pomace particle-filled GFRE composite specimens were determined at room temperature. The vibration test were occurred according to the ASTM E756. This system is based on a time domain technique that exhibits exponential decay characteristic of the free response of the structure to obtain damping ratio information. The damping ratio in composite materials is essential to avoid failure in the mechanical parts that are exposed to the vibration and it necessary to calculate the damping time **(**Figure 5**)** because it helps us to extend the life of these mechanical parts (ASTM E756).
The vibration properties were determined from the data of the testing machine using the Eqs. (1) to (3) below according to ASTM standard.

$$\delta = \frac{1}{n}\ln\frac{A_\circ}{A} \quad (1)$$

$$\xi = \frac{1}{\sqrt{1+\left(\frac{2\pi}{\delta}\right)^2}} \quad (2)$$

Material storage modulus ($E^{'}$) can be obtained from Euler-Bernoulli beam theory as:

$$\omega_1 = \frac{1.875^2}{2\pi L^2}\sqrt{\frac{E\prime I}{\rho A}} \quad (3)$$

Where δ is the logarithmic decrement, A_o is the maximum magnitude of first cycle and A is the maximum magnitude of nth cycle and ξ is the damping ratio.
Loss modulus of the beam ($E^{''}$) can be found using storage modulus. Relationship between loss and storage modulus is given in equation 4:

$$E^{''}(\omega) = 2E^{'}(\omega)\xi(\omega) \quad (4)$$

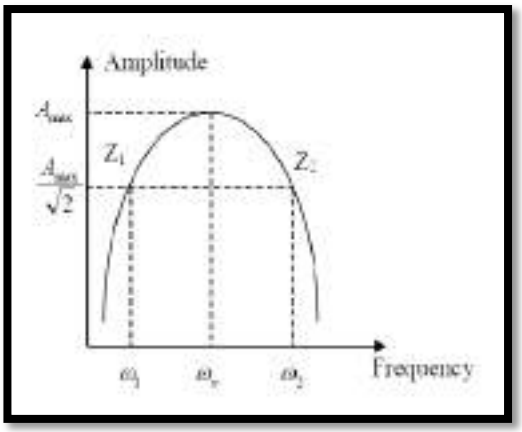

Figure 5 Method for determining maximum amplitude – frequency.

The experimental method used for specimens' analysis to calculate damping ratios and natural frequencies of GFRP composite. Accelerometer for output signal acquisition, impact hammer for stimulus force signal, data acquisition card device and the specimen analysis explain in Figure 6.

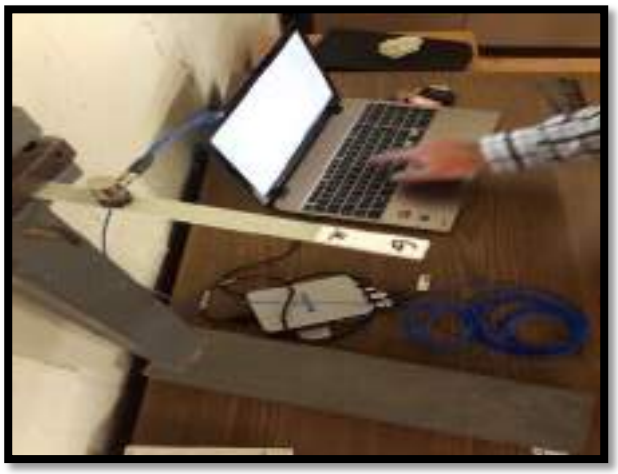

Figure 6. Data card, Accelerometer device, and impact hammer

RESULTS AND DISCUSSIONS

The variation of natural frequency values with damping characteristics of the composite laminates are given in Table 2. The Figures 7 to 10 show the vibration and damping properties. The results imply that the increase in modulus causes a trend of increase in the natural frequency (Liao and Wells 2011). However, increase in stiffness may not lead to increase in the damping ratio, since the damping characteristic of the structures strictly depend on viscoelastic characteristic, which means the better absorption of vibration energy and good storage modulus (Alsaadi et al. 2018). It is clear that the addition of olive pomace particles significantly improves the storage modulus about by 13.84% for GFRP-OP 5 composite, while loss modulus increases about by 74.21% for GFRP-OP_{10} composite. This means that addition of olive pomace

particles enhances the energy dissipation capacity of the structure followed by a decrease of the stiffness.

Table 2 Vibration results of the glass fiber reinforced epoxy composite filled with olive pomace.

Composite type	OP content (wt%)	Natural frequency, ω_n (Hz)	Damping ratio, ξ	Loss modulus È Gpa	Storage modulus Ē Gpa
GFRP	0	37.98	0.239	8.363	17.48
GFRP-$OP_{0.5}$	0.5	44.59	0.185	9.175	24.8
GFRP-OP_1	1	36.33	0.250	6.367	12.7
GFRP-OP_2	2	39.63	0.271	8.309	15.3
GFRP-OP_5	5	44.51	0.278	1.105	19.9
GFRP-OP_{10}	10	44.59	0.407	1.457	17.9
GFRP-OP_{15}	15	42.94	0.296	6.793	11.5

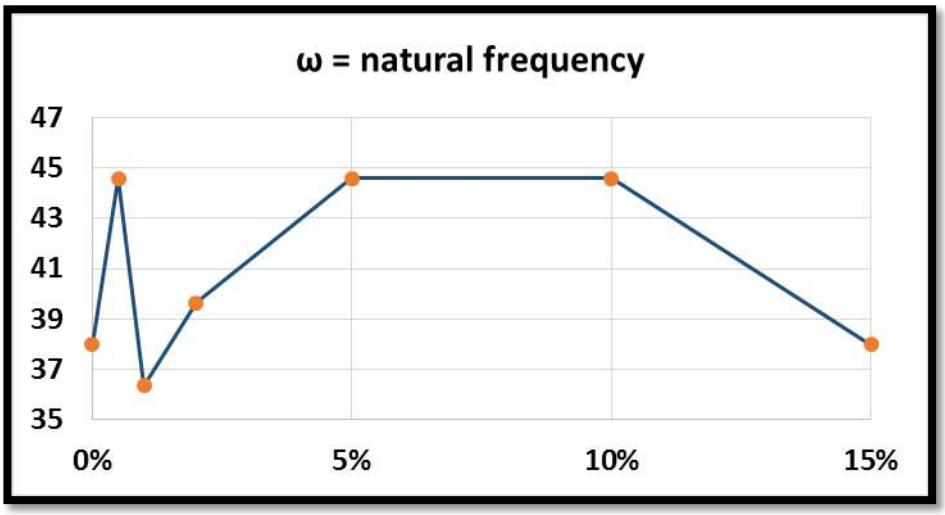

Figure 7 natural frequency - Particle content (wt%) diagram of the glass fiber reinforced epoxy composite filled with olive pomace.

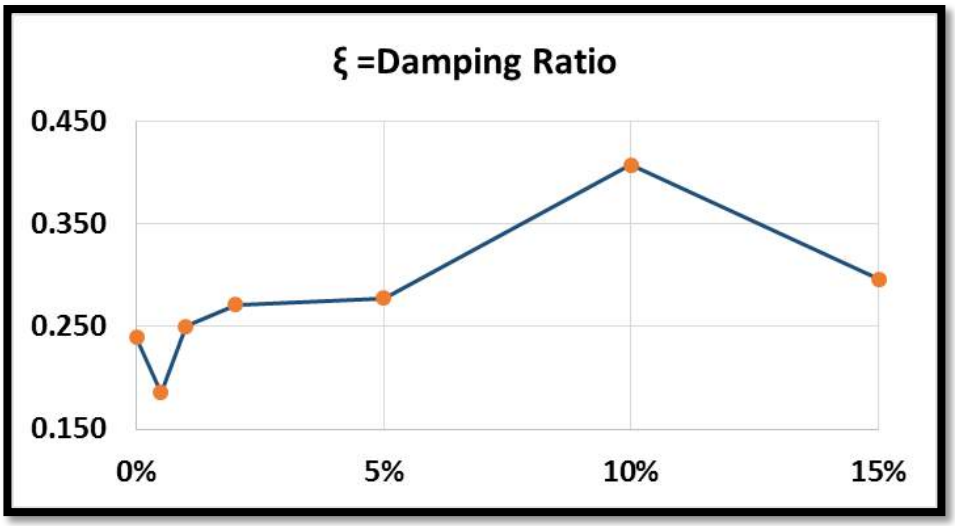

Figure 8 Damping Ratio - Particle content (wt%) diagram of the glass fiber reinforced epoxy composite filled with olive pomace.

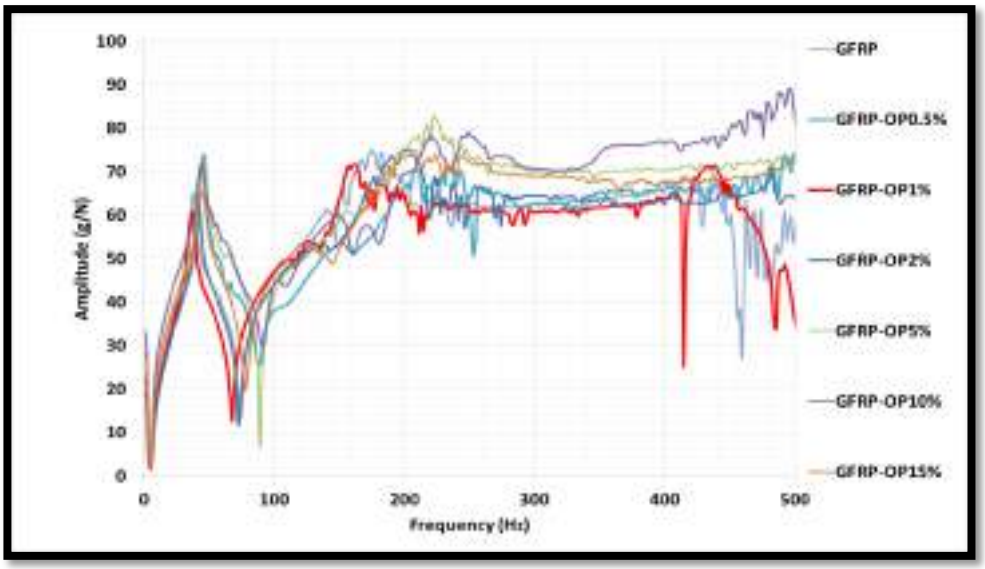

Figure 9 Amplitude – Frequency diagram of the glass fiber reinforced epoxy composite filled with olive pomace.

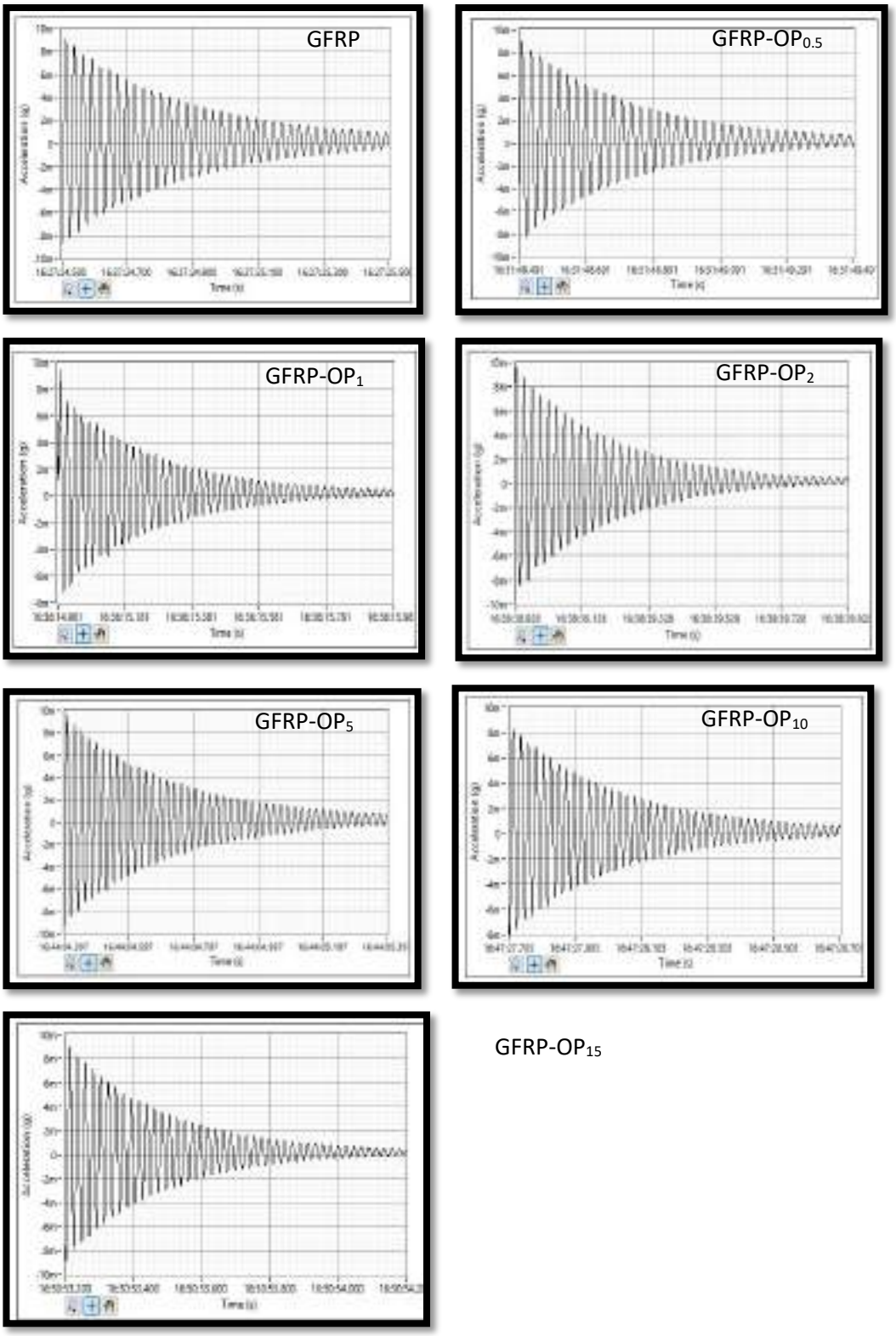

Figure 10 Time responses of samples.

CONCLUSIONS

The effects of olive pomace industrial waste particles with variation in contents on natural frequencies and damping properties of the glass fabric/epoxy composites

were examined experimentally. The maximum damping ratio is obtained at 10 wt% of olive pomace. The damping ratio is increased to 0.407 higher by 70% than GFRP composite. The maximum storage modulus value is obtained at 0.5 wt% of olive pomace. The Loss modulus is increased to 24.76 GPa with increment of 40.5 % higher than GFRP composite. The maximum loss modulus is obtained at 10 wt%. The storage modulus is increased to 83.63 GPa with increment of 74.2 % higher than GFRP composite.

REFERENCES

Alsaadi, M., Bulut, M., Erkliğ, A., & Jabbar, A. (2018). Nano-silica inclusion effects on mechanical and dynamic behavior of fiber reinforced carbon/Kevlar with epoxy resin hybrid composites. Composites Part B: Engineering.

Alsaadi M, Erkliğ A, Albu-khaleefah K. Effect of Pistachio Shell Particle Content on the Mechanical Properties of Polymer Composite. Arabian Journal for Science and Engineering. 2018;43(9):4689–4696.

Alsaadi M, Ugla AA, Erklig A. A comparative study on the interlaminar shear strength of carbon, glass, and Kevlar fabric/epoxy laminates filled with SiC particles. Journal of Composite Materials. 2017;51(20):2835-44.

Alsaadi M, Erkliğ A. A comparative study on mode I and mode II interlaminar behavior of borax and SiC particles toughened S-glass fabric/epoxy composite. Arabian Journal for Science and Engineering. 2017 Nov 1;42(11):4759-69.

Alsaadi M, Erkliğ A. Effect of perlite particle contents on delamination toughness of S-glass fiber reinforced epoxy matrix composites. Composites Part B Eng 2018;141:182-190.

ASTM E756. E756 - 05(2017) Standard Test Methods for Measuring Vibration Damping Properties of Materials.

Bulut M, Alsaadi M, Erklig A. A comparative study on the tensile and impact properties of Kevlar, carbon, and S-glass/epoxy composites reinforced with SiC particles. Materials Research Express. 2018, 5(2), 025301

Bulut M, Alsaadi M, Erkliğ A. Tensile and impact characterization of S-glass/epoxy composite laminates containing microscale borax, perlite, and sewage sludge ash particles. Journal of the Brazilian Society of Mechanical Sciences and Engineering. 2018;40(4):199.

Liao, Y., & Wells, V. (2011). Modal parameter identification using the log decrement method and band-pass filters. Journal of Sound and Vibration, 330(21), 5014-5023.

Chandra, R., Singh, S. P., & Gupta, K. (1999). Damping studies in fiber-reinforced composites–a review. Composite structures, 46(1), 41-51.

Finegan, I. C., & Gibson, R. F. (1999). Recent research on enhancement of damping in polymer composites. *Composite Structures*, ***44***(2), 89-98.

Hwang, S. J., & Gibson, R. F. (1987). Micromechanical modeling of damping in discontinuous fiber composites using a strain energy/finite element approach. Journal of engineering materials and technology, 109(1), 47-52.

Qutaiba , A. (2011). Investigation into the modes of damage and failure in natural fiber reinforced epoxy composite materials (Doctoral dissertation, University of East London).

Misra, S., Misra, M., Tripathy, S. S., Nayak, S. K., & Mohanty, A. K. (2002). The influence of chemical surface modification on the performance of sisal-polyester biocomposites. Polymer Composites, 23(2), 164-170.

Mohammed, A. A. (2015)" Investigation of Tensile and Impact of Composite Materials Reinforced with Natural Materials. The Iraqi Journal for Mechanical and Material Engineering, Vol.15, No2.

Karmaker, A. C., & Shneider, J. P. (1996). Mechanical performance of short jute fiber reinforced polypropylene. Journal of materials science letters, 15(3), 201-202.

Rodrigo, B., Serrano, L., & Labidi, J. (2012). Valorization of some lignocellulosic agro-industrial residues to obtain biopolyols. Journal of Chemical Technology and Biotechnology, 87(2), 244-249.

Termonia, Y. (1990) Tensile strength of discontinuous fiber-reinforced Composites. *Material Science*, **25**:4644-4650.

Ichazo, M. N., Albano, C., Gonzalez, J., Perera, R., & Candal, M. V. (2001). Polypropylene/wood flour composites: treatments and properties. Composite structures, 54(2), 207-214.

SIMULATION OF GASIFICATION PROCESS USING RESTRICTED CHEMICAL EQUILIBRIUM METHOD

Mahmut Caner ACAR
ITU Faculty of Mechanical Engineering
acarma@itu.edu.tr

Yakup Erhan BÖKE
ITU Faculty of Mechanical Engineering
boke@itu.edu.tr

ABSTRACT: Gasification process could be efficiently used to create useful gas mixture which is called synthesis gas or briefly, syngas, by gasifying the carbonaceous materials (such as biomass and coal). The syngas is mainly composed of hydrogen, carbon monoxide, carbon dioxide, methane and nitrogen. The percentage of each component in this gas mixture affects the quality and heating value of the syngas. Therefore, it is important to predict the syngas composition accurately. In this study, a simulation model has been developed using Aspen (Advanced System for Process Engineering) Plus to predict the syngas composition and gasifier performance under different operating conditions. The developed model is based on Gibbs free energy minimization. Also, restricted chemical equilibrium method was applied to arrange the model results with the experimental data. Results showed good agreement between simulation prediction and experimental data. Maximum deviation was about %7 for CO_2 composition. Sensitivity analysis and optimization study were carried out after the model validation process for different steam to biomass (S/B) and equivalence ratios (ER). The amount of H_2 and CO_2 increase while CO and CH_4 decrease with rising S/B ratio. The S/B ratio has a positive effect on gas yield and cold gas efficiency (CGE) and negative effect on low heating value (LHV). ER increases the CO_2 composition and conversely decreases the H_2 and CH_4 compositions that cause to drop gas yield, CGE and LHV. However, CO composition maintains almost the same level in terms of ER. For the same S/B ratios, increasing ER degrades the gasifier performance because of the decreasing LHV and CGE.

Key words: Gasification, restricted chemical equilibrium, syngas, simulation model.

DESIGN AND ANALYSIS OF INDUSTRIAL HEAT TREATMENT FURNACE

Haydar KEPEKCI
Beykent University
haydar893@gmail.com

ABSTRACT: Industrial furnaces are the technical units that provide a number of properties to metallic materials and that are placed in the interior or are continuously loaded to provide industrial applications for the purpose of raising the process temperature to the process temperature and keeping it at the required temperature. Industrial furnaces are frequently used in the glass industry, chemical plants, laboratories, paper, textile industry and metal industry. For this reason, they are of great importance. In this study, varieties of industrial furnaces which are of great importance for industrial enterprises, processes performed in these furnaces, fuels used in furnaces and furnace building materials are discussed. It also describes how an oven is designed in detail and heat transfer calculations of a sample oven using refractory bricks. Drawings of the designed oven were drawn using the SolidWorks program.

Key words: Industrial Furnaces, Heat Treatment, Refractory Bricks, Heat Transfer, SolidWorks.

INTRODUCTION

Metals have become indispensable materials of our life from the past to the present day. However, due to operating conditions, it is always a big problem that metals do not carry optimum properties. For this reason, people needed heat treatment.

Heat treatment; By applying the heating, standby and cooling stages of metals, the properties of the materials are changed in the desired manner. In thermal processes, the change of properties should be done only in the form of internal structure change, not dimensionally. Furnaces were needed to make these changes.

In this study, the design of an industrial furnace is explained. It is desired that the designed furnace be heated up to 1500 ^{o}C and the internal volume should be 10 liters. First of all, the materials that can withstand the temperature have been researched and the ones that are suitable have been selected.

It has been decided to use refractory bricks that can withstand such a high temperature for the walls of the furnace. The refractory brick catalogs have been examined, one of them is preferred for this project. Subsequently, the type of mortar was determined to hold the bricks.

For the heating, resistance temperature which can reach 1500 degree temperature is chosen. Among the resistance wires to be used at high temperature; The Super NC model of the Kanthal brand has been found suitable.

Then the heat transfer coefficients and some properties of the materials we have decided to use have been investigated and the necessary information has been reached. Mathematical calculations have been made in line with this information and the design

has been completed in general terms. The heat treatment furnace with the required design measurements is drawn on the computer using the SolidWorks program.

Heat Treatment

"Heat treatment"; in metal materials, it refers to proper property changes in solid state with temperature changes. In heat treatment, "heating" means heating parts to a certain temperature, "waiting" in waiting for a suitable time at this temperature, and "cooling" in the case of lowering the temperature to room temperature in accordance with a certain program. [1]

Features that can be changed in heat treatment;

- The hardened structure which by any method can be softened. Machinability in the material is increased.
- In the inner structure of the material, more homogeneous and fine grain is obtained.
- The inhomogeneous distribution of alloying elements which can remain on the surface after casting and rolling can be largely eliminated by heat treatment.
- It is possible to provide grain roughness with the aim of facilitating the machining.
- By cold forming, the elongated crystals in the shaping direction are transformed into a smaller and spherical form. The material is softened and the cold formability is gained again.
- By austenite stabilization in the steels, the quality is increased. Thus, resistance to cold and corrosion can be increased.
- A glossy surface can be provided to prepare the material surface for surface coating operations such as enamel. [2]

Definition of Furnace

The technical units that are placed inside or permanently charged with the materials that heated economically and raise the process temperature and hold the required time at this temperature are called Furnace. Generally, ovens are heated to 300 degrees Celsius and those for higher temperatures are called Furnace.

Energy requirements in industrial furnaces are supplied as chemical energy through incineration via the burning of solid, liquid or gaseous fuels. It can also be used physical energy in the form of electrical resistance, arc or induction heating.

According to the purpose of using the furnaces; we can separate two main groups as melting and heating furnaces. In general, use places can be listed as follows;

- Melting and refining furnaces of iron and other metal alloys
- Heating ovens for hot forming of metals
- Furnaces for heat treatment of metals
- Enrichment and earthing furnaces in ore preparation
- Furnaces used in the ceramic and brick production

- Glass industry furnaces

- Laboratory furnaces [3]

Furnace Building Materials
Refractory materials and hot-resistant metal alloys are used as building materials in industrial furnaces. The structure of the refractory materials consists of oxide minerals such as SiO_2, Al_2O_3, and Mg, which are formed by interconnections such as carbide, boron and nitrile. They are very resistant to high temperature, temperature changes and oven atmosphere.
As the metal material, heat resistant steel cast iron, copper and its alloys and resistance materials are used. Since copper and its alloys are not heat resistant, they must be absolutely cooled during use. In the outer parts of the furnace, the unalloyed steels are also used as construction materials. [4]

Refractory Materials
It is a kind of operating materials that should be used absolutely everywhere that working at high temperatures. There is a constant need for refractory materials. Since these materials have a specific service life, they have to be renewed at regular intervals.

Heat Generation in Fuel-Heated Furnaces
Wood and charcoal from solid fuels are rarely used in industrial furnaces due to their high price and low thermal furnace. Other fuels are preferred in the oven to provide better temperature distribution and automatic control.
When using gas or fuel, the following advantages are achieved when operating the furnace:
- Easy transport with the pipe under pressure
- Fuel and air can mix very well, so work with lower air count
- Providing heat supply using more burners
- Provide a more appropriate flame form, depending on furnace characteristics
- The fuels in the gas phase completely ashless, and the fuel is partly ashless. [3]

METHODS

Designed Furnace Intormation
Furnace Internal Volume: 10 dm^3
The maximum temperature at which the furnace can rise: 1500 ^oC

Table 1. Technical Data of Brick [5]

Item of Selected Brick	JM 28
Classification Temperature	1540 ^oC
Bulk Density	0.9 g/cm^3
Thermal Conductivity	0.37 W/m.K
Chemical Analysis	%67 Al_2O_3
Common Size of Brick	230 x 114 x 65 mm

Type of grout to be used: SÖRHARÇ A190 HSK

Table 2. Wire Information [6]

Item of Selected Wire	Kanthal Super NC
Classification Temperature	1800 °C
Chemical Analysis	$MoSi_2$ + Alüminyum Silisyum
Bending Force (1550 °C'de)	450 Mpa
Compression Force	1400-1500 Mpa
Bulk Density	5.6 g/cm^3
Fracture Strength	3-4 MPa
Hardness	9 GPa
Thermal Conductivity	20 – 600 °C'de: 30 W/Mk 600 – 1200 °C'de: 15 W/Mk

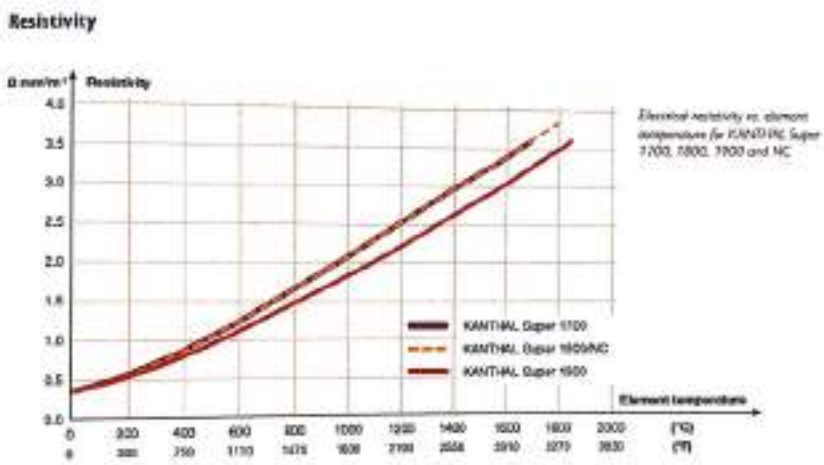

Fig 1. The Resistivity-Temperature Graph for Finding Wire Diameter Resistance [6]

From at the above graph, wire diameter resistance has been found for 1500 °C as 3.3 Ω mm^{2}m^{-1}

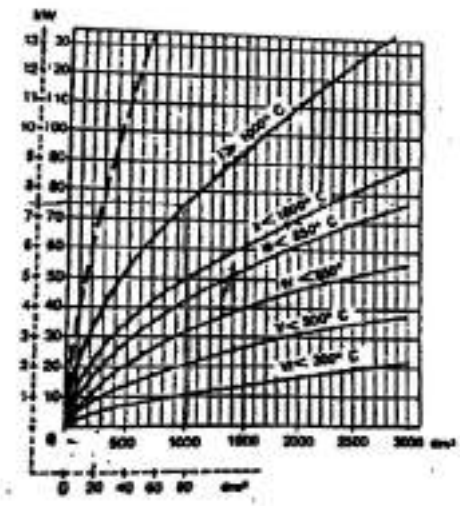

Fig 2. Graph of Furnace Power Depending on Volume [7]

From at the above graph, Furnace Power has been found 7.5 KW

Calculations of Wire

Surface Load: 1.2 W/cm^2

Because it is the trifle current, the power from a faze;

F/3 = 7500/3 = 2500 W

Wire diameter: (1/2.91) x [(F/U)^2 x (p/q) x C_t] ^ (1/3)

d= (1/2.91) x [(2500^2/2500 x 3.3) x (3.3/1.2)] ^ (1/3)

d= 4.38 mm

Table 3. Properties of Resistive Wires According to Diameter and Type [7]

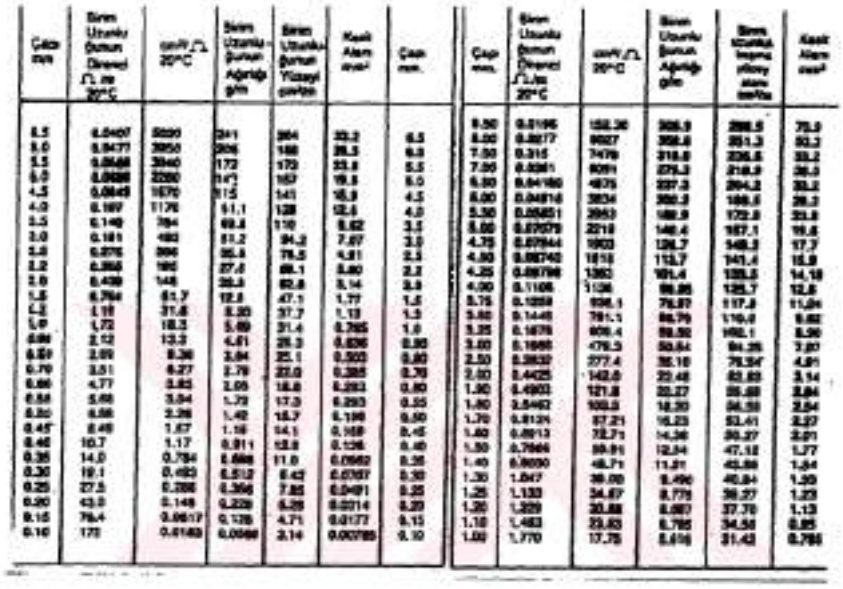

From at the above graph, 1-meter wire resistance has been found 0.0649 Ωm and 1-meter wire weight has been found 115 g/m.

Total wire size: 1 = R_{20} / R_m = 3.3 / 0.0649 = 50.847 m

Because the current is triplet;

l_t : 1 x 3 = (50.847 x 3) = 152.541 m

Total wire weight (G_{tot}): (152.541 x 115) = 17542.215 gr= 17.54 kg

Specification of spiral gauges = D/d= 6

D: Spiral diameter

d: Wire diameter = 4.38 mm

D/4.38 = 6

D= 26.28 mm
Number of turns (W): [1000 x l_t] x [(D-d) x π]
W: [1000 x 152.541] / [(26.28-4.38) x π]
W: 2217
Closed spiral length (L_w): W x d
L_w: (2217) x (4.38) = 9710 mm
Open spiral length (L) = W x S
S: Pitch
S/d: 3
S: 3 x 4.38 = 13.14
L: 2217 x 13.14 = 29131 mm

Computation of Heat Transfer
k: Thermal conductivity [W/mK]
h: Heat transfer coefficient [W/m^{2}K]
q_x: Unit heat transfer amount [W]
R: Thermal resistance [K/W]
Δ_X: Material thickness [m]
U: Total heat transfer coefficient
R= 1/ (U x A) = 1/A ($1/h_A + \Delta_{x1}/k_1 + \Delta_{x2}/k_2 + \Delta_{x3}/k_3 + \Delta_{x3}/k_3 + \Delta_{x4}/k_4 + 1/h_B$)
q_X= U x A x (T_A-T_B) formulas are used.
The values that we have are,
h_{air} : 17 [W/m^{2}K]
k_{brick} : 0.37 [W/mK]
$k_{glass\ wool}$: 0.038 [W/mK]
$k_{shit\ metal}$: 58 [W/mK]

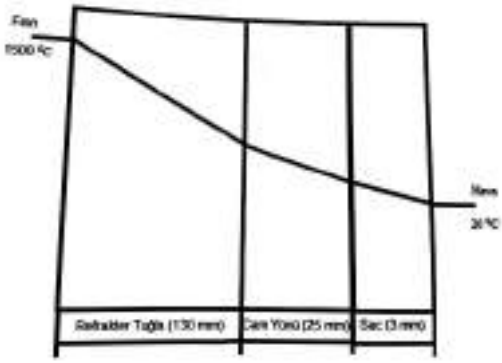

Fig 3. Two-Dimensional View of the Side, Rear, Bottom and Top Surfaces

R= 1/A ($1/17 + 130.10^{-3}/0.37 + 25.10^{-3}/0.038 + 3.10^{-3}/58 + 1/17$)
R= 1/A ($0.0588 + 0.3513 + 0.6578 + 5.1724.10^{-5} + 0.0588$)
R= 1/A (1.1267) [K/W]

The amount of heat transfer through the side surfaces (for a surface)
Area (A)= 171 x 275 = 47025 [mm^2] = 0.0470 [m^2]
R= 1/A (1.1267) = 1/0.0470 (1.1267) = 23.97 [K/W]
q_X = (T_A-T_B) / R= (1500-20) / (23.97) = 61.73 [W]

The amount of heat transfer through the rear surface
Area (A) = 171 x 214 = 3694 [mm²] = 0.037 [m²]
R = 1/A (1.1267) = 1/0.037 (1.1267) = 30.45 [K/W]
$q_X = (T_A - T_B) / R = (1500-20)/(30.45) = 48.60$ [W]
The amount of heat transfer through the Bottom and Top
Area (A) = 214 x 275= 58850 [mm²] = 0.058 [m²]
R = 1/A (1.1267) = 1/0.058 (1.1267) = 19.42[K/W]
$q_X = (T_A - T_B) / R = (1500-20) / 19.42 = 76.18$ [W]

The amount of heat transfer through the Front Surface (hatch)

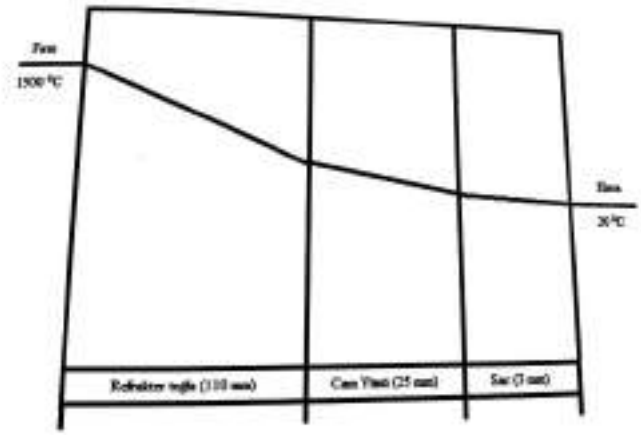

Fig 4. Two-Dimensional View of the Front Surface

Area (A) = 171 X 214 = 36594 [mm²] = 0.0365 [m²]
$R = 1/A\ (1/17 + 110.10^{-3}/0.37 + 25.10^{-3}/0.038 + 3.10^{-3}/58 + 1+/17)$
R= 1/A (1.07267) [K/W]
R= 1/0.0365 (1.07267) = 29.3127 [K/W]
$q_X = (T_A - T_B) / R = (1500-20) / (29.3127) = 50.49$ [W]

Total Heat Transfer
$q_{tot} = 2(q_{side}) + q_{rear} + 2(q_{bottom\text{-}top}) + q_{hatch}$
$q_{tot} = 2\ (61.73) + (48.60) + 2(76.18) + (50.49)$
$q_{tot} = 374.91$ [W]

Enclosure Sheet Metal Exterior Surface Temperature
$q_{tot} = (T_{Enclosure\ Sheet\ Metal} - T_B) / (1/17) = 374.91$
$T_{Enclosure\ Sheet\ Metal} - 20 = 22.05$
$T_{Enclosure\ Sheet\ Metal} = 42.05$ [°C]

RESULTS AND FINDINGS

The size of this furnace designed by various calculations is determined as 473x657x470 [mm]. The amount of heat passing through the side surfaces of the designed furnace; 61.73 W for each surface, 48.60 W of heat from the rear surface, the amount of heat passing through the floor and ceiling surfaces; 76.18 W for each surface, 50.49 W of

heat passing through the front surface and 374.91 W of total heat transfer. Furthermore, the temperature of the casing sheet is predicted to be 42.05 ^{o}C.

CONCLUSION

In this study, an industrial heat treatment furnace was designed using refractory brick, glass wool and sheet metal for insulation. JM28 brick has been used in this design, which has an internal volume of 10 litres (214x171x275 [mm]) and can reach a maximum temperature of 1500 °C. Also a maximum temperature of 1540 °C, a thermal conductivity of 0.37 W/mK, and a wire capable of reaching a maximum temperature of 1800 °C were used.
Drawings of the designed oven were drawn using the SolidWorks software. Besides, as this PID control system, Eurotherm 2704 is preferred.[8] More precise measurement values can be obtained due to the use of this control system.

REFERENCES

Prof. M. Ali Topbaş, Çeliğin Isıl İşlemi, Yıldız Teknik Üniversitesi Publications:250, İstanbul, 1992.
Prof. M. Ali Topbaş, Isıl İşlemler, Prestij Basın Publications, İstanbul, 1993
Prof. M. Ali Topbaş, Endüstri Fırınları, Kurtiş Publications, İstanbul, 1991
Nuri Özden, Refrakter Malzemeler ve Döner Ateş Tuğlaları, Türkiye Çimento Sanayi, Ankara, 1982
Retrieved September 11, 2018 from http://www.ceceramicfiber.com/Products/DJM28Insulatingbrick.html
Retrieved September 11, 2018 from https://www.kanthal.com/globalassets/kanthal-global/downloads/furnace-products-and-heating-systems/heating-elements/mosi2-heating-elements/s-ka058-b-eng-2012-01.pdf
Osman Nuri Çelik, Nitrürasyon Tav Fırını Dizaynı ve Nitrürasyonu Etkileyen Parametlerin İncelenmesi, Master's Graduate Thesis, Anadolu Üniversitesi, 1989
Retrieved September 11, 2018 from https://www.eurotherm.com/products/temperature-controllers/multi-loop/2704

APPENDIX

Fig 5. General Appearance of the Designed Furnace

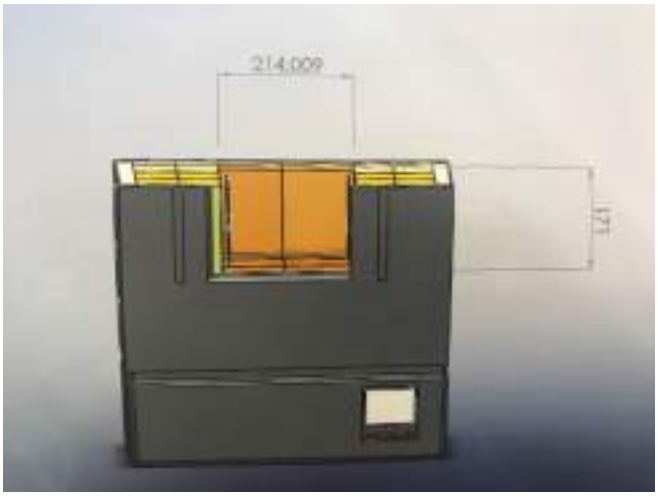

Fig 6. x-axis Cross-Sectional View of the Designed Furnace

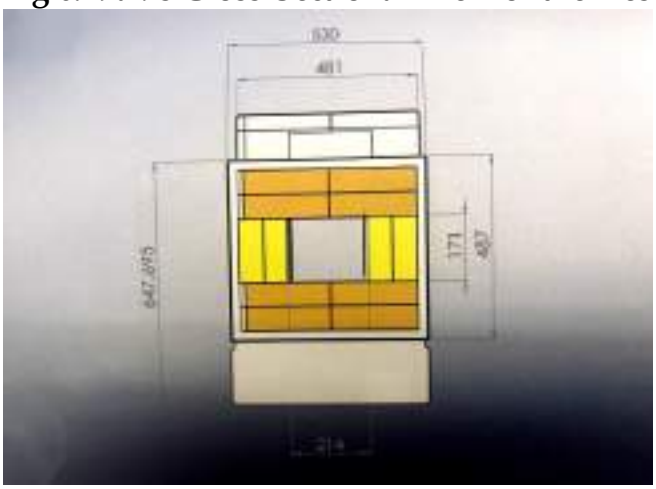

Fig 7. y-axis Cross-Sectional View of the Designed Furnace

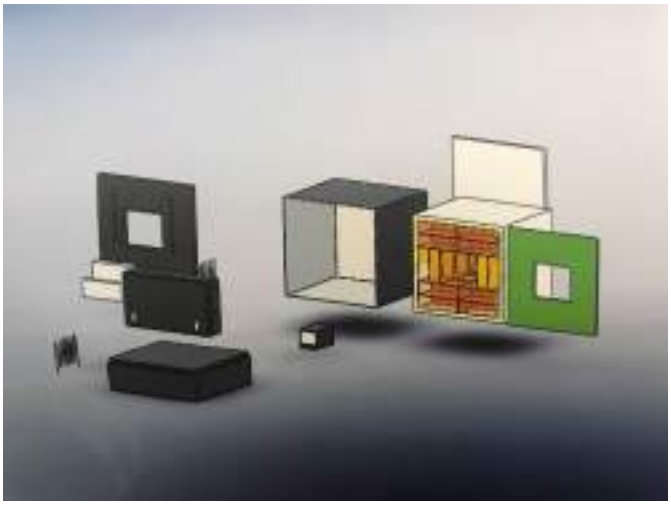

Fig 8. View of the Components of the Designed Furnace

FRESH PROPERTIES OF STEEL FIBER-REINFORCED SELF-COMPACTING CONCRETE

Sallal R. Abid*, Muammar H. Jebur, Ahmed A. Abbod, Samera Q. Kadhum, Noor A. Abdulhasan, Riyam Q. Hussein, sallal@uowasit.edu.iq, Wasit University/ College of Engineering / Civil Engineering Department

ABSTRACT: Self-compacting concrete (SCC) is a successful alternative for the conventional concrete in concrete works that include complex formwork and reinforcement details, especially for deep sections where external vibration is difficult to perform. SCC is known as highly flowable concrete that shows no potential of segregation or blocking around reinforcement. However, the presence of fibers is known to adversely influence the SCC fresh properties. This paper summarizes a case study on trial mixtures of SCC with two basic design strengths of 30 and 50 MPa and with different dosages of micro-steel fibers. The adopted volumetric contents of steel fiber are 0.5, 0.75, and 1.0%. Four fresh tests were used to evaluate the filling ability, passing ability, and stability of the SCC. These are the slump flow, T_{50}, ΔJ-ring, and rapid penetration tests. The test results showed that the inclusion of steel fiber adversely affects the desirable fresh properties of SCC and this effect increases as the fiber content increase. Several trial mixtures were tested and adjusted for each of the fiber contents. The adjustments were carried out by increasing the fine materials and reducing the coarse aggregate or in some cases by adding additional dosages of superplasticizer. As a result, eight SCC mixtures were introduced with different nominal design strengths and different fiber contents.

INTRODUCTION

Self-compacting concrete, which is also known as self-consolidating concrete, is a comparatively new type of concrete mixtures that can be considered as one of the major revolutions which had happened in the concrete industry during the recent decades. It was initially fabricated and developed by scientists in Japan during the late 1980's. SCC can be described as the concrete mixture that must be easily flowed, placed, and consolidated due to its own weight homogenously without any bleeding or segregation and without external vibration. This property gave SCC several advantages such as the more freedom in the design of concrete section size and reinforcement density, minimizing the construction time, reducing its cost, providing safer casting environment, decreasing the level of noise, enhancing the concrete surface finishing, and promoting the structure durability.

Like an ordinary concrete, SCC is manufactured from the mixing of cement, water, and aggregate but superplasticizer is an essential material to provide higher workability. Many mineral additives can be added to SCC mixture to increase the workability, control the content of cement, and consequently reduce the hydration heat. Stone powder, silica fume, fly ash, or ground blast furnace slag can be added to SCC mixture. Fibers also can be added to the SCC mixture. Steel and synthetic fibers were used in SCC in order to improve the concrete mechanical properties and minimize the segregation.

The fresh SCC mixtures must be fabricated to fulfill several requirements. Three essential properties should be obtainable, which are the filling ability, passing ability,

and segregation resistance. Easy and rapid tests should be applied in the site to give an important indication about the flowability of SCC mixtures. Filling ability can be tested by slump flow test, V funnel, and T_{50} test [1]. Filling ability tests are useful to estimate the horizontal flow of concrete in the open space if there is any obstacle. Passing ability is another SCC property which can give a sign of concrete ability to pass through obstructions such as reinforcement bars. Passing ability can be examined by many tests such as J-ring, L-box, and U-box [2, 3] test methods. The third essential fresh property of SCC is the resistance of segregation or stability, which can be studied by column or rapid penetration tests [4, 5]. Segregation tests provide a reliable estimation of whether SCC segregation is likely to occur.

Sahmaran et al. [6] studied the workability of steel fiber reinforced SCC. Two types of steel fibers were examined. The first is straight fibers (OL 6/16) with 6 mm and 37.5 length and aspect ratio, respectively. The second is (ZP 305) hooked ended with 30 mm and 55 length and aspect ratio, respectively. Hybrid fiber reinforcement was also used. Fibers were added with constant amount of 60 kg/m^3. Test results showed that there is a possibility to prepare SCC with 60 Kg/m^3 steel fibers, although some of the mixtures exceeded the maximum limits of fresh properties recommended by EFNARC [3]. To obtain better flowability for SCC mixtures with steel fiber reinforcement, mixture paste should be enlarged and that can be achieved by the increment of cementitious materials content, sand content, and the addition of admixtures. SCC with larger amount of (ZP 305) fibers had higher flowability, passing ability, and viscosity. Mixtures with only (OL 6/16) showed the highest compressive strength for both 28 and 56 days. On the other hand, the samples of equal quantity of the both types of fibers exhibited the highest splitting tensile strength.

Aslani and Nejadi [7] examined the mechanical properties of SCC which contains both steel, polypropylene and hybrid fibers. Four SCC mixtures were prepared and tested. One was a plain SCC, one was made up with 30 kg/m^3 of (RC-80/60 BN) steel fibers, one with 5 kg/m^3 of (Synmix 65) polypropylene (PP) fibers, while the third mixture was a hybrid reinforced SCC that contained 15 kg/m^3 and 3 Kg/m^3 of steel and PP fibers, respectively. Tests that carried out on the fresh concretes showed that all mixtures had passed the slump flow and T_{50} tests but exceeded the upper limits for J-ring, V-funnel, and L-box except the first mixture. At 28 and 90 days, the last mixture showed the highest compressive strength and modulus of elasticity, while the second mixture showed the highest tensile strength and modulus of rupture.

El-Dieb [8] studied the durability and mechanical properties of ultra-high strength SCC which was manufactured from local materials with various contents of (0, 0.08, 0.12 and 0.52%) of (HELIX 5-25). The length of this type of fiber is 25 mm, while its aspect ratio is 50. Slump flow test was used to evaluate the effect of steel fibers addition on fresh SCC mixture flowability. The results showed that all mixtures gave an acceptable flowability according to EFNARC [3] and ACI 273 [9], but the flow ability was affected by the addition of steel fibers. About 12% flowability reduction was recorded with the largest fiber amount. When a certain slump value is needed to stay constant after fibers addition, admixture quantity must be regulated. From compressive strength tests for samples after 90 days, it can be concluded that the compressive strength of SCC directly related to the steel fiber addition.

As it is shown in the reviewed literature, only limited number of researches are available on the fresh properties of SCC incorporating steel fibers. In this study, the effects of steel fibers on several workability fresh properties in addition to the early

age (7 days) compressive and tensile strengths of SCC are examined. Steel fibers of 15 mm length and 0.2 mm diameter were used in three different dosages. Slump flow, T_{50}, J-ring, and column segregation tests were used to evaluate the fresh concrete properties. The main goal of this research is to present steel fiber reinforced SCC concrete mixtures that pass the basic fresh concrete requirements of SCC.

EXPERIMENTAL WORK

Materials

Type 42.5 Portland cement was used in this study with different contents depending on the desired strength. The coarse aggregate was local siliceous gravel from Wasit province/Iraq, while local sand was used throughout all SCC mixtures as fine aggregate. Table 1 shows the grading of the coarse and fine aggregates. Fixed content of lime stone powder was also included in all mixtures. Silica fume was only used with high strength SCC mixtures. The characteristics of the cement and the lime stone powder are shown in Table 2. The used fiber was straight micro steel fiber with diameter of 0.2 mm, length of 15 mm (aspect ratio = 75), and tensile strength of 2600 MPa. The HRWR agent was Sika ViscoCrete-5930.

Table 1 Grading of the fine and coarse aggregates

Sieve size (mm)	**Fine (% Passing)**	**Coarse (% Passing)**
19	100	100
12.5	100	68
9.5	100	30
4.75	93.2	0
2.36	65	-
1.18	50.6	-
0.6	42	-
0.3	12	-
0.15	0	-

Table 2 Characteristics of cement and limestone powder

Oxide (%)	**Cement**	**Limestone Powder**
SiO_2	21.04	1.38
Fe_2O_3	5.46	0.12
Al_2O_3	2.98	0.72
CaO	63.56	56.1
MgO	2.52	0.13
SO_3	2.01	0.21
f-CaO	0.76	-
Loss on ignition (%)	1.38	4.56

SCC Mixtures

Two concrete grades were adopted as basic design strengths of the SCC mixtures in this research. The nominal design strengths of these mixtures are 30 and 50 MPa with

constituents' weights per cubic meter as shown in Table 3. These mixtures were designated as M30-0 and M50-0, respectively, where 0 refers to zero fiber content. None of the basic design mixtures contains steel fiber. The limestone powder was used in constant content of 67 kg/m^3 for all mixtures, with and without steel fiber, while the silica fume was also fixed at 67 kg/m^3 for all M50 mixtures. Three different steel fiber dosages of 0.5, 0.75, and 1.0% of the mixture volume were adopted for the M30 and M50 mixtures.

Table 3 Weights per cubic meter of the basic mixtures

Gradient (kg/m^3)	**M30-0**	**M50-0**
Cement	392	525
Sand	1039	907
Gravel	574	518
Silica fume	-	67
L.S. powder	67	67
Water	181.3	190
S.P.	9.3	17

Fresh SCC Tests

To consider a flowable concrete as a SCC it should possess three characteristics, filling ability, passing ability, and stability against segregation of aggregates. Thus, the produced concrete should fill the formwork without any external vibration and without showing any signs of aggregate segregation. This concrete should also pass through any reinforcing grid smoothly. Several tests were adopted by several researchers and standards to test the three characteristics. ACI 237 [9] adopts the ASTM C1611 [1] slump flow test to measure the filling ability of SCC. This test is similar to the standard ASTM slump test, yet, the slump is measured horizontally for the flowable concrete not vertically as for conventional concrete. Using the slump flow test, another SCC test can be obtained, which is the T_{50} test. The T_{50} measurement is used as an indication of the mixture viscosity. The time required to reach a flow diameter of 500 mm is the T_{50} of the mixture.
According to ACI 237 [9], the passing ability through the steel reinforcement is measured either using the J-ring or the L-box test. The J-ring was used in this research for this purpose, which is also a flow test of the fresh SCC from a conical mold, however, through vertical reinforcing bars as shown in Fig. 1. After the spreading of the SCC, the diameter is measured twice and perpendicularly. The average of the two diameters is the index of the J-ring test. The difference between the flow diameter through the J-ring and that of the slump flow measures the degree of passing obstruction of the steel reinforcement. Finally, the stability of the SCC mixture against the segregation of the aggregate was tested using ASTM C1712 [4] static rapid penetration test. In this test, a special apparatus with hollow cylinder attached to a central vertical metal rod are placed on a fresh SCC-filled inverted cone as shown in Fig. 2. The test starts with releasing the cylinder to freely penetrate the fresh concrete in the cone under the own weight of the assembly. The depth of this penetration is used as an index to evaluate the segregation of the mixture. Table 4 shows the acceptable limitations of four tests based on different standards.

Table 4 Limitations of fresh tests of different standards

Test	Limitations			Notes
	ACI 237	EFNARC	ASTM	
Slump flow (mm)	450-760	650-800	480-680* Or 530-740**	ASTM C1611
T_{50} (sec)	2-5	2-5		ASTM C1611
ΔJ-ring (mm)		0-10	0-25 + 25-50 ++	ASTM C1621
Rapid Penetration (mm)			0-10 † 10-25††	ASTM C1712

* Single-operator precision ** Double-operator precision + No visible blocking ++ Minimal to noticeable blocking † Resistance to segregation †† Moderately resistance to segregation

Fig. 1 J-ring apparatus

Fig. 2 Penetration test

RESULTS AND DISCUSSION: COMPOSITION AND FRESH PROPERTIES OF TRIAL SCC MIXTURES

As previously introduced, the goal of this paper is to present SCC mixtures incorporating steel fibers and passing the basic fresh concrete requirements of SCC. As explained above, two nominal strength grades of 30 and 50 were considered for the basic mixtures (without fibers) and the fibrous mixtures. For each of which, the basic mixture design was used with a specific initial fiber content of 0.5 or 0.75%, for which four SCC fresh tests were conducted. Based on the results of these four tests, the mix design was modified to obtain a SCC mixture that passes the basic tests requirements. When this mixture design is reached, it is again tried and modified if required for the other fiber contents.

As it is known, lower strength SCC concretes are easier to be produced than higher strength ones. Moreover, the presence of fiber reduces the flowability of concrete

significantly. Therefore, the 30 MPa design strength mixture was tested first for the effect of inclusion of steel fibers. The weighted gradients of the mixture are shown in Table 3, which are also shown as volume percentage (per cubic meter) in Fig. 3. It should be mentioned that the volumetric mix proportions are presented as pie charts for all mixtures. The weights of all gradients were presented as volumetric percentages considering an air content of 2% as recommended by EFNARC [3]. It should also be noted that the steel fiber content was not presented in these pie charts as this content is fixed for each trial mixture.

The slump flow, ΔJ-ring, and penetration test results of the basic 30 MPa mixture were 750, 5, and 5 mm, which are all within the standard limitations given in Table 4, while the T_{50} record was 2.55 seconds which also reflects good SCC flowability. Starting with the same gradient proportions, 0.75% of steel fiber was added to mixture. The addition of steel fiber is known to adversely affect the fresh properties of concrete, which was obviously achieved in this mixture. The slump flow, T_{50}, and penetration measurements were acceptable. However, the ΔJ-ring was increased noticeably from 5 mm to 22 mm, which is out of limit specified by EFNARC [3] and close to that specified by ASTM C1621[2]. This means that the mix still flowable and stable, yet, blocking around steel reinforcement is probable. To avoid blocking, it is preferable to reduce the volume of coarse aggregate and replace it with fine materials. Therefore, the cement was increased by 20 kg/m^3 and the sand was increased by 24 kg/m^3, while the gravel was reduced by 71 kg/m^3. The water and superplasticizer were also changed accordingly. Fig. 4 shows the pie chart of the volumetric percentages of the second trial. Comparing this trial mix with its preceding one, the flow slump was increased and the T_{50} was decreased, while the ΔJ-ring was decreased to 14 mm. Fig. 5 compares the results of the four tests for the two trials.

Trial 2 mixture (M30-0.75) was then used with 0.5% steel fiber (M30-0.5) and was successfully passing the required limitations of filling ability, passing ability, and stability tests as shown in Fig. 6. However, when 1.0% of steel fiber was used with this mixture (Fig. 4), the fresh properties were adversely affected. It should be noted this volumetric content is relatively high for SCC. For the first trial mix, the slump flow was decreased to 570 and the T_{50} was increased to 18 seconds, which exceeds the limitation of 5 seconds suggested by ACI 237 [9] and EFNARC [3]. Moreover, the ΔJ-ring record was 70 mm. These records reflects sharp drop in the filling and passing ability of this mixture. Therefore, this trial was followed by two more trials in which the cement was increased slightly by 3 and 2 kg/m^3 increments, while the fine and coarse aggregate, water, and superplasticizer contents were adjusted accordingly. The fresh properties of the second mixture were also inadequate, while those of the third trial mix were within the limitations of SCC. The volumetric percentages of Trial 3 mix, which took the designation M30-1.0, are shown in Fig. 7, while the records of the four tests of the three trial mixes are shown in Fig. 8.

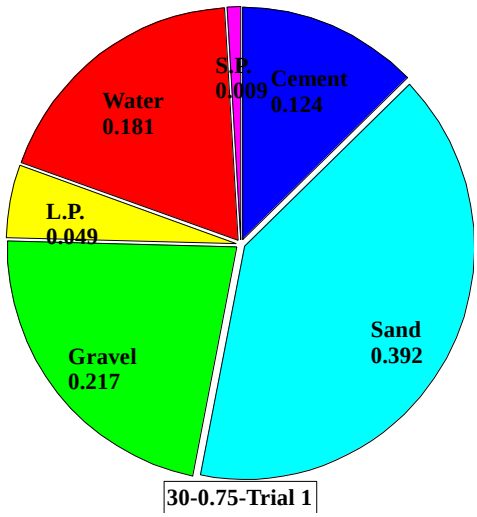

Fig. 3 Mix proportions of Trial 1-30 MPa-0.75% SF

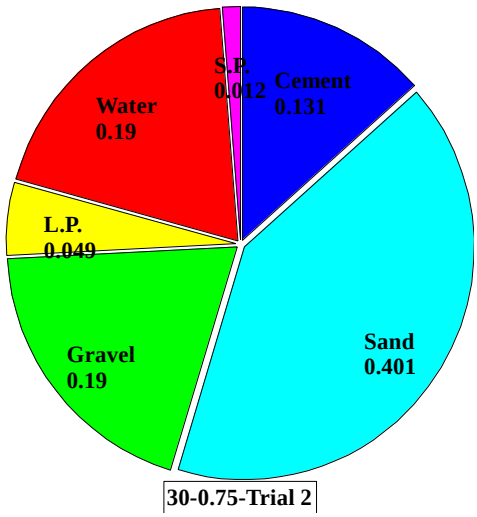

Fig. 4 Mix proportions of Trial 2-30 MPa-0.75% SF

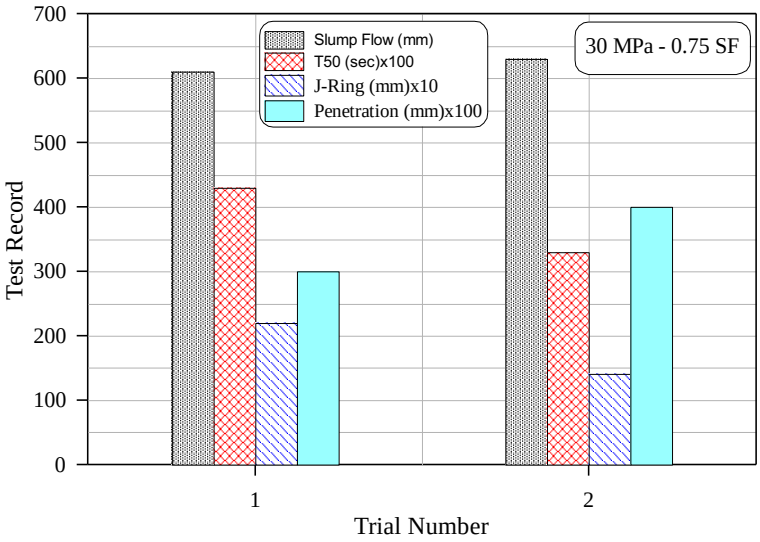

Fig. 5 Fresh test records - 30 MPa - 0.75% SF

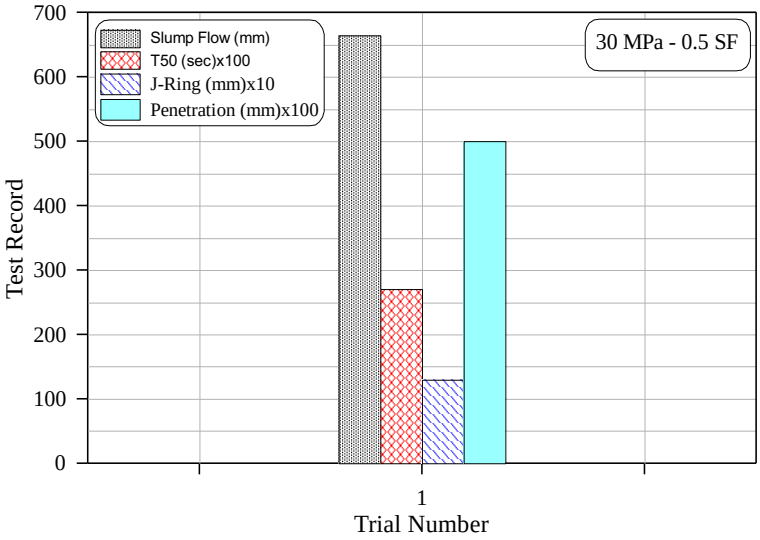

Fig. 6 Fresh test records - 30 MPa - 0.5% SF

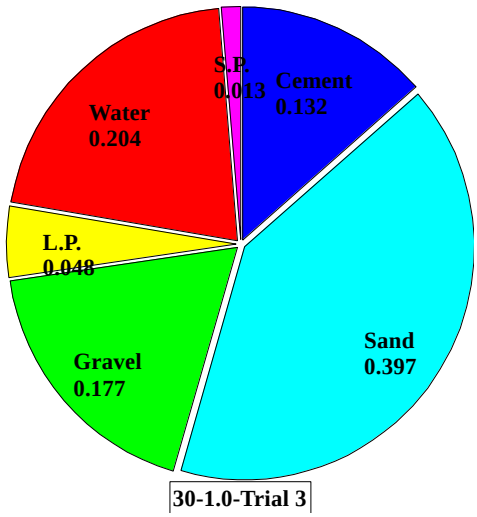

Fig. 7 Mix proportions of Trial 3- 30 MPa- 1.0% SF

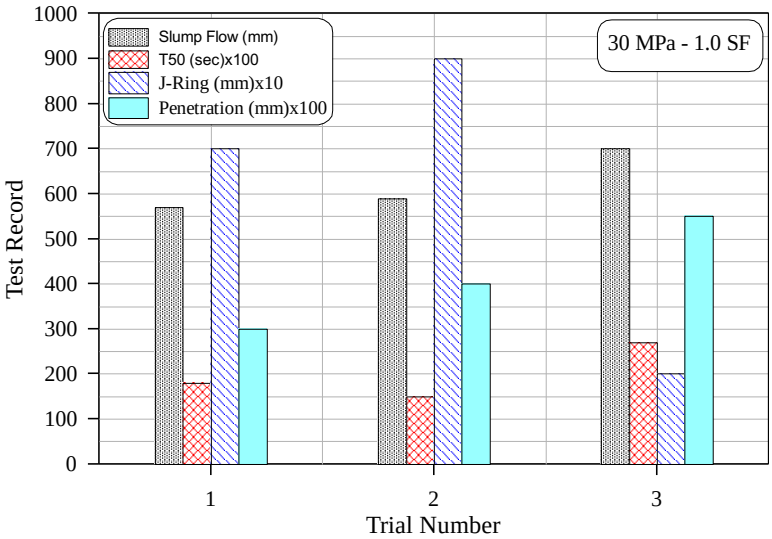

Fig. 8 Fresh test records - 30 MPa – 1.0% SF

The same procedure was adopted for trial mixes of M50 mixtures. The fresh tests records of M50-0 mixture were 615, 3, and 9 mm for the flow slump, ΔJ-ring, and the penetration tests, respectively, while the T_{50} was 4.9 seconds. As fiber was added, the fresh properties were altered. The M50-0 mix proportions were used for M50-0.5 by simply adding 0.5% of the steel fiber. This addition led to the increase of both T_{50} and penetration records. The mix was simply adjusted by increasing the water content of the mixture as shown in Fig. 9. This adjustment enhanced the fresh properties of the mixture, especially the penetration record, which decreased from 20 mm to 9 mm as shown in Fig. 10. However, the T_{50} record still slightly higher than the 5 seconds limit by only 1 second, which can be accepted with a slump flow record of 700 mm. The mix proportions of the approved M50-0.5 were then used with a steel fiber content of 0.75%. However, the increased steel fiber content adversely affected the ΔJ-ring and the T_{50} measurements. The ΔJ-ring record jumped to 45 mm and the T_{50} record increased to 8 seconds. In the second trial (Fig. 11), a specific quantity of coarse aggregate was replaced by an equivalent quantity of fine aggregate keeping the other gradients constants. For this mixture (M50-0.75), the ΔJ-ring and the T_{50} were decreased to acceptable values and the slump flow increased as shown in Fig. 12. The

approved mixture (M50-0.75) was used as the first trial of (M50-1.0) that contains 1.0% of steel fiber. For this trial, the ΔJ-ring and T_{50} records were slightly increased as shown in Fig. 13, however, these values were still in the acceptable ranges.

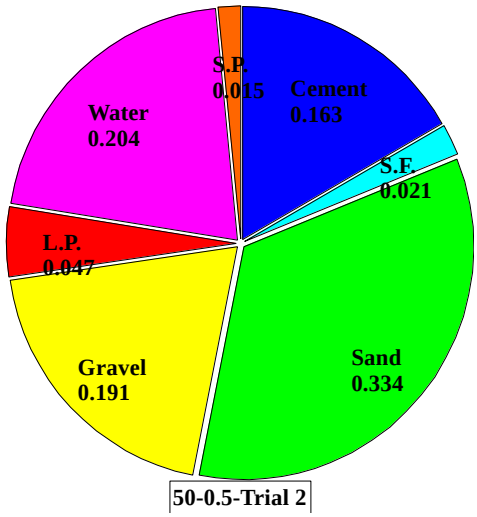

Fig. 9 Mix proportions of Trial 2- 50 MPa- 0.5% SF

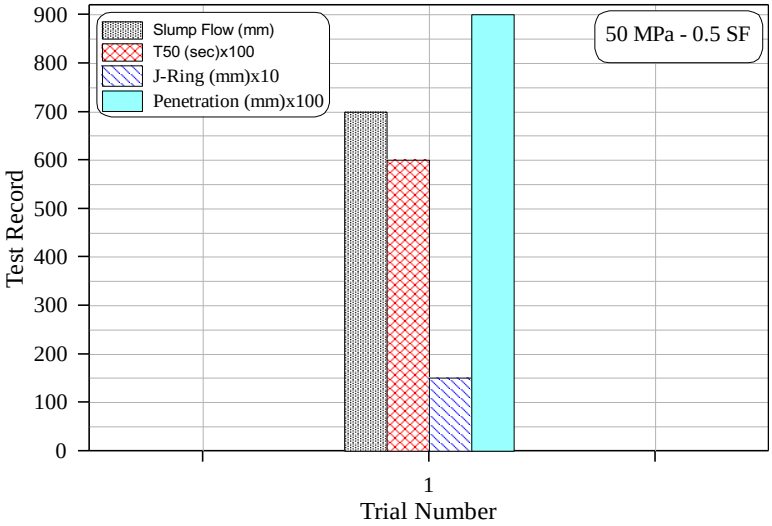

Fig. 10 Fresh test records - 50 MPa - 0.5% SF

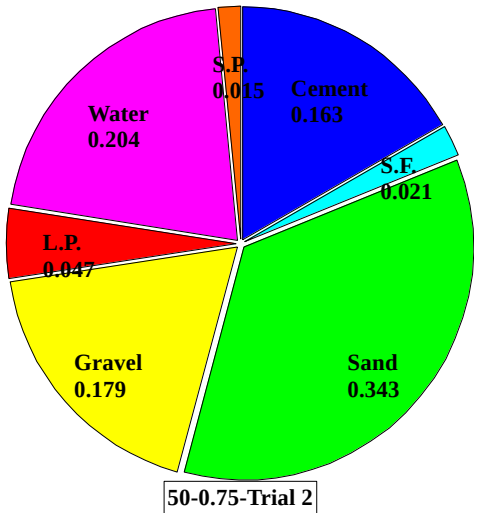

Fig. 11 Mix proportions of Trial 2- 50 MPa- 0.75% SF

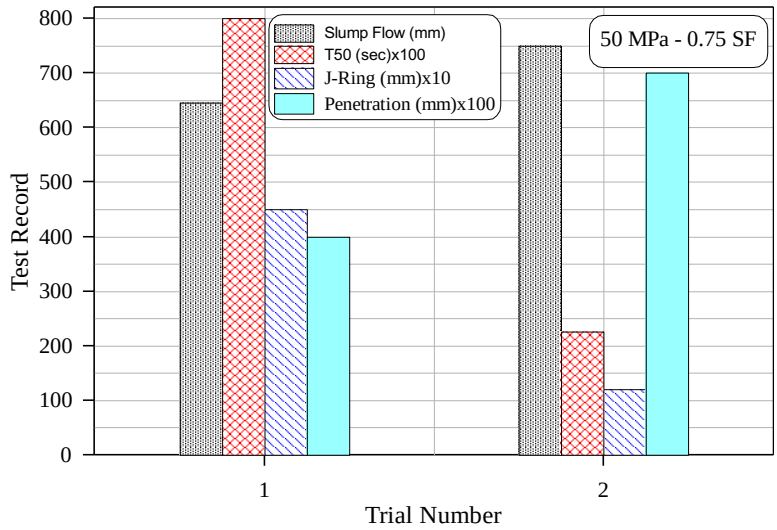

Fig. 12 Fresh test records - 50 MPa - 0.75% SF

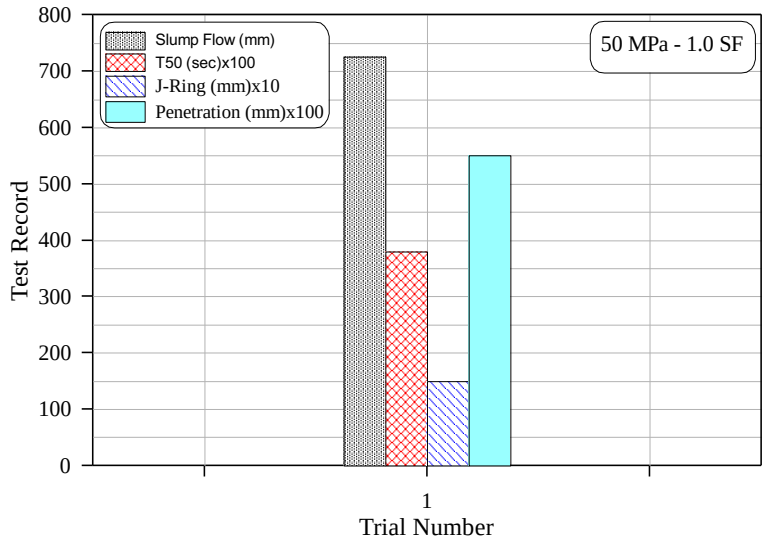

Fig. 13 Fresh test records - 50 MPa – 1.0% SF

RESULTS AND DISCUSSION: FRESH AND HARDENED PROPERTIES OF PASSED SCC MIXTURES

The trial mixtures that were considered acceptable according to the records of the four fresh SCC tests are compared in this section in terms of these tests. The weighted gradients of the adopted fibrous mixtures (M1-0.5, M1-0.75, M1-1.0, M2-0.5, M2-0.75, and M2-1.0) are listed in Table 5. It should be noted that among each mix grade (30 or 50 MPa), the fiber content is not the only variable parameter, as cement, fine aggregate, coarse aggregate, and in the case of M30, water and superplasticizer are also variables. Thus, the effect of concrete grade or fiber content on the fresh properties of SCC cannot be clearly judged based on the presented records. Fig. 14 compares the four test results of the two grades considering 0.5% steel fiber, while Figs. 15 and 16 show these comparisons for steel fiber contents of 0.75 and 1.0%, respectively. When the three figures are observed and compared it is concluded that no obvious trends can be

distinguished for the presented results. This again can be attributed to the variation of the other gradients of the mixtures with the steel fiber. It is important to remind here that the aim of this paper is not to study the influence of the inclusion of steel fibers on different grades SCCs, which is already an understood effect. This research is a case study to introduce different moderate strength SCCs incorporating low to moderate contents of steel fibers. Figs. 14 to 16 show obviously that the introduced fibrous mixtures are successful as self-compacting concretes.

Fig. 17 compares the 7-day compressive strength records for the eight mixtures, while Fig. 18 shows this comparison for the 28-day compressive strength. It is obvious from the two figures that M50 mixtures gained higher compressive strength values than their corresponding M30 ones. However, the effect of fiber content on compressive strength for each grade of concrete is not obvious, but it generally decreases with 0.5% steel fiber and increases with the higher steel fiber contents. Moreover, the compressive strength of the 1.0% steel fiber content was the highest for both ages and both concrete grades among the other fiber contents. The compressive strength was between 34.3 MPa and 37.3 MPa for all M30 fiber contents at age of 28 days, while it was in the range of 46.9 MPa to 61.8 MPa for M50 mixtures.

The results of the splitting tensile strength for the two concrete grades are shown in Figs. 19 and 20 at ages of 7 and 28 days, respectively. It is shown in Fig. 19 that the splitting tensile strength increases with the increase of fiber content for each grade of concrete. Similar trend of results is also shown in Fig. 20. The 7-day splitting tensile strength comparisons that are shown in Figs. 19 and 20 also reveal that the splitting tensile strength records were in general higher for M50 mixtures than their corresponding M30 mixtures. Such result is typical as the tensile strength develops with the development of concrete compressive strength, which increases with age.

Table 5 Weights per cubic meter of the fibrous mixtures

Gradient (kg/m³)	**M30-0.5**	**M30-0.75**	**M30-1.0**	**M50-0.5**	**M50-0.75**	**M50-1.0**
Cement	412	412	417	525	525	525
Sand	1063	1063	1052	907	931	931
Gravel	503	503	468	518	486	486
Silica fume	-	-	-	67	67	67
L.S. powder	67	67	67	67	67	67
Water	190	190	204	209	209	209
S.P.	13	13	14.3	17	17	17
Steel fiber	39	58.5	78	39	58.5	78

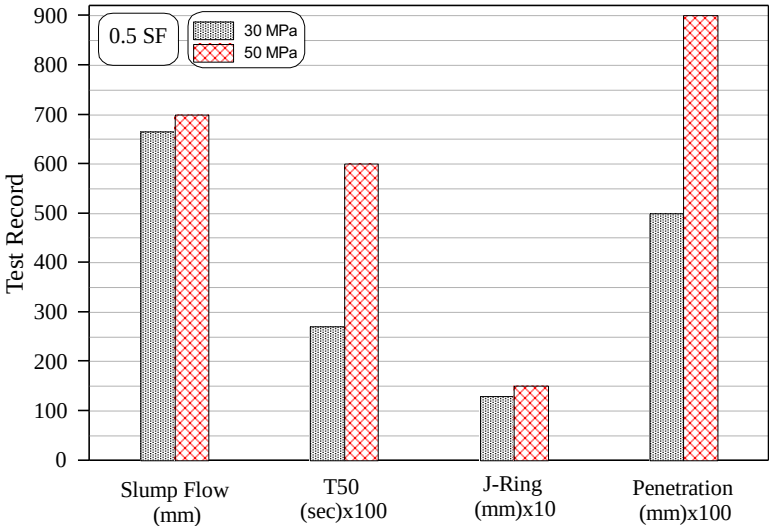

Fig. 14 Fresh test records – all strengths – 0.5% SF

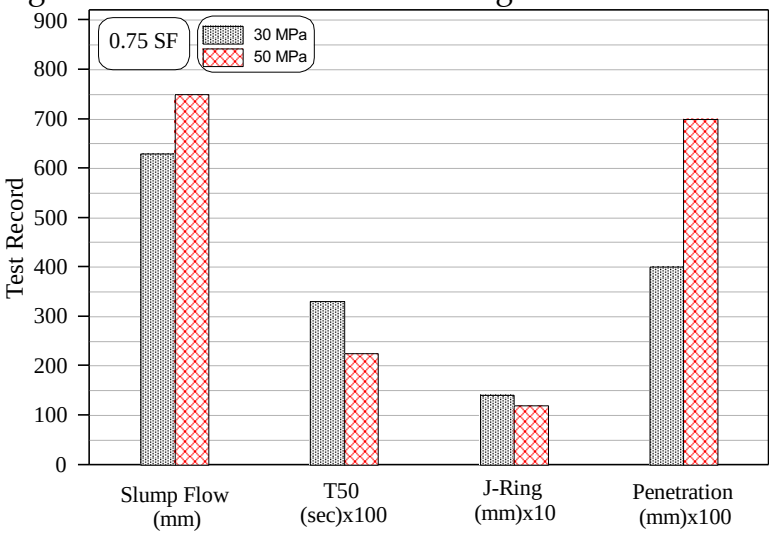

Fig. 15 Fresh test records – all strengths – 0.75% SF

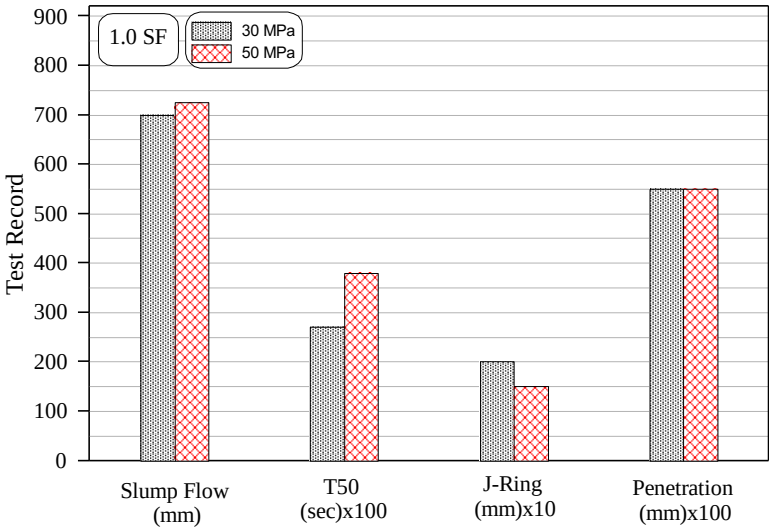

Fig. 16 Fresh test records – all strengths – 1.0% SF

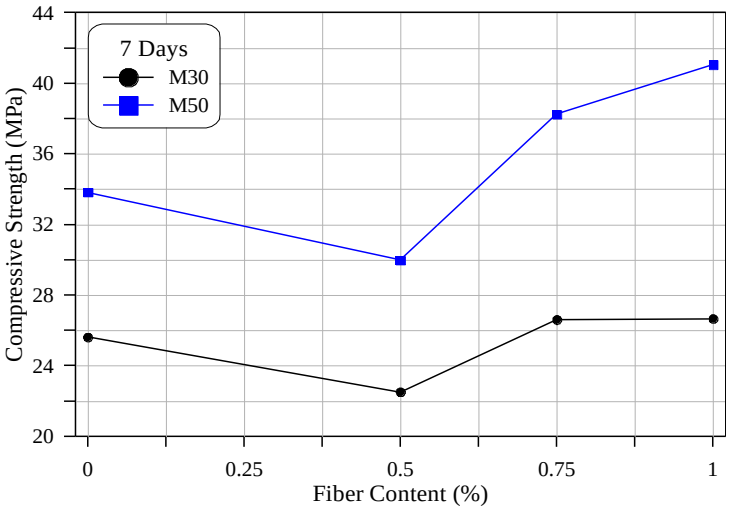

Fig. 17 7-day compressive strength records

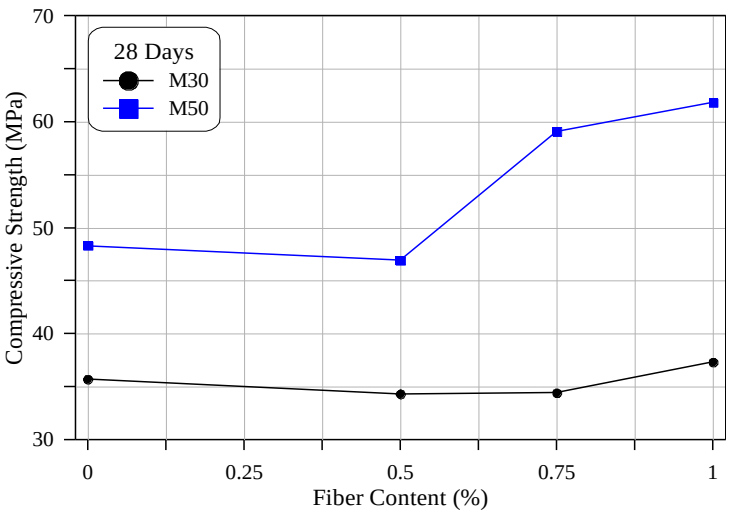

Fig. 18 28-day compressive strength records

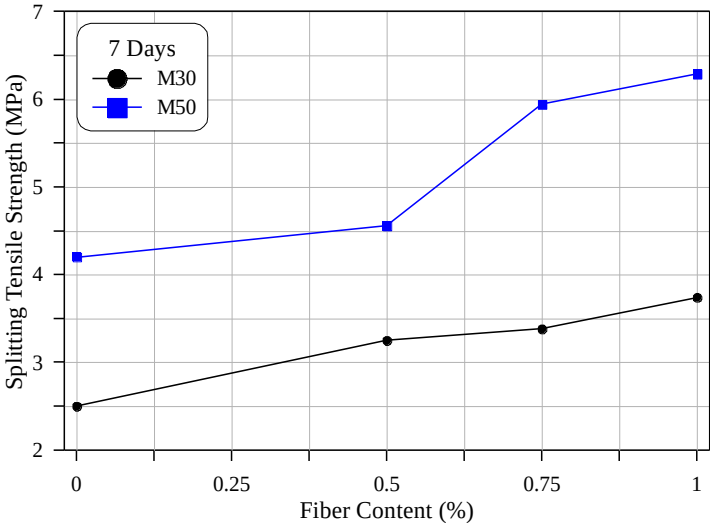

Fig. 19 7-day splitting tensile strength records

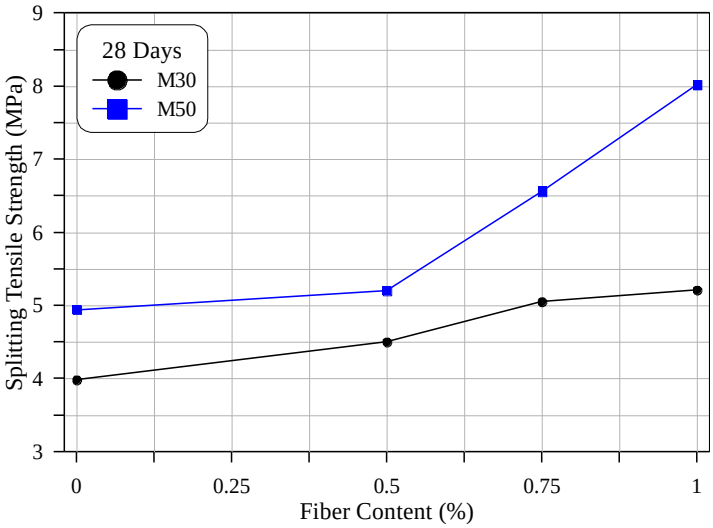

Fig. 20 28-day splitting tensile strength records

CONCLUSIONS

Several trial mixtures were mixed in this research to obtain SCC incorporating up to 78 kg/m^3 of steel fiber. Two mixtures with 30 and 50 MPa nominal design strengths were adopted as basic mixtures before the inclusion of steel fibers. The slump flow and T_{50} were used as standard tests to evaluate the filling ability of the produced SCC mixtures, while the ΔJ-ring and rapid penetration tests were used to evaluate the passing ability and stability of the SCC, respectively. The two basic mixtures were passed the four tests successfully.

The steel fiber was then added to these mixtures at different contents of 0.5, 0.75, and 1.0%. The inclusion of fiber was found to reduce the flowability and increase the potential blocking around steel bars. These behaviors were concluded from the decreasing of the slump flow, increasing of the T50 time record, and increasing in the difference between the J-ring flow diameter and slump flow diameter (ΔJ-ring).

To obtain SCC that meets the requirements of the four tests and contains steel fibers up to 78 kg/m^3, the gradients were adjusted in trial mixtures for each of the fiber contents at each concrete grade. The adjustments were mostly by increasing the finer materials (cement and sand) and reducing the coarse aggregate. The contents of water or superplasticizer were also adjusted in some trials for the same purpose. Consequently, for each of the two adopted concrete grades (M30 and M50), SCC mixtures with fiber contents of 0.5, 0.75, and 1.0% were introduced. The filling ability, passing ability, and stability against segregation for the six introduced fibrous mixtures were found acceptable according to the depended standards.

REFERENCES

1) ASTM C1611 (2014). Standard test method for slump flow of self-consolidating concrete. ASTM International, West Conshohocken, USA.
2) ASTM C1621(2014). Standard test method for passing ability of self-consolidating concrete by J-ring. ASTM International, West Conshohocken, USA.
3) EFNARC. 2002. Specifications and guidelines for self-compacting concrete. EFNARC, UK.
4) ASTM C1712 (2014). Standard test method for rapid assessment of static segregation resistance of self-consolidating concrete using penetration test. ASTM International, West Conshohocken, USA.
5) ASTM C1610 (2014). Standard test method for static segregation of self-consolidating concrete using column technique. ASTM International, West Conshohocken, USA.
6) Sahmaran, M., Yurtseven, A., Yaman, O. (2005). Workability of hybrid fiber reinforced self-compacting concrete. *Building and Environment*, 40, 1672-1677.
7) Aslani, F., Nejadi, S. (2013). Self-compacting concrete incorporating steel and polypropylene fibers: compressive and tensile strengths, modulus of elasticity and rupture, compressive stress-strain curve, and energy dissipation under compression. *Composites : Part B*, 53,121-133.
8) El-Dieb, A. (2009). Mechanical, durability and microstructural characteristics of ultra-high-strength self-compacting concrete incorporating steel fibers. *Materials and Design*, 30, 4286-4292.
9) ACI Committee 237R-07 (2007). Self-consolidating concrete. American Concrete Institute, USA.

DAILY HYDROGEN PRODUCTION EVALUATION USING SOLAR ENERGY IN BURSA, TURKEY

Kenan SAKA

Bursa Uludağ University, Vocational School of Yenişehir Ibrahim Orhan, Bursa, Turkey,
kenansaka@uludag.edu.tr

ABSTRACT: Hydrogen is considered the lightest, simplest and most plentiful element in the universe. It can be a source of new, renewable and almost the cleanest fuel of the future. Also solar energy has a significant share among renewable energy source. Especially photovoltaic power plants represent a good solution concerning electric energy supply. Turkey is looking for environment friendly renewable energy sources like most country. Photovoltaic power plants can be a sustainable energy source with huge potential for Turkey. Bursa province is located in the northwestern region and there are more efficient regions in terms of solar energy such as south region in Turkey. Soğuksu photovoltaic solar power plant is the first large scale power plant with 7 MW peak power in Bursa. In this study, generation values of a power plant were observed under actual operating conditions. The generation data showing the actual daily electricity generation values have been recorded in the library of the plant. This data have been used to investigation of daily hydrogen production performance of the power plant in theoretically. Proton Exchange Membrane (PEM) electrolyzer was selected for electrolysis of water. According to results, the maximum mass flow of hydrogen production can be 0.0625 $kgs^{-1}H_2$ for peak load and the electrolyzer can produce 1630 kg hydrogen in a clear summer day.

Key words: Hydrogen production, PEM electrolyzer, solar energy, electricity generation, Turkey

INTRODUCTION

The future energy economy will consist of many diversified and combined renewable energy technologies (Saadi et all. 2016). Global warming and climate change brings renewable energy sources to the forefront. Nowadays energy from fossil fuels may be inexpensive but the solar energy with hydrogen technologies are essential components of a sustainable energy future. Fossil fuels are finite in nature and a major source of greenhouse gas emissions. Hydrogen which is one of the most powerful fuels can be extracted from steam reforming through the process of electrolysis and it can be used either for storing or generating electricity in power systems. Although every location on the Earth receives sunlight, the amount received varies greatly depending on geographical location. Turkey is one of the world's best areas for sunlight and the number of the photovoltaic installations has increased significantly in Turkey (Hepbasli et all. 2010). Solar energy is common value of the whole world among renewable energy sources but share of countries in solar energy differs. In the literature many countries have analyses based on solar energy. Kumar and Sudhakar

(2015) conducted a performance evaluation of a grid connected 10 MWp photovoltaic power plant in India. They pointed out that grid connected photovoltaic systems are the best choice among renewable energy sources. Incekara and Ogulata (2017) have studied on the electricity generation plan of Turkey and they reported solar energy will have the second place in Turkey's electricity generation within fifteen years until 2030. Some analyses have been prepared for cities of Turkey. Boran et al (2010) have suggested the best location for a photovoltaic system to be installed in Turkey and they have taken into account sun hour, solar radiation, mean temperature, and topography as evaluation criteria. The result of the analysis has indicated that Bodrum should be selected as the best site for installing grid connected photovoltaic power plant.

Some studies have focused on the investigation of hydrogen production of a photovoltaic and thermal system. According to Cilogulları et al. (2017) 0.018 kg hydrogen can be produced daily with 1.28 m^2 photovoltaic and thermal system. Water electrolysis is a hydrogen production technique that has reached the stage of industrial exploitation. Used with PV, it offers a sustainable mean for hydrogen production (Boudries et al. 2014). Likkasit et al. (2018) have integrated solar energy into oil and gas industries to produce the hydrogen required in crude oil up grader processes. Pereira et al. (2017) have analyzed the electricity generation through a mini hydro plant and a photovoltaic system particularly sized for a location in Portugal. Proton Exchange Membrane (PEM) electrolyzer is a good chosen for electrolysis of water. Yilmaz and Kanoglu (2014) have thermodynamic evaluation of geothermal energy powered hydrogen production by PEM water electrolysis. In their study, energy capacity of the PEM electrolyzer is 3810 kW and mass flow rate of the produced hydrogen is 0.0340 kg/s.

Theoretically investigation of hydrogen production depends on actual electricity generation of the Soğuksu solar power plant has been presented in this study. The power plant is a photovoltaic and a grid connected type in the northwestern region of Turkey in the borders of Bursa province. It has started to electricity generation since 20th March 2017. Soğuksu solar power plant is the first large scale plant in the Bursa province. This point makes it important because photovoltaic investments will increase in case of success of the power plant. Monthly global radiation values of the region are below the average in Turkey. This means the power plant is not a pretentious investment. The electricity generation is very low on autumn and winter seasons under the effect of overcast weather. The generation values of the power plant were observed under real weather conditions and hydrogen production depends on actual electricity generation were also calculated in this study. The data are the actual generation data recorded by the power plant library and transmitted to the grid. Daily total electricity generation with hydrogen production capacity was demonstrated. The system which is investigated in this study is given in Figure 1 schematically. There are three main sections in the system. One of them is Soğuksu solar power plant where are necessary electricity is generated to produce hydrogen. The other section is solar collectors and water heater system. In this section the water will electrolyzed is preheated to 80 ^{o}C before enter to PEM electrolyzer. The last section is PEM electrolyzer where hydrogen is produced. There are explanations in detail in the next paragraphs for the sections.

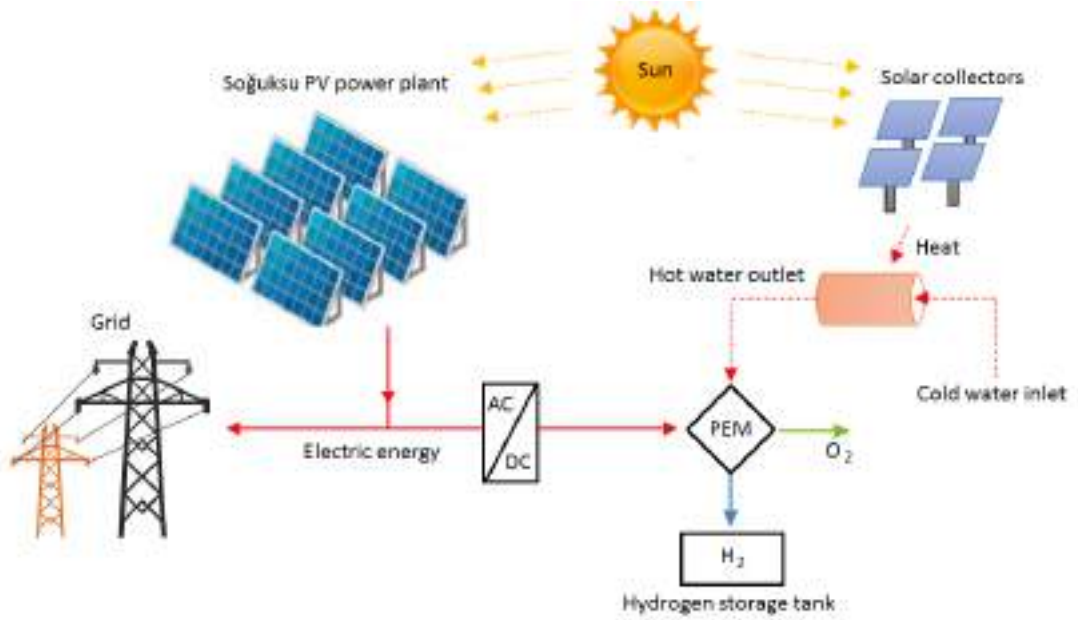

Figure 1. PV power plant aided hydrogen production system

Description and location of the Soğuksu power plant

Soğuksu solar power plant is a large solar field including seven different power plants each has 1 MWp capacity. There are 20 inverters in each 1 MWp scale power plant and each inverter has 10 strings. The photovoltaic solar panels connected to strings in series. Each string has 22 panels. In the plant installation a single type of panel was preferred. The properties of the panel used in the power plant which taken from producer catalog are given in Table 1. The type of panels preferred in the plant is not the most efficient panel type in the market. The commercial outlook of the panels was influential in the selection of this type.

Table 1. Properties of PV solar panels used in Soğuksu solar power plant

Model of the Panel	UP-M270P
Type	Polycrystalline Silicone
Power Rating	270 Watt
Peak Efficiency	16.6%
Number of Cells	60
Dimension of the Cells	156 mm X 156 mm
Length	1640 mm
Width	992 mm

Before installing of the power plant there are some processes must be taken in to account such as designing, constructing. Firstly a suitable area and the financing are necessary like in every investment. Soğuksu solar power plant has all the necessary processes and legal permits. Turkey government has some effective actions in terms of renewable energy. One of them is keep out of license the plants which is under 500 kW capacity. This condition also applies to solar power plants. But capacity of Soğuksu solar power plant is bigger than 500 kW so it can be accepted as big type power plant. The general characteristics of the power plant and its coordinates from satellite images

are shown in Table 2. Theoretically, the amount of generated electricity by a solar power plant is function of the panel surface area of the plant, the number of days it produces electricity, the panel and inverters efficiency used in the plant. Also it is directly related to the energy carried by the sunrays coming onto the power plant panels.

Table 2. General characteristics of Soğuksu solar power plant

Area where the power plant is installed	170000 m^2
Number of panels used	30800
Total panel surface area	50108 m^2
Total cell surface area	44972.9 m^2
Plant Power	7 MWp
Inverter Efficiency	97 %
Generation Commencement Date	20 March 2017
Plant Coordinates	40° 12′ 57′′ N 29° 25′ 50′′ E

Soğuksu solar power plant is located within the boundaries of Bursa province. Its geographical location is next to Yenişehir plain. In Figure 2, the map shows the location of the power plant and its satellite image. In the power plants conditions, there is no cooling application is performed on the panels. The location of the power plant has the advantage of natural ventilation as it is situated on a high hill relative to the plains.

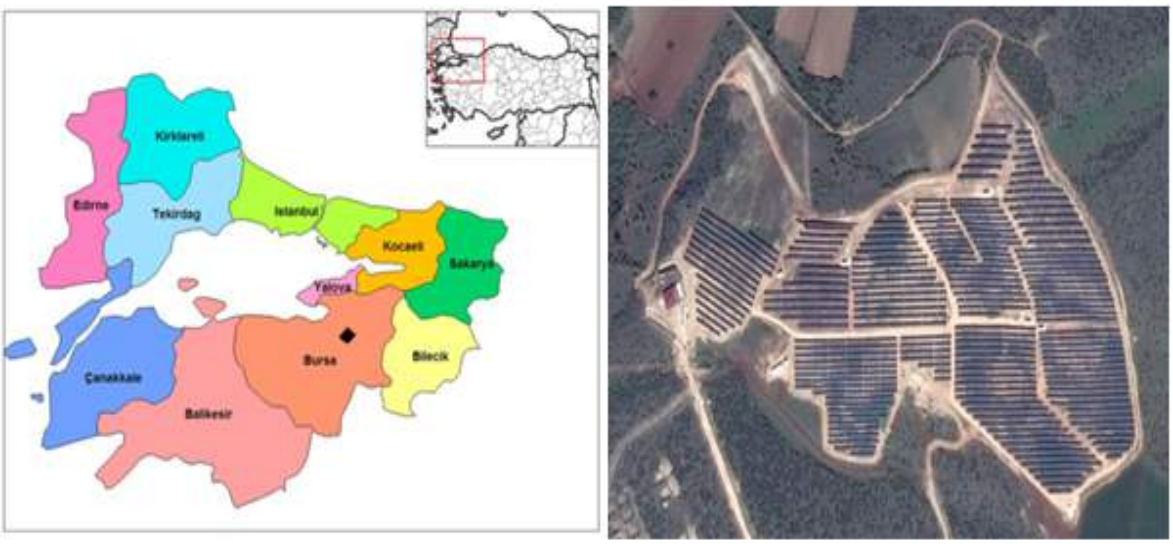

Figure 2. Location and satellite view of Soğuksu solar power plant

Proton exchange membrane (PEM) electrolyzer

In hydrogen production system, the PEM electrolyzers are built around a proton conductive polymer electrolyte. The schematic of PEM electrolysis section for hydrogen production is shown in Figure 1. Different PEM electrolyzer models can be designed. In this study Yilmaz and Kanoglu's (2014) model was used. According to this model, hydrogen can be produced at a rate of 0.0340 kg/s by using 3810 kW electricity power. With right proportion, the produced hydrogen will be 0,054 kg/s by

using 6 MW electricity power. This result has conformity with literature because Yuksel and Ozturk (2017) have reported the same result. Liquid water is fed to the preheater at a reference environment and is heated by the used solar collectors. Electricity and preheated water are supplied to the PEM electrolysis to drive the electrochemical reactions. Exiting from the cathode, produced H_2 (hydrogen) dissipates heat to the environment and cool down to the reference environment temperature.

Solar Aided Water Preheater System and Assumptions

Water which will be electrolyzed can inlet to PEM electrolyzer at any temperature. But water fed to the electrolyzer at higher temperature to increase the efficiency of the electrolyzer. There is no waste heat near of the Soğuksu power plant so there is three way to preheat the water. One of them is use electrical heater. This method is simple and easy but electrical heater will use %2 of the generated electricity approximately. The other method is use the water as coolant for solar panels. Efficiency of the panels and value of the generated electricity will increase as a result of this method. But the exact generated electricity value cannot be said without an extra analysis. In this study the data are the actual generation data recorded by the power plant library. The last method is use solar collectors to heat the water. This method was selected because it will not affect the generated electricity value. Soğuksu photovoltaic power plant has been established for electricity generation. The last phase of the electricity is AC before transmit to grid. Electrolyzers use the electricity in DC phase. There is added an extra AC-DC converter in the system as shown in Figure 1. This converter will cause decreasing on electricity value, it was neglected.

RESULTS AND DISCUSSION

According to solar potential map, the northwestern Anatolia region is not among the most sun soaked regions of Turkey. But Bursa province is in this region with Soğuksu photovoltaic power plant. Especially in winter, the effect of cloudy and overcast weather on the electricity generation of the power plant is significant. Generated electricity values by Soğuksu solar power plant was presented to literature (Saka et al. 2018). A summer day with clear skies can be described as the perfect day for a power plant. Figure 3 shows the changes in daily electricity generation with hydrogen production capacity on a clear day at the power plant.

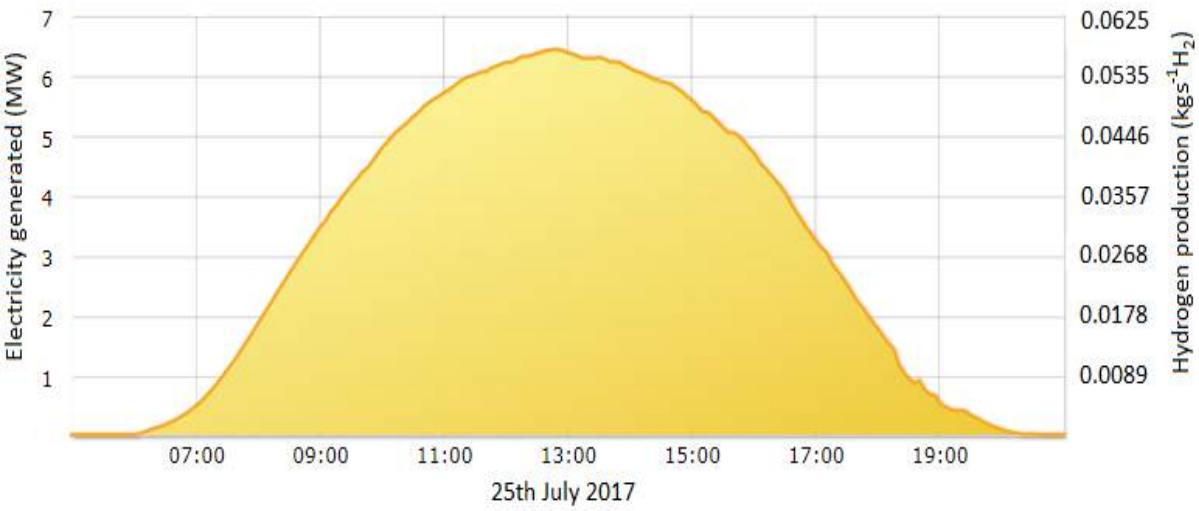

Figure 3. Distribution of the generated electricity with hydrogen production capacity in Soğuksu solar power plant on a clear summer day

In the distribution given above, the electricity generated in the power plant on July 25, 2017 is shown. Behavior of the graph is very close to a perfect day. The power plant started to wake up after 6:00 am in the morning. Before 13:00, the peak generation power reaches about 6.5 MW. The electrolyzer can produce 0.06 kg/s hydrogen for this loading approximately. Electricity generation continuing until 20:00 reached a total value of 50.74 MWh throughout the day. In terms of hydrogen production the electrolyzer can produce 1630 kg hydrogen in this day.

The generation distribution given in Figure 3 is an expectation. It is not always possible to talk about such a generation capacity especially in winter days. The daily generation distribution with hydrogen production capacity of a day that can be interpreted as a bad day is given in the Figure 4. The figure shows the effect of overcast weather on electricity generation distribution through a day.

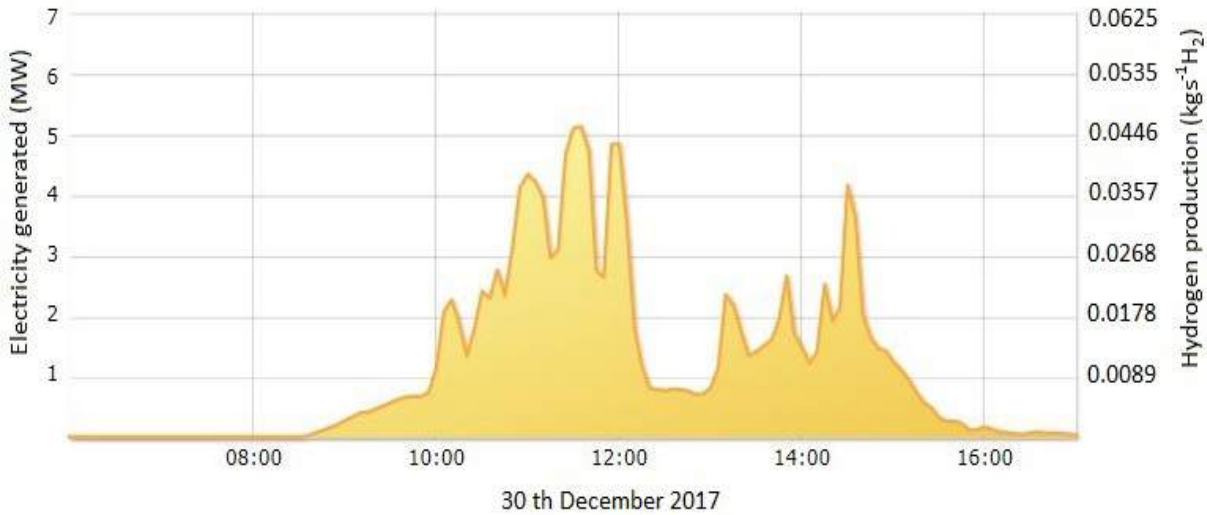

Figure 4. Effect of overcast weather on electricity generation and hydrogen production distribution in Soğuksu solar power plant

The generation values given in the figure belong to December 30, 2017. The weather conditions have significantly affected on electricity generation and hydrogen production. The fluctuations in electricity generation can be easily seen on the figure. 12.74 MWh of electricity was produced throughout the day and worse days were experienced during the period evaluated in this study. In terms of hydrogen production the electrolyzer can produce 410 kg hydrogen in this day approximately. Total hydrogen production will be revealed depending on the number of days with clear and overcast weather.

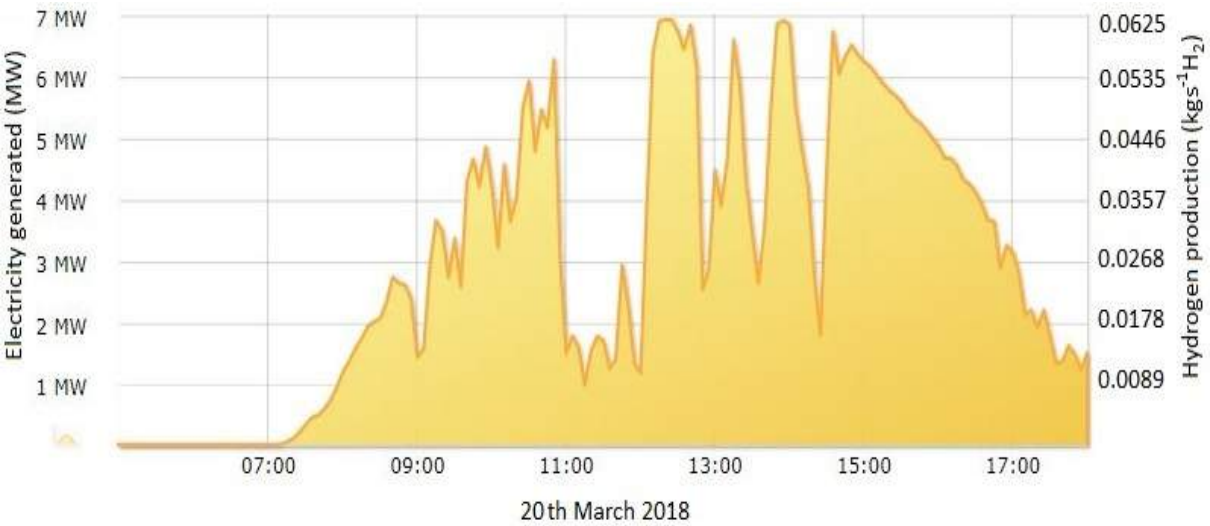

Figure 5. Distribution of the generated electricity with hydrogen production capacity in Soğuksu solar power plant with peak load

Figure 5 shows some instants that peak load is generated. The electrolyzer can produce 0.0625 kg/s hydrogen for peak loading. The perfect day which has peak load was not observed. Actually number of perfect days is very low so it is normal that both of them was not observed together. The generation values given in the figure belong to March 20, 2018. 36.74 MWh of electricity was produced throughout the day. The capacity of the electrolyzer can be 1180.3 kg hydrogen production approximately. Finally a very bad day will showed from winter.

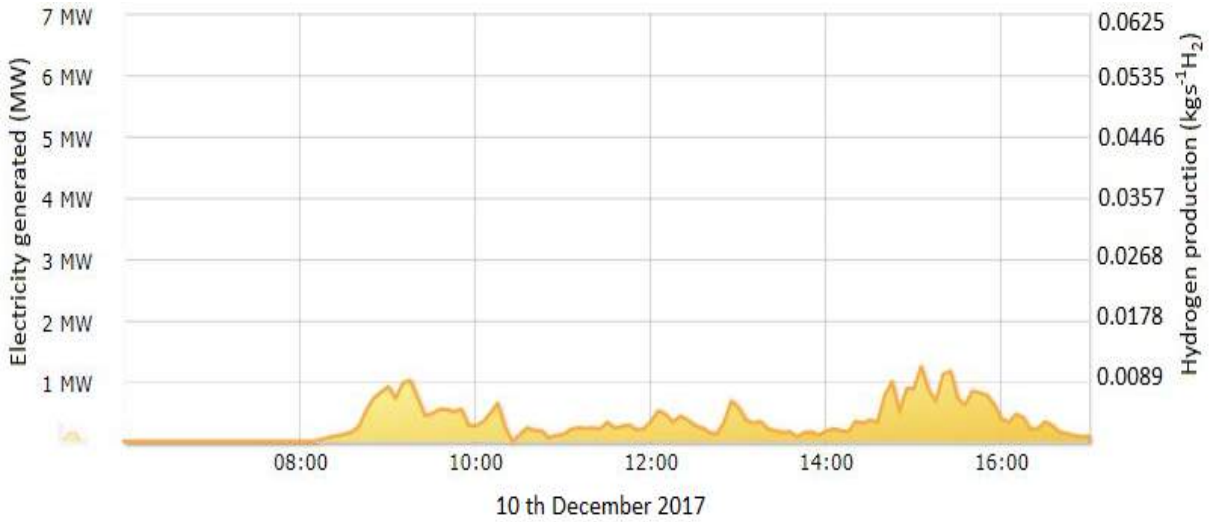

Figure 6. Distribution of the generated electricity with hydrogen production capacity in Soğuksu solar power plant on a winter day

Figure 6 shows distribution of the generated electricity with hydrogen production capacity in Soğuksu solar power plant on a winter day. The day is one of the bad days in terms of electricity generation. The generation values given in the figure belong to December 10, 2017. 3.39 MWh of electricity was produced throughout the day. The electrolyzer can produce 108.9 kg hydrogen in this day.

CONCLUSIONS

In this study, daily hydrogen production capacity depend on electricity generation of a photovoltaic grid connected solar power plant with 7 MWp installed power located in the north west of Turkey was performed. The power plant is the first solar power plant installed in the region in this scale. It has 30800 panels each generating 270 W of electricity. Daily electricity generation values of a power plant were observed under actual operating conditions and recorded in the library of the plant. This data was used to investigation of daily hydrogen production capacity of the power plant in theoretically. Proton Exchange Membrane (PEM) electrolyzer was selected for electrolysis of water. According to results, the maximum mass flow of hydrogen production can be 0.0625 $kgs^{-1}H_2$ for peak load and the electrolyzer can produce 1630 kg hydrogen in a clear summer day.

REFERENCES

Boudries, R., Khellaf, A., Aliane, A., Ihaddaden L., Khida F. (2014) PV system design for powering an industrial unit for hydrogen production. *International Journal of Hydrogen Energy,* 15188 – 15195.

Boran, F. E., Menlik, T., Boran, K. (2010). Multi-criteria Axiomatic Design Approach to Evaluate Sites for Grid-connected Photovoltaic Power Plants: A Case Study in Turkey. *Energy Sources, Part B: Economics, Planning, and Policy,* 5:3, 290 – 300.

Cilogluları M., Erden M., Karakilcik M., Dincer I., (2017). Investigation of hydrogen production performance of a Photovoltaic and Thermal System, *International Journal of Hydrogen Energy,* 42, 2547 – 2552.

Hepbaslı, A., Ulgen, K., Eke, R. (2004). Solar Energy Applications in Turkey. *Energy Sources,* 26:6, 551 – 561.

Saadi, A., Becherif, M., Ramadan, H. S. (2016). Hydrogen production horizon using solar energy in Biskra, Algeria. *International Journal of Hydrogen Energy,* 41, 21899 – 21912.

Incekara, C. O., Ogulata, S. N. (2017). Turkey's energy planning considering global environmental concerns. *Ecological Engineering,* 102, 589 – 595.

Kumar, B. S. Sudhakar, K. (2015). Performance evaluation of 10 MW grid connected solar photovoltaic power plant in India. *Energy Reports,* 1, 184 – 192.

Likkasit, C., Maroufmashat, A., Elkamel, A., Ku, H., Fowler, M. (2018). Solar-aided hydrogen production methods for the integration of renewable energies into oil & gas industries. Energy Conversion and Management. 395 – 406.

Pereira., C. A., Coelho, P. M. Fermandes, J. F., Gomes M. H., (2017). Study of an energy mix for the production of hydrogen. *International Journal of Hydrogen Energy,* 1375 – 1382.

Saka., K. Kaynakli, Ö., Yamankaradeniz. R. (2018) Bursa'da bulunan şebeke bağlantili bir pv güç santralinin günlük elektrik üretimi. IV. Uluslararası Katılımlı Anadolu Enerji Sempozyumu 18-20 Nisan 2018, Trakya Üniversitesi, Edirne, 1479 – 1485.

Yilmaz., C., Kanoglu, M., (2014). Thermodynamic evaluation of geothermal energy powered hydrogen production by PEM water electrolysis. *Energy,* 592 – 602.

Yuksel, E. Y., Ozturk, M., (2017) Thermodynamic and thermoeconomic analyses of a geothermal energy based integrated system for hydrogen production. *International Journal of Hydrogen Energy,* 2530 – 2546.

DESIGN and ANALYSIS of a MAGNETORHEOLOGICAL DAMPER

Ercan OLCAY[1], Alpay Tamer ERTÜRK[1]*, Fahri VATANSEVER[1], Sedat KARABAY[1]
[1]Department of Mechanical Engineering, Engineering Faculty, Kocaeli University
ercan.olcay@outlook.com, *tamererturk@gmail.com, fahrivatansever@gmail.com, sedat.karabay@kocaeli.edu.tr

ABSTRACT: Magnetorheological (MR) dampers are widely used in cost-effective semi-active vibration control systems. Upon designing of a MR damper electromagnetic circuit analysis has a great importance. In this paper, electromagnetic analysis of MR modified from a conventional damper was carried out using ANSYS Mechanical APDL software. The modification was performed on the rod of the parent damper using copper wire wound. In order to analyze the magnetic field generated by a copper wire wound an axisymmetric FEM model was used. Different levels of current intensity, MR fluid types and fluid gap size conditions configurated. Besides, magnetic flux densities and magnetic field strength of the modified damper were analyzed. According to the obtained results, the magnetic flux density increases with increasing current level and decreasing gap size.

Key words: MR Damper, FEM, vibration control

INTRODUCTION

Jacob Rainbow, who was a researcher from the US National Bureau of Standards, discovered magnetorheological clutch in 1948 [1]. MR dampers are commonly used for semi-active vibration control in automotive industry with the aim of a high comfort riding as well as defense industry to maintain high survivability. Besides, some constructions such as bridges have MR dampers for absorbing vibrations during an earthquake. MR dampers consist of three main parts including piston, coil and fluid carrier. The piston moves in oil and contributes to damping by its movement. The copper wire winding creates the coil which has a role to manage magnetic field intensity. The fluid carrier contains magnetic particles and the piston moves in the MR fluid. Electromagnetic circuit design has a vital role on the damper's performance. Several studies have been focused on the electromagnetic circuit design for this reason. Magnetorheological fluids used in the MR dampers have three different constituents. These are magnetic particles, carrier liquid and surfactants which are needed to design individually. Walid [2] studied four different piston shapes for maximizing the damping force with FEM analysis. This study reported that the shear forces provided along the MR fluid gap increased by increasing magnetic flux density. Li et al. [3] studied FEM analysis and simulation of a MR valve combined with a core, a wound coil and a cylinder-shaped flux return. In order to prevent the magnetic saturation, the valve weight was minimized. The Bingham plastic model was used to predict MR valve performance. The FEM results of the MR valve were showed that maximum block pressure was 1900 kPa. Zhang et al. [4] studied a FEM modeling of MR dampers. They focused on the magnetic saturation and utmost improvement for high damping forces. The results showed that the energy dissipation and controllable damping force play an important role of MR dampers. They were both related to magnetic flux

density. After optimization, the energy dissipation and the damping force were increased. Nguyen et al. [5] studied a geometry optimization of a MR valve constrained in a specific volume using the FEM owing to decreasing pressure. The pressure drop was investigated with the Bingham plastic model. A FEM model was used for optimization. Different types of MR valves; single-coil annular, multi-coil annular and annular–radial were optimized. According to the results, the two-coil annular MR valve provided the best valve ratio value while the annular–radial type provided the best pressure drop at the optimal design parameters. Domingueze et al. [6] studied the modeling and application of MR dampers. They used Bouc-Wen mathematical model which simulates the hysteresis behavior of the damper. FEM model of the MR damper was also developed. They obtained a relation between simulations and experimental data. The results show that the amplitude and the fundamental natural frequency of the response of the structure can be predicted by FEM [6]. Kumar and Mangal [7] studied on FEM analysis of a MR damper. They studied on geometrical parameters and the magnetic flux density at the clearance space of the damper using ANSYS software and calculated total damping force. According to their findings total damping force increases with increasing current. Krishna et al. [8] studied fluid an optimization of MR dampers for maximizing magnetic flux density with FEM analysis. They analyzed the magnetic flux density for different fluid gaps. The results showed that the fluid gap any value of less than 1.12 mm were increased magnetic flux density.

In this paper, a conventional damper was modified using a coil and analyzed with ANSYS Mechanical APDL software. Magnetic field variations were arranged as three different gap sizes (0.5, 1, 1.5 mm), four different current values (0.5, 1, 1.5, 2 A) and three different MR fluids (Lord 122 EG, 132 DG, 140 CG). It is aimed to determine that how magnetic field forms after using a coil modification of a traditional damper.

FEM Modeling of the Damper

Components and geometrical parameters of the designed damper are given in Fig 1.

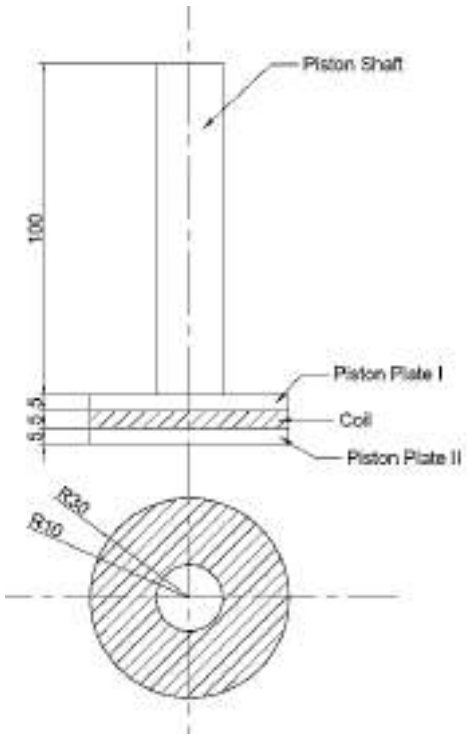

Figure 1. Components and Dimensions of the Damper

It's known that the magnetic circuit design has a very important role for magnetorheological properties of the damper. Viscosity and damping force are increases with increasing flux density in MR dampers. The ANSYS Mechanical APDL software was used in the study. Parallel flux boundary condition is applied to determine the magnetic field around the coil. In order to determine the current density, Eq. 1 is used. In Eq. 1, J_S is current density, N is the number of coils, I is current and A is cross-sectional area of the coil.

$$J_s = \frac{N \times I}{A} \tag{1}$$

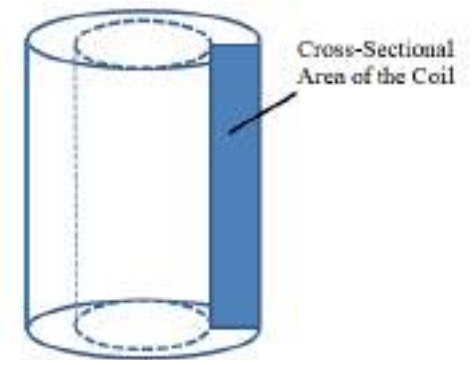

Figure 2. Cross-Sectional Area of Coil

A copper wire was used to forming the coil. The diameter of the wire was determined as 0.5 mm and winding was applied along the piston shaft. Thus 20 windings were obtained in one layer. Consequently, 40 layers were made owing to an increase in the cross-sectional area of the coil. When these values are applied in Eq. 1 with the parameters of 1 A, 800 turns and 200 mm^2, the current density;

$$J_S = \frac{800 \times 1}{200} = 4\ \mathrm{A}/mm^2 \tag{2}$$

The current density can be changed by changing the current. Designs for 0.5 - 1 - 1.5 and 2 A current values implemented in the study.

Table 1. Current Density Values for Applied Current Values

Current Value (A)	Current Density (A/mm²)
0.5	2
1	4
1.5	6
2	8

Magnetic field strength can be calculated using Eq. 3. In Eq. 3, H is magnetic field strength (A/m), N is the number of turns, I is current (A), l is the length of the coil (m).

$$H = \frac{N \times I}{l} \tag{3}$$

With using Eq. 3, the magnetic field strength can be calculated. Calculated magnetic field strength and current values are shown in Table 2.

Table 2. Current – Magnetic Field Strength Values

I(A)	H (A/m)
0.5	40000
1	80000
1.5	120000
2	160000

Various element types can be used for magnetic analysis in the ANSYS software. It is decided to use Plane13 element. It is a 2-D quadrilateral coupled-field-solid element and has four nodes. The Plane13 element has 2-D magnetic field and nonlinear magnetic capability for B-H curves [7]. Five steps were followed in the design; 1st creating the physical environment, 2nd modeling & meshing, 3rd applying loads & boundaries, 4th solution, 5th getting results and plots.

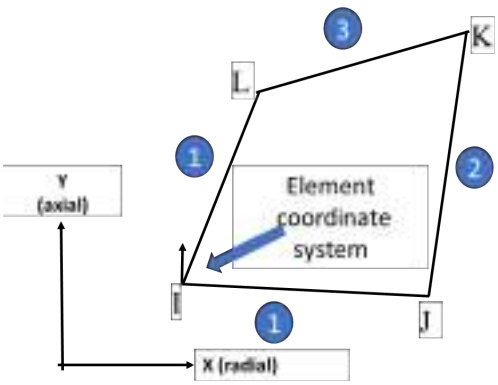

Figure 3. Plane 13 Element Description [7]

Design of Gap Size as 0.5 mm

The MR damper consists of different materials as copper, austenitic stainless steel, acrylic piston housing and MR fluid. Upon carrying out the magnetic analysis using FEM, some assumptions for magnetic permeability characteristics of the materials that are used in design of the damper were made. Relative permeability of copper, 304L austenitic stainless steel and acrylic were accepted as 1 [9, 10, 11] respectively. MR fluids have not magnetic relative permeability values; they have B-H curves. B-H curves have magnetic flux densities at different magnetic field strengths. The B-H curves of MR fluids were adapted from MRF-122EG [12], MRF-132DG [13] and 140 [14]. The plane 13 element allows entering these values in the material library. The change for magnetic calculations, The Magnetic-Nodal section was chosen in the preferences menu. Then, the element type was determined. After that, the materials (copper, silicone oil, steel) were created and set their relative magnetic permeability values and B-H curves. For magnetic calculations and design, the Magnetic-Nodal section was chosen, and the element type was determined.

Modeling & Meshing

For simplicity, a two-dimensional MR damper model was used. In this modeling section, firstly points, secondly lines and thirdly areas were created to prevent overlap. After these mentioned steps completed, model was created and meshed with the mesh tool. At this stage some points were added which were get from the AutoCAD design. For 0.5 mm gap size x_1, for 1 mm gap size design x_2 and for 1.5 mm gap size design x_3 were used. These points were shown in Table 4.

Table 4. In Active CS Points for Damper

Points	X_1	X_2	X_3	Y	Z
1	0	0	0	0	0
2	0.01	0.01	0.01	0	0
3	0.03	0.03	0.03	0	0
4	0.0305	0.031	0.0315	0	0
5	0.0335	0.034	0.0345	0	0
6	0.0335	0.034	0.0345	0.02	0
7	0.0305	0.031	0.0315	0.02	0
8	0.03	0.03	0.03	0.02	0
9	0.01	0.01	0.01	0.02	0
10	0	0	0	0.02	0
11	0.01	0.01	0.01	0.005	0
12	0.03	0.03	0.03	0.005	0
13	0.03	0.03	0.03	0.015	0
14	0.01	0.01	0.01	0.015	0

Modeling step was followed key points to lines and lines to areas before the meshing step. After the meshing step the working window was shown in Fig 4.

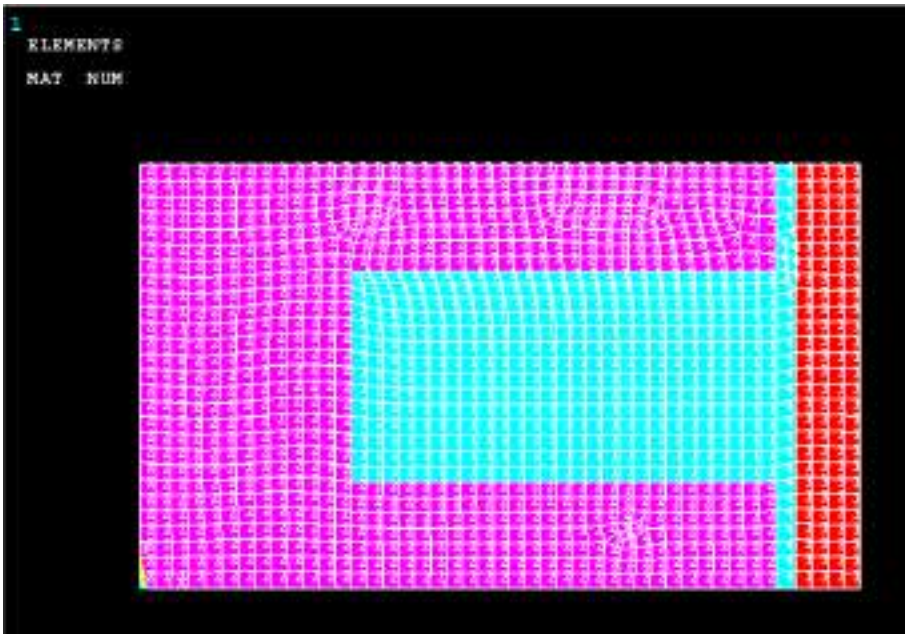

Figure 4. Working Window After Meshing Step

Applying Loads & Boundary Conditions

In ANSYS environment it's necessary to set boundaries. In this study it was assumed that the flux is parallel, and the boundaries set on the outer lines of the model. Then loads were applied due to J_S calculations which are shown in Table 1.

Solution

After applying boundary conditions and loads magnetic flux in the damper was analyzed. Magnetic flux gradient of 140 CG fluid, 0.5 mm gap size under 1.5 A condition is given in Figure 5.

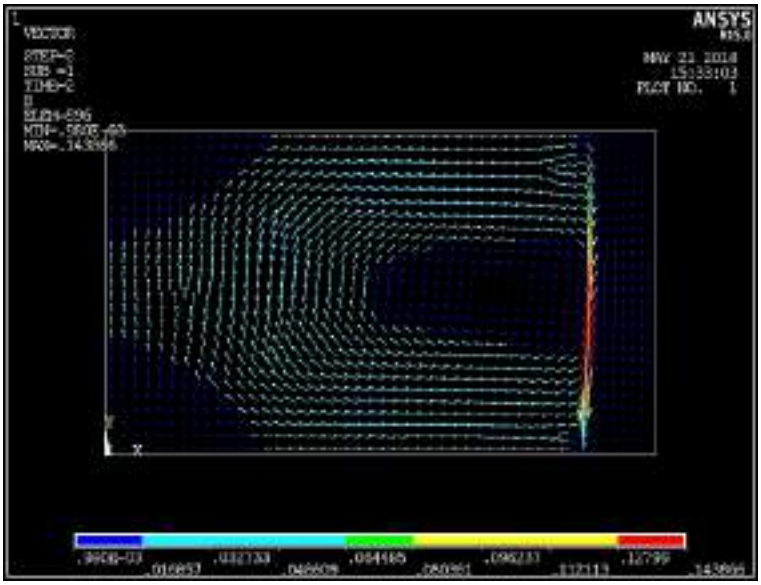

Figure 5. Magnetic Flux Gradient of 140 CG Fluid, 0.5 mm Gap Size Under 1.5 A

Design of gap sizes as 1 mm and 1.5 mm

ANSYS software does not allow modification after meshing. It is needed to remodel the system for different dimensions. So, the first step for 1 and 1.5 mm designs (creating a physical environment) was done in a new file. After that, the model was created again but this time x_2 and x_3 values were used and followed all the other steps respectively.

RESULTS

In this study a conventional damper was modified with the copper wound and then an axisymmetric FEM model was used. In the study the variables were defined as gap size, current and MR fluids. FEM modeling has the advantages of low cost and quick response compared with prototyping. The magnetic flux densities of the damper model were given in Table 4. It can be seen the magnetic flux density increases with increasing current value. This increasing trend is expected because the current parameter is a form of multiplier as given in Eq. 1.

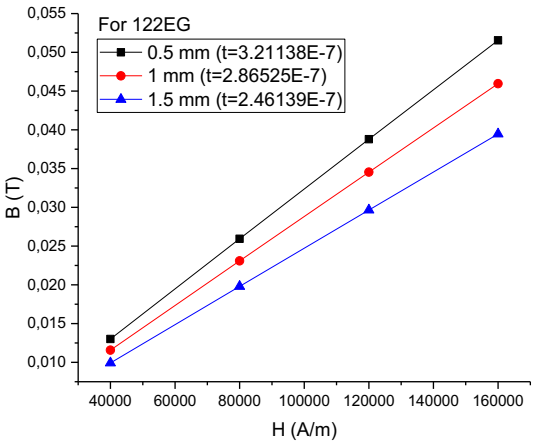

Figure 6. B-H Curve of the Damper Using Lord MRF-122 EG

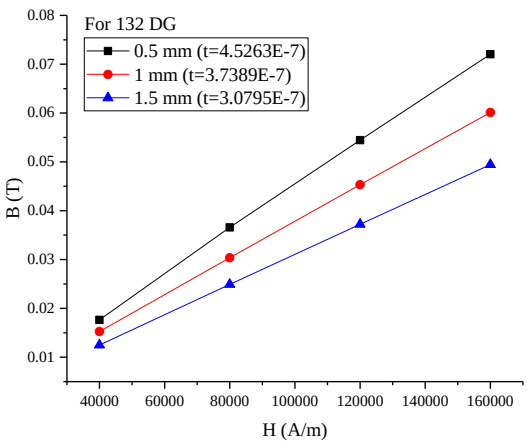

Figure 7. B-H Curve of the Damper Using Lord MRF-132DG

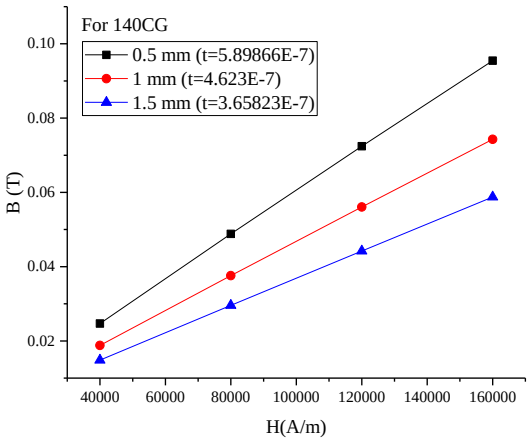

Figure 8. B-H Curve of the Damper Using Lord MRF-140CG

Increase in flow gap leads to more flux leakage, which results a decrease in magnetic flux density (Fig. 7). The magnetic flux density is perpendicular to the flow direction through the flange length that develops field dependent resistance on MR fluid flow. According to the results in Fig. 8 the smaller flange length causes bigger magnetic flux density on the MR fluid flow gap. Moreover, the magnetic flux density increases by increasing core diameter and core length. In both the cases, wrapping of more wire is required to construct the coil in order to produce more electromagnetic field. Therefore, the magnetic flux density increases gradually with increasing core length.

CONCLUSION

In this paper, a MR damper for vibration control application is designed and simulated. A conventional damper was modified with the copper wound and then an axisymmetric FEM model was used for analyzing to detect final effects on the model. Parallel flux boundary condition is applied to determine the magnetic field around the coil. The current density is changed from 2 to 8 A/mm^2 by arranging current values as 0.5 - 1 - 1.5 and 2A. The magnetic field strength and current values calculated according to the mathematical model. The simulation results indicate that the magnetic flux density increases with increasing current value. Increase in flow gap leads to more flux leakage, which results decrease in magnetic flux density.

REFERENCES

[1] Rabinow, J. (1948). Proceedings of the AIEE trans. *The Magnetic Fluid Clutch*, 67: 1308-1315.

[2] Walid, H. E. (2002). *Finite element based modeling of magnetorheological dampers.* September 23, 2002, M.Sc. Thesis, Virginia Polytechnic Institute and State University

[3] Guo, N., Du, H. & Li, W. (2003). Finite Element Analysis and Simulation Evaluation of a Magnetorheological Valve. *The International Journal of Advanced Manufacturing Technology*, 21, 438-445. https://doi.org/10.1007/s001700300051

[4] Zhang, H. H., Liao, C. R., Chen, W. M. & Huang S. L. (2006). A Magnetic Design Method of MR Fluid Dampers and FEM Analysis on Magnetic Saturation, *Journal*

of Intelligent Material Systems and Structures, 17(8-9), 813-818. https://doi.org/10.1177/1045389X06057537

[5] Nguyen, Q. H., Han, Y. M., Choi, S. B. & Wereley, N. M. (2007). Geometry Optimization of MR Valves Constrained in a Specific Volume Using the Finite Element Method, *Smart Materials and Structures*, 16(6), 2242-2252. http://doi:10.1088/0964-1726/16/6/027

[6] Dominguez, A., Sedaghati, R. & Stiharu, I. (2008) Modeling and Application of MR Dampers in Semi-adaptive Structures, *Computers and Structures*, 86(3-5), 407-415. https://doi.org/10.1016/j.compstruc.2007.02.010

[7] Kumar, A. & Mangal, S.K. (2014). Finite Element Analysis of Magneto-Rheological Damper, *Asian Journal of Engineering and Applied Technology*, 3, 42-46.

[8] Krishna, G., Kumar, H. & Gangadharan, K. (2017). Optimization of Magneto-Rheological Damper for Maximizing Magnetic Flux Density in the Fluid Flow Gap Through FEA and GA Approaches, *Journal of The Institution of Engineers (India): Series C*, 98(4), 533-539. https://doi.org/10.1007/s40032-016-0251-z

[9] Engineering ToolBox, (2016). *Permeability. online*. Retrieved from https://www.engineeringtoolbox.com/permeability-d_1923.html [Accessed 07 09 2018].

[10] A service provided by the SSAS Information Sheet No.2.81 British Stainless Steel Association, (2000). *Magnetic Properties of Stainless Steel online*. Retrieved from https://www.bssa.org.uk/cms/File/SSAS2.81-Magnetic%20Properties.pdf [Accessed 07 09 2018].

[11] Acrylic (PMMA) Clear Plastic Balls Retrieved from https://www.rgpballs.com/en/acrylic-pmma-balls/ [Accessed 22 05 2018].

[12] British Stainless Steel Association, LORD MRF-122DG fluid technical data Retrieved from http://www.lordmrstore.com/_literature_231216/Data_Sheet_-_MRF-122EG_Magneto-Rheological_Fluid [Accessed 07 09 2018].

[13] British Stainless Steel Association LORD MRF-132DG fluid technical data Retrieved from http://www.lordmrstore.com/_literature_231215/Data_Sheet_-_MRF-132DG_Magneto-Rheological_Fluid [Accessed 07 09 2018].

[14] British Stainless Steel Association LORD MRF-140G fluid technical data Retrieved from http://www.lordmrstore.com/_literature_231214/Data_Sheet_-_MRF-140CG_Magneto-Rheological_Fluid [Accessed 07 09 2018].

SUPERPLASTIC FORMING OF ALUMINUM ALLOYS

Fahri VATANSEVER[1]*, Alpay Tamer ERTÜRK[1], Sedat KARABAY[1]
[1]Department of Mechanical Engineering, Engineering Faculty, Kocaeli University
fahrivatansever@gmail.com, tamererturk@gmail.com, sedat.karabay@kocaeli.edu.tr

ABSTRACT: Superplastic forming (SPF) process is an advanced manufacturing technique for fabricating complex shaped parts. This process is used to form aluminum parts for low volume productions especially in aerospace, rail, and automotive sectors. Superplasticity refers to the ability of metals exhibiting extensive elongations prior to failure. Having a very small grain size of the raw material microstructure is needed to achieve this forming property. In addition that the material must be formed at elevated temperatures and at low strain rates. In this study, process conditions required for SPF are indicated for aluminum alloys. Besides, advantages and disadvantages of the forming process are compared with the conventional forming methods.

Key words: aluminum alloys, superplastic forming technique, strain rate sensitivity, microstructure

INTRODUCTION

Polycrystalline materials such as aluminum are generally exhibit low elongation at break when exposed to tensile stress. However, some of these materials may exhibit a very large neck free elongation under certain conditions [1]. This large neck free elongations occurs at least 400% and often exceed 1000% that is defined as "superplasticity" [1-3]. An example of this neck free elongation is given in Fig. 1.

It is accepted that a material must have two characteristic properties in order to considered as a superplastic material [4-7]. First, the material must have a very small grain size (d<10 μm) and the forming process should be conducted at elevated temperatures ($T>0.5T_m$ where T_m is the melting point) [4-7]. As a general practice, grain growth occurs at elevated temperatures in metals. It is favorable to use two-phase materials where presence of two separate phases leads to a significant inhibition in grain growth [1, 3, 5].

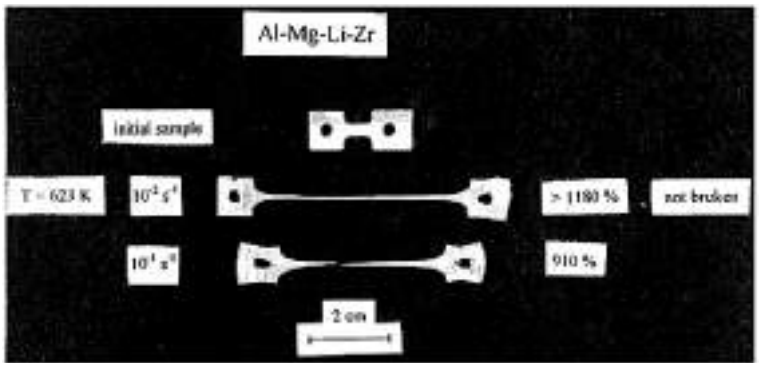

Figure 1. The First Example of High Strain Rate Superplasticity Reported in the Literature for an Ultrafine-Grained Al-Mg-Li-Zr Alloy in 1997 [3]

Using SPF technique very complex and curved parts can be produced with minimal initial investment cost. In order to obtain high elongation without failure, it is necessary to work with low strain rates in the range of 10^{-5} to 10^{-2} s^{-1} [8]. The forming time of a material using SPF technique ranges from twenty minutes to several hours according to the geometry of final product due to low strain rates [8]. SPF is used to manufacturing of components for planes, trains, automobiles and a whole lot more despite high production durations [9] as shown in Fig. 2 with the advantages of [2, 10-12]:

- Greater design of freedom - producing ability for complex shapes,
- The ability to build large assemblies with fewer pieces,
- Lower manufacturing costs for low and medium volume productions,
- Reduced weight and component count,
- Shorter lead time from design to delivery of the produced part,
- Elimination of springback forces.

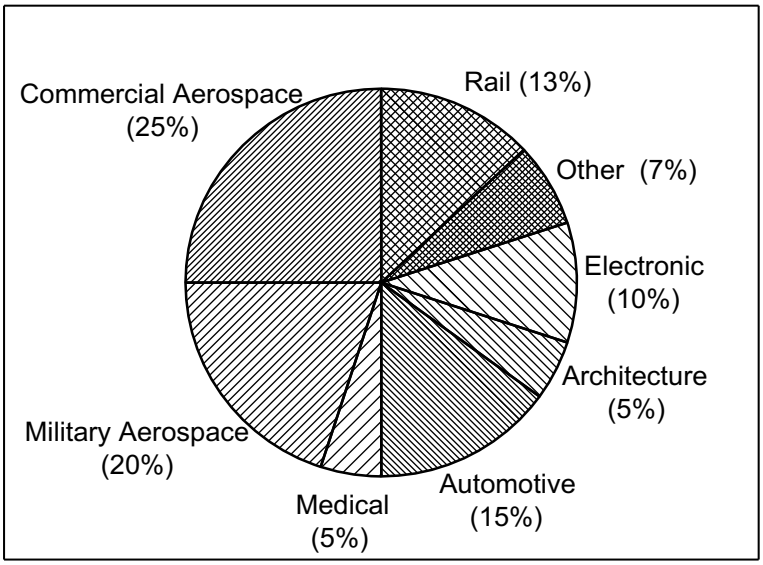

Figure 2. Using Areas of Superplastic Formed Aluminum Materials [10]

METHODS

Various SPF techniques as simple female forming, drape forming, male forming, backpressure forming and diaphragm forming used in industry [10]. Mostly using one of these techniques is the simple female forming which's schematic is given in Fig. 3. In this technique, a heated superplastic sheet is clamped around its edge and stretched into the heated cavity tool using gas pressure [10]. Upon using this technique tooling is significantly less expensive than that for a conventional stamping [12]. It must be considered that the parameters such as temperature, strain rate, gas pressure and clamping force must be controlled precisely [9].

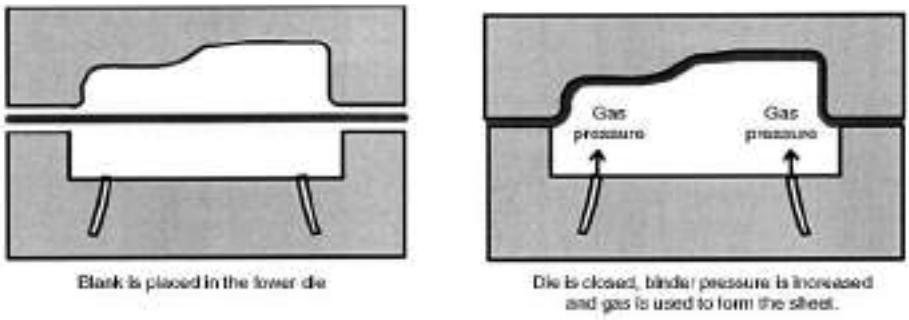

Figure 3. Schematic of the Simple Female SPF Technique [12]

Many alloy systems such as duplex eutectics, eutectoids (Zn-Al, Al-Cu, Al-Si, Al-Ca, Al-Pd) and standard alloys such as 7075, 7050, 2219, 6082, 8083 have been studied with SPF[10]. Among these alloys, only a limited number of aluminum alloy have become commercially available as listed in Table 1 with their compositions and typical mechanical properties [10].

Table 1. Composition and Properties of SPF Aluminum Alloys Currently in Use [10]

Alloy	Composition	Yield Strength (MPa)	UTS (MPa)	Elastic Modulus (GPa)	Density (kg/m^3)
2004	Al-6%Cu-0.4%Zr	300	420	74	2.83
2090	Al-2.5%Cu-2.3%Li-0.1Zr	340	450	79	2.57
2095	Al-4.7%Cu-0.37%Mg-1.3%Li-0.4%Ag-0.14%Zr	585	620	78	2.7
5083	Al-4.5%Mg-0.1%Cr	150	300	72	2.67
7475	Al-5.7%Zr-2.3%Mg-1.5%Cu-0.2%Cr	500	550	70	2.8
8090	Al-2.4%Li-1.2%Cu-0.6%Mg-0.1%Zr	350	450	78	2.55

2004, 5083 and 7475 aluminum alloys among the alloys given in Table 1 represent 90% usage of SPF owing to excellent superplastic formability, weldability, heat-treatability properties of 2004 alloy, corrosion resistance and durability properties of 5083 alloy, heat-treatability and strength properties of 7475 alloy [11].
It was mentioned that three key factors of SPF are small grain size, elevated processing temperatures and low strain rates. In Fig. 4(a) graphs of σ-$\dot{\varepsilon}$ and $(\Delta L/L_0)\%$-$\dot{\varepsilon}$ of a two-phase Zn-22%Al eutectoid alloy where the average spatial grain size is 2.5 µm and the testing temperatures in a range of 423-503 °K are given. The upper plot shows the measured elongations to failure and the lower plot shows the flow stress as a function of different strain rate values. It is obvious from the lower plot, different strain rate values divide the graph into three well-defined regions as I, II and III having different strain rate sensitivity values. The data in the upper plot shows that the material exhibits higher superplastic ductilities in region II where the tensile elongations extend up to nearly 3000% [5]. Mohamed [6] defined these regions as the low stress region (Region I), the superplastic region (Region II) and the high stress region (Region III) as given in Fig. 4(b).

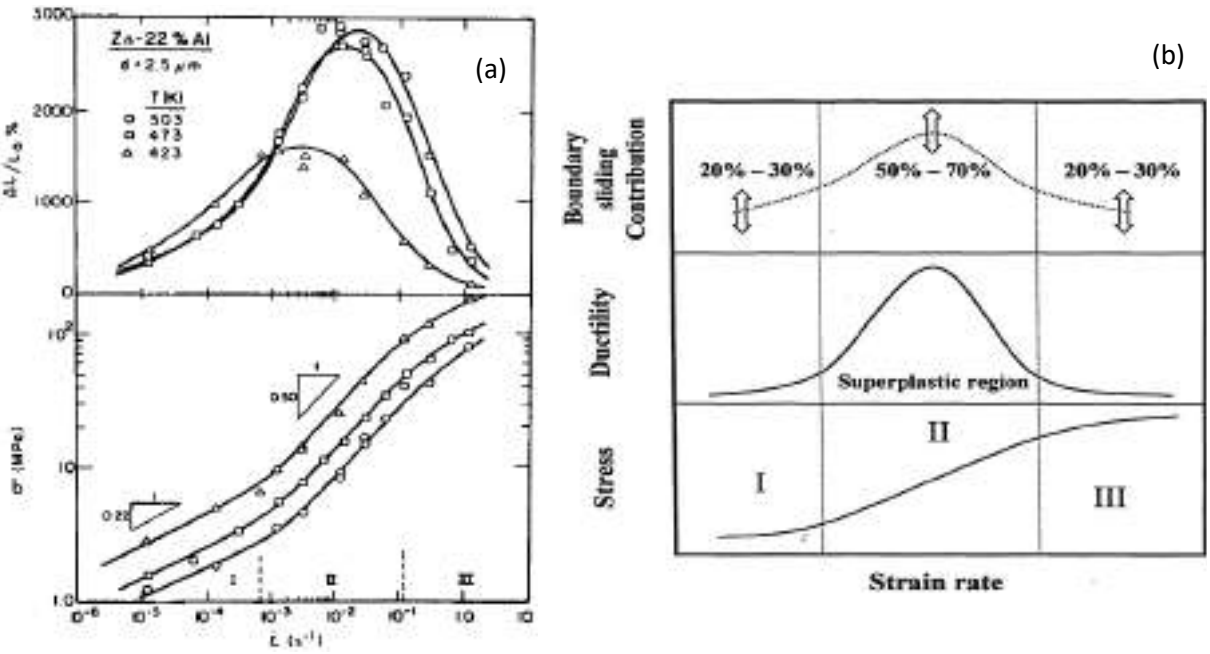

Figure 4. (a) Variation of the Elongation to Failure (Upper) and the Flow Stress (Lower) with the Imposed Strain Rate for a Zn-22%Al Eutectoid Alloy Tested Over a Range of 423-503 °K Temperatures [5], (b) a Schematic Representation for the Characteristics of Micrograin Superplasticity [6].

It's evident that superplastic regime is displaced to faster strain rates when the grain size of the material is reduced [13]. In other words, as long as obtaining nanometer level grain sizes, strain rate of the SPF may be increased [13]. Conventional manufacturing techniques such as casting and extrusion do not provide the small grain size needed for SPF. In order to achieve small grain sizes necessary to SPF, different production techniques such as equal channel angular pressing (ECAP), high pressure torsion (HPT) multi-directional forging, twist extrusion, cyclic extrusion-compression, friction stir processing (FSP), repetitive corrugation and straightening (RCS), constrained groove pressing (CGP), cylinder covered compression, accumulative roll-bonding (ARB) are used [4]. While this advanced manufacturing processes making SPF possible, at the same time increase production costs. Achieving severe plastic deformation on a material, ECAP has been mostly used method among the others using for obtaining small grain size. There is a sample of SPF application for producing dome form parts using raw billets processed by ECAP in Fig. 5.

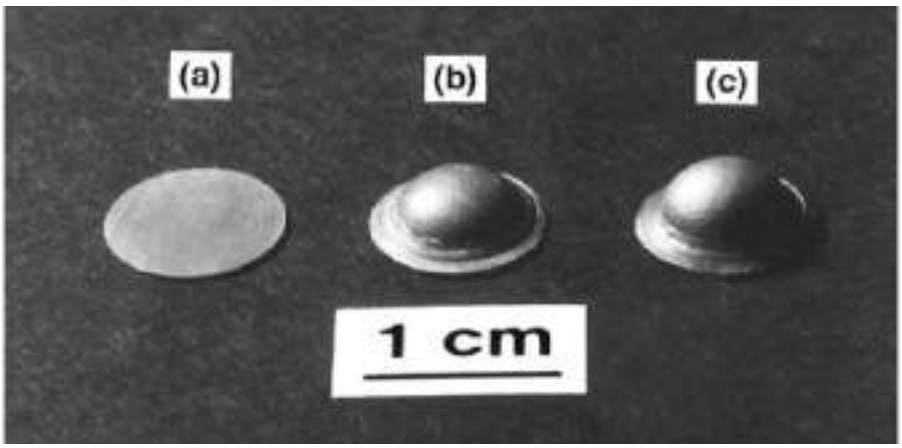

Fig. 5. Domes Produced by SPF in Disks of the Al-3%Mg-0.2%Sc Alloy Cut From Billets Processed by ECAP: (a) Initial Condition Without SPF, (B) and (C) were Held at 673 °K Under a Gas Pressure of 1 Mpa for 30 and 60 S, Respectively [1, 13]

CONCLUSION

- SPF is a production technique used to manufacturing complex shaped parts from aluminum sheets.
- Upon using SPF it is required to precise control of many critical parameters such as temperature, strain rate, applied gas pressure and clamping force.
- While it is advantageous that using SPF for low volume productions in the terms of production costs, for high volume productions SPF loses its advantage against traditional production techniques such as sheet metal forming, stamping and welding.

REFERENCES

[1] Langdon, T. G. (2009). Seventy-five years of superplasticity: Historic developments and new opportunities. *Journal of Materials Science*, *44*(22), 5998-6010.

[2] Barnes, A. J. (1999). Superplastic Aluminum Forming - Expanding Its Techno-Economic Niche. *Materials Science Forum*, *304-306*, 785-796.

[3] Langdon T. G. (2013), Achieving superplasticity in ultrafine-grained metals, *Mechanics of Materials, 67, 2-8.*

[4] Valiev, R. Z., & Langdon, T. G. (2006). Principles of equal-channel angular pressing as a processing tool for grain refinement. *Progress in Materials Science*, *51*(7), 881-981.

[5] Kawasaki, M., & Langdon, T. G. (2007). Principles of superplasticity in ultrafine-grained materials. *Journal of Materials Science*, *42*(5), 1782-1796.

[6] Mohamed, F. A. (2011). Micrograin superplasticity: Characteristics and utilization. Materials, 4(7), 1194-1223.

[7] Mikhaylovskaya, A. V., Kotov, A. D., Pozdniakov, A. V., & Portnoy, V. K. (2014). A high-strength aluminium-based alloy with advanced superplasticity. Journal of Alloys and Compounds, 599, 139-144.

[8] Babu, S. R., Deivanayagam, S., & Aravind, M. (2014). Determination of material parameters during superplastic forming of AA 5086 alloy. *Procedia Engineering*, *97*, 1379-1386.

[9] Barnes, A. J. (2007). Superplastic forming 40 years and still growing. *Journal of Materials Engineering and Performance*, *16*(4), 440-454.

[10] Barnes, A. J. (2001). Industrial Applications of Superplastic Forming: Trends and Prospects. Materials Science Forum, 357-359, 3-16.

[11] Sanders, D. (2001). The current state-of-the-art and the future in airframe manufacturing using superplastic forming technologies. Materials Science Forum, 357, 17-22.

[12] Friedman, P. A., Luckey, S. G., Copple, W. B., Allor, R., Miller, C. E., & Young, C. (2004). Overview of superplastic forming research at ford motor company. Journal of Materials Engineering and Performance, 13(6), 670-677.

[13] Horita, Z., Furukawa, M., Nemoto, M., Barnes, A., & Langdon, T. (2000). Superplastic forming at high strain rates after severe plastic deformation. Acta Materialia, 48(14), 3633-3640.

THE EFFECT OF GREEN ROOF ON URBAN HYDROLOGIC CYCLE

Bülent TOKATLI
University of Gaziantep
bulent@teknocev.com.tr

Soner Çağatay BAĞÇACI
Karamanoğlu Mehmetbey University
scbagcaci@kmu.edu.tr

Nermin ŞARLAK
Karamanoğlu Mehmetbey University
nsarlak@kmu.edu.tr

ABSTRACT: It has been observed that urban land cover is dominated by impervious surface in recent years. That is, urbanization increases the amount of surface runoff as much as urban heat island effect and alters the flow regime of water supply. To remedy these negative effects, green roof has been suggested by several researchers. The main objective of this study was to evaluate its performance on reducing stormwater runoff in Gaziantep. The mathematical model was developed to simulate the stormwater response of hypothetical extensive green roof with 40 mm growing media depth during warm season (April-October) from 2008 to 2010. The hypothetical green roof managed to retain 58% of total observed precipitation during the study period. In addition, the ratio of total evapotranspiration to total precipitation was determined as 0.60. In this study, it was managed to numerically express the effect of green roof performance on stormwater retention when applied in Gaziantep.

Key words: extensive, green roof, stormwater retention, urbanization

KENTSEL HİDROLOJİK DÖNGÜDE YEŞİL ÇATI ETKİSİ

ÖZET: Son yıllarda şehir arazi kullanımında geçirimsiz yüzeylerin hakim olduğu gözlenmektedir. Yani, şehirleşme ısı adası etkisi kadar yüzey akış miktarını artırmakta ve su kaynakları akım rejimini değiştirmektedir. Kentleşmenin negatif etkilerini azaltmak için yeşil çatı pek çok araştırmacı tarafından önerilmektedir. Çalışmanın başlıca amacı, Gaziantep ili yağmur suyu kaynaklı akışın azaltılmasında yeşil çatının performansını değerlendirmektir. Matematiksel model, 2008-2010 yılları ılıman sezon (Nisan-Ekim) süresince 40 mm yetiştirme ortamı derinliğine sahip hipotetik ekstensif yeşil çatının yağmur suyuna tepkisini benzetim kurmak için geliştirildi. Hipotetik yeşil çatının çalışma süresi boyunca gözlemlenen toplam yağışın %58'ini tutmayı başardığı tespit edilmiştir. Ayrıca, toplam buharlaşma-terleme miktarının toplam yağışa oranı 0.60 olarak belirlenmiştir. Bu çalışmada, yeşil çatının Gaziantep ilinde uygulandığında yağmur suyunu tutmadaki etkisinin sayısal olarak ifade edilmesi başarılmıştır.

Anahtar sözcükler: ekstensif, yeşil çatı, yağmur suyu tutma, kentleşme.

GİRİŞ

Türkiye artan nüfus yoğunluğu ile birlikte gelişmekte olan bir ülkedir. Ülkemizde, 1980 yılında yapılan nüfus sayımına göre 44 736 957 kişinin yaklaşık 20 milyonu şehirlerde yaşarken, bu sayının 2016 yılında yaklaşık 74 milyon kişiye ulaştığı Türkiye İstatistik Kurumu (TÜİK) tarafından tespit edilmiştir (TÜİK, 2017). Bu sonuçlar kırsal kesimden şehirlere ciddi bir göç akımının olduğunu göstermektedir. Kentlerde artan nüfus beraberinde bina (konut, hastahane, okul vb.), yol (kara, hava, demir) ve otopark alanları yapılmasını zorunlu hale getirmiştir. Söz konusu ihtiyaçları karşılamak için ise önceden otlak, mera veya tarım arazisi olan geçirimli alanlar imara açılmakta ve geçirimsiz alanlara dönüştürülmektedir. Geçirimli alanların şehirlerde azalması, özellikle kısa süreli ani yağışlardan sonra kentsel selin oluşmasına yol açarken, geçirimli alanlarda toprak ve bitki tarafından tutulabilen yağış, geçirimsiz alanlarda doğrudan akışa geçmektedir. Son yıllarda ülkemizde bu tip sellerin oluşmasında artış gözlemlenmektedir. 2016 Aralık ayında Mersin ilimizde 24 saatte düşen 155.8 mm yağışdan sonra oluşan kentsel selin neden olduğu maddi zararın yaklaşık 48 milyon TL olduğu belediye yetkilileri tarafından açıklanmıştır. Ayrıca sel felaketinde iki vatandaşımız hayatını kaybetmiştir. 2017 Temmuz ayında İstanbul'da 2 saatte metre kareye düşen 91 kg yağış zor anlar yaşatmış, maddi hasarlara ve yaralanmalara neden olmuştur. Kentlerde yağmur suyu drenaj sistemleri bulunsa bile, şiddetli yağışlardan sonra oluşan akışı gidermede yetersiz kaldıklarından istenmeyen sonuçlarla karşılaşılmaktadır.

Kentleşmenin beraberinde getirdiği ısı adası ve doğrudan akışa geçen yağışın neden olduğu olumsuzlukları gidermek için sunulan alternatif çözüm önerilerinden biri yeşil çatıdır. Uzun yıllardır kuzey Avrupa ve Amerika'da uygulanma alanları bulan yeşil çatı sistemleri, ektensif (seyrek) ve intensif (yoğun) olmak üzere iki tiptir. Ektensif yeşil çatı tipi, intesif çatı tipine göre daha hafif, daha sığ yetiştirme ortamı derinliğine sahip (<150 mm) ve daha az bakım gerektirir (Martin, 2008). Yetiştirilen bitki olarak tercih edilen, su olmadan çok uzun süre var olabilme yetisine sahip *Sedum* türleridir. Fotosentez yapmada kullanacağı karbondioksiti almak için gece gözeneklerini açabildiğinden, gündüz terleme esnasında kaybedeceği suyu muhafaza edebilmektedir (Starry ve ark., 2014). Bitkinin ekilip yetişebilmesi için gerekli suyu tutabilecek ve kökleri için uygun alanı sağlayabilecek yetiştirme ortamını saksıya benzetirsek, uygun derinliğe ve çatılardan binaya suyun sızmasını engellemek için kauçuk gibi yalıtım malzemelerinin serilmesi gerekir (Martin, 2008).

Yeşil çatıların, düşen yağışın yüzey suları oluşturmasını azalttığını ortaya koyan literatürde deneysel ve teorik pek çok çalışma mevcuttur. Connelly ve Liu, Kanada' da 100 m^2'lik binada tesis ettikleri 75 mm yetiştirme ortamına sahip çeşitli *Sedum* türleri yetiştirilen yeşil çatının yağmur sularını tutma performansını ölçüm yaparak gözlemlemişlerdir (Connelly ve Liu, 2005). 11 yağışsız geçen günden sonra 4 saat 23 dakikada yağan 12.19 mm yağışın %95'in yeşil çatı tarafından tutulduğunu saptamışlardır. Takip eden 13, 14 ve 15. günde yağan yağış ile doygunluğa ulaşma

noktasına gelen yeşil çatı sisteminin su tutma performansının %17'lere kadar düştüğünü tespit etmişlerdir. VanWoert ve ark., bitki yetişen ve yetişmeyen iki ektensif yeşil çatının yağmur suyu tutma yetisini araştırmışlardır (VanWoert ve ark., 2005). İki aylık çalışma süresinde yağan toplam yağışın %60'ının yeşil çatı tarafından alıkonduğu bulunmuştur. Ayrıca çalışmada bitki yetişen ve yetişmeyen ektensif yeşil çatının çok az farklılık gösterdiği saptanmıştır. Bu durum bize buharlaşmanın su dengesinde ne kadar dominant olduğunu vurgulamaktadır. Ekşi ve Uzun, İstanbul Üniversitesi yerleşkesinde 10.2 m^2'lik alana sahip ekstensif yeşil çatı sistemi kurmuşlar ve Aralık 2010- Kasım 2011 arası gözlem yapmışlardır (Ekşi ve Uzun, 2016). 2 Temmuz- 11 Ağustos 2011 tarihleri arasında yağışsız geçen 39 günün ardından 24.6 mm düşen yağışın yeşil çatı sisteminden 14 saat sonra %67 oranında tutularak akışa geçtiğini gözlemlemişlerdir. Carter and Rasmussen, Georgia Üniversitesinde tesis ettikleri çalışma alanında Kasım 2003- Kasım 2004 arasında yeşil çatının yağmur suyunu tutma performansını gözlemlemişlerdir (Carter and Rasmussen, 2006). Yağış yükseklikleri 0.28'den 8.43 cm aralığında değişen 31 yağış olayını incelemişlerdir. Yeşil çatının küçük yağışların (<2.54 cm) %90'nını tuttuğunu, buna karşılık daha büyük yağışların (>7.62 cm) %50'sini tutabildiğini tespit etmişlerdir. Geleneksel klasik çatılara nazaran yeşil çatının akış hidrografında sağladığı geciktirme 17.9 dakika olarak saptanmıştır. Toprak Koruma Servisi (SCS) yağış akış modellemesinde gereken eğri sayısını (CN) kendi çalışmaları için 86 olarak belirlemişlerdir. CN için yüz değerinin su yüzeyini temsil ettiği düşünülürse, yeşil çatının su tutma kapasitesinin yüksek olduğu anlaşılmaktadır. Çalışmalarında toprağın önceki nem durumunu göz önüne almamışlardır. Akımın oluşmasında toprağın nem durumu oldukça etkili olduğundan, çalışmanın sonuçları yorumlanırken bu durum göz önünde tutulmalıdır. Konu ile ilgili yapılan teorik çalışmalarda yeşil çatının performansını saptamada su dengesi modelinin kullanıldığı anlaşılmaktadır. Hilten ve ark., toprak nem simulasyonu olan Hydrus-1D paket programını yağmur suyunu geciktirmede yeşil çatı performansını göstermek için kullanmışlardır (Hilten ve ark., 2008). Modelin girdi verileri tarla kapasitesindeki hacimsel su, bitki kuruma noktası, potansiyel buharlaşma-terleme ve yağıştır. İlgili veriler 37 m^2'lik 10 cm yetiştirme ortamına sahip farklı *Sedum* bitkilerinin yetiştiği modüler olarak yerleştirilen yeşil çatıda ölçülerek elde edilmiştir. Çalışmada küçük yağışların (<2.54 cm) tamamının tutulduğu, daha büyük yağışlardan oluşan akışların geciktirildiği saptanmış ve yeşil çatı performansının yağış şiddetine bağlı olduğu vurgulanmıştır. 5 ve 7.93 cm arasında değişen yağış yükseklikleri için geciktirme zamanının yaklaşık 12 saat olduğu bulunmuştur. Prowell, kütlenin korunuma dayanan rezervuar modelini yeşil çatı için kullanmıştır (Prowell, 2006). Model sisteme giren (yağış vb.) ve sistemden çıkanların (akış, buharlaşma, terleme vb.) oluşturduğu +/- depolama miktarlarının belirlenmesi üzerinedir. 18 yağış olayını inceleyerek modelden ve gözlem yaparak ölçtüğü akış ve tutulan yağış verilerini kıyaslamıştır. Küçük yağışların tutulmasında model ile gözlem arasında bir fark saptanmamış, fazla yağış olduğunda modelden bulunan gecikme zamanı ölçüm ile elde edilenden daha fazla bulunmuştur. Çalışmada sedum bitkisinin ekilip ekilmemesinin tutma ve geciktirmede etkisi olmadığı sonucuna varılmıştır. Martin, Waterloo (Kanada) iklim verilerini kullanarak hipotetik yeşil çatının yağmur suyu tutma performansını teorik olarak araştırmıştır (Martin, 2008). Çalışma zamanı süresince alınan toplam yağışın yalnızca %29'unun akışa geçtiğini saptamıştır.

Gaziantep Büyükşehir Belediyesi 2012 yılında "Gaziantep Kilis Yolu ve Çevresi Vizyon Planı" kapsamında ekolojik kent uygulama tasarım rehberi hazırlamıştır (GBB, 2012). Bu şekilde doğa ile uyumlu, ekonomik olarak etkin sürdürülebilir bir kent vizyonu oluşturmaya çalışılmıştır. Tasarım rehberinde çatı tipi olarak yeşil çatı önerilmiş ve gerekçe olarak çatı yüzeyindeki ısı farkını azaltarak enerji verimliliği sağladığı, emisyonları/gürülüyü emdiği ve estetik yeni kullanım alanları oluşturduğu sunulmuştur. Bu çalışmada ise, teorik ve deneysel olarak performansı ortaya konulmuş yeşil çatının Gaziantep ilinde uygulandığında yağmur suyunu tutmadaki etkisinin sayısal olarak ortaya konulması hedeflenmiştir.

YÖNTEM

Çalışma Alanı

Gaziantep sıcak-kuru iklim tipinde; yaz ayları sıcak ve kurak geçerken kış ayları çok soğuk değildir. 17261-Devlet Meteoroloji İşleri istasyonu (37^o04^1 Kuzey, 37^o23^1 Doğu) Ocak 2000- Aralık 2011 dönemi verileri baz alındığında ortalama günlük kış ayları sıcaklığı 5.2 ^oC ve yaz ayları sıcaklığı 27.9 ^oC olarak ölçülmüştür. Aynı dönem ortalama yağmurlu gün sayısı seksenbirken, kar yağışlı gün sayısı dokuzdur. En fazla yağış Aralık 2010' da 66.5 mm olarak ölçülmüştür.

Çalışmada kar yağışı olan günlerden kaçınmak için 2008'den 2010 yılına kadarki Nisan-Ekim ılıman sezon 214 günlük meteorolojik veri kullanıldı. Söz konusu döneme ait toplam yağış yüksekliği 338.8 mm ve yağışlı gün sayısı 79'dur.

Çalışma, hipotetik ekstensif yeşil çatı üzerinde teorik olarak gerçekleştirilmiş olup, çeşitli Sedum türünün ekildiği varsayılarak yetiştirme ortamı derinliği 40 mm olarak belirlenmiştir.

Su Dengesi Yaklaşımı

Su dengesi yaklaşımı yağış ile artan, buharlaşma-terleme ve akış ile azalan yeşil çatı yetiştirme ortamında depolanabilen su miktarına dayanmaktadır.

$$D_i=D_{i-1}-P_i+R_i+BT_{a,u,i} \quad (1)$$

eşitlikteki D_i (mm) i zamanı sonunda yetiştirme ortamındaki su eksikliğini, P_i (mm), R_i (mm) and $BT_{a,u,i}$ (mm) sırasıyla i zamanı süresince gerçekleşen yağış, akış ve standart olmayan koşullarda buharlaşma-terleme miktarını ifade etmektedir. D_{i-1} i zamanından bir önceki zamandaki su eksikliğini göstermektedir. Bilindiği üzere terleme kökler aracılığı ile bitkinin topraktan besin elementleri ile aldığı suyu, yapraklarındaki stomaları (gözenekleri) karbondioksit almak için açtığında kaybetmesi olayıdır. Buharlaşma ise açık su yüzeylerinden olan su kaybıdır. Bitki kaplı alanlarda buharlaşma ve terlemeyi ayrı ayrı hesaplamak zor olduğundan, buharlaşma-terleme miktarı literatürde mevcut ampirik yöntemler ile belirlenebilmektedir. Birleşmiş Milletler Gıda ve Tarım Örgütünün (FAO) 1998 yılında bir grup uzmanın katılımı ile

hazırladığı FAO-56 Penman-Monteith buharlaşma-terleme hesabı, pek çok araştırmacı tarafından ölçülmüş değerlere en yakın sonuç verdiği ortaya konulmuş ampirik bir yöntemdir (FAO-56, 1998). Potansiyel buharlaşma-terleme miktarı söz konusu yöntem kullanılarak tahmin edilmiştir. Standart olmayan koşullarda buharlaşma-terleme miktarı, $BT_{a,u,i}$ (mm) aşağıdaki eşitlikten hesaplanmaktadır:

$$BT_{a,u,i}=k_c*k_s*BT_{o,i} \quad (2)$$

eşitlikteki k_c, k_s ve $BT_{o,i}$ sırasıyla bitki katsayısı, su stresi katsayısı ve 12 cm boyunda tamamen alfafa veya çim örtüye sahip alanda, su sıkıntısı yaşanmayan dönemde standart koşullar altındaki potansiyel su tüketimidir. k_c katsayısı alfafa veya çim haricindeki bitkilerden gerçekleşen su tüketimini belirlemede önem arz etmektedir. Bitkinin su stresi altında olmadığı (k_s=1) standart koşullardaki su tüketimi $BT_{a,i}$ olarak ifade edilmektir. k_s katsayısı bitkinin su alabilmesine göre aşağıdaki eşitlikten hesaplanabilmektedir:

$$k_s=FKS-D_{i-1}/FKS-HMS \quad (3)$$

eşitlikteki FKS, faydalı kullanılabilir su yüksekliği (mm) ve HMS herhangi bir zorlama olmaksızın bitki tarafından rahatça alınabilen hali hazırdaki mevcut su yüksekliğidir (mm). Yetiştirme ortamında HMS'den daha fazla su eksikliği yaşandığı zamanlarda bitki su stresi yaşayacağından, bu noktadan itibaren k_s değeri birden küçük olacaktır, diğer zamanlarda herhangi bir su stresi oluşmayacağından değeri birdir.

Su dengesi yaklaşımı ile akış hesaplama aşamaları aşağıda maddeler halinde özetlenmiştir:

1. Başlangıçdaki su eksikliği belirlenir. Hesaplamanın başında yeşil çatı sistemi doygun kabul edilirse, su eksikliği sıfırdır.

2. Su eksikliği HMS ile kıyaslanır. D_{i-1}<HMS ise k_s birdir.

3. Hesaplama yapılan zamanda meteoroloji istasyonunda ölçülmüş yağış olup olmadığına bakılır. Yağış yok ise buharlaşma-terleme miktarı kadar su eksikliğinde artma oluşacaktır. Sisteme dahil olan su bulunmadığından akış ve tutulan su miktarı sıfırdır.

4. Yağış ölçülmüş ise, ölçülen yağış yüksekliği D_{i-1} ile kıyaslanır. Yağış yüksekliği D_{i-1}'den büyük değilse yeşil çatı sisteminde akış oluşmayacak ve ortamdaki su eksikliği buharlaşma-terleme miktarı kadar artarken yağış kadar azalacaktır ($D_i=D_{i-1}-P_i+BT_{a,u,i}$). Akış miktarı sıfır olurken, tutulan su miktarı yağış yüksekliği kadardır.

5. Yağış yüksekliği D_{i-1}'den büyük ise yeşil çatı sistemindeki su eksikliği giderildikten sonraki miktar kadar akış ($R_i=P_i-D_{i-1}$) oluşabilecektir ve ortamdaki su eksikliği buharlaşma-terleme miktarı kadar olacaktır ($D_i=BT_{a,u,i}$). Tutulan miktar ise D_{i-1} kadardır.

BULGULAR

Hipotetik yeşil çatı sisteminde tutulan ve akışa geçen su miktarını tespit etmedeki ilk adım yetiştirme ortamı derinliğine karar verildikten sonra k_c, FKS ve HMS değerlerini belirlemektir. Sedum mix için önerilen bitki katsayısı 0.53'tür (Starry ve ark., 2014). Maksimum FKS sedum bitkisi solma miktarı göz önüne alınarak, yetiştirme ortamı derinliğinin %30'u olarak alınmıştır (Martin, 2008). HMS derinliği bitkiden bitkiye değişmesine rağmen FKS'nin %30-70'i alınabilindiğinden, bu çalışmada FKS'nin %50'si olacak şekilde seçilmiştir. Çalışmamızda yetiştirme ortamı derinliğinin 40 mm seçildiği dikkate alındığında, FKS=12 mm ve HMS=6 mm'dir. Su dengesi yaklaşımı ile akış hesaplama aşamaları takip edilerek, hipotetik yeşil çatıda tutulan ve akışa geçen su miktarları 2008-2010 Nisan-Ekim ılıman sezonu için hesaplanmıştır. Her bir yıl için hesapların başladığı ay Nisan olduğundan, Şubat ve Mart aylarında yağan kar ve yağmurları ihmal etmeme adına yeşil çatı sistemi her bir yılın başlangıç adımında doygun kabul edilmiştir. Ayrıca FKS'den daha büyük derinliklerden bitki su alamayacağından terleme gerçekleşmeyecektir. Bu sebepten maksimum su eksikliği 12 mm olacak şekilde hesaplamalar yapılmıştır.

Bitkinin yaşayacağı su stresinin buharlaşma-terleme miktarı üzerindeki etkisini göstermek adına çalışmamızda 2009 yılı için hesaplanan $BT_{a,i}$ ve $BT_{a,u,i}$ değerleri Şekil 1'de gösterilmiştir. Şekil 1'den de görüleceği gibi yetiştirme ortamındaki su eksikliğinin az olduğu başlangıç zamanlarında değerler eşittir. Su eksikliği HMS değerini aşmaya başladığı andan itibaren değerler farklılaşmaya başlamıştır. Yağışsız geçen günlerin etkisi ile yetiştirme ortamında artan su stresinin buharlaşma-terleme miktarında oluşturduğu azalmanın dikkate alınması gerektiği Şekil 1 ile vurgulanmaya çalışılmıştır.

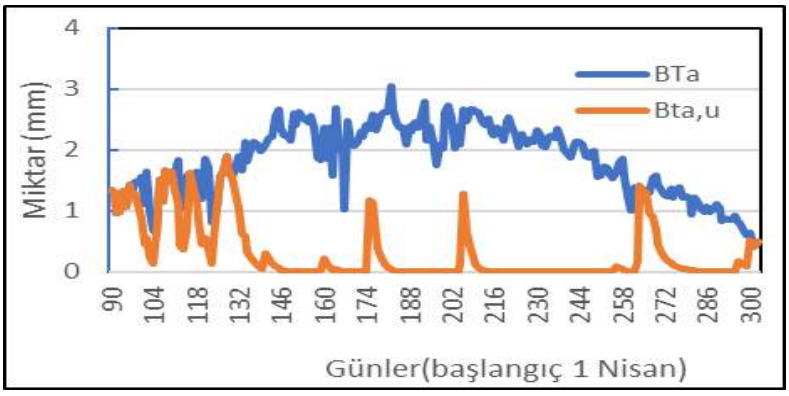

Şekil 1. 2009 Yılına Ait BTa ve BTa,u Kıyaslaması

$BT_{a,i}$ hesaplamalarında ortamda su bulunup bulunmadığına bakılmadığından sıfırdan büyük değerler elde edilmiştir. Ancak yağışsız geçen günlerin etkisi ile yetiştirme ortamında yeterli su bulunmadığında buharlaşma-terlemenin gerçekleşme imkanı azalmakta ve hatta bazı zamanlar hiç oluşmamaktadır. Şekil 1'den görüleceği gibi $BT_{a,u}$ değeri ilk olarak 31 Mayıs günü sıfır değerine ulaşmıştır. 1 Nisan-31 Mayıs tarihleri arasında gerçekleşen buharlaşma-terleme miktarı 59.60 mm olarak

hesaplanırken, su stresinin dahil edilmediği durumdaki miktar 98.90 mm olarak hesaplanmıştır. 22 Temmuzda maksimum faydalı su kullanım derinliğine ulaşan su eksikliği 24 ve 25 Temmuzda yağan toplam 3 mm yağış ile azalmış ve kazanılan miktar yağışsız geçen takip eden 27 günde terleme ile kaybedilmiştir.

Şekil 2'de seçilen yetiştirme ortamı derinliğinin yeşil çatı su tutma kapasitesi üzerindeki etkisi görülmektedir. Yetiştirme ortamı derinliği arttıkça su tutma kapasitesinin artacağı bilinen bir durum olmasına rağmen, çalışma bölgemiz için 150 mm den sonra derinliğin su tutma kapasitesi üzerinde etkisi olmadığı saptanmıştır. Seçilen bölgenin ılıman sezonda az yağış alması ve sıcaklıkların etkisiyle buharlaşma-terleme miktarlarının fazla olması bu sonuca ulaşılmada etkili olduğu düşünülmektedir. Çalışma dönemi süresince ölçülen toplam yağış miktarı 338.8 mm'dir. Klasik çatı kullanılması durumunda düşen yağışın doğrudan akışa geçeceği düşünüldüğünde, 150 mm yetiştirme ortamına sahip yeşil çatıdan akışa geçen miktarın 53.8 mm olacağı Şekil 2'den görülmektedir. Bu da bize çalışma bölgesi için yeşil çatı tarafından sağlanan akışdaki maksimum azalmanın %84 olacağını ifade etmektedir.

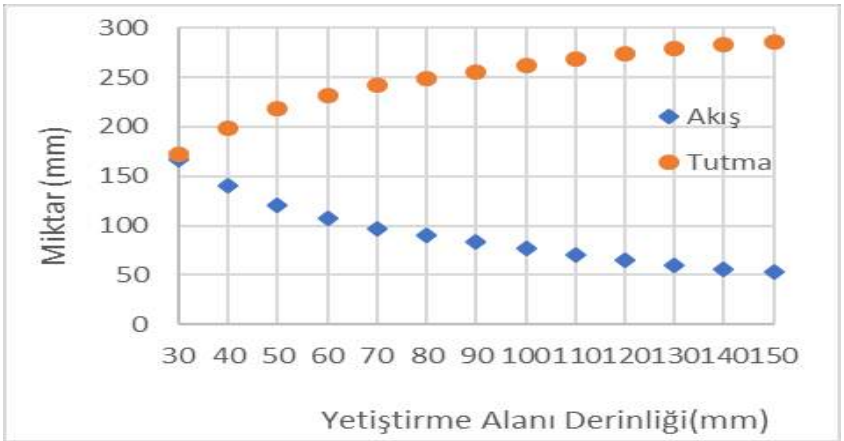

Şekil 2. Hipotetik Yeşil Çatı Yetiştirme Ortamı Derinliğinin Toplam Akış Tutma Miktarına Etkisi

Eşitlik 1'de verilen su dengesi denklemindeki bileşenler ve yeşil çatının yağışı tutma performansları sadece akışın tespit edildiği tarihler için Tablo 1'de özetlenmiştir. Çalışma döneminde gözlemlenen 79 yağışlı günün 58 gününde akış oluşmamaktadır. Akış oluşan 21 günde alınan toplam 229.9 mm'lik yağışın 11.20 mm'si 28 Ekim 2009 tarihinde gözlenmiştir. Yağış o tarihe kadar yetiştirme ortamında hesaplanan 7.22 mm'lik su eksikliğini gidermiş ve sistem doygun hale ulaştığından 3.98 mm akış oluşmuştur. 28 Ekim'i takip eden yağışlı geçen üç günde sistem doygun olduğundan yetiştirme ortamında tutulan su bir gün önce buharlaşma-terleme ile kaybedilen su miktarı kadardır.

Tablo 1'den görüleceği üzere akış genelde Nisan, Mayıs, Eylül ve Ekim aylarında oluşmuştur. Yazın sadece 25 Haziran 2010 tarihinde oluşmuştur. Söz konusu tarihe kadar oluşan 9.70 mm'lik su eksikliği o gün yağmış olan 18 mm'lik yağış ile giderilmiş ve düşen yağışın %46'sı akışa dönüşmüştür.

Yeşil çatının yağışı tutma performansı (TP) Tablo 1'de son kolonda yüzdelik olarak verilmiştir. Tutma performansı yeşil çatı tarafından alıkonulan yağış yüzdesi olarak hesaplanmıştır. Tablo 1'den görüleceği üzere hipotetik yeşil çatıda tutulan toplam miktar 89.10 mm'dir. Ancak akışın oluşmadığı 58 günde düşen 108.9 mm yağışlarında yetiştirme ortamında tutulduğu hesaba katıldığında, sistem tarafından tutulan miktar 198 mm olarak hesaplanmıştır. Kısacası çalışma dönemi süresince düşen yağışın %58'i yeşil çatı sistemi tarafından tutulurken, %42'si akışa geçmektedir.

Tablo 1. Hipotetik Yeşil Çatı Su Dengesi Model Sonuçları

Tarih	P (mm)	$BT_{a,u}$ (mm)	D_{i-1} (mm)	D_i (mm)	R (mm)	Tutma (mm)	TP (%)
01.04.2008	1.90	1.20	0.00	1.20	1.90	0.00	0.00
16.05.2008	13.50	0.09	11.72	0.09	1.78	11.72	86.82
14.09.2008	18.00	0.00	12.00	0.00	6.00	12.00	66.66
24.09.2008	17.00	0.93	6.21	0.93	10.79	6.21	36.51
27.09.2008	3.20	0.86	3.01	0.86	0.19	3.01	94.10
30.09.2008	11.90	1.07	2.98	1.07	8.92	2.98	25.05
22.10.2008	10.60	0.22	9.75	0.22	0.85	9.75	92.00
16.04.2009	15.50	0.62	1.93	0.62	13.57	1.93	12.44
17.04.2009	15.10	1.52	0.62	1.52	14.48	0.62	4.10
06.05.2009	3.60	1.05	0.93	1.05	2.67	0.93	25.94
28.10.2009	11.20	0.51	7.22	0.51	3.98	7.22	64.44
29.10.2009	7.20	0.41	0.51	0.41	6.69	0.51	7.08
30.10.2009	15.10	0.43	0.41	0.43	14.69	0.41	2.69
31.10.2009	5.40	0.50	0.43	0.50	4.97	0.43	7.94
08.04.2010	28.03	0.43	9.16	0.43	19.14	9.16	32.36
09.04.2010	1.60	1.19	0.43	1.19	1.17	0.43	26.89
12.04.2010	8.50	0.83	2.22	0.83	6.28	2.22	26.16
13.04.2010	1.60	1.51	0.83	1.51	0.77	0.83	51.61
01.05.2010	15.80	0.48	8.57	0.48	7.23	8.57	54.26
02.05.2010	6.90	1.39	0.48	1.39	6.42	0.48	6.93
25.06.2010	18.00	0.83	9.70	0.83	8.30	9.70	53.86

SONUÇ

Yeşil çatıdan oluşacak akış, yağış kadar buharlaşma-terleme ve yetiştirme ortamındaki su eksikliği miktarlarının fonksiyonudur. Su eksikliği miktarının sıfır, yani sistemin suya doygun olduğu zamanlarda yeşil çatıya düşen yağış, akış üretmektedir. Bu durumda yeşil çatının klasik (kiremit) çatı gibi davranacağı ve düşen yağışın tamamının akışa geçeceği düşünülebilir. Ancak yeşil çatının suya doygun olduğu zamanlarda dahi buharlaşma-terleme ile su kaybedildiğinden, klasik çatıdan oluşacak akış miktarından daha az akış oluşturmaktadır. Çalışma dönemi süresince düşen yağışın %58'i yeşil çatı sistemi tarafından tutulurken, %42'si akışa geçmektedir. Sistemdeki depolamadan dolayı akış hidrografında pik debide azalma ve oluşma

zamanında gecikme yaşanacağı açıktır. 40 mm yetiştirme ortamı derinliğine sahip hipotetik yeşil çatıdan buharlaşma-terleme ile kaybedilen miktar 202.76 mm'dir. Bununla birlikte toplam oluşabilecek akış yüksekliği 140.8 mm olarak hesaplanırken, sistemde tutulabilen yağış miktarı 198 mm olarak tespit edilmiştir. Hipotetik yeşil çatının yağış tutma performansı her yıl için başlangıç koşulu olarak sistemin doygun olduğu kabul edilmiş olmasına rağmen %58 olarak belirlenmiştir. Yağışı tutma kapasitesi yetiştirme ortamı derinliği artırılarak ve başlangıç doygunluk koşulu değiştirilerek artırılabilecektir. Yeşil çatının tek başına kentsel selin oluşmasını önlemesi beklenmese dahi yaşanılan sorunları azaltabileceği açıktır. Sonuç olarak, "Gaziantep Kilis Yolu ve Çevresi Vizyon Planı" kapsamında ekolojik kent ve uygulama tasarım rehberinde önerilen yeşil çatının yağmur suyunu tutabilme performansı bu çalışma ile sayısal olarak ortaya konulmuş bulunmaktadır. Akış katsayısı ekolojik kent yağmur suyu drenaj sisteminin planlamasında gerekli olan dizayn debisinin hesaplanmasında kullanıldığında ülke ekonomisine de katkı sağlanmış olacaktır.

KAYNAKLAR

Carter, T. L., & Rasmussen, T. C. (2006). Hydrologic behavior of vegetated roofs. *Journal of the American Water Resources Association, 42(5), 1261-1274.*

Connelly, M., & Liu, K. (2005). Green Roof Research in British Columbia-an Overview: *3rd North American Green Roof Conference: Greening rooftops for sustainable communities, 4-6 May,* Washington, DC, USA.

Ekşi, M., & Uzun, A. (2016). Assessment of Green Roof Systems in terms of Water and Energy Balance. *Journal of the Faculty of Forestry Istanbul University, 66(1), 119-138.*

FAO-56 (1998). Crop evapotranspiration. http://kimberly.uidaho.edu/water/fao56/fao56.pdf (Erişim Tarihi: 24.03.2017).

Gaziantep Büyükşehir Belediyesi (2012). Gaziantep Kilis Yolu Ekolojik Kent Uygulama Tasarım Rehberi, 232 s. Gaziantep.

Hilten, R. N., Lawrence, T. M., & Tollner, E. W. (2008). Modeling Stormwater Runoff from Green Roofs with HYDRUS-1D. *Journal of Hydrology, 358(3), 288-293.*

Martin, B. K. (2008). The dynamic stormwater response of a green roof. The University of Guelph, PhD Thesis, 149s, Canada.

Prowell, E. S. (2006). An analysis of stormwater retention and detention of modular green roof blocks. The University of Georgia, MSc Thesis, 98s, Athens, Georgia, USA.

Starry, O., Lea-Cox, J. D., Kim, J., & Van Iersel, M. W. (2014). Photosynthesis and Water Use by Two Sedum Species in Green Roof Substrate. *Environmental and Experimental Botany, 107, 105-112.*

TÜİK (2017). Türk İstatistik Kurumu. http://www.tuik.gov.tr/PreTablo.do?alt_id=1059 (Erişim Tarihi: 24.03.2017).

VanWoert, N. D., Rowe, D. B., Andreen, J. A., Rugh, C. L., Fernandez, R. T., & Xiao, L. (2005). Green Roof Stormwater Retention: Effects of Surface, Slope, and Media Depth. *Journal of Enviromental Quality, 34 (3), 1036-1044.*

EFFECTS OF POSTHARVEST OXALIC ACID THE TREATMENT ON 'HİCAZNAR' POMEGRANATE ARILS QUALITY AND CHILLING INJURY

Ayşe Tülin ÖZ Tuğçe CEREN
Osmaniye Korkut Ata University Engineering Faculty, Food Engineering Department
Karacaoğlan Campus 80000 Osmaniye
aysetulinoz@osmaniye.edu.tr

HİCAZNAR' NAR TANELERİNDE DERİM SONRASI ÜŞÜME ZARARININ VE KALİTESİ ÜZERİNE OKSALİK ASİT UYGULAMASININ ETKİSİNİN BELİRLENMESİ

'Hicaznar' nar meyveleri tanelenme işleminden sonra üç farklı konsantrasyonda kontrol (0mM), 2,5mM ve 5mM oksalik asit (OA) olacak şekilde 10 dk daldırma yöntemi ile yapılan uygulamanın ardından polivenilpropilen (PVPP)(250 gr) kutulara paketlenerek, 5°C'de %90 nispi nem koşullarında 20 gün süreyle muhafaza edilmiştir. Yapılan OA uygulamasının etkisini belirlemek amacı ile başlangıç günü (0.gün) dâhil olmak üzere 4 gün aralıklarla muhafaza sonuna kadar 'Hicaznar' nar meyve tanelerinin kalite değişimleri belirlenmiştir. OA uygulanan 'Hicaznar' nar meyve tanelerinin kontrol ile kıyaslanması sonucunda üşüme zararı üzerine etkileri istatistiki olarak anlamlı bulunmuştur ($p<0,05$). Maya ve küf gelişiminin muhafaza başlangıç ile sonuç değerlerinin rakamsal olarak birbirine çok yakın olduğu ve uygulamalar arasındaki farkın istatistiki açıdan anlamlı olmadığı belirlenmiştir.

Anahtar Kelimeler: 'Hicaznar' nar tanesi, oksalik asit, üşüme zararı

ABSTRACT:
'Hicaznar' pomegranate arils were treated with oxalic acid (OA) at three different concentrations as 0 mM 2.5mM and 5mM then stored at 5°C and 90% relative humidity for 20 days. Effects of the OA treatment quality changes of 'Hicaznar' pomegranate fruit arils were determined until the end of storage the 4 day intervals. According to our findings, OA treatment were statistically significant on pH and TA (titratable acidity), total soluble solids (%), chilling injury (%) values however it was no statistically significant effect on weight loss, gas composition (O_2/CO_2) measurement (%), arils texture change, arils color value (L, a, b, C, h°). It was determined that the initial and final values of yeast and mold growth are very closed to each other numerically and that the difference between applications is not statistically significant.

Key words: 'Hicaznar', arils, oxalic acid, chilling injury, microbial quality
'

1. GİRİŞ

Nar meyvesinin doğal yapısında bulunan biyoaktif bileşenlerin son yıllarda insan sağlığı üzerindeki olumlu etkilerinin öneminin farkına varılması, depolama alanları ve gıda teknolojisindeki önemli gelişmeler sonucu nar meyvesine olan talebin iç ve dış piyasada artması nedeniyle ülkemizde nar üretiminde önemli artışlar kaydedilmiştir.

Türkiye'de 2017 yılı verilerine göre toplam 502 606 ton (TUİK, 2017) nar üretimi gerçekleşmiştir. Nar meyvesinin hem iç ve hem de dış piyasada tüketiminin artırılması, piyasaya daha uzun süre kaliteli ürün sunulması ile mümkün olabilecektir. Piyasanın istediği kalitede ve uzun bir pazarlama yelpazesine sahip olabilmesi için, ticari olarak en çok kullanılan teknolojilerden birisi de soğukta muhafaza yöntemidir. Nar meyvelerinin soğukta muhafazasını ve meyve raf ömrünü sınırlandıran en önemli sorunların başında ise su kayıpları, üşüme zararına bağlı fizyolojik bozukluklar (meyve tane kahverengileşmesi) ve diğer fiziksel bozuklukların yanında fungal kaynaklı bozulmalar gelmektedir (Selçuk ve Erkan, 2014). Bununla birlikte nar meyvesinin özellikle 4 °C altı ve 10 °C üstündeki muhafaza sıcaklıklarında kalite ve ürün kayıplarının görülme sıklığı artar. Narlar için depolama sıcaklığı 5 ila 7,5 °C arasında ve raf ömrü ise çeşidine bağlı olmakla birlikte 8 ila 16 hafta arasında değişir (Fawole ve Opara, 2014; Fawole ve Opara, 2013; Arendse, vd., 2014). Nar depolamada raf ömrünü sınırlandıran en önemli sorunların başında su kayıpları, üşüme zararı, fiziksel bozuklukların yanında fungal kaynaklı bozulmalar gelmektedir. Depo sıcaklığının 5 °C üzerinde olduğu durumlarda fungal bozulmanın şiddetinin arttığı bilinmektedir. Az işlenmiş meyveler ve sebzelere tüketim kolaylığından dolayı son yıllarda ciddi bir tüketici talebi oluşmakla birlikte özellikle nar gibi soyulma zorluğu olan meyveler için az işlenmiş ürün uygulamaları önem arz etmektedir. Fiziksel olarak orijinal formundan değiştirilmiş olmasına bağlı olarak nar tüm ürünlere kıyasla daha kısa bir raf ömrüne sahiptir özellikle fizyolojik aktiviteye bağlı olarak mikrobiyal gelişmeyi hızlandırarak ürün kalitesinin daha hızlı bozulmasına neden olmaktadır (Adiani, vd., 2018). Muhafaza sırasında meydana gelen özellikle fungal bozulmaları önlemek amacı ile kullanılan sentetik fungisitlerin kullanımının yoğunlaşması ve mikrobiyel patojenlerin dirençlerinin artmasına sebep olmaktadır. Bu nedenlerden yola çıkılarak fizyolojik ve fungal bozulmaları engellemek amacıyla tüm ve taze kesilmiş ürünleri korumak için sentetik katkıların kullanımındaki endişelerin artması ile ısıl işlem, modifiye atmosfer, UV-C ışığı ve organik kökenli doğal maddeler gibi bazı alternatif yöntemleri kullanmaya yöneltmiştir (Maghoumi, vd., 2013). Doğal bileşiklerin hasat sonrası uygulamalarında enzim aktivitesi üzerindeki etkilerinin meyve sebzelerde, fungal çürümeyi ve fizyolojik bozuklukları olumlu yönde etkilediği bilinmektedir. Bununla birlikte, tüketicilerin kimyasal kullanımının azaltıldığı doğal alternatif uygulamalara yönelimi artış göstermiştir. Bu uygulamalar arasından özellikle OA uygulamasının kullanımı son zamanlarda önem kazanmaya başlamıştır. Fakat fungal bozulmalara karşı direnç sağlayan ve meyve üşüme zararı üzerinde önemli etkiler gösteren OA uygulamasının hasat sonrası depolama süre ve kalitesindeki etkilerini araştırmaya yönelik çalışmalar sınırlı sayıdadır. OA, bitkilerde doğal olarak bulunan bitkileri ve çevresel strese karşı direnci artıran organik bir asittir (Liang, vd., 2009). Tabiatta; sodyum tuzu halinde kuzukulağı bitkisinde, kalsiyum tuzu olarak ravent bitkisinde ve birçok başka bitkinin hücre özsuyunda bulunur. OA meyvelerde hasat sonrası kaliteleri ile ilgili etkileri yapılan çalışmalarla belirlenmiştir ve muz meyvesinin olgunlaşmasına, litchi meyvesinin kızarması ve muzda üşüme zararına karşı direnci arttırdığı belirlenmiştir (Yörük, vd., 2002, Zheng, vd., 2007(a); Huang, vd., 2013).

2. MALZEME VE YÖNTEM

2.1 Materyal

2.1.1 Bitkisel Materyal

Çalışmada bitkisel materyal olarak yaygın şekilde yetiştiriciliği yapılan hem iç pazar hem de dış pazarda talep gören bir çeşit olan 'Hicaznar' nar meyve çeşidi kullanılmıştır. Çalışmada kullanılacak olan 'Hicaznar' nar meyveleri ticari olarak yetiştiriciliği yapılan Mersin ilinin Tarsus ilçesinde bulunan nar bahçelerinden temin edilmiştir.

2.2 Yöntem

2.2.1 Oksalik Asit (OA) Uygulaması

Çalışmada 'Hicaznar' nar meyve bahçelerinden alınan hastalıksız ve muhafazaya uygun, homojen olan meyveler tanelenerek üç farklı Oksalik Asit (OA) (0 mM, 2,5 mM ve 5 mM) konsantrasyonunda, 10 dk süreyle daldırma işlemine tabii tutulmuştur. Yapılan uygulamalar Kontrol, OAI: Oksalik asit uygulamasının 2.5mM konsantrasyonu ve OAII: Oksalik asit uygulamasının 5mM konsantrasyonu olarak değerlendirilmiştir. Daldırma işlemlerinden sonra, tanelenmiş nar meyveleri üzerlerindeki suyun uzaklaştırılması için oda koşullarında kurutma kâğıtları üzerinde fazla suyu uzaklaştırmak amacı ile 60 dk bekletilmiştir.

2.2.2 Meyve Tanelerinin Ambalajlanması ve Depolanması

OA uygulanmış ve kontrol grubu nar meyve taneleri 250 g'lık PVPP kaplar içerisine alınmış ve +5°C'de % 90±5 nispi nem koşullarında 20 gün süreyle depolanmıştır. Denemede 'Hicaznar' nar meyve taneleri muhafaza periyodu süresince 4 gün aralıklarla depolanan meyvelerde uygulamanın etkilerini belirlemek amacı ile periyodik olarak fiziksel, biyokimyasal ve mikrobiyal analizler yapılmıştır. Fiziksel olarak yapılan analizler; ağırlık kaybı (%), O2/CO2 (%), meyve rengi (L,a, b, Hue ve Chroma), meyve sertliğidir (N). Biyokimyasal olarak yapılan analizler; SÇKM (%), titre edilebilir asit miktarı, pH, ile toplam maya küf sayımı (logkob/g) ve toplam mezofilik aerobik bakteri sayımı (logkob/g) yapılarak sonuçlar değerlendirilmiştir.

2.3.1 Muhafaza Süresince Yapılan Analizler

2.3.1.1 Ağırlık Kaybı

Derimden sonra, denemeye alınan tüm tanelenmiş nar meyvelerinde ağırlık kayıpları 4 gün aralıklarla yapılan tartımlar sonunda belirlenmiştir. Ağırlık kaybı, 'Hicaznar' nar meyve tanelerinin başlangıç ağırlığından son ağırlığının çıkarılıp ilk ağırlığına oranlanması ile hesaplanmış olup yüzde olarak ifade edilmiştir.

2.3.1.2 Nar Meyvelerinde Tane Sertliği

Meyve tane sertliği, meyveler tanelendikten sonra tekstürel değişimler CT3 model tekstür analiz cihazı kullanılarak (CT3 model, Brookfield Engineering Labs. Inc. 11 Commerce Boulevard Middleboro, MA 02346, 1031 USA) ölçülmüştür. Sonuçlar N olarak ifade edilmiştir.

2.2.1.3 Suda Çözünen Toplam Kuru Madde Miktarı

Suda çözünen toplam kuru madde miktarı analizi dijital refraktometre (Krüss, HR Series, A. Krüss Optronic, Hamburg, Germany) kullanılarak yapılmıştır. Nar suyunda bulunan kuru madde miktarı % olarak ifade edilmiştir.

2.2.1.4 pH Değeri veTitre Edilebilir Asitlik Miktarı

Nar meyve suyu dijital (CG 710 pH meter) pH metrenin cam elektrodu örneğe daldırılarak pH değeri ölçülmüştür. Nar meyve suyundan bulunan titre edilebilir asitlik (TA) sonuçları narda baskın olan sitrik asit cinsinden verilmiştir. Sonuçlar g/100mL olacak şekilde aşağıda verilen denklem yardımıyla hesaplanmıştır.

2.2.1.5 Gaz bileşimi ölçümü (O_2 ve CO_2)

Meyvelerin PVPP kutu içerisindeki gaz kompozisyonu değişimleri checkpoint O_2/CO_2 gaz analiz cihazı (PBI-Dansensor, Ringsted, Denmark) ile 4 gün aralıklarla ölçülmüştür.

2.2.1.6 Meyve Tane Rengi (L, a*, b*, C, h°) Değerleri

Meyve tane renginin belirlenmesinde meyve eti yüzeyindeki 1cm'lik bölgeden Minolta renk ölçer (Model CR-400, Konica Minolta, Tokyo, Japonya) cihazının kullanımı ile L (parlaklık), a* (+kırmızı-yeşil), b* (+sarı-mavi) modunda yapılmıştır Chroma değeri ve Hue açı değeri (Voss, 1992)' a göre yapılmıştır.

2.2.1.7 Üşüme Zararı Miktarı

Üşüme zararı nar taneleri zararlanmış ve sağlam olacak şekilde gruplandırılmıştır ve bu gruplandırmadaki üşüme zararı sonucu yaralanmış nar taneleri yüzde ile ifade edilerek üşüme zararı (%) değerleri belirlenmiştir.

2.2.1.8 Mikrobiyolojik Analizler

Stomacher torbasının içerisine sterilize 45 ml peptonlu buffer dilüsyon sıvısı (Merck, Amanya) konulup üzerine 5 g nar örneği steril koşullarda alınıp Stomacherde homojenize edilerek Ulukanlı ve Karadag, (2010)'a göre yapılmıştır. Sonuçları bu iki paralelin ortalaması alınarak logkob/g olacak şeklinde ifade edilmiştir).

2.2.1.9 Toplam Mezofilik Aerobik Bakteri Sayımı

Tanelenmiş nar örneklerinde toplam aerobik mezofilik bakteri sayısının belirlenmesi amacıyla (Anonim, 2001; Anonim, 2004) kullanılmıştır.

2.2.1.10 Toplam Maya ve Küf Sayımı

Tanelenmiş nar örneklerinde bulunan toplam maya ve küf sayısının belirlenmesi amacıyla Anonim, (1989); Anonim, (2001)'e göre yapılmıştır.

2.2.1.11 İstatistiksel Analiz

Deneme 3 tekerrürlü olacak şekilde düzenlenmiş ve her bir tekerrürde her biri 250 g olan PVPP kutular kullanılmıştır. Veriler tek yönlü varyans (ANOVA) analizi ve Duncan testi ($P<0.05$) kullanılmıştır. İstatiksel değerlendirmeler IBM®SPSS® Statistics 19 (IBM, NY, USA) paket programı kullanılarak yapılmıştır.

3. BULGULARI VE TARTIŞMA

Tanelenmiş 'Hicaznar' nar meyve tanelerinin 3 farklı OA konsantrasyonlarında (kontrol, 2,5mM ve 5mM), daldırma yöntemi ile uygulama yapıldıktan sonra PVPP kutulara konularak soğuk hava deposunda (5 °C) 20 gün süre ile muhafaza edilmiş ve muhafaza süresince 0., 4., 8., 12., 16., ve 20. günlerde fiziksel, kimyasal ve mikrobiyolojik analiz yapılmıştır..

3.1Ağırlık Kaybı

Meyve ve sebzelerde hasat sonrası devam eden fizyolojik aktiviteler, solunum hızı ve terlemenin de etkisi ile ürünlerde raf ömrü süresince ağırlık kaybı meydana gelir. Meydana gelen ağırlık kaybı miktarı hem meyve görünüşü hem de ürün tat ve kalitesi üzerinde önemli bir etkiye sahiptir. Meyve ve sebzelerde hasat sonrası ağırlık kaybının pazarlanabilme kalitesi üzerinde önemli etkisinden dolayı bu oranın meyvelerde % 5'i geçmemesi istenir aksi takdirde ürün pazarlanamaz duruma gelir (D'Aquino, vd., 2010). OA uygulamasına tabi olan 'Hicaznar' nar meyve tanelerinde muhafaza süresince meydana gelen ağırlık kaybı miktarı Şekil 4.1'de gösterilmiştir. Uygulamalar arası % ağırlık kaybı değişimi sırası ile kontrol %0,21, OAI (2,5mM) %0,22 ve OAII (5mM) %0,26 olarak ölçülmüştür (Çizelge 4.1).

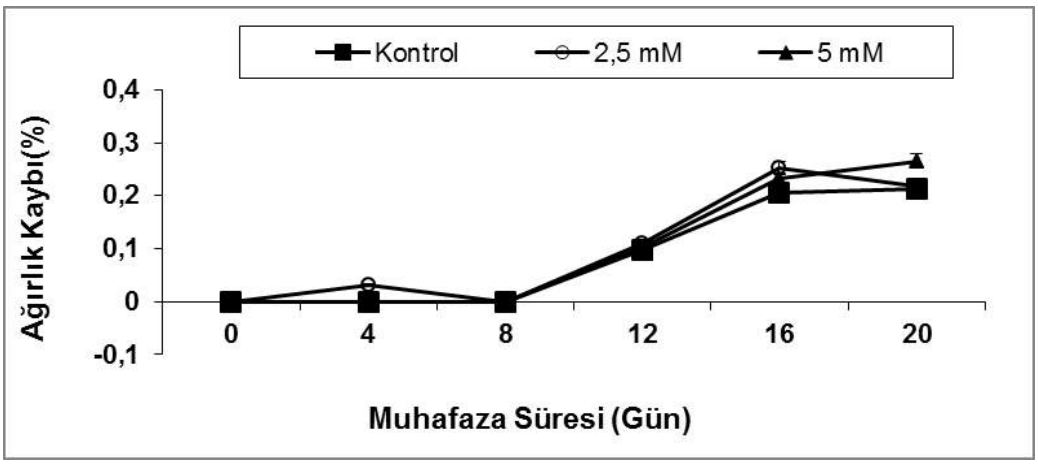

Şekil 1. OA uygulanan 'Hicaznar' nar tanelerinde ağırlık kaybı (%) değişimi

3.2 Gaz Bileşim Ölçümü (O_2 ve CO_2)

PVPP kutuları içerisine tanelenmiş nar meyvelerinin meyve solunum oranlarını periyodik olarak yapılan O_2/CO_2 (%) gaz bileşimi PBI dansensor cihazı ile belirlenmiştir. % O_2/CO_2 (0. gün) O_2 miktarı %19,3 civarındayken muhafaza süresince O_2 miktarında düşüş meydana gelmiştir. Muhafaza sonunda kontrol grubu meyvelerinin O_2 miktarı %14,2, OAI uygulaması yapılan örneklerin O_2 miktarı %14,3 ve OAII uygulaması yapılan nar tanelerinde ise O_2 miktarı %15,1 olarak ölçülmüştür (Şekil 4.2). Soliva-Fortuny, vd. (2004), O_2 seviyesinin, <% 2 altındaki bir düşüşün fermantasyon eşik limiti olduğunu anaerobik solunumla, sonuçlanacağını ve tat ve lezzeti olumsuz yönde etkileyebileceğini belirtmiştir.

% CO_2 miktarı muhafaza süresince ölçülmüş ve 0.gün CO_2 oranı %0,3'lerde iken %CO_2 miktarı özellikle muhafaza süresinin 12. gününde önemli bir artış göstererek en fazla %7'lere kadar ulaşmıştır. Martinez-Romero, vd. (2013)'nin yaptıkları çalışma dikkate alındığında tanelenmiş 'Mollar de Elche' çeşidi narlarda yaptıkları *Aloe vera* kaplama uygulamasında modifiye atmosfer ambalaj (MAP) koşullarında muhafaza ettiklerini ve 5–15 kPa CO_2 gaz bileşimi koşullarında depolama yapılabileceğini rapor etmişlerdir. Benzer şekilde çalışmamızda PVPP kutu içerindeki gaz bileşiminin de bu sınırlar içinde olduğu belirlenmiştir.

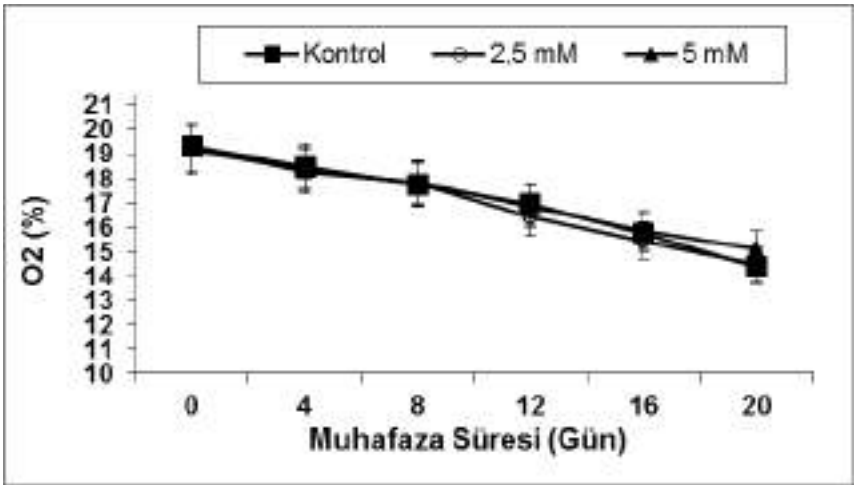

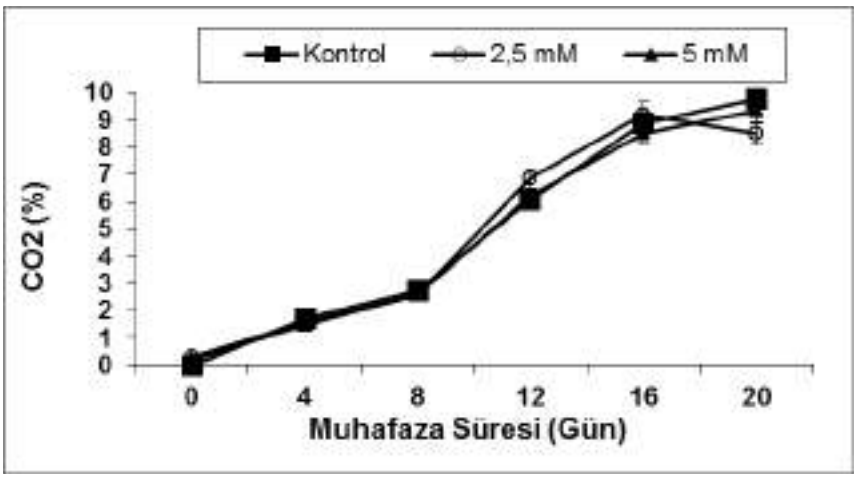

Şekil 2. OA uygulanan 'Hicaznar' nar tanelerinde O2 (%) ve CO2 (%) değişimi

3.3 pH Değeri ve Titre Edilebilir Asit Miktarı

Nar meyveleri muhafaza başlangıcında pH değerleri 2,3 olup muhafaza süresince önemli bir değişim olmamıştır 16. gün itibariyle pH değerlerinde düşüş meydana geldiği gözlemlenmiştir (Şekil 4.3). Bu meydana gelen değişimde yaşlılık, mikrobiyel bozulma ve raf ömrü süresi bitiminin etkilerinin olduğu düşünülmektedir. Nar meyvesindeki TA için sorumlu olan asıl organik asit sitrik asittir (Shahbaz, vd., 2014). TA miktarı %1,7 civarında iken muhafazanın 12. Gününde hafif bir düşüş eğilimi gösterse de muhafaza sonunda özellikle OAI ve OAII uygulaması yapılan meyve tanelerinde hafif bir artış görülmüştür (Şekil 4.3). Sayyari, vd. (2010) de 'Mollar de Elche' bütün nar meyvesinde yaptıkları OA uygulamasının titre edilebilirliği azalttığını bildirmişlerdir. Benzer şekilde Caleb, vd. (2014) de nar tanelerine pasif MAP'ın antiesmerleştirici ön muamele ile kombinasyon uygulamaları sonucunda TA'da muhafaza boyunca azalmalar gözlemlendiğini bildirmişlerdir.

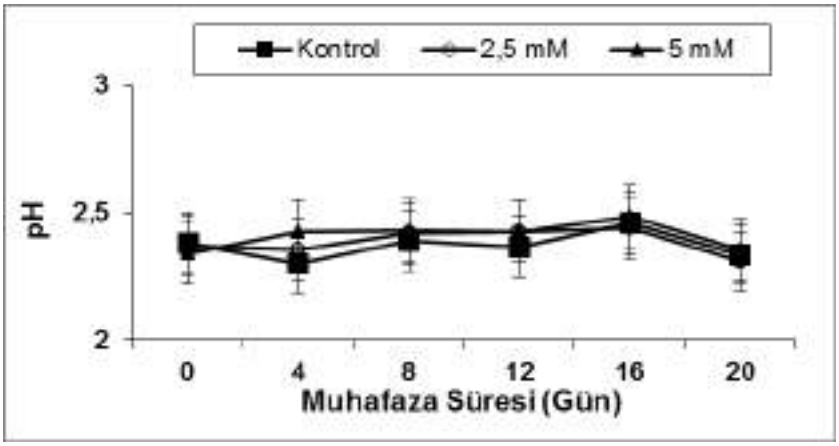

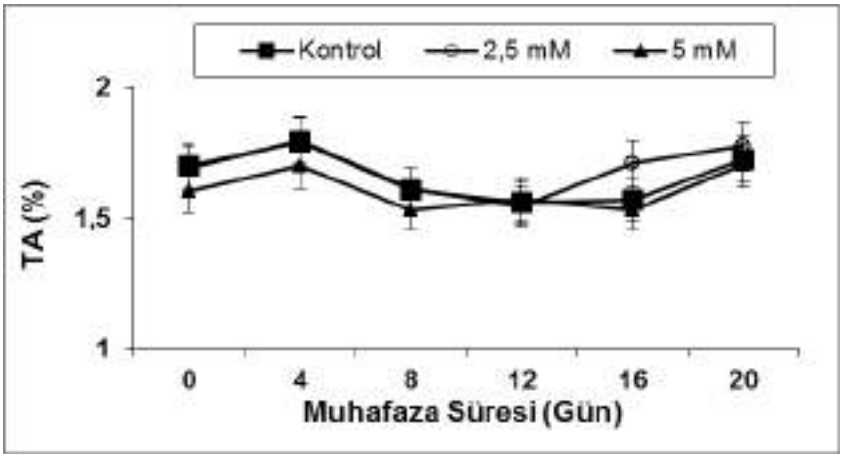

Şekil 3. OA uygulanan 'Hicaznar' nar meyve sularındaki pH ve TA (%) değişimi

3.4 Renk Değerleri (L, a*, b*, C, h°)

'Hicaznar' nar meyvesi gerek iç pazarda gerekse dış pazarda albeni olarak diğer nar çeşitlerine göre daha üstün özelliğe sahiptir. Meyve renk değerinin belirlenmesinde en yaygın olarak kullanılan özellikle L, a*, b* değerleridir (Üren, 1999). L meyvenin parlaklığını gösterir ve nar meyve tanelerinin L parlaklık değeri kontrol grubu meyvelerinde 0. gün değeri 22,72 iken OA uygulanan meyvelerde ise sırasıyla 26 ve 25,70 olarak ölçülmüş, muhafaza süresince düşüş eğiliminde olan L parlaklık değeri muhafaza sonunda kontrol grubu meyvelerinde 22,94 iken OA uygulamasının yüksek konsantrasyonundan en yüksek L değeri olan 24,37 elde edilmiştir (Şekil 4.4). Diğer nar meyve renk kalitesinde önemli bir renk değerleri olan kırmızı rengi gösteren +a değeri tüm uygulamalarda nar meyve tanelerinde muhafaza süresince artış eğiliminde olduğu ve bu artışın nar meyvesinin hasat sonrası ve olgunlaşması ile ilişkili olarak antosiyanin pigmentlerinin varlığından kaynaklandığı bilinmektedir (Martinez-Romero, vd., 2013). b* renk değeri meyvelerin +sarı ,- mavi renk değerini gösterir ve nar meyvesi b* renk değeri hafif artış eğiliminde olup başlangıç kontrol meyveleri b* değeri 8,38, OAI ve OAII uygulanan meyve tanelerinin sırası ile 7,26 ve 7,22 olarak ölçülmüştür. Muhafaza sonunda b renk değeri hafif artış eğiliminde olmuş ve sırası ile kontrol grubu 9,62 iken OA düşük dozunda 8,81 iken OA'nın yüksek konsantrasyonunda ise 10,86 olarak bulunmuştur (Çizelge 4.2).Ayrıca meyvenin renk tonunu gösteren kroma değeri olan C değeri hesaplanmış tüm uygulamalarda C renk değerinin muhafaza sonunda artış gösterdiği belirlenmiştir. Meyve nar taneleri hue açı renk değişimine olan etkisi istatistiki olarak anlamlı bulunmazken OA uygulamasının yüksek konsantrasyon uygulamasında 27,14 ile en yüksek hue açı değerine sahip olduğu belirlenmiştir (Çizelge 4.2).

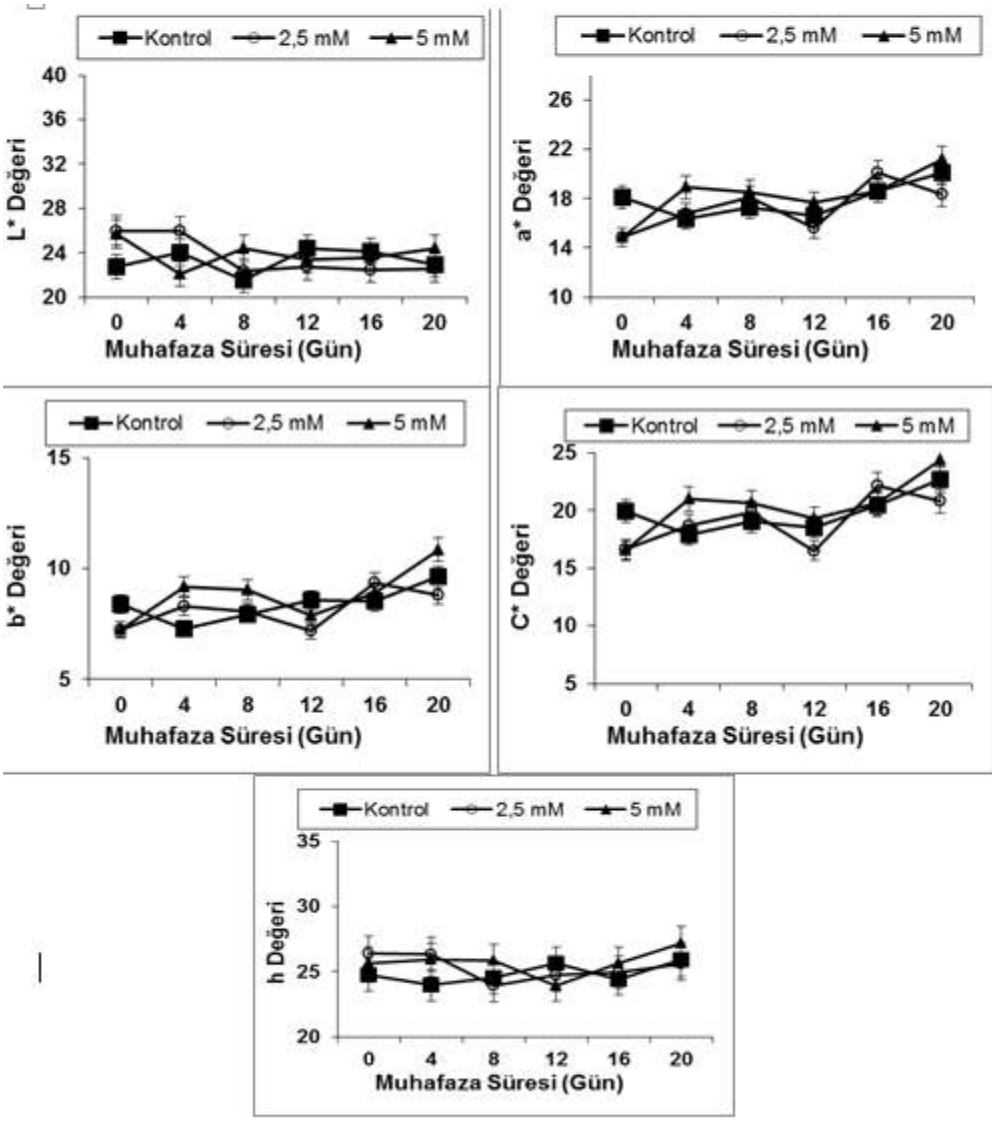

Şekil 4. OA uygulanan 'Hicaznar' nar tanelerinde renk değerleri değişimleri

3.5 Suda Çözünür Kuru Madde Miktarı

Meyvelerde SÇKM önemli bir kalite göstergesidir (Öz, vd., 2016). Polisakkaritler ve şekerler meyve tatlılığında ve meyve kalitesinde önemli bir yer tutar, meyvelerdeki şekerler ve asitler önemli ölçüde lezzet, kimyasal ve duyusal özellikleri etkiler (Shahbaz, vd., 2014).

'Hicaznar' nar meyve tanelerinde kuru madde miktarı muhafaza başlangıcında %15,6 civarında iken muhafaza süresince SÇKM'de düşüşler meydana gelmiştir. Ve muhafaza sonunda kontrol grubu meyve tanelerinde SÇKM %14,47 OAI uygulaması uygulanan meyve tanelerinde %14,8 ve OAII uygulaması uygulanan meyve tanelerinde ise %14,4 olarak belirlenmiştir (Çizelge 4.3). Bu sonuçlar doğrultusunda hem muhafaza süresi hem de uygulamaların SÇKM üzerindeki değişimleri istatistik olarak anlamlı bulunmuştur ($p<0,05$). Benzer şekilde Martinez-Romero, vd. (2013) da 'Mollar de Elche' çeşidinde yaptıkları *Aleo vera* kaplama uygulamasında 8 günlük muhafaza süresince SÇKM değerinde düşüş meydana geldiğini fakat bu değişikliğin istatistiki olarak anlamlı bulunmadığını bildirmişlerdir. Sayyari, vd. (2010) de 'Mollar de Elche' narlarının 2 °C'de 84 günlük muhafazası sırasında meyvelerin SÇKM içeriği üzerinde hiçbir etkisinin olmadığını bildirmişlerdir.

Aynı zamanda her ne kadar nar meyvesinin solunum hızı düşük olsa da meyve raf ömrü süresince kuru madde miktarı düşüşü üzerine solunum hızı ve diğer biyokimyasal reaksiyonlar etkilidir. Dolayısıyla muhafaza süresi uzadıkça kuru madde miktarında düşüşler meydana gelmiştir (Şekil 4.5).

3.5 Nar Meyvelerinde Tane Sertliği

'Hicaznar' nar meyve tanelerinde tane sertliğini belirlemek amacıyla yapılan ölçümlerde muhafaza başlangıcında 4-5,5 N arasında olan meyve tane sertliği muhafaza süresi boyunca azalmıştır (Şekil 4.5). Muhafaza sonunda sırasıyla kontrol grubu meyve tanelerinde 3,3 N, OAI uygulanan meyve tanelerinde 3,5 N ve OAII uygulanan meyve tanelerinde ise 4 N olarak ölçülmüştür (Çizelge 4.3). Sonuçlar istatistiki olarak anlamlı bulunmasa da rakamsal olarak OA uygulanan meyvelerde uygulama yapılmayan kontrol grubuna göre yaklaşık 1 N kadar daha yüksek bir sertlik değerine sahip olduğu belirlenmiştir (Çizelge 4.3). Muhafaza süresi her ne kadar 20 gün süre ile incelenmiş olsa da 12. gün değerlerine baktığımızda sonuçların daha anlamlı olduğunu ve OAII uygulanan meyve tanelerinin tekstürel açıdan en yüksek değerde olduğu gözlemlenmiştir. Bu da OA uygulamasının meyve hücre duvarı yapısında ve meyve sertliğinde etkili olduğunu göstermektedir (Öz, vd., 2016). Benzer şekilde Caleb, vd. (2013) de tanelenmiş nar meyvelerinde yaptıkları MAP muhafazasında değişimin istatistiki olarak anlamlı olmadığı sonucuna varmışlardır. Ding, vd. (2007) mango meyveleri üzerine yaptıkları OA ve salisilik asit uygulamalarının, muhafaza sonucunda meyve sertliği üzerine açıkça bir etkisinin bulunmadığını bildirmişlerdir.

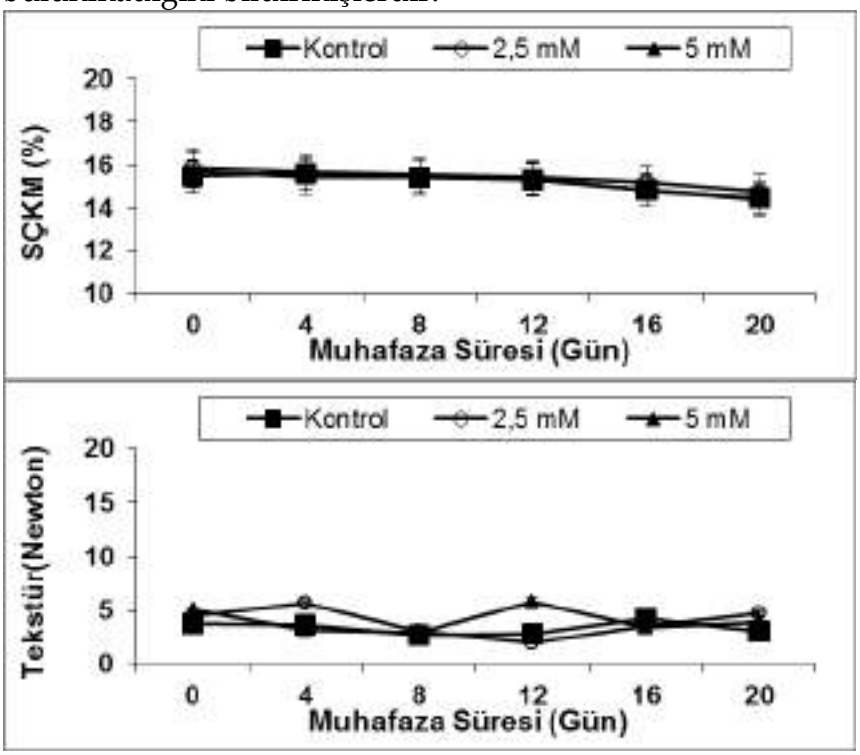

Şekil 5. OA uygulanan 'Hicaznar' nar tanelerinde SÇKM (%) ve tekstür (N) değerleri değişimi

3.6 Üşüme Zararı Miktarı

Meyve ve sebzelerde hasat sonrası raf ömrünü uzatmak amacıyla en çok kullanılan tekniklerden birisi soğukta muhafaza teknikleri olmakla birlikte, üşüme zararına hassas olan tropik ve subtropik meyvelerde, üşüme zararının ortaya çıkmasında

önemli bir risktir. Nar meyvesi de subtropik iklim meyvesi olduğundan düşük sıcaklıkta yapılan muhafazada üşüme zararına sebep olabilmektedir. Meyve 5 °C'nin altındaki sıcaklıklarda muhafaza edildiklerinde üşüme zararına maruz kalarak meyve kabuğun kahverengi renk değişikliği, yüzey çukuru ve duyarlılığına sebep olmakla birlikte ürünün metabolizmasını bozarak fizyolojik zararlanmalara neden olmaktadır bu da meyvenin hem iç hem de dış kalitesini olumsuz etkiler (Opara, vd., 2015).
Yapmış olduğumuz OA uygulamasının üşüme zararı üzerinde etkisi incelenmiş muhafaza süresi arttıkça üşüme zararında artışlar belirlenmiştir (Şekil 4.6). Muhafaza sonunda en fazla üşüme zararı %81 ile kontrol grubu meyvelerinde gözlenirken, OAI uygulamasında üşüme zararı %69, OAII uygulamasında ise üşüme zararı %64 olarak ölçülmüştür. OA uygulanan meyvelerde üşüme zararı kontrol grubu meyvelerle kıyaslandığında sonuçlar istatistiki olarak anlamlı bulunmuştur ($p<0,05$) ve OAII dozu en etkili uygulama olarak belirlenmiştir (Çizelge 4.4). Benzer şekilde Sayyari, vd. (2010)'nin yaptıkları çalışmadan elde ettikleri sonuçların çalışma sonuçlarımızı destekler yönde olduğu ve tüm nar meyvelerinden 'Mollar de Elche' nar çeşidinde OA uygulamasının üşüme zararını azaltmada polifenol oksidaz ve peroksidaz enzim aktivitelerini engelleyerek zararı kontrol altına alındığını belirlemişlerdir. Yine başka bir çalışmada mango meyvesine OA uygulamasının üşüme zararı üzerine etkilerinin belirlenmesinde, uygulama sonucunda soğukta meydana gelen hasarın azaltılması ve mango meyvesinin kalitesinin uzun süreli korunmasında olumlu sonuçlar alındığı bildirilmiştir (Li, vd., 2014). Sayyari, vd. (2011) de salisilik asit gibi organik kökenli uygulamaların kontrol uygulamalarına göre nar meyvelerinde üşüme zararı üzerinde olumlu etkileri olduğunu belirtmişlerdir.

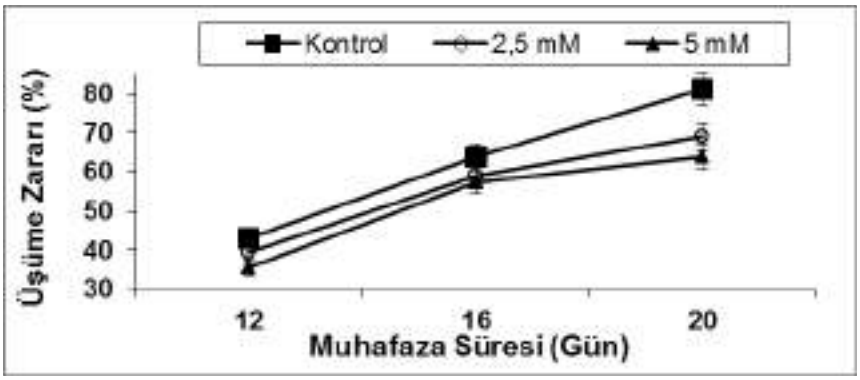

Şekil 6. OA uygulanan 'Hicaznar' nar tanelerinde üşüme zararı (%) değişimi

3.7 Mikrobiyolojik Değerler
Nar meyvesinde esas olarak çürüme neden olan *Alternaria spp.* ve *Aspergillus spp.* ile *Botrytis cinerea*'nın her ikisi, meyve bozulmasının en önemli nedenidir ve özellikle *Penicillium*, esas olarak muhafaza süresince ortaya çıkmaktadır (D'Aquino, vd., 2010).
3.7.1 Toplam Mezofilik Aerobik Bakteri Sayımı
Toplam aerobik mezofilik bakteri sayısı muhafaza sonu itibari ile kontrol grubu meyve tanelerinde 8,38, OAI uygulamasında 7,93 iken OAII uygulamasında ise 7,79 ile en düşük değer elde edilmiştir (Şekil 4.8). Bununla birlikte OA uygulanan meyvelerle kontrol grubu meyveleri arasındaki fark istatistiki olarak anlamlı bulunmuştur ($p<0,05$)(Çizelge 4.6).

3.7.2 Toplam Maya- Küf Sayımı

Toplam maya ve küf sayımı ise tüm uygulamaların 8 log kob/gr saptama limitleri aralığında bulunmuş ve istatistiki olarak anlamlı bulunmamıştır (Çizelge 4.6).

Caleb, vd. (2013)'de, maya ve küflerin aerobik mezofilik bakterilere kıyasla daha düşük pH değerlerinde yetiştiğini belirtmişlerdir ve gerek muhafaza başlangıcında ve gerekse muhafaza sonunda toplam maya küf miktarı kısmen de olsa toplam aerobik mezofilik bakteri sayısından daha fazla bulunmuştur.

Bazı ülkelerde taze kesilmiş meyve sebzelerde, maya ve küfün maksimum limiti 5 log.kob/gr dır. Çalışmamızda 12. günden sonraki muhafaza süresinde bu limitlerin aşılmış olduğu görülmektedir (Çizelge 4.6). Bu sonuçlar dikkate alındığında tanelenmiş nar meyvelerinin mikrobiyal kalite açısından muhafaza ömrünün 12 günden daha fazla olmasının bu yönüyle sakıncalı olabileceği sonucuna varılmıştır.

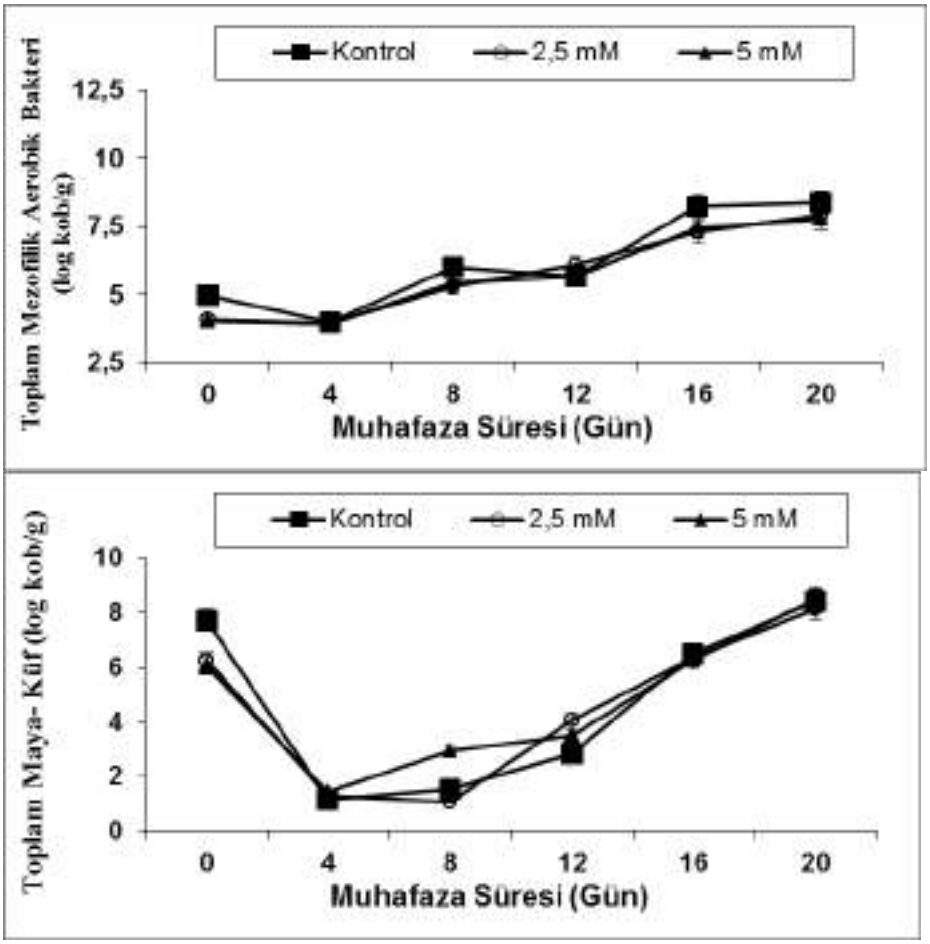

Şekil 7. OA uygulanan 'Hicaznar' nar tanelerinde Toplam Mezofilik Aerobik Bakteri (log kob/g) ve Toplam Maya- Küf (log kob/g) değerleri değişimi.

4.SONUÇLAR

Bütün 'Hicaznar' nar meyvelerinin kabukları soyularak tanelenmiş nar tanelerine üç farklı konsantrasyonda kontrol (0mM), 2,5mM ve 5mM OA olacak şekilde daldırma yöntemi uygulanan daha sonra PVPP (250 gr) kutulara paketlenen nar meyve taneleri, 5 °C'de % 90 nispi nem koşullarında 20 gün süreyle muhafaza edilmiştir. Yapılan OA uygulamasının etkisini belirlemek amacı ile başlangıç günü (0.gün) dâhil olmak üzere 4 gün aralıklarla muhafaza sonuna kadar nar meyve tanelerinin fiziksel, biyokimyasal

ve mikrobiyal kalite değişimlerini belirlenmiştir. Bu amaçla, nar tanesinde fiziksel kalite için ağırlık kaybı (%), O_2/CO_2 gaz bileşimi ölçümü (%), renk (L, a, b, C, h°) ölçüm değerleri, pH, TA (%) miktarı, SÇKM (%), tane sertlik (N) miktarı, üşüme zararı (%) miktarları belirlenmiştir. Mikrobiyal kalite değişimleri için ise toplam mezofilik aerobik bakteri (logkob/g) ve maya-küf (logkob/g) miktarı belirlenmiştir.

Bulgularımıza göre, derim sonrası tanelenmiş nar meyvelerine yapılan OA uygulamasının etkilerinden ağırlık kaybı, her üç uygulamada da depolama süresine bağlı olarak artış göstermiştir. Hem depolama süresinin etkisi hem de uygulamaların etkisi istatistiki açıdan önemli bulunmuştur ($p<0,05$). Uygulamanın gaz bileşimi (O2/CO2 (%)) değişiminin istatistiki olarak anlamlı olmadığı belirlenmiştir. Muhafaza başlangıcından sonuna kadar geçen süre boyunca O_2 miktarında azalma görülürken (%19,3 değerlerinden %14,5 değerlerine) CO_2 miktarında artış (%0,3 değerlerinden %9,3 değerlerine) gözlemlenmiştir. Bu değişimin nar tanelerinde solunum hızının sınırlı olmasından kaynaklandığı sonucuna varılmıştır.

Meyve suyu pH değişimi tüm uygulamalarda düşüş eğiliminde olduğu ve TA miktarının muhafaza sonunda kontrol grubu dışında hafif artış eğiliminde olduğu belirlenmiştir. Bu kalite parametrelerinden TA ve pH değerlerine OA uygulamasının istatistiki açıdan anlamlı etkide bulunduğu saptanmıştır ($p<0,05$). Nar meyve tanesi renk (L, a*, b*, C, h°) ölçüm sonuçlarına göre özellikle L parlaklık değerinin genel anlamda düşüş eğiliminde olduğu ancak, a* kırmızı ve b* sarı değerleri ile C ve h° değeri üzerine etkileri değerlendirildiğinde tüm uygulamaların artış eğiliminde olduğu belirlenmiştir. L parlaklık ve hue açı renk değeri dışındaki tüm uygulamaların diğer renk değeri üzerinde OA uygulamasının istatistiki olarak önemli bulunmuştur ($p<0,05$). Diğer bir kalite parametresi olan meyve tane sertliği ölçümleri istatistiki açıdan anlamlı bulunmamış ancak muhafaza sonundaki en yüksek tane sertliği 3,99 ile OA uygulamasının yüksek konsantrasyon uygulamasında olup bunu 3,5N ile OA'in düşük konsantrasyonundaki uygulamasının takip ettiği görülmüştür. Nar tanesi SÇKM değeri istatistiki açıdan anlamlı bulunmuş ($p<0,05$) ve meyve tane SÇKM'si başlangıç değeri muhafaza sonuna doğru hafif düşüş eğilimi göstermiştir.

Nar meyve taneleri muhafaza sırasında düşük sıcaklıklara maruz kaldığında üşüme zararı olarak adlandırılan bir fizyolojik bozukluğa maruz kalmakta ve meyve pazarlanmasını olumsuz yönde etkileyen bir kalite sorunu ortaya çıkmaktadır. Bu üşüme zararının OA uygulanan meyveler ile kontrol grubu meyveleri kıyaslandığında uygulamanın üşüme zararına karşı ürünü koruduğu belirlenmiştir. En etkili sonuç ise OAII uygulanan meyve tanelerinde elde edilmiştir.

Nar meyve tanelerinin toplam mezofilik aerobik bakteri miktarının tüm uygulamalarda artış gösterdiği OA uygulanan nar tanelerinde ise kontrol grubu ile kıyaslandığında kısmen daha düşük olduğu ve kontrol grubu ile OA uygulamaları arasındaki farkın istatistiksel açıdan anlamlı olduğu görülmüştür ($p<0,05$). Ayrıca maya ve küf sayımında muhafaza başlangıcı ile muhafaza sonunda rakamsal değerlerin çok yakın olduğu ve farkın istatistiksel açıdan anlamlı olmadığı belirlenmiştir.

OA uygulamasının tanelenmiş nar meyvelerinde muhafaza ömrü her ne kadar 20 gün süreyle incelenmiş olsa da 12 günlük raf ömrünün gerek meyve kalitesi gerekse mikrobiyal kalite açısından daha sağlıklı olacağı sonucuna varılmıştır.

Meyve tane sertliği, pH, üşüme zararı, antosiyanin madde miktarı, antioksidan madde miktarı, toplam mezofilik aerobik bakteri sayısı, glikoz miktarı, toplam şeker miktarı ve bütün renk (L, a*, b*, C, h°) ölçüm değerlerinde OAII uygulama dozunun diğer

uygulamalara kıyasla daha etkili olduğu gözlemlenmiştir. Bu sonuçlar doğrultusunda OAII uygulama dozunun bir yüksek dozu bundan sonraki çalışmalar için yol gösterici olacağı düşünülmektedir. OA uygulamasının solisyon olarak uygulamakla birlikte kaplama metaryalleri içerisine dâhil edilmesi uygulamanın etkinliğinin daha da arttırabileceği sonucuna varılmıştır.

KAYNAKLAR

Adiani, V., Gupta, S., Ambolikar, R., Variyar, P. S.. Development of rapid method to assess microbial quality of minimally processed pomegranate arils using FTIR. Sensors and Actuators B 260, 800–807, 2018.

Akbaşlı, İ. T. Ahmet Yasevi University, Faculty of Medicine, 2015.

Anonim. Aerobic Plate Count, Bacteriological Analytical Manual (BAM) Chapter 3, 2001.

Anonim. Türk Standartları Enstitüsü Mikrobiyoloji-Maya ve Küf Sayımında Genel Kurallar, 25°C 'da Koloni Sayım Tekniği. TS 6580-ISO 7954. Türk Standardları Enstitüsü, Ankara, 1989.

Anonim. Türk Standartları Enstitüsü, Mikrobiyoloji - Gıda ve Hayvan Yemleri, Mikroorganizmaların Sayımı İçin Yatay Yöntem, 30°C'da Koloni Sayım Tekniği. TS 7703 EN ISO 4833. Türk Standardları Enstitüsü, Ankara, 2004.

Arendse, E., Fawole, O. A., Opara, U. L. Effects of postharvest storage conditions on phytochemical and radical-scavenging activity of pomegranate fruit (cv. Wonderful). Scientia Horticulturae, 169, 125-129, 2014.

Bozan, B., Tunalier, Z., Koşar, M., Altıntaş, A., Başer, K. H. C.,Comparison of ascorbic and citric acid contents in 'Emphasis Type', Proc. 11. Symp. Plant Origin. Crude Drugs, Ankara, 258, 1997.

Caleb, O. J., Aindongo, W. V., Opara, U. L., Mokwena, L. Effect of pre-treatment and modified atmosphere packaging on quality attributes and volatile composition of pomegranate arils ('Bhagwa'). In V International Conference Postharvest Unlimited 1079, 165-171, 2014.

Caleb, O,J., Mahajan, P,V., Opara, U,L., Witthuhn, C,R. Modelling The Respiration Rates Of Pomegranate Fruit and Arils. Postharvest Biology and Technology, 64, 49-54, 2012.

Caleb, O. J., Oparaa, U.L., Mahajan, P.V., Manley, M.,Mokwena, L.,, Tredoux, A.G.J.. Effect of modified atmosphere packaging and storage temperature on volatile composition and postharvest life of minimally-processed pomegranate arils (cvs. 'Acco' and 'Herskawitz'). Postharvest Biology and Technology 79 54–61, 2013.

D'Aquino, S., Palma, A.,, Schirra, M., Continella, A.,Tribulato, E., Malfa, S. L..Influence of film wrapping and fludioxonil application on quality of pomegranate fruit. Postharvest Biology and Technology 55, 121–128, 2010.

Deng, J., Bi, Y., Zhang, Z., Xie, D., Ge, Y., Li, W., Wang, J., Wang, Y.. Postharvest oxalic acid treatment induces resistance against pink rot by priming in muskmelon (*Cucumis melo* L.) fruit. Postharvest Biology and Technology, 106, 53-61, 2015.

Ding, Z. S., Tian, S. P., Zheng, X. L., Zhou, Z. W., Xu, Y. Responses of reactive oxygen metabolism and quality in mango fruit to exogenous oxalic acid or salicylic acid under chilling temperature stress. Physiologia Plantarum, 130(1), 112-121, 2007.

Fawole, O. A., Opara, U. L. Physicomechanical, phytochemical, volatile compounds and free radical scavenging properties of eight pomegranate cultivars and

classification by principal component and cluster analyses.British Food Journal, 116(3), 544-567, 2014.

Fawole, O. A., Opara, U. L. Effects of storage temperature and duration on physiological responses of pomegranate fruit. Industrial crops and products, 47, 300-309, 2013.

Gürsoy, N., Sarıkurkcu, C., Cengiz, M., Solak, M.H., Antioxidant activities, metal contents, total phenolics and flavonoids of seven Morchella species, Food and Chemical Toxicology, 47, 2381- 2388, 2009.

Holland, D., Hatib, K., Bar-Ya'akov, I. 2 Pomegranate: Botany, Horticulture, Breeding. Horticultural reviews, 35(2), 127-191, 2009.

Huang, H., Jing, G., Guo, L., Zhang, D., Yang, B., Duan, X. Effect of oxalic acid on ripening attributes of banana fruit during storage. Postharvest Biology and Technology, 84, 22-27, 2013.

Jin, P., Zhu, H., Wang, L., Shan, T., Zheng, Y. Oxalic acid alleviates chilling injury in peach fruit by regulating enerjy metabolism and fatty acid contents. Food Chemistry, 161, 87-93, 2014.

Elyatem, S. M., Kader, A. A. Post-harvest physiology and storage behaviour of pomegranate fruits. Scientia Horticulturae, 24(3-4), 287-298, 1984.

Kulkarni, A.P., Aradhya, S.M.. Chemical changes and antioxidant activity in pomegranate arils during fruit development. Food Chemistry, 93, 319-324, 2005.

Kurt, H., Şahin, G. Bir ziraat coğrafyası çalışması: Türkiye'de nar (Punica granatum L.) tarımı. Marmara Coğrafya Dergisi, 27, 551-574, 2013.

Li, P., Yin, F., Song, L., Zheng, X. Alleviation of chilling injury in tomato fruit by exogenous application of oxalic acid. Food Chemistry, 202, 125-132, 2016.

Li, P., Zheng, X., Liu, Y., Zhu, Y. Pre-storage application of oxalic acid alleviates chilling injury in mango fruit by modulating proline metabolism and energy status under chilling stress. Food chemistry, 142, 72-78, 2014.

Liang, Y., Strelkov, S.E., Kav, N.N.V. Oxalic acid-mediated stress responses in Brassica napus L. Proteomics 9, 3156-317, 2009.

Maghoumi, M., Gómez, P.A., Mostofi, Y., Zamani, Z., Artés-Hernández F., Artés, F.Combined effect of heat treatment, UV-C and superatmospheric oxygen packing on phenolics and browning related enzymes of fresh-cut pomegranate arils. LWT - Food Science and Technology 54, 389-396, 2013.

Martínez-Romero, D., Castillo, S., Guilléna, F., Díaz-Mula, H. M., Zapata, P. J., Valero, D., Serrano, M. Aloe vera gel coating maintains quality and safety of ready-to-eatpomegranate arils. Postharvest Biology and Technology, 86, 107–112, 2013.

Meda, A., Lamien, C. E., Romito, M., Millogo, J. & Nacoulma, O. G. Determination of the total phenolic, flavonoid and proline contents in burkina fasan honey, as well as their radical scavenging activity. Food Chemistry, 91, 571–577, 2005.

Miron, D., Schaffer, A.A. Sucrose phosphate synthase, sucrose synthase, and invertase activities in developing fruit of *Lycopersicon esculentum* Mill. and the sucrose accumulating *Lycopersicon hirsutum* Humb. and Bonpl. Plant Physiol. 95, 623-627, 1991.

Mphahlele, R. R., Fawole, O. A., Opara, U. L. Influence of packaging system and long term storage on physiological attributes, biochemical quality, volatile composition and antioxidant properties of pomegranate fruit. Scientia Horticulturae 211, 140–151, 2016.

Opara, U. L., Atukuri, J., Fawole, O. A.. Application of physical and chemical postharvest treatments to enhance storage and shelf life of pomegranate fruit-A review . Scientia Horticulturae 197, 41–49, 2015.

Öz, A. T., Kafkas, N. E., Bozdoğan, A. Combined effects of oxalic acid treatment and modified atmosphere packaging on postharvest quality of loquats during storage. Turkish Journal of Agriculture and Forestry, 40, 433-440, 2016.

Pedriali , C.A., Fernandes, A. U., Santos, P. A.,. Silva, M. M., Severino, D., Silva, M. B. Antioxidant activity, cito- and phototoxicity of pomegranate (Punica granatum L.) seed pulp extract . Food Science and Technology, 30, 1017-1021, 2010.

Razavi, F., Hajilou, J. Enhancement of postharvest nutritional quality and antioxidant capacity of peach fruits by preharvest oxalic acid treatment. Scientia horticulturae, 200, 95-101, 2016.

Rojanathammanee L., Puig, K. L., Combs, C. K. Pomegranate polyphenols and extract inhibit nuclear factor of activated T-cell activity and microglial activation in vitro and in a transgenic mouse model of alzheimer disease. J. Nutr, 143, 597-605, 2013.

Sayyari, M., Castillo, S., Valero, D., Díaz-Mula, H.M., Serrano, M. Acetylsalicylic acid alleviates chilling injury and maintains nutritive and bioactive compounds and antioxidant activity during postharvest storage of pomegranates. Postharvest Biology and Technology, 60, 136–142, 2011.

Sayyari, M., Valero, D., Babalar, M., Kalantari, S., Zapata, P.J., Serrano, M.Prestorage oxalic acid treatment maintained visual quality, bioactivecompounds, and antioxidant potential of pomegranate after long-term storage.at 2 ◦C. Journal of Agricultural and Food Chemistry, 58, 6804–6808, 2010.

Selcuk, N., Erkan, M. Changes in antioxidant activity and postharvest quality of sweet pomegranates cv. Hicraznar under modified atmosphere packing. Postharvest Biology and Technology, 92, 29–36, 2014.

Shahbaz, H. M., Ahn, J. J., Akram, K., Kim, H.Y., Park, E.J., Kwon, J.H. Chemical and sensory quality of fresh pomegranate fruits exposed to gamma radiation as quarantine treatment. Food Chemistry, 145, 312–318, 2014.

Singleton, V. L., Rossi, J. A. Colorimetry of Total Phenolics with Phosphomolybdic-Phosphotungstic Acid Reagents. American Journal of Enology and Viticulture,16, 144-158, 1965.

Soliva-Fortuny, R. C., Elez-Martínez, P., Martín-Belloso, OMicrobiological and biochemical stability of fresh-cut apples preserved by modified atmosphere.packaging. Innovative Food Science & Emerging Technologies, 5, 215–224, 2004.

Tapias, V., Cannon, J. R., Greenamyre, J. T. Pomegranate juice exacerbates oxidative stress and nigrostriatal degeneration in Parkinson's disease. Neurobiology of Aging, 35, 1162-1176, 2014.

Türkiye İstatistik Kurumu (TÜİK), 2017. Diğer meyveler üretim istatistiği, 2017.

Ulukanlı, Z., Karadağ, E., Bacteriological and fungal evaluation of some aromatic and taste giving herbs from Igdir region in Eastern Anatolia of Turkey, African Journal of Microbiology Research, 4 (2), 2397-2401, 2010.

Üren, A. Üç boyutlu renk ölçme yöntemleri. Gıda, 24(3), 193-200, 1999.

Vardin, H., Abbasoğlu, M. Nar ekşisi ve narın diğer değerlendirme olanakları. Geleneksel Gıdalar Sempozyumu, 23, 195-196, 2004.

Viuda-Martos, M., Fernández-López, J., Pérez- Álvarez, J. A. Pomegranate and its many functional components as related to human health: A review. Comprehensive Reviews in Food Science and Food Safety, 9, 635-654, 2010.

Voss, H.D., Relating colorimeter measurement of plant color to the royal horticultural society colour chart, Hort. Science, 27 (12), 1992.

Wang, Z., Cao, J., Jiang, W. Changes in sugar metabolism caused by exogenous oxalic acid related to chilling tolerance of apricot fruit. Postharvest Biology and Technology, 114, 10-16, 2015.

Wrolstad, R.E., Color and pıgment analyses ın fruit products, Station Bulletion, Agrıcultural Experimental Station Oregon State Univercity, Corvalli, 16, 1976.

Yorulmaz, A., Erinc, H., Tekin, A. Changes in olive and olive oil characteristics during maturation, Journal of the American Oil Chemists. Society, 90(5), 647-658, 2013.

Yörük, R. The inhibitory effect of oxalic acid on browning of banana slices (30G-18). In Annual Meeting and Food Expo. Anaheim, CA, 2002.

Zheng, X., Tian, S., Gidley, M., Yue, H., Li, B. Effects of exogenous oxalic acid on ripening and decay incidence in mango fruit during storage at room temperature. Postharvest Biology and Technology, 45, 281–284, 2007b.

Zheng, X., Tian, S., Meng, X., Li, B. Physiological and biochemical responses in peach fruit to oxalic acid treatment during storage at room temperature. Food Chemistry 104, 156-162, 2007a.

Zhu, Y., Yu, J., Brecht, K. J., Jiang, T., Zheng, X. Pre-harvest application of oxalic acid increases quality and resistance to penicillium expansum in kiwifruit during postharvest storage. Food Chemistry, 190, 537-543, 2016.

THIS PAGE IS INTENTIONALLY
LEFT BLANK

INFLUENCE OF GABA TREATMENT ON 'HİCAZNAR' POMEGRANATE ARILS QUALITY

Ayşe Tülin ÖZ, Şeyma HİÇYILMAZ

Osmaniye Korkut Ata University Engineering Faculty, Food Engineering Department
Karacaoğlan Campus 80000 Osmaniye
aysetulinoz@osmaniye.edu.tr

ABSTRACT: Whole pomegranate were peeled by mannually and arils of pomegranate fruits were treated by using three different GABA concentrations as control (0mM), 2.5mM and 5Mm then packed in 250 g PVPP boxes the pomegranate fruit were stored for 20 days at 5°C in the cold air storage at 90 % relative humidity. Physical, chemical (TSS, TA, pH, and TSS) and microbial quality of pomegranate arils were determined. Effects of the treatments measured every 4 days during storage. The effect of GABA treatment on pomegranate arils of weight loss (%), pH, titratable acidty (%), gas composition changes (O_2 / CO_2) (%), arils color (L,a, b,C, h^o) value, arils firmness (N), chilling injury (%), bacteria, yeast and mold (logCFU/g) growth were investigated during the storage period.
Key words: **'Hicaznar', pomegranate, arils, GABA, quality.**

FORECASTING OF PRIMARY ENERGY CONSUMPTION OF TURKEY AND SOME EUROPEAN COUNTRIES WITH GM(1,1) MODEL

Utkucan ŞAHİN
Muğla Sıtkı Koçman Üniversitesi, Teknoloji Fakültesi, Enerji Sistemleri Mühendisliği Bölümü, 48000, Muğla, Türkiye
usahin@mu.edu.tr

ABSTRACT: The aim of this study is to forecast primary energy consumption of Turkey and total European countries with Grey prediction method for the period 2017-2021. To achieve this, actual data of primary energy consumption from 2005 to 2016 was modelled by GM(1,1). The achievement of established GM(1,1) models on prediction was determined with the posterior error ratio (C) and mean absolute percentage error ($MAPE$) parameters. Results showed that the established GM(1,1) models were in good level for both total European countries and Turkey's primary energy consumption. Additionally, the average annual growth rate of Turkey's primary energy consumption for the period 2017-2021 was forecasted as 2.73%. The average annual reduction rate of primary energy consumption of total European countries was forecasted as 1.11%.

Keywords: Grey prediction method, Turkey, European countries, primary energy consumption

TÜRKİYE'NİN VE BAZI AVRUPA ÜLKELERİNİN BİRİNCİL ENERJİ TÜKETİMİNİN GM(1,1) MODELİ İLE TAHMİN EDİLMESİ

Utkucan ŞAHİN
Muğla Sıtkı Koçman Üniversitesi, Teknoloji Fakültesi, Enerji Sistemleri Mühendisliği Bölümü, 48000, Muğla, Türkiye
usahin@mu.edu.tr

ÖZET
Bu çalışmanın amacı, 2017-2021 yılları arasındaki Türkiye ve Avrupa'nın birincil enerji tüketimini Gri tahmin yöntemiyle tahmin etmektir. Bunu gerçekleştirmek için, 2005-2016 yılları arasındaki birincil enerji tüketimi verileri gri tahmin yöntemi GM(1,1) ile modellenmiştir. Oluşturulan GM(1,1) modellerinin, gerçek verileri tahmin etmedeki başarısı sonsal hata oranı (C) ve ortalama mutlak yüzde hata ($MAPE$) parametreleri ile ölçülmüştür. Sonuçlar, oluşturulan GM(1,1) modellerinin başarılı olduğunu göstermiştir. Buna ek olarak, 2017-2021 yılları arasında Türkiye'nin birincil enerji tüketiminde yıllık ortalama büyüme oranının %2.73 olacağı tahmin edilmektedir. Avrupa'nın toplam birincil enerji tüketiminin ise yıllık ortalama %1.11 oranında azalacağı tahmin edilmektedir.

Anahtar sözcükler: Gri tahmin modeli, Türkiye, Avrupa ülkeleri, birincil enerji tüketimi

GİRİŞ

Avrupa ile Asya arasında bir geçiş noktası olan Türkiye, enerji tüketimi ve stratejik konumundan dolayı enerji politikaları açısından önemli bir ülke durumundadır (Hamzacebi ve Es, 2014). Avrupa İstatistik Ofisi (Eurostat) verilerine göre, 2016 yılı sonunda Avrupa ülkelerinin birincil enerji tüketimi toplamı 1735.7 milyon ton eşdeğer petrol (MTEP) olarak gerçekleşirken, Türkiye 131.6 MTEP'lik birincil enerji tüketim değeriyle İtalya'dan sonra 5. sırada yer almıştır. 2005-2016 yılları arasındaki dönem değerlendirildiğinde, Türkiye'nin birincil enerji tüketimi 2008, 2009 ve 2013 yıllarında düşerken 2013 yılından sonra sürekli artmıştır (Eurostat, 2018).

Enerji talep tahmini, bütün dünyada karar vericiler tarafından kullanılan en önemli politika araçlarından biridir (Ediger ve Akar, 2007). Ayrıca, ülkelerin uzun, orta ve kısa vadeli dönemler için stratejik karar almalarında veri oluşturmaktadır (Suganthi ve Samuel, 2012). Literatürde çeşitli tahmin yöntemleri olmakla beraber Gri tahmin yöntemi basit ve güçlü olması sebebiyle enerji tahmini ile ilgili çalışmalarda tercih edilen bir yöntemdir (Ayvaz ve Kusakci, 2017). 1982'de Ju-long Deng tarafından geliştirilen Gri sistem teorisinin bir parçası olan ve en yaygın biçimde kullanılan Gri tahmin modeli ise GM(1,1)'dir (Hamzacebi ve Es, 2014; Deng, 1982). Literatürde, GM(1,1) modelinin Türkiye'nin enerji tahmininde kullanıldığı birçok çalışma vardır (Akay ve Atak, 2007; Hamzacebi ve Es, 2014; Boran, 2015; Ayvaz ve Kusakci, 2017).

Bu çalışmanın amacı, GM(1,1) modelini kullanarak 39 adet Avrupa ülkesinin toplam birincil enerji tüketimi ile 2016 yılı sonunda Avrupa'nın birincil enerji tüketiminde en çok payı oluşturan ilk 5 ülkenin 2017-2021 dönemi için birincil enerji tüketimini tahmin etmektir. Bu amacı gerçekleştirmek için, Avrupa İstatistik Ofisi'nin 2005-2016 dönemine ait birincil enerji tüketim verileri kullanılmıştır. Oluşturulan GM(1,1) modellerinin gerçek veriler ile arasındaki istatistiksel farklılıklar sonsal hata oranı (C) ve ortalama mutlak yüzde hata ($MAPE$) parametreleri ile ölçülmüştür.

YÖNTEM

GM(1,1) Modeli

Gri tahmin modeli aşağıdaki biçimde açıklanabilir (Zhan-li ve Jin-hua, 2011):

Adım 1: Mevcut veriler kullanılarak ham veri seti $x^{(0)}$ oluşturulur.

$$x^{(0)} = \{x^{(0)}(1), x^{(0)}(2), x^{(0)}(3), \dots \dots .., x^{(0)}(n)\} \quad (1)$$

Adım 2: Birinci dereceden toplam üretim operatörü oluşturulur.

$$x^{(1)}(k) = \{x^{(1)}(1), x^{(1)}(2), x^{(1)}(3), \dots \dots .., x^{(1)}(n)\} \quad (2)$$

Burada,

$$x^{(1)}(k) = \sum_{i=1}^{k} x^{(0)}(i) \qquad k = 1,2,3 \dots .., n \quad (3)$$

Adım 3: GM(1,1) modelinin biçimlendirmek için birinci dereceden gri diferansiyel denklemi oluşturulur.

$$x^{(0)}(k) + az^{(1)}(k) = b \quad (4)$$

$$\frac{dx^{(1)}}{dt} + ax^{(1)}(k) = b \quad (5)$$

Burada, a gelişme katsayısı, b sürücü katsayısı ve $k = 2,3,4, \dots .., n$'dir. $z^{(1)}(k)$ aşağıdaki denklem ile hesaplanır.

$$z^{(1)}(k) = \frac{x^{(1)}(k)+x^{(1)}(k-1)}{2} \qquad k = 2,3,4,\ldots\ldots,n \tag{6}$$

Adım 4: a ve b katsayıları en küçük kareler yöntemi kullanılarak aşağıdaki biçimde hesaplanır.

$$[a\ b]^T = [B^T B]^{-1} B^T Y \tag{7}$$

Burada,

$$B = \begin{bmatrix} -z^{(1)}(2) & 1 \\ -z^{(1)}(3) & 1 \\ -z^{(1)}(4) & 1 \\ \vdots & \vdots \\ \vdots & \vdots \\ -z^{(1)}(n) & 1 \end{bmatrix}, \quad Y = \begin{bmatrix} x^{(0)}(2) \\ x^{(0)}(3) \\ x^{(0)}(4) \\ \vdots \\ \vdots \\ x^{(0)}(n) \end{bmatrix} \quad ve \quad [a\ b]^T = \begin{bmatrix} a \\ b \end{bmatrix} \tag{8}$$

Adım 5: Elde edilen a ve b parametreleri aşağıdaki denklemde yerine konularak GM(1,1) modeli elde edilir.

$$\hat{x}^{(0)}(k+1) = (1 - \exp(a))\left(x^{(0)}(1) - \frac{b}{a}\right)\exp(-a * k) \tag{9}$$

Burada, $\hat{x}^{(0)}(1) = x^{(0)}(1)$ alınır.

Elde edilen GM(1,1) modelinin doğruluğunu test edebilmek için sonsal hata oranı (C) ve küçük hata olasılığı (p) parametreleri hesaplanmaktadır.

$$C = \frac{S_2}{S_1} \tag{10}$$

Burada, S_1 mevcut verilerin hata kareleri ortalamasını, $\bar{x}$ ise mevcut verilerin ortalamasını vermektedir.

$$S_1 = \sqrt{\frac{1}{n}\sum_{k=1}^{n}(x^0(k) - \bar{x})^2} \tag{11}$$

$$\bar{x} = \frac{1}{n}\sum_{k=1}^{n} x^0(k) \tag{12}$$

Burada, S_2 tahmin edilen verilerin hata kareleri ortalamasını, $\bar{x}$ ise tahmin edilen verilerin ortalamasını vermektedir.

$$S_2 = \sqrt{\frac{1}{n}\sum_{k=1}^{n}(x^0(k) - \bar{y})^2} \tag{13}$$

$$\bar{y} = \frac{1}{n}\sum_{k=1}^{n} \hat{x}^0(k) \tag{14}$$

Buna ek olarak, ortalama mutlak yüzde hata ($MAPE$) oranı ise aşağıdaki formülle hesaplanabilmektedir.

$$MAPE\ (\%) = \sum_{i=1}^{n}\left|\frac{u(i)-\hat{u}(i)}{u(i)}\right| x \frac{100}{n} \tag{15}$$

Burada, u mevcut verileri, $\hat{u}$ tahmin edilen verileri ve n ise veri sayısını belirtmektedir. Elde edilen C ve MAPE değerleri ile GM(1,1) modellerinin doğruluk derecesi Tablo 1'den belirlenir.

Tablo 1. Tahmin modellerinin doğruluk derecesi (Hamzacebi ve Es, 2014)

Sınıflandırma	$\boldsymbol{C}$	$\boldsymbol{MAPE}$

Mükemmel	≤ 0.35	≤ 1%
İyi	≤ 0.50	≤ 5%
Kabul edilebilir	≤ 0.65	≤ 10%
Yetersiz	> 0.65	> 10%

SONUÇLAR

Bu çalışmada, ülkelerin birincil enerji tüketiminin tahmininde 2016 yılı sonunda birincil enerji tüketim değeri (Avrupa İstatistik Ofisi verilerine göre) en çok olan Avrupa ülkeleri (Almanya, Fransa, Birleşik Krallık ve İtalya), 39 Avrupa ülkesinin toplamı ile Türkiye tercih edilmiştir. 2005-2016 yılları arasında Türkiye, Almanya, Fransa, Birleşik Krallık, İtalya ve Avrupa ülkelerinin toplam birincil enerji tüketim değerleri Avrupa İstatistik Ofisi'nin (Eurostat) veri tabanından (Eurostat, 2018) alınmıştır. Avrupa'nın toplam birincil enerji tüketiminin değerlendirilmesinde Şekil 1'de verilen toplam 39 ülke göz önüne alınmıştır. Elde edilen 12 yıllık veriler kullanılarak Eşitlik (9) yardımıyla ülkelere ait GM(1,1) modelleri oluşturulmuş ve bu modeller Eşitlik (16-21)'de belirtilmiştir. Bu eşitlikler yardımıyla, ülkelerin birincil enerji tüketimi 2017-2021 yılları için tahmin edilmiştir.

$$\hat{x}^{(0)}(k+1)\Big|_{Avrupa} = (1-e^{0.00883})(1845.4-212630)e^{-0.00883*k}$$
(16)

$$\hat{x}^{(0)}(k+1)\Big|_{Almanya} = (1-e^{0.00907})(317.3-35376)e^{-0.00907*k}$$
(17)

$$\hat{x}^{(0)}(k+1)\Big|_{Fransa} = (1-e^{0.0082})(260.2-31614)e^{-0.0082*k}$$
(18)

$$\hat{x}^{(0)}(k+1)\Big|_{Birleşik\ Krallık} = (1-e^{0.01872})(222.8-11932)e^{-0.01872*k}$$
(19)

$$\hat{x}^{(0)}(k+1)\Big|_{İtalya} = (1-e^{0.02292})(181.5-8193)e^{-0.02292*k}$$
(20)

$$\hat{x}^{(0)}(k+1)\Big|_{Türkiye} = (1-e^{-0.03826})(80.9+2154)e^{0.03826*k}$$
(21)

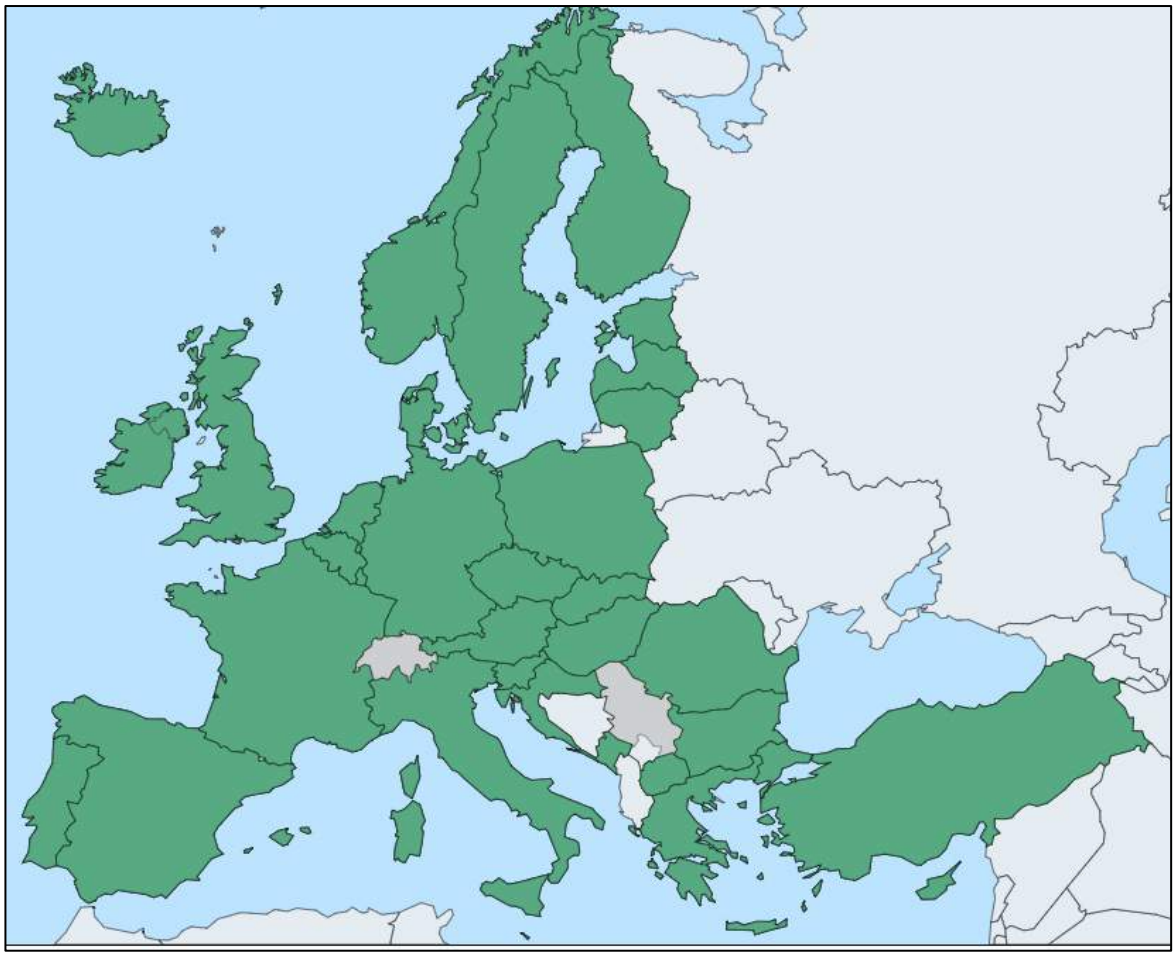

Şekil 1. Bu çalışma için Avrupa ülkelerinin toplamını gösteren harita (Avrupa İstatistik Ofisi'nden alınmıştır)

2005-2016 yılları arasındaki Türkiye, Almanya, Fransa, Birleşik Krallık, İtalya ve Avrupa ülkelerinin birincil enerji tüketimi verilerini tahmin etmek için oluşturulan GM(1,1) modellerinin gerçek verileri tahmin etmedeki başarısını ölçmek için sonsal hata oranı (C) ve ortalama mutlak yüzde hata oranı ($MAPE$) değerleri hesaplanmış ve sonuçlar Tablo 2'de verilmiştir. Buna göre, oluşturulan GM(1,1) modellerinin gerçek verileri tahmin etmede başarılı olduğu söylenebilir.

Tablo 2. Ülkelerin birincil enerji tüketiminin tahmin edilmesi için oluşturulan GM (1,1) modellerinin gerçek veriler ile arasındaki istatistiksel sonuçlar

Ülkeler	**Birincil Enerji Tüketimi (2005-2016)**	
	$\boldsymbol{C}$	$\boldsymbol{MAPE}$ **(%)**
Türkiye	0.25	2.70
Avrupa ülkelerinin toplamı	0.48	1.22
Almanya	0.62	1.94
Fransa	0.44	1.07
Birleşik Krallık	0.31	1.64
İtalya	0.28	1.81

Şekil 1'de belirtilen 39 ülkenin toplamına ait 2005-2016 yılları arasındaki Avrupa'nın toplam birincil enerji tüketim değerinin ve Eşitlik (17) yardımıyla oluşturulan tahmini

değerlerin yıllara göre gelişimi Şekil 2'de gösterilmiştir. Oluşturulan GM(1,1) modeline göre, Avrupa'nın toplam birincil enerji tüketiminin 2021 yılı sonunda 1623 milyon ton eşdeğer petrol (MTEP) olacağı başka bir ifadeyle birincil enerji tüketiminin 2017'den 2021 yılına kadar yılda ortalama %1.11 oranında azalacağı öngörülmektedir.

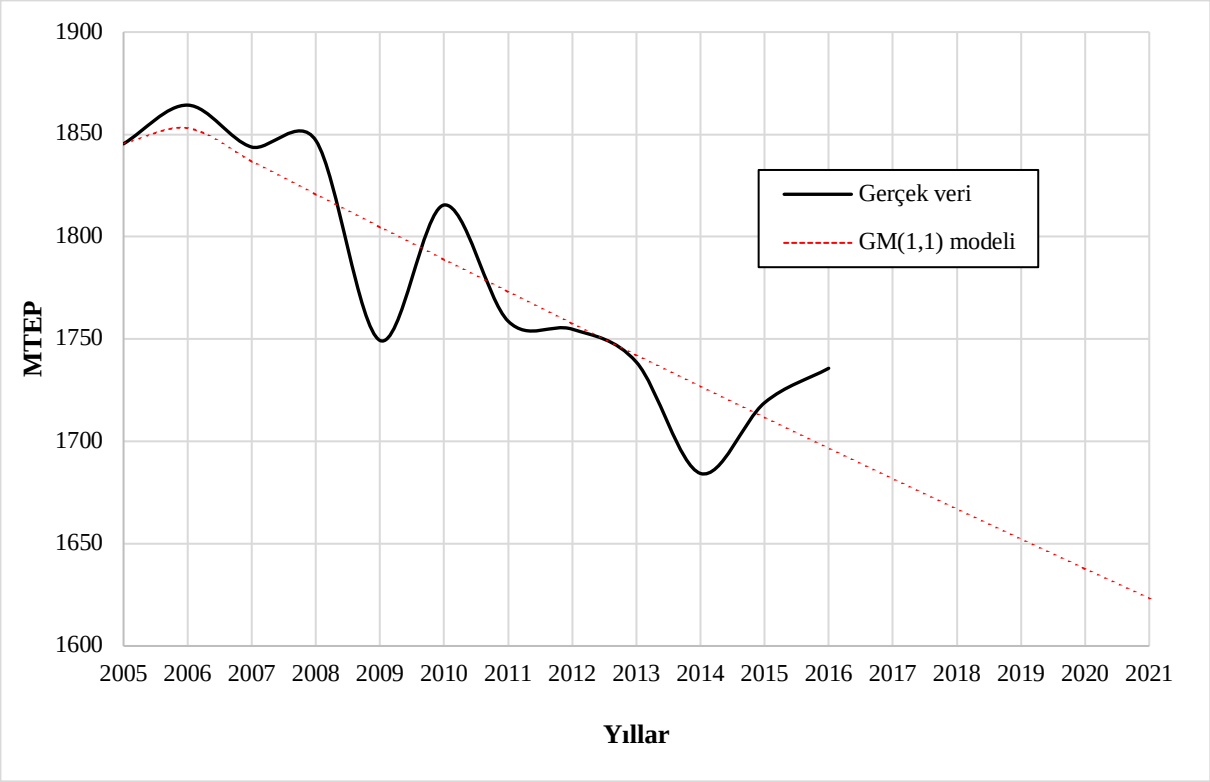

Şekil 2. GM (1,1) modeli ile 2005-2021 yılları arası Avrupa ülkelerinin toplam birincil enerji tüketiminin (MTEP) tahmin edilmesi

Avrupa İstatistik Ofisi'nin verilerine göre, 2016 yılı sonunda Şekil 1'de belirtilen 39 ülkenin toplam birincil enerji tüketimi 1735.7 MTEP olarak gerçekleşmiştir. Bunun en büyük payını sırasıyla %17.0'lık oranla Almanya, %13.6'lık oranla Fransa, %10.5'lik oranla Birleşik Krallık, %8.5'lik oranla İtalya ve %7.6'lık oranla Türkiye takip etmiştir. Eşitlik (17-21) yardımıyla oluşturulan GM(1,1) modellerine göre Almanya, Fransa, Birleşik Krallık ve İtalya'nın 2017-2021 yılları arasında birincil enerji tüketiminin azalacağı Şekil 3'te gösterilmiştir. Buna ek olarak, 2021 yılı sonunda Almanya, Fransa, Birleşik Krallık ve İtalya'nın Avrupa'nın toplam birincil enerji tüketiminin sırasıyla %17.0, %13.9, %10.1 ve %7.9'unu oluşturacağı öngörülmektedir.

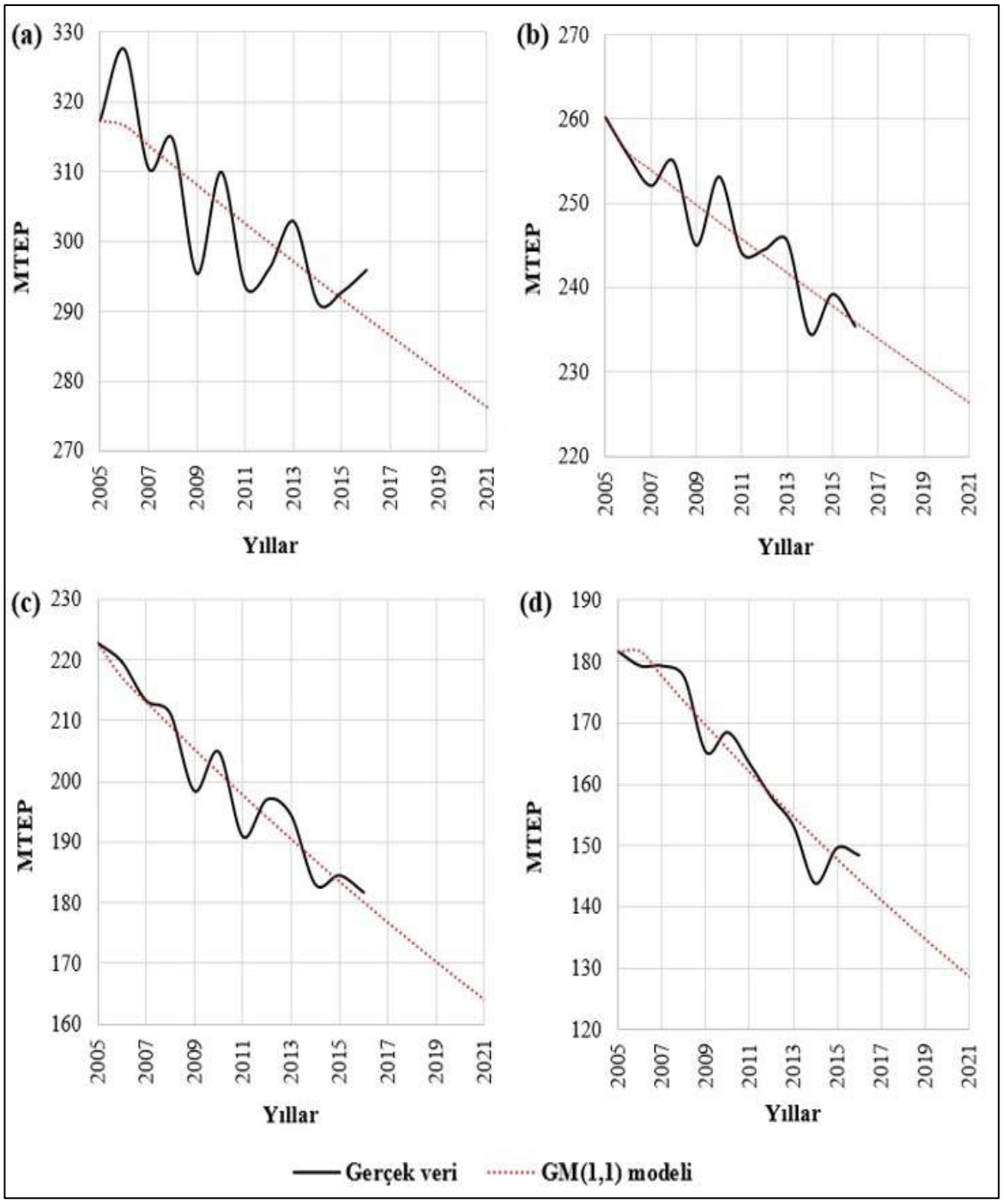

Şekil 3. Bazı Avrupa ülkelerinin (a) Almanya, (b) Fransa, (c) Birleşik Krallık ve (d) İtalya birincil enerji tüketiminin (MTEP) GM(1,1) modeli ile tahmin edilmesi

Türkiye'nin 2005-2016 yıları arasındaki birincil enerji tüketiminin yıllara göre gelişimi Şekil 3'te gösterilmiştir. Buna göre, 2005 yılından 2016 yılı sonuna kadar birincil enerji tüketiminin yılda ortalama %4.14 oranında arttığı sonucuna ulaşılmaktadır. Buna ek olarak, Eşitlik (21) yardımıyla oluşturulan GM(1,1) modeline göre Türkiye'nin birincil enerji tüketiminin 2017 yılı sonunda 132.8 MTEP, 2021 yılı sonunda ise 154.7 MTEP olacağı tahmin edilmektedir. Başka bir ifadeyle, 2016 yılı sonundan 2021 yılı sonuna kadar birincil enerji tüketiminin yılda ortalama %2.73 oranında artacağı öngörülmektedir. Bu sonuçlar, 2021 yılı sonunda Türkiye'nin birincil enerji tüketiminin Avrupa'nın toplam birincil enerji tüketiminin %9.5'ini oluşturacağını göstermektedir.

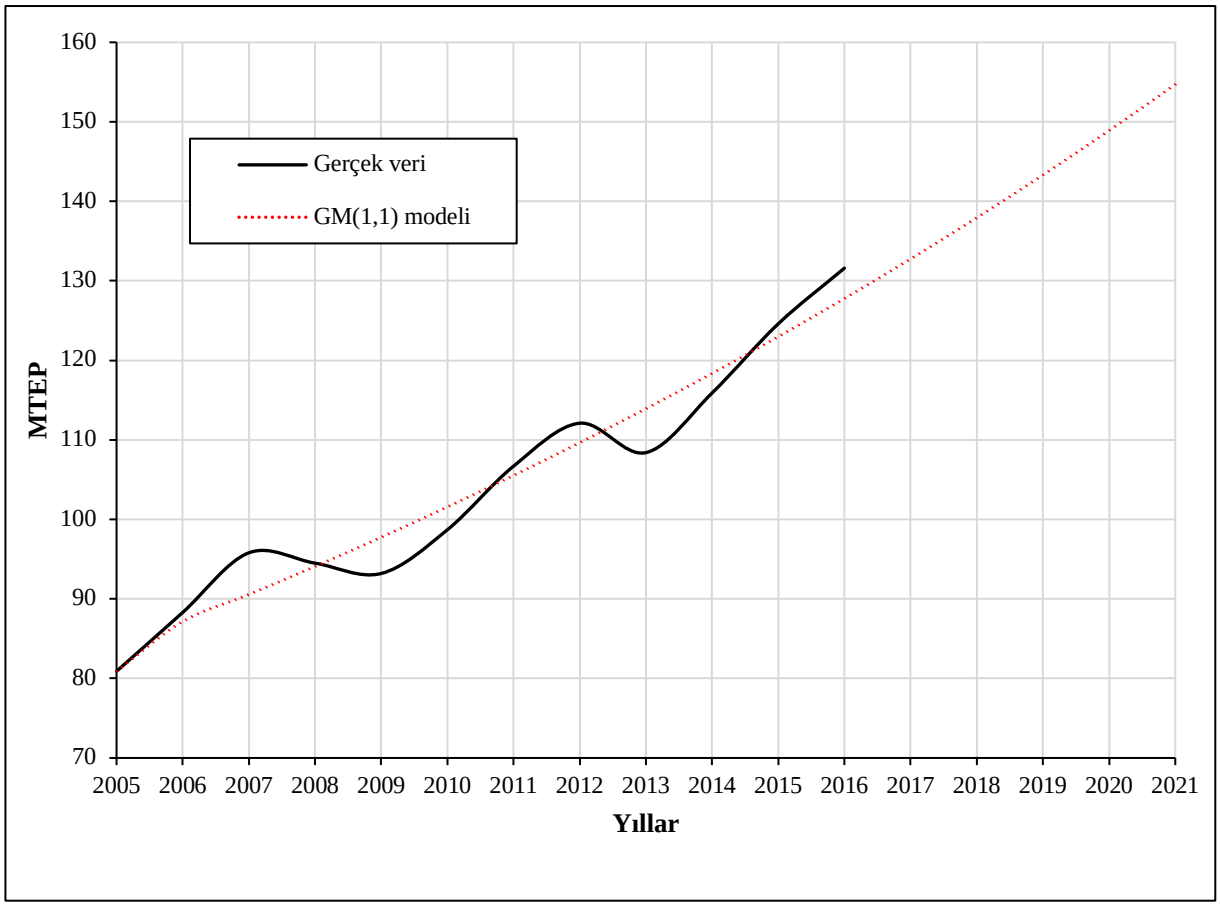

Şekil 4. GM(1,1) modeli ile 2005-2021 yılları arası Türkiye birincil enerji tüketiminin (MTEP) tahmin edilmesi

ÖNERİLER

Bu çalışmada, GM(1,1) modeli kullanılarak 2005-2016 yılları arasında Türkiye ve bazı Avrupa ülkelerinin birincil enerji tüketimi tahmin edilmiştir. Oluşturulan GM(1,1) modelleri ile 2017-2021 periyodu için ülkelerin birincil enerji tüketimi tahmin edilmiştir.

Sonuçlar;

Oluşturulan GM(1,1) modellerinin ortalama mutlak yüzde hata oranı (MAPE) değerleri %3'ün altındadır.

2017-2021 periyodu boyunca Almanya, Fransa, Birleşik Krallık, İtalya ve Avrupa'nın toplam birincil enerji tüketiminin azalacağı, Türkiye'nin ise birincil enerji tüketiminin artacağı öngörülmektedir.

2021 yılı sonunda Türkiye'nin birincil enerji tüketiminin Avrupa'nın toplam birincil enerji tüketiminin %9.5'ini oluşturacağı tahmin edilmektedir.

Bu çalışma, enerji kaynaklarına göre ayrılarak her bir enerji kaynağı için değerlendirilebilir. Buna ek olarak, farklı tahmin metotları kullanılarak çalışmanın sonuçları karşılaştırılabilir.

KAYNAKLAR

Akay, D., Atak, M. (2007). Grey prediction with rolling mechanism for electricity demand forecasting of Turkey. *Energy*, 32, 1670-1675.

Ayvaz, B., Kusakci, A.O. (2017). Electricity consumption forecasting for Turkey with nonhomogeneous discrete grey model. *Energy Sources, Part B: Economics, Planning, and Policy*, 12 (3), 260-267.

Boran, F.E. (2015). Forecasting Natural Gas Consumption in Turkey Using Grey Prediction. *Energy Sources, Part B: Economics, Planning, and Policy*, 10 (2), 208-213.

Deng, J. (1982). Control problems of grey systems. *Systems and Control Letters*, 1 (5), 288-294.

Ediger, V.Ş., Akar, S. (2007). ARIMA forecasting of primary energy demand by fuel in Turkey. *Energy Policy*, 35, 1701-1708.

Eurostat, 2018. < https://ec.europa.eu/eurostat/tgm/table.do?tab=table&init=1&plugin=1&language=en&pcode=sdg_07_10 >.

Hamzacebi, C., Es, H. A. (2014). Forecasting the annual electricity consumption of Turkey using an optimized grey model, *Energy*, 70, 165-171.

Suganthi, L., Samuel, A. A. (2012). Energy models for demand forecasting-a review, *Renewable and Sustainable Energy Reviews*, 16, 1223-1240.

Zhan-li, M., Jin-hua, S. (2011). Application of Grey-Markov model in forecasting fire accidents. *Procedia Engineering,* 11, 314-318.

DESIGN OF A LOW COST AND HIGH EFFICIENCY VERTICAL AXIS WIND TURBINE

Sohayb Abdul Karim
Gaziantep University
karim@gantep.edu.tr,

Khaled Hamoud
Gaziantep University
2khaledhamoud@gantep.edu.tr

ABSTRACT: This work focuses on manufacturing a vertical axis wind turbine with movable blades and experimenting the performance and comparing with non-movable ones. The aim was helping refugees living in camps of owing a small-scale source of energy at low cost and high efficiency. All processes were done using low budget workshop in order to develop a prototype as cheap as possible. The work was started by manufacturing a 6-blades prototype, from composite material fiberglass mate. A proposed mechanism installed at the blade joints allowing a circular motion on 35-degree angular sector. The mechanism eliminates the negative role of the blade while it is moving in the opposite direction of the wind. The experiments have proved the efficiency of the proposed mechanism. However, the turbine parameters at the first guess were not very successful. Therefore, another prototype was suggested and tested. Thus, the number of the blades was increased to ten blades instead of six. The blade chord was reduced to the half. In addition, the blade material was improved by using one layer of fiberglass cloth instead of using two layers of mate. The experimental results of the second model showed better synchronization between the motion of the blades about its own axis and the motion of the blade about the central axis because of reducing the inertial moments of the blades. Additionally, it shows smoother run, less noise, lower level of vibrations, and better response to wind. On the other side, it is more difficult to manufacture hence relatively higher cost. In conclusion, the movable blades model performs up to 20% better than fixed one.
Keywords: vertical axis wind turbine, composite material, fiberglass cloth, and mate.

INTRODUCTION:

Clean and renewable energy resources are an important issue for humanity since the rising of the global warming problem. One of the most creative solutions is implementing wind power. Turbines are successfully implemented to extract wind energy for more than five thousand years ago.

In spite of those huge steps that have been taken in the green energy, the humanity still suffering lack of clean and affordable energy in crises. Natural disasters or wars may lead to thousands of displaced people living in camps without any source of energy for lightening and communication purposes. In another word, there is a need to deliver power at affordable costs within the conditions of portability and capability of responding to emergencies without violating environmental constrains. Therefore, this project is an attempt to bridge this gap. In this contest, the work focuses on

designing an affordable, small-scale, portable, and environmentally clean source of energy to supply minimum requirements of electrical power for lightning, and communication purposes for displaced people and suggest a passive control mechanism to improve the performance of the selected type of turbine.

In the last century, the wind turbines have been witnessed dramatic improvements and wide usages. Various kinds and shapes have been developed and used.

Fundamentally, the turbines can be categorized into two types. Horizontal Axis Wind Turbine, (HAWT) and Vertical Axis Wind Turbine (VAWT). Horizontal axis types are more common, while the vertical axis wind turbines are very rare in spite of some advantages. In fact, every type has some advantages and disadvantages (M. Saad, 2014). To mention some advantages of the VAWT, it is easy to manufacture and install. The most important advantage of a VAWT is its ability to self-start (Aslam Bhutta et al., 2012). Structurally, the central shaft in the VAWT is subjected to the rotor weight. The weight is axisymmetric distributed about the shaft. This removes the bending moment hence, reduces the stresses. As a result, failures probability and running costs are less. From aerodynamically point of view, the VAWT reacts to wind from all directions. This eliminates the need to yaw directional mechanisms. This again reduces the operational costs. From another side, in the urban areas, the streamlines of wind are normally turbulent and changing directions. Therefore, in these circumstances, HAWT cannot appropriately respond to wind. Environmentally, VAWT is less damaging to the landscape. Practically, it is difficult to list all differences. However, differences are extensively discussed in the literature by many researchers. For example, Xin Jin et. al. in his review paper emphasized on the advantages of VAWT (Jin, Zhao, Gao, & Ju, 2014). They found that less researches on VAWT were carried out and have to be focused more; while HAWT was studied extensively (Jin et al., 2014). Robert Howell et. al. studied a small-scale VAWT and provided numerical results using CFD and experimental results using wind tunnel; three and two bladed rotors are compared as well. It was found that higher solidity gives higher performance (Howell, Qin, Edwards, & Durrani, 2010).

For those reasons, the VAWT type of wind turbine is to be focused in this project. However, there is also another issue need to be decided. It is related to the way by which the useful force is extracted from wind. Generally, vertical axis wind turbine can be classified into two classes based on the principle of extracting the useful force from the airflow. In more details, the profile of the blades generates lift and drag forces. Thus, some VAWTs use the lift to produce the useful torque, while other Turbines use the drag. Darrieus wind turbine is a typical example of the former while Savonius wind-turbine is an example of the later type (Shaheen & Abdallah, 2016)(Shankar, 1979). The lift type requires a careful design and aerodynamic shape for the blade to extract the maximum possible lift and the minimum drag. On the contrary, the lift force is not important for the case of the drag type. The drag needs to be maximized. In the most simple design of drag type, It is just a simple buckets connected to a rotating shaft. Clearly, the lift type VAWT is more efficient but from other side, it is more complex to design and to construct. Therefore, the question, which one is the more cost effective, is difficult to answer. Reviewing some researches published in this context in an attempt to lighten some related issues is useful. For example, Bedon et.

al. found that Darrieus vertical axis wind turbine based on Troposkein shape is efficient from aerodynamic and structural views. However this type found only in large-scale turbines (Bedon, Raciti Castelli, & Benini, 2014a)(Bedon, Raciti Castelli, & Benini, 2014b). On the contrary, Guoying Feng et al noticed that Darrieus suffered from problems in the energy market due to structural problems. As a results of that problem, some turbines were dismantled and related researches were closed (Feng, Liu, Daorina, & Gong, 2009). There is a tendency to focus researches on a small-scale VAWT. Accordingly, E M Budi et at studied a VAWT for a fishing boat he compared between Savonius rotor, and hybrid Savonius-Darrieus rotor (Budi, Banjarnahor, & Hanifan, 2017). Bhutta et al demonstrated the design methods and compared between Darrious and Savonius. It was found that VAWT is more appropriate for small-scaled wind turbine (Aslam Bhutta et al., 2012).

In an attempt to improve the performance of a vertical axis wind turbine, Y. C. Lim et. al suggested using omni direction guide vane (Lim, Chong, & Hsiao, 2013). Differently, Xiao, et. al. proposed to use a flaps, as shown in Figure 1, in order to increase the lift of VAWT lift-type. They carried out a numerical simulation to compare with fixed profile (Xiao, Liu, & Incecik, 2013).

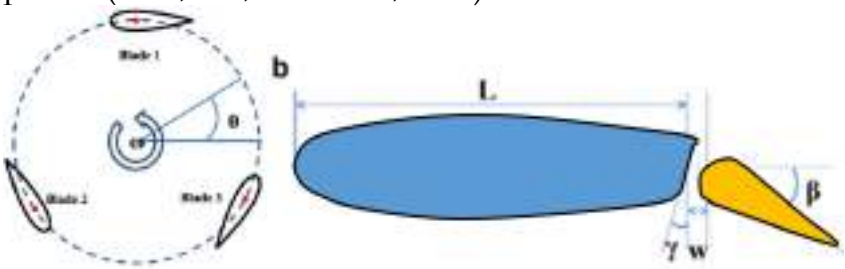

Figure 6 : Xiao et. al. proposed to use a flaps for Vertical axis wind turbine Lift type**(Xiao et al., 2013)**.

Svorcan, et. al. used vortex-wake model to simulate a lift type of small-scale VAWT as an approach to define the design paramters.

However, in this work, it was believed that using lift type requires more construction effort due to the complexity associated with the shape of the blade's profile. In addition, the flaps mechanism suggests more complexity both in construction and in running stages.

In the next paragraphs, a brief description of the design parameters and drawing geometry will be demonstrated using CAD applications; then a brief explanation of the construction process focusing on composite material elements; after that, the passive-control-mechanism installation process is explained, and then the assembly process is shown. In the last paragraph, a demonstration of the conducted experiments followed by a brief mathematical procedure formulated to estimate the mechanical power. Eventually, the conclusions and the recommendations are presented.

DESIGNING OF A VERTICAL WIND TURBINE PROTOTYPE

At the beginning, the first prototype was designed, manufactured, and tested. It was found that the performance could be improved by changing some parameters. Therefore, it was decided to design and manufacture another prototype.

The first prototype rotor diameter was 480 mm the blade length is 400 mm; the number of blades is six. The curvature of the blades was 130 mm while the width of the blade was 125 mm.

While the second prototype rotor diameter was 450 mm, the blade length is 400 mm the number of blades is 10,using the same curvature with half width 65 mm. another change was made by using one layer of fiberglass cloth instead of using two layers of fiberglass mat. These changes allowed increasing the number of blades without increasing the weight and the moment mass of inertia remains low. The most important geometry and differences between the two prototypes are shown in the table 1. While the table 2 shows a list of bolts and bearings used in assembling process.

Table 1 geometry of the most important components of two wind turbine prototypes

Part	First Prototype	Second Prototype
Central Shaft	Quantity 1 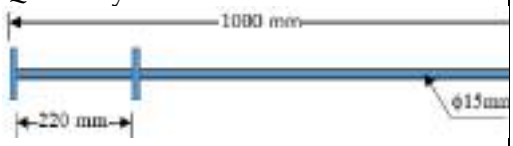	Quantity 1 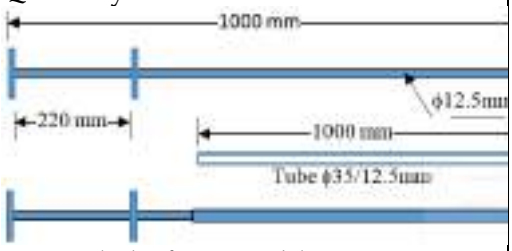 Central shaft assembly
Arms (connector)	Quantity 6x2=12 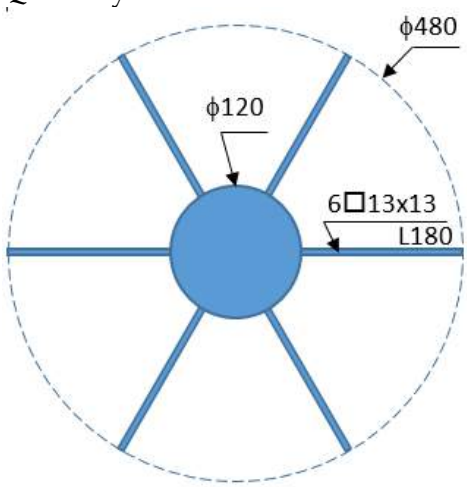 Arm cross section 13x13, Length 180mm	Quantity 10x2=20 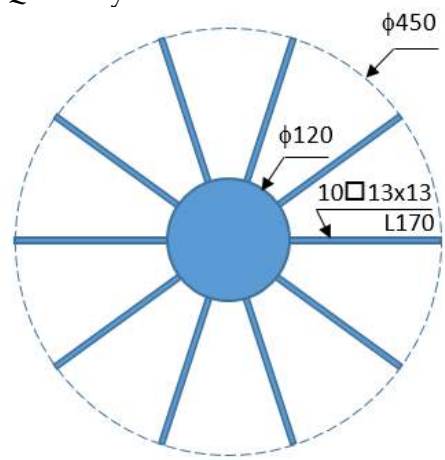 Arm cross section 13x13, Length 170mm
Blades	Quantity 6 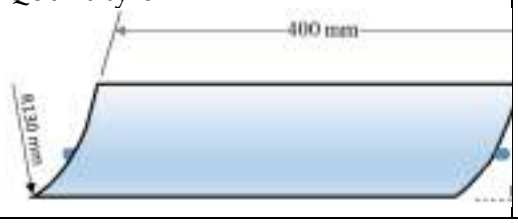	Qty 10 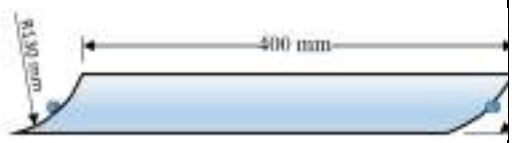

Table 2: list of bolts and bearings used in the two prototypes

Accessories	Qty	Dimension
Central shaft Bearing 6203 RS	2	17X40X12
Blade Bearings type 624 Z	20	4x13x5
self-drilling screws A	-	ϕ4.2 x 13 mm
self-drilling screws B	-	ϕ4.2 x 38 mm

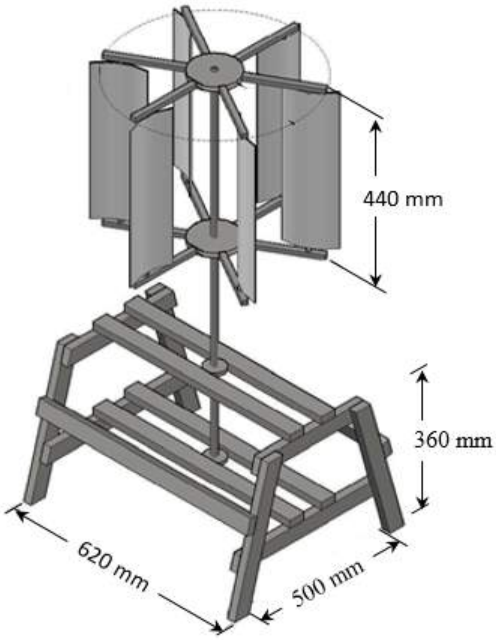

Figure 7: Three-D render of the assembly drawing of the first designed prototype of a VAWT

The dimensions of the central shaft of the first turbine prototype were ϕ15x1000 mm while the second prototype was ϕ12.5x1000 mm. In order to strengthen the central axis another tube was used to prevent vibration during the rotation. The dimension of the tube was ϕ12.5-ϕ32 x 700 mm. the length of the support tower was 220 mm in both prototypes.

VERTICAL AXIS WIND TURBINE CONSTRUCTION:

Blade Composite Material Construction Process

The most sensitive parts were the blades; therefore, a careful procedure was followed in order to produce accurate items. For these reasons, a mold consists of two components are designed and manufactured. The dimensions were chosen carefully to give the appropriate dimensions. The Figure 3 shows the manufacturing procedure of the blades. Briefly, the steps are as follow: a release film was painted to the internal surfaces of the mold; the first layer of mat was laid-up manually. Then the mixture, epoxy resin and a hardener, was manually added and uniformly distributed using a

roller. The same process was followed with the second layer. The upper mold was painted with release film and assembled with the lower parts. A pressure was applied using an external load for 24 hours in order to squeeze out all the excess resin and give enough time for curing. Figure 4 shows the two components of the used mold, and the produced items. It is used again to produce the blades for the second prototype.

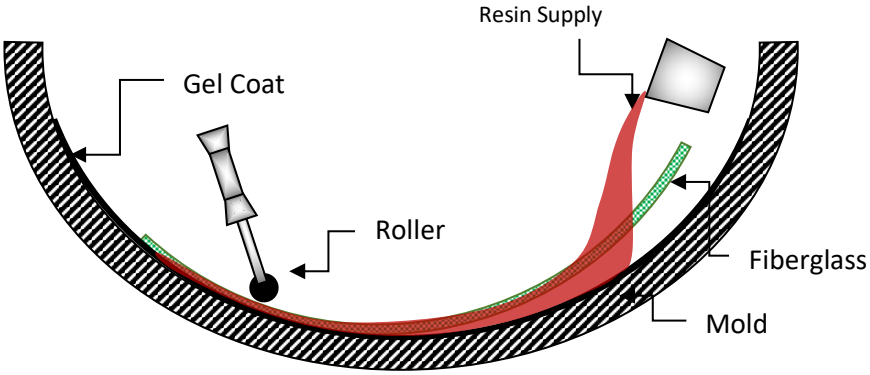

Figure 8: schematic drawing of the manual Lay-up process of the blades

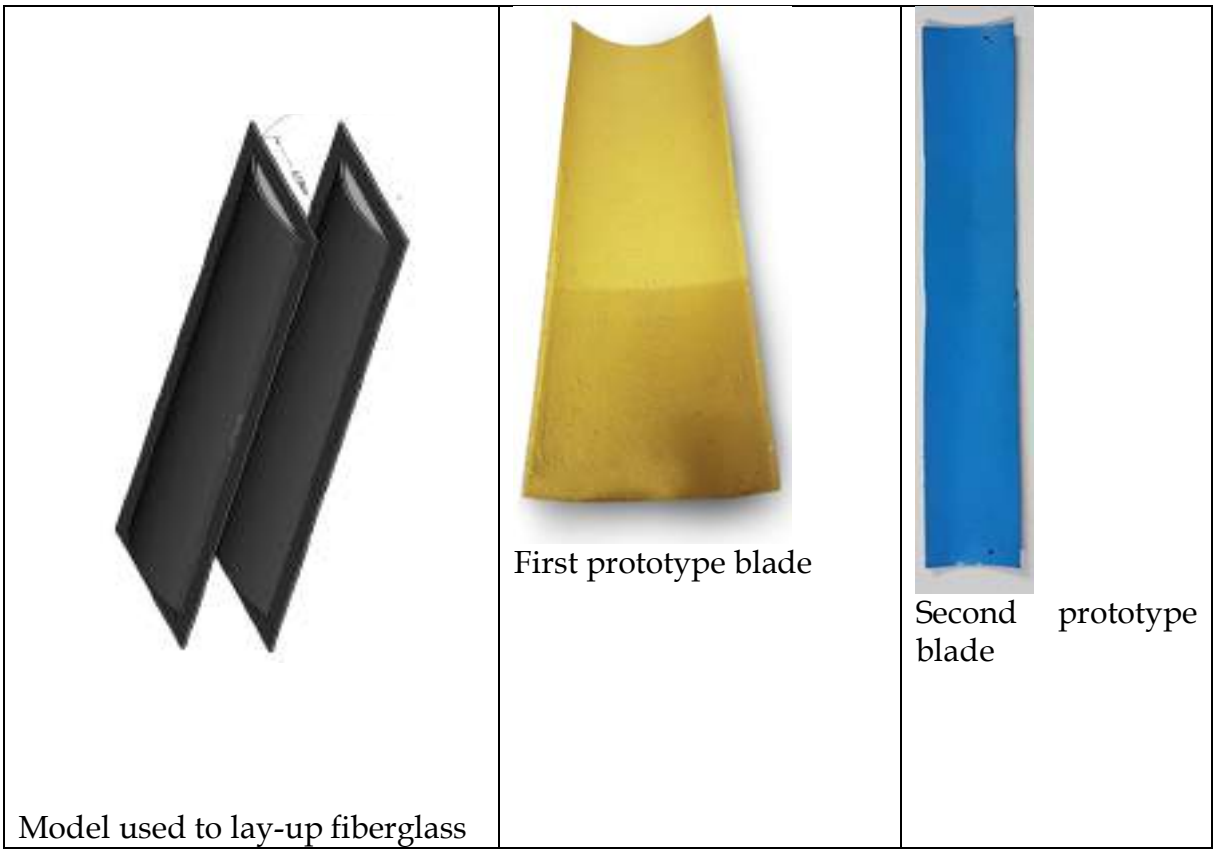

Figure 9: using the mold to make the blade from composite material

Passive Control Mechanism

The blade is rotating about the central axis of the rotor. Some blades produce a positive torque when the velocity vector sense agrees with the velocity vector of the wind while some other blades on the other side does not agree. Therefore, passive control mechanism is supplied such as to rotate the blades partially about their own axis. The purpose of the partial rotation is to reduce the blade projected area with respect to the

wind streamlines. This leads to reduce the drag force hence reducing the negative torque. Clearly, the position of the joints of the blade should be such as to produce a moment on the blade compatible with the rotation of the blade about the central axis. This may be achieved by locating the joints just forward of the symmetrical line of the blade and close to the central axis of the rotor. In this case, the drag force exerted by wind on the blade multiplied by the offset distance produces the control moments. The offset values were derived by using trial and error method, it was found that 20 mm offset value is enough to produce that moment on the blade to rotate for the first model and 10 mm for the second model. However, this value depends on the mass moment of inertia of the blade and the rotation speed of the rotor. For an accurate value, it is advised to optimize this value based on the parameters of a particular design. For this project, the joint is connected to blade using a bolt and a piece of metal sheet as shown in Figure 5.

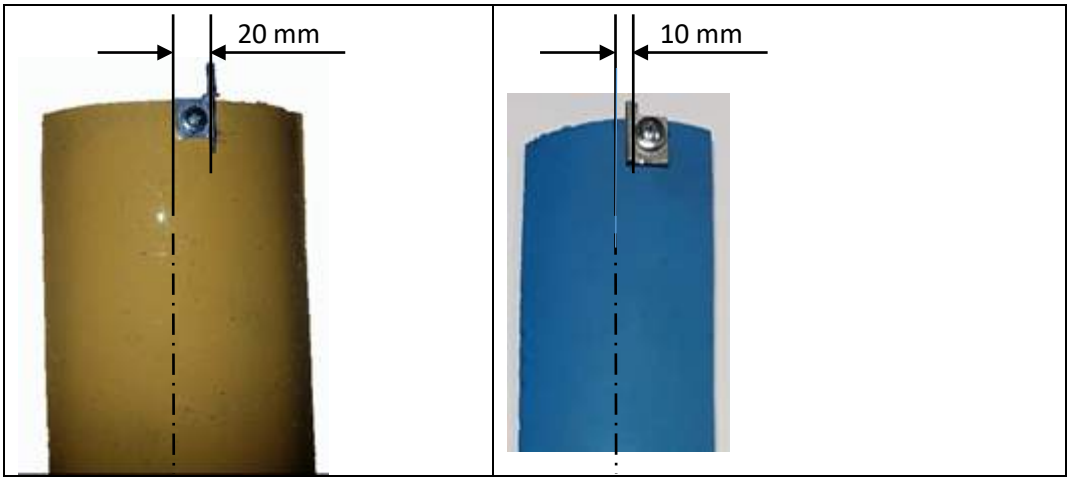

Figure 10: Blade Joint offset.

Another piece of steel sheet is formed and added to the joint as shown in Figure 6. The purpose of this configuration is to limit the motion on an angular sector of 35 degree. This value is also selected using a trial and error method. Bigger angle could lead the blade to lock while a smaller value reduces the freedom of the motion hence reducing the efficiency of the mechanism.

The angular limiter of blade rotation

Figure 11: motion limiter and assembly with the blade

Connecting Arms Assembly

The blades are connected to the central shaft using two wheels upper and lower. Every wheel consists of two circular sheets accommodating the central shaft bearing, 6203 RS. It is made of steel and riveted to the six arms that connecting the blades. In the second prototype, 10 arms are used as shown in Figure 7. The figure also shows a tiny bearing, type 624 Z, in order to reduce the friction of the joint during the motion of the blade about its own axis.

blade bearing, type 624 Z, and its fixture	The first prototype wheel and arms	The second prototype wheel and arms

Figure 12: The upper wheel connected to the blades supports (arms) for the two models

The two wheels are installed on the central shaft using two bearings. The shaft is provided with a tube in order to strengthen the axis during the rotation to avoid the vibrations noticed in the first model as shown in Figure 8. In addition, the blades are installed in the joint.

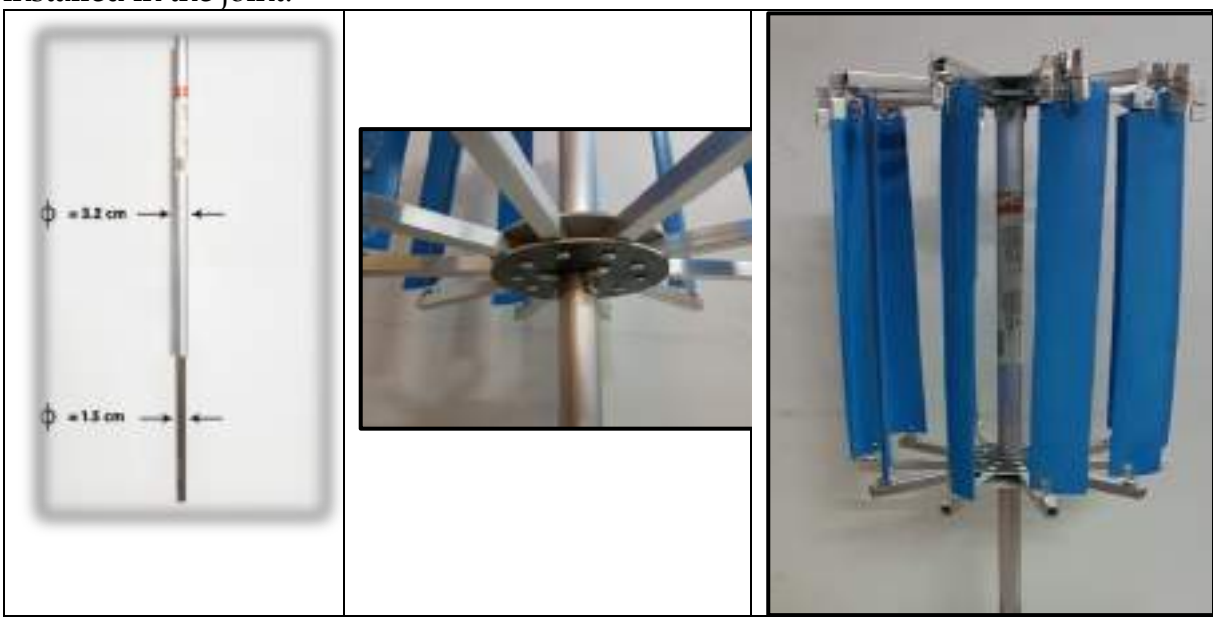

Figure 13: The wheel assembly with central shaft and the blades

In order to support the complete turbine in a vertical position, square-section bars have been assembled by bolts and rivets as shown in Figure 9. It provides support for the bearings of the two wheels and stabilizes the turbine during the rotation and it will accommodate the electric generator mechanism.

Figure 14: Final assembly of the two prototypes with bases

CONFIGURATION EXPERIMENTS

In order to reduce the costs, home fan had been used to generate the required wind, in addition to wind speed meter and rotation speed meter; it was possible to quantify the effects of the suggested mechanism on the overall performance in terms of rotational velocity of the rotor. Baring in mind that the model containing only the mechanical elements, it was not possible to estimate the amount of watts extracted by the turbine. However, the electrical generator can be found ready in the market.

Tachometer was used in order to measure the rotational speed of rotor, DT-2234A, the wind speed meter: Anemometer type VICTOR 816. This device can measure the wind speed until 30 m/s within the range of 10 – 45 C degree. The wind accelerated by a fan to air speed until 3.3 m/s.

EXPERIMENT RESULTS:

In order to eliminate any external wind effect, the experiments were carried out in a close and large workshop. The stream of wind was directed to wind turbine and measured using the anemometer every 5 seconds; in the same time a laser-beam, produced by the tachometer, is directed to the moving blades in order to measure the rotational speed of the rotor. The results are recorded and plotted as shown in Figure 10 at wind-speed 2.7 m/sec.

The test was repeated twice one using fixed blade configuration and another one using movable blades. During the experiments of the first model, two problems were noticed; the first one is that the motion of the blade was not always synchronized to the appropriate position. The second one is that the rotor at relatively high rotational speed causes the central shaft to vibrate. Therefore, in the second prototype, the mass of the blades is reduced, the central shaft was stiffened, and the number of blades is increased. Two more wind speeds were also tested; the wind speed 2.7 m/s is plotted in Figure 11. It shows the rotation speed of the wind turbine in two cases one fixed and the second movable blades. The other speeds were 3m/s and 3.3 m/s. They are plotted in Figure 12 and Figure 13 respectively.

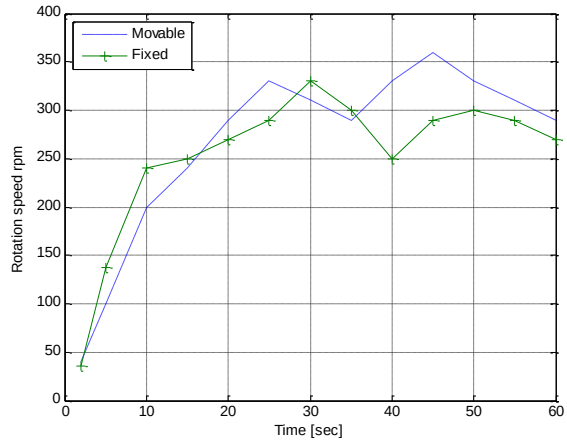

Figure 15: The rotational speed versus running time for the movable and the fixed blades turbine (1st. model) at wind speed, 2.7 m/s

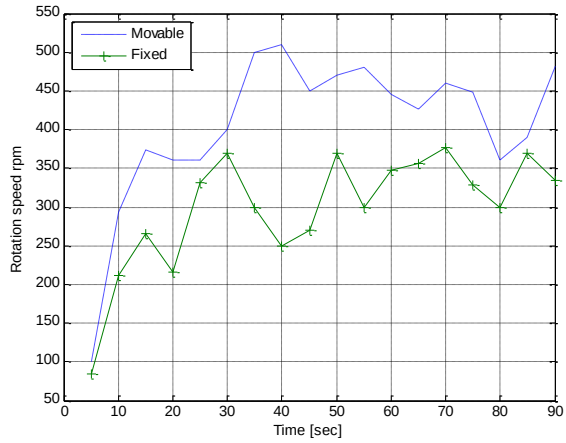

Figure 16: The rotational speed versus running time for movable and fixed blades turbine (2nd. design) at wind speed 2.7 m/s

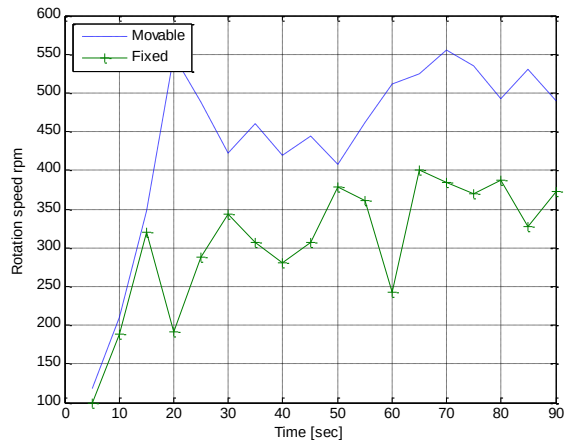

Figure 17: The rotational speed versus running time for the movable and fixed blades turbine (2nd. design) at a wind speed of 3 m/s

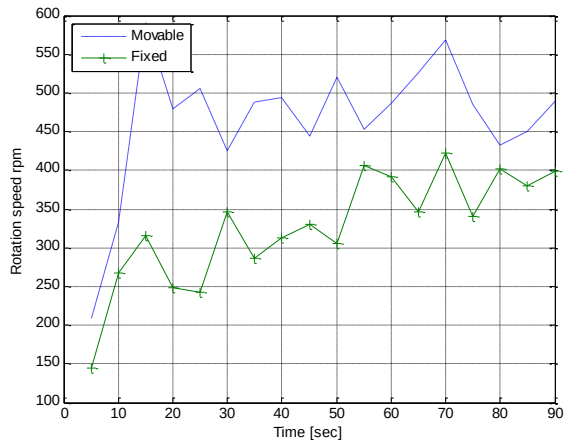

Figure 18: The rotational speed versus running time for the movable and fixed blades turbine (2nd. design) at a wind speed of 3.3 m/s

Clearly, in the first model the movable blades perform better than fixed blades turbine, the improvement is not significant. In the second model due to the modifications in

the design, the performance enhanced much better and at all wind speeds the improvement reaches up to 20%

ESTIMATION OF OUTPUT MECHANICAL POWER

Based on experimental results it is possible to estimate the extracted power by implementing the angular acceleration, α, evaluated from the time series of the rotation speed versus time. The useful torque cannot be calculated directly from the wind speed; but knowing the fact that the applied torque equals to the resistant torque generated by the inertia moment. Thus, it can be estimated as follow:

$$T = \alpha \cdot I, \qquad (1)$$

where, I is the mass moment of inertia of the rotating parts. It can be calculated using the weight and the geometry.
The total mass moment of inertia is calculated by equation 2.

$$I = I_{blades} + I_{arm} + I_{disk} + I_{shaft} \qquad (2)$$

For simplicity, the blades can be considered as concentrated mass at a particle at a distance R from the center of rotation, where, R is the radius of the rotor.

$$I_{blades} = N_{blades} \cdot m_{blades} \cdot R^2, \qquad (3)$$

where, N_{blades} is the number of blades, m_{blades} is the mass of the blade.

$$I_{arm} = 2N_{blades}\left(\frac{1}{12} \cdot L \cdot m_{arm} + m_{arm}\left(\frac{R}{2} - \frac{L}{2}\right)^2\right), \qquad (4)$$

where, L is the length of the arm, it is 0.170 m.

$$I_{disk} = \frac{1}{2} m_{disk} \cdot R_{disk}^2, \qquad (5)$$

there are two disks upper and lower one, in order to connect the arms to the central shaft.
After estimating the mass moment of inertia, the useful torque becomes known; the useful power can be estimated from equation:

$$P = T \cdot \omega\ , \qquad (6)$$

where, ω , is the sustained angular speed reached by the rotary at a certain tested wind speed. From the experimental results, the rotation speed of the second prototype is 450 rpm at 3.3m/sec.
Coding those relations using MATLAB code, the net mechanical power at 3.3m/sec was 30 watt.

CONCLUSION:

In this report, a brief description of the designing and the manufacturing of a vertical-axis wind-turbine prototype were presented. In an attempt to improve the performance of the turbine, a passive control mechanism is provided to the blades allowing a motion on an angular segment. This reduces the negative torque generated by the blades during returning shoot. Additionally, composite material was implemented in order to produce lightweight structure and reducing the costs of the manufacturing process. In a second attempt, the model is further improved by increasing the number of blades from 6 to 10; using one layer of fiberglass cloth, instead of using two layers of mat as well. For further weight reduction, the blades chord is reduced to half. After manufacturing and testing the second prototype, it was found two results. Firstly, the efficiency of the movable blades is higher than the fixed ones. Secondly, increasing the number of blades is producing a smoother run. The disadvantage of high number of blades is that the manufacturing costs are relatively higher and take longer time to make.

RECOMMENDATIONS

In future work, it is necessary to conduct more experiments at different wind speeds to estimate the starting and cut-off speeds and plot the characteristic P-V curve of the turbine; it defines the power change versus wind speed. Additionally, it is advised to simulate the wind turbine using numerical method to optimize the design parameters such as the number of blades, the blade's width, and the curvature of the blade. From other side, it is recommended to do research on designing the most appropriate electric generator in order to extract the maximum power with higher efficiency for this particular wind turbine.

REFERENCES

Aslam Bhutta, M. M., Hayat, N., Farooq, A. U., Ali, Z., Jamil, S. R., & Hussain, Z. (2012). Vertical axis wind turbine - A review of various configurations and design techniques. *Renewable and Sustainable Energy Reviews*, *16*(4), 1926–1939. https://doi.org/10.1016/j.rser.2011.12.004

Bedon, G., Raciti Castelli, M., & Benini, E. (2014a). Optimal spanwise chord and thickness distribution for a Troposkien Darrieus wind turbine. *Journal of Wind Engineering and Industrial Aerodynamics*, *125*, 13–21. https://doi.org/10.1016/j.jweia.2013.12.006

Bedon, G., Raciti Castelli, M., & Benini, E. (2014b). Proposal for an innovative chord distribution in the Troposkien vertical axis wind turbine concept. *Energy*, *66*(2014), 689–698. https://doi.org/10.1016/j.energy.2014.01.004

Budi, E. M., Banjarnahor, D. A., & Hanifan, M. (2017). Study of Vertical Axis Wind Turbine for Energy Harvester in A Fishing Boat. *IOP Conference Series: Earth and Environmental Science*, *75*(1), 012008. https://doi.org/10.1088/1755-1315/75/1/012008

Feng, G., Liu, Z., Daorina, B., & Gong, Z. (2009). Experimental research on vertical axis wind turbine. *Asia-Pacific Power and Energy Engineering Conference, APPEEC*. https://doi.org/10.1109/APPEEC.2009.4918357

Howell, R., Qin, N., Edwards, J., & Durrani, N. (2010). Wind tunnel and numerical study of a small vertical axis wind turbine. *Renewable Energy*, *35*(2), 412–422. https://doi.org/10.1016/j.renene.2009.07.025

Jin, X., Zhao, G., Gao, K., & Ju, W. (2014). Darrieus vertical axis wind turbine: Basic research methods. *Renewable and Sustainable Energy Reviews*, *42*, 212–225. https://doi.org/10.1016/j.rser.2014.10.021

Lim, Y. C., Chong, W. T., & Hsiao, F. B. (2013). Performance investigation and optimization of a vertical axis wind turbine with the omni-direction-guide-vane. *Procedia Engineering*, *67*(m), 59–69. https://doi.org/10.1016/j.proeng.2013.12.005

M. Saad, M. M. (2014). Comparison of Horizontal Axis Wind Turbines and Vertical Axis Wind Turbines. *IOSR Journal of Engineering*, *4*(8), 27–30. https://doi.org/10.9790/3021-04822730

Shaheen, M., & Abdallah, S. (2016). Development of efficient vertical axis wind turbine clustered farms. *Renewable and Sustainable Energy Reviews*, *63*(May 2018), 237–244. https://doi.org/10.1016/j.rser.2016.05.062

Shankar, P. N. (1979). *Development of vertical axis wind turbines. Proc. Indian Acad. Sci* (Vol. 2). Retrieved from https://www.ias.ac.in/article/fulltext/sadh/002/01/0049-0066

Xiao, Q., Liu, W., & Incecik, A. (2013). Flow control for VATT by fixed and oscillating flap. *Renewable Energy*, *51*, 141–152. https://doi.org/10.1016/j.renene.2012.09.021